

SOCIEDAD POLIMÉRICA DE MÉXICO

Advances in Polymer Science



Sociedad Polimérica
de México, A.C.

MACROMEX 2014

XXVII Congreso Nacional de la Sociedad Polimérica de México

***Nuevo Vallarta, México del 3 al 6
de diciembre de 2014***

Información Legal:

SOCIEDAD POLIMÉRICA DE MÉXICO, Año 13, No. 13, enero – diciembre 2014, es una publicación anual editada por la Sociedad Polimérica de México, A.C., Carretera Panorámica Prepa Pastita No. 12500, Barrio de la Alameda, C.P. 36000, Tel. 6641738928, <http://www.sociedadpolimerica.mx/portal/?p=memorias>, aliceac@tectijuana.mx.

Editor responsable: Dr. Ángel Licea-Claveríe. Reserva de Derechos al Uso Exclusivo No. 04-2015-052710244200-203, ISSN: 2448-6272, ambos otorgados por el Instituto Nacional del Derecho de Autor. Responsable de la última actualización de este número, Sociedad Polimérica de México, A.C., Carretera Panorámica Prepa Pastita No. 12500, Barrio de la Alameda, C.P. 36000, Tel. 6641738928, a cargo de la Dra. Beatriz García Gaitán, fecha última modificación, 6 de febrero de 2015.

Las opiniones expresadas por los autores, no necesariamente reflejan la postura del editor de la publicación.

Queda prohibida la reproducción total o parcial de los contenidos e imágenes de la publicación sin previa autorización de la Sociedad Polimérica de México, A. C.

COMITÉ EDITORIAL

***Angel Licea-Claveríe, Rubén González-Núñez
y Enrique Saldívar-Guerra***

PATROCINADORES



Prólogo	E. Saldívar-Guerra, A. Licea-Claverie y R- González-Núñez	1
Preface	E. Saldívar-Guerra, A. Licea-Claverie and R- González-Núñez	3

POLYOLEFINS

Ethylene polymerization via metallocenes: an experimental study ; by R. Infante-Martínez, E. Saldívar-Guerra, O. Pérez-Camacho and M. García-Zamora	5
Zirconocene aluminohydride/methylaluminumoxane clathrates for ethylene polymerization in slurry ; by B. Padilla-Gutiérrez, C. Ventura-Hunter, M. García-Zamora, S. Collins, A.N. Estrada-Ramírez and O. Pérez-Camacho	10
Study of kinetic behavior and reproducibility of ethylene polymerizations with zirconocene aluminohydride complexes ; by V.E. Comparán-Padilla, O. Pérez-Camacho, J.R. Infante-Martínez, M. García-Zamora and G. Cadenas-Pliego	15
Prediction of molecular weight distribution in chain growth polymerizations ; by R. Infante-Martínez, E. Saldívar-Guerra, O. Pérez-Camacho, M. García-Zamora and V. Comparán-Padilla	20
Rheological characterization of polyethylene resins used in extrusion blow-molded films ; by J. Gudiño-Rivera, R. Saldívar-Guerrero, N. Aguilar -Moreno, D.I. Rodríguez-Otamendi	24
Studies on rheological behavior of commercial blends involving LLDPE, LDPE and HDPE, using a torque rheometer ; by R. Leal, L. Martínez, J. Gudiño, R. Saldívar	29
Preparation and characterization of PE-clay-silver nanocomposites with different compatibilizers ; by M.C. Ibarra-Alonso, S. Sánchez-Valdés, E. Ramírez-Vargas, M.G. Méndez-Padilla and M. Lozano-Estrada	34

BIOMATERIALS

Human fibroblast viability on chitosan grafted lactic acid , by L.N. Sandoval Hernández, N. Vázquez, L. Tamay de Dios, C. Velasquillo and K. Shirai	39
Polymeric scaffolds for skin , by G. Ruiz-Velasco, F. Martínez-Flores, J. Morales-Corona and R. Olayo-González	43
Implantation of composed scaffold of PLA/HA coated with polypyrrole for generating neotissue-bone in rabbit: biological and mechanical evaluation ; by M.G. Flores-Sánchez, A.M. Raya-Rivera, R. González-Pérez, D.R. Esquiliano-Rendon, J. Morales-Corona and R. Olayo-González	48
Characterization of suspensions of iodine-doped polypyrrole (PPY-I) synthesized by plasma in bovine serum albumin (BSA) solutions ; by O. Fabela-Sánchez, L. Medina-Torres, S. Sánchez-Torres, H. Salgado-Ceballos, A. Morales, A.L. Álvarez, R. Mondragón, M.G. Olayo, G.J. Cruz, A. Díaz-Ruiz, J. Morales, C. Ríos and R. Olayo	53
Scaffolds produced by electrospinning, modified by plasma and mechanically evaluated to the regeneration of articular cartilage tissue ; by N.C. Islas-Arteaga, X.H. Gutiérrez-García, A. Raya-Rivera, J. Morales-Corona and R. Olayo-Gonzalez	58
PCU electrospun scaffolds for the vascular system ; by R. Vera-Graziano, L. Ávila Gutiérrez, R. Montiel-Campos, A. Raya-Rivera and A. Maciel-Cerda	63
Synthesis of carbon nanotubes for the development of polymer-supported carbon nanotubes hydroxyapatite nanofibers ; by R. Román-Doval, J. Morales Corona, R. Olayo-González and M. Ortega-López	68
Carbon nanoparticles embedded into electrospinning fibers of polylactic acid to improved their biocompatibility ; by E. Fragoso-Pérez, J. García-Hernández, J. Morales-Corona and R. Olayo	73
Synthesis of a bionanocomposite with pharmacological potential ; by F. Bedolla-Cázares, G. Rodríguez-García, R.E. del Rio, J.B. González-Campos and M.A. Gómez-Hurtado	78
Synthesis of poly(urea-amide)urethanes prepared with aminoacids ; by L.H. Chan-Chan, J.V. Cauich-Rodríguez, J.M. Cervantes-Úc and F. Hernández-Sánchez	83

Synthesis and characterization of biodegradable polyesters grafted starches by ring-opening polymerization; by Z.B. Cuevas-Carballo, S. Duarte-Aranda and G. Canché-Escamilla	88
Continuous system for the treatment of liquids, plasma process-biodegradable hydrogels; by D. Guevara-Ruiz, E. Almaraz-Vega, J. C. Sánchez-Díaz, M. A. Sánchez-Castillo, L. E. Cruz-Barba and A. Martínez-Ruvalcaba	93
Electrically controlled release of amoxicillin from polyacrylamide/polyaniline hydrogels; by C.J. Perez Martinez, Teresa del Castillo Castro and T.E. Lara Cenicerros	98
Nanogels with polyhexylacrylate core and polyethylene glycol (PEG) shell with potential as nano-biomaterials; by Y. Cerda-Sumbarda, A. Zizumbo-Lopez and A. Licea-Claverie	103
Precursor microemulsion to prepare core-shell polymeric nanoparticles for pharmaceutical applications. Formation, stability and cytotoxicity; by S.E. Flores-Villaseñor, R.D. Peralta, J.C. Ramírez, D. Ribeiro and T. Rodríguez	108
New high frequency relaxation in chitosan and PVA; by S. Kumar-Krishnan, E. Prokhorov, G. Luna-Barcenas, A. Mauricio-Sanchez and O. Arias de Fuentes	113
Estimation of surface free energy of poly(lactic acid) during UV-Grafting with N-vinylpyrrolidone; by M.H. Gutierrez-Villarreal, F.J. Rodríguez-Gonzalez and Y. Perera-Mercado	118

PRECISION POLYMER SYNTHESIS AND SMART POLYMERS

New amphiphilic molecules using RAFT polymerization; by I. Sáenz de Buruaga-Yurramendi, R. García-González, M.A. Macías-Contreras, R. Guerrero-Santos, H.M. Tello-Mañón	123
Temperature sensitive polymeric micelles by the self-assembly of poly(N-vinylcaprolactam)-b-poly(hexylacrylate) block copolymers prepared by RAFT; by O. Ruiz-Galindo, S.M. Ponce-Vargas, N.A. Cortez-Lemus and A. Licea-Claverie	128
Synthesis of Au nanoparticles coated with poly (N-isopropylacrylamide) folic acid functionalized; by G.D. García-Olaiz, N.A. Cortez-Lemus and A. Licea-Claverie	133
Synthesis of acrylamide-hexadecyl acrylamide block copolymers by RAFT emulsion polymerization; by S. Carro-Sánchez, V. González-Coronel, J. Cabello.Romero, J.V. Amador-Noya, J. Castillo-Tejas and F. López-Medina	138
Polymerization of styrene by reverse ATRP in scCO₂; by C.P. Rosales-Velázquez, J.R. Torres-Lubián, E. Saldívar-Guerra and E. Díaz-Barriga	143
Surface initiated NMP through a stable latex of block copolymers PAA-b-PS-b-PAA; by C. St Thomas, J.N Cabello-Romero, H. Maldonado-Textle, F. D'Agosto, B. Charleux, R. Guerrero-Santos	148
Development of new polymeric materials from ε-Caprolactam and starch; by M.G. Rodríguez-Delgado, F.J. Rodríguez-González and O. Pérez-Camacho	153
Polymerization fronts of acrylic monomers in deep eutectic solvents using microfluidics; by R. Becerra-Olivares, M. Zorrilla-Valtierra, J. Delgado, A. Vega, B. Mendoza-Novelo, C. Villaseñor and I. Quintero-Ortega	159
Oligomeric dispersants based on maleamic acid copolymers; by M. García-Zamora, M. Flores-Guerrero, M.T. Córdova-Alonso and O. Pérez-Camacho	164
Synthesis of crosslinked and functionalized polystyrene by miniemulsion polymerization: Particle size control; by A.N. Estrada-Ramírez, R.D. Peralta-Rodríguez, O. Pérez-Camacho and G. Cortez-Mazatán	168
Preparation and study of epoxy shape memory polymers; by M.L. Berlanga-Duarte, R. Acosta-Ortiz, A.E. Garcia-Valdez, L.A. Reyna-Medina and F. Aranda-Guevara	173

NANOCOMPOSITES AND BLENDS

Performance of zinc oxide as catalyst for the polymerization and grafting reactions in the microwave-assisted synthesis of poly(D,L-lactide)/zinc oxide nanocomposites; by H. Rodríguez-Tobías, G. Morales, J. Enríquez and D. Grande	178
Taking advantages of the unique properties at nanoscale of the zinc oxide for the development of functional polymer materials: from particle synthesis to final applications;	

by G. Morales, C. Espinoza-González, O. Rodríguez, A. García, H. Rodríguez-Tobías, D. Grande and G. Barreto	183
Nanocomposite of acicular rod-like ZnO nanoparticles and semiconducting polypyrrole photoactive under visible light irradiation for dye photodegradation; by V.M. Ovando-Medina R.G. López, B. E. Castillo-Reyes, J. E.A. Orozco, H. Martínez-Gutiérrez and P.A. Alonso-Dávila	188
Synthesis of TiO₂/polypyrrole nanocomposites photoactive under visible light using anionic and cationic surfactants; by B. E. Castillo-Reyes, V. M. Ovando-Medina, P.A. Alonso-Dávila, E. Perez and H. Martinez	193
Effect of synthesis conditions on morphology, crystallinity and thermal stability of magnesium hydroxide particles synthesized through the microwave-assisted technique; by H. Ortiz-Vázquez, G. Morales, O. Rodríguez-Fernández, C. J. Espinoza-González, D. Grande and L.G. Valdés-García	198
Preparation and characterization of polyethylene with nano-magnesium hydroxide as flame retardant; by E.N. Cabrera-Álvarez, L.F. Ramos de Valle and S. Sánchez-Valdés	203
Particle size effect of nano-CaCO₃ on thermal and mechanical properties on a nano-CaCO₃-PP composite; by D.S. Villarreal-Lucio, J.L. Rivera-Armenta, A.L. Martínez-Hernández, C. Velasco-Santos, J. Guerrero-Contreras, I.A. Estrada-Moreno and A.M. Mendoza-Martínez	208
Preparation and characterization of modified asphalt blends using SEBS/nanoclay; by S. Zapién-Castillo, M.Y. Chávez-Cinco, J.L. Rivera-Armenta, M. Mendoza-Martínez and B.A. Salazar-Cruz	213
Morphological and electrical properties of PE/carbon nanoparticles nanocomposites for thermal applications; by J.A. Valdez-Garza, V.J. Cruz-Delgado, J.G. Martínez-Colunga and C.A. Ávila-Orta	220
Evaluation of properties for nanocomposites (PE/carbon nanoparticles) for high temperature applications; by M.F. Rea-Escobedo, J.A. Valdez-Garza, V.J. Cruz-Delgado, J.G. Martínez-Colunga, C.A. Ávila-Orta, F. Chávez-Espinoza and M.G. Méndez-Padilla	225
The role of polymer's nature used as reducing agent in the synthesis of metal nanoparticles; by A. Pérez-Nava, J.S. Pérez-Campos, J.B. González-Campos, Y. López-Castro and J.A. Aviña-Verduzco	230
Silver nanoparticles by in-situ synthesis on a low density polyethylene film and their characterization; by L. Muñoz-Jiménez, L.F. Ramos-De Valle and S. Sanchez-Valdés	235
Morphological, mechanical and dielectric properties of PP/copper nanoparticles nanocomposites for thermal applications; by J.A. Velázquez de Jesús, J.A. Valdez-Garza, V.J. Cruz-Delgado, J.G. Martínez-Colunga, C.A. Ávila-Orta, G.F. Hurtado López, J.G. Rodríguez-Velazquez and M.G. Méndez-Padilla	240
In situ polymerization of ethylene with CNT and/or Cu nanoparticles using zirconocene aluminohydride complexes on heterogeneous phase; by C. Cabrera-Miranda, O. Pérez-Camacho, J.G. Martínez-Colunga, M. García-Zamora and C.A. Ávila-Orta	245
Effect of different nature nanoparticles surface modification on polymer nanocomposites thermal conductivity; by Y. Olivares-Maldonado, E. Ramírez-Vargas, L.F. Ramos-deValle and M.G. Neira-Velázquez	252
Pinewood residues/recycled HDPE composites to substitute medium density fiberboards: mechanical properties evaluation; by O. Rivero-Be, R.H. Cruz-Estrada, C.V. Cupul-Manzano, J.G. Carrillo-Baeza and E. Pérez-Pacheco	257
Effect of UV stabilizers on the mechanical properties of a pinewood residues/recycled HDPE composite; by J.M. Peraza-Góngora, R.H. Cruz-Estrada, C.V. Cupul-Manzano, J. Guillén-Mallete, M.A. Rivero-Ayala and J. Reyes-Trujeque	262
Structural sisal fiber-polyester composite laminate characterization; by U Ramirez-Barragán, J.P. Dominguez-Cruz, F. Estrada-De los Santos, M. Talavera-Ortega and O.A. Jiménez-Arévalo	267
Water absorption and mechanodynamic properties of composites based on thermoplastic starch/poly(lactic acid)/agave fiber; by F.J. Aranda-García, R. Gonzalez-Nuñez, C.F. Jasso-Gastinel and E. Mendizabal	272

Graphitic structures effect on the thermal conductivity of HDPE compounds; by E.E. Martínez-Segovia, L.F. Ramos de Valle, S. Sánchez-Valdés	277
Comparative study of plastic films bonded to cellulose as a bilayer materials; by M. Trujillo, A. Vargas, A. Maciel and M. Morales	283
Optimization of a polymer blend based on recycled polystyrene and styrene-butadiene rubber; by J. Veilleux and D. Rodrigue	288

ADVANCED POLYMER MATERIALS: OPTOELECTRONICS AND NANOMATERIALS

Mesomorphic and optical properties of ionic liquid-crystalline copolymers; by R.J. Rodríguez-González, C. de Santiago-Solís, O.L. Torres-Rocha, L. Larios-López, G. Martínez-Ponce and D. Navarro-Rodríguez	293
Morphology and conductivity tuning of polyaniline using short-chain alcohols by heterophase polymerization; by M.A. Corona-Rivera, V.M. Ovando-Medina, H. Martínez-Gutiérrez, F.E. Silva-Aguilar, E. Pérez, I. D and A. Carmona	298
Graphene oxides modification with poly(phenyleneethynylene)s by microwave-assist for solar cell applications; by G. Turlakov, E. Arias, I. Moggio, R.F. Ziolo, R.M. Jiménez and P. González-Morones	303
Synthesis and thermal properties of methacrylic polymers with a pendant zwitterionic moiety; by G. Guzmán, J. Cardoso, D. Nava and I. González	308
Morphological and electrochemistry properties of polymer electrolytes; by D. Nava, G. Guzmán, J. Cardoso and I. González	313
Au nanoparticles supported on aminopropyl functionalized silica particles as catalyst for the selective oxidation of styrene; by D.C. Martínez-Lejía, I. Moggio, J. Romero-García, C.A. Gallardo-Vega, E. Arias and J.R. Torres-Lubián	318
Nanoparticles of polymers synthesized by plasma polymerization; by M. Vasquez-Ortega, M. Ortega-Lopez, J. Morales-Corona and R. Olayo	323
Preparation of zinc oxide nanostructures and hybrid graphene/zinc oxide nanomaterials by a polysaccharide aqueous-based method; by M.B. Moreno-Trejo, Y. Agapito-Navarro, U. Márquez-Lamas, T. Lara-Ceniceros, J. Bonilla-Cruz and M. Sánchez-Domínguez	328

ADVANCED POLYMER MATERIALS: MEMBRANES

Sulfonation of commercial polysulfones UDEL and RADEL for membranes of reverse osmosis; by M.A. Yam-Cervantes, M.I. Loria-Bastarrachea, J.L. Santiago-García and M.J. Aguilar-Vega	333
Crosslinked PVA and PAAC membranes containing sulfonic acid groups: effect of cross-linking on the swelling degree and ion exchange capacity; by M.G. Aca-Aca, M.I. Loria-Bastarrachea, J.L. Santiago-García and M.J. Aguilar-Vega	338
Control of preparation process to form a sol-gel membrane deposited in plastic fiber optic for pH detection; by D.A. Razo-Medina, O. Ortiz-Jimenez, E. Alvarado-Méndez and M. Trejo-Durán	344
Pure gas permeation of membranes obtained from a novel polyimide (PI BTD-MIMA) /polibenzimidazole blends; by J.M. Pérez-Francisco, M.I. Loria-Bastarrachea, J.L. Santiago-García and M. Aguilar-Vega	349
Minimum parameters necessary for grow a thin film with a sol-gel method; by O. Ortiz-Jimenez, D.A. Razo-Medina, M. Trejo-Durán, E. Alvarado-Méndez, R.I. Mata-Chávez and M. Martínez-Rosales	354

POLYMER ENGINEERING, SIMULATION AND GENERAL TOPICS

Polystyrene pickering polymerization: mechanistic events; by L. I. García Damián, A. Rosas-Aburto, B. Fouconnier, A. Román-Guerrero and F. López-Serrano	359
Synthesis of core-shell resins for heavy-metal removal by seeded suspension copolymerization; by A. Tlilayatzí-Muñoz, S. Carro and J. Cardoso	364
Synthesis and characterization of macroporous resins from poly(4-vinylpyridine) and divinylbenzene functionalized by ampholyte groups; by J.A. Arcos and J. Cardoso	369

Synthesis of polymeric microcapsules for coatings applications; by A. Ortega-Carrizo, M.E. Velázquez-Sánchez, J.P. Acosta-Ramírez and I. Sáenz de Buruaga-Yurramendi	374
Synthesis of cis-1,4 poly(butadiene) in solution with styrene and their use as precursor rubber in high impact polystyrene by “in situ bulk” polymerization process; by G. Bosques-Ibarra, F. Soriano-Corral, F.J. Enríquez, R.E. Díaz de León and J.F. Hernández-Gómez	379
Polymerization of 1,3 butadiene in presence of styrene using neodymium versatate catalyst and synthesis of ABS by “in situ bulk” process; by P.A. de León-Martínez, F. Soriano-Corral, R.E. Díaz de León-Gómez, F.J. Enríquez-Medrano and J.F. Hernández-Gómez	384
Solution polymerization of methyl methacrylate in a ionic liquid employing cyclic multifunctional initiators; by K. Delgado-Rodríguez, G. Morales, P. Acuña, J. Enríquez and G.P. Barreto	389
Computational chemistry applied in the study of the structural properties in PEHD/wheat husk/ benzophenone composites; by N.A. Rangel-Vázquez and A.I. García-Castañón	394
Analysis of the absorption process of benzophenone in rice husk/polyethylene composites due amber and MM+ models; by N.A. Rangel-Vázquez and A.I. García-Castañón	398
A DFT study among interaction sites: NH₃⁺ of polymeric chitosan and SO₃⁻ of azoic colorant red 2; by J.H. Pacheco-Sánchez, B. García-Gaitán and R.E. Zavala-Arce	402
Rheological characterization and modeling of a water based perforation fluid; by A. Renteria, L. Medina-Torres, F. Calderas, O. Manero, A. Sánchez-Solís and C. Lira-Galeana	408
Rheological and structural characterization of hydrofobically modified polyacrylamide solution obtained by emulsion polymerization; by V.J. González-Coronel, S. Carro-Sánchez, N. Tepale-Ochoa, J. Cabello-Romero, J.V. Amador-Noya and E. Hench-Cabrera	411
Kinetic study of the thermal and thermo-oxidative degradation of ethylene-norbornene copolymers; by H.B. León-Molina, M. Gutierrez-Villarreal and R. Acosta	416
Thermal decomposition of pinacolone diperoxide (PDP) and diethyl ketone triperoxide (DEKTP) in methyl methacrylate and its further polymerization kinetic study; by K. Delgado-Rodríguez, G. Morales, J. Enríquez and G.P. Barreto	421
Development of low shrinkage polymers by using expanding monomers; by Ricardo Acosta-Ortiz, M. Sangermano , A.G. Savage-Gomez, A.E. Garcia-Valdez and M.L. Berlanga-Duarte	426
Degradation and characterization of polyethylene terephthalate (PET) for the elimination of lead (II) in water; by J.D. Estrada-Flores, N.A. Pérez-Rodríguez, M.G. Sánchez-Anguiano, P. Elizondo-Martínez and J. Rivera de la Rosa	431
Preparation and characterization of a thermoplastic matrix of poly-epsilon-caprolactone with chitosan for removal heavy metals from wastewater; by O. Velasco, M. Gimeno, R. Beristain, R. Rosas and K. Shirai	436
Effect of the height of the bed in a packed column with chitosan cryogels for sorption of Cu²⁺ ion; by A. Ostria-Hernández, A.J. Arcos-Arévalo, R.E. Zavala-Arce, P. Ávila-Pérez, E. Guibal, B. García-Gaitan and J.L. García-Rivas	441
Thin films of chitosan/pyrrolil quinone for adsorption of fluoride and nitrites; by M. Tapia-Juárez, J.B. González-Campos and L. Chacón-García	446
Synthesis of novel semiconducting polyurethane/polypyrrole/polyaniline composites for microorganism immobilization and wastewater treatment; by I.D. Antonio-Carmona, S.Y. Martínez-Amador and V.M. Ovando-Medina	451
Red 2 dye adsorption by chitosan-based bioadsorbent: a kinetic study; by R. Suárez-Reyes, A. Valdez-Zarco, C. Hernández-Tenorio, R.E. Zavala-Arce, J.L. García-Rivas, B. García-Gaitán	456
Sorption of fluorides using chitosan's cryogels; by A.J. Arcos-Arévalo, R.E. Zavala-Arce, P. Ávila-Pérez, B. García-Gaitán , J.L. García-Rivas and M.L. Jiménez-Núñez	461
Evaluation of the adsorption of red 2 dye in aqueous solution using chitosan-cellulose hydrogel beads; by J.I. Moreno-Puebla, C. Hernández-Tenorio, B. García-Gaitan, J.L. García-Rivas, R.E. Zavala-Arce and J.H. Pacheco-Sánchez	466

Encapsulation of extractants with biopolymers for palladium recovery; by T.I. Saucedo-Medina, R. Navarro-Mendoza, M. Dzul-Erosa, E. García-Vieyra, M. del Pilar González-Muñoz, E. Elorza.Rodríguez and E. Guibal	471
Thermodynamic parameters of fluoride ion adsorption by a biopolymer; by B.M. Millán-Olvera, J.L. García-Rivas, R.E. Zavala-Arce and B. García-Gaitán	476
Synthesis and characterization of some polymerizable surfactants (Surfmers); by M. González-Pluma, L.E. Elizalde-Herrera and E. Saldivar-Guerra	481
Degradation of plastics by plasma in a radio frequency reactor; by E. de J. Silva-Valenciano, M.G. Neira-Velazquez, Y.K. Reyes-Acosta, C.G. Hernández-Ramos, M.G. Mendez-Padilla	486
Metathesis depolymerization of chicozapote (manilkara zapota); by S. Reyes-Gómez and M. Tlenkopatchev	491

Prólogo, Macromex 2014, Trabajos en Extenso

Este volumen es una colección de trabajos presentados en la tercera versión del Simposio bianual Estados Unidos-México sobre Avances en Ciencia de Polímeros, Macromex 2014.

Las primeras dos ediciones de este simposio se llevaron a cabo en los años 2008 y 2011, respectivamente, y ambas fueron un éxito en cuanto a la calidad de los trabajos presentados y en cuanto a la variedad de interacciones entre científicos, principalmente de Estados Unidos y México, pero cada vez más de otros países.

Esta serie de conferencias nació como resultado de esfuerzos conjuntos entre la Sociedad Polimérica de México (SPM) y la división polímeros de la Sociedad Química Americana (ACS) con el objetivo de mejorar la cooperación e interacciones científicas entre investigadores de Estados Unidos y México. En la edición del 2011 también contamos con la participación de un grupo de científicos distinguidos del Canadá que contribuyeron significativamente a la calidad del evento. En la versión actual (2014) un grupo selecto de científicos canadienses también se unieron a los esfuerzos.

Macromex 2014 se llevó a cabo del 3 al 6 de diciembre de 2014 en Nuevo Vallarta, Nayarit, en la costa del pacífico mexicano. En el simposio se tuvo participación de 9 países en forma de 98 presentaciones orales y 197 carteles, sobrepasando los números de las dos versiones previas de este simposio.

Kris Matyjaszewski (Carnegie Mellon University), Rigoberto Advincula (Case Western Reserve University) y Kenneth Wynne (Virginia Commonwealth University) fueron presidentes del evento por parte de los Estados Unidos, mientras que Oliverio Rodríguez Fernández (Centro de Investigación en Química Aplicada, CIQA), Beatriz García-Gaitán (Instituto Tecnológico de Toluca) y Enrique Saldívar-Guerra (CIQA) fueron sus contrapartes por parte de México. Sin embargo el éxito del evento, como en las versiones anteriores, se debió al trabajo de un grupo más amplio de colegas que apoyaron tanto la organización como la realización del evento mismo.

Los polímeros y los materiales poliméricos son ya pieza fundamental de la vida moderna y de la tecnología, y los beneficios de su uso para la sociedad sobrepasan por mucho los posibles impactos negativos en el medio ambiente cuando sus desechos no son manejados de manera adecuada. Cada vez hay más aplicaciones avanzadas en campos relacionados con la solución a los grandes problemas de la sociedad que son investigados y materializados utilizando polímeros. Por ejemplo en los campos de fuentes alternativas de energía, aplicaciones biomédicas, tratamiento de aguas residuales, extracción de petróleo, separación de gases, por nombrar algunos. También, la búsqueda de respuestas a la preocupación por los efectos adversos para el medio ambiente por el uso de polímeros no biodegradables, es un área de investigación activa, principalmente investigando biopolímeros y biomateriales, aunque no exclusivamente.

La síntesis, modificación, caracterización y aplicación de materiales poliméricos en estas áreas, son el tema principal de los trabajos presentados Macromex 2014, de los cuales, la presente colección de trabajos es una muestra representativa.

Agradecemos a los autores que enviaron sus trabajos en extenso para publicación en el presente volumen.

En este volumen se incluyen 98 trabajos, los cuales están clasificados de la siguiente manera:

- Poliolefinas
- Biomateriales
- Síntesis precisa de polímeros y polímeros inteligentes
- Nanocompositos y mezclas
- Materiales poliméricos avanzados: Optoelectrónica y Nanomateriales
- Materiales poliméricos avanzados: Membranas
- Ingeniería de polímeros, simulaciones y tópicos generales

Los organizadores del evento agradecen el apoyo económico del Consejo Nacional de Ciencia y Tecnología (CONACYT-México), del Centro de Investigación en Química Aplicada (CIQA) y de la Universidad de Guanajuato.

Esperamos continuar con estos esfuerzos para organizar en el futuro la próxima edición de esta serie de conferencias exitosas.

Enrique Saldívar-Guerra, Angel Licea-Claverie y Rubén González-Núñez

Preface, Macromex 2014 Extended Abstracts

This volume is a collection of papers presented at the third version of the triannual Binational US-México Symposium on Advances in Polymer Science, Macromex 2014. The first and second editions of this conference took place in 2008 and 2011 respectively, and both were a success in terms of the quality of the papers presented and the rich interaction between scientists, mainly from US and México, but also increasingly from other countries. This series of conferences was born as a result of a joint effort of the Mexican Polymer Society (MPS) and the Polymer Chemistry Division of the American Chemical Society (ACS) aimed at increasing the cooperation and scientific interaction among researchers of US and Mexico. In the 2011 edition we also had the presence of a group of distinguished Canadian scientists who contributed significantly to the quality of the meeting. In this new version again, a selected group of Canadian researchers also joined the effort.

Macromex 2014 took place on December 3-6 of 2014 at Nuevo Vallarta, Nayarit, in the west coast of Mexico. The conference included participation from 9 countries in form of 98 oral presentations and 197 posters, surpassing in numbers the two previous versions of this conference.

Kris Matyjaszewski (Carnegie Mellon University), Rigoberto Advincula (Case Western Reserve University) and Kenneth Wynne (Virginia Commonwealth University) acted as chairmen on the US side, while Oliverio Rodríguez Fernández (Centro de Investigación en Química Aplicada, CIQA), Beatriz García-Gaitán (Instituto Tecnológico de Toluca) and Enrique Saldívar-Guerra (CIQA) were their counterparts on the Mexican side. As in the previous meetings however, the success of this meeting was due to the work of a larger group of colleagues who helped in its organization and during the conference itself.

Polymers and polymeric materials are already a fundamental piece of modern life technology and their benefits to society surpass by far their possible negative impacts on the environment when their residues are not handled in a proper way. Increasingly, advanced applications of polymers in fields related to the solution of the great problems of society are researched and materialized. This is true in the fields of alternative sources of energy, biomedical applications, water treatment, oil extraction, gas separation, etc. to name a few. Also, the response to the environmental concerns created by non-biodegradable polymers is an active area of research, mainly but not exclusively, via the investigation in biopolymers and biomaterials. The synthesis, modification, characterization and application of polymers and polymeric materials in these fields are the main subject of the papers presented at Macromex 2014, of which the works in this collection are a representative sample.

We thank those authors who provided their extended abstracts for publication in this volume.

In this volume 98 papers are included grouped in a classification as follows:

- Polyolefins
- Biomaterials
- Precision Polymer Synthesis and Smart Polymers
- Nanocomposites and Blends

- Advanced Polymer Materials: Optoelectronics and Nanomaterials
- Advanced Polymer Materials: Membranes
- Polymer Engineering, Simulation and General topics

The organizers of the meeting acknowledge the financial support of the National Council of Science and Technology (CONACYT-Mexico), the Center for Research in Applied Chemistry (CIQA) and the University of Guanajuato.

We look forward to the organization of the next edition of this successful series of conferences.

Enrique Saldívar-Guerra, Angel Licea-Claverie and Rubén González-Núñez

ETHYLENE POLYMERIZATION VIA METALLOCENES: AN EXPERIMENTAL STUDY

Ramiro Infante-Martínez, Enrique Saldívar-Guerra, Odilia Pérez-Camacho, Maricela García-Zamora

Centro de Investigación en Química Aplicada, Saltillo, Coahuila. México.

Author's email: ramiro.infante@ciqa.edu.mx

Abstract

An experimental study oriented to gather kinetic modelling data in the ethylene polymerization via metallocenes is reported. Also is illustrated the employment of two methods for determination of kinetic behavior and the instantaneous activity of Ziegler-Natta catalysts in the slurry polymerization of ethylene. Is described the basis of both methods as well as the required instrumentation for its implantation a laboratory level. An experimental program of polymerization with two different metallocenic systems was executed, showing that the direct (measurement of ethylene flow) as well as the calorimetric method (based on energy balances) give equivalent high quality information on the kinetic performance of the catalyst.

Introduction

The evaluation of a Ziegler-Natta catalyst is performed in reactors of complete mixing with an exchange heat jacket at an operation scale of 200 mL to 2 L. The operation is done in a semicontinuous way with constant pressure and controlled temperature (in the reactor or jacket) in ethylene atmosphere. The addition of ethylene is carried out in a continuous way by means of a deposit of higher pressure that the reactor pressure. Since the pressure of the reactor is constant, the flow of ethylene is controlled by the polymerization rate. The measurement of this flow gives directly the polymerization rate.

Additionally, the liberated heat by reaction can be used to estimate the reaction extent. This method (calorimetric) has been employed successfully in a variety of polymerization reactions.[1-6] Rincón et. Al.[1] and Esposito et. al.[2] studied the batch and semi-batch emulsion polymerization of vinylacetate in a 5 liters calorimetric type reactor. They used a Kalman type filter to estimate the heat transfer coefficient as well as the conversion evolution. Korber et. Al.,[3,4] working with a commercial calorimeter (RC1 from Mettler-Toledo) in the propylene polymerization via metallocenes, report comparable results between on-line calorimetry and propylene consumption measurement with a mass flowmeter. Altarawneh et. Al.[5] investigated the emulsion polymerization of Styrene via RAFT. They were able to monitor the conversion as well as the molecular weight using only calorimetric techniques. However, the reports of the use of calorimetry for monitoring the ethylene polymerization are scarce. In a recent report,[6] the calorimetric method has been used for the monitoring of ethylene polymerization via metallocenes in a laboratory reactor. The authors refer successful results when they develop a calorimetric observer and compare it with an estimation of ethylene consumption based on the pressure of an ethylene reservoir.

As the instrumentation required to implement a calorimetric monitoring technique on or off-line (that is: at the moment of the test or a posteriori) is standard and economically accessible to most laboratories (only temperature sensors in the reactor and the jacket are necessary), it is convenient to consider the applicability of the calorimetric method to the reaction rate monitoring of the

ethylene coordination polymerization and compare it with the most standard monitoring method (direct measurement of ethylene flow). The suitability of the calorimetric method for an accurate kinetic characterization should not be taken for granted for a given polymerization system, as it will depend on a number of variables, such as the polymerization enthalpy and reaction rate, as well as the dynamic behavior of the catalyst in the reaction system. In the present work, the standard and the calorimetric methods are established and implemented in order to determine the polymerization rate in the ethylene coordination polymerization.

The implementation of the calorimetric method is developed using notions and tools readily accessible to the chemical practitioner. The study is conducted in a bench scale polymerization reactor equipped for the ethylene flow measurement as well as for the reaction heat evolution estimation. Two metallocene type catalysts are used that illustrate the applicability of the kinetic monitoring techniques. It is also demonstrated how these kinetic studies provide essential information for a deeper understanding of the chemical and dynamic nature of the catalytic system and to compare different catalytic systems based on their kinetic performance. The application of the data obtained with these methods to modeling studies of the catalytic system will be a matter of future reports.

Experimental

Polymerization reactor

The experimental arrangement employed is shown in Fig. 1. It consists of a metallic-top, 600 mL glass PARR reactor provided with a glass jacket for heat exchange. The agitation is provided with a magnetically sealed mechanic drive. The reactor operation can operate at vacuum or light pressures (< 150 psig) at 150°C or lower temperatures. A constant temperature circulating bath is connected to the reactor jacket. The temperature measurements are taken with type T thermocouples. The system has 3 temperature sensors: the first at the reactor interior through a thermo-well; the second at the reactor jacket inlet; the third is exposed to the ambient.

Ethylene flow measurement

The ethylene flow entering the reactor is measured via an Aalborg gas flow-meter of 0 -500 mL/min flow range. The measuring principle of this instrument is based on the heat capacity determination of a small fraction of the total stream flowing through the apparatus. This flow fraction enters to a capillary provided with an electric resistance injecting a constant heat flow to the stream. Two high precision temperature sensors are located at the inlet and outlet of the capillary in order to determine the heat capacity of the stream. This heat capacity is directly related to the mass flow of gases flowing through the capillary and, by means of standardized constants, the ethylene mass flow can be obtained.

Data acquisition system

It is a National Instruments Field Point 2000 bank, consisting of an Ethernet module containing a microprocessor with associated peripherals; a thermocouple module; and an analog input signal module (configurable as current or voltage inputs). Optionally, a digital output module to implement feedback control can be added. The signals proceeding from the process (temperatures and ethylene flow) are transmitted to the data acquisition system where they are digitalized and directed to the supervisory control system (PC computer running LabVIEW software).

Supervisory control system

The supervisory control system implemented is based on the National Instruments LabVIEW 9 Software. It runs on a conventional personal computer with MS Windows environment. Conceptually, it constitutes the interface between the operator and the process. The operator actions and the process responses are performed and visualized through the supervisory control system. Its main functions are: i) Communication with the data acquisition system to update in real time all the variables of the process; ii) Display of the main variables of interest by means of windows and graphical objects; iii) Register of the process variables in the computer hard disk.

Isoperibolic operation

The reactor is operated with a constant jacket temperature (isoperibolic operation). This form of operation conveys the advantage of ease of implementation, as feedback control of the reactor temperature is not required, only control of the jacket temperature. This jacket temperature control can be simply accomplished by using a bath of controlled temperature integrated to the reactor jacket; the relatively large reservoir of the bath provides enough capacitance to absorb small disturbances that could create a deviation from the set point temperature. Also, in this operation modality, the reactor temperature evolution is a direct evidence of the thermal effect of the reaction, as described in the previous section.

Notice that, to the extent of our knowledge, the only other application of calorimetry [9] that has been reported for ethylene polymerization uses the isothermal instead of the isoperibolic modes, requiring a more elaborated control scheme than the simple one used here (isoperibolic) which only requires a constant temperature circulating bath that is a standard equipment in most laboratories.

Results and Discussion

Ethylene polymerizations using homogeneous (S1) and silica (SiO₂) supported heterogeneous (S2) catalytic systems, were conducted as described in the experimental part, in order to test the suitability of the calorimetric monitoring technique in ethylene coordination polymerizations run under a variety of kinetic conditions. Both homogeneous and heterogeneous systems were also studied in the presence of hydrogen as chain transfer agent in order to test if the calorimetric measurements could detect the rate-acceleration hydrogen effect previously reported for metallocene-based catalysts¹¹. The kinetic behavior at different polymerization conditions could then be compared by calorimetric measures transformed to activity (A), as discussed above.

Results of the kinetic monitoring realized in two polymerization tests with the catalytic system S1 and S2 are shown in Figure 1 and 2. Typical polymerization runs showing both monitoring methods are displayed. It can be seen that both methods reflect the same dynamic behavior of the catalysts.

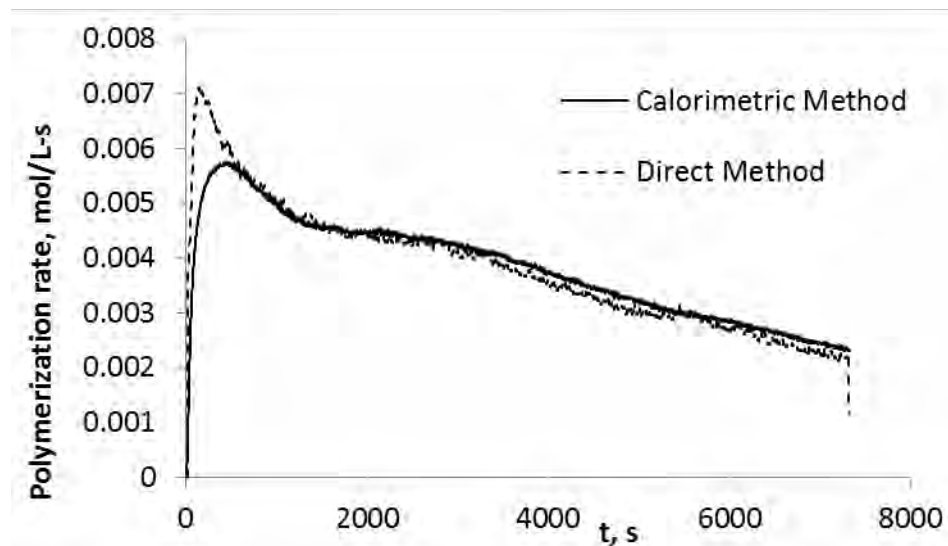


Figure 1. Polymerization test with catalytic system S1. Comparison of both monitoring methods.

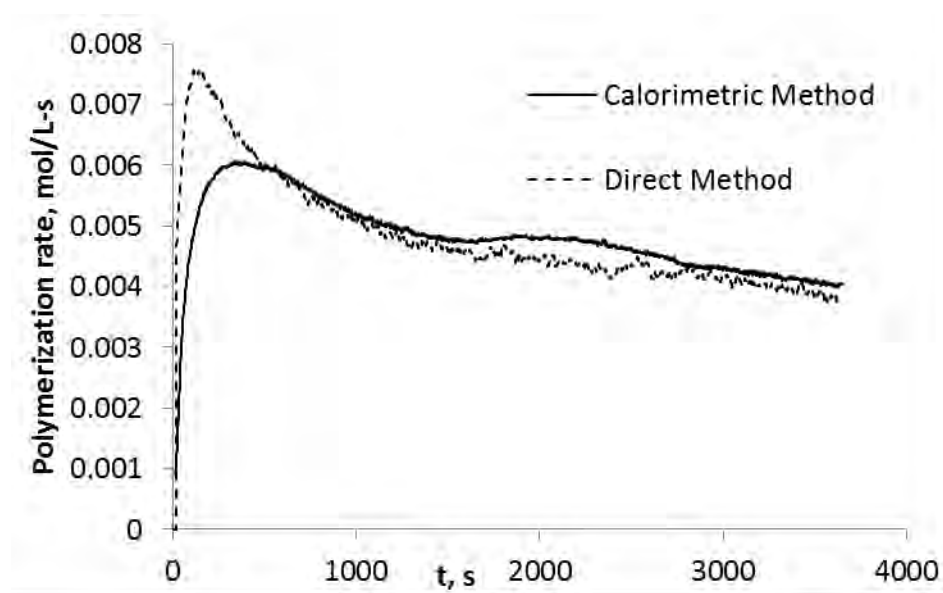


Figure 2. Polymerization test with catalytic system S2. Comparison of both monitoring methods.

Conclusions

It was characterized the kinetic behavior of two catalysts metallocenes with and without support by means of two techniques of monitoring that are mutually independent. These techniques can be employed simultaneously to increase the reliability of the test. The theoretical basis and sufficient experimental details are given to guide the implementation of both methods of monitoring in the coordination polymerization of ethylene at laboratory scale.

References

- [1] Rincon, F., Esposito M., Araujo P., Sayer C., Le Roux A. Macromolecular Reaction Engineering, 7(1), 24-35, 2013.
- [2] Esposito M., Sayer C., Machado R., Araujo, P. Macromolecular symposia 271, 38-47, 2008.
- [3] Korber F., Hauschild K., Fink G., Macromolecular Chemistry and Physics 202(17), 3329-3333, 2001.
- [4] Korber F., Hauschild K., Winter M., Fink G. Macromolecular Chemistry and Physics 202(17), 3323-3328, 2001.
- [5] Altarawneh I., Gomes V., Mourtada S. Polymer International, 58: 1427-1434, 2009.
- [6] Isse, V. F., Sheibat-Othman N., McKenna T.F.L. The Canadian Journal of Chemical Engineering, 88, 783-792, 2010.

Zirconocene Aluminohydride/Methylaluminoxane Clathrates for Ethylene Polymerization in Slurry

Benjamín Padilla-Gutiérrez,^a Carolina Ventura-Hunter,^b M. García-Zamora,^c Scott Collins,^d Alba Nidia Estrada-Ramírez^c and O. Pérez-Camacho^{*c}

^a Instituto Tecnológico de Saltillo, Venustiano Carranza 24000, Tecnológico, 25280 Saltillo, Coahuila, benjaminpadilla255@hotmail.com

^b Facultad de Ciencias Químicas, Universidad Veracruzana, Campus Coatzacoalcos, Av. Universidad Km 7.5 Col. Santa Isabel, C.P. 96535, caro_vethun@hotmail.com

^c Departamento de Síntesis de Polímeros, CIQA, Saltillo, 25250, Coahuila, México, odilia.perez@ciqa.edu.mx

^d Department of Chemistry, University of Victoria, P.O. Box 3065, Victoria, BC V8W 3V6, CANADA, scottcol@uvic.ca

Abstract

The main aim of this work is to obtain heterogeneous, zirconocene aluminohydride/methylaluminoxane (MAO) polymerization catalysts, without using inorganic carriers like silica. The syntheses of zirconocenium ion-based clathrates, formed from aluminohydride zirconocene complexes activated with MAO, are reported here. Several different approaches were examined for the synthesis of these clathrate compositions;¹ in one approach the catalyst (e.g. ¹PrCp₂ZrH₃AlH₂/MAO) was first prepared in toluene solution, and the clathrate phase then generated by addition of silicone oil. An alternate approach involved reaction of silicone oil or another clathrate-forming additive (e. g. KCl1¹) with MAO to form a solidified clathrate, and then introducing the zirconocene aluminohydride complex (e.g. ¹BuCp₂ZrH₃AlH₂). The clathrate catalysts were probed in the polymerization of ethylene in hydrocarbon slurry, without using additional co-catalyst (MAO), or at very low concentrations of modified MAO (MMAO 7, 13 wt% in IsoParE). The catalytic activities of the solid clathrate catalyst were compared as well as the morphology and properties of the polyethylenes synthesized in slurry.

Introduction

Zirconocene aluminohydrides are heterobimetallic complexes (Al-Zr) reported since 1970, as important intermediate compounds in organic syntheses or catalytic processes.² Several types of bridged and terminal Zr-H-Zr or Zr-H bonds were detected by infrared, but until 1997 Raston³ and Stephan⁴ confirmed by X-ray crystallography the presence of electron deficient bonds (bridged bonds, Zr-H-Zr or Zr-H-Al) as well as terminal hydride bonds (Zr-H and Al-H) stabilized as dimeric or higher nuclearity Zr-Al species. Since 2006 we reported the use of this kind of complex, as catalytic systems in coordination polymerizations and copolymerizations of olefins and α -olefins in homogeneous phase using different activators (MAO or boron compounds).⁵ As with most metallocenes, the zirconocene aluminohydrides were supported on porous silica, in order to obtain polyolefins of useful morphology in slurry polymerization processes.⁶ Different zirconocene aluminohydrides supported on silica produced very active systems (50-90 ton PE/molZr-hr), using MAO as co-catalyst, however the leaching of the catalysts was very evident because the fine particles produced in the reactors causing the fouling.⁷ According to several reports about studies of leaching in supported metallocenes, the trimethylaluminum (TMA) (always present in the MAO solutions) is highly reactive with oxygen, even with Si-O bonds of silica, causing fragmentation of the support, increasing the leaching of the catalysts.⁸ On the other hand, the use of silica as support for metallocene catalysts is restricted by several patents,⁹ which has motivated the searching of

alternative methods for using metallocenes and derivatives as the zirconocene aluminohydrides for the application in coordination polymerization in slurry.

In this work we studied the syntheses of zirconocenium ion-based clathrates, formed from aluminohydride zirconocene complexes activated with MAO, based on the reports of Sangokoya¹ for liquid clathrates using classical metallocenes (Cp_2ZrCl_2) and metallic salts of the first group (LiCl, NaCl or KCl), and the report of Pertti,¹ for preparing unsupported solid metallocene systems, using similar inorganic or organic salts and octamethyltrisiloxane (OMTS).

We tested two zirconocene aluminohydrides ($^n\text{BuCp}_2\text{ZrH}_3\text{AlH}_2$ and $^i\text{PrCp}_2\text{ZrH}_3\text{AlH}_2$) for the clathrate formation, using different approaches with two metallic salts (KCl and LiCl) and silicone oil.

Experimental

Synthesis of $^n\text{BuCp}_2\text{ZrH}_3\text{AlH}_2$ /MAO Clathrate

The zirconocene aluminohydride,⁴ was obtained from the corresponding $^n\text{BuCp}_2\text{ZrCl}_2$ (0.76 g, 1.87 mmol) in diethylether with 2.5 equivalents of LiAlH_4 (4.127 mL of 1M diethylether solution, 4.127 mmol), where the zirconocene aluminohydride was extracted in toluene (60 mL) or benzene (60 mL) having a stock solution of 3.11×10^{-5} mol Zr/mL. Apart in a 100 mL Schlenk, 2 g of MAO (without TMA) were dissolved in 10 mL of toluene or benzene, and then the corresponding amount of salt (KCl or LiCl) were added at 0°C, and the mixture was agitated during 12 hr. Two concentrations of salt were probed (10% and 30% in weight respecting to MAO). The MAO and the salt were mixed, until a viscous part, or second phase was observed (1-2 h). The solid material (clathrate) was reacted with 10 mL of zirconocene aluminohydride solution mixing during 24 h, then the mixture was ultrasonicated for 30 min and the viscous solution was introduced to the polymerization reactor, for probing the catalytic activity.

As for the clathrates prepared with silicone oil, this was previously dried with metallic sodium, refluxing 100 mL of silicone oil with 2 g of metallic sodium, during 4 h, and then the silicone oil was filtered under Ar atmosphere. 0.5 g of dry silicone oil was mixed with 5.19 g of solid MAO in 20 mL of toluene, during 12 h, and then an aluminohydride solution (5.66×10^{-5} mol Zr/20 mL toluene) was added to the mixture at 0°C. The clathrate formation was evident from the phase separation. The solution was decanted and the gel phase dried under vacuum for 2 h.

Synthesis of $^i\text{PrCp}_2\text{ZrH}_3\text{AlH}_2$ /MAO Clathrates

A stock solution of $^i\text{PrCp}_2\text{ZrH}_3\text{AlH}_2$ was prepared in toluene with a concentration of 2.65×10^{-6} mol Zr/mL. In this approach the aluminohydride was first activated with MAO, forming the cationic species (red or pink color), and the corresponding amount of silicone oil was dropped during 20 min, observing the clathrate precipitation as an oily phase. The toluene solution was decanted and the oil was dissolved in toluene and precipitated with hexane (1:4 v/v). The solid or oily phase was washed three times with hexane, and dried under reduced pressure for 2 h. The solid clathrate was analyzed by ICP determining the Al% and Zr%.

Ethylene Polymerization with Clathrates

Ethylene polymerizations were conducted in a 600 mL Parr reactor equipped with Ar and ethylene inlets, temperature control and mechanical agitation, as described in several reports for aluminohydride zirconocenes,⁶ using 3 mL MMAO as scavenger.

Results and Discussion

The zirconocene aluminohydride clathrates were prepared making several compositions and sequence additions, using salts (KCl or LiCl), silicone oil, MAO and zirconocene aluminohydrides ($^n\text{BuCp}_2\text{ZrH}_3\text{AlH}_4$ and $^i\text{PrCp}_2\text{ZrH}_3\text{AlH}_2$) based on the method reported by Sangakoya *et al.*¹ with some modifications. Table 1 and 2 describe the preparation conditions, and the polymerization results, respectively.

Table 1. Preparation conditions of clathrates $^n\text{BuCp}_2\text{ZrH}_3\text{AlH}_4/\text{MAO}/\text{KCl}$ or LiCl

Exp	Clathrate	salt	MAO/salt	MAO/Zr	Solvent	Time for clathrate formation
1	Clath 1	KCl	35	950	benzene	1h
2	Clath 2	KCl	35	900	toluene	1h
3	Clath 2	KCl	35	900	toluene	0.5 h
4	*Clath 3	KCl	35	900	toluene	1h
5	Clath 4	LiCl	17	900	toluene	2h
6	Clath 4	LiCl	17	900	toluene	2h

Clathrates formed as gel solution *Clathrate 3 formed inside the polymerization reactor

Table 2. Ethylene polymerizations using clathrates of $^n\text{BuCp}_2\text{ZrH}_3\text{AlH}_4/\text{MAO}/\text{KCl}$ or LiCl

Exp	Clathrate	Al:Zr	PE (g)	Activity KgPE/molZr·h	M _w (g/mol)	Đ
1	Clath 1	500	2.7	1630	98,800	2.4
2	Clath 2	500	3.4	4080	16,950	2.0
3	Clath 2	500	2.6	3150	19,300	1.7
4	*Clath 3	1000	5.2	3090	138,300	1.7
5	Clath 4	1800	4.5	1360	160,370	2.3
6	Clath 4	1800	10.0	2980	58,920	2.6

200 mL IsoParE ($i\text{C}_8$), T = 70°C, P_{C2} = 42 psi, 500 rpm, [Zr] = $1.4 - 9.1 \times 10^{-6}$ M

The clathrates prepared with KCl (Exp. 2) exhibited higher catalytic activities than that obtained with LiCl (Exp. 5 and 6) under the same procedure, however this first approach for clathrate preparation showed in all the cases gel formation, which was very difficult to introduce into the polymerization reactor. The fouling in the reactor was very evident suggesting that the metallocene was easily desorbed from the gelled clathrate in the presence of MAO.

In another procedure, silicone oil (0.5 mL) was first mixed with MAO (5.19 g/5 mL toluene), and then a toluene solution of zirconocene aluminohydride (5.6×10^{-5} mol/10 mL) was added drop wise at 0°C. Through this method the clathrate phase was separated, washed with more toluene, and dried under vacuum obtaining a pink powder. ICP analyses of the solid clathrate showed very low zirconium content (0.005 wt.%), 1.15 wt.% of Si, and 30.7 wt.% of Al. The ethylene polymerization results are shown in Table 3, where the polymerizations were carried out at different conditions, varying the solvent, Al/Zr ratio and ethylene pressure, keeping the same Zr concentration. Catalytic activities (Table 3) are higher than those obtained using salt-based clathrates, as well as the MW of the polymers, however, the wider dispersion of molar masses (Đ) could indicate polymerization in both heterogeneous and homogeneous phases.

In an alternate approach the activated catalyst ($^i\text{PrCp}_2\text{ZrH}_3\text{AlH}_2/\text{MAO}$) was first prepared in toluene solution, and the clathrate phase then generated by slow addition of silicone oil. The clathrate catalyst (pink solid) was tested in the polymerization of ethylene in hydrocarbon slurry, without using additional co-catalyst (MAO), or at very low concentrations of modified MAO (MMAO 7, 13 wt% in IsoParE). The polymerization conditions and results are presented in Table 4. Even the low Al/Zr ratio used (as obtained in the clathrate formation), the catalytic activities are higher than expected, compared to the clathrate evaluated in Table 1, where higher Al/Zr ratios were utilized.

The polymers obtained with this system show high MW and low dispersity of molar masses; however, formation of fine polymer particles, like emulsion (leaching) is more evident.

Table 3. Ethylene Polymerizations using the clathrate MAO/Silicone/ⁿBuCp₂ZrH₃AlH₄

Exp	Solvent	Al/Zr	P _{C2} (psi)	PE (g)	Activity (KgPE/molZr)	M _w (g/mol)	Đ
1	<i>i</i> C ₈	2000	42	5.7	4,000	102,400	3.2
2	<i>i</i> C ₈ : <i>n</i> Hpt	2000	42	7.1	5,100	153,460	3.6
3	<i>n</i> Hx	2000	42	4.2	3,000	73,830	3.0
4	<i>i</i> C ₈	2000	42	6.5	4,670	158,650	4.1
5	<i>n</i> Hx: <i>n</i> Hpt	2000	42	7.2	5,120	142,840	3.4
6	<i>n</i> Hx: <i>n</i> Hpt	4000	42	6.9	4,890	122,400	2.9
7	<i>n</i> Hx: <i>n</i> Hpt	6000	42	10.4	7,380	87,600	2.5
8	<i>n</i> Hx: <i>n</i> Hpt	4000	42	6.1	4,330	244,730	3.6
9	<i>n</i> Hx: <i>n</i> Hpt	3000	42	6.4	4,540	232,950	3.7
10	<i>n</i> Hx: <i>n</i> Hpt	3000	65	9.3	6,610	296,100	3.5
11	<i>n</i> Hx: <i>n</i> Hpt	3000	42	3.3	2,390	159,680	4.1
12	<i>n</i> Hx: <i>n</i> Hpt	3000	84	5.3	3,770	231,770	4.7

T = 70°C, [Zr] = 1.4×10⁻⁶, Al/Zr = 2000, 500 rpm, t = 1h, isooctane = *i*C₈, hexane: heptane, (*n*Hx:*n*Hpt 3:1), Isooctane:heptane (*i*C₈:*n*Hpt = 2:1).

Table 4. Ethylene Polymerizations using Clathrate MAO/ⁿBuCp₂ZrH₃AlH₄/Silicone Oil

Exp.	Solvent	Zr (10 ⁻⁶ mol)	Al/Zr	PE (g)	Activity (KgPE/molZr·h)	M _w (g/mol)	Đ
1	<i>i</i> C ₈	6.3	35	6.0	1,470	145,670	1.8
2	<i>i</i> C ₈ : <i>n</i> Hpt 2:1	2.8	35	2.3	1,250	176,390	2.0
3	<i>n</i> Hx: <i>n</i> Hpt 4:1	4.2	35	5.8	1,790	108,980	1.9
4	<i>i</i> C ₈ : <i>n</i> Hpt 4:1	4.4	35	3.8	1,300	146,370	2.0

T = 70°C, P_{C2} = 42 psi, 3 mL MMAO, 500 rpm, t = 1h, Isooctane (*i*C₈), Hexane:Heptane (*n*Hx:*n*Hpt), Isooctane:heptane (*i*C₈:*n*Hpt)

The fine particles formation in these polyethylenes, can be related to the homogeneous polymerization, where the aluminohydride zirconocene could be desorbed from the clathrate material, inside the polymerization reactor. According to the last results, the clathrate formed with silicone oil, where the metallocene is added after the mixture of silicone oil and MAO (8-10 wt. % Si/MAO), is the procedure which generated higher activity in ethylene polymerization and lower amount of fine polymer particles.

Conclusions

Zirconocene aluminohydrides were heterogenized through their clathrate species formed with silicone oil or KCl and LiCl salts, using several procedures, evaluated from the catalytic activity generated by the systems and the physical characteristics of the PE obtained.

The clathrate species prepared with silicone oil showed better results than the clathrates formed with salts, however, the procedures should be optimized, in order to get more stable zirconocene aluminohydride clathrates, avoiding its desorption at homogeneous phase.

Acknowledgments

The authors thank CONACYT México for financial support (Project No. 167901). Also thanks to Víctor Comparán, Guadalupe Méndez, Teresa Rodríguez, José Sánchez, Alejandro Espinoza and Sandra Ramos for technical support. And to Juan Uriel Peña and José Luis de la Peña for the electronic information supply.

References

- [1] a) Sangokoya, S. A. "Liquid clathrate aluminosilicate compositions" *US Patent 5,670,682* assigned to Albemarle Corp. **1997**, 8 pp. b) Pertti, E. "Process for preparation of an unsupported solid metallocene" *EP Patent 2,186,832 A1* assigned to Borealis AG, **2008**, 16 pp.
- [2] Wailes, P. C., Weigold, H. J. *J. Organomet.Chem.* **1970**, 24, 405-411.
- [3] K. Khan and C.L. Raston, *Organometallics*, **1997**, 16, 3252-3254
- [4] Etkin N., Hoskin A. J., Stephan D. W. *J. Am. Chem. Soc.* **1997**, 119, 11420-11424.
- [5] González-Hernández R.; Chai, J.; Charles, R.; Pérez-Camacho, O.; Kniajanski, S.; Collins, S. *Organometallics* **2006**, 25, 5366-5373.
- [6] R. Charles, R. González, E. Morales, J. Revilla, L. Elizalde, G. Cadenas, O. Pérez, S. Collins, *J. Mol. Catal. A: Chem.* **2009**, 307, 98-104.
- [7] V. Comparán Padilla, Thesis "Influencia de las condiciones de soporte de complejos aluminohidruros de zirconocenos" *March*, **2012**, Fac. Ciencias Químicas, Universidad Autónoma de Coahuila, México.
- [8] . N. Panchenko, V. A. Zakharov, E. A. Paukshtis, *J. Mol. Catal. A: Chem.* **2005**, 240, 33-39.
- [9] a) M. Chang "Method for preparing a supported metallocene-aluminosilicate catalyst for gas phase polymerization" *US Patent 4,937,301A* assigned to Exxon Chemical Patents Inc.,**1988**, 8 pp. b) M. Chang "Polymerization Process using a silica gel supported metallocene" *US Patent 5, 147,949 A* assigned to Exxon Chemical Patents Inc.,**1992**, 8 pp.

STUDY OF KINETIC BEHAVIOR AND REPRODUCIBILITY OF ETHYLENE POLYMERIZATIONS WITH ZIRCONOCENE ALUMINOHIDRIDE COMPLEXES

Víctor E. Comparán-Padilla*, Odilia Pérez-Camacho*, José R. Infante-Martínez, Maricela García-Zamora and Gregorio Cadenas-Pliego.

Centro de Investigación en Química Aplicada, Blvd. Enrique Reyna H. 140, Saltillo, Coahuila, México.

Abstract

In this work we studied the kinetic behavior and reproducibility of ethylene polymerizations using zirconocene aluminohydride complexes supported on SiO_2 and in solution. Homogeneous and heterogeneous systems activated with MAO were studied through their kinetic behavior, where the evolution of the polymerization rate, r_p , can be considered the fingerprint of the catalytic system.

Some variants in the polymerization reaction such as reaction time, co-monomer effect and hydrogen addition as transfer agent, were also studied. The polyethylenes obtained with both systems were analyzed and its characteristics compared by GPC, DSC and ^{13}C NMR. The Homogeneous system showed better reproducibility than the heterogeneous system.

Introduction

The high increase of polyolefin production has displaced some kind of commercial plastics that are less easy to manufacture or pose more problems for recycling or waste disposal. This increase is caused largely by new catalysts which are able to tailor the polymer structure and, by this, the physical properties. The metallocenes catalysts can produce many grades of polyolefins with precise control of microstructures, molecular weights (MW) and molecular weight distributions (MWD), as well as copolymers with homogeneous comonomer incorporation.^[1]

The majority of the metallocene catalysts in solution tend to be more active, but the homogeneous systems have severe problems in the operation of polymerization reactors, due mainly to the low bulk density of polymers obtained, that difficult the processing of the materials. Another disadvantage in polymerizations in solution is the great amount of MAO like cocatalyst necessary for activation and stabilization of the system. The heterogenization of this catalyst has been the technical and economical solution for correcting this problems, because can be obtained polymer with better morphology and bulk density.^[2] Porous silica (SiO_2) has shown by far the best results as support for this purpose, where the complexes can be stabilized and keep their activity, as in homogeneous phase. The usual method for supporting metallocenes, is through the previous modification of the silica with methylaluminoxane (MAO).^[3] A thermal pre-treatment of the silica is also required, for reducing its hydroxyl groups content, which could affect the MAO distribution on the surface, increasing the leaching or desorption of the metallocene, which is the main drawback of this method, affecting the morphology and bulk density of the polymer, since the leached catalyst is still active in solution in the presence of MAO.^[4] These differences of behavior between homogeneous and heterogeneous systems can be studied through kinetic behavior and the reproducibility in the ethylene polymerization reaction since the evolution of the polymerization rate, r_p , can be considered the fingerprint of the catalytic system, which can be used to understand the catalytic medium.^[5]

Frequently, at industrial level, activity values are used when comparing different catalysts; however, this information is lacking, because one same activity value can result from widely different kinetic behavior. For instances, a multisite catalyst could have the same activity as a single-site catalyst.^[6] Instantaneous activity values are better used to characterize a given catalyst. These are determined experimentally in low scale polymerization tests that report the instantaneous polymerization rate.^[7]

In this work we studied the kinetic behavior of the zirconocene aluminohydride complex supported on SiO_2 previously modified with methylaluminoxane (MAO), through the evaluation of ethylene

polymerization in heterogeneous and homogeneous phase using a low concentration of additional MAO as activator. We studied different catalytic media by comparing the kinetic polymerization data and reproducibility of the experiments. Some variants in the polymerization reaction such as reaction time, co-monomer and transfer agent were also studied. The polyethylenes obtained with homogeneous and heterogeneous system were analyzed by GPC, DSC and ^{13}C RMN. The Homogeneous system showed better reproducibility than the heterogeneous system.

Experimental

General data

All operations were carried out on a standard high vacuum line or in a dry-box under inert atmosphere. Toluene, diethyl ether, and 2, 2, 4-trimethylpentane, were reagent grade, distilled from the appropriate drying agents. MMAO-7 (13% isopar-E, Akzo Nobel), MAO (10% toluene, Aldrich) and LiAlH_4 (1 M, Et_2O , Aldrich) were used as purchased. The compounds $(n\text{-BuCp})_2\text{ZrCl}_2$ and $(\text{Cp}^*)_2\text{ZrCl}_2$ (Strem Chemicals) were used as catalyst precursors.

Synthesis of $\text{Cp}_2\text{ZrH}_3\text{AlH}_2$ complexes [$\text{Cp} = n\text{BuCp}$, Cp^]*

Complexes $(\text{Cp}^*)_2\text{ZrH}_3\text{AlH}_2$ and $(n\text{-BuCp})_2\text{ZrH}_3\text{AlH}_2$ were synthesized using the methods reported by Stephan and coworkers^[8a, b] varying the solvent and temperature of reaction. A suspension of $(n\text{BuCp})_2\text{ZrCl}_2$ (0.759 g, 1.876 mmoles) in 20 mL of ether was prepared in a 100mL Schlenk flask under Ar. A solution of LiAlH_4 in ether (1.01 M, 4.127 mL 4.127 mmoles) was added slowly at 0°C via syringe. After 15 min at 0°C , the suspension was mixed 15 min at room temperature, the mixture was filtered to remove LiCl and excess LiAlH_4 and the filtrate concentrated to dryness in vacuo to provide crude product, which was dissolved in 60 mL of toluene.

A similar procedure was used for $(\text{Cp}^*)_2\text{ZrH}_3\text{AlH}_2$, with the difference that this complex remained in a toluene solution and used directly in the polymerization reactions.

Thermal treatment of PQ silica

PQ silica was treated in a muffle furnace at 600°C for 6 h. After this, it was transferred to a 250 mL Schlenk vessel and cooled in vacuum for a further 8 h. Then a glass column (60x4 cm) was packed with dried PQ silica and heated in a tubular furnace to 600°C exposed with a flow of oxygen during for 2 h, then the powder was transferred to the Schlenk, cooled under a stream of argon to room temperature, and stored in a glove-box prior to use.

Impregnation of $n\text{BuCp}_2\text{ZrH}_3\text{AlH}_2$ on PQ silica/MAO

A fresh prepared toluene solution of $n\text{BuCp}_2\text{ZrH}_3\text{AlH}_2$ was added to a suspension of MAO modified PQ silica in toluene at 0°C under Ar atmosphere. The suspension was warmed to 25°C and stirred for 12 h under Ar. The supported catalyst was filtered under Ar and washed five times with dry toluene and dried in vacuum to provide a pink-colored powder, which turned pale yellow on exposure to air. The percentages of Zr and Al of the supported catalysts were determined by atomic absorption spectroscopy or by ICP analysis.

Polymerization procedure

The supported or soluble catalysts were activated using a 10 wt% toluene solution of MAO and in all the cases the solutions and suspensions were transferred by gas-tight syringe to the reactor. Polymerizations were carried out in a 600 mL Parr reactor equipped with mass flow meter and temperature control. The ethylene flow entering the reactor (polymerization rate, r_p) is measured via Aalborg gas flow-meter of 0–500 mL/min flow range and using a National Instrument C-DAQ connected to PC computer equipped with LabView software.

Results and Discussion

We investigated the behavior of two types of aluminohydride metallocene complexes: $(n\text{BuCp})_2\text{ZrH}_3\text{AlH}_2$ and $[(\text{Cp}^*)_2\text{ZrHAlH}_4]_2$ activated with MAO in ethylene polymerization reactions. The first complex was supported in SiO_2 previously modified with MAO, and the second one was tested in solution.

Table 1 also shows the characterization results of ethylene polymerizations using the heterogeneous catalyst.

Table 1. Ethylene Polymerizations using heterogeneous $(n\text{BuCp})_2\text{ZrH}_3\text{AlH}_2/\text{SiO}_2/\text{MAO}$.^a

No	Code ^b	H ₂ ^c	Oct. ^d	Time ^e	Activity ^f	Mw ^g (g/mol)	M _w /M _n ^g	Tm ^h (°C)	Tc ^h (°C)	% mol Oct. ⁱ
1	LLL	-	-	-	1869	60695	2.8	131.8	116.8	-
2	LLH	-	-	+	1077	90703	3.1	131.8	116.4	-
3	LHL	-	+	-	2063	17778	2.5	108.9	97.4	1.8
4	LHH	-	+	+	1558	26765	2.5	109.3	97.7	1.5
5	HLL	+	-	-	1221	7362	1.7	128.4	115.8	-
6	HLH	+	-	+	1088	7354	1.8	129.6	114.6	-
7	HHL	+	+	-	1869	7228	2	112.8	102	1
8	HHH	+	+	+	1609	7544	1.9	112.4	101.1	1.54

^a Conditions: 200 mL Isooctane, $[\text{Al}]/[\text{Zr}] = 2000:1$, 5 mL of 13 wt% MMAO in isoParE as scavenger, $P_{\text{C}_2\text{H}_2} = 42$ psig, $[\text{Cat}] = 3.09\text{--}3.37 \times 10^{-5}$ M, $T = 70^\circ\text{C}$, $t = 1$ or 2 h, 500 RPM, 0 or 13.3 mL 1-octene, 0 or 4.1 psig H₂. ^b L= low and H= high in H₂-Oct-Time. ^c with (+) or without (-) H₂. ^d with (+) or without (-) 1-octene. ^e 1 h (-) or 2 h (+). ^f Activity in Kg PE/mol of Zr*^h. ^g Determined from GPC chromatogram and universal calibration curve. ^h Determined from DSC. ⁱ Determined from ¹³C NMR spectrum.

For heterogeneous reactions, the amount of MAO contained in the support (modified silica) was determined to 12.7 %wt Al by atomic absorption (AA) analysis and was not considered in the Al/Zr ratio of the additional MAO used as activator. On the other hand, the zirconium content (2.15 % wt Zr) was determined by inductively couple plasma (ICP) analysis. The higher activities (Table 1) were observed at higher levels of co-monomer contents, low hydrogen contents at shorter reaction times. As expected, molecular weights (MW) of the polymers obtained with the supported catalyst decrease with the use of H₂ (transfer agent). The mixture C₂/H₂ 1000 psi/45 psi formed polyethylenes, around 7000 g/mol decreasing almost 80% of the original MW without H₂ (compare MW of Exp.1 and 5). The co-monomer effect contributed to increase the catalytic activity of the system as reported for several metallocenes, where the MW is less affected. The polydispersity of the polyethylenes is characteristic of these kind of single site systems, as well as the melting points for linear polyethylenes, except for the copolymerization reactions, where the melting points were shifted for more than 20 degrees to lower temperatures (108–112°C), as well as the crystallization points (97–102°C), with an average of co-monomer incorporation of 1.5% (determined by ¹³C NMR spectroscopy). Figure 1 show the kinetic behavior of ethylene polymerizations using the supported complex $[(n\text{BuCp})_2\text{ZrH}_3\text{AlH}_2/\text{SiO}_2/\text{MAO}]$ at 1 and 2 h of reaction time and varying comonomer (1-octene) and transfer agent (H₂).

Comparing Exp. 1-LLL and 8-HHH (Fig. 1), more differences in the kinetic can be observed. In the first case without H₂ and co-monomer (Exp.1-LLL), the initiation velocity is higher, but the activity decrease more rapid, than in Exp. 8-HHH, where the initiation is lower, but the ethylene consumption keeps almost constant during the 2 hours of reaction. In general, kinetic behavior of the ethylene polymerizations was not reproducible in the majority of the experiments, if we compare between experiments at 1 and 2 h (Fig. 1) with the same polymerization conditions (1-octene and H₂), only in the case of experiments 7-HHL and 8-HHH, using co-monomer, the kinetic curves are more similar at longer reaction times. The low reproducibility is attributed to the poor

dispersion of the zirconocene aluminohydride on the support, where the handled of the catalytic system for addition to the polymerization is difficult to reproduce.

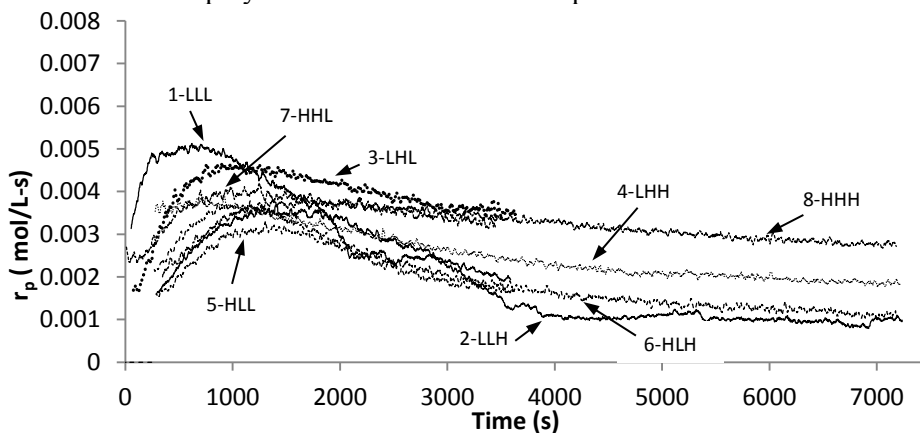


Figure 1. Kinetic behavior of ethylene polymerizations using $(n\text{BuCp})_2\text{ZrH}_3\text{AlH}_2$.

As for ethylene polymerizations in homogeneous phase we used the system $[(\text{Cp}^*)_2\text{ZrHAlH}_4]_2$, activated with additional MAO (Al:Zr) 2000:1. The polymerization reactions were conducted using 200 mL of Isooctane, at 42 psig of ethylene pressure or a mixture of ethylene/hydrogen 1000psi/45psi (C_2/H_2) and 70 °C of polymerization temperature. We varied reaction time, comonomer (1-octene) and transfer agent (H_2) in the polymerization reaction. The Table 2 shows the polymerization conditions and characterization results of polyethylenes obtained in homogeneous phase.

Table 2. Ethylene Polymerizations in homogeneous phase using $[(\text{Cp}^*)_2\text{ZrHAlH}_4]_2$.^a

No	Code ^b	H_2 ^c	Oct. ^d	Time ^e	Activity ^f	Mw ^g (g/mol)	M _w /M _n ^g	Tm ^h (°C)	Tc ^h (°C)	% mol Oct. ⁱ
9	LLL	-	-	-	7412	34316	2.9	131.8	119.1	-
10	LLH	-	-	+	5239	31632	3.2	132.4	118.8	-
11	LHL	-	+	-	14808	25954	2.7	130.2	113.7	0.79
12	LHH	-	+	+	11410	29760	2.9	127.8	115.2	3.86
13	HLL	+	-	-	15874	12056	2.6	129.7	124.1	-
14	HLH	+	-	+	13092	10417	2.3	129.5	123.8	-
15	HHL	+	+	-	29150	11695	2.5	126.4	113.2	0.47
16	HHH	+	+	+	23237	12001	2.3	127.2	113.9	4.70

^a Conditions: 200 mL Isooctane, [Al]/[Zr]= 2000:1, 5 mL of 13 wt% MMAO in isoParE as scavenger, $P_{\text{C}_2\text{H}_2}$ = 42 psig, [Cat]= 6.00173×10^{-6} M, T= 70°C, t= 1 or 2 h, 500 RPM, 0 or 11 mL 1-octene, 0 or 4.1 psig H_2 . ^b L= low and H= high in H_2 -Oct-Time. ^c with (+) or without (-) H_2 . ^d with (+) or without (-) 1-octene. ^e 1 h (-) or 2 h (+). ^f Activity in Kg PE/mol of Zr*^h. ^g Determined from GPC chromatogram and universal calibration curve. ^h Determined from DSC. ⁱ Determined from ^{13}C NMR spectrum.

As expected, the activities obtained with the homogeneous system in solution, are higher than that observed in heterogeneous phase (Tabla 1) and characteristics for these types of homogeneous systems. The activity increased when comonomer (1-octene) and agent transfer (H_2) were used in the experiments, this effect is more remarkable when both (1-octene and H_2) are used at the same time in the polymerization reaction. Moreover, the activity decreases with the reaction time, normally observed for this type of processes. Molecular weights (MW) of the polymers obtained in homogeneous phase decreased until three times when using H_2 as transfer agent. Polydispersity of the molar masses are characteristic for metallocenes, as well as Tm and Tc obtained in the thermal analyses. Kinetic curves at 1 and 2 h of ethylene polymerization in homogeneous phase are showed in Figure 2.

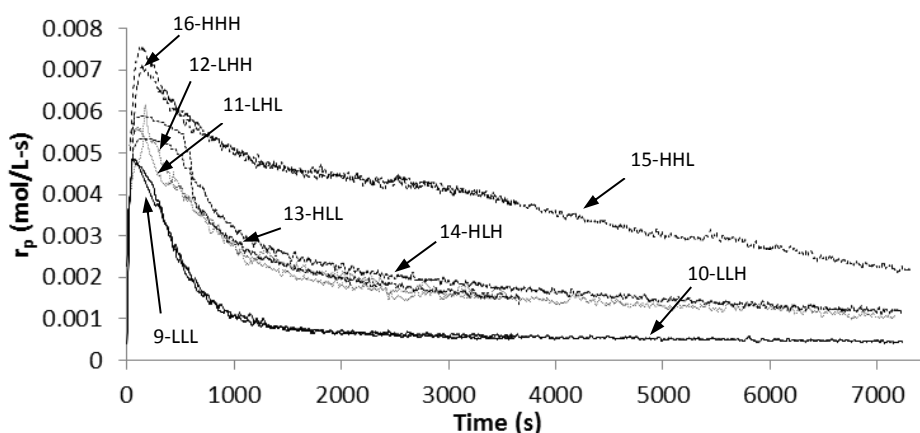


Figure 2. Kinetic behavior of ethylene polymerization using $[(Cp^*)_2ZrHAlH_4]_2$.

As can be observed, kinetic behaviors of ethylene polymerization are very similar in each pair of experiments (1h and 2 h) for instance 9-LLL and 10-LLH. This good reproducibility was attributed to the way of addition of the catalyst, where in solution, the zirconocene complex is easily handled for the polymerizations. Comparing with the heterogeneous reactions, the homogeneous system showed better reproducibility for each pair of experiments at 1 and 2 h. On the other hand, the kinetic behavior shows increase of r_p and in consequence of activity, when the comonomer and agent transfer are used in the polymerization reaction, besides when both are used together the increase is highest. This behavior is characteristic in this type of catalytic system.

Conclusions

Through the study of the kinetic behavior of zirconocene aluminohydrides systems for ethylene polymerizations, was probed the reproducibility of the experiments in homogeneous phase. As for the heterogenized similar system, the activity decreased, and the low reproducibility of the experiments was attributed to the poor dispersion of the zirconocene aluminohydride complex on the support.

Acknowledgements

The authors thank CONACYT México for financial support (Project No. 167901) and also thank Guadalupe Méndez, Teresa Rodríguez and José Sánchez for technical support.

References

- [1] Kaminsky W., Laban A. *Applied Cat. A: General* 222 (2001), 47-61.
- [2] Jacobsen G., Wijkens P., Jastrzebski J., Van Koten G., International Patent WO 96/28480, (1996).
- [3] a) Kaminsky W., Duttsche J., Maedler H., Miri M., Schlobohm M. (Hoechst AG). DE Patent 3240382, May 3, 1984. b) Kaminsky W., Madler H. (Hoechst AG). EP Patent 0307877, March 22, 1989.
- [4] Turunen J. P. J., Pakkanen T. T., *J. Appl. Poly. Sci.* 100 (2006), 4632-4635.
- [5] Infante J. R., Saldivar E., Pérez O., Comparán V. E., García M., *J. Appl. Poly. Sci.* 131 (2014), 40035.
- [6] Soares, J. B. P., McKenna, T., Cheng, C. P. In *Polyolefin Reaction Engineering*, Asua, J. M., Ed.; Blackwell Publishing, 2007, Chapter 2, pp 29–117.
- [7] Wu L., Lynch D. T., Wanke S. E., *Macromol.* 32 (1999), 7990-7998.
- [8] (a) Etkin N., Stephan D. W., *Organometallics* 17 (1998), 763–765.
(b) Etkin N., Hoskin A. J., Stephan D. W., *J. Am. Chem. Soc.* 119 (1997), 11420–11421.

PREDICTION OF MOLECULAR WEIGHT DISTRIBUTION IN CHAIN GROWTH POLYMERIZATIONS

Ramiro Infante-Martínez, Enrique Saldívar-Guerra, Odilia Pérez-Camacho, Maricela García-Zamora, Víctor Comparán-Padilla

Centro de Investigación en Química Aplicada, Saltillo, Coahuila. México

Author's email: ramiro.infante@ciqa.edu.mx

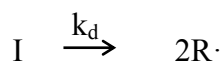
Abstract

This work presents results on the prediction of the molecular weight distributions (MWD) of chain growth polymerization using conventional software and hardware tools. The investigation focuses on two kinds of polymerization processes: free radical batch and continuous polymerization (LDPE); and coordination polymerization via metallocenes (HDPE). For both processes, kinetic models, consisting of sets of differential equations describing the dynamic behavior of all the chemical species in the reaction media, are presented. From these sets is possible to obtain the molecular weight distribution of the polymer[1,2,4]. The results confirm the idea that the complete MWD can be directly calculated with conventional hardware and software tools.

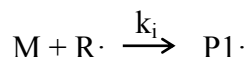
Introduction

As an example of a model for the chain-growth polymerization, the free-radical polymerization mechanism is illustrated[1].

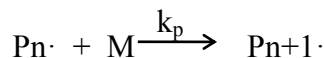
Initiator decomposition:



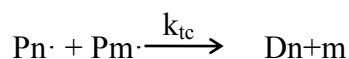
Chain initiation:



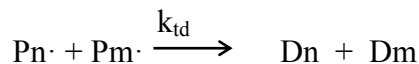
Propagation:



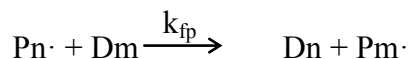
Termination by combination:



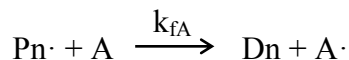
Terminación by disproportion:



Chain-transfer to polymer:



Chain-transfer to small species:



Where I = Initiator, R = Free-radical, M = Monomer, Pi = Live chain of length i, Di = Dead chain of i units, A = Chain-transfer agent (monomer, solvent, etc.), ki = Kinetic constant for reaction i.

Description of the full MWD is to translate the kinetic mechanism known or proposed in

equations describing the evolution of the concentrations of all the sizes of polymeric species. This results in a system of ordinary differential equations (ODE's) which must be resolved to know the evolution in time of the complete MWD[2,5].

Experimental

For the polymerization via metallocenes case, results of an experimental program conducted to obtain data for modelling purposes [3], are presented in Figure 1. In this program of 10 tests, the effect of 3 selected variables was analyzed: the reaction time; the concentration level of a chain-transfer agent, H₂; and the concentration level of a comonomer (1-octene).

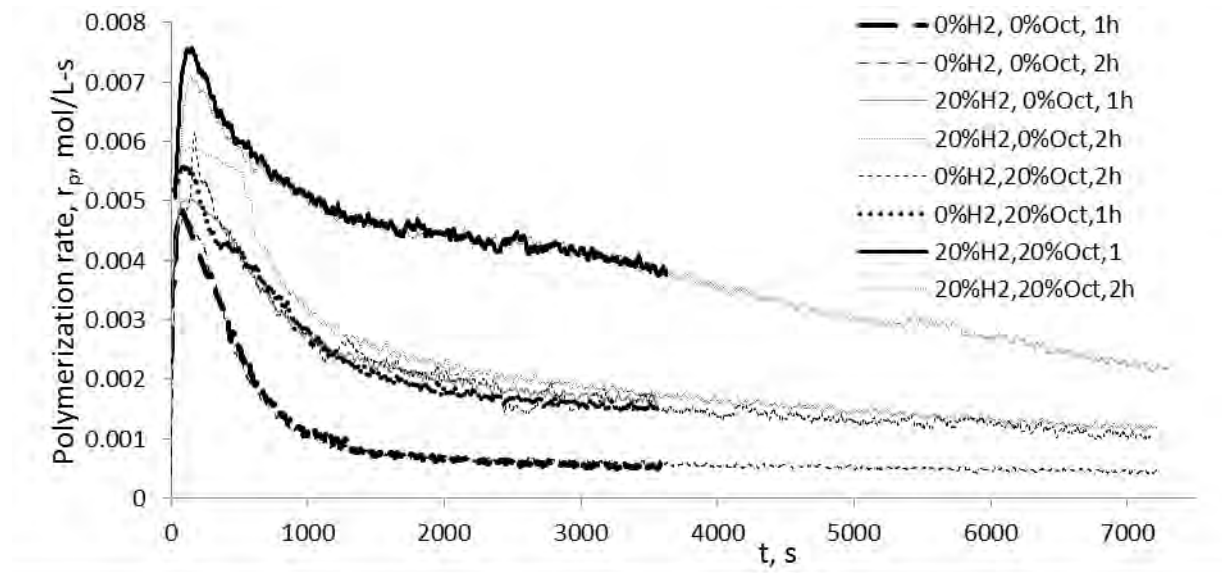


Figure 1. Polymerization tests of ethylene via metallocenes.

Results and Discussion

A. Free-radical polymerization model

The free-radical mechanism was illustrated with the ethylene polymerization case. The model includes chain transfer to polymer, which produces polymer with dispersity index > 2 as well as asymmetric distributions. These non-linear effects can be seen in Fig. 2 a) and b).

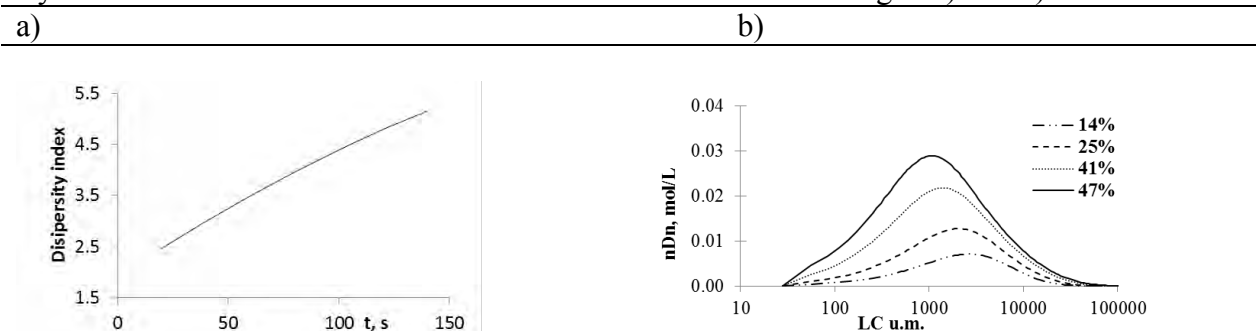


Figure 2. Simulation results for an ethylene polymerization run in a batch reactor. a) Evolution of the dispersity index. b) Molecular weight distributions during the simulated run.

B. Coordination polymerization

Typical results obtained during an ethylene polymerization test via metallocenes are presented in Fig. 3-5. Results of simulation are also presented, showing that the standard coordination model employed reproduces well the kinetic performance of the polymerization.

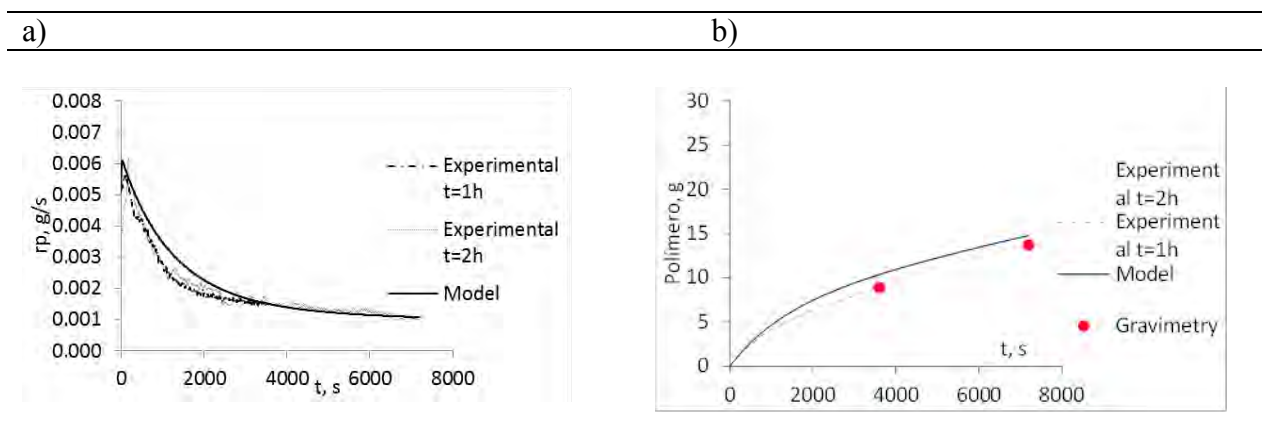


Figure 3. Experimental results of ethylene polymerization via metallocenes. Test conditions: 0% H_2 , 20% H_2 . a) Polymerization rate b) Accumulated polymer.

Experimental and simulation results for the MWD of the polymer in the ethylene polymerization via metallocenes are compared in Fig. 4. The agreement between them shows that the standard model also reproduces well the molecular weight distributions of this process.

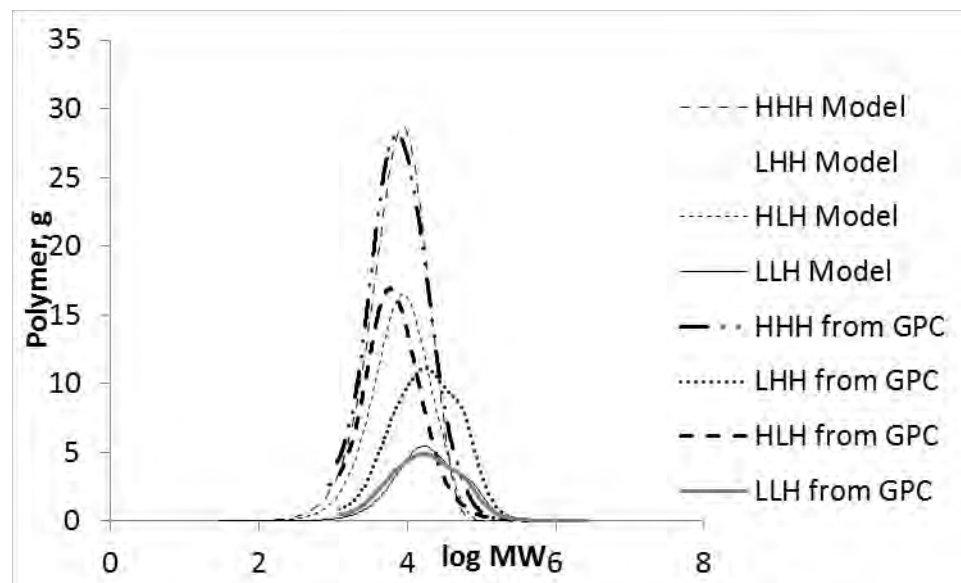


Figure 4. MWD of the polymer after 2 h of reaction. Four tests at different concentrations of H_2 and comonomer.

Table I. Code for the polymerizations runs showed in figure 4.

	H ₂	Comonomer
HH	20%	20%
LH	0%	20%
HL	20%	0%
LL	0%	0%

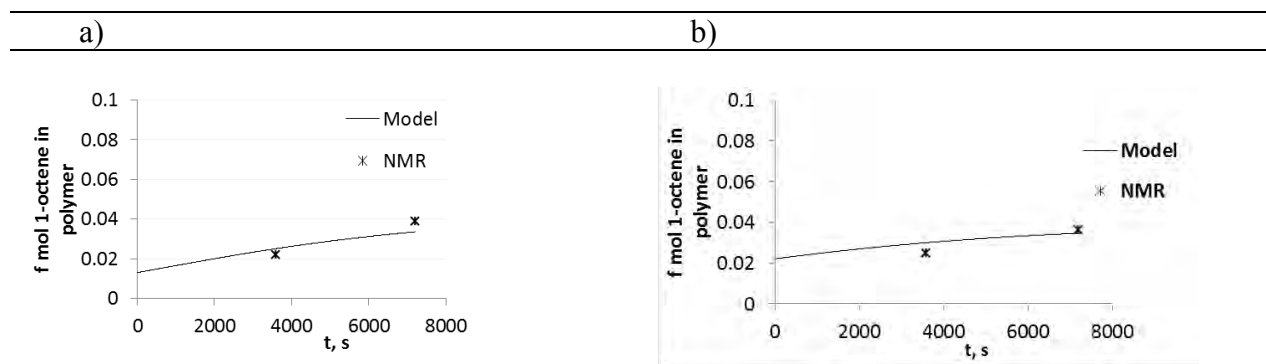


Figure 5. Copolymer composition in the ethylene polymerization via metallocenes. Simulation results _____ and Nuclear Magnetic Resonance (NMR) results (*). a) Tests with 0% of H₂ and 20% of comonomer. b) Tests with 20% of H₂ and 20% of comonomer.

Conclusions

It can be stated that the free-radical model for the ethylene polymerization including long-chain branching, captures the non-linear features characteristic of this polymer (low-density polyethylene, LDPE). With respect to the standard coordination model⁴ we can see that this model has the capability to reproduce the kinetic performance as well as the molecular weight distribution in the ethylene polymerization via metallocenes.

Both models can be implemented and solved for the direct molecular weight distribution calculation using standard software and hardware tools (MATLAB and personal computer).

References

- [1] J. M. Asua, Polymer Reaction Engineering, Blackwell Publishing, 2007.
- [2] J. B. P. Soares, "Mathematical modelling of the microstructure of polyolefins made by coordination polymerization: a review", Chem. Eng. Sci., 56, 4131-4153, 2001.
- [3] Infante M. Ramiro, Saldívar G Enrique, Pérez C. Odilia, Comparán P. Víctor, García Z. Marisela, "Kinetic monitoring methods for the Ethylene coordination polymerization in a laboratory reactor", Journal of Applied Polymer Science, Vol. 131,6, March 15, 2014
- [4] J.B.P. Soares, T.F.L. McKenna, Polyolefin Reaction Engineering, Wiley-VCH, 2012
- [5] Saldívar-Guerra.E., Infante Martínez R., Vivaldo-Lima E., Flores-Tlacuahuac A. "Returning to basics: Direct Integration of the Molecular-Weight Distribution Equations in Addition Polymerization", Macromolecular Theory Simulation, 19, 2010.

RHEOLOGICAL CHARACTERIZATION OF POLYETHYLENE RESINS USED IN EXTRUSION BLOW-MOLDED FILMS

Gudiño-Rivera J., Saldivar-Guerrero R., Aguilar -Moreno N. , Rodríguez-Otamendi D.I.

¹ Centro de Investigación en Química Aplicada C.I.Q.A., Laboratorio de Asistencia Técnica CIQA-PEMEX, Blvd. Enrique Reyna H. 140, P.O. Box 379, 25100, Saltillo, COAH., México, javier.gudino@ciqa.edu.mx, ruben.saldivar@ciqa.edu.mx.

Abstract

Polyethylene resins used in the formulation of films obtained by extrusion blow-molding were analyzed in order to correlate their chemical structure and rheology with their processability. A melt spinning technique (Rheotens test) was used to determinate and compare their melt strength and elongational viscosity using a strand acceleration of 24 mm/s², and similar initial conditions for all tests. A higher degree of branching causes a higher degree of strain hardening and a lower drawability of the melt. The elongational viscosities curves obtained by this technique were compared with those obtained using an extensional viscosity fixture (EVF) in an oscillatory rheometer.

Introduction

In the plastic industry linear and branched polyethylenes are mixed in the production of films to obtain a combination of properties and inherent advantages of these types of resins, such as good mechanical properties of linear low density polythene (LLDPE), and a good processability of low density polyethylene (LDPE). It is important to consider a balance between good resin processability and good mechanical properties of the film. In order to improve the processability of blends of polyethylenes is necessary a rheological testing of these materials considering its molecular structure, average molecular weights and polydispersity index (PI) [1]. Besides shear rheology, it is important to know and measure the elongational melt strength of the resins for extrusion blow molding process of the films in order to prevent sagging, fracture of the extrudate, and other problems during processing [2]. The elongational melt strength and extensional viscosity are more sensitive to structure differences of polymer materials than those in shear [3]. In this work, we study the shear and extensional viscosity of four different types of commercial polyethylenes, used in blends to obtain extrusion blow molded films, with respect to their molecular structures.

Experimental

Materials: The commercial polyethylenes used in this work were a low density polyethylene (LDPE), a linear low density polyethylene (LLDPE), a medium density polyethylene (MDPE), and a high density polyethylene (HDPE). **Characterization:** Average molecular weights and its distributions were measured in an Agilent PL-GPC 220 Gel Permeation Chromatograph with a viscosity, and light scattering detectors. The samples were dissolved in 1, 2, 4-Trichlorobenzene. Storage and loss modulus of the samples were measured in a TA Instruments RSA G2 Dynamic Mechanical Analyzer using a dual cantilever fixture to perform a standard temperature ramp from 30 to 130°C at a constant strain of 0.05%. Shear flow properties were determined using a Göttfert

Rheograph 25 Capillary Rheometer with a die having a length to diameter ratio (L/D) of 30:1 at 190 °C, and with a TA Instruments ARES G2 Oscillatory Rheometer, a frequency sweep with parallel plates at a constant strain of 1%, and a temperature of 190 °C. To study the extensional flow properties and extensional viscosity of the polyethylenes a Göttfert Rheotens 71.97 was used with a die having a length to diameter ratio (L/D) of 20:2 at 190 °C with a constant shear rate of 193.5 1/s, a start speed of 48 mm/s and a strand acceleration of 24 mm/s². Additionally, the extensional viscosity curves were obtained with a extensional viscosity fixture in a TA Instruments ARES G2 Oscillatory Rheometer at a temperature of 170 °C with a extension rate of 0.3 1/s.

Results and Discussion

In **Table 1** are summarized our results by G.P.C., melt flow index, density by column gradient, and zero viscosity by oscillatory rheometry in order to correlate physical characteristics and molecular structure of the polyethylene analyzed with their shear and extensional viscosity.

Table 1. Summary of physical and molecular characteristics of the polyethylene resins analyzed in this work.

Type of Polyethylene	MFI (g/10 min)	Density (g/cm ³)	η_0 (Pa.s)	Mw (g/mol)	Mn (g/mol)	PI
LDPE	1.94	0.921	8502.37	1.11E+05	4.33E+04	2.6
LLDPE	2.02	0.922	4293.98	1.08E+05	3.63E+04	3
MDPE	4.66	0.937	1928.48	9.85E+04	3.29E+04	3
HDPE	7.18	0.958	1458.64	8.55E+04	2.40E+04	3.6

According with these results, we observed that LDPE and LLDPE selected for blow molding film blends have similar densities, melt flow index values, and polydispersity indexes, but the values of zero viscosities determined by oscillatory rheometry are different. This difference in viscosity can be attributed to the LDPE has a molecular structure with a largest number of branches. MDPE and HDPE have higher MFI values and similar polydispersity indexes. Moreover despite having lower viscosities, we observe a strong correlation between density and storage and loss modulus. In **Figure 1** we observe that increasing density increases both modulus, especially the storage modulus which is related to the elastic portion of the polymer. The density is related to the crystallinity of polymers, at a higher density a polymer has a higher degree of crystallinity and therefore a greatest stiffness. MDPE and HDPE are used in films to increase its mechanical properties and are important components of the blend.

Figure 2 shows apparent shear and complex viscosities curves of the selected polyethylenes obtained at a standard temperature of 190 °C.

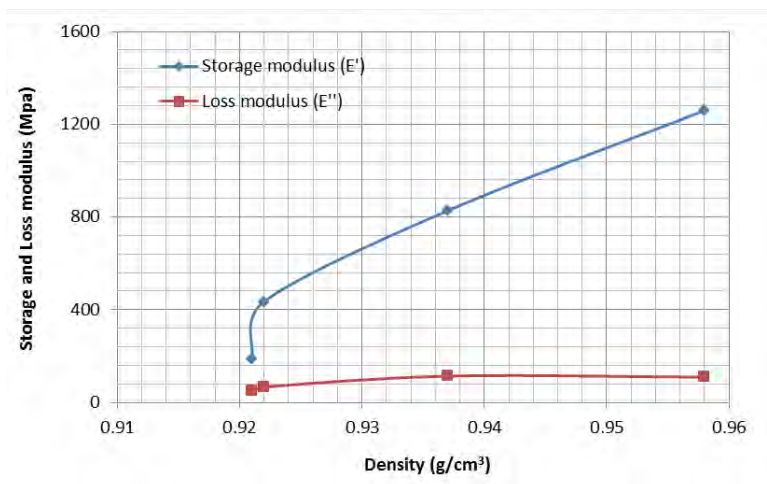


Figure 1. Variation of storage and loss modulus with density of polyethylene resins.

Despite having similar values of MFI, LLDPE has a higher viscosity of the melt in a range of high shear rates. It is for this reason that is used to improve the processability of the blend. In the complex viscosity curves, we observe a lower angular frequencies (less than 2 rad/s) LDPE has a higher viscosity than LLDPE due to a more branched structure. MDPE and HDPE have lower viscosities as we determined by MFI experiments.

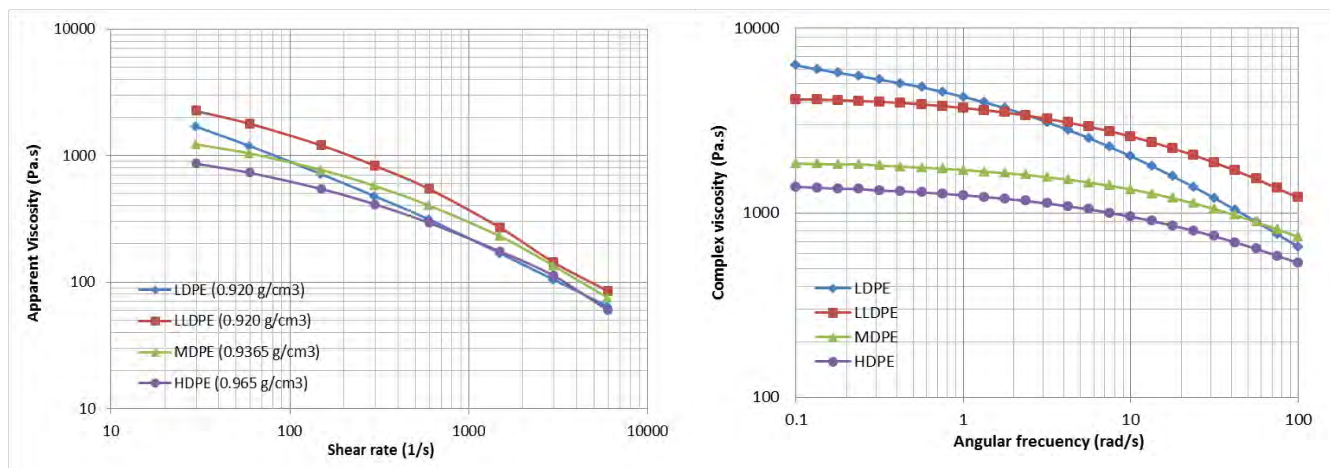


Figure 2. Apparent shear and complex viscosities of polyethylenes having similar polydispersities determined at 190 °C.

In **Figure 3** we reported the Rheotens curves of melt strength as a function of drawdown velocity for polyethylenes. At higher draw ratios the experimental curves start to oscillate, an effect called draw resonance, and all the extension of the curve is called drawability of the melt. We observe that with a higher density polymer experiment a lower melt strength (maximum force at rupture), but a higher drawability. There is a significant difference in the melt strength of LDPE and LLDPE, with similar MFI values and polydispersity indexes, again due to a largest number of ramifications.

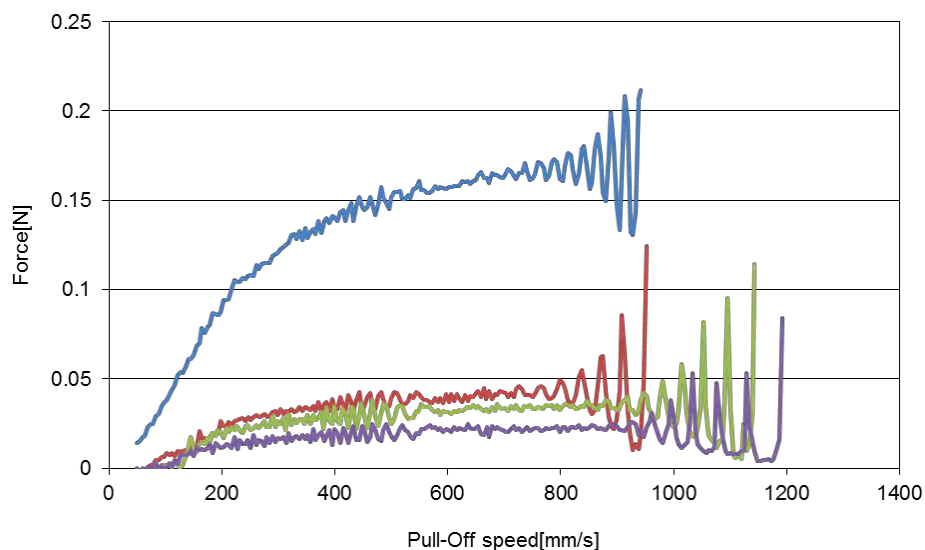


Figure 3. Rheotens curves measured at a constant acceleration of 24 mm/s^2 , LDPE (blue), LLDPE (red), MDPE (green), HDPE (purple).

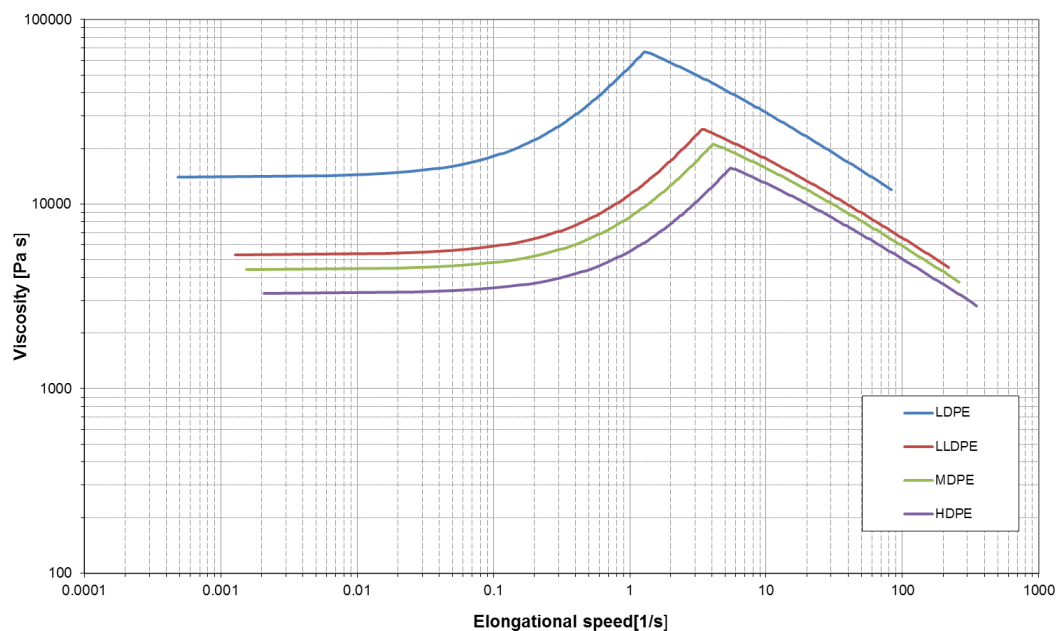


Figure 4. Apparent elongational viscosity calculated from Rheotens experiments in polyethylenes, LDPE (blue), LLDPE (red), MDPE (green), HDPE (purple).

In **Figure 4**, we observed the apparent elongational viscosities calculated from Rheotens experiments in polyethylenes. LDPE melts which have a high degree of long chain branching, showed a pronounced maximum in the elongational viscosity curve, and this viscosity is lower for a less branched polymer (MDPE and HDPE).

Finally, in **Figure 5**, we reported the elongational viscosity curves of the polyethylenes obtained with an extensional viscosity fixture (EVF). We observe the same behavior, than with the Rheotens test. LDPE has the higher elongational viscosity than LLDPE. LDPE and LLDPE are used for extrusion blow molding films to give a greater melt strenght to the blend.

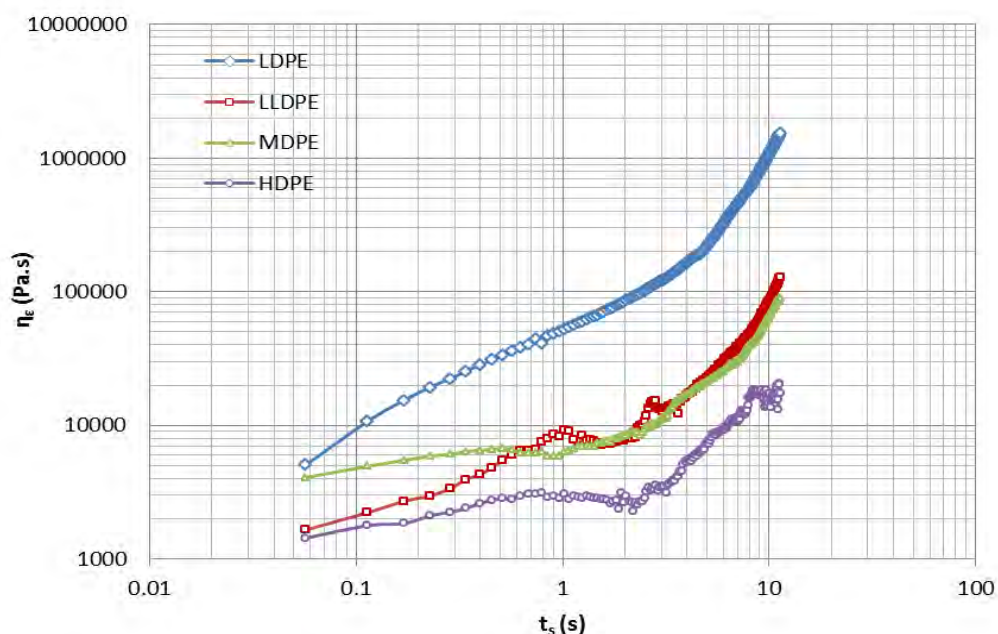


Figure 5. Elongational viscosity curves of polyethylenes at 170 °C with an extension rate of 0.3 1/s.

Conclusions

MDPE and HDPE resins are used in the formulations of blends for extrusion blow molding to improve their mechanical properties because with a higher density they have higher degrees of crystallinity. LDPE is used in the blends because it has lower viscosity at high shear rates and improves its processability. LDPE and LLDPE are used in these formulations to improve its melt strength and extensional viscosities due to a more branched structure.

Acknowledgements

We want to thank to CIQA and PPQ for allowing the experiments in their facilities at LAT in Mexico City.

References

- [1] Ariawan A.B., Hatzikiriakos S.G. Hatzikiriakos, S.K. Goyal, H. Hay, Adv. Polym. Tech., Vol. 20, No. 1, 1 (2001).
- [2] Keawkanoksilp C., Apimonsiri W., Patcharaphun S., Sombatsomopop N., J. of App. Polym. Sci., Vol. 125, 2187 (2012).
- [3] Bernnat A., Polymer Melt Rheology and the Rheotens Test, Universität Stuttgart (2001).

Studies on rheological behavior of commercial blends involving LLDPE, LDPE and HDPE, using a torque rheometer

Leal Rosalba^{1,2}, Martínez Laura^{1,2}, Gudiño Javier¹, Saldivar Rubén¹

¹ Laboratorio de Asistencia Técnica, Centro de Investigación en Química Aplicada, Eje Central Lázaro Cárdenas #152, Col. San Bartolo Atepehuacan, D.F.

² Students at the Escuela Superior de Ingeniería y Arquitectura Unidad Ticomán del Instituto Politécnico Nacional.

Abstract

In this work, selected grades of LLDPE, branched LDPE, and HDPE have been melt-mixed using commercial compositions for packing films. We use a torque rheometer for rheology analysis of individual polyethylenes and the blends. The results show that linear low density and high density PE have the higher torque during the fusion process (165 and 175 Nm respectively) while the branched low density PE has the lowest torque peak (124 Nm). The obtained blends (30% of LLDPE, 40% of LDPE and 30% of HDPE) showed a torque peak similar (30% less) to the LDPE making easy for processing, while in the steady state mixing the torque is maintained close to the LLDPE behavior (35.7 Nm) between the limits of parents polymers.

Introduction

Commonly in the packing industry is necessary to make films using different materials some times to achieve better properties or some others to reduce the prices talking about raw material cost or the amperage consumed during the process. In this case, a composition of 30% of LLDPE, 40% of LDPE and 30% of HDPE is the first step of the experiment because its industry acceptance and variations in the other two blends had the finality of understand specifically the influence of the LLDPE and the HDPE in the LDPE.

The present study offers the opportunity to understand how changing the composition of a different polyolefins in series of binary and ternary blends, performs an effect on the final rheological properties. Focusing the attention mainly in ternary blends comparing the results of the torque rheometer, melt flow index (MFI) and capillary rheometer as a function of the concentration of LLDPE and HDPE.

Experimental

The commercial national resins used in this experiment were Low Density Polyethylene known as LDPE (MFI=2g/10min), Linear Low Density Polyethylene with acronym LLDPE (MFI=2g/10min), and a High Density Polyethylene for short HDPE (MFI=8g/10min), these materials requires 165Nm, 175Nm and 124Nm respectably in order to do a fusion process.

In order to load the materials, a sensitive electronic read-out weighing machine, Ohaus Adventurer Pro was used. The density was necessary to obtain the weight of pellets, this data obtained in a density gradient column, which brand is AMETEK and has nine standards of density with values between 0.880 and 0.976g/cm³ at a temperature of 23°C according to the ASTM D1505.

Each blend composition was previously mixed in a mechanical shaking way before being fed at the torque rehometer.

The Brabender's Intelli-Torque Plasti-Corder equipped with mixer attachments was necessary to obtain the fusion behavior curve. The capacity of the mixer chamber used was 60% and the speed of rotors at 60rpm, temperature setting at 190°C and a period of 10 minutes. The ASTM D2538-02 focused in PVC but it is a reference to develop the experimentation with polyethylene.

After obtained the mixed blends they were cooling at atmospheric temperature and chopped in small pieces to finally be fed into next two rheological tests.

The Melt Flow Index was evaluated by a plastometer branded CEAST according to the norm ASTM D1238 at a work temperature of 190°C and a pressure of 2.16kg.

The capillary rheometry was made under the ASTM 3835 at an interval of shear rate of 12 to 2400 seg^{-1} . This test requires a Rheograph 25 brand GOETTTFERT with a 1mm capillary die and a relation $L/D=30$.

Results and Discussion

The first round of experiments consisted in analyze two groups of binary blends in the torque rheometer the first one composed by LDPE and LLDPE (ML), having a variation on the increase of the lineal polyethylene in a range of 30% at 60% in weigh. In addition, the second group contained LDPE and HDPE (MH) in the same concentration range.

As you can see in figure1 the load torque doesn't change too much between the ML and the MH blends. But the torque in the melt changes around 10 units, mainly because of the mayor melt index belonged to the HDPE which contributes in a better processability in this point.

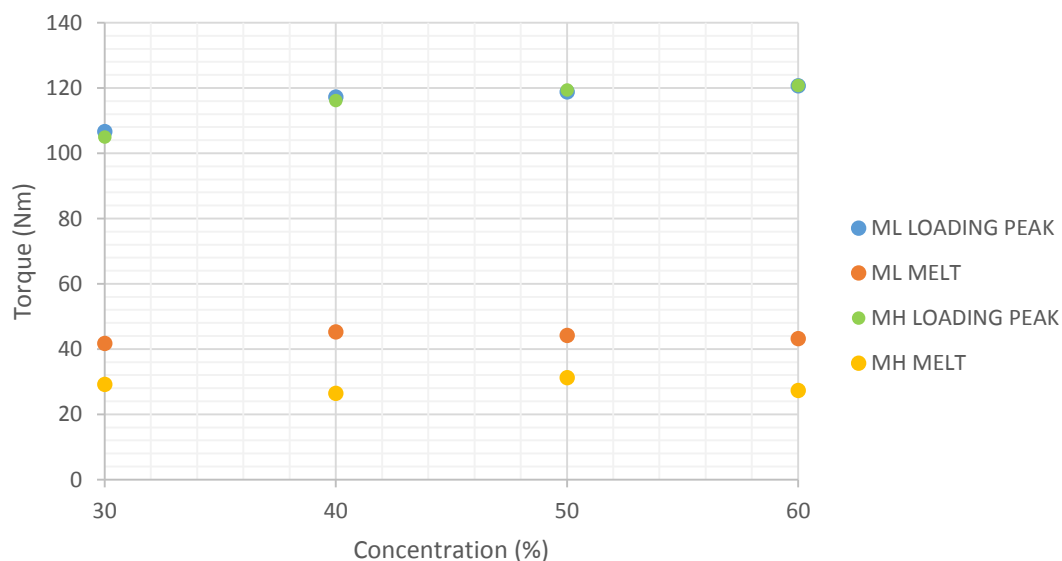


Figure 1. Binary mixtures torque behavior

The binary blends permit us look a proportional relationship between the blends compositions and the torque necessary at the beginning and the end of the fusion process. When the content of LLDPE goes up the load torque does as well and while the HDPE present increase in the blend it's visible at the very end of the test (once the mixture has been melted), how the torque goes down describing a inversely behavior.

After check the behavior of the binary blends in the torque rehometer, it was precisely to evaluate ternary blends, now with the three polyethylenes is important to determinate the effects of the formulation in rheological properties and compere the behavior exhibited in the previous mixes.

The next figure resumes the content of the tow variable polyethylenes in each blend and the torque recurred at the beginning and at the end of the tests, also, there is the melt index too. The units for the load peak and the melt index had been modify because in the first case the values were too bin and in the MFI the values in g/10min are too small to appreciate in the figure.

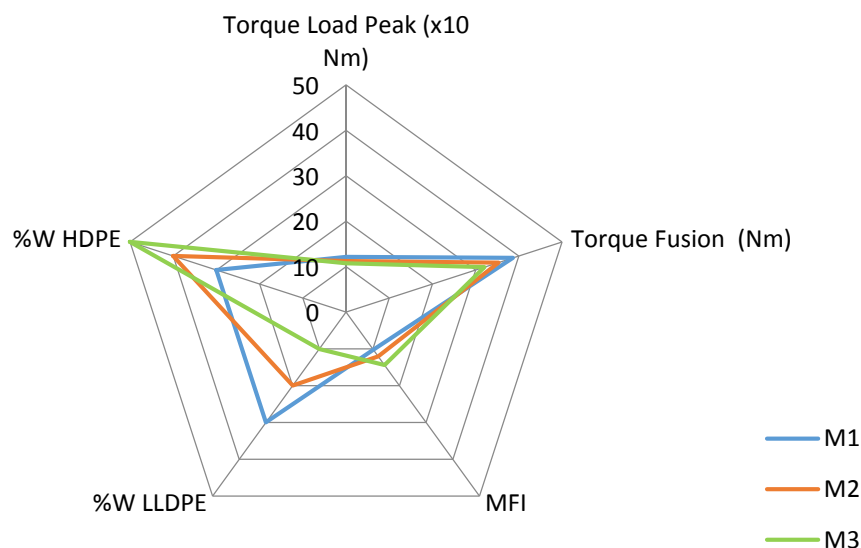


Figure 2. Rheological properties comparative

The spider web illustrate the moment when the LLDPE concentration rises the melt index decrees so that's why the torque rehometer needs more shear stress expressed in the torque as Nm to transport the blend inside the mixer chamber.

For the three mixtures exist a small variation in the values at the Load Peak due to the content of LLDPE, as this resin low its content on the mixtures the torque needed at the load peak goes in a minimal quantity down.

The MFI obtained for the mixes M1(1.7g/10min), M2(2.0g/10min) and M3(2.4g/10min) are unexpected, the mixes values doesn't achieve the MFI calculated by a simple mix rule in which case should have been 3.8,4.4 and 5g/10minutes respectively. Then the properties of the mixers differs from the row materials due to the branching arrangement between the three resins.

On the other hand, the figures 3 and 4 shows the curves of shear stress and apparent viscosity, bout in function of the shear rate for the ternary blends obtained thanks to the capillary rheology.

At first sight, the values are the same but observing there are differences between the three blends that make them parallel.

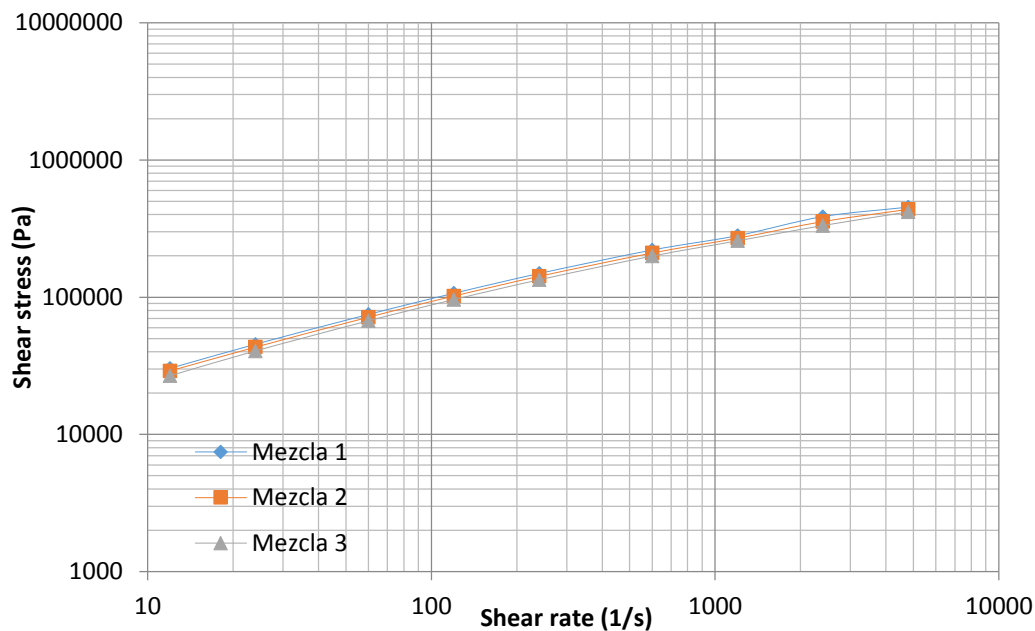


Figure 3. Shear stress for each blend

Viscosity curve shows a bigger difference making remarkable that the composition of the blends taking in count the increase of the HDPE (MFI=8g/10min) brings an easier way to flow through the capillary for the blends. This curve is a back off for the results of the melt flow index reported in figure2, the difference is that here the range of the shear rate is bigger.

As it was expected as the shear rate goes up the opposition to flow decreases.

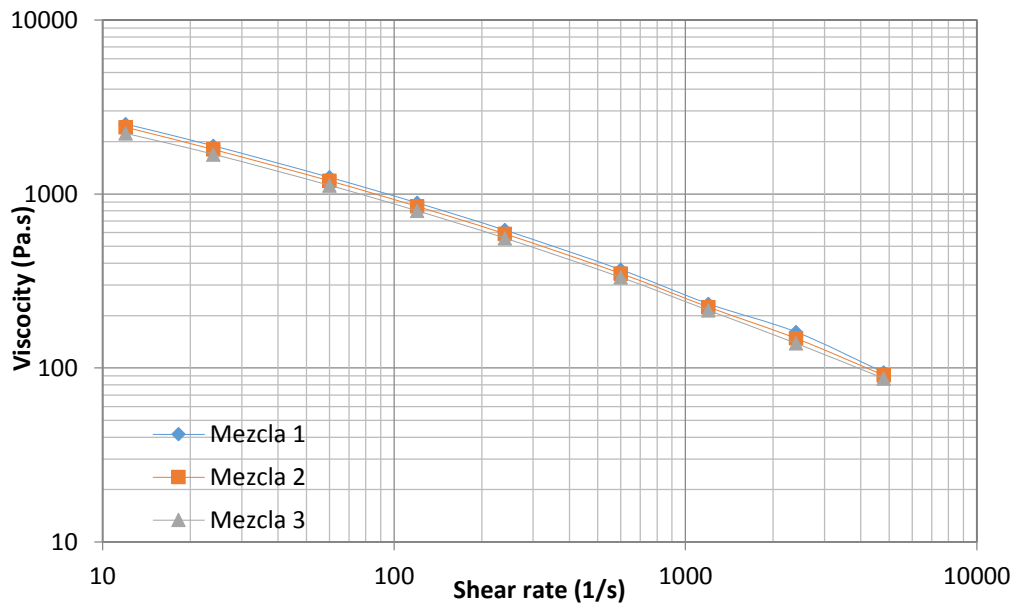


Figure 4. Registered viscosity for each blend

Conclusions

The load peak and the viscosity for the ternary blends had been influenced by the content of LLDPE, the experiment show a rise in these two properties as the LLDPE increase its proportion in the blend. One reason can be the molecular arrangement of the LLDPE, characterized by ordered small braches that gives crystallinity around 30-40% to the resin and in the blend, these branches have an interaction with the big branches present in the LDPE producing opposition to melt soon.

Another point is the fusion torque, which shows a tendency to go down when the HDPE increase its present even when this material achieves 80% of crystallinity and has a small molecular weight distribution. The key here is the MFI that possess the HDPE because of its almost none branching that once are melt can flow easily. In the blends as this resin increase its present, the LLDPE reduce interactions with the LDPE reducing the opposition to flow. The relationship between LDPE and HDPE is not that strong as the one existed in LLDPE/LDPE.

Acknowledgements

We want to thank CIQA and PPQ for financial support to carry out the research.

References

- Baojia Cheng, C. Z. W. Y. X. S., 2001. Evaluation of rheological parameters of polymer melts in torque rheometers. *ELSEVIER POLYMER TESTING*, 20(811-818).
- Cantú, D. R. B., 2014. *Los plásticos y sus características*. Saltillo: CIQA.
- IMPI, 1997. *Enciclopedia del Plástico*. Ciudad de México: s.n.
- Naoya Mieda, M. Y., 2011. Flow instability for binary blends of linear polyethylene and long-chain branching polyethylene. *ELSEVIER*, 166(231-240).
- Ogah, A. a. A. J., 2012. The effects of linear low density polyethylene(LLDPE) on the mechanical properties of high-density polyethylene (HDPE) film blends. *International journal of engineering and managemnt sciences*, Volume 3, pp. 85-90.
- Pemex Petroquímica, 2014. <http://www.ptq.pemex.com.mx/>. [Online].
- Zhengang J. Fan, M. C. W. P. C., 2002. A molecular dynamics study of the effects of branching characteristics of LDPE on its miscibility with HDPE. *ELSEVIER Polymer*, 43(1497-1502).

“PREPARATION AND CHARACTERIZATION OF PE-CLAY-SILVER NANOCOMPOSITES WITH DIFFERENT COMPATIBILIZERS”.

M.C. Ibarra-Alonso,¹ S. Sánchez-Valdés,¹ E. Ramírez-Vargas,¹ M. G. Méndez-Padilla,¹ M. Lozano-Estrada.¹

¹ Centro de Investigación en Química Aplicada, Blvd. Enrique Reyna 140, Saltillo, Coahuila 25253, México.

Abstract

The Itaconic acid was grafted onto the PE melt to obtain PEgAI, and then PEgAI was reacted with D to obtain PEgAID. This PEgMA was also reacted with DMAE to obtain PEgMAD. Chemical modification of PE was carried out by reactive extrusion. Synthesis and deposition of Ag-NPs was done using a sonochemistry technique by two different methods: In one method the nanosilver deposition was conducted over the different compatibilizers with the aim of forming a coordinate bond between the Ag-NPs and the polar groups of compatibilizer. These resulted in a better particle distribution of both silver and clay into PE. Characterization techniques indicated that an increase in the content of Ag-NPs, filler (clay and silver) dispersion and mechanical and antimicrobial properties were strongly affected by the type and concentration of the compatibilizer used.

Introduction

Hybrid nanocomposites, such multifunctional materials, have reached a high interest, both scientific and technological, mainly due to the bactericidal and fungicidal properties, in addition to good physical and mechanical properties as; thermal stability, improved gas barrier properties and fire resistance [1-4]. An important application where gas barrier properties, good mechanical and physical performance as well as antimicrobial properties are required; is in the packaging industry, specially for food packaging. However, it is an important challenge, the effective incorporation of metal and clay nanoparticles in polymeric materials, because these particles tend to agglomerate. PE is one of the most used polyolefin in the manufacture of flexible film due to its low cost, ease of processing and recycled facility. However due to lack of a polar group in its main chain, when trying to form hybrid nanocomposites based clay particles and silver, it is difficult to obtain an exfoliation and a homogeneous dispersion of these nanoparticles in the polymer matrix. One of the most effective solutions to overcome the formation of agglomerates and to improve its processability in hybrid systems is the use of compatibilizing agents, that is, polymers functionalized with polar groups that act as anchoring clay and metal nanoparticles to the polymer matrix, [3-9]. Currently in our working group has been published the use of polyolefins grafted with 2 [2 (dimethyl amino) ethoxy] ethanol (D) [13-14], to obtain new coupling agents. These coupling agents (PEgIAD and PEgMAD) were obtained taking advantage of the rapid reactivity of the hydroxyl groups of DMAE with carboxylic groups from the IA and MA. The amino group present in the structure of the coupling agent provides a functionality capable of acting as a ligand with respect to the silver particles [15, 16]. Based on the above grounds, it is proposed in this study; exploring the use of two types of coupling agents (PEgIAD and PEgMAD) that could provide a higher level of compatibility between the polymer matrix, clay and silver nanoparticles, in order to use them to obtain a hybrid nanocomposite polymer-clay-silver and determine their antimicrobial activity besides the mechanical physical properties and gas barrier.

Experimental

The materials used were: Low Density Polyethylene Grade 22004 PEMEX, with a melt index of 0.35-0.45g / 10 min and a density of 0.9210- 0.9230 g/cm³. The PEgIA, was obtained in our laboratory using the PE melt mixing using Itaconic Acid from Sigma-Aldrich and Dicumyl peroxide (PDC), from Sigma-Aldrich as initiator. The PEgIA obtained contains 1 wt% of IA.

The amino alcohol used; 2 [2 (dimethyl-amine) ethoxy] ethanol sigma-aldrich. Polyethylene grafted maleic anhydride (PEgMA) was acquired trade name of DuPontTM Fusabond® E226, with a melt flow rate of 1.75 g/10 min and a density of 0.93 g/cm³, containing 0.9% graft MA. Silver nitrate (AgNO₃), was used as the silver precursor, Scientific. In addition, other chemicals such as ammonium hydroxide (NH₄OH) and Ethylene glycol (C₂H₆O₂), sigma-aldrich. The organo-modified clay with octadecyl trimethyl amine used was; Nanomer I28E (Nanocor Inc.). The organoclay I28E, has a diffraction peak near $2\theta = d001$ to 3.84, which corresponds to a spacing of 2.30nm galleries. All reagents were of reagent grade and used without further purification.

Hybrid Nanocomposite Preparation

The different coupling agents were prepared as described in a previous work [4, 5]. The sonochemical technique was used for the synthesis and deposition of silver nanoparticles (Ag-NPs) in different coupling agents, this synthesis was carried out in the presence of ultrasonic radiation as described below. The PE was premixed with Itaconic Acid and Dicumyl peroxide within a Banbury batch mixing chamber (Brabender PL2000). After 2 min of mixing, the amino-alcohols (D) was added, in sealed PE bags, and the mixing was continued for 12 min at 180°C and 60 rpm, forming the PEgIAD. This compatibilizer was reacted using ultrasound with a solution of AgNO₃ 0.04 M and Ethylene glycol. Ammonium hydroxide was added in a ratio of 2:1 molar with respect to silver nitrate. The resin was washed with deionized water and allowed to dry at 80 °C for 24 hrs. These silver coated compatibilizer was loaded into the internal mixer for adding PE and nano-clay (Cloisite I28E), thus forming the different hybrid nanocomposites listed in Table 1.

Table 1. Hybrid composites description.

	Modified PE:	PEgA. (%weight)	I28E (%weight)	Plata* (%weight)	PE (%weight)
1A-IA	Itaconic acid (IA)	10	3	0.0011	86.998
2A-IA	Itaconic acid (IA)	15	5	0.0010	79.998
3A-IA	Itaconic acid (IA)	30	5	0.0037	64.996
1A-IAD	IA → Dimethyl-amino-ethoxy-ethanol	10	3	0.0022	86.997
2A-IAD	IA → Dimethyl-amino-ethoxy-ethanol	15	5	0.0050	79.995
3A-IAD	IA → Dimethyl-amino-ethoxy-ethanol	30	5	0.0089	64.991
1A-MA	Maleic Anhydride (MA)	20	3	0.0013	76.998
2A-MA	Maleic Anhydride (MA)	15	5	0.0020	79.997
3A-MA	Maleic Anhydride (MA)	30	5	0.0030	64.997
1A-MAD	MA → Dimethyl-amino-ethoxy-ethanol	10	3	0.0021	86.997
2A-MAD	MA → Dimethyl-amino-ethoxy-ethanol	15	5	0.0031	79.996
3A-MAD	MA → Dimethyl-amino-ethoxy-ethanol	30	5	0.0057	64.994

Results and Discussion

XRD Analysis

X-Ray diffraction spectras of silver nanoparticles in the presence of coupling agent are shown in Fig. 1a. The diffraction signal for I28E nano-clay appears about 3.84° which corresponds to a intergallery spacing of 2.30 nm. Increasing the content of coupling agent has less diffraction intensity signals, lower than those observed for the angles of clay, but still you can see the signal even for the highest concentration of PEgAI as coupling agent (30 wt%). Therefore diffraction signal about 3°, which approximately corresponds to a distance between layers of 2 nm for the sample with lower content of agent (1A-IA) is observed, corresponding to a slight increase in the separation galleries, when using AI as a coupling agent. This suggests that there was only a slight engagement with the AI content increases. This suggests that a nanocomposite with some degree of intercalation-exfoliation was obtained.

It can also be seen in Figure 1b, c, signals of about 38° and 44° , corresponding to the silver. These peaks show a slight increase as the content of PEGAI increases, which indicates a low coupling effect [6, 16, and 17].

The coupling agent (PEGIA), previously analyzed, which has limited capability to exfoliate nanoclay was modified again with amino-alcohol, to get the PEGIAD. The results obtained with this agent are presented in Figure 2. It is observed that with the increased content of PEGIAD, the diffraction signal for the I28E decreases. Only one slight shoulder on the signal can be observed at low levels of 15% and then this signal completely disappear for higher compatibilizer contents. Indicating that higher amounts of this compatibilizer promote more interaction with the nanoclay which destroys the crystallographic arrangement and obtaining a greater exfoliation compared with PEGIA. This coincides with that reported in previous studies [13-15 and 22] where the amino alcohol has the facility to interact with the hydroxyl groups present on the surface of the nanoclay facilitating the penetration of the polymer chains through the galleries of the clay separating and exfoliating them easier.

Regarding the signals characteristic for Ag NPs can be identified that the increased content of the coupling agent increases the intensity of the peaks at 2θ values around 38° and 44° , this difference in the intensity of the peaks, is related to the percent by weight of silver. This indicates that this coupling agent (PEGIAD), besides of its better influence on the degree of exfoliation-intercalation of the nanoclay it also has greater compatibility with Ag NPs, compared to IA grafted polyethylene. This was attributed to the existence of coordination attractions between silver nanoparticles and polar groups of the amino alcohol (D). So this interaction is carried out by the free amino groups in the agent, as can be shown in Figure 3, in which the unshared electrons of nitrogen present in the amine are bonded to metallic silver to form a complex moiety, as has been reported by other researchers [15-17].

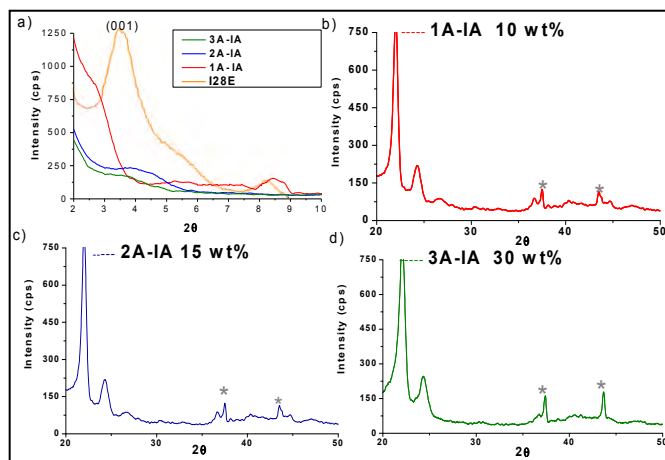


Figure 1. XRD patterns for: PEGIA.

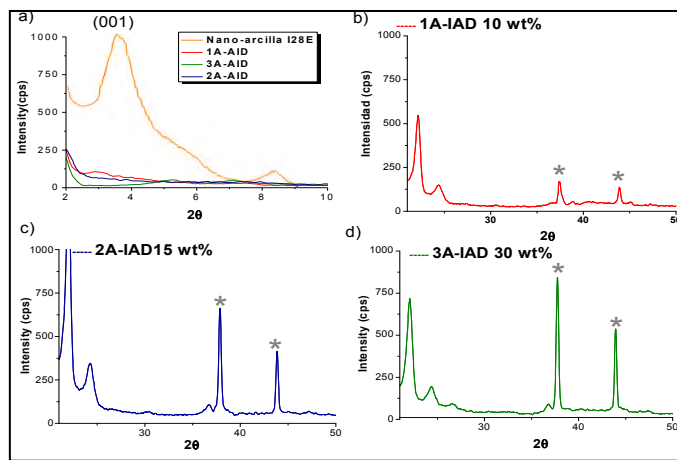


Figure 2. XRD patterns for: PEGIAD.

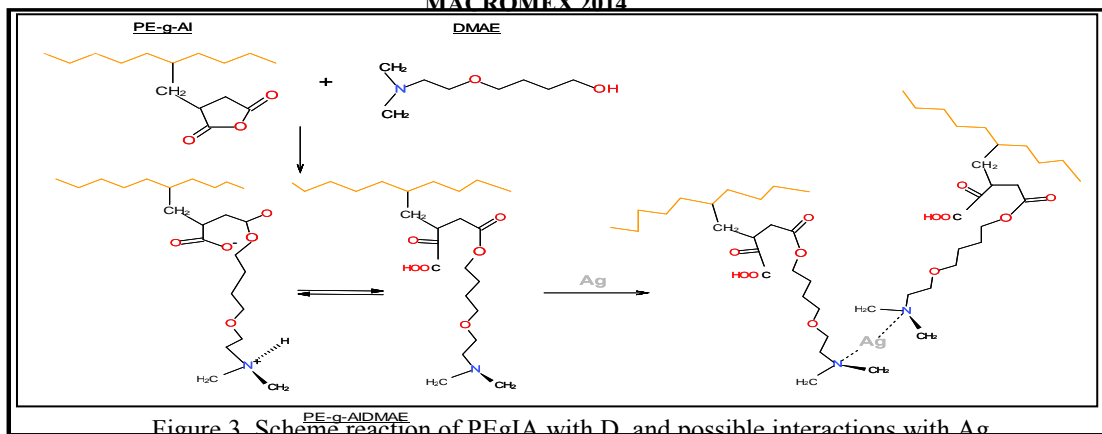


Figure 3. Scheme reaction of PEGIA with D, and possible interactions with Ag.

Antimicrobial Test (JIS Z 2801)

Antimicrobial results are presented in Figure 4a and c. Nanocomposites with 30wt% of the different coupling agents showed higher inhibition percentages, around 99%, and a value of antifungal activity (R) greater than 2. These results classified as an antimicrobial material according to Japanese Industrial Standard JIS Z 2801 [18].

For concentrations of 15 wt% of coupling agents based on amino-alcohol (2A-AMD and 2A-IAD), classified the test. However coupling agents with 10 wt%, evaluated against *Aspergillus Niger*, not classified in the standard. The nanocomposites with coupling agent 3A-IAD and 3A-MAD, rated 2.5 of antimicrobial activity due to their greater amounts of silver, according to the results of X-ray diffraction. The percentages of inhibition and antimicrobial activity obtained for the bacterium *Escherichia coli* (Fig. 4b and d) were greater than those induced by the fungus *Aspergillus Niger*. This is mainly because the Ag NPs are effective in the destruction of the cell membrane and inhibit the reproduction of bacteria. In the case of fungi *Aspergillus Niger*, is filamentous aspect, hindering the antimicrobial attack [19].

The coupling agent 3A-IAD, was the greatest inhibition presented for both the bacteria and fungus. We also observe that the coupling agent 3A-IAD, induced the major antimicrobial activity inhibition to both bacteria and fungus.

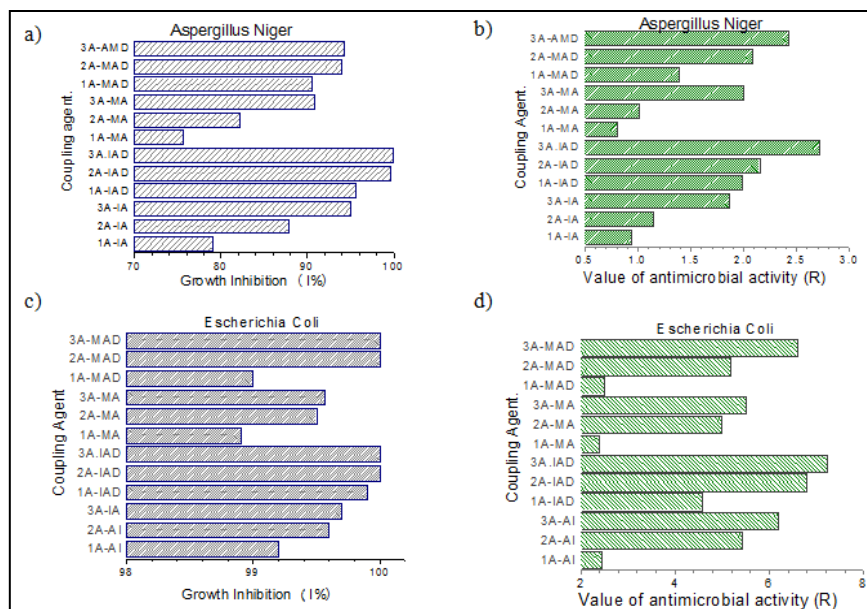


Figure 4. Growth inhibition and antimicrobial activity (R).

Conclusions

Nanocomposites prepared by the method of direct synthesis of Ag NPs on the coupling agents according to the analysis of X-ray diffraction, showed higher degree of exfoliation-intercalation. The coupling agent, 3A-IAD, had greater coupling by promoting exfoliation I28E clay in the nanocomposite. This result is attributed to the better interactions between silver and clay nanoparticles with the coupling agent. Characterization techniques allowed us to establish that the increase in the content of silver nanoparticles, is mainly attributed to the type and concentration of coupling agent. It was concluded that the systems where an increase was observed in the concentration of silver will permit higher inhibition values and antifungal activity. Finally it was concluded that for both methods evaluated, the coupling agent PEGIAD showed a higher content of silver nanoparticles and a higher degree of exfoliation of I28E clay, compared with other coupling agents (PEGIA, PEGMA y PEGMAD). The PEGIAD, proved an efficient coupling agent between the matrix, clay and silver NPs.

Acknowledgements

Authors wish to thank "Proyecto CONACYT 232753 Laboratorio Nacional de Materiales Grafénicos". Authors are grateful to the staff of CIQA: Josefina Zamora, Blanca Huerta, Silvia Torres, Concepcion Gonzales, Jesus Rodriguez, Francisco Zendejo, Fabian Chavez, Rodrigo Cedillo, Sergio Zertuche, Alejandro Espinosa, Anabel Ochoa, Marcelina Sanchez, Rosario Rangel, Sandra Ramos, Fabiola Castellanos, Irma Solis, Marcelo Ulloa, Efraín Alvidrez, Daniel Alvarado, Juan Peña and Jose Luis de la Peña, their help and technical assistance with this research.

References

- [1] Manias E, Touny A, et al. *Polymer Mater Sci Eng*, 82, 282-290 (2000).
- [2] M.L. Lopez ML, S. Sanchez, L.F. Ramos, *Polymer*, 57. 385-389 (2006).
- [3] D. Garcia, O. Picazo and J.C. Merino, *Eur Polymer J*, 39. 945-956 (2003).
- [4] M. Zanetti, S. Lomakin and Camino G, *Macromol Mater Eng.*, 1. 279-280 (2000).
- [5] H.R. Dennis, D.L. Hunter, D. Chang, S. Kim, et al. *Polymer*, 42. 9513-9518 (2001).
- [6] P.H. Nam, M. Okamoto, N. Hasegawa and Usuki A. *Polymer*, 42. 9633-9645 (2001).
- [7] K. Vande, P. Kiekens et al. *Macro-mol Mater Eng.*, 286, 237-241(2001).
- [8] M. Yazdani, H. Vega, R. Quijada. *Polymer*, 42. 4751-4756 (2001).
- [9] L. Cui, DR. Paul. *Polymer*, 48.1632-1652 (2007).
- [10] J.S. Parent, A. Liskova and R. Resendes, *Polymer*, 45. 8091-8094 (2004).
- [11] S. Sánchez, E. Ramírez, M.C. Ibarra, L.F. Ramos, et al. *Composites b*, 497-502 (2011).
- [12] M.J Wills, et al. *Polymer*, 48, 1632-1640 (2007).
- [13] M. Bin, K. Shameli, N. Azowa and M. Darroudi. *Australian Journal of Basic and Applied Sciences*, 4(7). 2158-2165 (2010).
- [14] R. Buddhadeb, P. Bharali, N. Karak. *Bioresource Technology*, 127. 175–180 (2013).
- [15] A. Travan, C. Pelillo, I. Donati, E. Marsich and T. Scarpa. *Biomacromolecules*, 10 (6), 1429–1435 (2009).
- [16] Y. Zhang, H. Peng, W. Huang, Y. Zhou, X. Zhang and DeYan. *J. Phys. Chem. C*, 112 (7). 2330-2346 (2008).
- [17] P.K. Khanna, N. Singh, S. Charan, et al. *Mater Chem Phys*, 93. 117-119. (2005).
- [18] Estándar Industrial Japonés. JIS Z 2801: E (2000).
- [19] K. Shameli et al. *International Journal of Nan medicine*, 5, 1067-1077 (2010).

HUMAN FIBROBLAST VIABILITY ON CHITOSAN GRAFTED LACTIC ACID

Laura N. Sandoval Hernández,¹ Nadia Vázquez,² Lenin Tamay de Dios,² Cristina Velasquillo,² Keiko Shirai^{1*}

¹Universidad Autónoma Metropolitana, Biotechnology Department, Laboratory of Biopolymers. Av. San Rafael Atlixco No. 186. Col. Vicentina, C.P. 09340. Mexico City. *Corresponding author e-mail: smk@xanum.uam.mx

² Biología. Instituto Nacional de Rehabilitación Mexico City.

Abstract

Key words: Chitosan, lactic acid, fibroblast.

Chitosan was prepared by heterogeneous deacetylation from chitin extracted by biological method (BCH). BCH was functionalized with lactic acid (LA) in the presence of catalyst and characterized by its LA incorporation rate, swelling behavior, erosion and fibroblasts viability. The maxima swelling and rate of erosion in DMEM was reached on the 4 d (1585.89%) and 6d (78.25%), respectively. The incorporation of LA was 43.62%. Spherical fibroblasts were observed until 2d of culture and the development of elongated fibroblasts was observed from 4d and, after 8d the cells formed networks. The LA grafted BCH showed adequate adherence and viability of human fibroblasts.

Introduction

Biopolymers are an excellent alternative to the materials currently used in areas such as medicine, pharmacy, agriculture, food among others. Chitosan is a biopolymer that has received much attention in recent years due to its biomedical applications, such as tissue engineering, in wound healing or excipient for drug delivery, based on their biodegradability, renewability and bioactivity [1,2]. Chitosan has been widely used in the formation of extracellular matrix (ECM) in the regeneration of tissue. These properties can be attributed to its structural similarity with the glycosaminoglycans of the ECM and simulate the activity of growth factors [3]. Poly (lactic acid) belongs to the family of aliphatic polyesters, and has excellent mechanical properties and is compatible with the human body; accordingly it has been used as scaffold and in implants [4]. Therefore, the aim of this work was to combine CH with polyesters in order to improve their mechanical properties without loss of bioactivity.

Experimental

Materials and Chitosan grafted lactic acid

BCH with $M_v = 274.8 \text{ g mol}^{-1}$ and $DA = 6.43 \pm 0.19\%$ was obtained by heterogeneous deacetylation of chitin extracted from lactic acid fermentation of shrimp wastes (*Litopenaeus vanameii*) [1]. Racemic D,L-lactic acid (D,L-LA) (85% aqueous solution) and *p*-toluene sulfonic acid (TSA) were obtained from JT Baker (Mexico) and Sigma Aldrich (USA), respectively.

Grafted copolymer of D,L-LA onto BCH (BCH-g-LA) with TSA % (ww^{-1}) was produced following the method reported by Espadín et al [2].

Mechanical properties of BCH-g- LA

Mechanical properties in terms of tensile strength on tension and on puncture [5, 6] in a SINTECH 1/S (MTS, USA) apparatus with a load cell of 100N. Samples were conditioned to 44% RH at 25 °C prior to analyses.

Swelling capacity and erosion of BCH-g- LA

Percent of swelling (%H) was determined by introducing dry films of 1 cm^2 in 5 mL of Dulbecco's Modified Eagle Medium (DMEM) at 37 °C and recording the weight of the sample every 24 h. Erosion percentage (%E) was determined during 14 d in DMEM [2].

Fibroblast attachment and viability

Films were sterilized with UV light for 10 min in a crosslinker (BLX-254 Vilber Lourmat, Germany), subsequently washed with phosphate buffered Saline (PBS) (Gibco), DMEM (pH 8, NaOH 0.01 M) DMEM and dried for 24 h at 25 °C. Samples were seeded with 60 μ L of a suspension of human dermal fibroblasts (hDFs) (1×10^5 cells mL^{-1}) and plated in 24-well cultures for 5 and 10 d, changing the medium every 24 h. For viability and cell attachment to the polymer with cells was washed with PBS and incubated with Hanks/P phenol medium with ethidium homodimer-1 (EthD-1) and calcein at 37 °C for 45 min (Invitrogen). Then, the solution was removed, washed with PBS and analyzed in a microscope with fluorescent light (Axio Observer A1, Carl Zeiss).

DAPI staining was using a mounting medium containing this compound. After completing the viability test were mounted with Vectashield Mounting Medium with DAPI, which stains the nuclei, then the sample was covered with a coverslip, and images were captured with a confocal microscope.

Results and Discussion

The synthesis of BCH-g-LA is based on the amide bond formation by dehydration of lactate amino chitosan salt formed by solubilizing the chitosan in lactic acid [2]. TSA was the reaction catalyst over the formation of ester bond, as the tosyl group acted as a protective group of amino group, avoiding protonation of chitosan by the impurities present in the lactic acid, causing the formation of the bond in less time than reaction without catalyst (Fig. 1).

^1H NMR analysis of the polymer was performed to determine the molar ratio (MR) and the percent molar fraction (% FM). 43.62% was determined as the FM of lactic acid in BCH-g-LA material, whereas the MR indicates that for every 7 lactyl units were incorporated 5 glycoside units of chitosan.

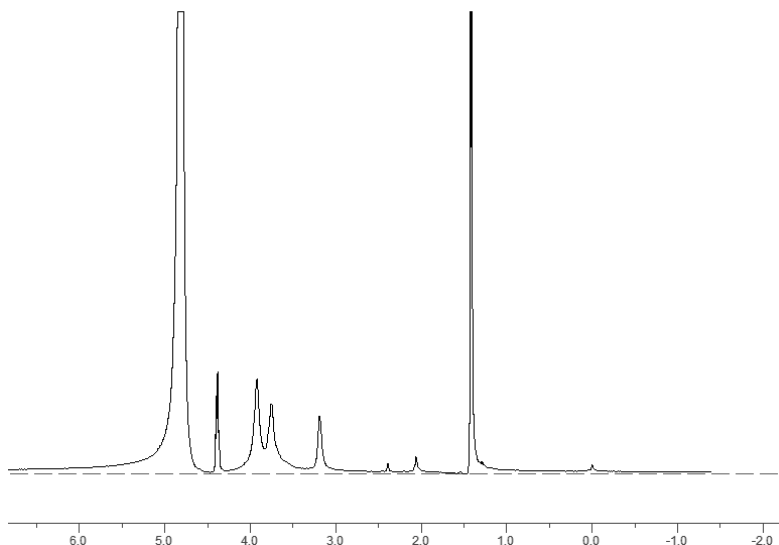


Figure 1. ^1H NMR spectrum of BCH-g-LA.

The grafted LA onto CH enhanced the mechanical properties in regard to the extension profiles and puncture testing in films, as it is shown in Table 1. BCH-g-LA was significantly more flexible and elastic (Young's modulus in tension = 105.6 MPa) than LA grafted chitosan materials prepared without TSA (Young's modulus = 48.20 MPa) [2]. As well, BCH-g-LA with TSA was more resilient and requires more effort to break (67.6 %) than materials prepared without TSA (56.9%) [2].

Table 1. Force fracture extension and puncture in BCH-g-LA

	Young's Modulus (MPa)	Elongation at break (%)	Maximum stress (MPa)
BCH-g-LA tension	105.6±2.14	67.60±5.57	1.92 x10 ³ ±12
BCH-g-LA puncture	2.94 x10 ⁴ ±1.63 x10 ³	96.90±2.96	3.47x10 ⁶ ±2.35 x10 ³

The results are averages of three determinations and their standard deviations

The swelling test was conducted to determine the absorption capacity of the material in DMEM at 37 ° C simulating physiological conditions. The swelling behavior depends on the relative magnitude of water diffusion, relaxation time of the material and the pH due to the protonation of the chitosan amino group [1]. The absorption capacity of the film in equilibrium was achieved on 9 d with a swelling 120.83± 13.31%. The degree of degradation of the material over time in DMEM at 37 ° C was determined as 78.25 ± 8.18% at 6 d.

Fibroblast Viability

Microscopic fluorescence analysis with calcein was carried out in BCH-g-LA materials seeded with fibroblasts at 2, 4, 8 and 15 d of hDFs. The viability of hDFs was determined, the micrographs showed at 2 d spherical living cells and few dead cells appeared on 4 d. hDFs alive remained spherical, but elongation was also observed. On 8 d live cells were elongated and dead cells remained in a lesser extent. At 15 d of culture the formation of networks of fibroblasts was evident. In addition, nuclei of these cells were noticed in blue color due to the dye DAPI, BCH-g-LA promoted adhesion and viability of human fibroblasts (Fig. 2).

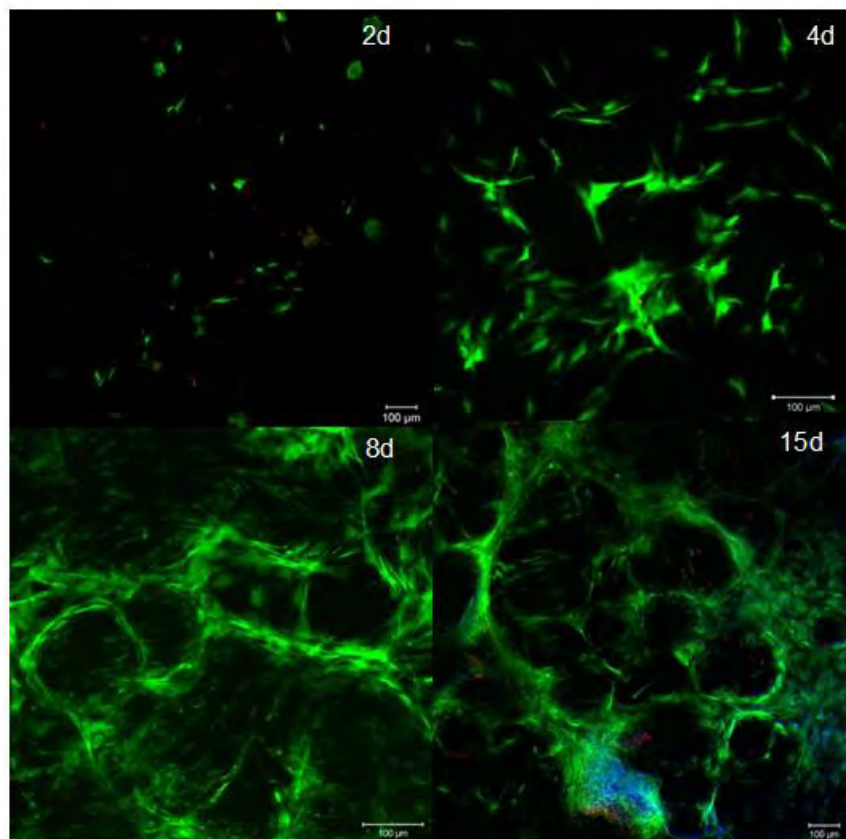


Figure 2. Human fibroblasts micrographs BCH-g-LA films, dyed by the method of calcein-MA, where the living cells are green, red-dead and nuclei are blue.

Conclusions

BCH-g-LA material presents degradation in short time and cytocompatibility. Latter based on their ability to promote adhesion and viability of human fibroblasts. The enhanced grafting procedure with the presence of p-toluene sulfonic acid catalyst give improved mechanical properties.

Acknowledgements

We thank National Council on Science and Technology (CONACYT) (Sectoriales No.161687) and Secretary of Science Technology and Innovation of Mexico City (SECITI) (PICSO12-152).

References

- [1] N. Pacheco, M. Garnica-Gonzalez, M. Gimeno, E. Barzana, S. Trombotto, L. David & K. Shirai, *Biomacromolecules*, 12, 3285–3290. (2011).
- [2] A. Espadín, N. Vázquez, A. Tecante, L. Tamay de Dios, C. Velasquillo & K. Shirai, *J. of Appl. Polym. Sci.*, 131,40252-40261 (2014).
- [3] T. Minagawa, Y. Okamura, Y. Shigemasa, S. Minami, Y. Okamoto. *Carbohydrate Polymers*, 67, 640-644. (2007).
- [4] L. Avérous. *Poly(lactic Acid: Synthesis, Properties and Applications*. In M. Naceur Belgacem, & A. Gandini, *Monomers, Polymers and Composites from Renewable Resources* (pp. 433-450). Great Britain: Elsevier Ltd. (2008).
- [5] ASTM D882-97. Standard test method for tensile properties of thin plastic sheeting. (2003).
- [6] N. Gontard, S. Guilbert, J. Cuq, *J. of Food Sci.*, 58, 206-211 (1993).

POLYMERIC SCAFFOLDS FOR SKIN

Ruiz-Velasco G.^{1*}, Martínez-Flores F.², Morales-Corona J.^{1**}, Olayo R.¹

¹ Departamento de Física, Universidad Autónoma Metropolitana, San Rafael Atlixco 186 Col. Vicentina A.P.09340, México D.F.

² Banco de Tejidos y Piel, CENIAQ-Instituto Nacional de Rehabilitación, Calz. México Xochimilco No. 289 Col. Arenal de Guadalupe C.P. 14389 México D. F.

*tucograce@yahoo.com.mx, **jmor@xanum.uam.mx

Abstract

The skin may be injured due to burns, skin cancer, diabetes, among others. To repair these injuries, treatments require skin grafts, and strict medical care. There is a high demand for healthy skin to be grafted onto the lesions and very limited availability. Tissue engineering combines polymeric biomaterials and cell cultures that develop skin substitutes to heal or recover the damaged area. In this paper the development of a polylactic acid scaffold coated with polypyrrole doped *in situ* with iodine by plasma polymerization is presented. The scaffold was characterized by standard techniques for polymers. Biological characterization was made by the culture of keratinocytes and human fibroblasts derived from skin.

Keywords: Polymeric Scaffolds, plasma polymerization, PPLA, PGA, PPy, skin.

1. Introduction

Burns and diseases are the main cause of skin lesions, and when this happens the body can not act fast enough to produce the necessary replacement cells. Injuries as diabetic foot ulcers may not heal and members must be amputees. The burn victims may die from infection, dehydration and blood loss plasma [1]. Autografts or allografts have been the handiest techniques for burn injuries. But when the injuries involve more than 60% of the body surface there is skin scarcity for the autografts, and in the case of allograft, rejection and infection are issues of great concern. Therefore, there is a growing demand for artificial skin to be used as a substitute for natural skin that has been damaged. Tissue engineering tops the search for a substitute for natural skin by building polymeric scaffolds in combination with cell culture and biologically active molecules to create functional tissues. The intention is to create polymer scaffolds to provide a 3D structure that gives mechanical support to the physiological load allowing the adhesion, proliferation and differentiation [2]. Once cells have been implanted, an ideal scaffold must stimulate production of extracellular matrix (ECM) so that it can later replace the damaged tissue. The polyglycolic acid (PGA) and polylactic acid (PLLA) are synthetic and biodegradable biopolymers, and have had extensive clinical application. They are usually used for the manufacture of polymer scaffolds [3]. Such scaffolds can be constructed as nonwoven mats (electrospun fibers), and they have multiple applications in tissue engineering because they have a very similar structure to the extracellular matrix [4]. The PGA and PLLA scaffolds are biodegradable and biocompatible, but an important feature is that they don't have cell recognition sites, thus the cells cannot anchor the scaffold. To modify this singularity of poor cell attachment, the scaffolds can be modified by physical or chemical means to give them these recognition sites [5]. Plasma treatment is a modifying method for surfaces by depositing a thin film; this gives a favorable response on cell anchorage. Plasma treatment only affects the surface of fibers without altering its bulk properties; in addition, this technique allows introducing functional groups to improve the biocompatibility properties of the scaffold. Plasma treatment of scaffolds of PGA and PLLA with pyrrole, doped with iodine generates a thin film, which is rich in positive charged amine groups, giving a better cell culture [6-8].

In this work, polymeric scaffolds of PLLA and PGA were modified by plasma polymerization of pyrrole to generate a surficial thin film of PPy-I. The morphological and surface properties are analyzed using, microscopy and FTIR-ATR. Subsequently the biological behavior was observed in cell cultures of primary human keratinocytes, fibroblasts derived from human skin, tenocytes and kidney embryonic cells.

2. Experimental Methods

2.1 Materials

Nonwoven fibers of PGA and PLLA BIOFELT® of CONCORDIAL MEDICAL in sizes 10x10 mm were used. The reactants were (Sigma-Aldrich): pyrrole $W_m = 67.09$ g/mol and Iodine with higher purity than 99%.

2.2 Plasma polymerization.

For plasma coating a cylindrical glass reactor was used with a volume of 1500cm^3 approximately, assembled with a vacuum system constituted by a mechanical vacuum pump and a cold trap of particles. The reactor is connected to an RF generator Dressler 1500. The film deposition was done at 18W, 1.5×10^{-1} Torr. and 30 min of synthesis reaction. Pyrrole monomer and iodine were evaporated to the reactor from separate containers. Figure 1 shows the reactor schemes.

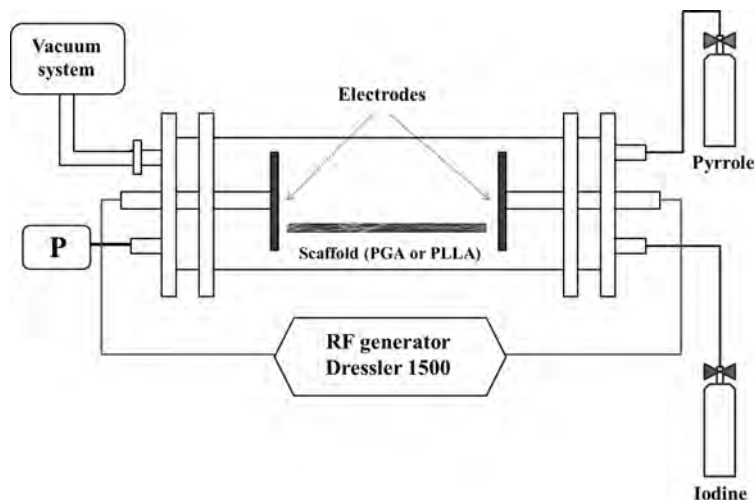


Figure 1. Diagram of the Plasma polymerization reactor.

2.3 Cell culture.

As cell culture medium fetal bovine serum (FBS) was used, samples were: FBS as Control, PPy-I/ PGA and PPy-I/PLLA in SFB. The pH levels were measured in the samples.

2.4 Sterility.

Scaffolds were immersed in an isopropanol solution by 20 min for disinfection, samples were dried in a sterile cabinet (HeraSafe Cabinet Class II Thermo-Kendro, Germany) for 10 min, then rehydrated with SFB for 1 hour. 2×10^6 cells were seeded in 6 wells boxes with fresh culture medium, and antibiotics were added. They were placed in an incubator with 5% of CO_2 , 21% of O_2 and 100% of moisture.

2.5 Growing.

Seeded cells were human primary keratinocytes, fibroblasts derived from human dermis, primary human tenocytes, and embryonic kidney cells line HEK 293. After 9 days, cell culture medium was replaced by one infected with nonreplicating adenovirus Ad-CMV-GFP for one hour. Then, the cells were washed, and the culture medium was changed to a fresh one, and maintained under these conditions for 24 hours.

3. Characterization and results.

3.1. Spectroscopy FT- IR- ATR

The analysis was performed with a Perkin-Elmer GX System with an ATR Smith diamond Durasample II. Figure 2(a) shows the FTIR spectrum of the PGA scaffold. The vibration of the O-H groups is in 3500cm^{-1} ,

and in 2961cm^{-1} are the vibration of the aliphatic group. The vibration of the carbonyl group is in 1738cm^{-1} , and in 1412cm^{-1} is the CH_3 bond. The vibration of the ester groups is located at 1084cm^{-1} . In 2(b) the FTIR spectrum of the PPy-I /PGA scaffold is presented. In 3311cm^{-1} the vibration of the primary and secondary amine groups can be seen, also in 2958cm^{-1} the aliphatic carbons are located.

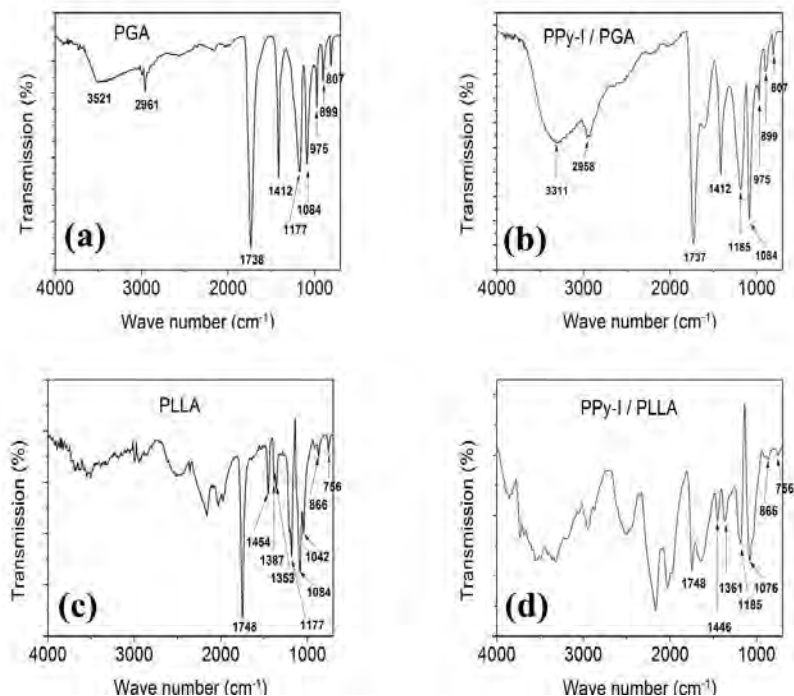


Figure 2. Spectra FT-IR-ATR of: (a) PGA, (b) PPy-I/PGA (c) PLLA and (d) PPy-I/PLLA.

Spectra of PLLA and PPy-I/ PLLA are shown in Figures 2(c) and 2(d) respectively. In 2(c) the $\text{C}=\text{O}$ group characteristic of PLLA is at 1748cm^{-1} . The asymmetric vibrations group $\text{C}-\text{H}$ is in 1454cm^{-1} and 1387cm^{-1} . The stretching vibration of the ester group $\text{C}-\text{O}$ is observed in 1084cm^{-1} . Figure 2(d) shows wide peaks, which are characteristic of the plasma polymerization. The PPy peaks can be identified again.

3.2 SEM

The micrographs of the scaffolds were taken with a Scanning Electron Microscope Field Emission JEOL JSM 7600F. Figure 3(a) and 3(b) show microscopy images SEM of PPy-I/PGA that show that the thickness of the fibers is homogeneous with dimensions around $25\mu\text{m}$ and randomly distributed throughout the space. It is also observed that there are broken fibers, indicating a chemical degradation process of the material. In 3(c) and 3(d) the PPy-I/PLLA scaffold is shown, it is observed that the fibers have an average size of around $30\mu\text{m}$. Figure 3(d) clearly shows the roughness of the fiber surface due to the plasma coating which has a thickness of about $3\mu\text{m}$.

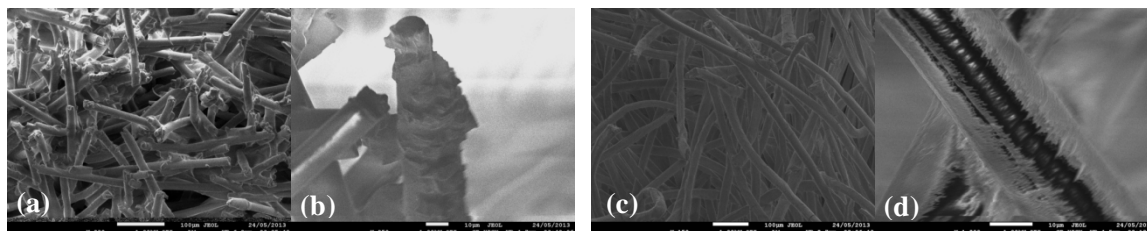


Figure 3. SEM images of the scaffolds of PPy-I/PGA and PPy-I/PLLA respectively, (a) $100\mu\text{m}$ and (b) $100\mu\text{m}$, (c) $100\mu\text{m}$ and (d) $10\mu\text{m}$.

3.3 pH and cell culture.

Table 1 shows the pH measurements. It is observed that there are no significant changes in the sample with just control medium. In the case of PPy-I/PGA there is a major change in 24 hours relative to the control sample, reflecting a change from 7.23 to 3.15 in, leading to significant effects on the cellular environment as all cells die in the course of this time, these scaffolds are degraded due to contact with the culture medium, making it a highly acid solution. For scaffolds PPy-I/PLLA no significant changes in pH are observed, this scaffold is very stable in the cell medium, allowing a better response to cell growth.

Table 1. Measurement of pH of the scaffolding function of time.

Time	Control	PPy-I/PGA	PPy-I/PLLA
24 hours	7.23	3.15	7.32
48 hours	7.50	3.66	7.64
72 hours	7.19	3.44	7.34
7 days	7.15	3.62	7.23

3.4 Confocal microscopy.

We used confocal microscopy LSM 100 Meta (Carl Zeiss, Germany) with an excitation source of argon of 488 nm and with an emission filter of 520 nm.

Figure 4 shows the 3D images of the four cell lines that were seeded on PPy-I/PLLA scaffolds. Luminescent points on the fibers show functional cells that are alive and infected with the adenovirus. 4(a) displays keratinocytes, showing a very good anchoring response and proliferation. 4(b) shows the good anchoring of the fibroblasts. Tenocytes in 4(c) show less cell proliferation, but they are capable of growing in the scaffold. In 4(d) kidney embryonic cells show good adhesion to the fibers.

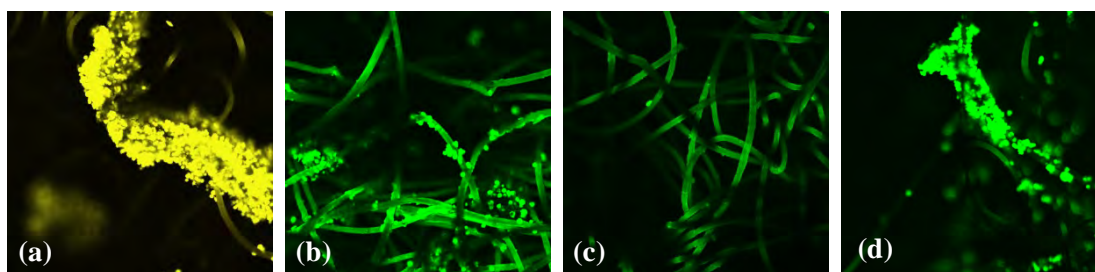


Figure 4. Confocal microscope images of cell growth on the fibers of PPy-I/PLLA. (a) keratinocytes, (b) fibroblasts, (c) tenocytes, and (d) an embryonic kidney cell line HEK-293.

4. Conclusions

Nonwoven PGA and PLLA scaffolds were plasma-modified with a surface thin film of PPy-I and studied. The results show that PLLA scaffolds covered with PPy-I have an excellent response to the cell culture, particularly of skin.

The PGA scaffold coated with PPy-I did not show a favorable response to the cell culture, showing a high degree of degradation and incrementing the pH therefore producing cell mortality.

Acknowledgements

The authors wish to thank: Consejo Nacional de Ciencia y Tecnología for partial support for the realization of this work through project CONACYT-15523 respectively and the Laboratorio de Microscopía de la UAM Iztapalapa.

References

- [1]. Ramos López C., Gan Acosta Antonio, Díaz R. Jorge L., “*Piel Artificial*”, Revista Colombiana de Tecnologías avanzadas, (2006), 2(8), 41-47, ISSN: 1692-7257.
- [2]. Shinji Oshima, Chihiro Suzuki, Rina Yajima, Yuya Egawa, Osamu Hosoya, Kazuhito Juny, Toshinobu Seki., “*The use of an Artificial Skin Model to study Transdermal Absortion of Drugs in Inflamend Skin*”, Biol. Pharm., 35, (2012), 203-209.
- [3]. Pathiraja A. Gunatillake, Raju Adhikari., “*Biodegradable synthetic polymers for tissue engineering*”, European Cells and Materials, 5, (2003), 1-16.
- [4]. Ruiz-Velasco G., Martínez-Flores F., Morales-Corona J., Olayo R., “*Andamios poliméricos electrohilados para la generación de una piel artificial*”, Tópicos especiales de Física: Encuentro de Estudiantes de Posgrado, UAM Iztapalapa, 2013.
- [5]. Jian Yang, Guixin Shi, Jianzhong Bei, Shenguo Wang, Yilin Cao, Qingxin Shang, Guanghui Yang, Wenjing Wang, “*Fabrication and surface modification of macroporous poly(L-lactic acid) and poly(L-lactic-co-glycolic acid) (70/30) cell scaffolds for human skin fibroblast cell culture*”, J Biomed Mater Res 62 (2002), 438–446.
- [6]. G. J. Cruz, J. Morales, R. Olayo, “*Films obtained by plasma polymerization of pyrrole*”, Thin Solid Films, 342/1-2, (1999), 119-126.
- [7]. E. Zúñiga-Aguilar, R. Olayo, O. Ramírez-Fernández, J. Morales, & R. Godínez, “*Nerve cells culture from lumbar spinalcord on surfaces modified by plasmapyrrole polymerization*”, Journal of Biomaterials Science Polymer, 25 (2014), 729-747.
- [8]. O. Ramírez-Fernández, R. Godínez, J. Morales-Corona, L. Gómez-Quiroz, M.C. Gutiérrez-Ruiz, E. Zúñiga-Aguilar, R. Olayo., “*Superficies Modificadas Mediante Polimerización por plasma para cultivo de Modelos Hepáticos*”, Revista Mexicana de Ingeniería Biomédica, 33 (2012), 127-135.

IMPLANTATION OF COMPOSED SCAFFOLD OF PLA/HA COATED WITH POLYPYRROLE FOR GENERATING NEOTISSUE-BONE IN RABBIT: BIOLOGICAL AND MECHANICAL EVALUATION

María Guadalupe Flores-Sánchez¹, Atlántida Margarita Raya-Rivera², Raquel González-Pérez², Diego Ricardo Esquiliano-Rendon², Juan Morales-Corona³ and Roberto Olayo-González³

¹*Departamento de Ingeniería Eléctrica, Posgrado de Ingeniería Biomédica, Universidad Autónoma Metropolitana, Unidad Iztapalapa, Av. San Rafael Atlixco 186, Col, Vicentina, Del. Iztapalapa, CP 09340, DF, México.*

²*Laboratorio de Ingeniería de Tejidos, Hospital Infantil de la Ciudad de México, "Federico Gómez", Mexico, D.F.*

³*Departamento de Física, Área de Polímeros, Universidad Autónoma Metropolitana, Unidad Iztapalapa, Av. San Rafael Atlixco 186, Col, Vicentina, Del. Iztapalapa, CP 09340, DF, México*

Abstract

This work presents the fabrication of porous matrices of Polylactic Acid (PLA) and hydroxyapatite (HA) coated with polymer of pyrrole doped with iodine, synthesized by plasma. The composite was made first by electrospinning, creating nanometric and micrometric fibers of PLA/HA from solutions at different concentrations and conditions of the spinner. The resulting porous materials are coated by plasma polymerization of pyrrole (PPy), favoring cell adherence and cell stimulation due to their chemical diversity. The scaffold made of PLA/HA/PPy were implanted underneath the back of rabbit for 30 days; the newly formed tissue is characterized by Scanning Electron Microscopy (SEM), and stress tests.

Introduction

A graft or bone substitute is usually needed to help repair a skeletal deficiency due to some type of trauma or disease such as osteosarcoma. Tissue Engineering is an alternative to generate synthetic bone providing the patient with the preservation of the gait, functional recovery and mobilization. Biomaterials that can be used as bone substitutes should possess osteoinductive, osteoconductive, resistance and biocompatibility, the latter is closely related to their surface properties; such materials can be found in polymeric materials that combined with ceramic materials are better to repair bone tissue. Polylactic acid (PLA) is a polymer having biodegradability and biocompatibility and hydroxyapatite (HA) is a ceramic that forms the bulk inorganic bone part, it is also biocompatible and resistant.

The Electrospinning technique is used for the manufacture of porous matrices, it consists in the application of a voltage ranging from 10KV to 30KV to create a strong electric field seeking to attract electrically charged particles of a polymeric solution from a nozzle system into a surface where it solidifies (collector) forming arrays of microfibers and nanofibers giving pores of different sizes. In this work the technique of Plasma Polymerization is used to synthesize films of polypyrrole (PPy) and modify the surface properties of the matrices of PLA/HA. Using polypyrrole is an advantage in the proliferation of bone forming cells (osteoblasts) due to their chemical diversity, inducing cell adhesion and stimulation. The samples were characterized by scanning electron microscopy (SEM). To test arrays of PLA/HA coated with polypyrrole, first the cultivation was carried out *in vitro*; this requires a biopsy of rabbit's femur marrow, then the interested cells (osteocytes, osteoblasts and osteoclasts) are extracted and a sequential seeding of the cells in the matrix is performed. Once the cells have been seeded, the culture is maintained *in vitro* for 7 days to then implant the cell-matrix structure *in vivo*, under the skin of the back of a rabbit (subcutaneous) for 30 days. Finally, it is important to evaluate the microstructure or neotissue and for this is necessary to characterize it morphologically by scanning electron microscopy (SEM). To evaluate the mechanical performance a voltage test is done.

Experimental

Solution Preparation

Two types of matrix M1 and M2 were manufactured, in order to make comparisons between these; for this were done two mixtures in proportions of 10 mL of solvent, 90% chloroform (9 mL) and 10% ethanol (1 mL); in each of these solutions PLA (1.8 g) was dissolved by gentle stirring for 5 hrs at room temperature. After this time HA was added at 18.1% and 35.7% to the resulting solutions for M1 and M2 respectively, and dissolved until obtaining homogeneous solutions.

Fabrication of polymeric matrices

Electrospinning system consists of an injection mechanism in which the polymer solution of PLA/HA is deposited. This solution travels from the positive electrode (the needle) to the collecting electrode that is a rotating drum of 7cm in length and 5 cm in diameter that is connected directly to the ground; when the solution solidifies forms matrices with nanofibers and microfibers of different lengths. The voltage applied to this kind of solution is of 25KV to 30KV, the voltage breaks the surface tension forming the Taylor cone at the tip of the needle. Needles of 0.9 mm diameter were used. The sample of interest was injected in a volume of 20 mL. The percentage of HA obtained in M2 (35.7%) is considerable as natural bone consists of 60% inorganic matter.

The matrices obtained are removed from the collector, dried at 42 ° C under vacuum for 4 days to remove the solvent (chloroform) excess. Each sheet was split into rectangular strips homers (1 cm wide x 3 cm long). Scanning Electron Microscopy was used to evaluate the morphology, porous structure, and integration of matrices.

Plasma Polymerization

Plasma polymerization technique was used for the deposition of a polypyrrole thin film and thus modify the surface of the matrices of PLA/HA, in order to facilitate the adhesion and proliferation of bone cells as polypyrrole is a cells growth stimulator due to its chemical diversity.

Arrays of PLA/HA, were placed in the center of the reactor, in which are two stainless steel electrodes separated by 10 cm, figure 1. The polymerization conditions were: 1.2×10^{-1} Torr, 13MHz and 18W for 30 min.



Figure 1. a) Plasma polymerization b) Covered with Polypyrrole Matrix.

Osteoblast culture in vitro

A male rabbit of 2 months of extrauterine life was used to obtain cells, New Zealand species whit 2.2 kg of weight, 3 mL of bone biopsy femur (figure 2 a) were taken. CTM mesenchymal stem cells were obtained by enzymatic digestion with collagenase II continuously stirred for a whole night, in α -MEM-F12 (1:1) supplemented with antibiotic-antimycotic and PBS 2%. These cells were maintained in culture dishes with Dulbecco's Eagle Modified medium, supplemented with 10% fetal bovine serum (DMEM/PBS). After 4-10 days of culture, no adherent cells were removed by changing the culture medium by fresh culture medium while the adherent cells were kept in culture under standard conditions of 37 ° C, 5% CO₂, and an humid environment.

Cell characterization was performed by immunohistochemistry in which different cell types are identified in the bone, such as osteoblasts, osteocytes and osteoclasts, this is achieved using specific antibody-tissue. The phenotype of osteoblasts and osteocytes were confirmed by used the Bon-Sialiprotein II antibodies. Once the cells of interest are obtained, they are seeded in a Lab-Tek 8 well plate until 70-80% confluence

has been reached and fixed with cold acetone for 5 min, then washed with PBS and incubated with the antibody polyclonal Bone Sialoprotein II for 1hr, (figure 2 b). Finally, counterstaining was performed with hematoxylin for 1 min and placed in the visible light microscopy to observe it, (figure 2 c).

Cells were cultured in petri dishes of 25 mL and when they reached 70% confluence were performed 3 passes to 2 new petri dishes with trypsin-EDTA solution for 1 min; to detach the cells from the Petri dish it was quenched with serum.

For seeding of cells in the PLA/PPy HA-matrix, these cells were centrifuged and the cell pellet was seeded at a concentration of 5×10^6 cells /well in a PBS/thrombin solution. Then a 0.5 cm^2 matrix was deposited in each well, (Figure 2 d), and incubated under standard culture conditions (37°C , $5\% \text{ CO}_2$), changing the medium depleted by fresh medium every 3 days until day 7, some matrix-cell structures were removed and were used for cell culture in vivo (implantation).

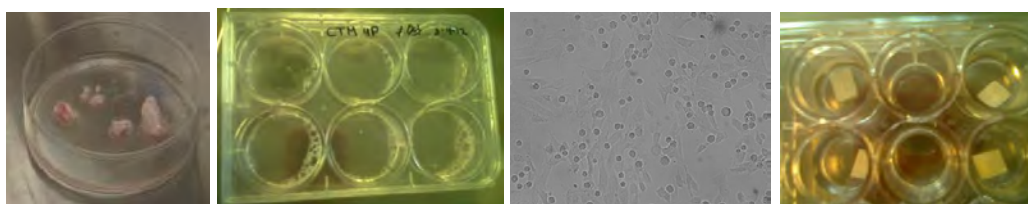


Figure 2. a) Bone biopsy, b) cells in multiwell cash deposited, c) Optical microscopy of osteoblasts attached to the housing, d) seeding matrices osteoblasts PLA / HA-PPy.

Matrix Implant PLA/HA and PLA/HA/PPy in back of rabbit

The implant of the matrices was made under the skin of the back of a male rabbit of 2 months of extrauterine life, species New Zealand. Under proper conditions of asepsis and antisepsis, the animal was calmed with an intramuscular injection of acepromazine (5 mg/kg) and ketamine (20 mg/kg); then was anesthetized with an intravenous injection of Pentobarbital Sodium (40 mg/kg). Then was locally anesthetized with Xylocaine. Subsequently the back of the animal was shaved to (figure 3 a) and an incision was made with a scalpel taking care not to injure anatomical structures. Arrays were wrapped in vicryl mesh in order to insert them (Figure 3 b).

Once inserted all matrices, the defect was closed in two layers with nylon or silk sutures, (figure 3 c) and was used micromizado aluminio, (figure 3 d) to seal, ultimately came the area disinfection and antibiotic was administered intraoperatively and for 3 days post-op.



Figure 3. PLA matrix implant / HA, PLA / HA / PPy. a) Shaving b) Insertion of matrices, c) 12 matrices introduced g) Seal with aluminum micromizado.

Mechanical Stress Testing

Mechanical tests were performed on the same day that were extracted from the animal, samples were placed in the clamps of the tensile machine being careful not to damage them, the speed was 0.5 mm/min , (figure 4) shows specific points in the course of this test from the start until the material-tissue breaks down for each of the matrices of interest also the graphs is showing stress-strain and Young's modulus (E).

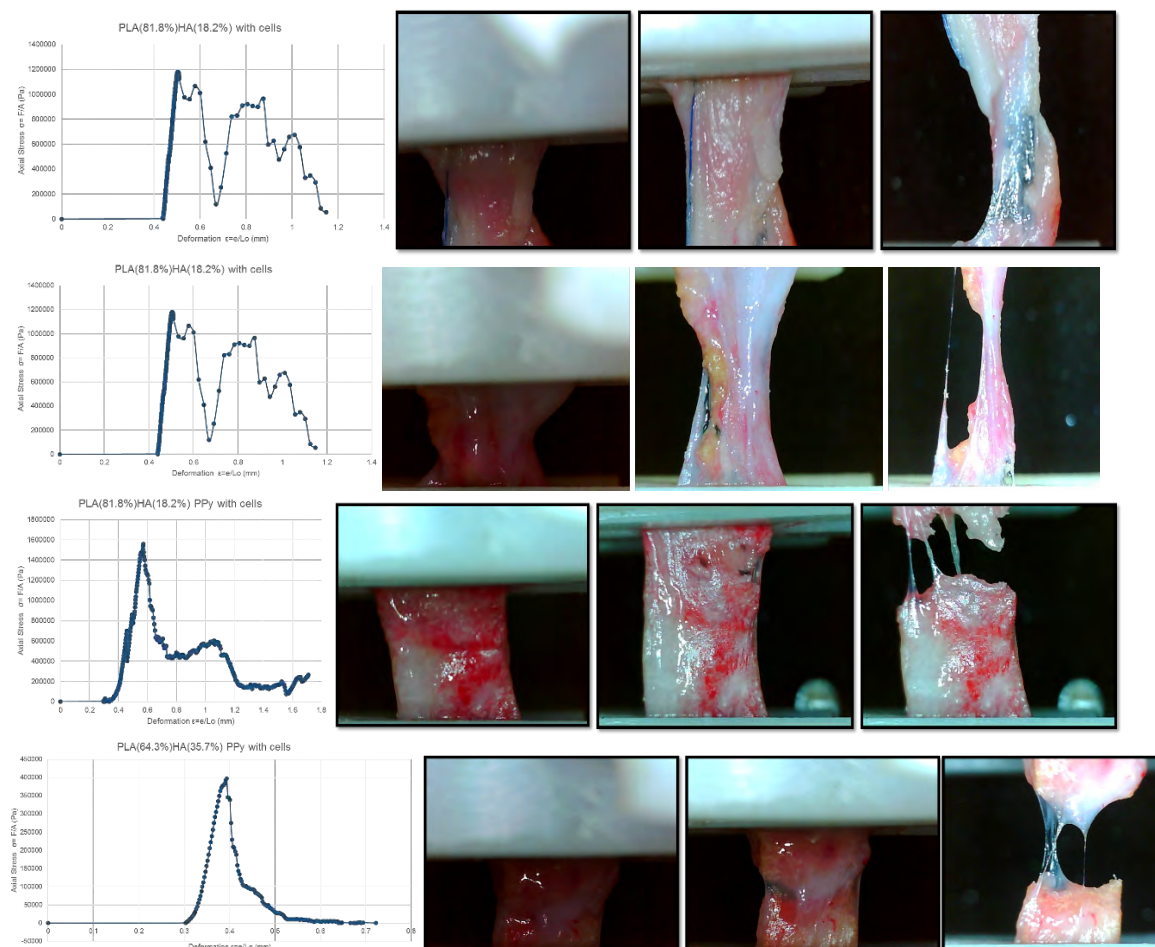


Figure 4. Tensile test, Young's modulus (MPa) a) 19.4 b) 10.1 c) 8.1 d) 6.76

Results and Discussion

The samples were analyzed by SEM; they exhibit "rough" areas because of HA aggregates. An important aspect to be noted is that HA aggregates are mainly in those fibers whose diameter is larger; the fiber diameters ranges from 800 nm to about 10 μm and pores with size from 10 μm to about 100 μm , which allows passage of osteoblasts and culture medium within the matrices, as the diameter of osteoblasts is 10 μm .

Morphological characterization of in vitro culture of osteoblasts were also performed by SEM; Figure 5 shows the matrices of interest with osteoblasts at day 7 of culture, where we can see the beginning of the adhesion of these bone cells, which tend to be in those areas where there are more hydroxyapatite, ie in rough areas, (figure 5 c), d)); another important aspect is that most cells adhere in the matrices that present polypyrrole than in those who lack in this, (figure 5 b), d)).

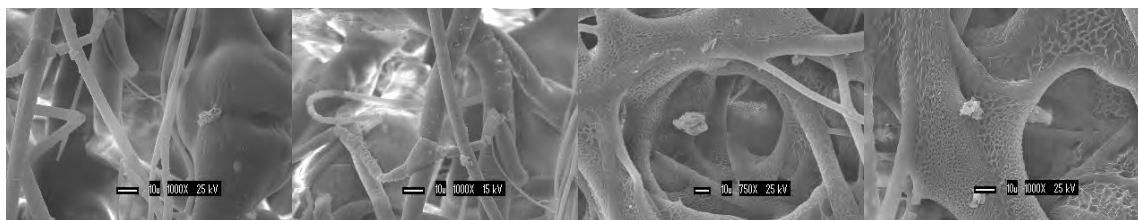


Figure 5. a) SEM of matrices, at day 7 of culture of osteoblasts in vitro. a) PLA/HA(18.2%) with cells,

b) PLA/HA(18.2%)/PPy with cells, c) PLA/HA(35.7%) with cells, d) PLA/HA(35.7%) PPy with cells.

Samples were taken at 30 days of being implanted Figure 6 emphasizes that there was no rejection of material by the animal, there was vascularization and tissue formation in matrix, indicating that the material effectively allowed the adhesion and proliferation of cells.

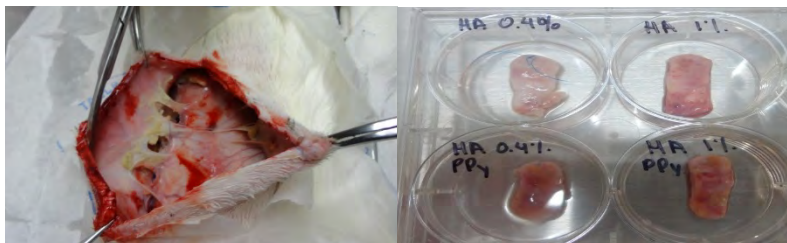


Figura 6. Removing the matrices for tensile test.

Tensile tests have shown that these matrices have low Young module, this precisely because the tissue is at an early stage of formation, however, it can be observed that matrices with lower percentage of HA have a higher module, which means that these matrices yield more to stretch more than those with more HA, and those matrices which have less hydroxyapatite are broken in the hourglass neck, while those which have more hydroxyapatite break of "coup" throughout its cross section.

Conclusions

This study confirms that the technique of electrospinning produces porous matrices of PLA/HA formed by fibers of diameters varying from 800 nm to 50 microns, variable lengths and pore size from 10 μm to 100 μm . Because of the versatility of the technique of electrospinning was possible to vary the conditions of deposit so that could be combined the properties of polylactic acid with hydroxyapatite, leading to a strong and flexible matrix result. The Biocompatibility of PLA and HA and the presence of Polypyrrole and matrices allowed to grow bone cells in vitro and in vivo, achieving good adhesion and cell proliferation without causing cytotoxicity or side effects. It is intended to extend the time of the implant to 3 and 9 months to observe the behavior of these matrices and realize again correspondent testing and comparisons.

Acknowledgements

The authors wish to thank: Consejo Nacional de Ciencia y Tecnología for partial support for the realization of this work through project CONACYT-15523 respectively and the Laboratorio de Microscopía de la UAM Iztapalapa.

CHARACTERIZATION OF SUSPENSIONS OF IODINE - DOPED POLYPYRROLE (PPY-I) SYNTHESIZED BY PLASMA IN BOVINE SERUM ALBUMIN (BSA) SOLUTIONS.

Fabela-Sánchez, O.¹; Medina-Torres, L.⁴, Sánchez-Torres, S.³, Salgado-Ceballos, H.^{6, 7}, Morales, A.⁹, Álvarez, A. L.¹, Mondragón, R.⁵, Olayo, M. G.⁵, Cruz, G. J.⁵, Díaz-Ruiz, A.⁸, Morales, J.², Ríos, C.⁸ y Olayo, R.²

*1*Depto. Ingeniería Eléctrica. *2* Depto. Física. *3* Depto. Biología Celular, Universidad Autónoma Metropolitana, México.

*4*Depto. Ingeniería Química, Universidad Nacional Autónoma de México, México.

*5*Depto. Síntesis y Caracterización, Instituto Nacional en Investigaciones Nucleares, México.

*6*Unidad de Investigación Médica en Enfermedades Neurológicas, Hospital de Especialidades, Centro Médico Nacional Siglo XXI, México.

*7*Centro de Investigación del Proyecto CAMINA A.C., México.

*8*Depto. Neuroquímica, Instituto Nacional de Neurología y Neurocirugía Manuel Velazco Suárez S.S.A. México.

*9*Centro Nacional de Investigación en Imagenología e Instrumentación Médica, Universidad Autónoma Metropolitana, México.

Abstract

The cellular interactions with natural and artificial surfaces are predominantly mediated by proteins adsorbed on the surface of biomaterials, which can be set biocompatibility. We used PPy-I as an implant in spinal cord injury and as a scaffold in cell culture; but understanding how the surface properties of PPy-I are affected by the presence of albumin protein is vital. Therefore, this work focuses on presenting the characterization studies of PPy-I under two different synthesis conditions, analyzing their properties by XPS, SEM and TEM; likewise, their behavior in different albumin solutions by means contact angle and its rheological properties. In this respect we found that the rheological properties and surface characteristics by contact angle were those that showed greater difference in contrast to certain other properties.

Introduction

Polypyrrole (PPy) has been widely studied due to its relative stability to environmental factors and its applications, for example, in biological systems has been selected as a material in the regeneration and protection of nerve tissue due to its semiconducting properties, ease of preparation and diversity of surface characteristics¹⁻³. Because of its surface chemical diversity, PPy is also susceptible to proteins adsorption, which has been studied actively because of its importance in the biomedical applications and tissues engineering^{4,5}. The techniques used to study protein adsorption fall into two categories: those applicable to particles systems and those usable with films or particles; the contact angle measured on proteins films could potentially be helpful in drawing some conclusions regarding the surface structure of these films⁵. Coupled with this, studies related to surface microscopy and elemental composition, add a battery of information on the understanding the interaction of the surface chemistry of polymers.

The rheological study of polymeric particles in suspension is a complex function of its physical properties and the stability of the suspended particles. The most important factors are particle volume fraction, particle shape, interactions between particles, proteins and particles - proteins, among others^{6, 7}. These properties are important to the emergence of new therapies of minimal invasive character that actually are required, a strategy is the microinjection of suspended particles^{8, 9}, such a strategy is contingent on properties that present the suspension from the rheological point of view. In this work, we have focused on analyzing the characteristics of two PPy-I biomaterials by techniques such as SEM, TEM and XPS, as well as the interaction between this biomaterial and albumin protein to determine its properties by contact angle and its rheometric properties in suspension.

Experimental

Plasma polymerization. The synthesis of PPy-I1 and PPy-I2 by plasma polymerization, was carried out in a flanged tube glass reactor as previously reported^{2, 10} and PPy-I2 was synthesized with a modification to introduce a stream of water vapor in the reactor, in both cases, an average power of 20 Watts with reaction times of 240 min. The products of the reaction that were not deposited as films were collected by a gas condenser cooled with liquid nitrogen.

Spectroscopy, elemental and surface analysis. The IR spectra of the film were taken with Perkin-Elmer FT 1600 spectrophotometer sample directly from the films. For the analysis of the samples once sprayed films, the equipment used were Jeol JSM - 5900LV (15 kV) for SEM, HRTEM Jeol 2100F (200 kV) for TEM and Thermo K-Alpha spectrometer with a monochromatic X-ray source of Al Ka (1486.6 eV) for XPS. **Protein adsorption test.** For the study of adsorption of bovine serum albumin (BSA) on the surface of the polymers of PPy-I, thin films of polymer deposited on slides were synthesized, which were submerged for 5 minutes in solutions of BSA dissolved in phosphate buffer solution (PBS, pH = 7.4), at increasing concentrations of 0 to 30 mg/mL, then the slides were washed with PBS to remove the excess protein. The slides were placed in a desiccator for subsequently performing the analysis of the contact angle. **Rheological test.** The rheological properties of the suspension of the polymers of PPy-I in BSA solutions were measured using a TA Instrument AR-G2 rheometer. The suspensions tested consisted 10 mg of PPy-I1 or PPy-I2 in 1 mL solution of BSA in PBS (pH = 7.4) at concentrations of 7, 14 or 21 mg/mL.

Results and Discussion

Elemental analysis. In the Table 1 presents the elemental analysis obtained from the polymers using XPS technique. The elements analyzed were carbon, iodine, nitrogen and oxygen and relations X/N, X/O where X represent any element respect to nitrogen or oxygen and they comparative relationship between PPy-I1 and PPy-I2. As shown in Table 1, there is an increased amount of iodine and oxygen in PPy-I1 than in PPy-I2, is necessary considerate that although in both polymers, iodine is considered a dopant and possibly some of the dopant atoms could be covalently linked to the polymer and others could be trapped among the chains in ionic interaction. Assuming the oxygen as reference and that this element is not part of the monomer pyrrole which consists only 4 carbons and 1 nitrogen, it was noted that PPy-I2, contained a minor amount of oxygen than expected due to synthesis conditions.

Table 1. - Elemental composition in % atomic of PPy-I1 and PPy-I2.

Element (X)	% atomic		Relation					
	PPy-I1	PPy-I2	A = (X/N) _{PPy-I1}	B = (X/N) _{PPy-I2}	A/B	C = (X/O) _{PPy-I1}	D = (X/O) _{PPy-I2}	C/D
Carbon	74.36	78.01	6.18	5.49	1.13	6.30	11.05	0.57
Iodine	1.81	0.73	0.15	0.05	3.00	0.15	0.10	1.48
Nitrogen	12.02	14.20	1.00	1.00	1.00	1.02	2.01	0.51
Oxygen	11.81	7.06	0.98	0.50	1.98	1.00	1.00	1.00
Total	100	100	*X represent to element					

Morphology analysis. Fig. 1 show the representative SEM and TEM micrographs of polymers PPy-I1 and PPy-I2. It is noted that in the images obtained by SEM the powders were constituted of particles of different sizes in a seemingly homogeneous surface, however, the images obtained by TEM was observed that both materials are made up of layers of different thicknesses which shows the process of synthesis is carried out by forming layer upon layer of material, interspersed with

areas rich pyrrole or iodine; as mentioned above iodine could be trapped among the chains without being linked to a specific site in the structure.

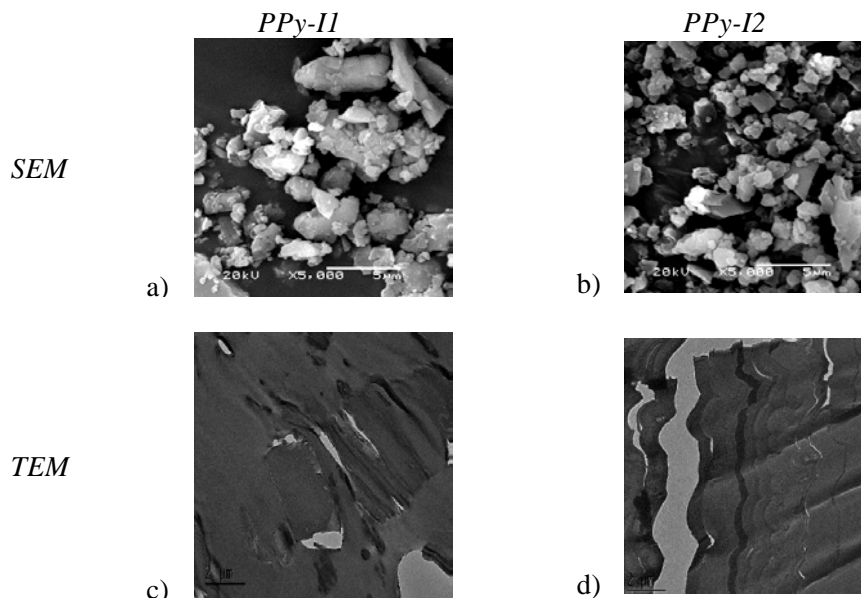


Fig. 1. - Representative SEM and TEM micrographs of polymers synthesized by plasma polypyrrole. In these micrographs is possible to observe different particle size obtained after spray the synthesized polypyrrole films, however, there is no visible difference between the polymer surface of PPy-I1 (a, c) and PPy-I2 (b, d).

FT – IR analysis. The IR analysis shows the PPy-I1 and PPy-I2 powders have structure with presence of O-H, N-H and C-H groups in the bands 3731 , 3192 and 2960 cm^{-1} . The next peak (2361 cm^{-1}) corresponds to an area where they can be localized absorption bands corresponding to multiple groups, such as $\text{C} \equiv \text{C}$, $\text{C} \equiv \text{N}$ bonds. This suggests the formation of new bonds due to the loss of hydrogen at the time of synthesis. On the other hand, the peak at 1615 cm^{-1} confirms the presence of nitrile bonds in the structure formation of polypyrrole, one can assume the presence of alcohol / acid groups because the bands 1417 and 1048 cm^{-1} in addition to the broadening of the peak at 3192 cm^{-1} and the presence of two peaks in the area 3731 cm^{-1} . It was also possible to observe two bands between 3400 cm^{-1} and 3500 cm^{-1} associated with primary amines, they could be related to peaks in the area from 1560 to 1640 cm^{-1} . Finally, presence an intense band at 678 cm^{-1} may associate with cis-disubstituted vinyl type bonds ($\text{C}=\text{CH}_2$) coupled with the peak at 734 cm^{-1} corresponding to CH_2 bonds. Both materials PPy-I1 and PPy-I2 above showed the peaks so it could be assumed that both have very similar surface functional groups.

Surface analysis. According to that reported in literature¹¹, contact angles near 46° indicates a lot of NH_2 groups on the surface, as is the case for PPy-I1 ($\theta = 50.82^\circ$); On the other hand, at higher angles ($\theta = 70.65^\circ$) are characteristic hydrophobic surfaces such as PPy-I2. As mentioned previously, due to synthesis by plasma energy, the chemical species present on the surface are varied and complex, which was corroborated by IR analysis of both polymers. It is notable that in the process of exposure to different concentrations of BSA there is a decrease in the contact angle measurement reaching a point of apparent stability⁵ in areas which could be associated with COOH groups for PPy-I1 which gives greater hydrophilicity, whereas for PPy-I2 decrease its initial hydrophobicity to present a related thread behavior NH_2 groups; said functional groups may be present in the main by the amino acid composition in the albumin and not only by the chemical diversity in the material surface. Likewise, it is to be remarked that PPy-I1 reaches a saturation

point quicker at low concentrations of BSA as compared to PPy-I2, which require higher concentrations to be saturated with the same protein.

Rheometry test. We observed solid-like behavior at low frequencies, should be understood as the independence of the elastic modulus in relation to the frequency at which is subject the suspension of PPy in BSA solution respect to the suspension of the polymer alone, that has a tendency to drop the elastic modulus when is exposed at low frequency; carried out at constant temperature of 37 ° C. Furthermore, it is evident that both polymers exhibit this type of behavior at concentrations of 14 and 21 mg/mL BSA in the range of 0.1 to 100 rad/s, probably due to its affinity for BSA as mentioned above.

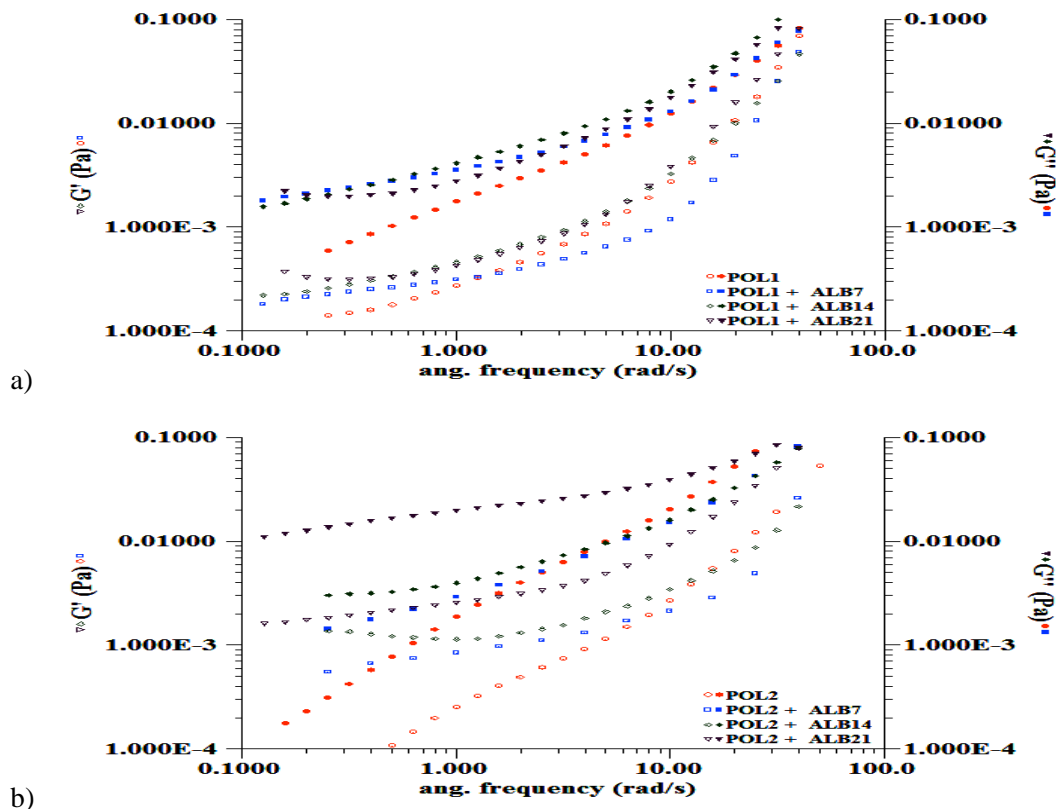


Fig. 2 – Rheological tests for combinations of BSA and PPy-I2 at $T = 37^{\circ}\text{C}$. Panel PPy-I1 (a) and PPy-I2 (b). In both cases, concentrations of 7, 14 and 21 mg/mL of BSA with or without 10 mg of polymer per mL suspended in PBS (pH= 7.4).

Conclusions. We have demonstrated a solid-like response of suspensions of PPy-I BSA solutions lower frequencies and under conditions close to body temperature. These responses are of great interest because albumin alone had a neuroprotective activity in spinal cord injury¹², in the same way, the PPy-I presented in previous studies such feature in injury models of the central nervous system¹³⁻¹⁵. Therefore, these results show that it would be of great interest to test its synergistic potential in this type of injury.

Acknowledgments

We appreciate the support provided by CONACyT through project CONACYT-15523 and Dr. José Sepulveda and Technical histologist Jorge Sepulveda.

References.

1. Z. Zhang, J. Dou, F. Yan, X. Zheng, X. Li and S. Fang, *Plasma Processes and Polymers*, 2011, **8**, 923-931.
2. J. Morales, M. G. Olayo, G. J. Cruz, M. M. Castillo-Ortega and R. Olayo, *Journal of Polymer Science Part B: Polymer Physics*, 2000, **38**, 3247-3255.
3. X. Wang, X. Gu, C. Yuan, S. Chen, P. Zhang, T. Zhang, J. Yao, F. Chen and G. Chen, *Journal of Biomedical Materials Research Part A*, 2004, **68A**, 411-422.
4. W. Li and S. Li, *Colloids and Surfaces A: Physicochemical and Engineering Aspects*, 2007, **295**, 159-164.
5. T. Białopiotrowicz and B. Jańczuk *Journal of Surfactants and Detergents* 2001, **4**, 287 - 292.
6. S. Mueller, E. W. Llewellyn and H. M. Mader, *Proceedings of the Royal Society A: Mathematical, Physical and Engineering Science*, 2010, **466**, 1201-1228.
7. E. A. Vogler, *Biomaterials*, 2012, **33**, 1201-1237.
8. M. D. Baumann, C. E. Kang, J. C. Stanwick, Y. Wang, H. Kim, Y. Lapitsky and M. S. Shoichet, *Journal of controlled release : official journal of the Controlled Release Society*, 2009, **138**, 205-213.
9. M. S. Shoichet, C. H. Tator, P. Poon, C. Kang and M. Douglas Baumann, in *Progress in Brain Research*, eds. M. J. Webber and M. Maass, Elsevier B. L., 2007, vol. 161, pp. 385-392.
10. G. J. Cruz, J. Morales, M. M. Castillo-Ortega and R. Olayo, *Synthetic Metals*, 1997, **88**, 213-218.
11. D. M. Keselowsky Bg Fau - Collard, A. J. Collard Dm Fau - Garcia and A. J. Garcia, *Journal of Biomedical Materials Research Part A*, 2003, **66A**, 247 - 259.
12. L. D. Cain, L. Nie, M. G. Hughes, K. Johnson, C. Echetebe, G. Y. Xu, C. E. Hulsebosch and D. J. McAdoo, *Journal of neuroscience research*, 2007, **85**, 1558-1567.
13. G. Cruz, G. Olayo, H. Salgado, A. Diaz, C. Rios, R. Olayo, J. Morales, A. Alvarez Mejía, R. Mondragón Lozano and A. Morales, in *Contribuciones del Instituto Nacional de Investigaciones Nucleares al avance de la Ciencia y la Tecnología en México*, eds. G. Duque Mojica, M. Jiménez Reyes, F. Monroy Guzmán, S. Romero Hernández and J. Serment Guerrero, ININ, México, 2010, ch. 1, pp. 11 - 28.
14. R. Olayo, L. Alvarez, R. Lozano, A. Escalona, C. Morales, J. Morales, M. G. Olayo, G. J. Cruz, C. Ríos, A. Díaz-Ruiz and H. Salgado-Ceballos, in *La Física biología en México: Temas selectos* eds. L. GarcíaColín, L. Dagdug and Picquart, Colegio Nacional, 2008, vol. 2, ch. 8, pp. 195 - 205.
15. R. Olayo, C. Rios, H. Salgado-Ceballos, G. J. Cruz, J. Morales, M. G. Olayo, M. Alcaraz-Zubeldia, A. L. Alvarez, R. Mondragon, A. Morales and A. Diaz-Ruiz, *Journal of materials science. Materials in medicine*, 2008, **19**, 817-826.

SCAFFOLDS PRODUCED BY ELECTROSPINNING, MODIFIED BY PLASMA AND MECHANICALLY EVALUATED TO THE REGENERATION OF ARTICULAR CARTILAGE TISSUE.

Nancy C. Islas-Arteaga¹, Xinhua Herón Gutiérrez García², Atlántida Raya-Rivera³, Juan Morales-Corona⁴,
R. Olayo⁴

^{1,2}Posgrado Ingeniería Biomédica, Universidad Autónoma Metropolitana, Unidad Iztapalapa, Apdo. Postal 55-534, Iztapalapa, México, D.F

³Hospital Infantil de México Federico Gómez, Depto. de Urología, Laboratorio de Ingeniería de tejidos. Del. Cuauhtémoc México, D. F

⁴Departamento de Física, Universidad Autónoma Metropolitana, Unidad Iztapalapa, Apdo. Postal 55-534, Iztapalapa, México, D.F. jmor@xanum.uam.mx

ABSTRACT: The loss of a tissue or its function due to birth defects, disease or trauma, is one of the most common and costly problems facing medicine, [1] this is the case of cartilage where previous studies have stated preliminarily the feasibility of constructing cartilage in vitro, however, the in vitro regenerated cartilage is currently unsatisfactory for clinical application because cartilage structure is not homogeneous, has insufficient mechanical properties and poor thickness. Despite two decades of research in cartilage tissue engineering, few products have passed the laboratory [2]. This paper is intended to form a new scaffold based on polylactic acid (PLA)-polycaprolactone (PCL) surface modified with polypyrrole-Iodo (PPy-I) looking improve their interaction with the matrix and coated with Aggrecan (AG) which is a important component of the extracellular matrix of native cartilage being a protein essential for normal tissue function [3] and their concentration favors defining how tissues during early development and properties mechanical thereof. Size and distribution of pore by scanning electron microscopy (SEM) were evaluated, and its chemical composition was evaluated by spectroscopy Infrared Fourier Transform Attenuated total reflectance (FTIR-ATR) in addition to mechanical tensile tests.

1.- Introduction

The cartilage is a network of entangled collagen and proteoglycans, which provide the mechanical support of tissue in vivo, however, they lack a blood supply thus have a low cell density with minimum potential for self-repair and therefore, damage to the cartilage rarely resolves spontaneously, which, if not treated, causes degeneration of surrounding cartilage and negative effects on the routine activities. There are numerous treatments that have been developed to repair cartilage damage typical examples: chondrocyte transplantation, mosaicplasty and microfracture. Given that no method used to repair damage to the cartilage, restore permanently the osteoarthritis, currently systems based on the implantation of cells cultured on biodegradable scaffolds are used, they are made with different biodegradable polymers and different techniques. Tissue engineering has been proved to be one of the most promising alternative therapies for articular cartilage defects, these treatments have produced satisfactory results, however, the literature also documents treatment failures [4][5][6]. In this work scaffolds of PLA-PCL surface modified by plasma polymerization of pyrrole and coated with AG are discussed.

2.- Materials and methods

2.1 Design and fabrication of PLA-PCL-PPyI scaffolds

A polymer solution of PLA ($M_v = 4531.75$) and a PCL ($M_v = 65112.65$) was prepared at 12% w/v having as a solvent a mixture of cloformo-ethanol (2:1) until a homogeneous mixture. The polymer scaffolds were produced by the technique of electrospinning, the polymer solutions were placed in 2 separate plastic syringes in a ratio of 70:30 PLA-PCL, an injector machine was used for simultaneous administration by applying pressure on the syringe plunger the needles at a distance of 20cm from the collector and a voltage of 24KV, a jet flow 0.129 ml/h.

2.2 Using the technique of plasma polymerization a film of Polipirrol- Iodo (PPy-I) was deposited on the scaffolds. Reagents used were Sigma Aldrich. The operating parameters of the reactor were: 8cm electrode spacing, power of 20W and 1.2×10^{-1} Torr pressure, applied continuously for one hour pyrrole and for 6 minutes intervals of iodine.

2.3 One of the coated substrates with PPy-I was immersed in a solution of aggrecan (AG) for 24 hours. Subsequently rinsed with distilled water for 10 minutes and allowed to dry at room temperature in a vacuum desiccator for 24 hours.

2.4 The chemical composition and adhesion of the AG protein on the scaffold was determined for FTIR-ATR with a Perkin-Elmer FT-IR-2000, equipped with an ATR accessory DuraSamplIR II TM Smiths Detection with crystal diamond. The morphology of the samples was studied using a scanning electron microscope JEOL JSM -7600F. The apparent area of the pores in the material was measure using the program ImageJ 1.46, using the SEM images.

2.5 An auricular cartilage biopsy was performed using a rabbit of the species New Zealand white and was conducted to cell expansion cultures for 3 weeks. Approximately 1.2×10^6 cells were deposited on the scaffolds and cultured for 7 days (*in vitro*) and 30 days (*in vivo*).

2.6 For the mechanical behavior, tensile tests of the cultured materials *in vitro* and *in vivo* were conducted in a home made universal machine, assays were carried out at 1 mm/min and of the Young's modulus, yield strength, maximum stress, ductility and tenacity were obtained.

3. Results and discussion

3.1 Plasma Polymerization

Plasma polymerization was used to modified the materials surface seeking improve their interaction with the matrix, and the cells because after treatment amines and carbonyl groups contribute to the anchoring and cell proliferation, besides immobilizing biomolecules [7].

3.2 Chemical composition.

Figure 2 shows the ATR-FTIR spectra performed of the materials obtained. The FTIR spectrum of PLA-PCL coated with PPy-I-AG without washing with distilled water (Fig.2a), where one may distinguish the representative peaks of the molecule AG, such as primary amines and stretching C=O in 1638 cm^{-1} , secondary amines in 1565 cm^{-1} , the stretching of sulfate in 1243 cm^{-1} [8]. Moreover, in the spectrum of the scaffold coated with PPy-I-AG washed with distilled water (Fig. 2b) have a peak located in 1665 cm^{-1} which is the Amine I, the stretching of the C=O and Amine II.

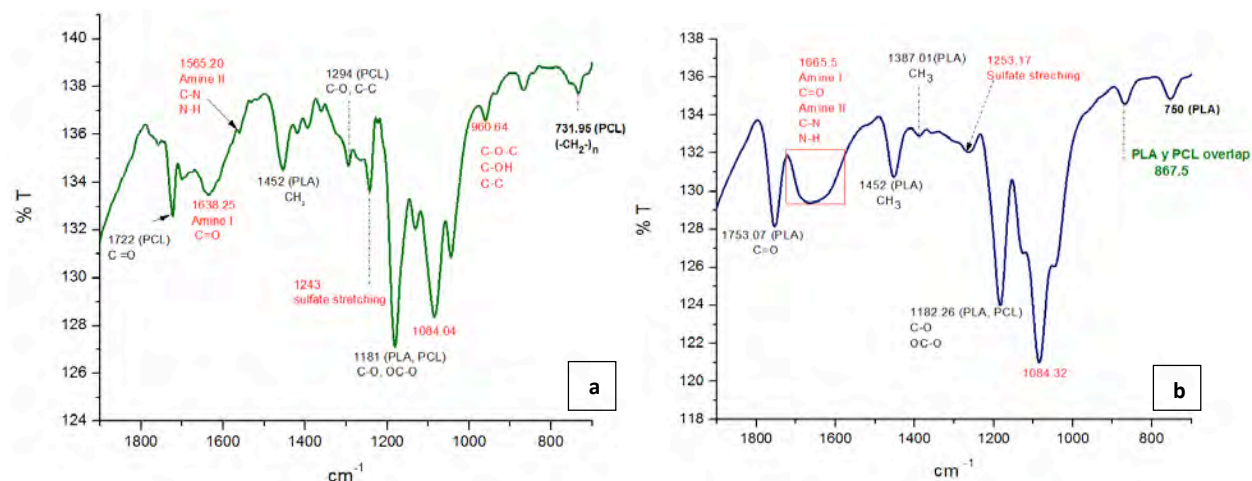


Fig. 1 ATR-FTIR spectrum obtained from the scaffold surface coating PPy-I-AG.
a) before washing with distilled water b) after washing with distilled water.

3.3 Scanning Electron Microscopy.

The PPy-I coated membrane forms film between several fibers, which improves the definition of pores, as showed in Fig.4a, thereby improving support cell proliferation promoting both 2D and 3D. Moreover the PPy-AG coated scaffold (Fig. 4b) shows well-defined structures due to the way in which both the sugar and sulphate content in the AG protein are accommodated, which leads to the phenomenon known as biomineralization that is the formation of ordered inorganic crystals [9].

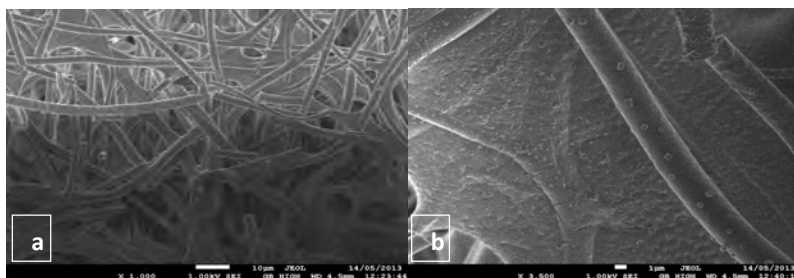


Fig. 2 SEM image of the membrane produced by electrospinning of PLA / PCL surface coating with PPy-I-AG after washing with distilled water a) 1000X, b) 10 000 x, c) 3500X.

3.4 Porosity.

For the PLA-PCL pores of $5\mu\text{m}^2$ to $521\mu\text{m}^2$ were found with an average of $100\mu\text{m}^2$. The average size of the chondrocyte is $30\text{-}40\mu\text{m}^2$ so the materials contains the necessary porosity for the suspension and deposition of cells.

3.5 Tensile test.

The mechanical properties of the scaffolds generated are essential, because this will have clinical use. It is reported that the hyaline cartilage has a tensile modulus of 0.2-4.90MPa, breaking strength of 0.15MPa [10]. The results of mechanical strength tests of each sample are shown below:

Material	Young's modulus (MPa)	Yield strength (MPa)	Maximum stress (MPa)	Ductility (%)	Tenacity (MPa)
In vitro					
PLA-PCL-PPy n=1	19.33	0.04	2.26	88.9	0.59
PLA-PCL-PPy-I-AG n=1	7.6	0.1	1.35	66.77	0.29
In vivo					
PLA-PCL-PPy n=1	0.39	0.0014	0.19	131.02	0.01
PLA-PCL-PPy-I-AG n=1	0.18	0.09	0.10	207.71	0.13

Table 1 Results of tensile tests.

The results of *in vitro* culture indicate that the material with protein AG adhesion affects the mechanical properties; generating less elastic and less impacts support comparison containing without protein.

The mechanical properties of PLA-PCL-PPy-I-AG *in vivo* shows promising mechanical properties, even if your module is the lowest of the 2 materials 0.18MPa, is very close to that reported for tensile value in cartilage [10] in addition to having a yield strength of 0.08MPa, the ductility or deformation capacity before fracture was 200% and greater toughness and plastic deformation of 0.13MPa having a greater plastic deformation before failure suffer, considering a ductile material or not fragile.

4. Conclusions.

Infrared spectra of PLA-PCL-PPy-I-AG show representative peaks of AG protein on the scaffolding, even after being subjected to a wash with distilled water, the morphology indicates that has porosity to proliferation and cell differentiation also exhibit mechanical properties that give a promising scaffold for use in tissue engineering conditions, however there are still multiple evaluations including longer periods of culture *in vivo* and histological evaluations and characterization of the quality of tissue formed on the scaffold (mechanical properties). Currently these studies are in development their results soon will be exposed.

Acknowledgements

The authors wish to thank: Consejo Nacional de Ciencia y Tecnología for partial support for the realization of this work through project CONACYT-15523 respectively and the Laboratorio de Microscopía Electrónica de la UAM-Iztapalapa.

References.

- [1]. Falke , G. F., & Atala, A. (2000). Reconstrucción de tejidos y órganos utilizando ingeniería tisular. Arch Argent Pediatr (Archivos Argentinos de Pediatría), 98(2), 103-115.
- [2]. Yingying Zhang, Fei Yang , Kai Liu a, Hong Shen , Yueqian Zhu , Wenjie Zhang, Wei Liu a,b, Shenguo Wang , Yilin Cao, Guangdong Zhou. : “The impact of PLGA scaffold orientation on in vitro cartilage regeneration”, Biomaterials, vol.33(10), pp. 2926-2935. Abr. 2012.
- [3]. Roughley, P. J. (2006). The structure and function of cartilage proteoglycans. *European Cell and Materials*, 12, 91-101.
- [4]. Chung, C., & Burdick, J. A. (2008). Engineering cartilage tissue. *Advanced Drug Delivery Reviews*, 243-262.
- [5]. Álvarez, E., Ripoll , P., Restrepo, A., & Forriol , F. (Abr-Jun. de 2010.). “Revisión de la reparación del cartílago. Posibilidades y resultados”. *Revista Trauma*, 21(2), 217-134.
- [6]. Goro Ebihara, M. S. (Mayo de 2012.). “Cartilage repair in transplanted scaffold-free chondrocyte sheets using a minipig model”. *Biomaterials*, 33(15), 3846-3851.
- [7]. Morales, J., Osorio, C., Montiel, R., Vázquez, H., Olayo, R., Olayo, M., y otros. (2008). Autoensamble de capas de polímeros iónicos sobre polietileno funcionalizado por plasma de pirrol. *Superficies y vacío*, 21(3), 1-4.
- [8]. Camcho, N., West, P., Torzilli, P., & Mendelson, R. (2000). FTIR Microscopic Imaging of Collagen and Proteoglycan in Bovine Cartilage. *Biopolymers*, 62(1), 1-8.
- [9]. Arias, J. L., Neira, C. A., Arias, J. I., Escobar, C., Boderó, M., David , M., y otros. (2004). Sulfated polymers in biological mineralization: a plausible source for bio-inspired engineering. *Journal of Materials Chemistry*(14), 2154-2160.
- [10] Saey Tuan Barnabas, H., Ekaputra, A., Hui, J., & Hutmacher, D. (2010). An electrospun polycaprolactone–collagen membrane for the resurfacing of cartilage defects. *Polymer International*, 59(6), 808-817.

PCU ELECTROSPUN SCAFFOLDS FOR THE VASCULAR SYSTEM

Ricardo Vera–Graziano 1*, Lizeth Ávila Gutiérrez 1, Raúl Montiel-Campos 2, Atlantida Raya-Rivera 3, Alfredo Maciel–Cerdal

1 Instituto de Investigaciones en Materiales, UNAM, Apdo. Postal 70-360, CP 04510, D.F. México. graziano@unam.mx

2 Dr. Raúl Montiel Campos, División de Ciencias Básicas e Ingeniería, UAM-Iz, San Rafael Atlixco 186, Vicentina, 09340 Ciudad de México, D.F. luar@xanum.uam.mx

3 Hospital Infantil Federico Gómez, Calle Dr. Márquez 162, Cuahtemoc, 06720 México, D.F. atlantidaraya1@yaqhoo.com

Abstract

Electrospun scaffolds show useful characteristics in regenerative medicine such as physical properties; nanometric diameters; high surface/volume ratio; adhesion and growth of living cells. Poly(carbonate-urethane) electrospun tubular scaffolds mixed with fibronectin were studied for the regeneration of small diameter blood vessels (<0.5 mm). Tube walls were made of nanofiber layers to mimic the functions of blood vessels. Electrospinning induced important changes in the morphology and mechanical properties of the poly(carbonate-urethane) as determined by GPC, MALLS, FTIR, NMR, XRD, SAX, SEM, DSC, DMA, and micro-mechanical analysis. Proliferation of HEK293 cells increased with the amount of fibronectin in the poly(carbonate-urethane) nanofibers.

Introduction

Tissue engineering is a demanding branch of regenerative medicine and requires that the biomaterials used be productive and innovative [1]. A common strategy in tissue engineering is the use of biomaterials to mimic the functions of native tissues, which may promote cell growth and extracellular matrix generation and match the resultant mechanical properties with those of the target tissue [2–6].

According to the World Health Organization, cardiovascular diseases represent one of the main causes of mortality in developed and developing countries. Intensive research is directed in the area of synthetic vascular prosthesis for the treatment of vascular diseases such as arterial obstruction, episcleral venous pressure (EVP), aneurisms, etc. [7].

There is an increasing need of vascular constructs due to the limited availability of natural grafts and the fast rate of atherosclerosis in some of these grafts. Both biodegradable and biostable materials are often required for the treatment of vascular diseases. Biodegradable polymers such as poly(glycerol-sebacate) and copolymers of poly(glycerol-sebacate) and poly(ϵ -caprolactone) are investigated for the reconstruction and regeneration of blood vessels affected by aneurysms and related diseases [8,9]. Biostable poly(urethanes) and poly(carbonate urethanes) are studied as medical devices for treatment of small diameter (<6 mm diameter) blood vessels [10, 11]. We focus here on the study of biostable poly(carbonate urethanes).

Polycarbonate urethanes (PCUs) are an improvement over the polyurethanes used now for making biostable implantable medical devices. They are characterized by very good mechanical properties, similar to polyether urethanes. PCUs have outstanding hydrolysis and ageing resistance as compared to PEUs of the same hardness, which may undergo cracking on the surface of implanted materials. Acute and chronic inflammatory responses of the PCUs and PEUs are similar [12–13]. The general structure of a segmented poly(carbonate urethane) is shown in Figure 1.

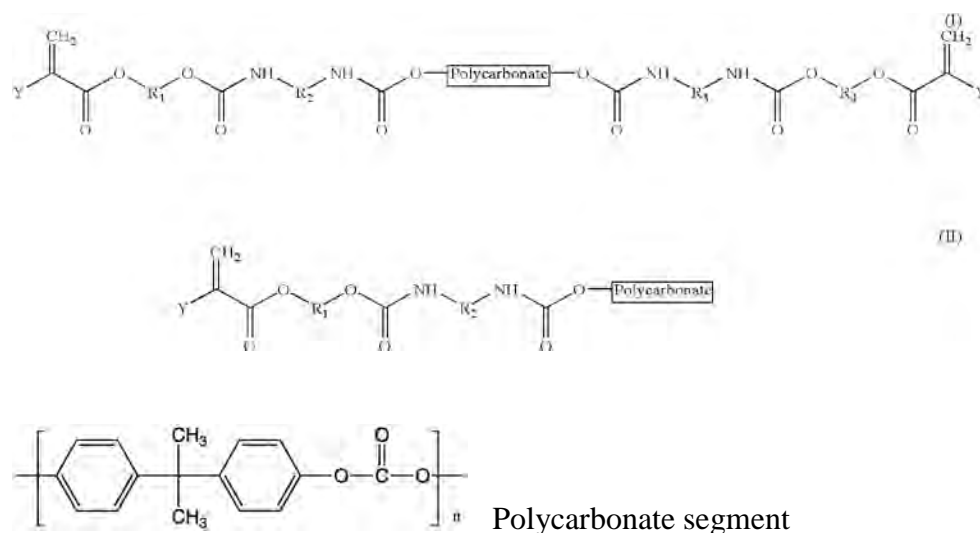


Figure 1. Scheme of two segmented poly(carbonate-urethane) polymers

PCUs of this type are constructed, at the molecular level, using hard and soft segments, and this allows control of the glass transition temperature and the mechanical properties at 37°C. To improve the compatibility of polyurethanes with blood, some methods were used to change the hydrophobicity of the PCUs and to make their surface more similar to natural tissue by adsorption of albumins, endothelial cells, or phospholipids (particularly phosphorylcholine compounds) [14]. Among the several techniques to produce scaffolds, electrospinning is one of the most useful, simple and versatile methods for controlling the structural parameters of fibrous scaffolds such as composition, fiber orientation, diameter, texture porosity of the nanofiber meshes and mechanical properties [6]. Electrospinning is capable of fabricating fibers with nanometer scale diameters that yield very high specific surface area – up to one to two orders of magnitude higher than micrometer scale fibers produced by conventional melting and dry/wet spinning methods.

Experimental

Materials. PCU (polycarbonate-urethane) (Bionate® II, 55D, kindly provided by DSM), human plasma fibronectin and HFP (1,1,1,3,3,3 hexafluor-2-propanol) of Sigma Aldrich.

Electrospinning. Solutions of (10% w/v) PCU in HFP with 0.5, 5% and 19% w/w fibronectin (FN) were processed in a custom made electrospinning set-up to make the scaffolds [6]. Typical process conditions were: flow rate 0.2 ml/h (injector, KD Scientific, USA), temperature 34°C, applied DC voltage 15kV (Power supply, Spellman, USA) and injector collector gap 30cm. A static aluminum copper plate was used to make 2D random fiber meshes. A rotating custom made shaft collector (Figure 1a) with both variable rotating speed and uniform displacements in the longitudinal axis of the shaft was used to make the uniform tubular (3D) scaffolds of 0.2 and 0.5mm inner diameter, and fiber diameters below $0.17 \pm 0.02 \mu\text{m}$.

Results and Discussion

Chemical structure. Fibronectin (FN) is a high-molecular weight (~440kDa) glycoprotein found in the extracellular matrix and blood plasma. It is composed of two nearly identical disulfide

(SO4-2) bound polypeptides. Fibronectin serves as a general cell adhesion molecule by anchoring cells to collagen.

The FTIR-ATR spectra of PCU and PCU-FN nanofibers were obtained after the scaffolds were immersed (by 72hrs) and rinsed with distilled water. The di-sulfur bridging of the two units of fibronectin was observed at 590 cm^{-1} in the PCU-FN spectrum, revealing that fibronectin molecules could not be dissolved in water because they are entangled with the PCU chains.

Morphology.- The morphology of the nanofibers (previously coated with gold) was observed by SEM (JEOL-JSM-7600F, at 20kV) (Figure 2). Nanofiber diameters range between 0.17 and 0.5 μm and pore sizes between 10-30 μm at the foreground plane (Image-J software).

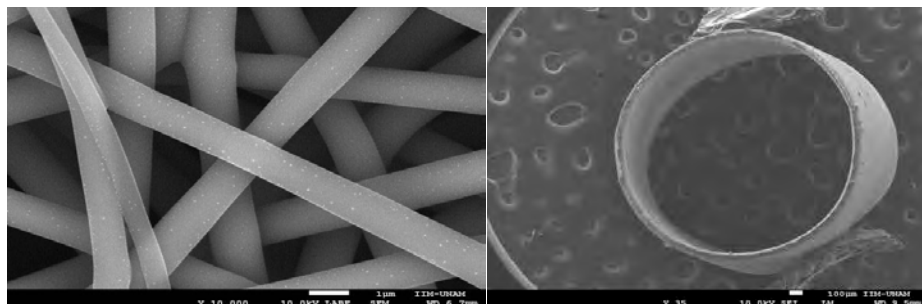


Figure 2. (a) SEM micrograph of PCU-FN fibers (10,000 X). (b) Tubular scaffold $\phi = 0.2$ mm.

Transitions.- Thermal transitions of PCU-FN nanofibers were determined by DSC (TA Instruments DSC 2910) and compared with those of Bionate II PCU 55D (product sheet, DSM). Two glass transition temperatures (T_g), were observed at -22.4°C and -0.4°C . Furthermore, the segments formed micro phases as shown below. A melting temperature, T_m , is also observed at 181°C . These transitions were also observed by DMA (TA Instruments DMA Q800). The damping curves show evidence of the two-phase behavior that would be expected if there was significant phase separation of hard and soft segments [15]. These results confirmed that nanofibers are composed of soft and hard domains and that the soft domains are semicrystalline structures. Thermal transitions of fibronectin were also studied by DSC. Two transitions, observed at 59°C and 83°C , correspond to denaturalization of the glycoprotein [16,17].

Crystalline structure.- The solid state structure of PCU in bulk is different from that of the nanofibers. A sharp peak at a Bragg angle (2θ) equal to 20.6° (WAXD Siemens D-500) was observed in bulk in contrast to the diffuse hill observed in the nanofibers. PCU in bulk is clearly semicrystalline [18, 19] while nanofibers apparently present lateral order suggesting that atomic and molecular organization of the PCU is strongly dependent on the processing conditions.

Based on reports about PCU nanofibers having crystalline structures [20], our samples were analyzed by small angle X-Ray scattering (SAXS Xenocs, mod. Xeuss). Results show two different ordered structures: one corresponds to the poly(urethane) hard segments with a mean size of 46 nm and the other to the poly(carbonate) soft segments with a mean size of 2.58 nm. The interplanar distances of the hard and soft segments were 5.47 nm and 0.43 nm, respectively.

Mechanical properties.- Stress-strain behavior of the samples was determined in tension according to ASTM standard D1708. (MTS Minibionix 858, at a strain rate of 10 mm/min, with a load cell of 110 N and a linear variable differential transformer (LVDT) (± 50 mm)). Data were registered by a software programmed in Lab-VIEW [21].

Fibronectin makes the PCU-FN scaffolds stiffer and thus less deformable than PCU. The ultimate strength and ultimate elongation at break of Bionate II PCU 55D (product sheet, DSM) are 61.8

MPa and 372 respectively. The modulus of elasticity of PCU-FN (10%FN) was 20.5 ± 2 MPa; about twice of the reported modulus of PCU nanofibers [22].

Hydrophobicity.-The effect of fibronectin on the hydrophobicity of the PCU scaffolds was determined by measuring the contact angles of water (Θ) on the scaffolds under the sessile drop method in a Ramé-hart goniometer 100-07-00. PCU scaffolds were highly hydrophobic $\Theta = 125.3 \pm 5.4^\circ$. Fibronectin changes completely the hydrophobic character of PCU. The contact angle in PCU scaffolds with the glycoprotein was reduced down to zero as the amount of fibronectin increased up to 10% on the surface of the nanofibers.

Both FTIR and EDS-SEM analysis, performed after the scaffolds were immersed and rinsed in water, evidenced that the fibronectin molecules remain and are well dispersed in the bulk and on the surface of the PCU nanofibers. It is then expected that entanglement of fibronectin and PCU chains (both are macromolecules) prevents the dissolving effect of water on the glycoprotein during proliferation of endothelial cells in-vitro. It is also expected that in this way permanence of fibronectin is enhanced after implantation of the scaffold in the organism.

Biocompatibility.- MTT assays were performed to determine cell viability. Human embryonic kidney 293 cells (HEK293) were cultured on the scaffolds during 14 days. Confluency of cells was observed by optical microscopy (Figure 3). In comparison with PCU scaffolds, cell proliferation in PCU-FN scaffolds increased 37% at 5% FN and 81% at 10% FN after 14 days.

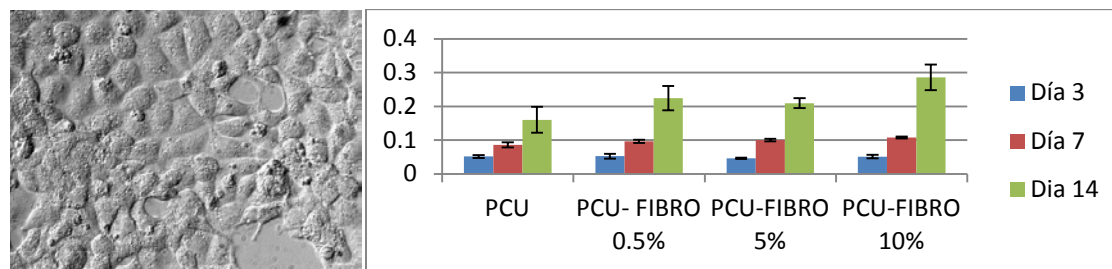


Figure 3. (a) Confluency of HEK293 cells after 14 days of culture (b) cell viability test.

Conclusions

The PCU and PCU-FN 3D (tubular) scaffolds intended for regeneration of small arteries (between 0.5 and 0.2 mm inner diameter) were obtained by electrospinning. The tube wall is formed by nanofiber layers that mimic the morphology of blood vessels. PCU and PCU-FN high quality scaffolds were obtained HFP, under electrospun controlled conditions.

The morphology of PCU electrospun nanofibers differs from that observed in bulk. PCU nanofibers contain phase domains of nanoscopic size, with domains constituted of single types of structural units. The types of domains comprise hard poly(urethane)- and soft- poly(carbonate) segment phase domains. In contrast, PCU in bulk contains crystals of microscopic size. Morphology and thus elastic properties of the scaffolds depend strongly on processing.

Fibronectin modified drastically the hydrophobic character of PCU scaffolds because the glycoprotein and the PCU mix together at molecular level. Scaffolds with FN at 10% were completely hydrophilic. Furthermore, entanglement between FN and PCU chains prevents the dissolving effect of water on the glycoprotein.

Both PCU and PCU-FN scaffolds showed good cell viability. Cell proliferation increased with the amount of fibronectin in the nanofibers. HEK293 cells showed good adhesion and proliferation on scaffolds made of small fiber diameters ($0.17 \pm 0.02 \mu\text{m}$) and pore sizes of 1-2 μm .

Acknowledgements

The authors thank Mikhail Zolotukin for helpful advice, Francisco Sánchez Arevalo for the mechanical analysis, Omar Novelo Peralta for SEM analysis, Humberto Vázquez Torres for SWAX analysis, Adriana Tejeda Cruz for XRD analysis, Damaris Cabrero Palomino for DSC analysis, Gerardo Cedillo Valverde for NMR analysis Salvador López Morales for GPC analysis, Miguel Canseco Martínez for FTIR analysis, Diego Ricardo Esquiliano Rendón and Raquel González Pérez for cell viability tests advice.

This project has been supported by DGAPA-UNAM (Grant IN108913) and CONACYT (Grant CNPq 117373).

References

- [1] Barnes CP, Sell SA, Boland ED, Simpson DG, Bowlin GL (2007) *Adv Drug Deliv Rev* 59:1413.
- [2] Agarwal S, Wendorff JH, Greiner A (2008) *Polymer* 49:5603.
- [3] Persson M, Cho S-W, Skrifvars M (2013) *J Mater Sci* 48:3055.
- [4] Reneker DH, Yarin AL (2008) *Polymer* 49:2387.
- [5] McClure M, Simpson DG, Bowlin GL (2012) *J Mech Behav Biomed Mater* 10:48.
- [6] Gomez-Pachon EY, Sanchez-Arevalo FM, Sabina-Ciscar FJ, Maciel-Cerda A, Montiel Campos R, Batina N, Morales-Reyes I, Vera-Graziano R, (2013) *Mater Sci* 48:8308–8319.
- [7] Global atlas on cardiovascular disease prevention and control. Geneva, World Health Organization, 2011.
- [8] S Sant, D Iyer, AK Gaharwar, A Patel, A Khademhosseini. (2013) *Acta Biomaterialia* 9:5963- 5973.
- [9] Monrroy AA, Montiel-Campos R, Vera-Graziano R. *Macromex* 2014, ID-45.
- [10] Stokes K, Mc Venes R, Anderson JM. (1995) *J Biomater Appl* 9:321–354.
- [11] A. Szelest-Lewandowska,¹ B. Masiulani,¹ M. Szymonowicz,² S. Pielka,² D. Paluch², (2007) *Journal of Biomedical Materials Research Part A* DOI 10.1002/jbm.a.
- [12] Tanzi MC, Mantovani D, Petrini P, Guidoin R, Laroche G. J (1997) *Biomed Mater Res* 36:550-559.
- [13] Mathur AB, Collier TO, Kao WJ, Wiggins M, Schuber MA, Hiltner A, Anderson JM.(1997) *J Biomed Mater Res* 36:246–257.
- [14] Ishihara K, Iwasaki Y. (2000) *Polym Adv Technol* 11:626–634.
- [15] S.C. Scholes, I.C. Burgess, H.R. Marsden, A. Unsworth, E. Jones, N. Smith, (2006) *Proc. Inst. Mech. Eng. [H] J. Eng. Med.* 220, 583–596.
- [16] Wallace D.G., (1981). *Arch. Biochem Biophys*, 515-524.
- [17] Niedzwiadek WE (1988). *Biochemistry*, 7116-7124.
- [18] Hernandez Rebeca, J. W. (2008). Wiley InterScience.
- [19] Roger Wesley Bass. (2011) PhD Thesis, University of South Florida.
- [20] Jintang Guo, Meihua Zhao, Yan Ti, Bo Wang (2007) *J Mater Sci*, 42:5508–5515.
- [21] Sanchez-Arevalo FM, Pulos G (2008) *Mater Charact* 59:1572.
- [22] Arjun G.N. (2011). *Society for Biomaterials*, 11-18.

SYNTHESIS OF CARBON NANOTUBES FOR THE DEVELOPMENT OF POLYMER-SUPPORTED CARBON NANOTUBES-HYDROXYAPATITE NANOFIBERS

Román Doval R.^{a*}, Morales Corona J.^c, Olayo R.^c, Ortega López M.^{a,b}

^a*Programa de Doctorado en Nanociencias y Nanotecnología. Centro de Investigación y de Estudios Avanzados del IPN. Av. IPN 2508, San Pedro Zacatenco, México D.F. C. P. 07360, México.*

^b*Sección de Electrónica del Estado Solido-Departamento de Ingeniería Eléctrica. Centro de Investigación y de Estudios Avanzados del IPN. Av. IPN 2508, San Pedro Zacatenco, México D. F. C. P. 07360, México.*

^c*Departamento de Física Universidad Autónoma Metropolitana, Ave. San Rafael Atlixco No 186, Iztapalapa, Vicentina, México D. F. CP 09340, México.*

ABSTRACT

Multiwalled carbon nanotubes were synthesized by chemical vapor deposition using ferrocene as a precursor. After a purification process, the carbon nanotubes were oxidized and then functionalized with chemicals carboxyl-containing groups. Subsequently the nanotubes were incorporated in a previously prepared hydroxyapatite-PLA mixture to obtain nanofibers by electrospinning. The HRSEM results from polymer showed a high porosity structure on the fibers, this kind porosity benefits the cell osteoinduction. The FTIR study showed bands corresponding to phosphate, PLA, hydroxyl, carboxyl groups, which demonstrates that all initial precursors were effectively incorporated. In addition, X-ray studies revealed the presence of $C_{16}H_{30}CaO_4$ crystalline phase.

INTRODUCTION

Bone grafting or bone substitute are commonly required to help or complement the repair of bone tissue, this tissue is a specialized connective tissue that consist for cells and extracellular calcified components forming the bone matrix. The manufacture of artificial materials that mimic the structure and properties of natural bone is a challenge. Hydroxyapatite is chemically similar to the mineral component of bone; this is one of the few materials that are classified as bioactive, which means that it will support bone growth and osseointegration when is used in applications of this tissue [1]. Another materials, which have been given attention, are carbon nanotubes (CNTs) due to their novel mechanical and electronic properties. Carbon nanotubes have a nanoscale tubular structure; this structure has carbon-carbon bonding of sp^2 type that makes one of the strongest materials known. By other hand, the carbon nanotubes have such a low density as graphite, tensile strength, excellent flexibility and low density, so the carbon nanotubes are ideal to the production of high strength materials and lightweight such as bone. These characteristics compared with other scaffolding materials such as polymers and peptide fibers; the carbon nanotubes are better [2]. However, carbon nanotubes are cytotoxic by themselves and therefore have to undergo to a purification and functionalization process to have related functional groups to hydroxyapatite.

This work we report the purification and functionalized of CNTs that were obtained by CVD technique and the preparation of CNTs and hydroxyapatite solution in a polymeric matrix to do a composite for bone application.

EXPERIMENTAL SECTION

Sample preparation

Multiwalled carbon nanotubes (MWCNT) were obtained by chemical vapor deposition (CVD) using ferrocene. These CNTs were purified to eliminate byproducts, catalytic residues and amorphous carbonaceous species.

The purification process consists of placing carbon nanotubes in a flask and adds a mixture of nitric acid (HNO₃) and 65% sulfuric acid (H₂SO₄) at 95% for 5 h at a temperature of 55 °C under magnetic stirring. Subsequently the reaction with sodium hydroxide (NaOH) was neutralized, once treatment time of CNTs with acids and neutralization is completed, centrifuged in a Hettich centrifuge Rotina mark 420R for 30 minutes, the sample was washed with deionized water, ethanol and acetone and then in the centrifuge for 30 min. Finally, it was dried under vacuum at 50 °C for 12 h.

After being purified and chemically functionalized, the nanotubes were incorporated in a previously prepared solution of polylactic acid-Chloroform with hydroxyapatite. The resultant product was used as precursor solution for the electrospinning process.

The electrospinning conditions were as follow: keeping the needle – collector distance at 10 cm, the process was carried out at 40 °C, at a voltage needle-collector of 20 kV, and a injection rate of 15 ml/h.

The final product was characterized by means of electron scanning microscopy in a Zeiss (HRSEM-AURIGA), FTIR spectroscopy (Perkin Elmer spectrum GX) and attenuated total reflectance (ATR) in a range 4500-700 cm⁻¹, and X-ray diffraction (D8 Advance X-ray diffractometer, Brunker) using a copper target (1.541Å), in the 2θ =20-80 interval in 0.02 steps. The diffraction peaks were identified using the EVA database.

RESULTS AND DISCUSSION

The process of chemical functionalization of carbon nanotubes with treatment of concentrated acid has observed that generate defects. However these defects (breakage of bonds) can react and result in functional groups such as hydroxyl (OH) and carboxyl (COOH). The functionalization and purification process was performed to eliminate dangerous byproducts and avoid the carbon nanotubes cytotoxicity, as required for biological application.

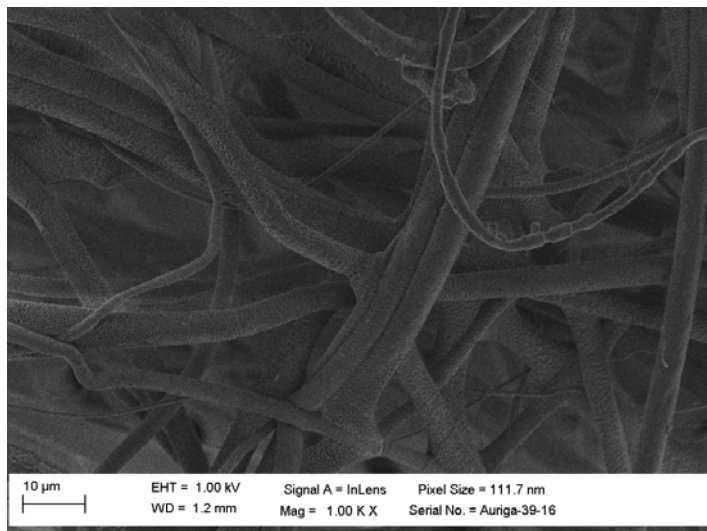


Figure 1. - HRSEM image of electrospun to from a polymer matrix with hydroxyapatite and CNTs.

The electrospung composite was analyzed by scanning electron microscopy. Where we can observe the polymeric fibers. Figure 1 displays the fibrous morphology whit fibers, which have a diameter of 1-5 microns. In Figure 2 we can observe to detail the morphology of the fibers, they have a porous surface texture which serves to cell growth.

Figure 3 shows a typical IR spectrum in the $4500\text{-}500\text{ cm}^{-1}$ range. It displays the absorption bands corresponding to the functional groups present in the prepared composite. The band in the interval $760\text{-}740\text{ cm}^{-1}$ represents an aromatic ring, the band at $1100\text{-}1000\text{ cm}^{-1}$ corresponds to the presence of the phosphate group (PO) [4], the band at $1410\text{-}1260\text{ cm}^{-1}$ corresponds to hydroxyl groups, the band in the interval $1800\text{-}1500\text{ cm}^{-1}$ corresponds to PLA and $\text{C}=\text{C}$, $\text{C}=\text{O}$ [5], the band in the interval $3200\text{-}2800\text{ cm}^{-1}$ corresponds to the CH bonds, the band at $3500\text{-}3750\text{ cm}^{-1}$ corresponds to the OH bonds.

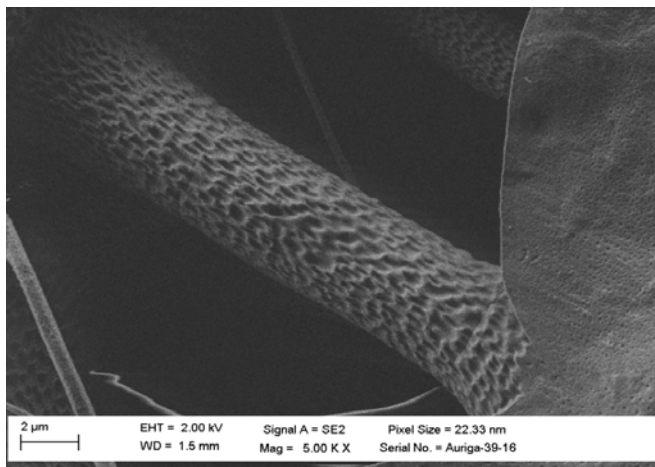


Figure 2. - SEM image of electrospinning to from a polymer matrix with hydroxyapatite and CNTs.

The X-ray helps us to know the crystalline phase that we have in our composite formed by electrospinning. The result of X-ray is shown in figure 4 where we can observe the spectrum from the sample. There is a well defined peak and other two peaks bad defined but those peaks are the first peak complement. Those peaks are related to a crystalline phase of calcium in presence of carbon, oxygen and hydrogen. With this relation we can confirm that we have the crystal phase ($C_{16}H_{30}CaO_4$). If the peak has his base open like in the figure, we can predict that there are nanofibers of nanometers or a few microns size. To complement the information will be made as future work the characterization by SAX.

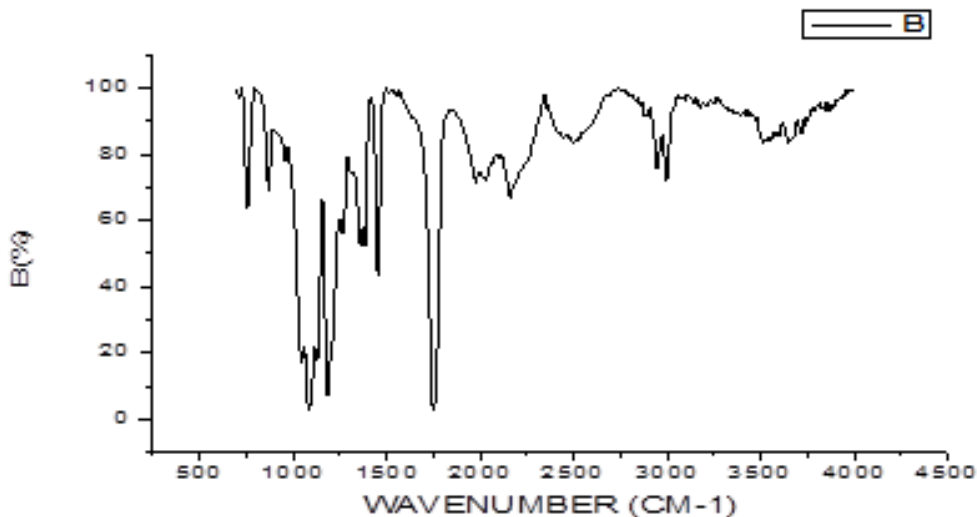


Figure 3. - FTIR of electrospinning from composite.

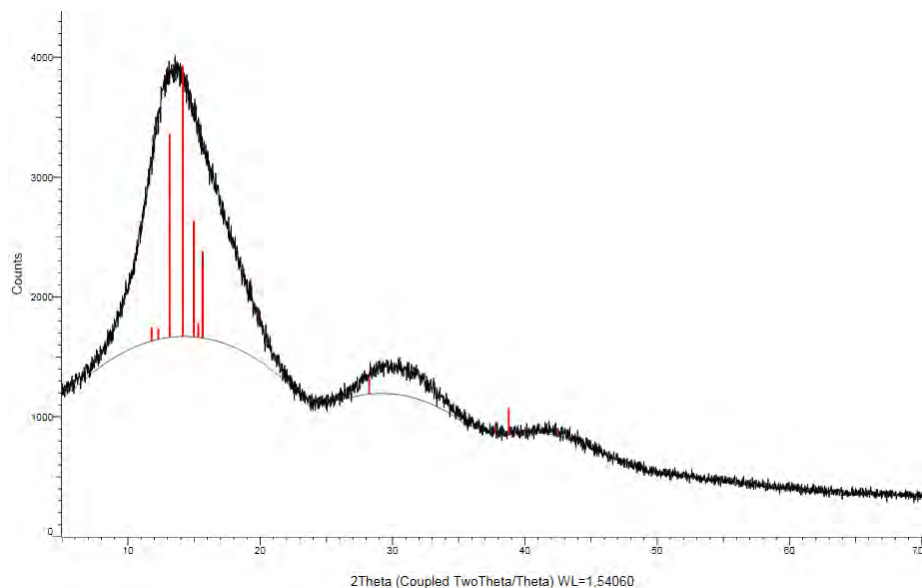


Figure 4. - X-ray spectrum the electrospinning from composite.

CONCLUSION

In conclusion for the electrospinning of the composite is investigated as the carbon nanotubes were functionalized to introduce them with hydroxyapatite in the polymer matrix of polylactic acid (PLA). The results showed good porosity that benefits cell growth of osteoblasts, and FTIR study has provided a wealth of information on the functional groups in our electrospinning composite like a good properties for the osteoinduction. The X-ray study has complemented the composite information that show a phase of crystallinity of the hydroxyapatite in the presence of carbon.

Acknowledgements

The authors wish to thank to Consejo Nacional de Ciencia y Tecnología for partial support for the realization of this work through project CONACYT-15523.

REFERENCES

- [1].- A.B. Martínez-Valencia*, H.E. Esparza-Ponce, Caracterización estructural y morfológica de hidroxiapatita nanoestructurada: estudio comparativo de diferentes métodos de síntesis, Superficies y Vacío 21(4) 18-21, diciembre de 2008.
- [2]. - Bin Zhao, Hui Hu, Swadhin K. Mandal, and Robert C. Haddon*, A Bone Mimic Based on the Self-Assembly of Hydroxyapatite on Chemically Functionalized Single-Walled Carbon Nanotubes, Chem. Mater. 2005, 17, 3235-3241.
- [3]. - Zheng-Ming Huang*, Y.-Z. Zhang, M. Kotakic, S. Ramakrishna, A review on polymer nanofibers by electrospinning and their applications in nanocomposites, Composites Science and Technology 63 (2003) 2223–2253.
- [4].- R. M. Trommer, L. A. dos Santos, C. P. Bergmann, Técnica alternativa para obter recobrimentos de hidroxiapatita (Alternative technique to obtain hydroxyapatite coatings), R. M. Trommer et al. / Cerâmica 53 (2007) 153-158.
- [5].- Carmen Rosales¹*, Marcos Sabino, Rosestela Perera, Héctor Rojas y Numalbert Romero, Estudio de mezclas de poli (ácido láctico) con polipropileno y nanocompuestos con montmorillonita, ISSN: 0255-6952, ISSN: 2244-7113 Rev. LatinAm. Metal. Mat. 2014; 34 (1): 158-171.

CARBON NANOPARTICLES EMBEDDED INTO ELECTROSPINNING FIBERS OF POLYLACTIC ACID TO IMPROVED THEIR BIOCOMPATIBILITY.

Erika Fragoso-Pérez, José García-Hernández, Juan Morales-Corona, R. Olayo.

Departamento de Física, Área de Polímeros, Universidad Autónoma Metropolitana, Unidad Iztapalapa.

Av. San Rafael Atlixco 186, Col. Vicentina, CP 09340, D.F., México.

Abstract

Biodegradable polymer scaffolds such as the polylactic acid, PLA, allow the growth of different cell types such as hepatocytes, keratinocytes, and neurons. To support the neoformation of tissues it is necessary to incorporate into the polymer scaffold specific cell type, growth factors, genes or carbon nanoparticles that provide biochemical signals which cells are capable of decode. In this work the fabrication of polymeric scaffolds of PLA through electrospinning technique containing carbon nanoparticles is presented. The thickness of the fibers is studied according to the rate of injection of the polymer solution 3mL/h, 5mL/h and 7mL/h. The fibers characterization was done with FT-IR, SEM, DSC, and SAX.

Introduction

Electrospinning polymeric scaffolds are useful in tissue engineering, and the fiber diameter is in the range of micrometers to nanometers. The electrospun scaffold can be made of biodegradable polymers such as polylactic acid (PLA). These scaffolds tend to degrade due to hydrolysis reactions in physiological conditions within the body, and is completely removed by metabolic pathways. In this type of scaffold can grow different cell types as liver cells, keratinocytes and neurons. To increase biocompatibility of such scaffolds carbon nanoparticles can be addicionated.

In this work the electrospinning polymeric scaffolds of PLA with carbon nanotubes immersed are studied. Using scanning electron microscopy the thickness of the fibers is studied according to the rate of injection of the polymer solution, 3mL/h, 5mL/h and 7ml/h. The composite materials were characterized by infrared spectroscopy (FT-IR), scanning electron microscopy (SEM) and low-angle (SAXS) and wide-angle x-ray diffraction.

Experimental section

12 Solutions, each with 1.2 g of PLA and 9 mL of chloroform (CHCl_3), and 1 mL of ethanol ($\text{CH}_3\text{CH}_2\text{OH}$) were prepared. Three of these solutions were used for each scaffold so four scaffolds were fabricated. Different amount of carbon nanotubes were added to three of the samples. Solutions with nanotubes were placed in an ultrasound machine for a better dispersion of the nanotubes. Table 1 shows the composition and the injection rate of the electrospinning for the four scaffolds made, and Table 2 shows the experimental condition of the electrospinning machine, These parameters are kept constant, and the injection rate is changed as shown in Table 1. Fig. 1 shows the experimental setup of the electrospinning process.

Table 1 Electrospinning scaffolding composition.

Scaffold	PLA (g)	Chloroform (mL)	Carbon nanotubes (g)	Injection rate (mL/h)
1	3.65317	27	0	5
2	3.66214	27	0.005482	3
3	3.65995	27	0.099975	5
4	3.69639	27	0.048961	7

Table2. Electrospinning process parameters.

Displacement "x" of the needle	2.7 cm/min
Applied Voltage	15.22 kV
Collector ratio	1519 rpm
Distance between the needle and collector	12 cm
Temperature	40°C

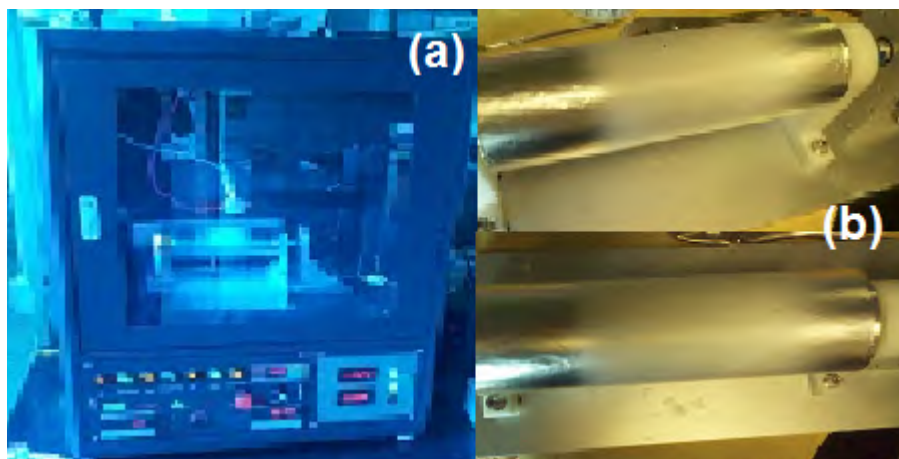


Fig. 1. Electrospinning process

Characterization

SEM microscopy

In the Fig. 2 the PLA polymeric scaffold without carbon nanotubes is shown. It can be appreciated that the fibers are uniformly distributed throughout the surface and are reasonably aligned, possibly due to the

high rotation rate of the collector, forming small beads of material indicating that the polymer is not completely dried in the travel between the needle and the collector. Fig. 2 (b) shows an amplification of the previous image showing that the fiber diameter is uniform around 400-nanometer diameter, here the alignment of the fibers can better be seen. In 2 (c) a fiber diameter of 4 microns is shown, this fiber shows a series of marks possibly by interaction of the air on the fiber as it travels towards the collector.

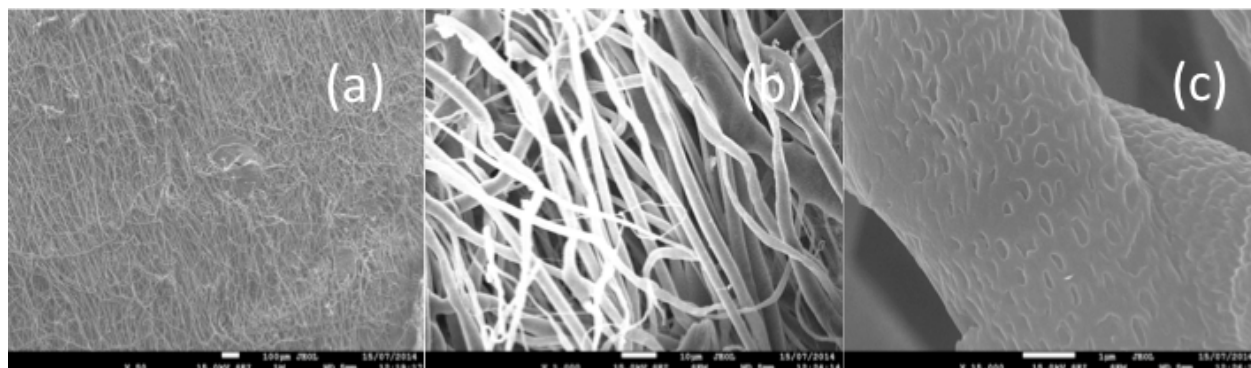


Fig. 2. Figure 2 Images of PLA scaffold.

Fig. 3 shows a cross section of the scaffold 3 with carbon nanotube embedded into of the fibers of PLA. In Fig. 3 (a) can be seen carbon nanotubes with a diameter of about 50 nm dispersed on the fiber. Figure 3 (b) shows some nanotubes out of the fiber. These images show that carbon nanotubes are embedded in a polymeric matrix of PLA.

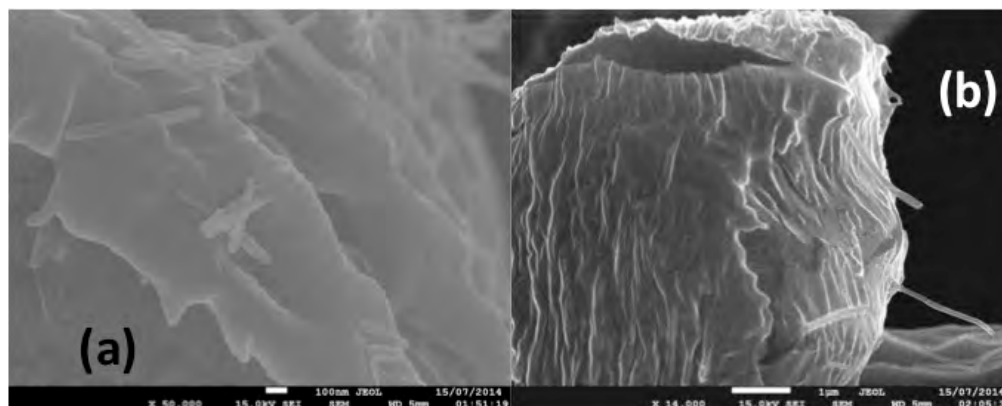


Fig. 3 PLA electrospun fibers with carbon nanotubes embedded in the polymer matrix.

Small-angle X-ray diffraction (SAXS)

In Fig. 4 the diffraction pattern of electrospun scaffolds is shown. The images indicate a horizontal orientation of the nanofibers. With increasing the content of nanotubes patterns becomes longer in the vertical direction, possibly due to the orientation of the nanotubes. This orientation is due to the electrospun process.

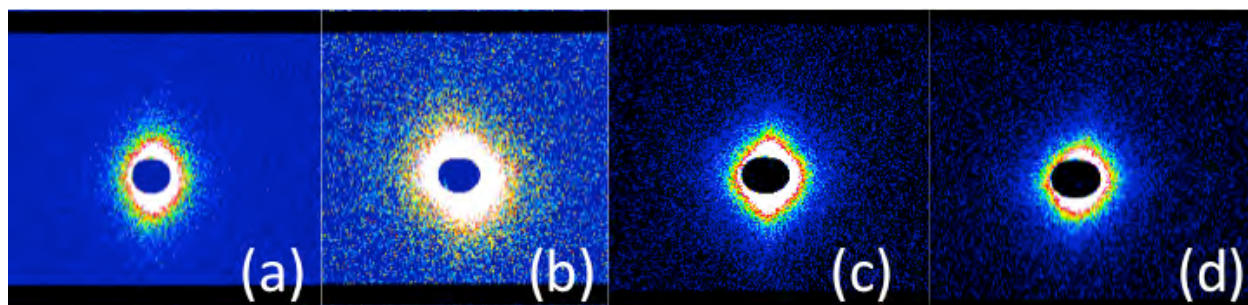


Fig. 4 XRD of small angle scattering (SAXS) of the scaffolds 1, 2, 3 and 4 respectively.

XRD

Fig. 5 shows the XRD diffractogram of PLA scaffold injected at a 5 mL/h rate, containing 0.099g of carbon nanotubes. A large peak at $2\theta = 16.8^\circ$, characteristic of the crystalline portion of the PLA can be seen, using Bragg's law this peak corresponds to a 5.9 Å interplanar space. Typical graphite peaks ($2\theta = 45, 58$) are also observed in the diffractogram. The last 2 peaks centered in $2\theta = 65$ and 70° correspond to the Ni in the catalyst used in the carbon nanotubes synthesis.

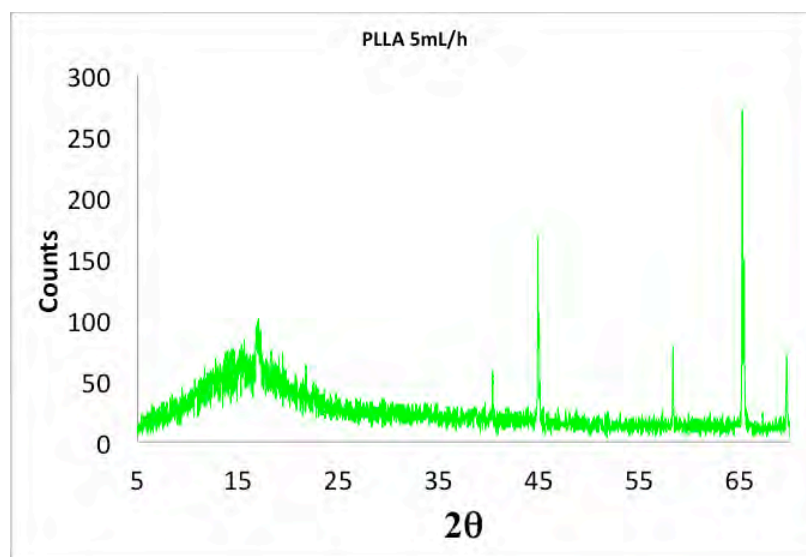


Fig. 5 XRD spectrum of PLA scaffold with 0.099g of carbon nanotubes.

FTIR-ATR spectroscopy.

In Fig. 6 the FTIR spectrum of PLA scaffold, sample 3, can be seen. The FTIR spectra of the others samples is similar. The peak centered in 3550cm⁻¹ show the vibration of OH group. In 2948 cm⁻¹ the aliphatic carbon vibration can be appreciated. The stretching of C=O group is presented in 1775cm⁻¹ and the asymmetric deformation of the C-H group is show in 1458cm⁻¹. The skeletal vibration is presented in 1190 cm⁻¹ y 1090cm⁻¹, C-H, C-O. In the peak of 873cm⁻¹ is the =CH₂ out of the plane deformation vibration. The C-O-C stretching vibration is appreciated in 758cm⁻¹.

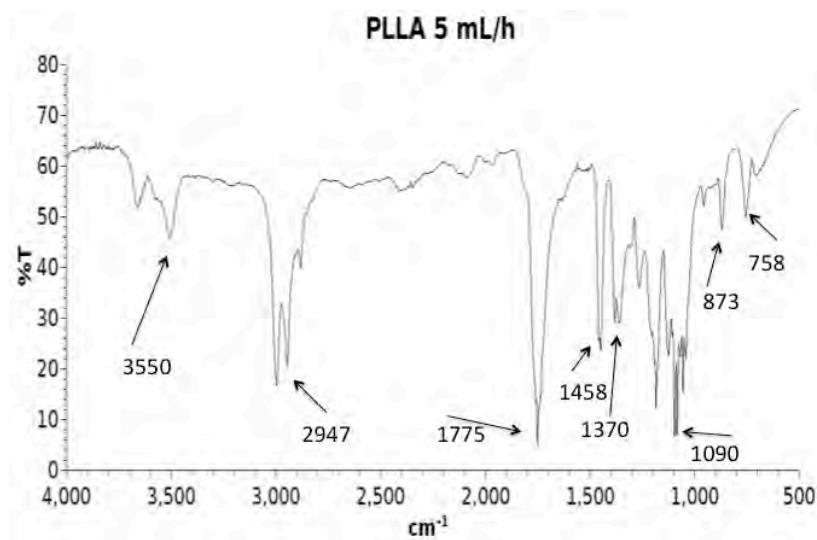


Fig. 6 FT-IR spectrum of the PLA scaffold, injected to ratio of 5mL/h with 0.099g of carbon nanotubes.

Conclusions

PLA scaffolds were electrospun with carbon nanotubes embedded in the polymer matrix. The FT-IR results show characteristic vibrations of the PLA. The XRD show a peak centered 16.8° indicates that the material is crystalline and shows signals characteristic of multiwall carbon nanotubes, also has peaks corresponding to the metal which was a catalyst for the production of the nanotubes. SAXS indicates that scaffolds have an alignment in the horizontal direction. SEM shows the incorporation of the nanotubes into of the PLA fibers.

Acknowledgements

The authors wish to thank to Consejo Nacional de Ciencia y Tecnología for partial support for the realization of this work through project CONACYT-15523 and the Laboratorio de Microscopía Electronica de la UAM Iztapalapa.

References

- (1) Fang, M.; Jinsheng, Z.; Xiaoping, Y.; Xiangying, O.; Shen, Z.; Xiaoyang, H.; Qi, Ma.; Jiqui, L.; *Biomacromolecules* **2007**, 8, 3729-3735.
- (2) Hillmann, G.; Steinkamp-Zucht, A.; Geurtsen, W.; Gross, G.; Hoff-mann, A. *Biomateriales* **2002**, 23, 1461.
- (3) Kenawy, E. R.; Layman, J. M.; Watkins, J. R.; Bowlin, G. L.; Matthews, J. A.; Simpson, D. G.; Wnek, G. E. *Biomaterials* **2003**, 24, 907.

SYNTHESIS OF A BIONANOCOMPOSITE WITH PHARMACOLOGICAL POTENTIAL

Fernando Bedolla-Cázares, Gabriela Rodríguez-García, Rosa E. del Rio, J. Betzabe González-Campos and Mario A. Gómez-Hurtado

Instituto de Investigaciones Químico Biológicas, Universidad Michoacana de San Nicolás de Hidalgo, Morelia, Mich. Mexico.

Abstract

Nanofibers of Chitosan (CTS) containing silver nanoparticles (AgNPs) and the synthesized metal complex $[Ag_2-(\text{affinin})](NO_3)_2$, were obtained by Electrospinning. The CTS/AgNPs and CTS/Affinin-AgNPs solutions used to electrospun nanofibers were generated by sunlight photoreduction of either the precursor salt or the metal complex using the own biopolymer as reducing agent. The synthesis of nanoparticles from the metal complex as well as from $AgNO_3$ salt was confirmed by UV-Vis spectroscopy, while the metal complex was characterized by IR, NMR spectroscopy and Mass spectrometry. SEM analysis showed nanofibers with diameters of 150-1000 nm with small empty spaces between them and little presence of beads. This bionanocomposite will be subject to biological evaluation to analyze its pharmacological potential.

Introduction

Bionanocomposites are nanostructures with potential technological applications. Nowadays, the development of nanocomposites with organic/inorganic base is a fast growing research area, promoting the generation of materials with new and improved properties compared to their macrocomposites counterparts. Among bionanocomposites, there are those prepared from a biopolymeric basis with applications towards sustainability, eco-efficiency and industrial ecology. The justification for their use is mainly based on their intrinsic properties since they are renewable resources [1], in addition to their potential antibacterial activity, biodegradability and biocompatibility [2].

In polymers diversity, nanofibers have been prominent because of their mechanical properties and their ability to support cell growth and encapsulate chemicals [3]. Currently the generation of nanofibers by electrospinning method has been described, this recent technique involves the formation of fibers at nanometric scale by applying a voltage to a polymer solution that possess the physical and chemical properties necessary to form stronger, durable and elastic fibers [4]. Such technique opens the possibility to generate nanocomposites of complex composition.

Chitosan, the second most abundant natural biopolymer after cellulose is one of the most widely used biopolymers in the production of nanofibers because its biodegradability, non-toxicity and biocompatibility. Chitosan has received particular interest in pharmaceutical and medical applications because of their physical, chemical and mechanical properties, and its capability to combine with other chemicals to improve the structure-activity relationship [5]. However, the electrospinning of chitosan represents a significant challenge due to its miscibility properties. This biopolymer has been combined with other polymers and compounds for the synthesis of composites in the form of nanofibers, nonetheless, their combination with natural products has been little explored. In this sense, affinin is a bioactive natural compound formed by an unsaturated fatty acid bonded to isobutylamide residue [6], some researchers have highlighted their biological activity as a powerful oral anesthetic [7], analgesic [8] and anti-inflammatory compound [9] besides being used as an antimicrobial agent, thus being an attractive alternative to be combined with chitosan.

In the same way, metal nanoparticles (NP's) have received special attention; especially those from gold and silver because of their unusual properties compared to other metals and their important

applications in catalysis, optics, sensing and as antimicrobial agents, [10]. It is known that silver ions have potent biological activity widely applied in some medicine fields [11]. In particular, the preparation of nanoparticles of metals immobilized in various matrices is an interesting research area due to the excellent synergistic effects that could be achieved [12].

Therefore, the combination of chitosan, affinin and silver nanoparticles to produce a composite in the form of nanofibers represents an attractive alternative to achieve a synergistic-potentiated material with potential biological activity. This work describes the synthesis of CTS/affinin-AgNPs nanofibers composite where nanoparticles were generated by sunlight photoreduction from either AgNO_3 and affinin- $[\text{Ag}_2(\text{affinin})](\text{NO}_3)_2$ complex. At the same time, the determination of the electrospinning optimal parameters for obtaining nanofibers with good quality from this novel combination and the $\text{AgNO}_3[\text{Ag}_2(\text{affinin})](\text{NO}_3)_2$ complex characterization are presented.

Experimental

Chilcuague or “Raíz de Oro” roots were purchased from the Sonora’s market in Mexico City. Air-dried ground roots (43 g) were extracted with hexane (250 mL) for 3 days and filtered to finally yield 761 mg of a yellowish oil, which was subsequently column-chromatographed using silica gel eluting with hexane-EtOAc (7:2).

Affinin complexation reaction was carried out with AgNO_3 salts in CH_3CN , affinin was added in a 2:1 (AgNO_3 :affinin) ratio and the reaction was refluxed for 24 h. Subsequently, the crude reaction was concentrated and washed with hexane, CH_2Cl_2 , and finally with CH_3CN in order to remove remaining unreacted materials. From this process an amorphous brown solid was obtained which was further characterized by NMR, IR and Mass spectrometry.

Additionally, chitosan 2 wt% solutions (in acetic acid aqueous solution 1 wt%) containing affinin- AgNO_3 , $[\text{Ag}_2(\text{affinin})](\text{NO}_3)_2$ metal complex (75 $\mu\text{g/mL}$) and others with different concentrations of AgNO_3 salt (1, 5 and 10 mM) to compare with it, were exposed to sunlight during 2 h in order to obtain AgNPs by photoreduction. The AgNPs presence was verified by UV-Vis spectroscopy.

Chitosan-AgNPs solutions were poured into Petri dishes and dried at 74°C during 8 h for solvent evaporation to obtain thin films; these films were re-dissolved into a TFA- CH_2Cl_2 (7:3) solution and finally processed in a NaBond® Electrospinning unit.

Results and Discussion

Once Chilcuague’s extract was column-chromatographed, the resulting isolated product was characterized by NMR 1D and 2D, these results (not shown) corresponds to affinin structure in agreement to previously reported data [13]. Afterwards, the complexation reaction was assayed with a mix of affinin and AgNO_3 ; the product obtained by the complexation reaction showed different appearance as well as physical and chemical properties (such as the boiling point and solubility) compared to those of the starting compounds.

The IR spectra of affinin and the resulting product of complexation reaction (Figure 1) showed significant differences in the transmittance percent ratio (ΔT) between C-H and C=C stretching bands; the IR spectrum of affinin showed a $\Delta T = 18\%$ for the bands at 2924 cm^{-1} and 1668 cm^{-1} , while the IR spectrum of the reaction product showed a $\Delta T = 1\%$ for the bands at 2929 cm^{-1} and 1637 cm^{-1} .

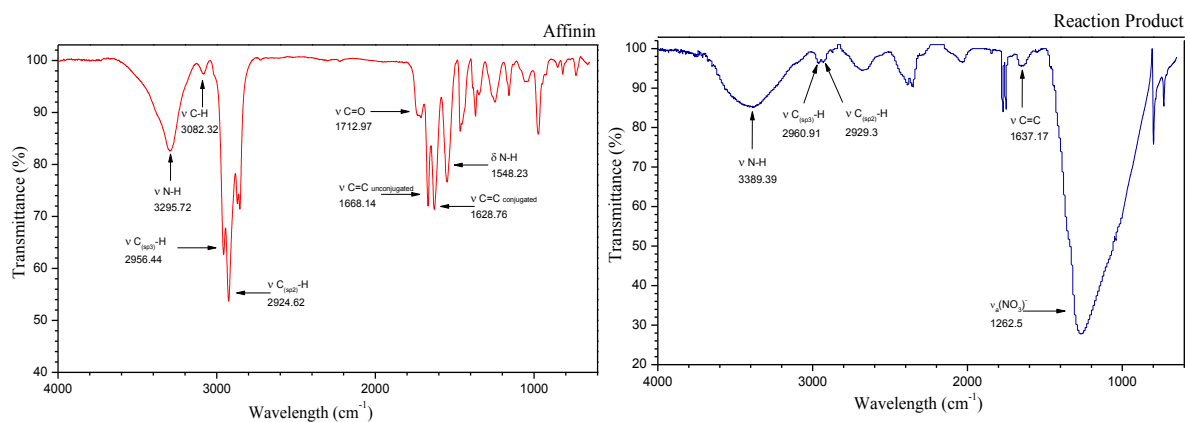


FIGURE 1. IR spectra of affinin and AgNO_3 -affinin complex.

The mass spectrum (not shown) of the reaction product obtained by electrospray produced a molecular ion $[\text{M}^+ + \text{H}_2\text{O} + \text{Na}]$ 599 m/z which corresponds to the $[\text{Ag}_2\text{-(affinin)}](\text{NO}_3)_2$ complex. This complex will be subsequently used to produce CTS/affinin/AgNPs to produce synergistic-potentiated composite in the form of nanofibers with potential biological activity.

The silver nanoparticles were synthesized by sunlight photoreduction, their presence was confirmed by UV-Vis spectroscopy due to the existence of the characteristic absorption band located between 390-420 nm [14]; these bands were similar in all chitosan solutions containing $[\text{Ag}_2\text{-(affinin)}](\text{NO}_3)_2$ metal complex (75 $\mu\text{g/mL}$) and AgNO_3 salts (1, 5 and 10 mM) (Figure 2).

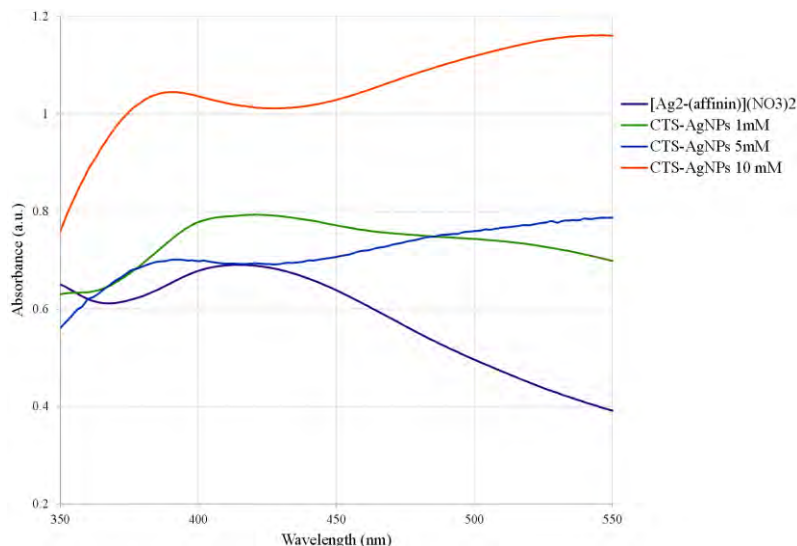


FIGURE 2. UV-Vis spectra of chitosan solutions containing AgNPs from either the $[\text{Ag}_2\text{-(affinin)}](\text{NO}_3)_2$ metal complex or AgNO_3 salts.

On the other hand, the electrospinning processing parameters (chitosan concentration, type of solvent, collector distance, mass flow, temperature and voltage) were varied for each case: pure CTS, CTS/Affinin and CTS/AgNPs from AgNO_3 to find the optimal set that consistently produced good quality nanofibers. The nanofibers obtained with the optimal parameters had good strength and thickness to be easily removed from metal collector (Figure

3A). SEM micrographs showed homogenous fibers randomly oriented with diameters between 150-1000 nm (Figure 3B) and minimal or no bead formation, these makes them suitable to support another bioactive compounds like affinin in this case (Figure 3C).

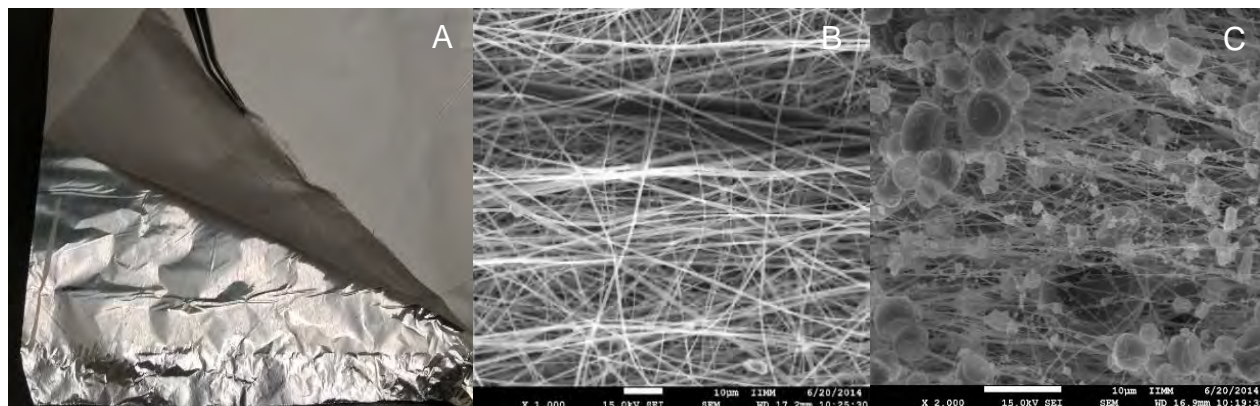


FIGURE 3. A) Chitosan nanofiber being separated from the planar collector, B) Homogeneous Chitosan nanofibers randomly oriented C) Chitosan nanofibers acting as structural support for affinin clusters.

The optimal set of electrospinning processing parameters to produce chitosan-[Ag₂-(affinin)](NO₃)₂ coordination complex are currently under investigation.

Conclusions

Natural affinin was successfully isolated and used to obtain the [Ag₂-(affinin)](NO₃)₂ coordination complex to be subsequently combined with chitosan solutions in order to obtain a synergistic-potential material with potential biological activity from the combination of chitosan, affinin and AgNPs. The synthesis of AgNPs was achieved in chitosan solution through sunlight photoreduction of AgNO₃, without the addition of stabilizing or reducing agents and the optimal set of electrospinning processing parameters including chitosan concentration, type of solvent, collector distance, mass flow, temperature and voltage for pure CTS, CTS/Affinin and CTS/AgNPs were obtained producing good quality nanofibers. Finally, it was observed that in CTS/Affinin composite, CTS serves as structural support for affinin clusters.

References

- [1]. D. L. Kaplan, Springer, First Edition. New York (1998).
- [2]. M. Rinaudo, *Prog. Polym. Sci.*, **31**: 603-632 (2006).
- [3]. W. Gamboa, O. Mantilla, V. Castillo. VII Congreso de la Sociedad Cubana de Bioingeniería, La Habana, Cuba, (2007).
- [4]. J. D. Schiffman, C. L. Schauer. *Polymer Reviews* **48**:317-352 (2008).
- [5]. L. Martinová, D. Lubasová. *RJTA Vol. 12 No. 2*. 72 (2008).

- [6]. J. Molina-Torres, R. Salgado-Garciglia, E. Ramírez-Chávez y R. Del-Rio. *Biochem. Syst. Ecol.* **24**: 43-47 (1996).
- [7]. J. Molina-Torres, A. García-Chávez. **20**: 377-387 (2001).
- [8]. Rios MY, Aguilar-Guadarrama AB, Gutiérrez M del C. *J Ethnopharmacol.* Mar 21; 110 (2): 364-7 (2007)
- [9]. I. Hernández, Y. Lemus, S. Prieto, J. Molina-Torres, G. Garrido. *Boletín Latinoamericano y del Caribe de Plantas Medicinales y Aromáticas.* **8**: 160-164 (2009).
- [10]. F. Zeng; C. Hou; S. Z. Wu; X. X. Liu; Z. Tong; S. N. Yu, *Nanotechnology*, **18**: 1-8 (2007).
- [11]. H. Y Kang, M. J. Jung, & Y. K. Jeong, *Korean Journal of Biotechnology and Bioengineering*, **15**, 521–524 (2000).
- [12]. S. Manna; S. K. Batabyal; A. K. Nandi, *J. Phys. Chem. B*, **110**, 12318–12326 (2006).
- [13]. J. Calle, A. Rivera, M. T Reguero, R. E. Del Rio, y Joseph-Nathan, P. *Rev. Latinoam. Química* **19**, 94-97 (1988).
- [14]. M. H. El-Rafie, M. E. El-Nagggar, M. A. Ramadan, M. M. G. Fouda, S. S. Al-Deyab, & A. Hebeish, *Carbohydrate Polymers*, **86**:630–635 (2011).

SYNTHESIS OF POLY(UREA-AMIDE)URETHANES PREPARED WITH AMINOACIDS

Chan-Chan Lerma Hanaiy,^{1,2} Cauch-Rodríguez Juan Valerio,¹ Cervantes-Úc José Manuel,¹ Hernández-Sánchez Fernando.¹

¹ Centro de Investigación Científica de Yucatán, A. C. 130 Chuburná de Hidalgo, Mérida Yucatán.

² Universidad de Sonora- Cátedras CONACYT, Luis Encinas y Rosales, Centro, Hermosillo, Sonora.

Abstract

Diamines and dicarboxylic acids have been used as chain extender for obtaining poly(urea)urethanes and poly(amide)urethanes for biomedical applications. In this study three series of poly(amide-urea)urethanes (PUAUs) with different hard segment content were synthesized from polycaprolactone diol (soft-segment) and 4,4'-methylenebis(cyclohexyl isocyanate) (HMDI) and amino acids (hard-segment). Hard segment models, prepared with HMDI and amino acids without polycaprolactone, revealed the formation of urea and amide bonds by solid-state ¹³C-NMR and FTIR, in agreement with the PUAUs composition. Additionally, PUAUs containing arginine and glycine showed elastomeric behavior and higher molecular weight than those containing aspartic acid.

Introduction

Diamines and dicarboxylic acids have been used as chain extenders rendering poly(urea)urethanes and poly(amide)urethanes but in search of more biocompatible materials, molecules of biological importance such as amino acids have also been suggested as hard segment (either as diisocyanates or chain extenders) [1].

Derivatives from amino acids and other aliphatic diisocyanates have been used in the synthesis of biodegradable polyurethanes with the aim of substituting aromatic diisocyanates in order to avoid toxic and carcinogenic degradation products. For the same purpose, polycaprolactone (PCL) is widely used as soft segment because their hydrolizable ester groups and because their degradation products can be metabolized by the body [2].

In order to understand how single amino acids can be incorporated within PUAUs, three series of polyurethanes were prepared, varying the rigid and soft segment content, and then physicochemically characterized. The amino acids were chosen on the basis of their different pH behavior and the presence of different functional groups that can react with isocyanate groups. Alkaline L-arginine, neutral glycine and acidic L-aspartic acid as well as butanodiamine (BDA) were incorporated separately into the polyurethane backbone as chain extenders. 4,4'-(methylen-bis-cyclohexyl)diisocyanate (HMDI), an aliphatic diisocyanate, was used as the other component of the rigid segment. Polycaprolactone diol, a biodegradable polyester approved by the Food and Drug Administration was used as soft segment.

Experimental

PCL diol (Mn= 530 and 2000), HMDI, L-arginine monohydrochloride (R), glycine hydrochloride (G), L-aspartic acid (D), BDA and stannous octoate were purchased from Sigma-Aldrich. Dimethyl formamide anhydrous (DMF, Fluka) and tetrahydrofuran (THF, JT Baker) were used

as solvents in the synthesis or film preparation.

Three polyurethanes with different hard segment (HS) content were prepared: 100% HS (X-Model series, without PCL diol), 54-59% HS (X-530 series, with PCL diol Mn=530 Da) and 24-26% HS (X-2000 series with PCL diol Mn=2000 Da). Where X refers to each chain extender (L-arginine=R, Glycine=G, L-aspartic acid=D, Butanediamine=BDA).

2.1 Synthesis conditions

Reactions were conducted in a glass reactor with stirring at 60°C and nitrogen atmosphere. Before reaction, monomers and DMF were dried at 60°C and reduced pressure for minimum 12 h or dried using molecular sieves.

Hard segment model compounds (100% HS) were prepared by one-step reaction. HMDI (4 mmol), Tin(II) 2-ethylhexanoate (30 µg) and chain extender (4 mmol) were dissolved in 15 ml of DMF (HMDI:Chain extender molar ratio= 1:1). After this period of time, the polymer in solution was precipitated in cold water and kept overnight. Finally, the polymer was thoroughly washed, filtered, and dried at 60°C and reduced pressure.

The PUAUs were synthesized by a two-step procedure using a molar ratio of 1:2.05:1 (PCL diol:HMDI:chain extender). In the first step, PCL diol (Mn=530 or 2000) was mixed with a molar excess of HMDI under stirring. The time of prepolymerization and the concentration of catalyzer were 1 h and 0.1% respectively for PCL 530 but 4 h and 0.3% when PCL 2000 was used. In the second step, the chain extender was added and the reaction was stopped after 2 h. The polymer in DMF solution was precipitated in cold water and thoroughly washed with distilled water to eliminate residual monomers. Finally, the precipitate was filtered and dried at 60°C under reduced pressure.

2.2. Measurements

Solid state ¹³C (150.8 MHz) cross polarization (CP) / magic angle spinning (MAS) NMR spectra were recorded at 22 °C on a Varian/Agilent PremiumCompact 600 NMR spectrometer with rotors of ZrO₂ (diameter 4.2 mm). $\pi/2$ pulse of 2.0 µs, 1.0 ms of contact time and 5.0 s of recycle delay were used. Chemical shifts (ppm) were determined relative to external adamantane (38.4 ppm).

¹H (599.8 MHz) and ¹³C{¹H} (150.8 MHz) NMR spectra were recorded at 25 °C on a Varian/Agilent PremiumCompact 600 NMR spectrometer with $\pi/4$ pulse of 4.30 and 4.35 µs for ¹H and ¹³C respectively. DMSO-d₆ was used as solvent and chemical shifts (ppm) were determined relative to internal TMS (0.0 ppm).

Infrared spectra of the SPUs were obtained with a Thermoscientific Nicolet 8700 FTIR (Madison, WI) in the spectral range from 4000 to 600 cm⁻¹ averaging 50 scans with a resolution of 4 cm⁻¹.

Thermal characterization was carried out by differential scanning calorimetry (DSC 7 from Perkin-Elmer) using 5 mg of polymer encapsulated on aluminum pans. The polymers were heated from -100 to 160 °C at 10 °C min⁻¹ under nitrogen atmosphere. Dynamic mechanical analysis was performed with a DMA 7 from Perkin-Elmer in the extension mode. Strips of 15 x 3.5 x 0.1 mm were heated from -100 to 100°C at 5 °C min⁻¹ using a static force of 90 mN and a dynamic force of 70 mN at 1 Hz. Thermogravimetry analysis was conducted by means a TGA7 from Perkin-Elmer heating since 50°C to 700°C at 10°C/min under nitrogen atmosphere.

Molecular weight was determined by gel permeation chromatography (GPC) using an Agilent 1100 GPC-SEC system equipped with Zorbax PSM (60S and 1000S) coupled columns and a refractive index detector (Agilent technologies). HPLC grade DMF was used as eluent with a flow rate of 1ml/min at 50°C and the calibration curve was obtained with 1 mg/ml polystyrene

molecular weight standards in the range from 1,050 to 420,600 g/mol.

Tensile mechanical properties of the PUAUs were measured on a mechanical testing machine (MINIMAT) using a 200 N load cell and a cross-head rate of 50 mm min⁻¹. Samples of 15 x 2 x 0.11 mm were obtained according to ASTM D-412. The Young's modulus at 100% (E100), tensile strength (σ) and strain to failure (ϵ) were reported.

Results and Discussion

Based on the synthesized model compounds and data reported in literature Figure 1 shows the suggested reaction scheme between chain extenders and the isocyanate group. Urea groups were formed during their reaction with amines. However, carboxylic acid react first to form unstable carbamic carboxylic anhydride and then amide and urea groups by irreversible elimination of carbon dioxide [3].

¹³C CP/MAS spectra (data not showed) exhibited broad characteristic peaks. Around 157 ppm, in the carbonyl region, urea groups (-NH-CO-NH-) in BDA-Model were observed. Polymer prepared with HMDI and the aminoacid (G-Model, R-Model and D-Model) amine group reacted

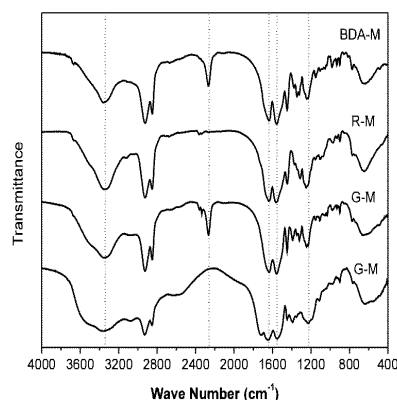


Figure 2. FTIR spectra of hard segment models

(C=O, at 1630 cm⁻¹) in another urea molecule [4].

In addition to urea appearance, the broad band around 3400 cm⁻¹ (corresponding to asymmetric stretching modes of carboxylic group) decrease in intensity indicating that carboxylic acids are able to react. The peak around 1400 cm⁻¹ characteristic to amino acids [5] are observed in G-M because residual carboxylic acid. D-M also show this peak and another at 1700 cm⁻¹ while the broad band at 3400 cm⁻¹ remained because of the two carboxylic acids present in aspartic acid. Residual isocyanate groups (-N=C=O at 2274 cm⁻¹) were detected when bifunctional chain extenders were used, but that band disappear when tri-functional amino acids were used.

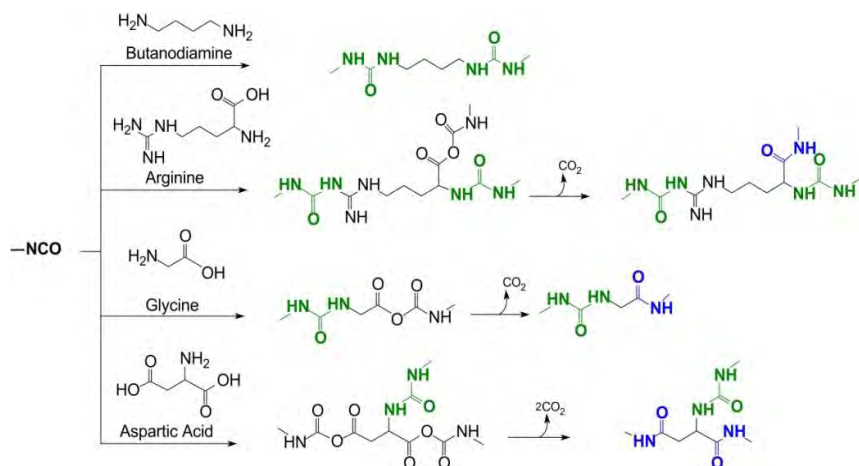


Figure 1. Suggested mechanism of Chain extension reaction.

^1H NMR and ^{13}C NMR of PUAUs in DMSO- d_6 (data not shown) were also used for the chemical characterization of PUAUs. Hard segment signals were more intense in 530 series because of its higher concentration. Hard segment protons corresponding to aliphatic cyclohexyl rings of HMDI, were observed between 0.5 and 2 ppm. The downfield at 7.01 and 6.91 ppm are assigned to urethane groups which were formed during first step of synthesis. Protons of urea groups formed during the second step of the polymerization are assigned in the range of 5.8 to 5.4 ppm. Additionally, protons of HMDI adjacent to urethane groups ($-\text{O}-(\text{C}=\text{O})-\text{NH}-\text{CH}<$) could be seen at 3.48 and 3.15 ppm, based on the correlation spectroscopy (COSY).

FTIR spectra of PUAUs of 530 series and 2000 series (Figure 3) showed a broad carbonyl band composed for two overlapping bands, one at 1730 cm^{-1} assigned to carbonyl absorptions from the ester group of the PCL, and the other one at 1708 cm^{-1} assigned to carbonyl from the urethane bond. Also, spectra showed the commonly called

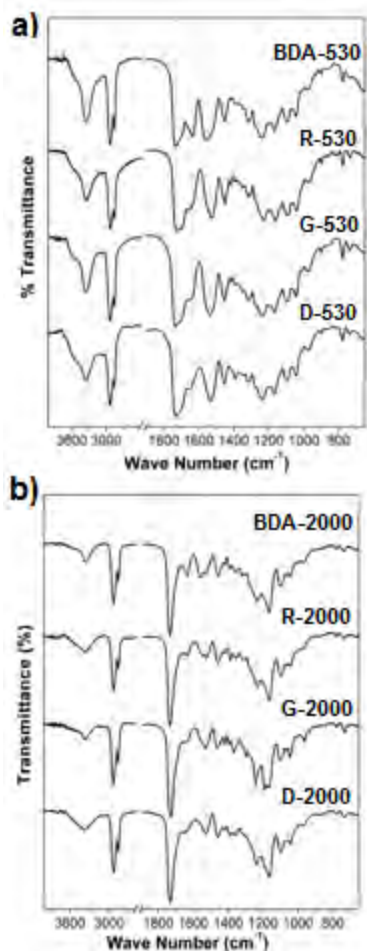


Figure 3. FTIR spectra of:
a) series 530 and b) series 2000

‘amide bands’ as hard segment models since these are characteristic to urethane, but also to urea and amide groups [6]. Urea bonds were confirmed by a band at 1636 cm^{-1} and formed exclusively from the reaction of amine group of chain extenders. This signal was more intense when BDA was used because their two amine groups. This band was also intense for arginine as it can form urea groups from the reaction of a primary amine and the guanidine amine. Glycine and aspartic acid showed less intense bands because there is only one amine group available in the amino acids. Amide bond observed in hard segment models were completely overlapping by carbonyl of PCL.

Chain extension was also confirmed by GPC analysis. R-530 and G-530 exhibited high molecular weights while D-530 showed low molecular weight because of the difference in reactivity of the carboxylic acid groups. A similar trend was observed in the 2000 series.

Thermal properties are summarized in Table I. Analysis of their thermal behaviour provides important information about phase segregation i.e. glass transition and melting point of the soft and hard segments. The TGA thermograms of PUUs showed thermal stability up to 300°C . After this temperature, all polymers exhibited a major weight loss before 400°C .

PUAUs showed elastomeric behavior, except for D-2000 which was rigid and brittle (see Table I). The higher modulus and tensile strength in series 2000 can be associated partly to the PCL as its crystalline phase may act as physical crosslinker in a similar manner to that normally attributed to the hard segment [7,8]. Other factors that explain the elastomeric properties include a higher phase separation along with their higher molecular weight. In contrast, the D-2000 exhibited the lowest mechanical properties due to its low degree of chain extension as shown by its low molecular weight and low urea bond formation.

Table I. Thermal and mechanical properties of PUAUs.

Sample	Thermal Properties							Mechanical Properties		
	T α (°C)	T g (°C)	ΔC_p	T m (°C)	C (%)	Td1 (°C)	Td2 (°C)	E100 (MPa)	σ_{max} (MPa)	ϵ_{max} (%)
BDA-2000	-43	-51.9	0.43	53.9	16.3	375	474	2.09±0.2	22.40±3.5	982±103
R-2000	-39	-51.1	0.41	53.0	27.6	358	457	4.26±0.8	38.00±5.4	1586±167
G-2000	-34	-50.8	0.28	52.7	34.3	335	465	3.85±0.4	13.80±1.5	1216±87
D-2000	-33	-51.9	0.29	61.0	38.9	346	447	---	---	---
BDA-530	29	2.8	0.18	-	-	336	454	1.85±0.49	2.40±0.14	327±28
R-530	28	3.0	0.43	-	-	344	449	0.58±0.20	1.60±0.50	667±84
G-530	26	4.9	0.30	-	-	332	442	0.79±0.19	2.11±0.14	571±73
D-530	30	4.6	0.26	-	-	351	455	0.93±0.1	0.94±0.15	116±08

Conclusions

Hard segment models prepared with HMDI and amino acids showed many similarities to hard segment model prepared with HMDI and BDA. Spectroscopic characterization confirmed formation of urea and amide groups from the reaction of isocyanate groups with amine and carboxylic acid respectively.

Diisocyanate groups reacted with arginine, glycine and aspartic acid to a different extent in order to form different types of polyurethanes. Reactions with arginine and glycine rendered poly(urea)urethanes with high molecular weight and elastomeric properties. In contrast, aspartic acid form poly(urea amide)urethanes with molecular weight and poor mechanical properties.

Acknowledgements

This work was supported by FOMIX-CONACYT 170132 and CONACYT 169398. NMR experiments were conducted at facilities at the Laboratorio Nacional de Nano y Biomateriales (LANNBIO), CINVESTAV-IPN Mérida (projects FOMIX-Yucatán 2008-108160 and CONACYT Lab-2009-01 No 123913).

References

- [1] P. Król, Prog. Mater. Sci., 52, 915-1015 (2007).
- [2] A. Marcos-Fernández, G. A. Abraham, J. L. Valentín, J. San Román, Polymer, 47, 785-98 (2006).
- [3] G. R. Stark, Biochemistry, 4, 1030-6 (1965).
- [4] C. Wu, J. Wang, P. Chang, H. Cheng, Y. Yu, Z. Wu, et al., Phys. Chem. Chem. Phys., 14, 464-8 (2012).
- [5] M. Wolpert, P. Hellwig, Spectrochim. Acta A Mol. Biomol. Spectrosc., 64, 987-1001 (2006).
- [6] G. G. Suchkova, L. I. Maklakov, Vib. Spectrosc., 51, 333-9 (2009).
- [7] G. A. Skarja, K. A. Woodhouse, J. Appl. Polym. Sci., 75, 1522-34 (2000).
- [8] R. G. J. C. Heijkants, R. V. Calck, T. G. van Tienen, J. H. de Groot, P. Buma, A. J Pennings, et al. Biomaterials, 26, 4219-28 (2005).

SYNTHESIS AND CHARACTERIZATION OF BIODEGRADABLE POLYESTERS GRAFTED STARCHES BY RING-OPENING POLYMERIZATION

Zujey Berenice Cuevas-Carballo,¹ S. Duarte-Aranda,¹ G. Canché-Escamilla*¹

¹ Centro de Investigación Científica de Yucatán, A. C. Calle 43, No. 130, Chuburná de Hidalgo, 97200, Mérida, Yucatán, México. *E-mail: gcanche@cicy.mx

Abstract

In this work, granular starch grafted with polycaprolactone (PCL) was obtained by using the N-methylimidazole (NMI) as catalyst. The effect of the relations starch/monomer (50/50, 75/25 and 25/75), and catalyst content (12.5%, 25% and 37.5%) were studied. The graft parameters were determined; and the grafted starch were characterized by infrared spectroscopy (FTIR), thermogravimetric analysis (TGA), differential scanning calorimetry (DSC) and scanning electron microscopy (SEM). The higher percentage of grafting (68%) and of addition (40%) was obtained for reactions with relation starch/monomer 50/50 and 25% catalyst. The FTIR and DSC analysis confirmed the presence of PCL in the grafted starch.

Introduction

Over the past few decades, biodegradable polymers have been considered as an attractive solution to the problems caused by the non-degradable synthetic polymers. Starch is an inexpensive polysaccharide, completely biodegradable and is synthesized by a large number of plants [1]. Its use in the production of biodegradable materials to replace synthetic polymers can simultaneously reduce dependence on oil and help reduce the problem of plastic waste [2]. However, applications of manufactured products from thermoplastic starch (TPS), are limited by their low water resistance and poor mechanical properties [3]. Due to the foregoing, starch is mixed with other natural or synthetic polymers to improve their properties and processability [4]. Another approach to overcome the shortcomings of thermoplastic starch, is starch modification, for example, by grafting monomers (such as styrene [5] and methyl methacrylate [6]) to the backbone of the starch. However, in almost all cases, the graft chains are not biodegradable and grafted thermoplastic starches are partially biodegradable [7].

Another effort in the chemical modification of starch, has been the polyester graft chain, such as polycaprolactone (PCL) [8] and polylactic acid (PLA) [9], on starch through reactions of functional groups or through polymerization by ring opening monomer with the starch as a site of initiation of polymerization. Graft copolymers of starch-g-PCL and starch-g-PLA presented improved mechanical performance and may be completely biodegradable by bacteria under natural conditions. Therefore, these graft copolymers can be used directly as thermoplastics or as compatibilizers in the compounds materials based on starch-PCL or starch-PLA mixtures [10].

In this paper the results of the synthesis and characterization of starch grafted with biodegradable polyester polycaprolactone (PCL) using the N-methylimidazole (NMI) catalyst are presented.

Experimental

Corn starch Unilever México was used. The ϵ -caprolactone monomer (ϵ -CL) with 97% purity and the catalyst N-methylimidazole (NMI) were reagent grade from Sigma-Aldrich. Starch particles were grafted according to a method reported in the literature [11]. The procedure was as follows: the starch (dry basis), the ϵ -CL monomer and catalyst NMI were placed into a 250mL glass reactor; equipped with a mechanical stirrer and a condenser. The reactor was placed in a glycerin bath at

150° and the mixture was stirred for 2h. The polymerization yield was determined gravimetrically. In Table 1, the formulations used for obtaining polycaprolactone grafted starch are shown.

Table 1. Formulations used in grafting reactions of the polycaprolactone onto the starch.

		REACTIONS				
Code		St-g-PCL1	St-g-PCL2	St-g-PCL3	St-g-PCL4	St-g-PCL5
		1st	2nd	3rd	4th	5th
Materials	Starch [g]	5	5	5	5	5
	ε-Caprolactone (ε-CL) [g]	5	5	5	2.5	7.5
	N-Methylimidazole (NMI) [g]	0.625	1.25	1.875	1.25	1.25

Graft parameters determination

Extraction with toluene was conducted to dissolve remains ε-CL monomer, the catalyst and the polymer ungrafted chains (homopolymer) [11]. Graft parameters are determined using the weights before and after extraction [12, 13], by the following equations.

$$\text{Graft (\%)} = \left[\frac{\text{PCL grafted weight}}{\text{Starch weight}} \right] \times 100 = \left[\frac{W_{\text{insolfrac}} - W_{\text{st}}}{W_{\text{st}}} \right] \times 100 \quad (1)$$

$$\text{Addition (\%)} = \left[\frac{\text{PCL grafted weight}}{\text{Total weight copolymer St-g-PCL}} \right] \times 100 = \left[\frac{W_{\text{insolfrac}} - W_{\text{st}}}{W_{\text{insolfrac}}} \right] \times 100 \quad (2)$$

$$\text{Grafting Efficiency (\%)} = \left[\frac{\text{PCL grafted weight}}{\text{PCL formed weight}} \right] \times 100 = \left[\frac{W_{\text{insolfrac}} - W_{\text{st}}}{W_{\text{homop}} + (W_{\text{insolfrac}} - W_{\text{st}})} \right] \times 100 \quad (3)$$

Where $W_{\text{insolfrac}}$ is the weight of the product obtained after extraction, in grams (g); W_{st} is the weight of starch loaded in the reaction, in grams (g); and W_{homop} is the weight of the homopolymer formed in the reaction, in grams (g).

Characterization

FTIR analysis of starch and grafted starches was performed in a Nicolet 870 Fourier transform infrared spectrophotometer, in a wave number range from 4000 to 400cm⁻¹, with 16 scans and a resolution of 4 cm⁻¹. TGA thermograms were obtained on a thermogravimetric balance Perkin Elmer TGA-7, in a temperature range from 40 to 700°C, with a heating rate of 10°C/min. Differential scanning calorimetry analysis was performed on a Perkin Elmer DSC-7. The runs were carried out in a temperature range of -120 to 0°C, with a heating rate of 10°C/min. Morphology of the particles was performed using a JEOL 6360LV SEM. The particles were cover with a gold surface layer to improve contrast.

Results and Discussion

Table 2 show the graft parameters obtained after the extraction with toluene. Reactions with the higher amounts of catalyst (25% and 37.5% by weight relative to the monomer) had similar parameter values graft, with graft percentage values of 68-64%, addition rate of 40 %, and grafting efficiency of 88-72%. An increase in the amount of monomer, keeping constant the amount of catalyst (25%) resulted in a decrease of the values of the parameters graft. It is known that the

kinetics of the reaction is faster for a higher amount of catalyst and a solid paste forms rapidly. This phenomenon limits the stirring and diffusion of the monomer into the starch and implies that the experiment should be performed in a short time [11].

Table 2. Effect of reaction conditions on the graft parameters.

Code	Relation St/mono.	Amount of catalyst (g)	Amount of monomer (g)	Graft (%)	Addition (%)	Grafting efficiency (%)
St-g-PCL1	50/50	0.625 (12.5%)	5	13	11	28
St-g-PCL2	50/50	1.25 (25%)	5	68	40	88
St-g-PCL3	50/50	1.875 (37.5%)	5	64	39	72
St-g-PCL4	50/25	1.25 (25%)	2.5	42	30	92
St-g-PCL5	50/75	1.25 (25%)	7.5	21	18	22

St-g-PCL1-5: 5g starch, 150°C, 2h of polymerization, bulk polymerization.

In Figure 1 FTIR spectra of the starch, PCL homopolymer and starches grafted with polycaprolactone are shown. The spectrum of the starch has a wide band in the region between 3700-3000cm⁻¹ and a peak at 1645cm⁻¹ corresponding to stretching and bending of the –OH group, respectively [14]. It also shows two signals at 2930cm⁻¹ and 2890cm⁻¹ corresponding to the asymmetric and symmetric stretching of –CH₂ group, respectively [15]. For the spectrum of PCL homopolymer, intense peak at 1730cm⁻¹ is observed corresponding to the stretching of C=O group of the polycaprolactone [14, 15]. Characteristics signals from –CH₂ group can also be seen, but with a slight shift of the signal due to the asymmetric stretching at 2940cm⁻¹ and a third signal at 2870cm⁻¹ corresponding to the bending/stretching effect of –H attached to C=O, both at the same time [15]. These signals are clearly noticeable in the spectrum grafted starch, confirming the graft of polycaprolactone (PCL) on the starch chains. It is also observed that the signal increases with increasing amount of NMI in the reaction, which is consistent with the highest values of graft parameters obtained.

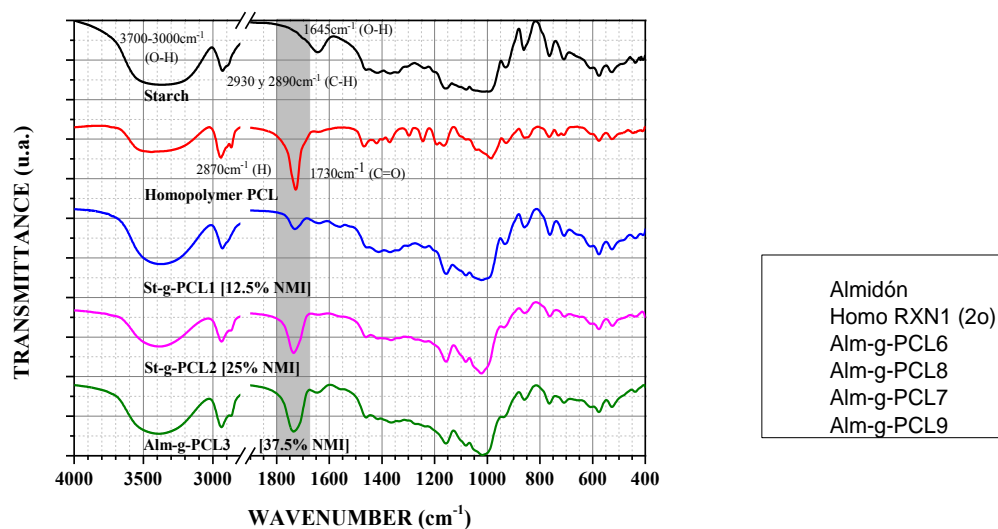


Figure 1. FTIR starch, PCL homopolymer and starch grafted with PCL at different concentrations of the catalyst NMI.

In Figure 2 TGA thermograms from starch, PCL homopolymer and grafted starches with PCL are shown. It can be seen in the TGA thermogram of the starch has an initial mass loss of 9% in the range of 40 to 150°C, which corresponds to desorption of water. The main degradation is observed in the range from 280 to 370°C, with a sharp drop in mass caused by the thermal degradation of the amylose and amylopectin chains [16], yielding a residual mass of 11% at 700°C. PCL homopolymer have a lower initial mass loss of 3% than starch; and the primary degradation is observed from 395 to 455°C. PCL thermal degradation of the polymer chains initiated at approximately 260°C [17]. TGA thermograms from grafted starch show less water loss indicating lower hydrophilic character due to the presence of the PCL. Only one decomposition zone is observed in the range of 260-400°C for grafted starch with the smaller amount of catalyst and 260-456°C for larger amount of catalyst, which indicates that both polymers are thermally decomposed in the same area.

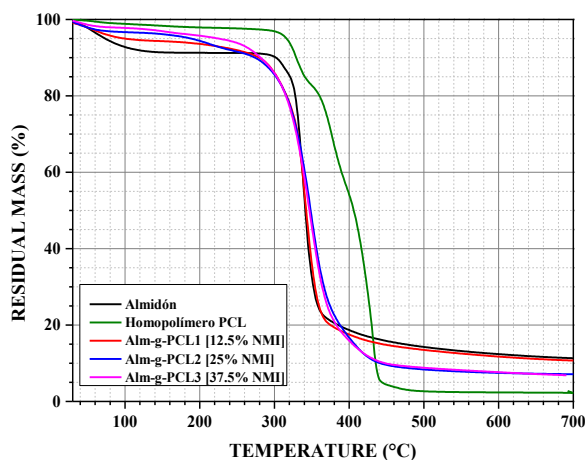


Figure 2. TGA graphs starch, PCL homopolymer and starch grafted with PCL at different concentrations of NMI.

Figure 3 shows DSC thermograms of starches grafted with PCL in the range of -100 to 0°C. PCL is a semicrystalline polymer which has three thermal transitions, a transition of the first order at about 60°C which corresponds to melting endotherm; second order transition, glass transition temperature -60°C; and exothermic crystallization peak around -25°C [17].

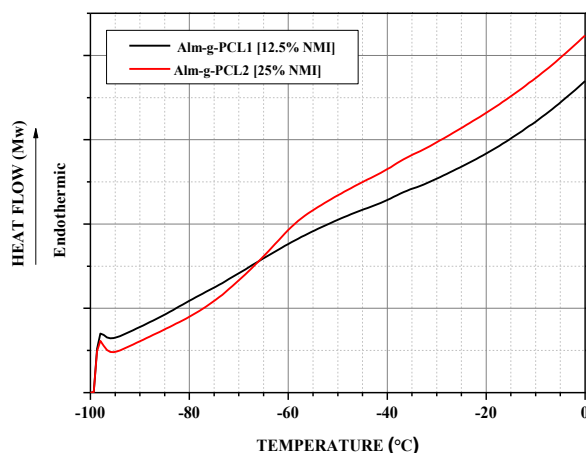


Figure 3. DSC thermograms of starches grafted with PCL to different amounts of catalyst.

In Figure 4, SEM micrographs of the granules of starch and grafted starches obtained with different amount of NMI are observed. The starch granules (Fig. 4a) are in the form of polyhedral with pin holes and equatorial grooves. For grafted starch particles (Fig. 4b-4d), it can be seen that in general the granular structure of starch is maintained, although clusters are observed. Its surface exhibits a certain roughness, which is attributed to the graft polymer on the granules [11, 12]; this roughening, and the tendency to agglomerate was less evident for starches grafted with a smaller amount of catalyst.

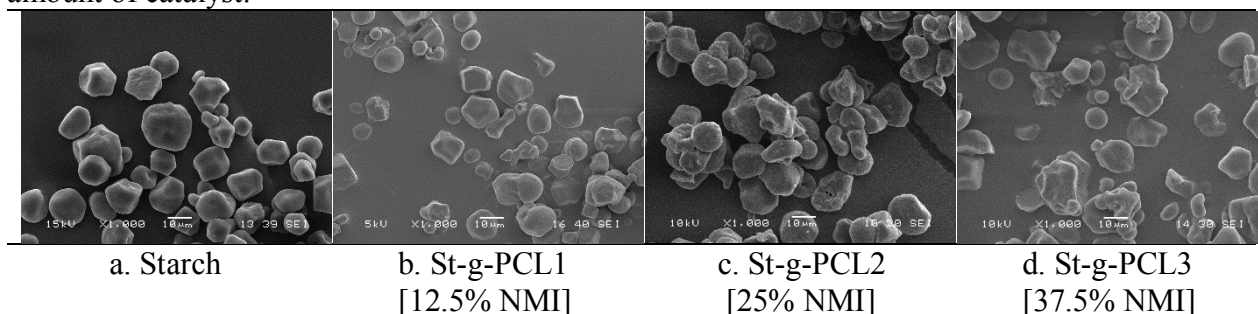


Figure 4. SEM micrographs of starch grafted with polycaprolactone.

Conclusions

Granular starch with grafted ϵ -CL monomer was obtained and verified by different physicochemical techniques. The grafted chain produced changes in the surface of these particles. Because PCL is grafted in different proportions by modification of the concentration of catalyst or monomer, materials that exhibit different characteristics can be obtained.

Acknowledgements

Cuevas-Carballo thanks the Mexican Council of Science and Technology (CONACyT) for financial support during her PhD studies.

References

- [1] Zerroukhi, A., et al. (2012). *Starch/Stärke*, 64, 613-620.
2. Shi, Q., et al. (2011). *Polymer Degradation and Stability*, 96, 175-182.
3. Ren, J., et al. (2009). *Carbohydrate polymers*, 77, 576-582.
4. Da Róz, A. L., et al. (2011). *Industrial Crops and Products*, 33, 152-157.
5. Kaewtatip, K., et al. (2010). *Journal of Thermal Analysis and Calorimetry*, 102, 1035-1041.
6. Li, M.-C., et al. (2012). *Journal of Applied Polymer Science*, 125, 405-414.
7. Canché-Escamilla, G., et al. (2011). *Carbohydrate polymers*, 86, 1501-1508.
8. Rutot, D., et al. (2000). *Composite Interfaces*, 7, 215-225.
9. Wootthikanokkhan, J., et al. (2012). *Journal of Applied Polymer Science*, 126, E388-E395.
10. Chen, L., et al. (2005). *Polymer*, 46, 5723-5729.
11. Najemi, L., et al. (2010). *Starch/Stärke*, 62, 147-154.
12. Chen, L., et al. (2005). *Carbohydrate polymers*, 60, 103-109.
13. Vera-Pacheco, M., et al. (1993). *Journal of Applied Polymer Science*, 47, 53-59.
14. Moreno-Chulim, M. V., et al. (2003). *Journal of Applied Polymer Science*, 89, 2764-2770.
15. Colthup, N. B., et al. (1990). Elsevier, United States of America.
16. Mano, J. F., et al. (2003). *Journal of Materials Science: Materials in Medicine*, 14, 127-135.
17. Elzubair, A., et al. (2006). *Journal of dentistry*, 34, 784-789.
18. Singh, N., et al. (2003). *Food Chemistry*, 81, 219-231.

Continuous system for the treatment of liquids, plasma process - biodegradable hydrogels.

D. Guevara-Ruiz^{1*}, E. Almaraz-Vega¹, J. C. Sánchez-Díaz¹, M. A. Sánchez-Castillo², L. E. Cruz-Barba¹, A. Martínez-Ruvalcaba.¹

¹Departamento de Ingeniería Química, Centro Universitario de Ciencias e Ingenierías, Universidad de Guadalajara, Blvd. M. García Barragán #1451, C. P. 44430 Guadalajara, Jalisco, México.

²Facultad de Ciencias Químicas, Universidad Autónoma de San Luis Potosí, Av. Manuel Nava #6 Zona Universitaria, C. P. 78210, San Luis Potosí, S.L.P., México.

*E-mail: guevararuiz@hotmail.com

Abstract

The plasma processing involves different techniques of modification of a compound. The ability to modify materials precursors used for the synthesis of hydrogels capable of removing dissolved substances in a liquid body is investigated. Ligno-cellulosic materials are used to ensure the biodegradability thereof. This modification and removal technique works together with a reaction system in which it is possible to give plasma treatment directly to a liquid. We demonstrate that the modification of the materials alters swellable hydrogels, and it is possible to conduct reactions within the liquid using the plasma reactor.

Introduction

The industrial effluents contain various organic chemicals that cause toxicological and environmental problems. Generally, treatment involves the removal of suspended solids, as well as various methods for removing the color produced by the dye or colorant, and the organic and inorganic agents are dissolved in the effluent.

The use of natural polymers such as cellulose in the preparation of hydrogels is of great importance in the food and pharmaceutical area. Cellulose is a carbohydrate insoluble in water natural. High rigidity and insolubility in most solvents is due to the hydroxyl groups of the anhydroglucose, which form strong hydrogen bonds to increase its crystallinity. [1] To solubilize the cellulose is necessary to incorporate various substituents in the structure of the anhydroglucose to decrease its degree of crystallinity. Moreover, mixtures of biopolymers and synthetic polymers are particularly important because they can be used for biomedical applications [2].

The plasma processing involves different materials processing techniques using cold plasmas to modify the properties thereof. Treatments may be superficial, either by coating with a thin film of other materials or by altering the surface chemical structure of the base material, or by volumetric modification treatments on the chemical form or composition of the original material, which is made using partially ionized gases, generically called "plasma". The surface modification techniques using plasmas permit adapting the surface properties of the treated materials to service conditions, satisfying functional requirements impossible to meet by the base material [3].

The interest of the study of techniques able to clean or reduce toxic compounds that are thrown to the environment is of great importance. At present the problem that cause this type of effluent reaches enormous proportions, hence are intended to find new methods and techniques to existing alternatives, to reduce costs and increase efficiencies. Starting from this trend seeks to create a system which involves continuously various techniques including adsorption and elimination using hydrogels through a plasma system. Starting by the synthesis and characterization of the hydrogels using cellulose derivatives, which is capable of adsorbing some metal ions [4]. Besides making the

modification of materials precursors by plasma treatment to alter its properties. And, moreover, the design, construction and validation of the plasma reactor in solution (PRS) for treating liquids.

Experimental

Reagents.

The materials used are listed below: sodium carboxymethyl cellulose (CMCNa) from Sigma-Aldrich, hydroxyethyl cellulose (HEC) from Sigma-Aldrich, analytical grade acetic acid from Sigma, Products Selectopura bidistilled water, and oxygen (O₂) extra dry, 99.5% purity, INFRA SA de CV

Plasma treatment of the precursor materials.

The properties of the polymers used in hydrogel synthesis are selectively modified by a surface treatment in a system of dielectric barrier discharge (plasma system), with oxygen as the precursor gas [5,6], which gave rise to phase reactions heterogeneous polymer surface for the introduction of oxygen containing functional groups such as carboxyl, carbonyl, hydroxyl, etc.

Synthesis of hydrogels.

Hydrogels in the form of film of CMCNa / HEC were sintered by the solvent evaporation technique. The composition of the synthesized gel is 2% total solids with a ratio of 3: 1 weight ratio CMCNa: HEC varying the amount of AC with respect to the total solids. These conditions were used to synthesize modified hydrogels from each of the treatments used materials. CMC-T / HEC-T-T CMC / HEC-NT and NT-CMC / HEC-T: the hydrogels according to the following combinations were synthesized. Where CMC-T is treated with plasma sodium carboxymethylcellulose, CMC-NT is sodium carboxymethyl cellulose untreated HEC-T and HEC-NT, equal but for the hydroxyethyl cellulose. The same procedure for the study of the kinetics of swelling continues.

The swell (H) for each sample at a given time (t) was calculated using the following equation:

$$H = \frac{w_t - w_0}{w_0} [=] \frac{g \text{ water}}{g \text{ xerogel}} \quad \text{where } w_t \text{ is the weight of the sample at a time } t \text{ and } w_0 \text{ is the initial weight of}$$

the material without hydrate (xerogel).

Design, construction and validation of the PRS.

The PRS consists of two zones. The first reaction zone is constituted by a source of AC power that can regulate the voltage, frequency and power applied to the reactor; the body of the reactor is a pyrex glass tube; electrodes are made of stainless steel with tube-tip configuration. The second feed zone is where the flow rate of gas entering the reactor is controlled, is used as oxygen-argon gas precursor. The variables to be observed are: the reaction time (1, 3 and 5 minutes), the inter-electrode distance (IED) (1-3 mm), the flow of gas (5, 10 and 20 ccs) and power (50 , 70 90 and 100%). Liquid and solid reaction products are analyzed by IR and UV spectroscopy.

Results and discussion

The treatments were designated according to the duty cycle used in accordance with the following tabulation:

Duty cycle	45%	37.5%	30%	22.5%	15%
Number of treatment	1	2	3	4	5

Thus, the CMCT1 label corresponds to the sodium carboxymethyl cellulose modified by treatment No. 1, and similarly all other tags are interpreted.

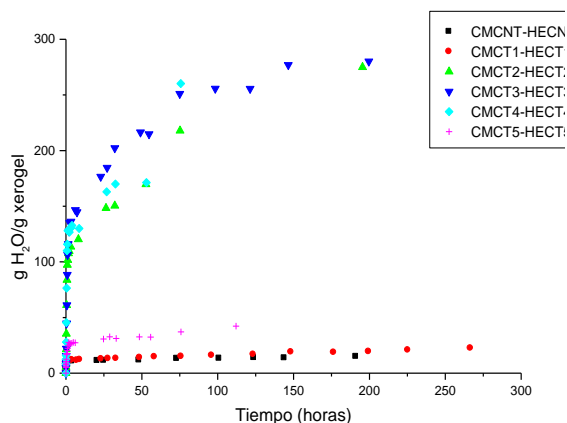


Figure 1 Comparison of the swelling kinetics of the CMCNT-HECNT and CMCT-HECT sample.

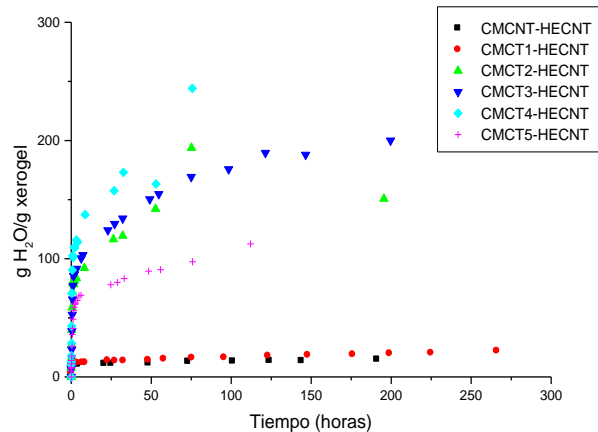


Figure 2 Comparison of the swelling kinetics of the CMCNT-HECNT and CMCT-HECNT sample.

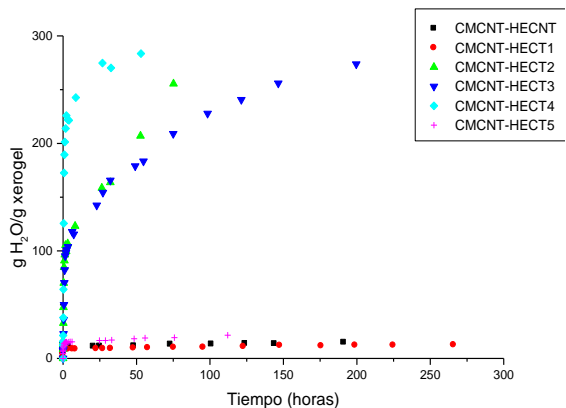


Figure 3 Comparison of the kinetics of swelling and CMCNT-HECNT CMCNT-HECT sample.

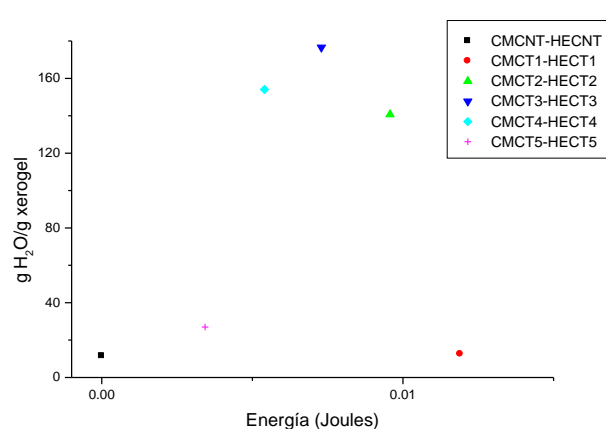


Figure 4 Swelling to a maximum time of 24 hours. Comparison HECNT CMCNT-and-HECT FCTC.

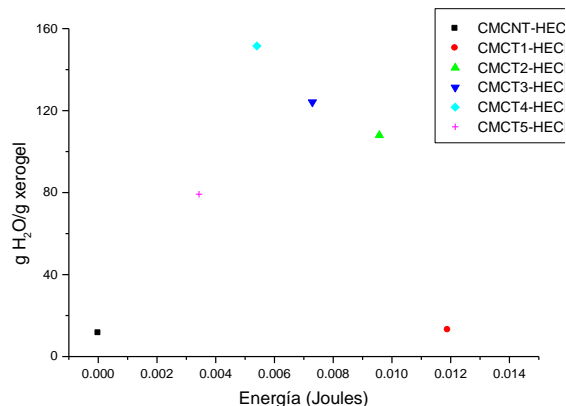


Figure 5 Comparison HECNT CMCNT-and-HECNT FCTC.

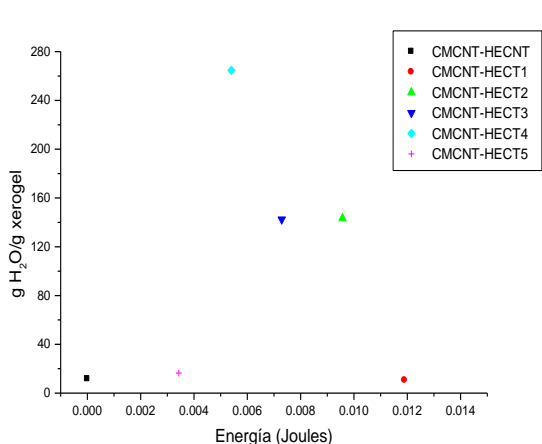


Figure 6 Comparison of CMCNT-HECNT and CMCNT-HECT.

Figure 1 shows the comparison processing carried out, with a control sample synthesized under the same experimental conditions. It can be seen that all the samples synthesized with modified

Third US-Mexico Meeting "Advances in Polymer Science" and XXVII SPM National Congress
Nuevo Vallarta, December 2014

materials showed greater swelling than the control sample, remaining stable for the same period of time. It can also be seen that the treatment 1 and treatment 5 no significant change compared to the control, while the other three treatments including appear similar behavior. It is important to note that the maximum swell which is record-treated sample 3 is about 10 times that of the control sample. Figure 2 shows that in the material synthesized with the modified treatment 5 had an intermediate swelling powder, in addition to the swellings were lower than those achieved in the case of the CMCT-HECT combination. Data for CMCNT-HECT combination shown in Figure 3 can be seen that in this case the sample synthesized with 5 treatment products again behaved similarly to the control manner, as treatment 1. The results of this combination are very similar to those of the CMCT-HECT combination. The swelling is controlled by the amount of crosslinking and other factors such as the added groups by the use of the HEC. In the above figures it can be seen that there is a significant effect when the HECT, either in combination with CMCNT or CMCT, as when used HECNT occur swellings smaller is used. In general the increase in swelling capacity after modifying the material, due to the introduction of hydrophilic groups on the surface of the powder, thus improving its solubility separately and their ability to swell as hydrogels. In Figures 4, 5 and 6, the kinetics of swelling to 24 hours is showed, in each of the graphs a peak is seen, this shows that the swelling capacity is related to the energy supplied in the reactor, and that behavior is nonlinear, which may be due to surface-induced crosslinking groups that are deposited in the dust, by increasing the number of groups, the crosslinking and the material strength increases, but decreases swelling capacity.

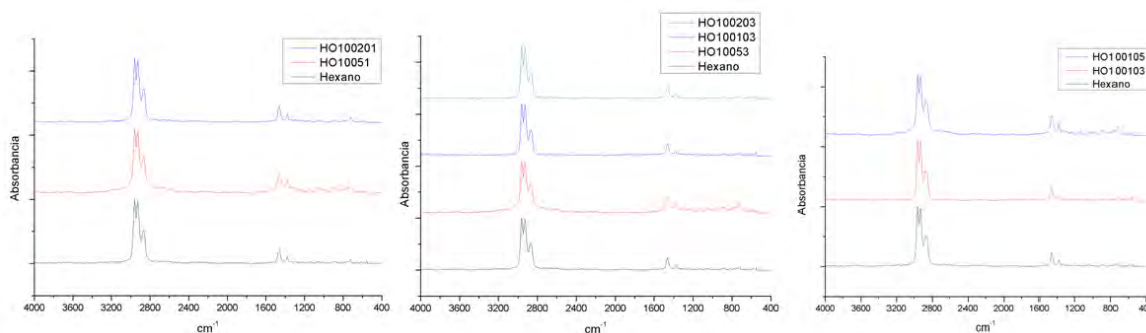


Figure 7 FTIR spectra obtained by comparing the pure hexane with the treated samples.

Hexane as the treatment of type reaction in the RPS, with variables marked above took place. The body of the reactor with 25 ml of pure sample is loaded, it is held upright, the gas is introduced through a tube-shaped electrode, while the other electrode is shaped tip. The necessary gas flow and IED are adjusts. Frequency is set to the power source until the formation of the arc, initiating the reaction. In the reaction three products are obtained, gas, solid and liquid. FTIR analysis for the remainder of the reaction liquid is made. In Figure 7, the spectra obtained are presented for each of the samples, labeled as follows: H (hexane) O (oxygen), 100 (power) 20-10-5 (gas flow) 5-3-1 (time). No significant change was not looked, which can be interpreted in different ways, one of which is that the reaction products remain overlapped on the same spectrum of the untreated sample, this because during the reaction can fragment the molecule hexane into shorter chain hydrocarbons, or it may be a separate accommodation, as branches. In either of the above cases, the bonds in the molecule are the same, so that the FTIR technique provides no meaningful information of the remaining liquid. Another option is that there is not a high concentration of a product in the remaining liquid, which would indicate that all the reaction products are in solid or gaseous state.

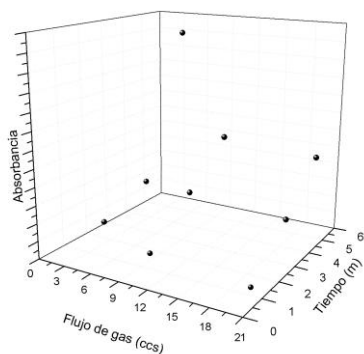


Figure 8 Maximum absorbance point for olive oil samples treated with Argon.

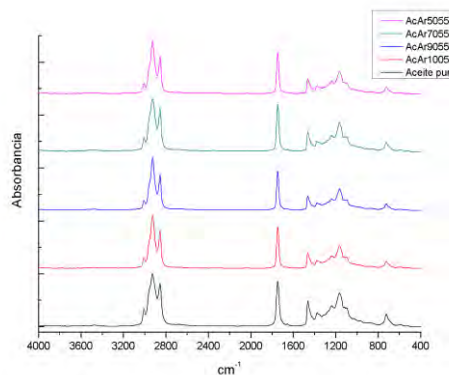


Figure 9 FTIR olive oil treated with Argon.

For the power variation is performed treating olive oil using Argon gas as precursor. A run of experiments varying the gas flow and time to peak power is made. The samples were analyzed using the technique of UV. In Figure 8, the absorbance of each of the samples, where you can see a peak corresponding to the lower gas flow and increased reaction time is shown. Figure 9 shows the FTIR analysis of the oil, by varying the power, no significant change is seen. This is due to the same reasons discussed above.

Conclusions

Surface modification of the sodium carboxymethyl cellulose and hydroxyethyl cellulose was achieved, which is reflected in the improvement of the mechanical strength of the materials, and also enhance the swelling capacity of the hydrogel, in some cases, by a factor of ten.

The relationship between power supplied and the swelling of the samples allowed to find a peak of the swelling capacity at a time.

The reactor designed can be used for the treatment of organic compounds. The reactions result in three types of products, gas, solid and liquid. FTIR analysis of the liquid does not provide a clear identification of the products, so that a more accurate technique is needed.

The modification of ligno-cellulosic materials, in this case in the form of hydrogel, gives us the ability to place functional groups capable of removing contaminants, this coupled with the ability to decompose organic compounds in the PRS, lays the foundation for continuous removal system of pollutants involving the two techniques.

References.

- [1] Park, J. S., Ruckenstein, E., *Carbohydr polym*, 46, 373 (2000).
- [2] Park, J. S., Park, J. W., Ruckenstein, E., *Polymer*, 42, 4271 (2000).
- [3] Rodrigo, A., *Rev. Argent Nuclear*, 8:57, 31-42 (1996).
- [4] Yanmei Zhou, Qiang J., *J Mater Sci* 47:12, 5019-5029 (2012).
- [5] Lugo Vega, C., "Modificación superficial de materiales mediante el uso de un reactor rotatorio de plasma DBD a presión atmosférica" Tesis de Maestría en Ingeniería Química, Universidad Autónoma de San Luis Potosí, (2011).
- [6] Guevara Ruiz, D., "Modificación de materiales celulósicos para la síntesis de hidrogeles biodegradables novedosos" Tesis de Maestría en Ingeniería Química, Universidad de Guadalajara, (2012).

ELECTRICALLY CONTROLLED RELEASE OF AMOXICILLIN FROM POLYACRYLAMIDE/POLYANILINE HYDROGELS

Cinthia Jhovanna Perez Martinez ^{a,b}, Teresa Del Castillo Castro^c, Tania Ernestina Lara Cenicerros^d.

^aCentro de Investigación en Materiales Avanzados, S. C.- Unidad Chihuahua, C.P. 31109 Chihuahua, Chihuahua, México.

^bDepartamento de Ciencias Químico Biológicas, Universidad de Sonora, C.P. 83000 Hermosillo, Sonora, México.

^cDepartamento de Investigación en Polímeros y Materiales, Universidad de Sonora, C.P. 83000 Hermosillo, Sonora, México.

^dCentro de Investigación en Materiales Avanzados, S. C.- Unidad Monterrey, C.P. 66600 Apodaca, Nuevo León, México.

Abstract

In a novel approach, submicro/nanofibers of Polyaniline (PANI) were prepared by chemical polymerization in the presence of L-glutamic acid (AG). Subsequently, PANI structures were loaded with therapeutic doses of amoxicillin. Then, the suspension of drug-loaded polymer was incorporated into Polyacrylamide (PAAm) hydrogel during the formation of the semi-interpenetrating network. The composite hydrogel of PAAm/PANI were stimulated electrically to evaluate the release of the antibiotic.

Introduction

Stimuli-responsive materials are of great interest in the field of biotechnology and biomedicine. Drug delivery systems based on controlled release under an electrical stimulus offer the promise of new treatments, as the iontophoretic transdermal patch, for chronic diseases that require daily injections for precise doses of medication. The composites obtained from the dispersion of particles of an electroconductive polymer in a hydrogel matrix are potential electroactive systems because they can retain the electrical properties attained by the electroconductive polymer and the capacity of adsorption/desorption of large volumes of water of the hydrogel feature. This work presents the preparation of semi-interpenetrating network of polyacrylamide (PAAm) and polyaniline (PANI) and the kinetics of release of amoxicillin, a first choice of broad-spectrum antibiotics, from the composite by electrical stimulus.

Experimental

Synthesis of PANI

PANI was synthesized by a chemical-oxidative polymerization of aniline in the presence of the L-glutamic acid (AG) using ammonium persulfate APS as oxidant. The molar ratio of aniline:AG:APS was 1:0.25:1. The solution was cooled at 5°C in an ice bath under nitrogen atmosphere and it was kept under moderate stirring for 24 h. After reaction, the resulting mixture consisting of dark-green suspension of PANI was rinsed thoroughly with deionized water in a Buchner funnel until the filtrate became neutral. The PANI suspension was reserved for TEM and loading/releasing studies of amoxicillin.

Characterization

The morphology of synthesized PANI was studied by TEM using a JEOL2010F microscope. PANI suspensions were re-dispersed in deionized water through sonication and adequate portion was transferred to copper grids for the analysis.

Loading of amoxicillin

For the loading of amoxicillin, 25 mL of PANI suspension (0.0148 g mL^{-1}) were mixed with 5 mL of an aqueous solution of the drug (0.2 g mL^{-1}). After stirring for 24 h, the resultant mixture was carefully transferred to dialysis tubing (acetate of cellulose, purification capacity M.W. > 12,000). The dialysis tubing was then put into 500 mL of deionized water at room temperature for removing the drug that was not adsorbed on PANI structures. The dialysis solution was periodically replaced with fresh deionized water until the amoxicillin release was below 0.1%.

Incorporation of amoxicillin-loaded PANI particles into polyacrylamide hydrogel

An aliquot of suspension of amoxicillin-loaded PANI was mixed by magnetic stirring with 10 mL of an aqueous solution of (AAm)/bisacrylamide (MBAAm) (58:2), subsequently adding an initiator agent (APS) and a reaction catalyst (TEMED). The mixture was placed in a cylindrical mold. Before the gelation point was reached, a thin copper electrode was introduced in the center of the composite hydrogel. The system was kept at room temperature to complete the process of polymerization and gelation. The preparation of the composite hydrogel [PAAm/(PANI-amoxicillin)] is illustrated in Figure 1.

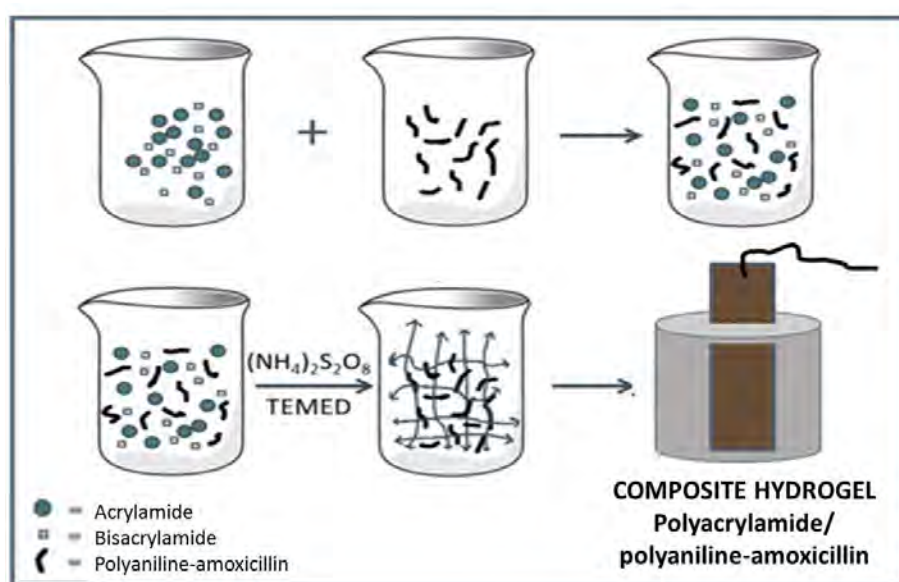


Figure 1. Representation of preparation of semi-interpenetrating network of polyacrylamide (PAAm) and amoxicillin loaded-polyaniline (PANI-amoxicillin).

Controlled release of amoxicillin by electrical stimulus

The study of drug release by electric stimulus was performed at 25°C , placing the electrode-containing composite hydrogel and uncoated identical electrode in a phosphate-buffered saline solution at pH 7. For the release study, potentials of 5 V (DC power supply Agilent, model E3632A) were applied for 1

minutes between the two electrodes in intervals of 60 minutes. Aliquots of the release medium were taken before and after application of each potential to determine the concentration of delivered drug. The concentration of the amoxicillin was quantified by UV-visible spectroscopy (Perkin-Elmer Lambda 20) at 273 nm, using a calibration curve previously made.

Results and Discussion

Figure 2 showed the TEM images of PANI obtained by the chemical-oxidative polymerization of aniline in the presence of GA. Images revealed fibrous structures with diameters between 100 to 300 nm.

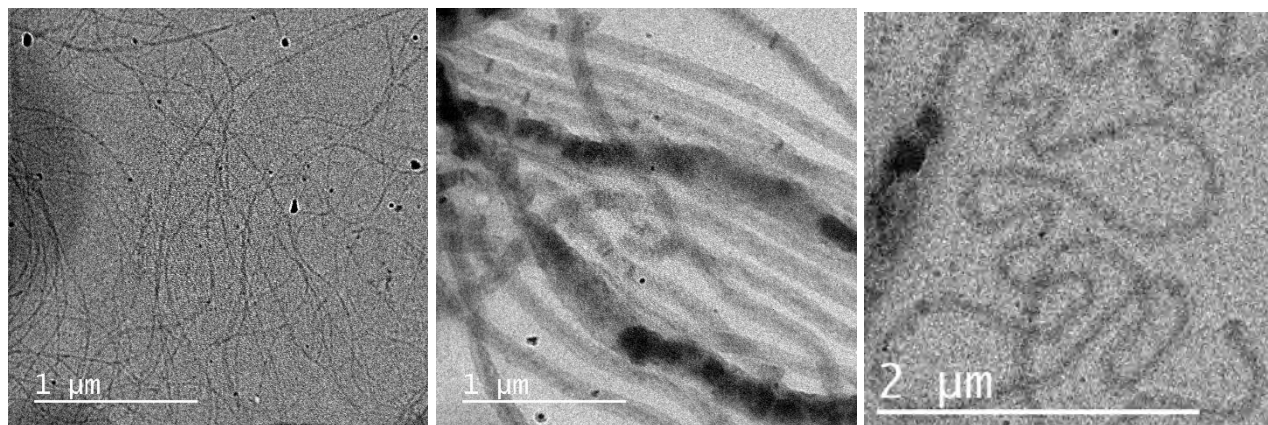


Figure 2. TEM images of nanofibers of PANI synthesized by oxidative polymerization with APS in the presence of GA.

The fiber-like morphology of PANI and its polar nature favors the adsorption of amoxicillin. A therapeutic dose of the drug was added to the suspension of PANI. Un-bonded amoxicillin was removed by dialysis against deionized water and the effective amount of loaded drug was founded to be 80 wt.%, which confirmed the efficiency of the drug adsorption onto PANI particle surface.

The entrapment of amoxicillin-loaded PANI into PAAm network produced composite hydrogels which preserved their geometry once they were removed from molds.

Figure 3 shows the kinetics of amoxicillin release from composite when the hydrogel-coated electrode was connected to the negative pole of the power supply. It was found an immediate increase of amoxicillin release after the first voltage application. Negligible changes in medium concentration were detected until the application of next stimulus. Similar “ON-OFF” release pattern was observed in the subsequent cycles of application and removal of the electrical potential difference.

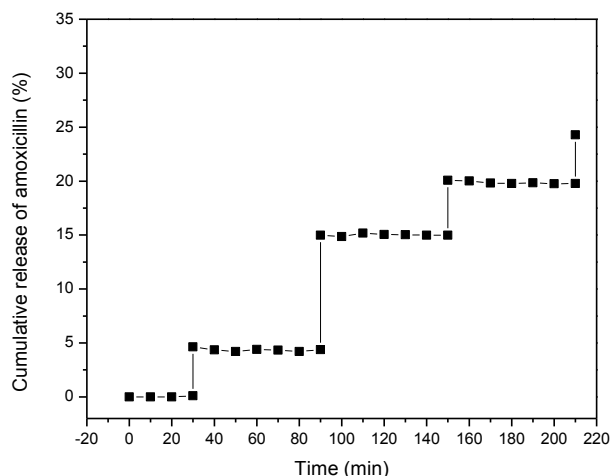


Figure 3. Release of amoxicillin from composite hydrogel of PAAm/PANI under electrical potential application (5V). Composite hydrogel is in cathode.

Figure 4 shows the kinetics of amoxicillin release when the hydrogel-coated electrode was connected to the positive pole of the power supply. After application of the first voltage, the composite hydrogel starts the process of drug release. The amoxicillin concentration increased at a constant rate regardless of subsequent application of electrical stimulus. Furthermore, the cumulative release at the end of the experiment was significant lower than the value obtained when composite hydrogel was placed in the cathode site (Figure 3).

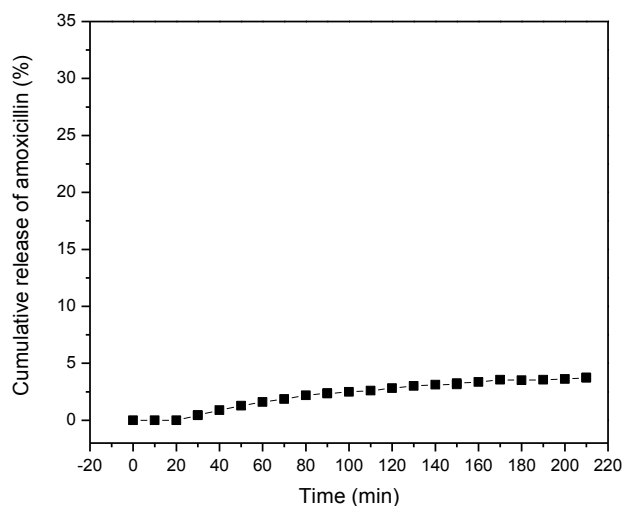


Figure 4. Release of amoxicillin from composite hydrogel of PAAm/PANI under electrical potential application (5V). Composite hydrogel is in anode.

The difference between results of Figures 3 and 4, which were obtained under the same conditions of voltage, time and number of electrical stimulus application can be associated to the change of the overall

net charge within PANI upon reduction or oxidation. The electric-field-driven movement of amoxicillin is discarded because it exists as zero net charge molecule at neutral pH. The electrochemical reduction of PANI caused changes in the charge density of particles, with the synergistically release of noncovalently bonded amoxicillin molecules.

The above results of electrically controlled amoxicillin release, particularly those of Figure 3, showed a cumulative release up to approximately 25% of the drug content, which demonstrated the suitability of the system for drug delivery applications such as iontophoretic systems.

Conclusions

The chemical oxidative synthesis of aniline in the presence of amino acid produced submicro/nanostructures of cylindrical profile. The polyaniline presented fibrillar morphology with diameters in submicro and nanometric scale, which efficiently adsorbed therapeutic doses of amoxicillin. Electroconductive composite hydrogel can be obtained by the entrapment of amoxicillin-loaded polyaniline in polyacrylamide network. The antibiotic molecules can be subsequently released (or sustained) from composite hydrogel in response to application (or removal) of electrical stimulation. This tuning release profile can lead to promising drug delivery applications such as implantable devices and iontophoretic systems.

Acknowledgements

This work was supported by the Consejo Nacional de Ciencia y Tecnología (CONACYT), México (Grant Ciencia Básica 2012-N°180280). The authors thank Ramón Iñiguez (Laboratorio de Microscopía Electrónica de Transmisión-UNISON) for TEM images. C.J. Pérez-Martínez acknowledges CONACYT for the scholarship during this study.

References

1. M.M. Castillo-Ortega, T. Del Castillo-Castro, V.J. Ibarra-Bracamontes, S.M. Nuño-Donlucas, J.E. Puig, P.J. Herrera-Franco. *Sensors and Actuators B* 125, 538–543 (2007).
2. C. L. Medrano Pesqueira, T. del Castillo-Castro, M. M. Castillo-Ortega, J. C. Encinas. *Journal of Polymer Research* 20, 71-79 (2013).
3. Issa A. Katime, Oscar Katime, Daniel Katime. *Anales de la Real Sociedad Española de Química* 35-50, (2005).
4. D. E. Rodríguez-Félix, C. J. Pérez-Martínez, M. M. Castillo-Ortega, M. Pérez-Tello, J. Romero-García, A. S. Ledezma-Pérez, T. Del Castillo-Castro, F. Rodríguez-Félix. *Polymer Bulletin* 68, 197–207 (2012).
5. Pérez-Martínez, C. J.; del Castillo-Castro, T.; Castillo-Ortega, M. M.; Rodríguez-Félix, D. E.; Herrera-Franco, P. J.; Ovando-Medina, V. M. *Synth. Met.* 184, 41 (2013).
6. M. Shaolin, Y. Yang, *Phys. Chem*, 112, 11558–11563 (2008),.
7. J. Nan-rong, L. Epstein, A. J. Mater. Chem, 18, 2085–2089 (2008),.
8. S. Qunhui, P. Myung-chul, D. Yulin, *Mat. Lett*, 61, 3052–3055 (2007).
9. K. Lalani, Story, J. Greg, Bertino, F. Massimo, S. K. Pillalamarri, D. Frank, D. Xu-Sheng, Z. Cui-Feng, W. Gong-Tao, M. Yiu-Wing, *Chem. Mater*, 20, 3806–3808 (2008).

NANOGELES WITH POLYHEXYLACRYLATE CORE AND POLYETHYLENE GLYCOL (PEG) SHELL WITH POTENTIAL AS NANO-BIOMATERIALS

Y. Cerda-Sumbarda^{1,a}, A. Zizumbo-Lopez^{1,b} and A. Licea-Claverie^{1,c*}

¹*Instituto Tecnológico de Tijuana, Centro de Graduados e Investigación en Química; A.P. 1166, Tijuana, B.C., México, C.P. 22000.*

a-nanosumbarda@gmail.com b-azizumbo@tectijuana.mx c-aliceac@tectijuana.mx

Abstract

In this project a synthetic approach has been developed for the preparation of amphiphilic nanogels formed by a hydrophobic viscoelastic polymeric core of poly(*n*-hexylacrylate) (PHA) and a shell of the biocompatible hydrophilic polymer polyethylene glycol (PEG). Nanomaterials, containing PEG as coating, have gain great interest since “PEGylated” biomaterials, are provided with a layer of “invisibility” against the immune system. A “soap-less” emulsion polymerization methodology was used for the nanogels preparation where methacrylate functionalized PEG (PEGMA) acts as stabilizer for the monomer droplets. Results show that the nanogels diameter depends on the mass ratio of PEGMA to HA and can be tunned from 26 nm to 116 nm by decreasing PEGMA in the recipe.

Introduction

Nanosized hydrogels (nanogels) are polymer nanoparticles consisting of three-dimensional networks, that are able to retain a large amount of water in their swollen state[1]. Over the past decades, significant progress has been made in the field of hydrogels as functional biomaterials. Hydrogel matrices comprise a wide range of natural and synthetic polymers held together by a variety of physical or chemical crosslinks. Nanogels are interesting for a wide field of applications ranging from: drug delivery, fillers for composites, tissue engineering, coatings and self-healing materials, to compatibilizers, sensors and catalysts.

There are various methods for obtaining nanogels either by high energy irradiation or chemically. Nanogels were prepared, for example, by the emulsification-evaporation technique[2] and through water in oil microemulsion.[3] On the other side nanogels were also prepared by irradiation of hydrogel-forming monomer solutions or irradiation of preformed polymers.[4] An example is the formation of intramolecular nanogels from linear polymers, by irradiation with pulses of accelerated electrons. This method allows to synthesize monomer absent nanogels.[5] Photopolymerization has provided also good results to develop this type of architecture.[6] Another method for preparing nanogels is the chemical method; this method is a copolymerization reaction with crosslinking between one or more monomers and a multifunctional monomer, which is present in very small amounts joining large molecular weight chains through their multifunctional groups.

Experimental

Preparation nanogels

With the goal to obtain nanogels with different sizes, the following synthetic parameters were varied: Ratio of *n*-hexylacrylate (HA) to polyethylene glycol methyl ether methacrylate (PEGMA, MW 1100 g/mol) and the concentration of crosslinker ethyleneglycol dimethacrylate (EGDMA).

The concentration of the free-radical initiator ammonium persulphate (APS) was 2 mol% with respect to HA in all cases. An example of the synthetic procedure is described in detail below for the case of the nanogels with mass ratio HA:PEGMA 70:30. In a 100 mL Schlenk flask, 0.15 g (1.36 mmol) of PEGMA dissolved in 48 mL of deionized water were added; next 0.35 g (22.43 mmol) of HA monomer was mixed into that solution under vigorous stirring. Then 10.57 μ L (0.56 mmol) of EGDMA was added. The flask was then capped with a rubber stopper. The mixture was placed under vigorous stirring while it was deoxygenated by flushing nitrogen for 20 minutes using a needle. Afterwards, nitrogen flow was stopped and the closed flask was placed in an oil bath preheated at a temperature of 85 °C. The mixture was allowed to stabilize to the temperature for 30 minutes under gentle stirring. Afterwards 5 mL of an aqueous solution of APS initiator (0.448 mmol) were injected through the stopper and the stirring increased to be vigorous. This is taken as the start of polymerization. The system was allowed to react for 60 minutes under vigorous stirring and at a constant temperature of 85 °C. Afterwards the flask was removed from the oil bath and allowed to cool down to room temperature by submerging it in 1 L of cold water to terminate the reaction. The nanogels were purified by the following methodology; first to remove unreacted HA monomer, petroleum ether was added into a beaker with a magnetic stirrer and allowed to stir for 2 h. Afterwards it was allowed to phase separate to discard the organic phase. The monomer free aqueous product was further purified by dialysis using Spectra/Por® Dialysis tubing with a MWCO: 12 to 14.000 g / mol. For dialysis, the aqueous product poured into the dialysis tubing was submerged into a beaker containing 4 L of deionized water for 5 days, changing the water daily. Water was then eliminated from the purified aqueous product by using a rotary evaporator operating at 40 °C and high vacuum. Finally the product was dried using a vacuum oven at 40 °C for 12 h to obtain dried nanogels.

Characterization methods

Nanogels were characterized by Fourier transform infrared spectroscopy (FTIR) Spectrum 400, FT-IR/FT-NIR Spectrometer (Perkin Elmer); dynamic light scattering (DLS) ZetaSizer Nano-ZS model ZEN3690 (Malvern Instruments); nuclear magnetic resonance spectroscopy (NMR) 200 MHz, Varian Mercury; differential scanning calorimetry (DSC) 2920 Modulated DSC (TA Instruments) and thermogravimetry (TGA) SDT 2960 Simultaneous DSC–TGA(TA Instruments).

Results and Discussion

Five emulsions were obtained starting with different mass ratios of PHA:PEGMA. Table 1 shows the sizes obtained by DLS for each of the products. Results show that as the content on PEGMA increases the hydrodynamic diameter (D_h) decreases; this demonstrates that PEGMA acts as emulsion stabilizer with the advantage that it is retained (chemically attached) to the nanogel surface forming a shell. A similar behavior has been reported in the literature regarding nanogels of poly(N-isopropylacrylamide) [7].

Figure 1 illustrates the distribution of sizes in the nanogels. In most cases monomodal distribution of sizes are observed while the width of the distributions increases with increasing PEGMA content, and therefore, decreasing diameter of the nanogels. Furthermore, it can be observed that where a 50:50 mass ratio of HA:PEGMA was used, a second distribution is formed at higher sizes, although not to a great extent. This let us to suggest that when the content of PEGMA is greater than needed to stabilize the emulsion excessive PEGMA promotes other interactions such as nanogels to nanogel reaction which leads to aggregate formation; therefore the distribution is bimodal.

Table 1. Effect of mass ratio of comonomers on D_h results of nanogels synthesized at $T = 85^\circ \text{C}$; in 60 min reactions using 2.5 mol% of EGDMA^{a)} and 2 mol% of APS^{b)}.

PHA:PEGMA ^{c)}	D_h Z average (nm)	D_h Intensity (nm)	D_h Volume (nm)	PDI
100 : 0	104.9	115.9	90.94	0.086
80 : 20	71.44	78.32	61.07	0.074
70 : 30	59.76	70.97	43.97	0.144
60 : 40	57.66	69.55	40.88	0.173
50 : 50	22.77	26.2	10.16	0.362

a) and b) with respect to HA, c) the total weight of the comonomers is 0.5g .

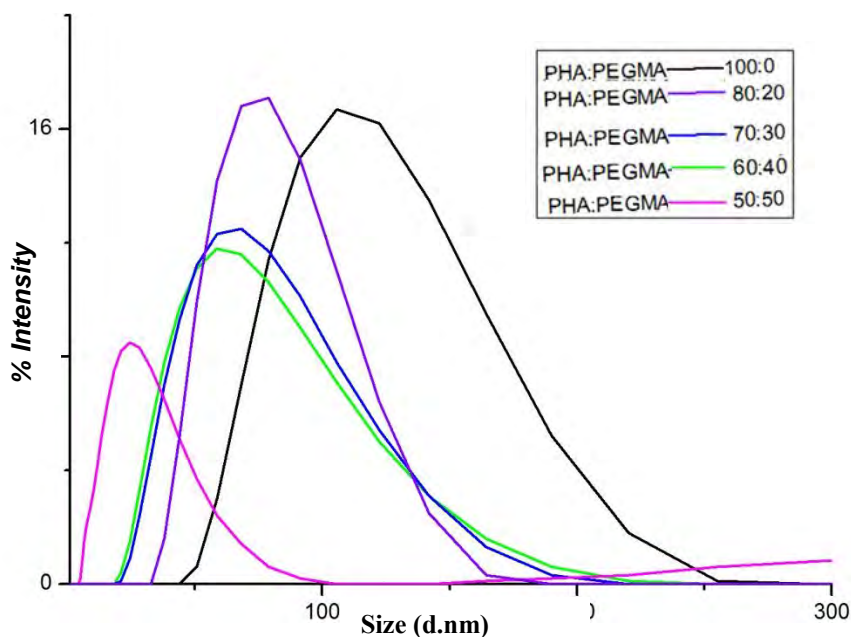


Figure 1. Effect of concentration of PEGMA in the D_h of poly(HA) nanogels crosslinked with EGDMA.

The effect of crosslinker content was studied varying its concentrations from 1.5 mol% up to 4.5 mol% of EGDMA with respect to HA. Table 2 shows the main results from this investigation. As the EGDMA content increases the size of the obtained nanogel also increases. A rationale for understanding this effect, is that the crosslinker is not highly hydrophobic, therefore, certain amount of it is distributed in the whole reaction medium. Excessive amount of crosslinker will tend to bridge nanogels into larger particles, since the core of the nanogels are highly hydrophobic. It is also noteworthy that the size increase is larger as the crosslinker content increases, than by decreasing the PEGMA (stabilizer) content, while the polydispersity remains in acceptable values.

Table 2. Effect of crosslinker content on D_h results of nanogels synthesized at $T = 85^\circ \text{C}$; in 60 min reactions using a ratio of HA: PEGMA of 60:40 and 2 mol% of APS^{b)}.

EGDMA mol% ^{a)}	D_h Z average (nm)	D_h Intensity (nm)	D_h Volume (nm)	PDI
1.5	55.27	65.43	38.93	0.197
2.5	57.66	69.55	40.88	0.173
3.5	113.2	125.3	101.4	0.089
4.5	153.6	176.0	150.3	0.112

a) and b) with respect to HA.

To determine the real composition of the nanogels ^1H -NMR spectroscopy was used. In Figure 2 the ^1H -NMR spectrum of the nanogel prepared using a HA:PEGMA ratio of 60:40, with 2.5 mol% EGDMA is shown.

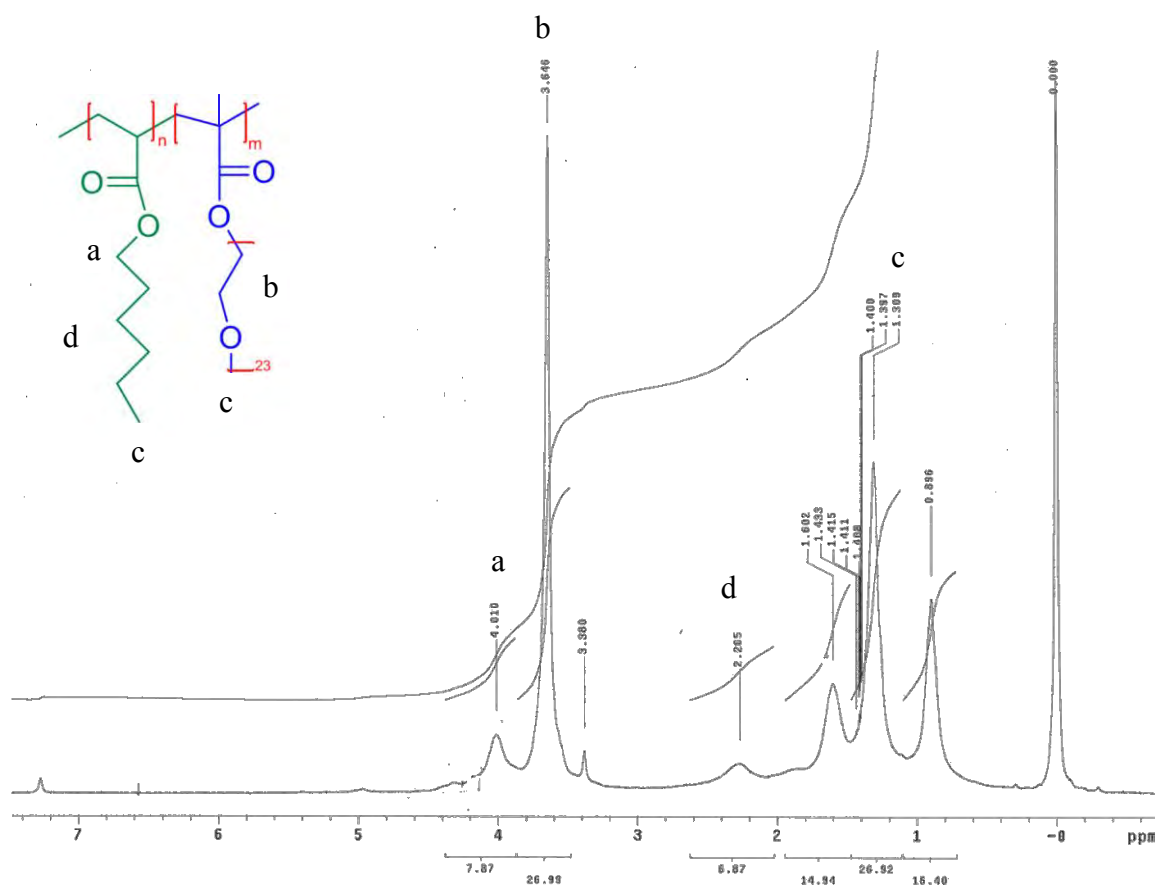


Figure 2 ^1H -NMR analysis of nanogels prepared with a HA:PEGMA ratio (60:40) and 2.5 mol% EGDMA.

Characteristic signals corresponding to PEGMA units and to poly(HA) units, can be observed. Nanogel composition was calculated using the signal corresponding to methylene linked to the ester oxygen of HA at ~ 4 ppm and the methylene signal of the PEG attached to oxygen at ~ 3.6 ppm. This calculation reveals that the nanogel contains 63 mass% of poly(HA) and 37 mass% of PEGMA, which coincides greatly with the theoretical content as prescribed by the synthesis recipe.

Conclusions

It has been shown that core shell nanogels with a core of poly(n-hexyl acrylate) and a shell of polyethylene glycol can be prepared by a surfactant-free (soap-less) emulsion polymerization method. A variety of nanogels of sizes ranging from 26 nm to 176 nm were prepared with good PDI and monomodal size distributions varying different parameters such as ratio of HA:PEGMA and concentration of crosslinker. The real composition of the nanogels is close to the expected one from the recipe, however a little bit higher content on HA was observed by ^1H -NMR. Further characterization results from thermal analysis (not discussed here) confirm the identity and core-shell architecture of the prepared nanogels. Due to their sizes and PEGylated shell, this nanogels have potential to be used as biomaterials.

Acknowledgements

This investigation is supported by the grant No. 174378 CONACYT-CNPq México-Brasil en Nanotecnologías 2011. We thank I.A. Rivero for NMR measurements.

References

- [1] Salgado-Rodríguez, R. New smart temperature sensitive gels and methacrylic derivatives containing pH hydrophobic spacers. Doctoral Thesis in Chemical Sciences, Instituto Tecnológico de Tijuana, Centro de Graduados e Investigación, Tijuana, B.C., **2003**, p 40-43.
- [2] S. Kadlubowski, J. Grobelny, W. Olejniczak, M. Cichomski, and P. Ulanski, *Macromolecules* **36**, 2484-2492 (2003).
- [3] S. Vinogradov, E. Batrakova, and A. Kabanov, *Colloids Surf., B: Biointerfaces* **16**, 291-304 (1999).
- [4] M. Shahiner, W.T. Godbey, G.L. McPherson, V.T. John, *Colloid. Polym. Sci.* **284**, 1121-1129 (2006).
- [5] P. Ulanski and J. Rosiak, *J. M. Nuclear Instruments and Methods in Physics Research*, **151**, 356-360 (1999).
- [6] L. Wen-Chuan, L. Yuan-Chung and C. I-Ming, *Macromol. Biosci.* **6**, 846-854 (2006).
- [7] J. Oh, S. Bencherif and K. Matyjaszewski, *Polymer*. **50**, 4407-4423 (2009).

PRECURSOR MICROEMULSION TO PREPARE CORE-SHELL POLYMERIC NANOPARTICLES FOR PHARMACEUTICAL APPLICATIONS. FORMATION, STABILITY AND CYTOTOXICITY

Sergio E. Flores Villaseñor,¹ René D. Peralta,¹ Jorge C. Ramírez,¹ Daniele Ribeiro,² Tiago Rodrigues.²

¹*Departamento de Procesos de Polimerización Centro de Investigación en Química Aplicada (CIQA), Blvd. Enrique Reyna No. 140, Saltillo Coahuila, México.*

²*Universidade Federal Do ABC, Centro de Ciências Humanas e Naturais, Rua Santa Adelia, 166. Santo André, SP, Brasil.*

e-mail for corresponding author: senrike.floresv@gmail.com

Abstract

The preparation of biocompatible normal microemulsions (ME) with different oil phases (peppermint oil, trans-anethole, vitamin E, jojoba oil) and stabilized with d- α polyethylene glycol succinate (TPGS-1000) and isobutanol (iso-BuOH) is presented. Results of average particle diameter determination, D_p , by dynamic light scattering, indicated $6 \leq D_p \leq 15$ nm and spherical morphology. These ME showed excellent colloidal stability (-40 and + 40 °C) and, without any drug loaded, decreased dramatically, 60 - 90 %, in 24 hours, the viability of leukemia cells (K562). The ME will be loaded with anti-cancer drugs and coated with a pH-sensitive biocompatible polymeric shell to prepare drug delivery nano-devices.

Introduction

The concept of microemulsion was introduced by Professor Jack Shulman at Columbia University in 1943. "A microemulsion is a system of water, oil and amphiphile which is a single, optically isotropic and thermodynamically stable liquid solution"[1,2,3]. ME have at least three components: a polar and a nonpolar liquid phase (water and oil, respectively) and a suitable surfactant frequently in combination with a co-surfactant such as a short chain aliphatic alcohol[4]. Systems devoid of co-surfactants are the "ternary systems" and those requiring co-surfactants are the "pseudoternary" systems (where the surfactant and co-surfactant are taken together as a single phase)[5,6].

The surfactants are amphiphilic molecules with a polar (hydrophilic) head and a nonpolar (hydrophobic) tail, and the co-surfactants can be short chain alcohols, amines and similar substances. The dispersions are formed when oil, water and surfactant/co-surfactant are mixed in appropriate proportions[5].

ME posses some unique characteristics such as thermodynamic stability (imparting long shelf life), compartmentalized polar and non-polar dispersed nano-domains, ease of preparation, low viscosity, ultralow surface tension and optical transparency[6], forms spontaneously with an average droplet diameter between 10 and 100 nm, and have a definite boundary between the oil and the water phases where the surfactant is located[6]. Due to the existence of both polar and non-polar microdomains, both hydrophilic and lipophilic drug molecules could be solubilized, encapsulated and stabilized in these microscopically heterogeneous and macroscopically homogeneous systems[6].

Oil in water microemulsions have been proposed as aqueous based delivery vehicles for a range of drugs[4]. In this case, the ME should be less viscous for intravenous application so as not to cause pain on injection, and it should not be hemolytic[5].

The biocompatible microemulsion system is a relatively new “drug delivery system” for pharmaceutical application. A significant number of microemulsion systems is reported in the literature, but the systems are of divergent composition. This poses a hurdle to data correlation and meaningful clinical uses[6]. ME systems have considerable potential to act as drug delivery vehicles by incorporating a wide range of drug molecules due to the facts that: they are thermodynamically stable and inexpensive, they are used in a wide range of pharmaceutical and cosmetic formulations, they are used as a vehicle for topical, oral, nasal and transdermal applications, they act as penetration enhancers and super-solvents of drugs, they have long shelf life, wide applications in colloidal drug delivery systems for the purpose of drug targeting and controlled release, also the ME can be sterilized by filtration[3].

ME are prepared by the spontaneous emulsification method (phase titration method) and can be studied with the help of phase diagrams. Construction of phase diagrams is a useful approach to study the complex series of interactions that can occur when different components are mixed. Pseudoternary phase diagrams are constructed to find the different zones including the microemulsions zone, in which each corner of the diagram represents 100 % of the particular component. The region can be separated into W/O, bicontinuous or O/W ME by simply considering the composition, that is whether it is oil rich or water rich[3].

ME are an attractive technology platform for the pharmaceutical formulator since they are thermodynamically stable, possess excellent solubilization properties, and their formulation is a relatively straightforward process. These properties as well as their ability to incorporate drugs of different lipophilicity stand out as an appropriate system for drug delivery intravenously, e.g., paclitaxel[6].

Experimental

2.1 Materials

TPGS-1000, iso-BuOH, trans-anethole and (\pm) tocopherol (Vitamin E) were purchased from Sigma Aldrich, peppermint oil was commercial grade (Productos del Roble de Guadalajara, Jalisco, México) and de jojoba oil commercial grade (Pranarom, Pranarom España s.l., Sant Cugat del Vallès), leukemia cells (K562) were provided from Natural and Human Sciences Center from the Federal University of ABC, Brasil. 3-(4, 5-dimethylthiazol-2-yl)-2, 5-diphenyltetrazoliumbromide (MTT) was obtained from Sigma Chemical Co. (St. Louis, MO, USA). Dulbecco's modified eagle medium (DMEM), penicillin and fetal bovine serum were obtained from Invitrogen (Ontario, Canada).

2.2 Methods

2.2.1 Preparation of Microemulsions

A set of ME were prepared by the titration method. A ratio of water to surfactant 90/10 (w/w) was used to obtain a micellar solution. The oily phase (peppermint oil, trans-anethole, vitamin E and jojoba oil) was added dropwise until a change in turbidity was detected visually, indicating that the limit of the microemulsion region had been reached. Then, enough micellar solution was added to turn the system transparent.

2.3 Characterization of microemulsions

2.3.1 Mean droplet size

The droplet size of the ME was measured by dynamic light scattering (DLS) (Nanotracer wave, Microtrac) at 25 °C.

2.4 Stability test.

The microemulsions were subjected to a colloidal stability test: heating (40 °C) and freezing (-40 °C) cycles for 24 hours analyzing the droplet size, these cycles were carried out during 21 days.

2.5 Cytotoxicity test

Cytotoxicity tests were carried out for all the ME prepared, using a cell culture of leukemia cells during 24 hours with a medium DMEM at 10 % FBS and 1 % penicillin. The tests were carried out placing 2×10^6 cells into a 96 wells plate with 200 μL of cell suspension for adherence; they were kept in storage during 24 hours at 37 °C, under 5 % CO_2 . After this time, different volumes of microemulsions were added to the wells. The plates were stored under the same conditions mentioned above. After 24 hours contact time of the microemulsion with the cells, the MTT assay was carried out to determine the viability[7,8].

Results and Discussion

3.1 Microemulsions preparation

Phase diagrams were the point to start work with the objective to determine the macroscopic phase behavior of the ME and to compare the effect of different oil phases. To illustrate the results, the pseudo ternary diagram water/trans-anethole/TPGS-1000/iso-BuOH will be shown and only the boundaries between the single and multi-phase regions were identified as shown in Figure 1.

The short chain alcohol iso-BuOH (cosurfactant) was combined with d- α tocopherol polyethylene glycol 1000 (surfactant) to form the ME. With iso-BuOH partially incorporated in the polar parts of the lipid layers, there is an increase in the area of each lipid molecule polar head group. As a result, the spontaneous curvature of the lipid layers towards the oil changes, thereby decreasing the stability of the lamellar liquid crystalline phase and increasing the isotropic single phase region that is seen with systems containing lecithin:buthanol[9].

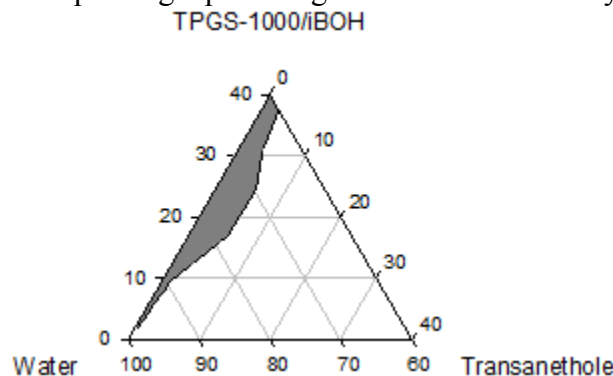


Figure 1. Pseudo ternary phase diagram composed of water, trans-anethole, TPGS-1000 and iso-BuOH as surfactant and co-surfactant (51:49 w/w), respectively. All the systems were prepared at 25 °C. The grey area represents the o/w microemulsion region.

Pseudo ternary phase diagrams were prepared for each oil phase, and four transparent ME with droplet sizes between 6 and 15 nm were selected. These nanometric droplets sizes enables ME to be sterilized by filtration[3].

3.2 Stability Test

All the ME were subjected to freezing-heating (-40 and + 40 °C) cycles, with the objective to determine the colloidal stability under thermal stresses. The stability test is one of the most

important tests for ME in the pharmaceuticals area due to the fact that the drug preparation must be stable and keep the quality specifications and this test allows know the kind of changes occurring in the microemulsion during storage under different environmental conditions. The Official Mexican Standard (NOM-073-SSA1-2005) sets that for a known drug the stability test must be for a long time in cycles of 30 °C and 2 °C during a year. In this work the stability test was run in a short time but under more extreme conditions. The results are shown in Figure 2.

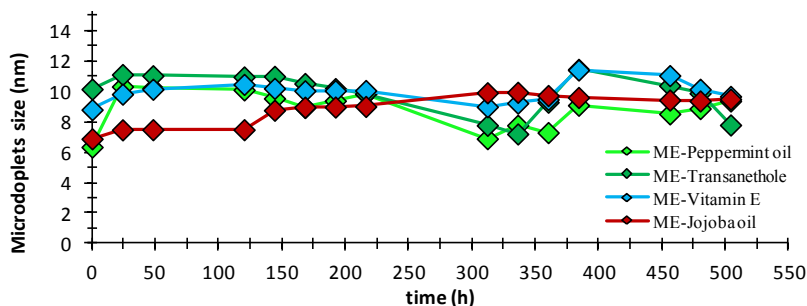


Figure 2. Evolution of the droplet size in microemulsions under freezing-heating (-40 and +40 °C) cycles during 21 days.

It can be observed in Figure 2 that all the ME were stable during 21 days under extreme conditions (2-3 nm variation between day 0 and day 21). This behavior is good for the ME because shows that these systems do not lose their integrity when subjected to temperature stress and retain their size which is a desirable feature to be used as drug delivery systems.

3.3 Cytotoxicity of microemulsions

All the ME were tested in leukemia cells (K562). After 24 hours of treatment with the ME the MTT assay was used to determine the cell viability and the results are plotted in Figure 3.

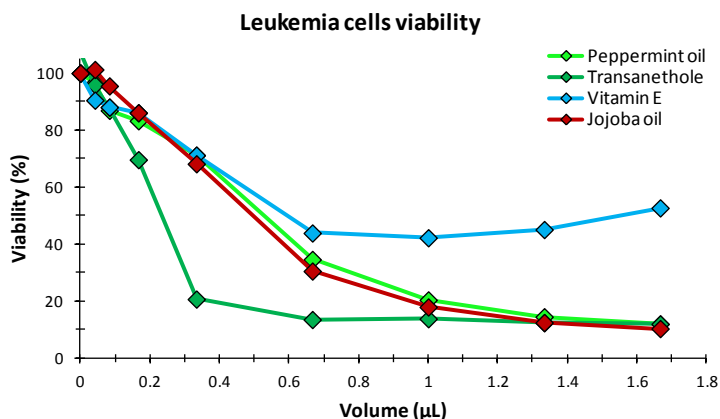


Figure 3. Percent cell viability versus volume of ME added to the wells. Cells were incubated at 37 °C. MTT assay was used to determine cell viability at 24 hours after the treatment.

As can be observed in Figure 3, viability of the cells decreases more drastically with the transanethole microemulsion, where at 0.3 μL the viability is around 20 %, whereas peppermint oil and jojoba oil ME reached the same viability at 1 μL of microemulsion. A less drastic effect was observed for the vitamin E microemulsion which was the less effective versus the leukemia cells, reaching only 50 % of annihilation as the maximum. The observed behavior can be due to the

interaction between de oils with the surfactant (TPGS-1000) at it is reported in the literature that trans-anethole, peppermint oil, vitamin E and jojoba oil are anticancer compounds[10,11,12]. Also the presence of TPGS-1000 has been reported that is capable to induce apoptosis in different culture cancer cells[13]. The important point to mention is that ME without drug are having activity against leukemia cells. These results are good because these ME are composed by essential oils and in consequence are totally Cremophor EL free.

Conclusions

It was possible to prepare ME with different essential oils (peppermint oil, trans-anethole, vitamin E and jojoba oil) and TPGS-1000 as surfactant. All the ME were optically transparent, thermodynamically stables and the droplet sizes were around 6 – 15 nm, and the most important point to mention is that all the ME prepared are totally Cremophor EL free.

In the stability test the variation in droplet size was around 3 nm in all systems, indicating that ME are stable.

In the cytotoxic evaluation the microemulsion prepared with trans-anethole showed the major cytotoxic effect, in other words, with less quantity of microemulsion (0.3 μ L) a major annihilation of leukemia cells (87 %) is reached.

Acknowledgements

Federal University of ABC, Brasil for the cytotoxic assays in leukemia cells (K562). CONACYT Grant CB – 2011/168472. Fellowship to SEFV from CONACYT for his Ph. D. studies at CIQA.

References

- [1] T.P. Hoar and J. H. Schulman, *Natura Letters to the editors*.152, 102 (1943).
- [2] I. D. Lindman and Björn, *Colloid Surf. A-Physicochem. Eng. Asp.*, 391-392 (1981).
- [3] K. S. Kumar, D. Dhachinamoorthi, R. Saravanan, U. Gopal, V. Shanmugam, *Int. J. Pharm. Sci.*, 10 (2), (2011).
- [4] J. L. Burguera and M. Burguera, *Talanta*, 96, 11-20 (2012).
- [5] S.P. Moulik, *J. Pharm. Sci.*, 97 (1), 22-45 (2008).
- [6] S. Gupta, *Curr. Sci.*, 101 (2), 174-189 (2011).
- [7] Type A, Collection C. MTT Cell Proliferation Assay Instruction Guide, 1-6 (2011).
- [8] Lab W and P. Proliferation Assay: MTT Protocol, 3-4 (2007).
- [9] K. Shinoda, M. Araki, A. Sadaghiani, A. Khan, B. Lindman, *J. Phys. Chem.*, 95, 989-993 (1991).
- [10] F. Bakkali, S. Averbeck, D. Averbeck, M. Idaomar, *Food Chem. Toxicol.*, 46 (2), 446-475 (2008).
- [11] Y. Nakagawa, T. Suzuki, *Biochem. Pharmacol.*, 66 (1), 63-73 (2003).
- [12] R. Truhaut, B. L. Bourhis, M. Attia, R. Glomot, J. Newman, J. Caldwell, *Food Chem. Toxicol.*, 27 (1), 11-20 (1989).
- [13] T. Weber, M. Lu, L. Andera, H. Lahm, N. Gellert, M. W. Fariss, V. Korinek, W. Sattler, D. S. Ucker, A. Terman, W. Erl, U. T. Brunk, R. J. Coffey, C. Weber, *Clin. Cancer. Res.*, 8, 863-869 (2002).

NEW HIGH FREQUENCY RELAXATION IN CHITOSAN AND PVA

S. Kumar-Krishnan¹, E. Prokhorov¹, G. Luna-Barcenas¹, A. Mauricio-Sanchez¹, O. Arias de Fuentes^{1,2}

¹ CINVESTAV del IPN, Unidad Queretaro, Mexico.

² Instituto de Ciencia y Tecnología de Materiales de la Universidad de La Habana, Cuba.

Abstract

In this work, for first time, a high frequency ($1 \cdot 10^9$ - $3 \cdot 10^9$ Hz) relaxation process has been observed in chitosan and PVA films in the temperature range of 4⁰C to 130⁰C. This relaxation exhibits negative activation energy below the glass transition temperature and positive values at above Tg. The high frequency relaxation process and its temperature dependence can be attributed to the interaction of the bounded water and the changes of energy and freedom of movement of side molecular chains groups. This conclusion has been supported by in-situ FTIR measurements. A possible scenario of this relaxation and dynamics of molecular motion is proposed.

Introduction

Chitosan and poly(vinyl alcohol) (PVA) are used in a wide variety of applications which include the biomedical field, sensors, the food industry, and fuel cells, among others. Because of all the above applications, it is important to fully characterize the properties of these polymers in solid state. Some of these properties include their physical, physicochemical and dielectric relaxations, including the molecular mobility that occurs within the polymeric structure in both wide frequency and temperature ranges.

It is noteworthy that both polymers exhibit high water absorption due to interaction of side groups (OH in PVA and OH/NH₂ in chitosan) with water molecules mainly through hydrogen bonding. The amount of water in hygroscopic materials, such as chitosan and PVA is generally a dominant factor in their performance as biomaterials. The plasticizing effect drastically affects the Tg and related α -relaxation, which corresponds to the segmental motion of chains [1, 2].

Additionally, very complex supramolecular structures of hygroscopic polymers with intra and intermolecular hydrogen bonds depend upon of water content such that it can give rise to the appearance a new relaxation process in the high frequency domain. It has been previously reported a dielectric relaxation at 1 GHz frequency for different hygroscopic solids [3]. The polymer chain restricts the orientation of water molecules such that the collective motions of the macromolecule-water are distorted giving rise to relaxation times about 100 times as slow as that of pure water [4]. This relaxation can be attributed to the breakage of hydrogen bonds between adjacent water molecules in thin films in microwave frequencies. The high frequency dielectric relaxation in the aqueous solutions of biopolymers [4] and in the PVA aqueous solutions [5] have been previously observed. However, to the best of our knowledge, there is no report in the literature about the molecular origin of the dielectric relaxation properties of chitosan and PVA films in the gigahertz (GHz) frequency range. High frequency dielectric relaxations are important to fully understand the physicochemical and electrical properties of polymer material including the molecular mobility, dielectric relaxation and hydrogen bonding structure. Dielectric spectroscopy is a relevant technique to probe translational or rotational molecular motions and hydration properties with high sensitivity [6].

The objective of this work is to investigate the temperature-dependent dielectric relaxation behaviors of chitosan and PVA films in the frequency range of 1 MHz to 3 GHz and temperature range of 4 to 130⁰C using dielectric spectroscopy.

Experimental

Chitosan (CS), 86% of degree of deacetylation ($M_w = 350,000$ g/mol) and PVA ($M_w = 89,000$ – $98,000$ g/mol) was purchased from Sigma-Aldrich. CS films were obtained by dissolving 1 wt % of CS in a 1 wt % aqueous acetic acid solution with subsequent stirring to promote dissolution. To remove acetic acid, chitosan films were immersed into a 0.1M NaOH solution during 30 min and washed with distilled water until neutral pH. PVA films were obtained by the dissolution of a known amount of PVA in water to obtain a 7.8 wt % solution under stirring. The films with thickness *ca* 40 μm have been prepared by the solvent-cast method. A thin layer of gold was vacuum-deposited onto both film's sides to serve as electrodes.

Dielectric spectroscopy measurements were carried out using Impedance Analyzers Agilent E4991A (in the frequency range 10^6 – 3×10^9 Hz). The high frequency measurements were carried out in the cell in the bench-top temperature chamber SU-261. FTIR was performed on a Spectrum GX (Perkin–Elmer) with in situ temperature controller in the temperature range of 25°C to 110°C .

Results and Discussion

Figure 1 shows a typical dependence of the dielectric loss (ϵ'') with frequency of as-prepared chitosan (Fig. 1a) and PVA (Fig. 1b) films with water content *ca* 6–10 wt. % (according to TGA measurements) at four different temperatures. The dielectric loss (ϵ'') in both films shows a well-pronounced maximum at frequencies between 0.5–3 GHz. The fitting of the complex permittivity in chitosan and PVA films were carried out using the well-known Cole-Cole empirical model:

$$\epsilon^* - \epsilon_\infty = \frac{\epsilon_s - \epsilon_\infty}{[1 + (j\omega\tau)^\alpha]}$$

where $\epsilon_s - \epsilon_\infty$ and ϵ_∞ are the dielectric relaxation strength and the dielectric constant in the high frequency limit, respectively; τ is relaxation time. The exponents α introduce a symmetric broadening of the relaxation.

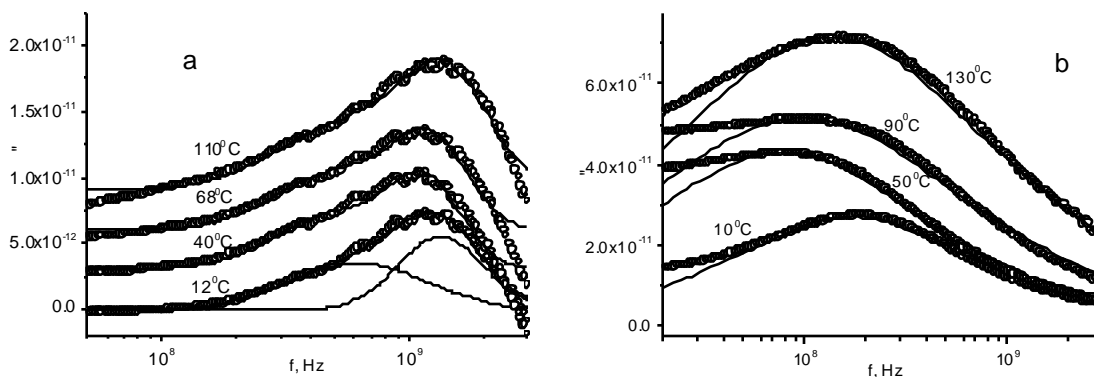


Fig. 1. Dielectric loss factor (ϵ'') versus frequency for chitosan (a) and PVA (b) films measured at the indicated temperature (continuous-lines: fitting using Cole-Cole model).

In the case of PVA films one symmetrical relaxation process has been observed with a maximum at frequency *ca.* 1.8×10^8 Hz. In the chitosan films, due to non symmetrical shape of the dependencies of the dielectric loss with frequency, the impedance response has been calculated as the sum of two Cole-Cole contributions with two maximum frequencies *ca.* 5.8×10^8 and 1.3×10^9 Hz (tagged as p1 and p2).

Figures 2a and 2b show the dependencies of relaxation time *versus* reciprocal temperature for chitosan (peaks 1 and 2). Fig. 2c shows dependence of relaxation time *versus* reciprocal temperature for PVA film in the process of heating.

Below the glass transition temperature (54°C for chitosan and 65°C for PVA, respectively) the temperature dependence of relaxation time τ for both polymers can be described by Arrhenius-type dependence: $\tau = \tau_0 \exp(E_a/RT)$ (where E_a is activation energy), with negative activation energy indicated on Fig. 2. Above the glass transition temperature the activation energies change slope from negative to positive values. Values of glass transition temperatures have been determined from low frequency dielectric measurements ($0.1\text{--}10^5$ Hz) by using the methodology previously described by our group [1, 2, 7].

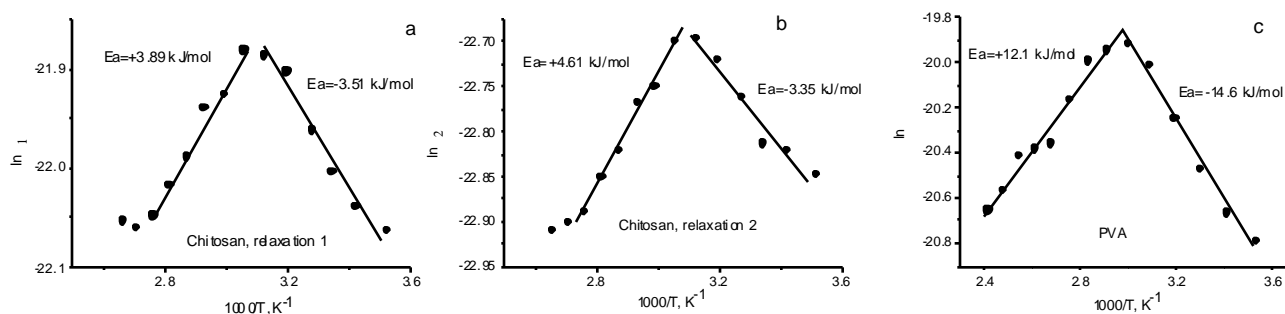


Fig. 2. Temperature dependence of relaxation times versus $1/T$ for chitosan film (a and b) and for PVA (c). Lines represent Arrhenius-type dependence fitting.

To understand which groups of chitosan and PVA are responsible for high frequency relaxation, we carried out temperature-dependent FTIR measurements on films under the same heating process (analogously to dielectric spectroscopy measurements). Figure 3 shows FTIR spectra of chitosan (Fig. 3a) and PVA (Fig. 3b) films in the process of heating at the temperature indicated on graph.

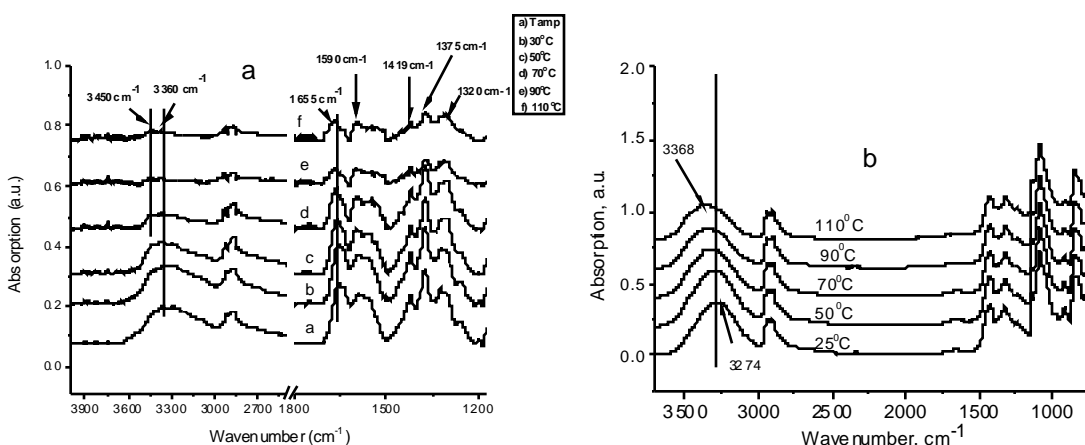


Fig. 3. FTIR Spectra of chitosan (a) and PVA (b) films in the process of heating

For the case of chitosan films, during the process of heating, there are two relevant changes observed: 1) reduction of intensity and broadening of the band centered at 3360 cm^{-1} which shifts to 3440 cm^{-1} and 2) the band at 1635 cm^{-1} shifts to 1655 cm^{-1} . These changes could be reflecting the change of the hydrogen bonded structure of the chitosan film due to elimination of adsorbed water [8] and the breaking of intra-chain hydrogen bonds between water molecules and NH or OH

groups in the chitosan molecule.

The main changes observed in FTIR spectra of PVA films during the process of heating are the shifting of band at 3274 cm^{-1} to higher wave number values (3368 cm^{-1} at 110°C). According to the literature [9], this band is associated with stretching vibration of $-\text{OH}$ groups due to interaction with both inter and intra-molecular hydrogen bonds.

In summary, FTIR measurements show that bonding structure of $-\text{OH}/\text{NH}_2$ in chitosan and OH side groups in PVA change with temperature; therefore these groups are likely to be responsible for observed high frequency relaxation process.

Negative activation energies at the MHz frequency range have been observed in hydrated lysozyme, in hydrate collagen and calcified and decalcified bone. Most explanations for this negative activation phenomenon that are reported in the literature are based on the suggestion that the activation process involves the breaking of a hydrogen bond between surrounding molecules and a water molecule and the formation of more stable hydrogen bonds between reoriented water molecules [10]. On the other hand, high frequency relaxation at the frequency $5.6 \cdot 10^8\text{ Hz}$ has been observed in the aqueous PVA solutions at room temperature [5] and it has been identified as the exchange of hydrated water molecules to the OH groups of the PVA monomer units. This frequency is remarkably close to the frequency $1.8 \cdot 10^8\text{ Hz}$ at which we observed the high frequency relaxation in PVA solid films.

Additionally, the molecular dynamics simulation of OH side groups in poly(vinyl alcohol) [11] considers a motion of these groups between two sites separated by an energy barrier which appears due to the presence of intermolecular and intramolecular hydrogen bonds. In PVA the presence of intermolecular and intermolecular hydrogen bonds are responsible for hydroxyl side groups to have two energy minima with difference in energy of 5.5 kJ/mol and only 8% of groups have average energy 10 kJ/mol . This value of energy is close to the value of positive activation energy ($+12\text{ kJ/mol}$) observed in PVA films at the temperatures above the glass transition temperature.

In the case of chitosan two relaxations processes have been observed which can be related to changes in the structure of chitosan; it has two $-\text{OH}$ and a $-\text{NH}_2$ side groups. Investigations of chitosan and chitosan in acetate form allowed us to conclude that process 1 (p1) relates to relaxation of $-\text{OH}$ side groups and relaxation process 2 (p2) can be related to relaxation of NH_2 side groups [7].

Based upon the above analyses, it is possible to propose a plausible scenario of high frequency relaxation and dynamics of the molecular motions in chitosan and PVA films.

At temperatures below glass transition temperature, negative activation energy can be related to the reorientation of intermolecular hydrogen bonds between water and OH/NH_2 in chitosan and OH groups in PVA. This effect changes the symmetry of hydrogen bonding of the side groups and, as a result, energy of these groups is lowered; consequently, a negative activation energy is observed. At temperatures higher than T_g the amplitude of the random thermal motions of chains increases leading to breaking of hydrogen bonds between water molecules and OH/NH_2 in chitosan and OH groups in PVA. Additionally, upon further heating (according to TGA measurements) the loss of water affects the molecular relaxations of lateral groups thus exhibiting normal relaxation processes with positive activation energy.

Conclusions

For the first time, a new relaxation process in the gigahertz frequency range has been reported in chitosan and PVA films using impedance spectroscopy. Upon heating and below the glass transition temperature, both polymers exhibit an Arrhenius-like dependence with negative

activation energy due to the disruption of the symmetry of hydrogen bonding between water molecules and OH/NH₂ side groups. Upon further heating (above the glass transition) the activation energy changes slope from negative to positive values due to breaking of hydrogen bonds between water molecules and OH/NH₂ groups and water evaporation. This relaxation of side groups exhibits normal process with positive activation energy.

Acknowledgements

This work was partially supported by CONACYT of Mexico. The authors are grateful to J.A. Muñoz-Salas for assistance in electrical measurements.

References

- [1]. J. González-Campos, E. Prokhorov, G. Luna-Bárcenas, A. Fonseca-García, I.C. Sanchez. J. Polym. Sci., Part B, 47, 2259 (2009).
- [2]. J. Betzabe Gonzalez-Campos, Z.Y. Garcia-Carvajal, E. Prokhorov, G. Luna-Barcenas, et al., J. Appl. Polymer Sci., 125, 4082 (2012).
- [3]. J.H. Christie, S.H. Krenek, I.M. Woodhead, Biosystems. Eng., 102, 143 (2009).
- [4]. Y. Hayashi, N. Shinyashiki, S. Yagihara, J. Non-Cryst.Solids, 305, 328 (2002).
- [5]. Y. Satokawa, T. Shikata, Macromolecules, 41, 2908-2913 (2008).
- [6]. F. Kremer and A. Schonhals, Broadband dielectric spectroscopy, (Springer, 2003).
- [7]. S. Kumar-Krishnan, E. Prokhorov, M. Ramirez, et al. Soft Matter, (2014).
- [8]. A. Nogales, T.A. Ezquerro, D.R. Rueda, F. Martinez, J. Retuert, J. Colloid. Polym. Sci., 275, 419 (1997).
- [9]. A. Uda, S. Morita, Y. Ozaki, Polymer, 54, 2130 (2013).
- [10]. R. Pethig, Annu. Rev. Phys. Chem., 43, 177 (1992).
- [11]. A. De La Rosa, L. Heuxa, J.Y. Cavaille, K. Mazeau, Polym. 43, 5665 (2002).

Estimation of Surface Free Energy of Poly (lactic Acid) during UV-Grafting with N-Vinylpyrrolidone

Mario H. Gutierrez-Villarreal¹, Francisco J. Rodríguez-Gonzalez¹, Yibran Perera-Mercado¹
Centro de Investigación en Química Aplicada¹, Departamento de Procesos de Transformación de Plásticos, Blvd. Enrique Reyna Hermosillo N° 140, Col. San José de los Cerritos, C.P. 25294, Saltillo, Coahuila México.

Abstract.

The surface free energy (SFE) of polylactic acid (PLA) during grafting with N-vinylpyrrolidone (NVP) was determined from contact angle measurements using the vOCG, Fowkes', and Owens-Wendt methods (Harmonic and Geometric mean approximation equations). A good correlation between the results of the three methods was found. Polymer film was obtained by melt extrusion and grafted with NVP using UV light and benzophenone (BP) as photoinitiator. Comparison of SFE results with those from the literature for pristine PLA showed that the correlation depends on the method used for contact angle determination and the properties of the liquids used for this measurement. This finding might promote the rational design of surface modification of biocompatible films.

1. Introduction

In recent years there is a growing interest on the use of polymers derived from renewable resources in different fields; with respect to the biomedical field, the biocompatibility of polymers is critically dependent on surface properties; processes such as cell adhesion and protein adsorption on polymer surfaces are generally accepted to be influenced by polar and dispersion components of surface free energy. Some research groups have studied the interactions of different types of cultured cells or blood proteins with various solid substrates (mainly polymers) with different grade of wettability to correlate the relationship between surface free energy and cell or blood compatibility [1,2]

Poly(lactic acid) (PLA) has been widely investigated for biomedical applications because it is biodegradable, bioresorbable, and biocompatible [3,4]. This polymer has several applications in tissue and surgical implant engineering, like production of: artificial ligaments, hernia repair meshes, scaffolds, screws, surgical plates, and suture yarns [5,6]. To make this material more attractive for some applications, some properties should be improved, namely surface free energy [7].

The knowledge of surface tension is thus of great interest for every domain involved in understanding these mechanisms mainly on topics related with the biomedical and pharmaceutical applications. The aim of the present work is to determine the change of SFE of the PLA surface film during grafting process with NVP and to examine differences on SFE values between various methods of evaluation.

The value of the contact angle θ with water indicates how hydrophobic the surface is: a large contact angle (or small $\cos \theta$) corresponds to a hydrophobic surface, whereas a small contact angle (or large $\cos \theta$) implies a hydrophilic surface

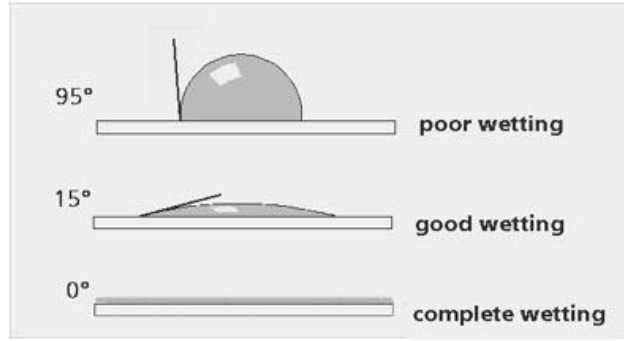


Fig. 1 Wetting grade of a surface

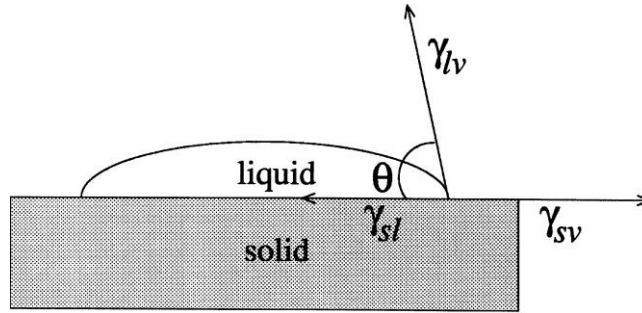


Figure 2. Equilibrium between solid, liquid and gas

2. Experimental Procedure

2.1 van Oss–Chaudhury–Good Approach

Determination of the surface energy of solids by the vOCG method requires the use of three probe liquids. The set of the measuring liquids has to include two bipolar liquids and one apolar. [8]. In this approach are recognized two types of energy: the dispersive energy also called the *Lifshitz–van der Waals energy* where ($\gamma_s^{LW} = \gamma_s^d$) and the polar surface energy, which is called the *acid/base surface energy* where ($\gamma_s^{AB} = \gamma_s^p$), it is calculated from the acid/base property. That is, the electron acceptor/donor or hydrogen bond donor/acceptor properties (γ_s^+ , γ_s^-) of the solid as follows:

$$\gamma_s^p = \gamma_s^{AB} = 2[\gamma_s^+ \gamma_s^-]^{0.5} \quad (1)$$

As a result, the total surface energy is expressed in terms of three surface-energy parameters (γ_s^{LW} , γ_s^+ , γ_s^-):

$$\gamma_s^{TOT} = \gamma_s^{LW} + \gamma_s^{AB} = \gamma_s^{LW} + 2[\gamma_s^+ \gamma_s^-]^{0.5} \quad (2)$$

Thus, three probe liquids will be required to determine the total surface energy of polar solids with this method.

2.2 Owens and Wendt approach

The measurement of surface energy of a film by this approach implies to divide the surface energy of a solid surface into dispersive and polar components [9, 10].

Dispersive component arises from molecular dispersive interactions generated by movement of electrons around an atom or molecule. Polar component results from polar interactions such as hydrogen bonds, covalent bonds and dipole–dipole interactions. This method was initially proposed by Girifalco and Good in 1957 [11] to estimate the surface tension of polymers from the contact angle measurements with water and methylene iodide.

Considering dispersion and hydrogen bonding-dipole components of the surface tension, they obtained the more general form for the equation:

$$\gamma_L(1+\cos\Theta) = 2(\gamma_s^d \gamma_l^d)^{1/2} + 2(\gamma_s^p \gamma_l^p)^{1/2} \quad (3)$$

The surface tension of a solid can then be determined by using this equation applied for two liquids: this approach is also commonly named the two-liquids method.

2.3 Fowkes' approach

According to Fowkes [12] who considers that the total free energy at a surface is the sum of contributions from the different intermolecular forces at the surface, the surface tension can be described by:

$$\gamma = \gamma^d + \gamma^p \quad (4)$$

where γ^d is the dispersive and γ^p is the polar part of the surface tension. The polar component includes various dipole interactions, hydrogen bonding and metallic bonding. This assumption, reflecting the intermolecular energy between two materials, results from the sum of a dispersion component and a polar component. This method is applied for a system where only London dispersion forces operate between two contacting phases S and L then, the work of adhesion is given by the following equation:

$$W_{SL}^d = 2(\gamma_s^d * \gamma_l^d)^{0.5} \quad (5)$$

This expression is equivalent with the Young-Dupre $W_{SL} = \gamma_L(1+\cos\Theta)$ equation so that

$$\gamma_s^d = (1/4\gamma_l^d) [\gamma_L^2 (1 + \cos \theta)^2] \quad (6)$$

2.4 Experimental

2.4.1 Materials

PLA pellets 3001D were supplied by Cargill Dow LLC, 1-vinyl-2-pyrrolidinone (Aldrich) was purified by vacuum distillation before using. The photoinitiator benzophenone (BP) was analytical grade used without further purification, diiodomethane -99% (Aldrich) was used as received.

2.4.2 Sample Preparation

Preparation of PLA film was carried out by melt extrusion process in absence of additives, the nominal film thickness was 30 μm . A sample (5 x 5 cm^2) was prepared for UV irradiation, where a UV processor (Model No. 60000; Oriel Corporation) was used. The processor was equipped with a 100-W mercury arc lamp (Model No. 8261; Oriel Corporation) having a wavelength range of 232-500 nm and intensity of $\sim 25 \text{ mW/cm}^2$ at 365 nm.

2.4.3 Grafting Polymerization Procedure

Photografting procedure was carried out using the method followed by Ping Deng and coworkers [26], in our work a 10 μl sample of water solution (75 wt % of monomer and 3 wt % of benzophenone) pre-purged with nitrogen, was deposited between two PLA films with a microsyringe and pressed into a thin and even liquid layer. The system was laid on the holder under nitrogen atmosphere and irradiated with UV light, keeping a distance from the UV lamp to the films of 30 cm. The irradiation time was varied in order to control the degree of polymerization. A control film was prepared following the same procedure without UV irradiation.

3.0 Results and Discussion

3.1 Contact Angle

Pristine PLA film exhibits a water contact angle of $72^\circ \pm 1^\circ$ and after 10 minutes of irradiation, a value of $36.6^\circ \pm 1^\circ$ was obtained, which indicates a substantial modification of the PLA surface during the irradiation process. A reduction of $\sim 25\%$ from the original value after the first minute clearly shows that NVP grafting occurred immediately after UV exposure.

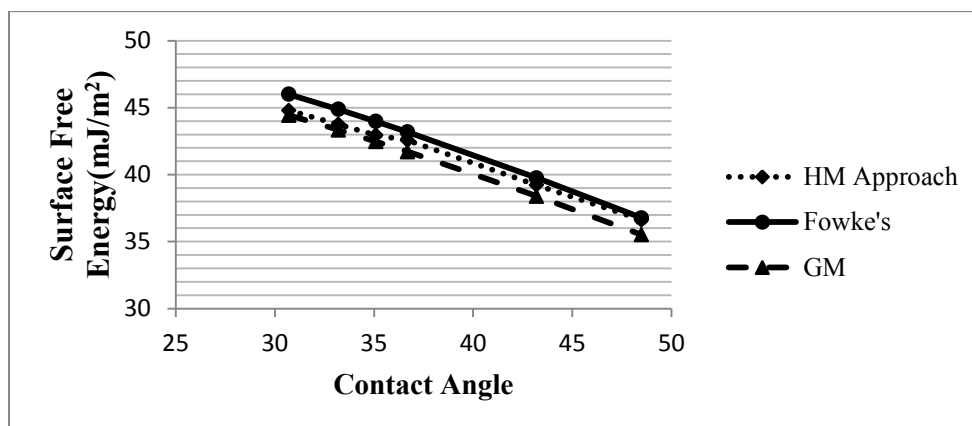
Table I Surface Tension Data of Liquids Used for Contact Angle Measurements

Probe liquid	γ_L (mJ/m ²)	γ_L^d (mJ/m ²)	γ_L^p (mJ/m ²)
Water	72.8	21.8	51
Glycerol	63.4	33.4	30
Diiodomethane	50.8	48.5	2.3

Table II Surface Free Energies (mJ/m²) values calculated with three different methods using Diiodomethane as non-polar liquid.

Time in minutes	Contact Angle	Fowke's Method	Harmonic Mean Method	Geometric Mean Method
0	30.7	46.01	44.80	44.44
1	33.2	44.87	43.76	43.34
3	35.1	43.97	42.95	42.47
5	36.7	43.18	42.57	41.71
7	43.2	39.76	39.22	38.40
9	48.5	36.77	36.63	35.51

Fig. 3 Comparison of surface free energy for grafted PLA versus Contact Angle with HM, Fowke's and GM methods using Diiodomethane as non-polar probe liquid.



4.0 Conclusions

The SFE values of the NVP grafted PLA films calculated under different approaches, show a little difference between them that could be related to different performing conditions of the CA measurements, the nature of the selected liquids used in the CA measurements and to existing differences in the mathematical formulae used; however, the fact that different approaches show the same tendency with similar values, the use of these methods will allow to understand surface tensions of biopolymers. Surface tension characterization of biodegradable films by contact angle measurements appear thus to be a good way to know mechanisms involved in hydration properties of materials.

References

1. P.B. van Wachem, T. Beugeling, J. Feijen, A. Bantjes, J.P. Detmers, W.G. van Aken *Biomaterials* 6:403–8 (1985).
2. J.H. Lee, J.W. Lee, G. Khang, H.B. Lee. *Biomaterials* 18: 351–8. (1997).
3. R. Drumright, P. Gruber, D. Henton, *Adv. Mater.* 12 1841 (2000).
4. H. Tian, Z. Tang, X. Zhuang, X. Chen, X. Jing, *Prog. Polym. Sci.* 37 237 (2012).
5. S. Ramakrishna, J. Mayer, E. Wintermantel, K.W. Leong, *Compos. Sci. Technol.* 62 1189. (2001).
6. I. Armentano, M. Dottori, E. Fortunati, S. Mattioli, J.M. Kenny, *Polym. Degrad. Stab.* 95 2126 (2010).
7. T. Desmet, R. Morent, N. De Geyter, Ch. Leys, E. Schacht, and P. Dubruel; *Biomacromolecules*, Vol. 10, No. 9, (2009).
8. C.J. van Oss, M.K. Chaudhury, R.J. Good, *Sep Sci Technol*, 24, 15–30. (1989).
9. J.H. Han, Y. Zhang, R. Buffo, J.H. Han (ed) *Innovations in food packaging*. Elsevier Academic Press, New York, pp 45–59 (2005).
10. V.P. Cyras, L.B. Manfredi, M.T. Ton-That, A. Vazquez; *Carbohydr Polym* 73:55(2008)
11. E.P. Kalogianni, T. Savopoulos, T.D. Karapantsios, and S.N. Raphaelides, *Colloids and Surfaces. B: Biointerfaces*. 35: 159-167. (2004)
12. F.M. Fowkes, *Attractive forces at interfaces*. *Industrial and Engineering Chemistry*. 56: 40-52.(1964)

NEW AMPHIPHILIC MOLECULES USING RAFT POLYMERIZATION

Isabel Sáenz de Buruaga Yurramendi,¹ Rafael García González,¹ Miguel Ángel Macías Contreras,² Ramiro Guerrero Santos,² Héctor Manuel Tello Mañón¹

¹ Centro de Investigación en Polímeros. Marcos Achar Lobatón 2, Tepexpan. Edo. Mex. México. CP 55885.

² Centro de Investigación en Química Aplicada. Blvd. Enrique Reyna 140, Col. San José de los Cerritos, Saltillo Coahuila. México. CP 25294.

Abstract

A series of random copolymers composed of acrylic acid, styrene and a fluorinated monomer were prepared through RAFT polymerization in view of their possible uses as additives for paints. The monomer addition protocol, temperature and the molar ratio RAFT transfer agent-initiator were varied in trials targeting final solid content of 30 percent and full conversion. The hydrophilic lipophilic balance (HLB) was dependent of the entire incorporation of all involved monomers and projected to be close to 14. At this value, products dilute readily in water and could be used directly in technological applications. The outcome of this experimentation was materialized by some materials with promising properties. Therefore, these materials were optimized to evaluate their performance as additives for color concentrates. In this step, the molecular weight and the narrow molar mass distribution provided by the RAFT process were correlated to their performance.

Introduction

Fluorinated polymers have been extensively used in a broad range of applications including chemical, electronic and mechanical devices, due to its unique properties such as chemical inertness, resistance to solvents, low friction coefficient, repelling properties (non adhesive) which might prevents bacteria from binding to it, biocompatibility, low water absorption, thermal stability until about 260 °C at atmospheric pressure, non flammability, electrical insulating properties, weathering resistance and high radiation resistance. The properties observed in fluorinated polymers arise for the presence of stable and strong C-F and low dipolar moment of the bond.

Even though they are considered as a low volume consume product, and not as a commodity, the demand for fluoropolymers is huge; in 2011, it hit \$7.25 billion. New uses and applications for fluoropolymers are being developed constantly, and as a result, the demand continues to grow. In the particular case of fluorinated coatings, the North American market was valued at \$0.4b in the year 2013, growing at 8.4% annually, and is projected to reach \$0.6b by the end of the year 2018. Fluoropolymers Coating Additives market is expected to grow to 37.8% by the end of the year 2018.¹

Since the invention of TEFLON, different fluorinated polymers have been developed from new fluorinated monomers. However, most of the monomers used were insoluble and high temperature curing processes were required. One of the recent solutions to produce soluble fluorinated polymers was the development of Fluoresters which are similar to common methacrylate monomers, but with the properties of fluorine containing monomer. Unlike polymers whose main chain contains fluorine, this polymer contains fluorine in its side chain. An example of this fluoresters is the 2,2,2-Trifluoroethyl methacrylate (TFEMA) which is a colorless liquid that can be copolymerize with ordinary vinyl monomers such as acrylic esters, styrene, vinyl acetate, and other fluorine-containing acrylic esters, both in solution or in emulsion polymerization process.

The TFEMA can be copolymerized with a wide range of comonomers such as vinyl ethers, *N*-vinylpyrrolidone, methyl methacrylate, methyl acrylate, *n*-butyl methacrylate, methacrylonitrile, acrylonitrile, methyl vinylidene cyanide, styrene. In contrast to other Fluorester like *tert*-butyl- α -trifluoromethylacrylate (TBTFMA), TFEMA can be easily homopolymerized by radical processes. It was also used in grafting polymerization with poly(methyl methacrylate).²

In contrast to many investigations concerning the radical copolymerization of trifluoromethacrylates, several works have been reported during last decade using controlled radical polymerization (CRP) techniques to produce several kind of fluoropolymers. Actually, CRP has attracted attention as a powerful tool to control polymer structures (molecular weight distribution and composition). It has been predicted that the marked of materials obtained by CRP might reach until \$20 billion/year during next years.³

CRP has been investigated since the middle of 1990's leading to several techniques well developed nowadays. This includes some techniques such as nitroxide-mediated radical polymerization (NMP), atom transfer radical polymerization (ATRP), iodine transfer polymerization (ITP), reversed iodine transfer polymerization and reversible addition-fragmentation chain transfer (RAFT).

The interest of this works relays on the potential production of fluorinated molecules through the powerful tool of CRP. Due to their mild conditions, CRP and particularly RAFT polymerization might allow to synthesize different fluoropolymers with interesting applications in the coatings formulation. The aim of this investigation is to explore synthesis of some fluorinated polymers prepared by RAFT polymerization and evaluate its performance as additives for color concentrates such as carbon black, red oxide (inorganic) and blue ftalocianine (organic).

Experimental

The main goal activities of the investigation can be divided in the synthesis of fluorinated copolymers in solvent and aqueous median, and their evaluation as additives in color concentrates.

1. Synthesis of random copolymers via RAFT in organic media

As a reference synthesis, three different experiments were performed using dioxane as organic solvent. A water soluble tritiocarbonate was used as RAFT agent, and a water soluble molecule was used as initiator. Styrene (S), Acrylic acid (AA) and 2,2,2-Trifluoroethyl methacrylate (TFEMA) were used as received without purification. The theoretical mol ratio of ingredients was AA:S:TFEMA:CTA:Initiator 60:10:5:1:0.5 (exp. 1), 70:6:4:1:0.5 (exp. 2), 75:3:2:1:0.5 (exp. 3). Experiments were performed in closed vial adding all the ingredients, degassed during 30 min. with N₂. Reaction was done at 60°C during 12 hours.

2. Synthesis of random copolymers via RAFT in aqueous media.

As in the synthesis in organic media, the reaction was performed at 30% solids w/w and same initiator and RAFT agent were used. The theoretical mol ratio of ingredients was AA:S:TFEMA:CTA:Initiator 60:10:5:1:0.5. Reactions were performed in a 100 mL round bottom flask. Deionized water was initially added and degasses during 30 min. with N₂. Initiator solution, NaOH (equimolar) and monomer mixture were transfer to the flask filled with purged water and reaction started at 60°C during 24 hours. In some cases initiator solution was dosed in time during the reaction. The products obtained were dried and mutilated with trimethylsilyldiazomethane (TMDAM) to render the polymers soluble in THF before they were analyzed by GPC and ¹H-NMR. Different studies were performed to find the best possible conditions to control molecular weight and composition. In this case different reaction temperatures (60, 70 y 80 °C), RAFT:Initiator ratios (1:1.05, 1:1.07, 1:1) and solid content were evaluated. Furthermore a kinetic study was performed to predict how monomers are added in the polymer chain during the RAFT mediated polymerization.

3. Performance as Additives for color concentrates

The last activity consisted in the evaluation of two prototypes as additives for color concentrates. Carbon Black, Red Oxide (Fe₂O₃) and Blue (Ftalocianine) were selected because they represent families of analogous pigments of interest in the coating industry. The dispersion test basically was made by grinding a pigment in water media together with the addition of the fluoropolymers. The tinting strength was an indication of the performance of the fluoropolymer as additive for pigment dispersions when the color concentrates prepared were applied in two different coatings systems: water and oil based.

Results and Discussion

1. Synthesis in organic media.

As shown in results (Table 1), there was a good agreement between theoretical and experimental composition of the molecules determined by ¹H-NMR. Molecular weight determination was performed by GPC to demonstrate that reaction proceed under control (Fig. 1). The kinetic results showed lately (section 2.1) confirmed this fact.

Tabla 1. Random Copolymer of AA, S, TFEMA

Exp.	t (h)	Conversion (%) ^a	Composition AA:S:TFEMA (%w/w) ^b	M _n ^c	Đ ^c
1	16	25	68:17:15	7,800	1.2
2	3	86	77:12:11	8,200	1.2
3	2	93	86:6:8	7,300	1.3

^a Gravimetrically, ^b ¹H NMR, ^cGPC

Solubility test also showed that the copolymers with an AA content of 90% w/w were completely soluble in water meanwhile those with 80% w/w or less were insoluble.

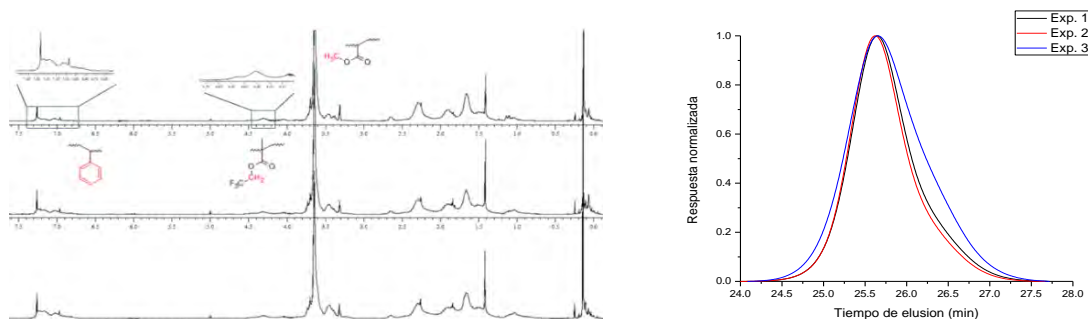


Figure 1. ^1H NMR and GPC analysis to determine composition and Mol. Weight

2. Synthesis in Aqueous Media

In comparison with the process in organic solvent, synthesis of polymers in aqueous media had to be optimized to have better control. Temperature, RAFT / Initiator ratio and solid content were adjusted until acceptable control in molecular weight and composition was obtained. In this cases it has to be demonstrated the sole formation of a kind of copolymers and avoid formation of homopolymers from different monomers due to its different water solubility. Results summarized in table 2 showed the characteristics of some of the fluoro-polymer obtained. Those with better control on polydispersity (one only MW distribution), and composition were selected to be evaluated as additives for color concentrates. One of the most important results of different variables studies confirmed that the ratio RAFT/Initiator is a key factor in polymer structure control at fixed temperature and solid content.

2.1 Kinetics

The kinetic study was made in a NMR tube to follow on line monomer instantaneous conversion. This study was made during the synthesis of poly(AA₅₉-S₇-TFEMA₇) with a $M_n = 6,000$ g/mol. Reaction was made in DMSO- d_6 . 1,3,5-trioxano was used as Internal Standard⁴.

Table 2. Variation of [RAFT]/[CVA] ratio.

Exp.	[RAFT] / [CVA] ratio	t (h)	Content NV theor. (%w/w)	Content NV exp. (%w/w)/conversion (%) ^a	Composition AA:S:TFEMA (%w/w) ^b	M_n^c	\bar{D}^c
1	1:0.5	24	30	18/90	78:11:20	5,900	1.3
2	1:0.7	24	30	24/80	81:9:10	4,400	1.3
3	1:1	24	30	12/77	76:10:14	4,300	1.3

Theoretical composition AA:S:TFEMA 59:7:7. Temperature 60 °C, ^a gravimetric, ^b ^1H NMR, ^c GPC

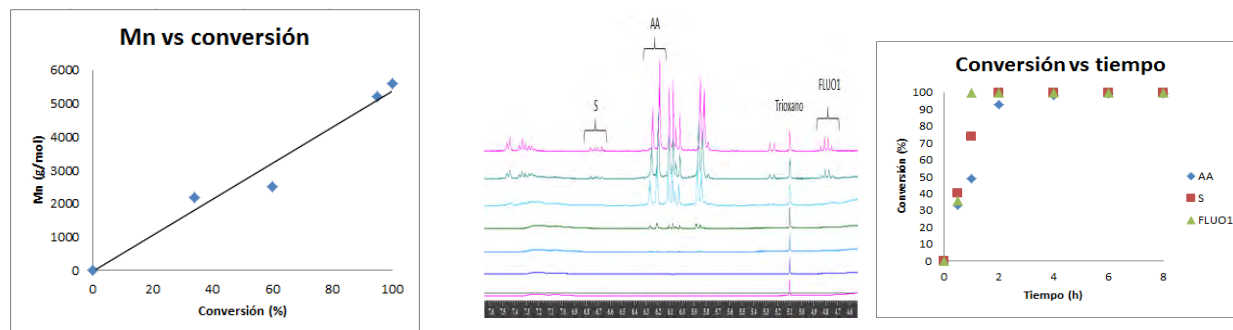


Figure 2. Left: Molecular weight evolution for the best [RAFT]/[CVA] ratio conditions. Rx. Temp. 60°C. Right: a) ^1H NMR spectra. b) Kinetic analysis.

In figure 2 (Right) an overlap of the ^1H NMR spectra obtained in time are shown including the peaks assigned to the different monomers present. Analysis of kinetic measurements showed that AA is incorporated faster in the polymer chain than the other monomers present. Due to the characteristics of the RAFT agent used, a random copolymer with an hydrophobic center and more hydrophilic sides might be expected.

3. Properties as additives in color concentrates

The copolymers with the following structure $\text{P}(\text{AA}_{59}\text{-S}_7\text{-TFEMA}_7)$ were evaluated as additives for color concentrates. Carbon Black, Red Oxide and Phthalocyanine Blue dispersions are tested in a water based paint and in an oil based paint. Two different polymer concentrations were used. Particularly, in Black and Red fluoropolymers showed their best performance when the pigment concentrate is applied in water based coating. In the case of the blue concentrate, it had a lower efficiency than the other pigments formulated with the same fluoropolymer. The performance of the blue concentrate applied in an oil based coating had a acceptable performance when higher amount of fluoropolymer was used. However, black and red concentrates had a poor performance.

Conclusions

It can be conclude that synthesis of random fluoropolymers were obtained satisfactory by RAFT polymerization and their performance as additives for color concentrates (Carbon Black, Red Oxide and Blue) was explore for two different coatings systems: water and oil based. It is important to mention that very low amount of hydrophobic fluor-containing monomer was sufficient to give hydrophobic character to the polymer tested as additive for color concentrates.

Acknowledgements

Centro de Investigación en Polímeros-Grupo COMEX, Centro de Investigación en Química Aplicada and CONACYT for the financial and technological support.

References

- [1] Laura Wood, Research and Markets, **2013**.
- [2] PCIMAG. SEP. **2000**.
- [3] Ameduri Bruno, *Macromolecules* **2010**, 43, 10163–10184
- [4] Mellon, V.; Rinaldi, D.; Bourgeat-Lami, E.; D'Agosto, F. *Macromolecules* **2005**, 38, 1591

TEMPERATURE SENSITIVE POLYMERIC MICELLES BY THE SELF-ASSEMBLY OF POLY(N-VINYLCAPROLACTAM)-B-POLY(HEXYLACRYLATE) BLOCK COPOLYMERS PREPARED BY RAFT

O. Ruiz-Galindo,¹ S.M. Ponce-Vargas,^{1#} N.A. Cortez-Lemus,¹ and A. Licea-Claverie,^{1*}

¹Centro de Graduados e Investigación en Química, Instituto Tecnológico de Tijuana. A. P. 1166. Tijuana, B. C. 22000, México.

E-mails: oscaruizbc@hotmail.com, sandramponcev@gmail.com, ncortez@tectijuana.mx, aliceac@tectijuana.mx

Current Address: Universidad Autónoma de Baja California, Facultad de Ciencias Químicas e Ingeniería, Tijuana, B.C. México.

Abstract

In this work the controlled polymerization of *N*-vinylcaprolactam (NVCL) with a trithiocarbonate CTA was exploited for the preparation of NVCL homopolymers; NVCL statistical copolymers with *N*-vinylpyrrolidone, hexyl acrylate and 2-methacryloyloxibenzoic acid; also for the preparation of PNVCL block copolymers with poly(*n*-hexylacrylate) using RAFT methodology. Polymers were obtained with controlled molecular weight and dispersity and characterized by NMR and DSC. Studies of water solutions by dynamic light scattering and turbidimetry showed that the lower critical solution temperature of the system was adjusted to higher temperatures by statistical copolymerization with hydrophilic monomers. Polymeric micelles were formed by dispersion in water of the block copolymers prepared.

Introduction

Stimuli-responsive polymers are attractive because of their various applications such as biomaterials, chemical sensors, textiles and optical systems.[1] Two well documented stimuli in chemical environments include pH and temperature; in the case of the latter there is a phase separation upon heating and the polymer exhibits a lower critical solution temperature (LCST) which depends of interactions between the polymer and its solvent. Poly(*N*-vinylcaprolactam) (PNVCL) is water soluble, thermo-sensitive polymer that has been widely studied recently for its potential use as biomaterial since it has proven to be non-toxic and biocompatible,[2] although it's been the focus on recent studies, there is still a need for more scientific publications regarding its properties as biomaterial.

The polymerization of NVCL via reversible addition fragmentation chain transfer (RAFT) has been studied, furthermore it has been shown that employing 4-cyano-4-(dodecylsulfanylthiocarbonyl)sulfanyl pentanoic acid as chain transfer agent (CTA) it's a way to obtain the intended polymer with a controlled molecular weight and an acceptable dispersity.[3] Since the intention of this work is to obtain different types of block and random copolymers, the need for a flexible chain transfer agent that can be used for the different types of monomers to be polymerized is a high priority. These characteristics make a trithiocarbonate RAFT agent ideal for this study.

The interest of copolymerization of NVCL serves two purposes in this study; first, block copolymerization of hexyl acrylate gives the polymer an amphiphilic property which in a water dispersion forms a micelle like structure that by means of changes in concentration exhibits a critical micelle concentration (CMC).[4] Second, random copolymerization can be used to tailor the LCST of PNVCL as shown in previous studies.[5]

Experimental

Polymer synthesis

For all polymers (random copolymers, block copolymers and PNVCL), 1,4-dioxane was used as a solvent, along with 2,2'-azobis(cyanopentanol) (ACP) azo type initiator and the trithiocarbonate RAFT agent. N-vinylpyrrolidone and 2-(methacryloyloxy)benzoic acid (2-MBA) were used as co-monomers of random copolymers, while hexyl acrylate (HA) was used in block copolymerization, maintaining as base component of polymers mainly NVCL. The reaction conditions and characterization for all these polymers is the same, while the purification step differs from PNVCL to copolymers. The synthetic procedure is described in one example: NVCL polymerization. A mixture of NVCL (1 g, 7.19 mmol), CTA (0.012 g, 0.0308 mmol), ACP (0.0015 g, 0.0062 mmol) and 1,4-dioxane (1 ml) was weighted and transfer to an ampule. Cycles of freeze-vacuum-thaw were used to remove all oxygen from the reaction, and then the ampule was sealed with a flame in an argon atmosphere, the ampule was submerge in an oil bath at 70 °C with magnetic stirring for about 24 hours. The polymerization was stopped by cooling at room temperature (25 °C). When it comes to purification, NVCL polymers were purified by precipitation of the polymer with ethyl ether to remove the remaining NVCL monomer; copolymers were purified by first precipitation of polymers with petroleum ether to remove the monomers in the solution, followed by dissolution with an excess of methanol and petroleum ether, after its centrifugation the precipitate was discarded and cold water was added to the solution followed by another centrifugation, this time the precipitate was kept and was dried under vacuum. The polymerization yield was obtained gravimetrically.

Measurements

The molecular weight and polydispersity were obtained by gel permeation chromatography (GPC). The measurements were made in a solution of tetrahydrofurane at room temperature. The $dn/dc = 0.109$ value was used for PNVCL obtained from literature.[6] The phase behavior (LCST) was determined by turbidimetry on a DR/890 portable colorimeter and confirmed by dynamic light scattering (DLS) on Zetasizer NanoSZ. 1w% copolymer solutions in buffers of different pH-values were prepared by stirring in ultrasonic bath followed by stirring the solution. The solutions were filtered off before measurement using 0.45 microns nylon filters.

Results and Discussion

Since the objective of this investigation was to obtain NVCL based copolymers with different co-monomers, a CTA capable of the controlled polymerizing various families of monomers needed to be chosen, because of these characteristics a trithiocarbonate CTA was used since it has medium chain transfer ability. The structures of the monomers and CTA used are shown in Figure 1. Block copolymers were synthesized starting with a macro-chain transfer agent (macro-CTA) of poly(NVCL) or from a macro-CTA of random copolymers of NVCL with NVP or with 2-MBA. In the case of copolymerization the majority of the copolymer contains NVCL and a minority content of NVP or 2-MBA, while hexyl acrylate was used to form the block copolymer as it gives the polymer amphiphilic properties. Table 1 summarizes the results from homopolymerization as well as random copolymerization and block copolymerization of NVCL.

Table 2 shows the LCST values determined for random copolymers as well as for PNVCL in water and in a buffer at physiological pH (7.4). In all cases modifications of the LCST were found with the incorporation of a co-monomer in a random copolymer; while for the block copolymer, almost no change of LCST was observed.

Table 2. LCST of copolymers in phosphate buffers at physiological pH (7.4) and in water.

Sample	Polymer	LCST (°C)	Solution
1	Poly(NVCL)	32	pH 7.4
1	Poly(NVCL)	34	Water
2	Poly(NVCL-co-NVP _{3.1 %})	36	pH 7.4
3	Poly(NVCL-co-NVP _{9.2 %})	36	pH 7.4
4	Poly(NVCL-co-NVP _{15.2 %})	38	pH 7.4
5	Poly(NVCL-co-2MBA _{4.6 %})	44	pH 7.4
6	Poly(NVCL-co-HA _{5 %})	27	pH 7.4
7	Poly(NVCL-b-HA _{14 %})	32	Water

As we can see in Table 2, LCST increases as the content of hydrophilic co-monomer NVP (with similar structure to NVCL) also increases. In the case of the acid co-monomer 2MBA, results show that the LCST increases since at pH 7.4 the acid units are ionized given the fact that this pH value is higher than the pKa of the acid. The contrary was observed with inclusion of the hydrophobic co-monomer HA in the random copolymer; the LCST drastically dropped. Since the LCST depends on the nature of the solution, in water solutions the LCST of polyNVCL increased as compared to the buffer conditions, while the block copolymer containing the hydrophobic HA co-monomer drop the LCST but not by much. It can be seen that the changes of the LCST on a polymer depends on the solution they are in as well as on the co-monomer content and type. Figure 2 shows a comparison of size distributions by volumen for samples 1 and 7 in water. As it can be seen, the hydrodynamic diameter (D_h) increases from 7 nm to 113 nm as a result of self-assembly of the block copolymers, and also showing only one distribution for both polymers.

Conclusions

Random and block copolymers of PNVCL were prepared using RAFT co-polymerization with acceptable molecular weights and dispersity.

Different kinds of co-monomers were successfully introduced ‘randomly’ into a NVCL copolymer. The composition of the random copolymers induces changes on the LCST of PNVCL. It was found that it’s possible to increase the LCST-value incorporating hydrophilic or acid co-monomers (NVP and 2MBA), or it can be decreased by incorporating hydrophobic co-monomers (HA). These results also confirms that in random copolymers there are drastic changes in the LCST, while in block copolymers the LCST only changes slightly. Monodisperse micelle like formation was confirmed by DLS for PNVCL-b-PHA.

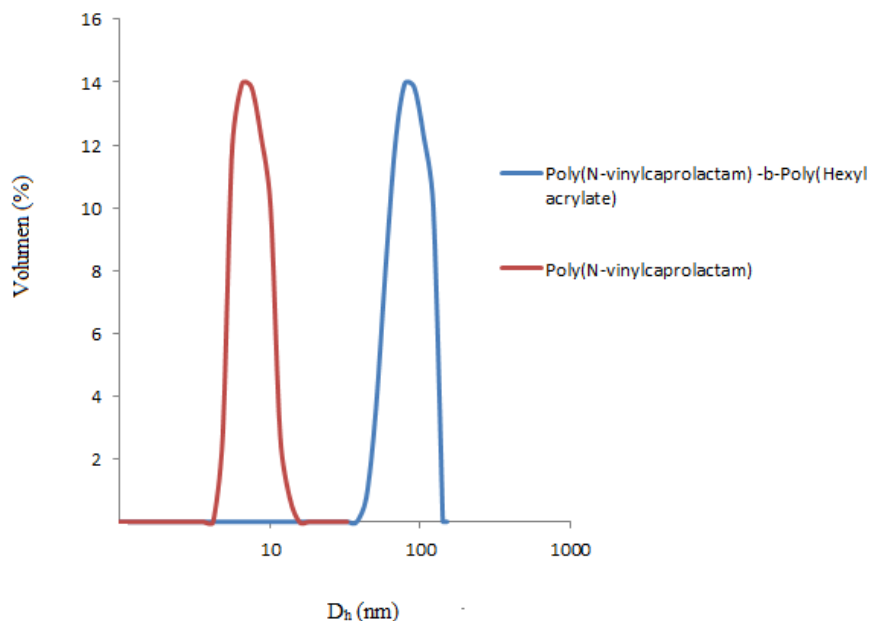


Figure 2. Size distributions by volume obtained by DLS for PNVCL and PNVCL-*b*-PHA at 20 °C.

Acknowledgements

This investigation was supported by the National Council of Science and Technology of Mexico (CONACYT) through the grant CB-2012-C01-178709. We thank I.A. Rivero for NMR-measurements.

References

- [1]. Genzer, J., Zauscher, S., Stamm, M., Stuart, M.A.C., Szleifer, I., Minko, S., Winnik, F., Urban, M., Tsukruk, V.V., Muller, M., Luzinov, I., Ober, C., Sukhorukov, G.B., *Nature Mater.* 9, 101-113 (2010)
- [2]. Vihola H., Laukkanen A., Valtola L., Tenhu H., *Biomaterials* 26, 3055-3064 (2005).
- [3]. Ponce-Vargas S.M., Licea-Claverie A., Cornejo-Bravo J.M., *Memorias del XXIII Congreso Nacional de la SPM*, 474-478 (2010).
- [4]. Picos-Corrales, L.A., Licea-Claverie, A., Arndt, K.F., *React. Func. Polym.* 75, 31-40 (2014)
- [5]. Boyko, V., Richter, S., Grillo, I., Geissler, E., *Macromolecules* 12, 5266-5270 (2005)
- [6]. Beija M., Marty J. D., Destarac D., *Chem. Commun.* 10, 2826-2828 (2011)

SYNTHESIS OF AU NANOPARTICLES COATED WITH POLY (N-ISOPROPYLACRYLAMIDE) FOLIC ACID FUNCTIONALIZED

G.D. García-Olaiz¹, N.A. Cortez-Lemus^{1*} and A. Licea-Claverie¹

¹*Instituto Tecnológico de Tijuana, Centro de Graduados e Investigación en Química; A.P. 1166, Tijuana, B.C., Mexico, C.P. 22000*

Abstract

In this work, we prepared folate-functionalized RAFT PNIPAAm using Reversible Addition-Fragmentation Chain Transfer Polymerization (RAFT) for covered AuNPs. An important aspect of this work is the determination of the lower critical solution temperature (LCST) for the folic acid-functionalized PNIPAAm, which is of fundamental importance in the potential biomedical application. Some polymer therapeutics can be functionalized using this strategy, and is highly versatile for functionalizing RAFT polymers. To date, few transfer agents that incorporate biomolecules in structure and can be vectorized. Gold nanoparticles have generated interest in the medical area due to its use in photothermal therapy against cancer.

Introduction

The gold nanoparticles coated with thermosensitive smart polymers are nanohybrids can have a number of potential applications in fields such as controlled release of drugs, photothermal therapy, nanoelectronics, sensors and catalysis.[1] The gold nanoparticles (AuNPs) have interesting properties due to their size, unlike their bulk counterparts, however a stabilizing agent needed not agglomerate and lose their nanometer size.[2] Thermoresponsive polymers have received large interest as stabilizing agents for nanoparticles, because there can display ligand functionality and presenting a lower critical solution temperature in aqueous solutions.[3]

Poly *N*-isopropylacrylamide (PNIPAAm) is one of the most important thermosensitive polymer and of greatest interest, because its phase transition temperature its 32.8 °C, that is close to the physiologic temperature.[4] On the other hand, a number of studies demonstrate that drug transporters nanosystems superficially decorated with folate ligand moieties show a very high affinity for tumor cells versus normal cells.[5]

Experimental

Phase 1: Trithiocarbonate synthesis.

The synthesis was carried out using a technique found in the literature.[6] 1-Dodecanethiol (7.7 g, 38 mmol) was added dropwise to a suspension of sodium hydride (60% in mineral oil, 1.575 g, 39.5 mmol) in 75 mL of ethyl ether anhydride at 0 °C for 2 h. The reaction mixture was cooled to 0 °C and carbon disulfide (3.0 g, 39.5 mmol) was added. The product was obtained for filtration and used in the next step without purification (10.03 g, 87.9% of yield). Then the dodecyl trithiocarbonate was suspended in 170 mL of ethyl ether. Solid iodine was gradually added by portion-wise addition (4.25 g, 16.5 mol). Then the reaction mixture was stirred at room temperature for 1 h. White sodium iodide which was removed by filtration. The dark yellow filtrate was washed with aqueous sodium thiosulfate solution (5x100 mL) to remove excess iodine. The solution was dried with sodium sulfate, filtered and evaporated to leave a yellow solid of 5.93 g (32% yield).

This product (2.77 g, 5.0 mmol) was dissolved in ethyl acetate (80 mL) and mixed with 4,4-azobis(4-cyanovaleric acid) (ACVA) (2.1 g, 7.49 mmol) and then heated in reflux for 20 h. After removing the solvent in vacuum, the crude product was dissolved in DCM, extractions with water (3 x 100 mL) were made and evaporated to remove the solvent. The product obtained was purified by recrystallization from cold hexane (12 h in the refrigerator) (Figure 1).

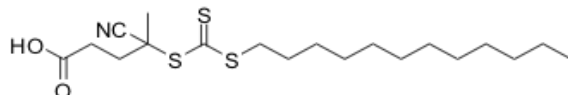


Figure 1. Structure of trithiocarbonate.

Phase 2: Trithiocarbonate ester activation.

To carry out the union of trithiocarbonate, synthesized above with folate, is required to activate the trithiocarbonate ester. To a solution of trithiocarbonate (370 mg, 0.950 mmol) in 20 mL of chloroform were added dimethylaminopyridine (DMAP) (1.6 g, 0.095 mmol), *N*-hydroxysuccinimide (120 mg, 1.045 mmol). Then, dicyclohexylcarbodiimide (0.215 g, 1.045 mmol) dissolved in 5 mL of dichloromethane were added to this solution slowly. The reaction was stirred by 20 h. The byproduct (urea) was filtered off and the filtrate was concentrated.

Phase 3: Trithiocarbonate link to Folate: CTA

To carry out the coupling reaction of folic acid to the trithiocarbonate-NHS, 7 mL of pyridine (86.6 mmol), ethylenediamine unprotected folate (386 mg, 799 mmol) and trithiocarbonate-NHS (415 mg, 840 mmol) were added to 30 mL of DMSO. The reaction mixture was stirred for 24 h at room temperature. It was purified by precipitating with ethyl ether, decanting and evaporating. Figure 2 shows the final structure of folate-CTA.

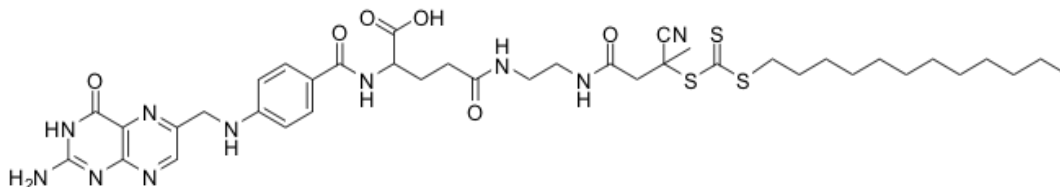


Figure 2. Chain transfer agent (CTA).

Polymerization of N-isopropylacrylamide

In a 10 mL ampoule containing a magnetic stir bar, monomer (28.8 mmol), azo initiator (0.155 mmol), CTA-folate trithiocarbonate (0.778 mmol) were dissolved in 2 mL of dimethylformamide; then argon was bubbled for 20 min the vial. Vacuum and freeze cycles were performed (in triplicate) and the ampoule was sealed with a gas torch. Then, the solution was placed in an oil bath with magnetic stirring at 70 °C. After reaching the polymerization time, the polymerization was removed from the oil bath and placed in a bath of acetone/dry ice to stop the reaction by cooling. Ethyl ether to precipitate the product was used for purification of the polymer, decanted and evaporated under reduced pressure.

Preparation of Gold Nanoparticles coated

Gold nanoparticles were synthesized according to the methodology of Destarac and collaborators.[7] In a beaker with 94 mL of distilled water and filtered under stirring, were added 250 μ L of a solution of NaOH (1 mol L⁻¹) and 5 mL of a solution of HAuCl₄ (1x10⁻² mol L⁻¹). Subsequently the pH was adjusted to 7.5. Were added drop by drop to 500 mL of NaBH₄ (0.1 mol L⁻¹). The solution changed to dark red. To make the coating of the gold nanoparticles was added 2 mg of polymer in 4 mL of gold nanoparticle solution and placed under stirring for 12 h. Not conduct any separation or purification process of coated and uncoated AuNPs polymer.

Characterization methods

The following characterization methods were used: chromatography permeation gel (GPC) mobile phase of THF, spectroscopy Fourier transform infrared (FT-IR), ^1H NMR and ^{13}C NMR analysis in DMSO, UV-visible spectroscopy and dynamic light scattering (DLS).

Results and Discussion

Table 1 show that the molecular weights (relative to theoretical GPC) is very close to plan. Although the polydispersity are higher for the reactions referred to as G-PNI27 and G- PNI25.

Table 1. Results of polymerization of NIPAAm with RAFT agent containing folate.

Reaction ^a	NIPAAm : CTA : AIBN	Concentration monomer/solvent (mol/L)	Mn (g/mol) _{theoretical}	Mn (g/mol) _{GPC}	PDI (Mw/Mn)	Solvent	Time h
G-PNI25	1450 : 4 : 1	4	37165	48000	1.6	DMF	2.5
G-PNI26	1450 : 4 : 1	1	37165	36820	1.2	DMF	2.5
G-PNI27	1450 : 4 : 1	1	37165	38770	1.5	DMF	3

* The conversions are estimated at 20-35%.

By decreasing the monomer concentration, it is possible to get closer to the theoretical molecular weight. Also, the polymerization time plays an important role because with increasing time increasing the molecular weight as well as the polydispersity. Also, it is important to clarify through a comprehensive literature search; there are no reports of PNIPAAm by RAFT incorporating folic acid following the methodology proposed here.

UV-spectrum of transfer agent coupled with folic acid

The presence of folate in the PNIPAAm-folate incorporated throughout the CTA synthesized was confirmed by UV-Vis spectroscopy. Figure 3 shows absorption at 380 nm corresponds to the free folic acid. Same band was observed in the PNIPAAm containing folate segment. This band was absent for pure PNIPAAm telechelic polymer according to the expected results.

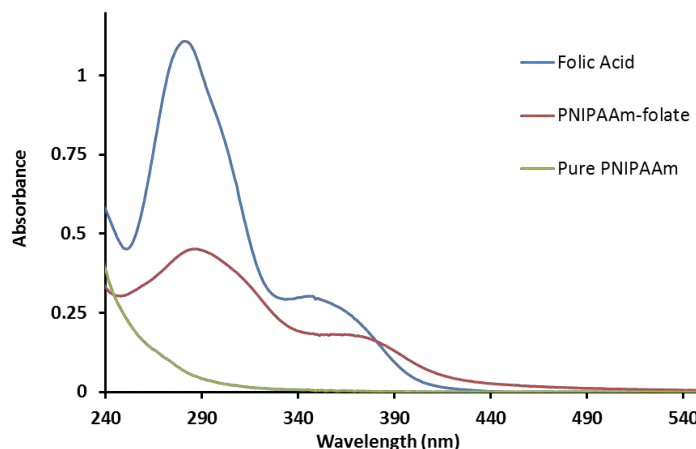


Figure 3. UV-vis spectrum of PNIPAAm-folate, pure PNIPAAm and folic acid.

^{13}C NMR (200 MHz, $\text{DMSO-d}^6\text{-CDCl}_3$) chain transfer agent spectrum.

In Figure 4, ^{13}C NMR of CTA showed at 217 ppm the signal corresponding to carbonyl carbon characteristic of trithiocarbonate group (assigned as 1), confirming trithiocarbonate coupling 2-folate ethylenediamine fragment. Carbonyls for the carboxyl group and amides are located from 174 to 170 ppm (assigned as 2-6). The methyl carbon of the aliphatic chain can be observed at 14 ppm (assigned as 2-6).

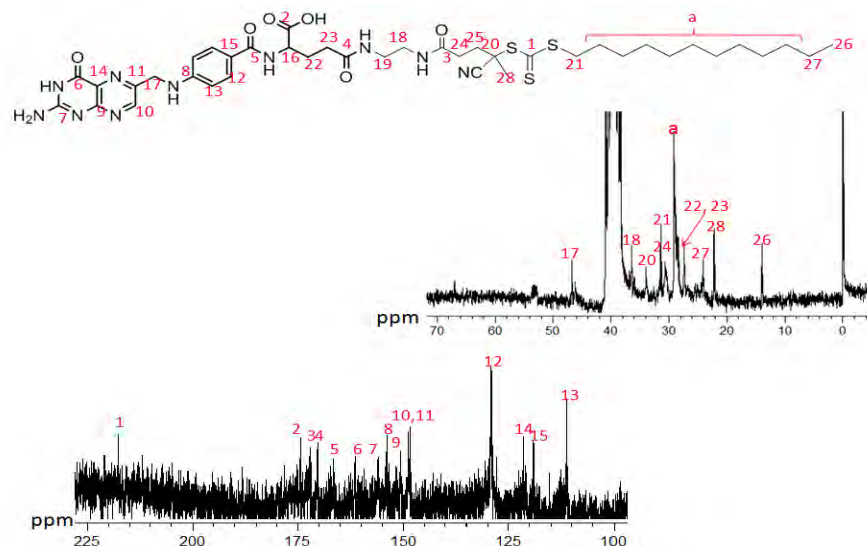


Figure 4. ^{13}C NMR (200 MHz, $\text{DMSO-d}^6\text{-CDCl}_3$) spectrum of chain transfer agent.

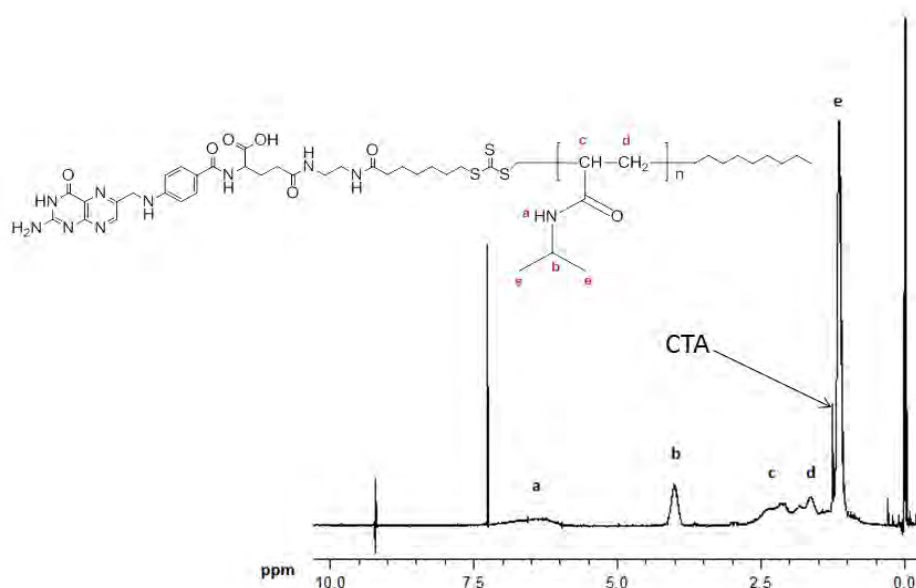


Figure 5. ^1H NMR (200 MHz, CDCl_3). PolyNIPAAm spectrum.

^1H NMR (200 MHz, CDCl_3) PNIPAAm-FOLATE spectrum

The general structure of the PNIPAAm containing folate was confirmed by ^1H NMR (Figure 5), where signals from the polymer and from the multifunctional CTA, can be observed at 1.23 ppm (aliphatic chain of CTA).

Analysis of Lower Critical Solution Temperature (LCST) of PolyNIPAAm

Analysis was performed on dynamic light scattering (DLS) in there was obtained a temperature of 30.8 °C which corresponds to that reported in the literature for the polyNIPAAm.

Dynamic light scattering characterization.

The sizes of the pure polymers dissolved in water and the coated nanoparticles were measured. Is possible see that the hydrodynamic diameter showing each gold nanoparticle.

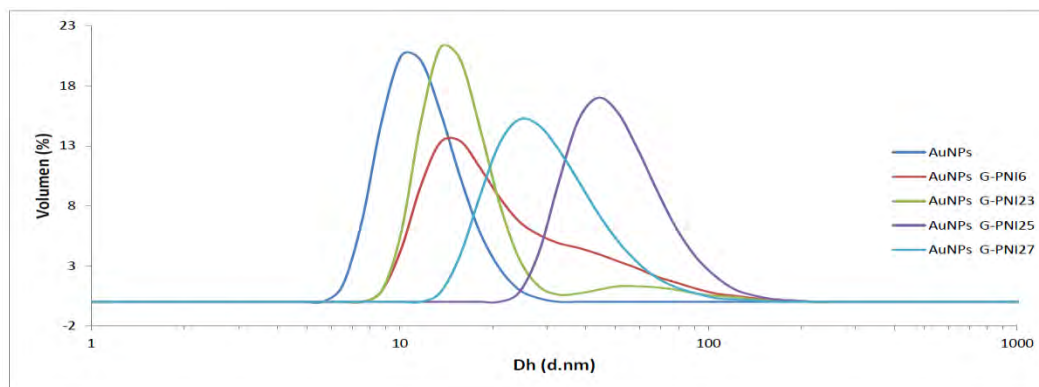


Figure 6. Comparing sizes of gold nanoparticles coated with polymers used by DLS.

Conclusions

Herein we describe the synthesis of folate-functionalized CTA employed for the controlled polymerization of NIPAAm. It was possible to obtain a complete assessment of the ability of controlling the polymerization chain transfer agent synthesized by polymerization of *N*-isopropylacrylamide. Gold nanoparticles were synthesized in a size of 12 nm successfully, and that was achieved coat them with some samples of the polymers obtained in this work. The polymer was shown to work as an agent that prevents aggregation of gold nanoparticles because adding the polymer to stop the color change reflecting the growth of the nanoparticles

Acknowledgements

This investigation is supported by the National Council of Science and Technology of Mexico (CONACYT) through grant SEP-CONACYT (CB-2012-C01-178709).

References

- [1] M. Beija, J. Marty, M. Destarac, *Chem. Commun.*, 47, 2826–2828 (2011).
- [2] X. Z. Hu, L. Zhou, C. Gao, *Colloid Polym Sci*, 289, 1299-1320 (2011).
- [3] S. Bokern, J. Getze, S. Agarwal, A. Greiner, *Polymer*, 52, 912-920 (2011).
- [4] N. Cortez, R. Salgado, A. Licea, *J. Polym. Sci. Part A: Polym Chem*, 48, 3033-3051 (2010).
- [5] K. S. Soppimath, D.C.W. Tan, Y.Y. Yang, *Mater*, 17, 318 (2005).
- [6] G. Moad, Y. Chong, A. Postma, E. Rizzardo, S. Thang, *Polymer*, 46, 8458-8468 (2005).

SYNTHESIS OF ACRYLAMIDE-HEXADECYL ACRYLAMIDE BLOCK COPOLYMERS BY RAFT EMULSION POLYMERIZATION

Shirley Carro Sánchez,¹ Valeria González-Coronel,² Judith Cabello Romero,³ José Víctor Amador Noya,¹ Jorge Castillo Tejas,¹ Friné López-Medina¹

¹ *Universidad Autónoma de Tlaxcala, Facultad de Ciencias Básicas, Ingeniería y Tecnología. Calzada Apizaquito S/N. 90300, Apizaco, Tlaxcala, México.*

² *Benemérita Universidad Autónoma de Puebla. Facultad de Ingeniería Química, Av. San Claudio y 18 Sur, Col. San Manuel Ciudad Universitaria, 72520, Puebla, Puebla, México*

³ *Centro de Investigación en Química Aplicada. Blvd. Enrique Reyna #140, 25253. Saltillo, Coahuila, México.*

Abstract

Acrylamide–hexadecyl acrylamide block copolymers were synthesized via RAFT in inverse emulsion polymerization. A trithiocarbonate was used as RAFT-agent. Two different synthesis routes were proposed. Also the effect of the kind of initiator was investigated. AIBN (2,2'-azobis(isobutyronitrile), soluble in the continuous phase) and ACVA (4'-azobis (4-cyanopentanoic acid)). RMN results show a mayor incorporation of the hydrophobic monomer when a post-polymerization is performed. Regarding the effect of the kind of initiator, for the macroagent synthesis no effect was observed, however, for the synthesis of the copolymers a mayor incorporation of the hydrophobic monomer when AIBN is used.

Introduction

Controlled radical polymerization has been applied to prepare polymers and block copolymers with well-defined structures and possible reactivation for further chain extension. Reversible addition-fragmentation chain transfer (RAFT) polymerization seems well-suited for polymerizing acrylamide (AM) derivatives [1, 2]. Most reports focus only on the controlled polymerization of N-isopropylacrylamide and acrylamide [2]. Reversible addition–fragmentation chain transfer (RAFT) polymerization is a very promising method, because wide varieties of RAFT agents allow the control over almost all monomers possibly to polymerize under conventional experimental conditions, such as in emulsion system [3,4]

For AM RAFT polymerization trithiocarbonates chain transfer agents, CTA, are preferred to obtain macroCTA of AM by solution polymerization. Thomas et al. tried five different CTA and they found that for polymerizations mediated by trithiocarbonate CTA reactions rates are faster. Cao and Zhu [5] prepared triblock copolymers of N-alkyl substituted acrylamides by RAFT polymerization also employing a trithiocarbonate CTA, finding that this is also a good choice to synthesize macro CTA for N-alkyl monosubstituted acrylamide.

Acrylamide and their derivative copolymers are of special interest because they produce hydrophobically associating polymer. At the present, amphiphilic copolymers have been prepared by RAFT solution polymerization. There are scarcely reports about their synthesis by emulsion polymerization.[6] Water-in-oil (inverse) emulsion polymerization is one of the ideal methods for obtaining polyacrylamide based polymers with high molecular weight and low viscosity. An inverse emulsion, however, cannot be simply considered as an analogy to conventional emulsion in which the water is replaced by the oil and the hydrophobic monomer by the hydrophilic monomer. The kinetic mechanism of inverse emulsion polymerization can be affected by many factors such as initiators, surfactants and oils [7]. In this work Acrylamide–hexadecyl acrylamide block copolymers were synthesized via RAFT in inverse emulsion polymerization using a trithiocarbonate as CTA as an alternative to produce amphiphilic block copolymers.

Experimental

All solvents and reagents were employed without further purification. The water was distilled and

deionized. Acrylamide (AM, Aldrich 99% purity) was used as hydrophilic monomer and (HDAM) as hydrophobic comonomer. 4,4'-azobis(4-cyanovaleric acid) (ACVA, Aldrich 99% purity) or 2,2 azobisisobutironitile (AIBN) as initiator and SPAN 80® (non-ionic emulsifier, sorbitan monoleate, Aldrich) as surfactant. MacroCTA of AM was obtained as follows. Batch inverse emulsion copolymerizations were carried out at 80°C, using a thermostated water bath, in a 500 ml glass reactor equipped with thermometer and mechanical stirrer. For emulsion polymerizations continuous phase (51 wt%) was prepared dissolving in toluene the hydrophobic comonomer, initiator, CTA and surfactant (12% wt relative to monomer). Finally macroCTA of AM was washed with a acetone/methanol solution. The mixture was washed several times until turbidity disappeared. The material was filtered and dried in a vacuum oven at 50°C for 48 h.

To synthesize PAM-HDAM copolymers two different methods were tried. In first method, one step method, after macroCTA of PAM synthesis HDAM monomer was added immediately and copolymerization proceeded during 3 hr. After this time, copolymer was washed, filtered and dried. For the second method, two steps method, the purified macroCTA of AM is added to aqueous phase and polymerization proceed as it was indicated before.

Samples were withdrawn periodically from the reactor for the conversion and molecular weight analysis. Conversion was followed by gravimetric technique. The copolymers cannot be characterized by size exclusion chromatography in water, due to aggregation phenomena. However macroCTA of PMA, homopolymer from AM, prepared under identical experimental conditions was measured. The viscosity-average molecular weight, M_v , of copolymers was calculated from $[\eta] = 6.31 \times 10^{-3} M_v^{0.8}$ [8]. Limiting viscosity number $[\eta]$ was determined with Ubbelohde viscometer in water at 25°C.

To verify the hydrophobic comonomer ¹H NMR spectrum were recorded on a Bruker Avance 300 spectrometer at 300.15MHz in deuterium oxide (D₂O). The chemical shifts were referenced to TMS. The hydrophobe content was calculated from the relative integrated area of peak corresponding to the protons of terminal CH₃ group.

Results and Discussion

Results of RAFT inverse emulsion polymerizations of acrylamide with AIBN or ACVA as initiator and ACVA are shown in Figure 1. As it can be seen fractional conversion is lower for AIBN polymerization. The M_v of poly(acrylamide) when AIBN was employed was much higher than that for ACVA polymerization at the end of the reaction. (AIBN= 167000 /mol; ACVA= 37 100). The different concentration ratio of RAFT agent and AM in the reactions sites lead to a different controlled behavior. This can be attributed to the long time interval that the oligoradical take to enter droplets and initiate polymerization. Besides, RAFT agent is mainly located in the droplets. Similar results were obtained by Qi et al. and Ouyang et al. [9,10]

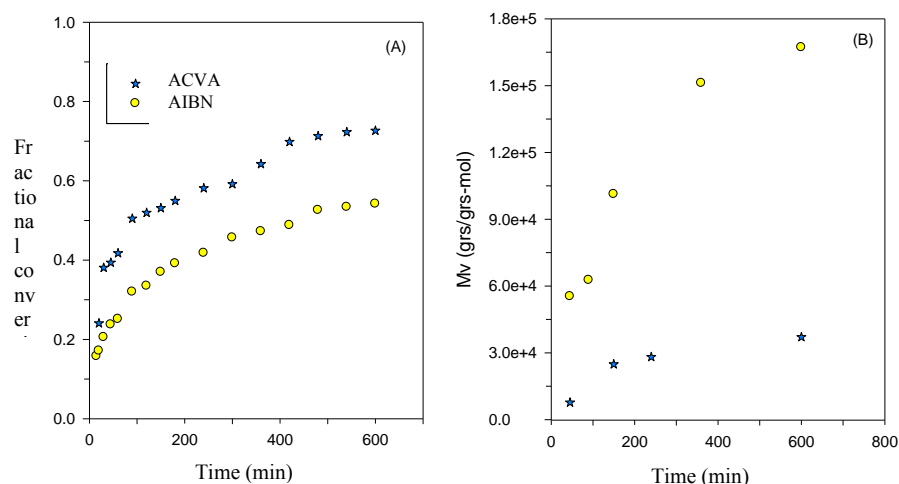


Figure 1. Evolution of conversion and molecular weight for acrylamide RAFT polymerization using AIBN or ACVA as initiator.

In Figure 2 and 3 RMN spectrums for copolymerizations are shown. When method 1 is used for AIBN a signal in 1.12 ppm (C, Figure 2 a) corresponding to HDAM indicates an adequate incorporation of the hydrophobe comonomer. However, for ACVA a signal corresponding to HDAM signal cannot be seen. This behavior could be explained by the difference in reactions sites. HDAM is soluble in organic phase and in the case of ACVA radicals are growing in the aqueous phase, in this case HDAM cannot reach this radicals. For method 2, HDAM signal is present for both initiators, but, in this case, a mayor incorporation of HDAM is achieved when ACVA is used. When macroCTA is added as a reagent, initiator is dissolved in organic phase, then it HDAM radicals are generated and, when ACVA is used, this initiator is also soluble in aqueous phase reactivating macroCTA chains.

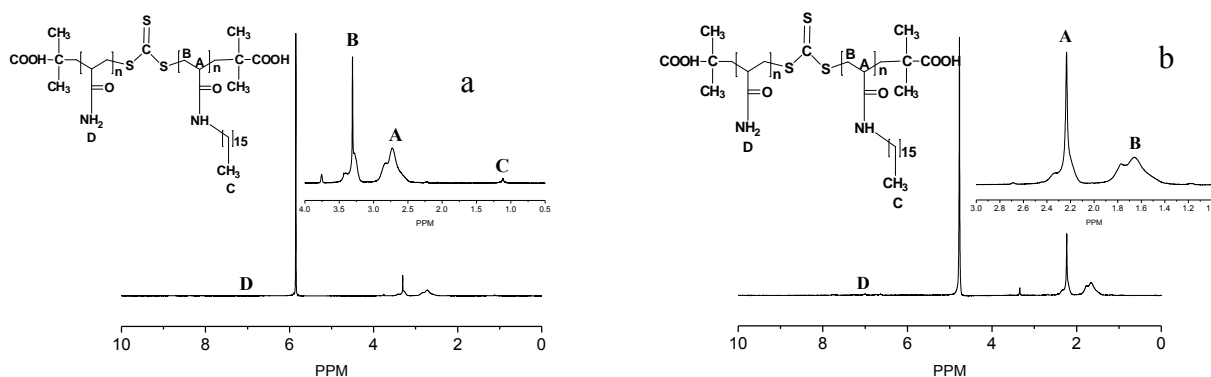


Figure 2. ¹H NMR spectrums of HDAM-co-AM polymerized by method 1 (a) AIBN and (b) ACVA)

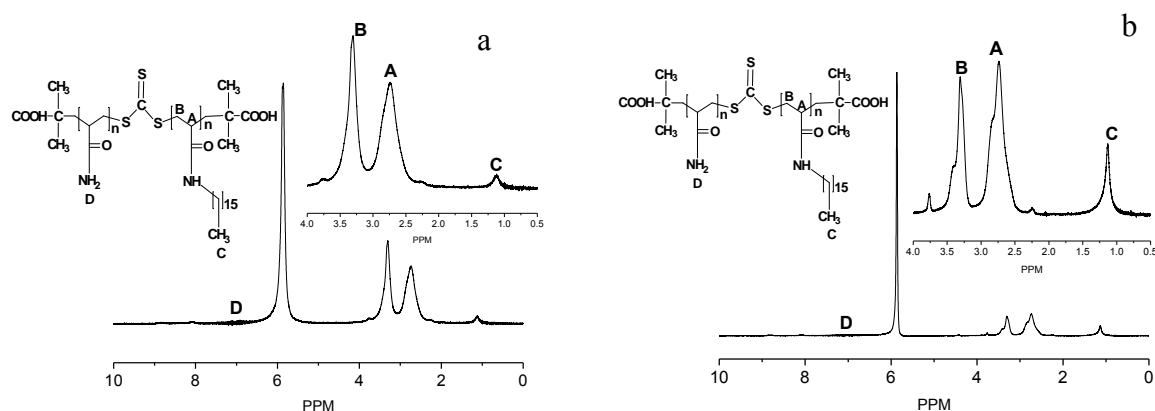


Figure 3. ^1H NMR spectra of HDAM-co-AM polymerized by method 1 (a) AIBN and (b) ACVA)

Table 1 shows the molecular weight for the copolymers, obtained by the two methods. For the two steps copolymerization an increase in M_v was observed showing that macroCTA can chain-extended. As it can be seen the two steps method is more suitable to obtain block copolymers.

Table 1. Viscometric molecular weight for the different polymers obtained.

Polymerization	AIBN (M_v ; g/mol)	ACVA (M_v ; g/mol)
MacroCTA	16700.00	37100.00
PAM-HDAM, method 1	18600.00	21800.00
PAM-HDAM, method 2	62500.00	47700.00

Conclusions

RAFT polymerizations of hexadecyl acrylamide has been successfully carried out in the presence of a trithiocarbonate CTA. Macro-CTA of AM can be used to be subsequently chain-extended with other acrylamide-based monomers to form diblock copolymers. When the oil-soluble initiator AIBN was used to replace ACVA, a less extent of comonomer was incorporated to the AM chain-

Acknowledgements

Authors thanks financial support to PROMEP; project 103.5/12/2116.

References

- [1] G. Moad, E. Rizzardo, and S. H. Thang. Aust. J. Chem. 58, 379 (2005).
- [2]. S. Perrier, P. Takolpuckdee, J. Westwood, and D. M. Lewis. Macromolecules, 37, 2709 (2004)
- [3] J. Chiefari, R.T.A. Mayadunne, C.L. Moad, G. Moad, E. Rizzardo, A. Postma, M.A. Skidmore, S.H. Thang, Macromolecules 36, 2273 (2003).
- [4] Y.K. Chong, J. Krstina, T.P.T. Le, G. Moad, A. Postma, E. Rizzardo, S.H. Thang, Macromolecules 36, 2256 (2003).
- [5] Y. Cao, X. Zhu. Canadian Journal of Chemistry. 85, 407 (2007)
- [6] Y.Chen, W.Luo, Y. Wang,C. Sun, M. Han, C. Zhang, J. Colloid Interface Sci. 369, 46 (2012)
- [7] J. Chiefari, Y. Chong, F. Ercole, J. Krstina, J. Jeffery, T. Le, R. Mayadunne, G. Meijs, C. Moad, G. Moad, E. Rizzardo, S. Thang, Macromolecules. 31, 5559 (1998)

- [8] J. Klein, W.M. Kulicke, Colloid and Polymer Science. 258, 719-732. (1980)
- [9] G. Qi, C. Jones, F. Schork. Macromolecular Rapid Communications. 28,1010 (2007)
- [10] L. Ouyang, L. Wang, F. Schork. Polymer. 52,63, (2011)

POLIMERIZATION OF STYRENE BY REVERSE ATRP IN scCO_2 .

Rosales-Velázquez, Claudia Patricia;¹⁾ Torres-Lubián, José Román;¹⁾ Saldívar-Guerra, Enrique;²⁾ Díaz-Barriga, Enrique.³⁾

1) Department of Polymer Synthesis, claudia-rosales@hotmail.com; roman.torres@ciga.edu.mx; 2) Department Polymerization Processes, enrique.saldivar@ciga.edu.mx; 3) Department of Microscopy, enrique.diazbarriga@ciga.edu.mx; Center of Research and Applied Chemistry, Blvd. Enrique Reyna 140, Col. San José de los Cerritos, Saltillo Coah., C.P. 25294, México.

Abstract

Dispersion polymerization of styrene in scCO_2 by reverse ATRP was studied using a catalyst of Ru (III) $\text{Cp}^*\text{RuCl}_2\text{P}[4\text{-C}_6\text{H}_4\text{-(CH}_2)_2(\text{CF}_2)_5\text{CF}_3]_3$ (1), AIBN as initiator and a block copolymer of polystyrene and polytridecafluoro octylmethacrylate (PSt-b-PTDFM) as steric stabilizer. Polystyrene obtained in different reaction conditions, showed that the conversion reached 80 %, with molecular weights of about 15,000 g/mol, indicating that the PSt chains grew around a DPn of 144. NMR analysis of PSt gives evidence of the chain-end functionalization with the fragment derivative from AIBN used as an initiator. The surfactant was present in the polymers even after re-precipitation. The effect of the pressure, temperature and the type of surfactant used, on polystyrene morphology, was studied.

Introduction

Carbon dioxide attains the supercritical state at near-ambient temperature ($T_c = 31.2^\circ\text{C}$) and a relatively moderate pressure (73.8 bar). Supercritical CO_2 (scCO_2) offers many mass transfer advantages over conventional organic solvents due to its gas-like diffusivity, low viscosity, and surface tension. The use of scCO_2 as a polymerization medium has promising advantages with respect to conventional solvents.¹

Conversely, most industrially important hydrocarbon-based polymers are relatively insoluble in scCO_2 . As an illustration, polystyrene is insoluble in scCO_2 even at 225°C and a pressure of 2100 bar. However, CO_2 acts as a plasticizing agent for PSt, and this phenomenon facilitates the diffusion of monomer inside the swollen polymer phase during a heterogeneous polymerization.²

Heterogeneous polymerization is generally divided into four categories, depending on the solubility of the monomers and initiators in the continuous phase and the addition of surfactants or stabilizing agents.² In the case of polymerization under scCO_2 conditions, many reports showed that it occurs under dispersion polymerization where both the monomer and initiator are soluble in the continuous phase but the resulting polymer is insoluble. As a result, the precipitated product is stabilized by a suitable surfactant, resulting in stable microparticles.

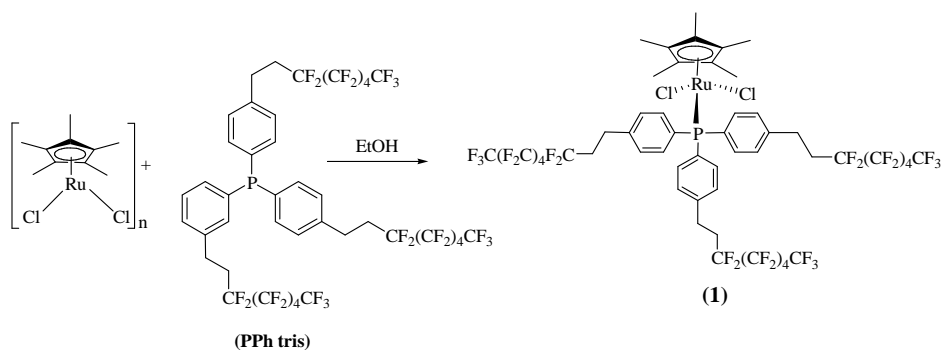
Studies over ATRP and his variants (ARGET, ICAR, REVERSE) conducted in scCO_2 are scarce, however the interest for using this green solvent in control radical polymerization is growing. Some recent reports concerning the ATRP in scCO_2 are: the synthesis of poly(2,2,2-trifluoroethyl methacrylate) by supported ATRP,³ the synthesis of PMMA by ATRP using a catalyst ligated to a polymeric ligand having a dual role, the complexation and the stabilization of the growing PMMA particles⁴ and the synthesis of well-defined graft copolymers of P(MMA-co-HEMA) with poly(ϵ -caprolactone) by means of ATRP in scCO_2 in conjunction with enzymatic ring opening polymerization.⁵

Experimental

Materials. Styrene (St, 99% Aldrich) was vacuum-distilled from calcium hydride, 3,3,4,4,5,5,6,6,7,7,8,8,8-Tridecafluorooctyl methacrylate (TDFMA, 97% Aldrich) was purified by passage through an alumina column, 2,2-Azobisisobutyronitrile (AIBN) was recrystallized twice from methanol and carbon dioxide gas was provided by INFRA and was used as received.

Synthesis of Ru(III) $\text{Cp}^*\text{RuCl}_2\text{P}[4\text{-C}_6\text{H}_4\text{-(CH}_2)_2\text{(CF}_2)_5\text{CF}_3\text{)]}_3$ (**1**).

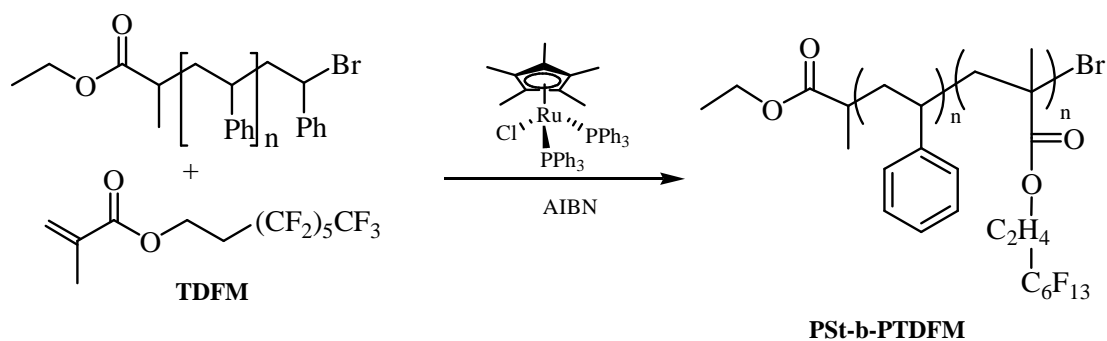
In a 100 mL flask equipped with magnetic stirring the paramagnetic compound of ruthenium (III), $[\text{Cp}^*\text{RuCl}_2]_n$ 300 mg (0.97 mmol) and $\text{C}_{42}\text{H}_{26}\text{F}_{39}\text{P}$ 1.2 g (1.52 mmol) in 30 mL EtOH were placed. The reaction was stirred at room temperature under argon atmosphere for 1.5 h, then the reaction crude was filtered under vacuum, followed by a series of washings with EtOH and ether, then was brought to dryness, obtaining a powder of brick red with a yield of 72 % (1.1 g) which was characterized by ^1H -RMN (300 MHz, CDCl_3 ; r.t.; δ =ppm), 24.8 (ws, 15H); 14.6 (ws, 2H); 9.3 (ws, 2H); 6.65 (ws, 6H); 4.5 (ws, 3H); 3.3 (ws, 7H); mp: 150°C. Scheme 1 shows the stoichiometry of the synthesis of compound **1**.



Scheme 1 Stoichiometry synthesis of $\text{Cp}^*\text{RuCl}_2\text{P}[4\text{-C}_6\text{H}_4\text{-(CH}_2)_2\text{(CF}_2)_5\text{CF}_3\text{)]}_3$ (**1**).

Synthesis of PSt-*b*-PTDFM 81/19.

A Schlenk tube was charged with 6.5 mg (0.0081 mmol) of complex $\text{Cp}^*\text{RuCl}(\text{PPh}_3)_2$ as catalyst, 222 mg (0.022 mmol) of macroinitiator styrene (experimental M_n of 13900 g/mol, IPD= 1.12 and 90 % of functionality), 0.3 mg (0.000189 mmol) of AIBN as initiator-reducer, 267 μL (0.00092 mol) of (TDFMA) and 1 mL of toluene as solvent. The solution was freeze- pump-thaw degassed three times and finally the tube was placed in an oil bath at 90°C. The polymerization was stopped after 48 hours, removing the Schlenk from the oil bath and cooled in ice water. The crude reaction was dissolved in chloroform and the copolymer precipitated in methanol, and then filtered. The copolymer obtained was dried at 40 °C for one night. The base fluorinated monomer conversion was 52%, determined gravimetrically. The copolymer obtained was a cream-colored powder with a molecular weight of 27200. The same procedure was followed for the 77/23 copolymer composition with gravimetric molecular weight of 35950.



Schema 2. Synthesis of block copolymer PSt-*b*-PTDFMA for ATRP-ICAR.

Dispersion Polymerizations using PSt-*b*-PTDFM as surfactant.

The polymerizations were conducted in a cylindrical steel reactor of 25 mL of volume. The reactor was charged with AIBN (3.9 mg, 2.37×10^{-5} mol), complex **1** (3.9 mg, 2.41×10^{-5} mol), surfactant (PSt-*b*-PTDFM 81/19, $M_n = 27226$, 39 mg, 1.44×10^{-6} mol) and a magnetic spinning bar under vacuum, styrene (772 mg, 7.42×10^{-3} mol) addition to the system was purged with an argon, the reactor was charged to a pressure of about 80 bar. To pressurize the reactor with CO₂ a mechanical/manual pump was used which allowed increasing the pressure until a desired value. Later, the reactor was heated at 130 °C, using a hot plate, reactions were performed at different pressures. At the end of the reaction time, the reactor was cooled to room temperature and slowly depressurized until atmospheric pressure, and the crude reaction mixture was dissolved in chloroform and the polymer precipitated in methanol. The yield was determined gravimetrically.

Polymer Characterization

Molecular weights of the resulting polymers were determined by using Hewlett Packard 1100 size exclusion chromatograph (SEC). The SEC equipment had three PLgel 5-10 μ m columns (pore size 10^6 , 10^5 , 10^3 ; 300×7.5 mm) and one PLgel 10 μ m guard column (50×7.5 mm) supplied by Polymer Laboratories. Tetrahydrofuran was used as eluent at 1.0 mL min⁻¹ at 40 °C. Molecular weights were determined relative to polystyrene standards (1×10^6 - 400 Daltons), NMR spectra were recorded on a Jeol Eclipse 300 instrument operating at 7.05 T in CDCl₃ solvent at 25 °C, for ¹H at 300 MHz and referenced to internal CHCl₃. The morphology of the polymer particles was determined with scanning electron microscope (SEM) (JEOL-5410LV). The number-average particle size and particle size distributions were determined by measuring the diameters of particles in the SEM images.

Results and Discussion.

Firstly, we conducted the polymerization of St by reverse ATRP in scCO₂, changing the pressure in the system and maintaining the temperature, the reaction time, the weight ratio of St/volume of reactor = 6.0 wt-% and the kind of steric stabilizer constants. The results are showing in Table-1.

As can be observed (from entries 1 to 4), the final conversion and the M_n (SEC) decrease with increasing CO₂ pressure, and the dispersity values increased. This suggests that the PSt particles are better stabilized at 1100 psi of critical pressure, and the polymerization control is better too at the same critical pressure since the dispersity value is the lowest.

Table-1. Results of St polymerization by reverse ATRP in scCO₂.^{a)}

Entrance	Pressure (PSI)	Conversion (%) ^{b)}	Mn(th) ^{c)}	Mn(SEC)	Đ ^{d)}	Dn (μm) ^{e)}	PSD ^{e)}
1	1100	68	10274	15752	1.35	—	—
2	2400	29	4762	9448	1.8	—	—
3	4200	11	12562	2702	3.8	—	—
4	6400	5	914	1986	4.6	—	—
5	0	86	13914	35144	3.14	—	—
6^{f)}	1100	69	11300	7660	19.7	—	—

a). Temperature = 130°C, reaction time = 20 h., a steric stabilizer of PSt-*b*-PTDFM (81/19 molar composition) and Mn = 27226. b). Determined gravimetrically. c). Mn(th) = [St]/2[AIBN]*%conv.*104. d). Determined by SEC. e) Dn= particle diameter, PSD = particle size distribution. Not yet determinate f). Conducted without catalysts **1**.

DeSimone reports a little increase in the conversion and the Mn with the CO₂ pressure increase, during the radical polymerization of styrene in scCO₂.⁶ Here we found a contrary effect and it's likely because the catalyst (**1**) has a CO₂ philyc property, which makes it separate from the particle centers preventing their growth. The experiments (entries 5 and 6) were conducted in order to evaluate the properties of PSt obtained in bulk without CO₂ pressure (entrie 5) and without catalyst (entrie 6). As it can be seen, the dispersity values were too high suggesting the loss of polymerization control and indirectly showing that the inverse ATRP has a role in the mechanism of polymerization. Following, we studied the effect of temperature in the molecular weight, conversion and the control of the St polymerization, maintaining the pressure and the reaction time constant. We show the summarized results in Table.2.

Table-2. Results of St polymerization by reverse ATRP in scCO₂, changing the temperature.^{a)}

Entrance	Temperature (°C)	Conversion (%) ^{b)}	Mn(th) ^{c)}	Mn(SEC)	Đ ^{d)}	Dn (μm) ^{e)}	PSD ^{e)}
1	130	68	10274	15752	1.35	-	-
2	110	48	7882	13508	1.16	-	-
3	90	10	1642	7023	1.3	-	-

a). Pressure = 1100 psi, reaction time = 20 h., a steric stabilizer of PSt-*b*-PTDFM (81/19 molar composition) and Mn = 27226. b). Determined gravimetrically. c). Mn(th) = [St]/2[AIBN]*%conv.*104. d). Determined by SEC. e) Dn= particle diameter, PSD = particle size distribution. Not yet determinate

With the temperature decreasing in the radical polymerization we observe the decrease in the conversion and the Mn, but the polymerization control is better since the polydispersity values decrease.

Conclusions:

The reverse ATRP polymerization of St in scCO₂ was conducted with a moderate conversion, with a Dpn in average 150 and with acceptable polymerization control since the dispersity values were narrow.

Acknowledgements: The authors thank the financial support from CONAYT by the project No. CB-2009-131103.

References:

- (1) Canelas, D. A.; Betts, D. E.; DeSimone, J. M. *Macromolecules* **1996**, 29, 2818.
- (2) Zetterlund, P. B.; Kagawa, Y.; Okubo, M. *Chemical Reviews* **2008**, 108, 3747.
- (3) Grignard, B.; Calberg, C.; Jerome, C.; Wang, W.; Howdle, S.; Detrembleur, C. *Chemical Communications* **2008**, 5803.
- (4) Grignard, B.; Jerome, C.; Calberg, C.; Jerome, R.; Wang, W.; Howdle, S. M.; Detrembleur, C. *Chemical Communications* **2008**, 314.
- (5) Villarroya, S.; Zhou, J.; Thurecht, K. J.; Howdle, S. M. *Macromolecules* **2006**, 39, 9080.
- (6) Canelas, D. A.; DeSimone, J. M. *Macromolecules* **1997**, 30, 5673.

Surface initiated NMP through a stable latex of block copolymers PAA-*b*-PS-*b*-PAA

Claude St Thomas¹, Judith N Cabello-Romero¹, Hortensia Maldonado-Textle¹,
Franck D'Agosto², Bernadette Charleux², Ramiro Guerrero-Santos¹

1. Centro de Investigación en Química Aplicada (CIQA), Blvd. Enrique Reyna 140. Saltillo, Coahuila, MEXICO, CP 25100

2. de Lyon 1, CPE Lyon, CNRS UMR 5265, Equipe LCPP Bat 308F, 43 Bd du 11 Novembre 1918, F-69616 Villeurbanne, France

Abstract

The applicability of *RN*, a new inifer, in emulsion polymerization to obtain stable latexes was investigated. Such inifer was used to initiate a homopolymerization of AA in dioxane to form macroagentNMP/RAFT which was used in a surfactant-free emulsion polymerization of styrene or butyl acrylate. Latexes obtained were used to trigger out NMP polymerization from the surface by activating the alkoxyamine end groups. In the case of 4-sodium sulfonate styrene a reorder of the spherical assembled structures was observed.

Introduction

The Reversible Deactivation Radical Polymerization RDRP (1) [including Nitroxide-Mediated Polymerization (NMP) (2), Atom Transfer Radical Polymerization (ATRP) (3), and Radical Addition-Fragmentation Transfer (RAFT) (4) techniques] is an efficient process to prepare well-defined macromolecular architectures from vinyl monomers. The RDRP techniques can be used to form nano-objects as spheres, cylinders, vesicles, etc. through polymerization-induced self-assembly strategy vernacularly known as PISA (5) which involves the formation of amphiphilic block copolymer in an aqueous media⁶. Indeed, PISA is centered on the ability of such copolymers to build-up supra-macromolecular arrangements having potential use in different areas as: biomedicine, biomaterials, microelectronics, photo electronics materials, and catalysts⁷. For this reason, an increasing number of papers using RDRP techniques to succeed PISA have appeared in the last decade.

On account of his versatility, RAFT polymerization has revealed very attractive to trigger out well-defined polymers and successfully implemented to carry out PISA. However, in spite of the great number of monomer combination and structures, recently some attention has been devoted to combine RAFT with others RDRP techniques (8) in order to access to even more complex architectures. For instance, combined systems including ATRP/RAFT (9), RAFT/NMP (10), (11) or RITP/RAFT (12), have been reported. It must be remembered, that individual RDRP techniques are mainly differentiated by their ability to polymerize preferentially some families of monomers with a strong dependency on structures of control agent. The use of molecules having the capacity to regulate efficiently two or more RDRPs open the way to unusual polymer structures able to develop remarkable morphologies. In the case of PISA it can lead to a variety of nanoparticles such as micelles, vesicles or fibers.

Recently we reported the preparation of amphiphilic block copolymers via RAFT with a dithiobenzoate having an alkoxyamine as R group (10). To achieve the procedure, two separated steps or even in one-pot system was required. In both cases, a water soluble homopolymer was first prepared and then, used as macroRAFT agent in aqueous polymerization of hydrophobic monomers to yield copolymers with still active alkoxyamine groups at one chain-end.

In the present report, we describe a route to synthesize of symmetric and well-defined amphiphilic copolymers from a new dual RAFT/NMP controller. A new dialkoxyamine trithiocarbonate (RN) (13) was synthesized and used in a solution polymerization of α,ω -dialkoxyamine-poly(acrylic acid) trithiocarbonate which was utilized subsequently in a surfactant free emulsion polymerization of styrene or butyl acrylate. For the first time, the obtained latex was used, to trigger out SIP by cleavage the alkoxyamine end-groups attached to PAA block copolymer in the surface of the nano-sized particles. Given that NMP initiated with TEMPO alkoxyamines is restricted to styrenic monomers, styrene and 4-sodium styrene sulfonate were used at 130 °C to form long-haired nanoparticles which reorganize to form rubbions or micelles.

Experimental

Conversion of AA was determined by ¹H NMR spectra carried out in DMSO-*d*₆ at room temperature (Brucker DRX 300). For the latexes, hydrophilic monomers consumption was followed by gravimetric analysis. Before analysis, the polymers were modified by methylation of the carboxylic acid groups using trimethylsilyl diazomethane.

The particle size was measured by dynamic light scattering (NanoZS from Malvern Instruments) and TEM. In order to preserve particle shape, latexes containing PBA were observed by (cryo-TEM).

Polymerization

Synthesis of PAA MacroRAFT/NMP agent (Step1).

In a typical experiment (with targeted M_n , ca. 11,000; 6,000 and 7,000 g mol⁻¹), the procedure was the following; in a two-necked round-bottom flask equipped with a condenser 56 mg of **RN** (69 x 10⁻⁶ mol L⁻¹) and 2.3 mg of ACPA (8.2 x 10⁻⁶ mol L⁻¹) were dissolved in 6.3 mL of dioxane and 1.96 g of AA (0.027 mol L⁻¹). 0.326 mg of 1, 3, 5- trioxane (0.0036 mol L⁻¹) was added as an internal reference for NMR analysis. The monomer conversion was determined by ¹H NMR spectroscopy of the crude reaction medium diluted with DMSO-*d*₆ by the relative integration of the protons of 1,3,5- trioxane and the double-bond protons of monomers. Also a kinetic follow of AA polymerization in the presence of RN was also carried out. (See samples in Table 1)

Table 1. RAFT polymerization of acrylic acid mediated by **RN**.

Entry	PAA- RN code	[AA] / [RN]	[RN] / [ACPA]	<i>t</i> (h)	Conv ^a (%)	$M_{n,th}^b$ (g mol ⁻¹)	$M_{n,SEC}^c$ (g mol ⁻¹)	\bar{D}^c
1 ^d	PAA- RN 1	300	10	7	63	14,480	10,400	1.3
2 ^d	PAA- RN 2	300	10	8	61	14,000	10,770	1.3
3 ^d	PAA- RN 3	185	10	8	49	7,340	8,040	1.2
4 ^e	PAA- RN 4	155	4.3	5	77	9,400	8,820	1.2
5 ^e	PAA- RN 5	150	5.0	4.5	39	5,050	4,100	1.2
6 ^e	PAA- RN 6	150	4.5	5	71	8,670	8,040	1.2

^aMonomer conversion was determined by ¹H NMR. ^bTheoretical $M_n = ([AA]_0 \times \text{conversion} \times M_{AA}) / [RN]_0 + M_r$. ^cNumber-average molar mass and \bar{D} determined by SEC in THF with PMMA standards. ^dCarried out in water 55% (v/v), ^eCarried out in dioxane 70% (v/v). T = 70 °C

RAFT Surfactant Free Emulsion Polymerization Procedure (Step 2).

In a typical experiment, 500 mg of styrene was added to a solution of previously synthesized A4 ($M_n = 11,000$ g mol⁻¹) and water content was adjusted. At that point, 1 mL of an aqueous solution of ACPA (concentration = 6.9 mg mL⁻¹ neutralized by 7 mol equiv of NaHCO₃) was added to the reaction mixture. The medium was purged with argon during 30 min and the round-bottom flask was immersed in oil bath thermostated at 80 °C. Stable latexes PAA-b-PS-b-PAA or PAA-b-PBA-b-PAA were obtained. Similar molar ratios were utilized to polymerize BA using PAA-**RN** with a minor amount of styrene, ca. 10% (¹⁴). Results are reported in Table2.

Table 2. RAFT emulsion polymerization of S and BA mediated by different PAA-**RN**

Entry	Macro-CTA/M	<i>t</i> (h)	DP _{n,th}	Conv ^a (%)	$M_{n,SEC}^b$ (g mol ⁻¹)	\bar{D}^b	D_h^c	Poly ^c	D_n	D_w/D_n^d
L1	PAA 1/S	8	650	70	53,400	1.7	55	0.12	45	1.15
L2	PAA 6/S	8	500	60	39,500	1.6	50	0.19	43	1.11
L3	PAA 5/S	8	800	85	73,000	2.2	53	0.11	38	1.12
L4	PAA 6/S	5	900	70	62,500	1.7	51	0.10	40	1.09
L5	PAA 5/BA	5	400	52	25,200	1.8	30	0.38	23	1.07
L6	PAA 6/BA	8	550	60	39,700	1.7	34	0.19	30	1.21

^aMonomer conversion was determined gravimetrically. ^bNumber-average molar mass and dispersity determined by SEC in THF after methylation using PS standards. ^c \bar{D}_h were obtained by dynamic light scattering (DLS). ^d D_w/D_n were obtained by transmission electron microscopy. T = 80 °C ; pH = 3.05.

Surface Initiated Polymerization through NMP from latex nanoparticles Procedure (Step 3).

Polymerization of SSNa and S were achieved in an autoclave reactor. In a typical experiment 138 mg of SSNa (0.00067 mol L⁻¹) was added to the latex L2 (291 mg, 7.4x 10⁻⁶ mol). The mixture was degassed with three freeze-pump-thaw cycles and heating in autoclave under argon at 130 °C overnight. Polymers obtained were characterized by TEM.

Results and Discussion

Synthesis of PAA MacroRAFT/NMP agent (Step 1).

It starts with the RAFT polymerization of AA with **RN** to form a PAA macro-iniferters (**PAA-RN**) which were subsequently chain extended using styrene or butyl acrylate under surfactant-free emulsion polymerization conditions at 80 °C to produce stable latexes. As described in the experimental section, a series of PAA-RN were prepared with different monomer concentrations keeping the molar ratio RN / ACPA = 10. An inhibition of about 3h is observed in this polymerization as it can be seen in Figure 1a for an experiment carried out using a molar ratio: Monomer / **RN** / ACPA = 300 / 1 / 0.1 which correspond to polymers PAA-**RN** 1 and PAA-**RN** 2 in Table 1.

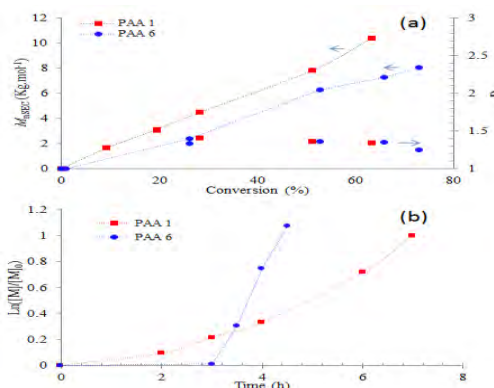


Figure 1. Kinetics of acrylic acid RAFT polymerization mediated by **I** (a) Conversion vs. M_{nSEC} and (b) Conversion vs. time; $T = 70^\circ\text{C}$. Solvent; water (PAA-**I** 1) and dioxane (PAA-**I** 6).

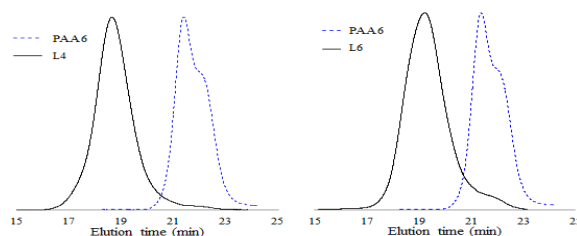


Figure 2. (a) SEC trace of PAA 6 and its corresponding block copolymer **L4**, (b) SEC curve of PAA 6 and its corresponding block copolymer **L6**.

The molecular weights increased and D decrease with conversion as shown in Figure 1a and 1b. In experiments A4-A5, D was improved but the experimental M_n retains the same discrepancy which was attributed to chain transfer to dioxane²⁶. In fact, the SEC traces corresponding to PAA-**RN** show a shoulder in the low molar mass region suggesting that a small fraction of dead-end chains were formed. Nevertheless, a living character was observed in all these cases indicating the incorporation of RN to PAA which was supported by the fact that these polymers are effective precursors of block copolymers.

Surfactant free Emulsion RAFT Polymerization

Amphiphilic block copolymers were obtained using S or BA as hydrophobic monomer in Surfactant Free Emulsion polymerization as reported by Charleux (15) starting from the PAA. These polymerizations were carried out under RAFT conditions with molar ratios of $[\text{PAA}] / [\text{M}] = [1] / [400]$ or $[1] / [1000]$. In the case of styrene retardation ($< 1\text{h}$) was observed whereas with BA neither retardation nor inhibition was detected.

Remarkably in this case, stable latexes were formed irrespectively of conversion, molecular weight of PAA or hydrophobic monomer. As it can be seen, the SEC traces presented in Figure 2, an entire shift toward high molecular weight is produced after hydrophobic chain extension of PAAs. High conversion is obtained in almost all cases and M_{nth} is well adjusted to M_{nExp} (see Table 2) albeit, D increases significantly. As it can see, block copolymers show asymmetrical SEC traces which are assigned to dead-end chains mentioned above. Indeed, a small peak corresponding to such non-functionalized chains is observed in Figure 2b in both, PAA-**RN** and PAA-b-PBA-b-PAA SEC traces.

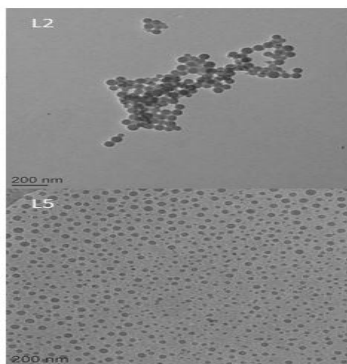


Figure 3. TEM images of latex **L2** and cryo-TEM images of latex **L5**.

All latexes obtained were also characterized by TEM (Fig. 3). The diameters averages D_h obtained by DLS (Table 2) are slowly higher than diameters obtained by TEM due to the hydrodynamic effect. For all latexes the average diameter was calculated to be 68 nm. However, using the same PAA two different sizes can be obtained demonstrating the influence of length chain of hydrophobic segment in nanoparticles obtained. Self-assembled micelles of block copolymers: PAA-b-PS-b-PAA were observed by TEM (Figure 3a), whereas for PAA-b-PBA-b-PAA a cryo-TEM was used to preserve original form of nanoparticles (Figure 3b).

The ^1H NMR characterization of amphiphilic block in deuterium oxide or DMSO- d_6 is presented for latex L2 in Figure 5. As we can observe in the Figure 4a, the block copolymers dissolved in DMSO- d_6 exhibit peaks corresponding to PS at 7.3 to 6.2 ppm as well as PAA peaks at 2.1 to 2.4 ppm. Also the methyl groups of alkoxyamine peak appearing at 0.8 ppm and the methyne proton α to the alkoxyamine at 5.2 ppm are observed.

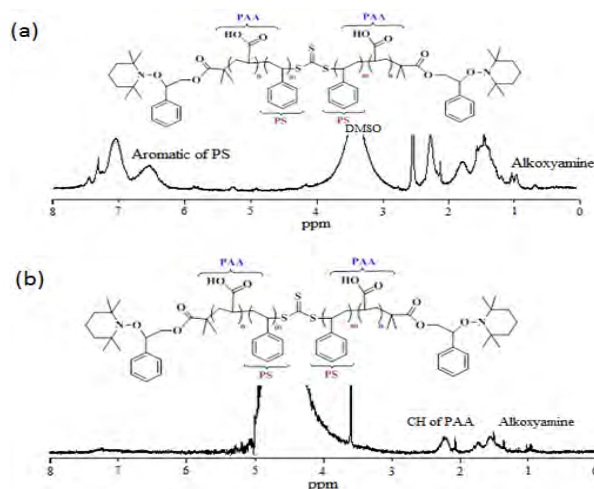


Figure 4. (a) ^1H NMR of latex L2 in DMSO- d_6 , (b) ^1H NMR of Latex L2 in D_2O

In the Figure 4b, the ^1H NMR spectrum of the same latex dissolved in D_2O is presented. In this case only the PAA peaks at 2.1 ppm and CH_3 at 0.9 ppm attributed to methyl groups of alkoxyamine are observed. The disappearance of the PS peaks at 7.3 ppm is explained by demixion this hydrophobic chain in water to form encapsulated PS cores by and hydrophilic shell of PAA. According to these results we can reasonably admit that the formation of block copolymers PS-b-PAA-b-PS was succeeded.

Surface Initiated Polymerization through NMP from latex nanoparticles (Step 3)

Considering that latexes are composed of RDRP- active self-assembled amphiphilic triblock copolymers with functional alkoxyamine end- group (see Figure 4), it should be possible to chain extend their hydrophilic tail located on the surface of particles. In order to do so, latexes were heated at 130 $^{\circ}\text{C}$ to form styryl radicals by cleaving the alkoxyamine end-group in the presence of monomers.

The case of SIP of SSNa, this is a water soluble monomer; the polymerization mediated by the alkoxyamine groups linked in hydrophilic corona of nanoparticles could lead to interesting double hydrophilic shell. To avoid distortions of spherical particles we chose latex L2 prepared with S to ensure that the heating does not affect its form even if the heating is above the glass transition temperature of polystyrene). It was predicted that at 130 $^{\circ}\text{C}$ the alkoxyamine decomposes to generate an initiating radical which get started SIP of SSNa in water. Taking into consideration that only few reports refer to NMP of SSNa (16) a blank experiment was also carried out without monomer to compare.

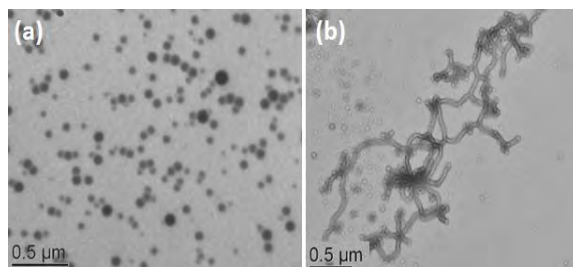


Figure 5. TEM images of latex L2 before (a), and after (b) SSNa surface initiated polymerization via NMP.

In both cases, the experiments ran without any noticeable change, i.e. the latex exhibited a typical light scattering blue color before and after reaction. Samples were taken, diluted and placed in copper grids for TEM observation. As it can be seen in Figure 5, the effect of SSNa polymerization is noticeable in the alteration of self-assembled structures. The transformation of nano-spheres to nano-cylinders is certainly favored by the change of the HLB value of assembled chains and the softening of the polystyrene core during thermal treatment.

Conclusions

It has been demonstrated that RN is an effective chain transfer agent in the formation of self-assembled polyacrylic acid block copolymers prepared through surfactant-free emulsion polymerization. Well-defined nanoparticles were observed in TEM which were tested in a surface initiated polymerization of styrene or SSNa. The SEC traces and microscopy analysis strongly suggest that polymers growth was produced from the surface and the change in the hydrophilic/lipophilic balance of block copolymers induced a new organization of chains. Thus, the multiblock copolymer PSSNa-*b*-PAA-*b*-PS-*b*-PAA-*b*-PSSNa leads to nano-cylinders.

Acknowledgements

Éric Auger, ONA YTF, p f fu “É Sup u -Physique É qu” E/ ; ; F p j fu B-2008-1-04. Thanks are given to all people who helped me in this step, specially: Hortensia Maldonado-Textle, Judith N. Cabello-Romero, Guadalupe Tellez-Padilla, Jesus Angel Cepeda-Garza, Xuewei Zhang, Julien Parvole, and Edgar Espinosa.

References

- 1 Jenkins, A. D.; Jones, R. G.; Moad, G.; *Pure Appl. Chem.* **2010**, 82, 483–491
- 2 Georges, M. K.; Veregin, R. P. N.; Kazmaier, P. M.; Hamer, G.K. *Macromolecules*, **1993**, 26, 2987-2988. (b) Hawker, C. J., Bosman, A. W. and Harth, E. *Chem. Rev.*, **2001**, 101, 3661-3688.
- 3 Matyjaszewsky, K. and Xia, J. *Chem. Rev.*, **2001**, 101, 2921-2990
- 4 Rizzardo, E., Moad, G., Thang, S. US Patent, WO **98/01478**; (b) John Chiefari, J., Chong, Y. K., Ercole, F., Krstina, J., Jeffery, J., Le, T. P. T., Mayadunne, R. T. A., Meijs, G. F., Moad, C. L., Moad, G., Rizzardo, E. and Thang, S. H. *Macromolecules*, **1998**, 31, (16), 5559-5562.
- 5 Blanz, A., Ryan, A. J., Armes, S. P. *Macromolecules*, **2012**, 45, 87–99
- 6 Mai, Y.; Eisenberg, A. *Chem. Soc. Rev.*, **2012**, 41, 5969-5685
- 7 Zehm, D.; Ratcliffe, L. P. D.; Armes, S. P. *Macromolecules*, **2013**, 46, 128-139
- 8 Moad, G.; Rizzardo, E.; Thang, S. H. *Aust. J. Chem.* **2012**, 65, 985-1076
- 9 Nicolay, R.; Kwak, Y.; Matyjaszewski, K.; *Macromolecules*, **2008**, 41, 4585–4596.
- 10 St Thomas, C.; Maldonado-Textle, H.; Rockenbauer, A.; Korecz Laszlo, Nagy, N.; Guerrero-Santos, R.; *J of Polym. Sci. Part A: Polym. Chem.* **2012**, 50, 2944–2956.
- 11 Favier, A.; Luneau, B.; Vinas, J.; Laissaoui, N.; Gimes, D; Bertin, D. *Macromolecules*, **2009**, 42, 5953–5964.
- 12 Enriquez-Medrano, J. F.; Maldonado-Textle, H.; Hernandez-Valdez, M.; Lacroix-Desmazes, P.; Guerrero-Santos, R. *Polym Chem.*, **2013**, 4, 978-985.
- 13 St Thomas, C.
- 14 Chenal, M.; Bouteiller, L.; Rieger, J. *Polym. Chem.* **2013**, 4, 752-762
- 15 Brusseau, S.; Boyron, O.; Schikaneder, C.; Santini, C. C.; and Charleux, B. *Macromolecules*, **2011**, 44, 5590-5598.
- 16 (a) Brusseau, S., Belleney, J., Magnet, S., Couvreur, L., Charleux, B., *Polym. Chem.* **2010**, 1, 720-729 ; (b) Bagryanskaya, E., Brémond, P., Edeleva, M., Marque, S. R. A., Parkhomenko, D., Roubaud, V., Siri, D., *Macromol. Rapid Commun.* **2012**, 33, 152-157

Development of New Polymeric Materials from ϵ -Caprolactam and Starch

M.G. Rodríguez-Delgado¹, F.J. Rodríguez-González, O. Pérez-Camacho.

Center for Research in Applied Chemistry, Blvd. Enrique Reyna 140, Saltillo, Coahuila 25253, México.

ABSTRACT

The anionic ring-opening polymerization of ϵ -caprolactam was carried out in the presence of 3, 6 and 9 % granular starch. Polymers were characterized by ¹H RMN and FTIR, whereas the interfacial characteristics of the compounds were assessed through the selective separation of PA6 and starch phases by SEM. PA6 conversion decreased from 80 to 40 % and the molecular weight varied between 14,947 and 3,500 g/mol when the content of starch was increased from 3 to 9 %, respectively. On the other hand, the existence of PA6 signals in the fraction of starch granules were detected by ¹H RMN and FTIR, and SEM micrographs showed good interfacial adhesion and the presence of PA6 onto the surface starch granules. These results evidenced by the first time the formation of starch-g-PA6 copolymer from anionic ring-opening polymerization.

Keywords: starch; nylon 6; starch copolymers; anionic ring-opening polymerization.

1. Introduction

Anionic polymerization of ϵ -caprolactam has been extensively investigated, which is well known that occurs at faster rates than the classical hydrolytic polymerization process, reaching the equilibrium conversion in only few minutes[1][2]. The presence of anionically activated monomer and activator, are essential conditions for starting the anionic polymerization of ϵ -caprolactam[3]. Moisture inhibits the anionic polymerization, eliminating the active primary amine, where the catalyst also reacts with moisture prior to the initiator[4]. Therefore, the anionic polymerization of ϵ -caprolactam should be carried out after drying raw materials. On the other hand, natural polymers like starch, cannot satisfactorily replace the functional and physical properties of synthetics plastics[5]. Due to its high hydrophilicity being constituted by a large number of OH groups in its structure, starch cannot be easily processed[6]. In order to solve these problems, the modification of starch was studied by physical or chemical modifications with other polymers[7]. The chemical modification includes graft copolymerization extensively used in the modification of starch as an efficient method to improve its properties[6]. The difficulty in the graft copolymerization is the content of water and OH groups in the starch, because most of the catalysts are sensitive to the moisture or OH groups[8]. Several graft copolymers of starch with vinyl polymers, as acrylamide, methacrylamide, acrylic acid, methacrylonitrile, styrene, and polyethylene, have been reported, among others[9]–[16]. These materials have been produced with redox initiators for the generation of free radicals, generally employ potassium persulfate ($K_2S_2O_8$), ceric ammonium nitrate (CAN) and Fenton reagent (H_2O_2/Fe^{2+}). In this type of reactions, the graft copolymerization is always accompanied with homopolymerization of vinyl monomers, which reduces grafting efficiency[11]. On the other hand, several researchers have carried out studies on the synthesis of starch copolymers with grafted biodegradable polyesters as polylactic acid (PLA) and polycaprolactone (PCL), which confer thermoplastic properties, and improved the physical properties of starch[17]. Starch copolymers are generally obtained by polycondensation or ring-opening reactions [7], [17]–[19] in bulk or suspension [8], [20], using catalysts based on octanoate $Sn(Oct)_2$ and stannous chloride $SnCl_2$, titanium tetrabutoxide $Ti(OnBu)_4$ and aluminum isopropoxide $Al(OiPr)_3$ among others. In this work we carried out the anionic synthesis of CM in the presence of starch using sodium caprolactamate (NaCM) and N-acetylcaprolactam for obtaining a starch copolymer with PA6 grafts with the purpose of studying the parameters governing the formation of PA6 grafted on the starch and its effect on the structure of the copolymer of starch-g-PA6.

Experimental

2.1 Materials

Potato starch was supplied by ADM/Ogilvie, ϵ -caprolactam (CM), acetyl caprolactam (ACM), formic acid, anhydrous trifluoroacetic acid and tetrahydrofuran supplied by Sigma-Aldrich and a concentrated sodium caprolactamate (NaCM) in CM at 18.5%w supplied by Brüggemann Chemical.

2.2 Anionic polymerization of caprolactam

In a Schlenk container were placed 21.76g of CM and 4.28g of NaCM/CM, while, in a Schlenk flask ball were placed 30g of CM, 1.5811g of ACM and the corresponding amount of starch (3, 6 and 9%). The container and flask ball were maintained at 100°C under magnetic stirring and argon bubbling to dry and degasify the reagents. The temperature was increased to 130°C and the melted materials of the Schlenk and flask ball were mixed to start the polymerization. The mixture solidified in 5 min and the reaction product was deactivated with methanol, then methanol was decanted, and the product was extracted with formic acid. Then the polymer (PA6 with starch) was precipitated with methanol, filtered and washed several times. Finally the solid was dried in a vacuum oven at 70°C, until constant weight to determine the conversion and the percentage of insoluble.

2.3. Gel permeation chromatography (GPC)

The molecular weight of PA6 was obtained by gel permeation chromatography, performed in an Alliance 2695. Samples were dissolved in a mixture of tetrahydrofuran and anhydrous trifluoroacetic acid (98:2). As mobile phase HPLC grade tetrahydrofuran was used at 30°C, the injection volume was 25 μ L.

2.4. Infrared Spectroscopy Attenuated total reflectance (ATR)

The infrared analysis of PA6-starch was carried out by IR-ATR spectroscopy performed in a Magna-IR Spectrometer 550 from Nicolet running a background and 100 scans for each sample.

2.5. Proton nuclear magnetic resonance (^1H NMR)

PA6-starch copolymer could be demonstrated by ^1H RMN performed in a Jeol Eclipse 300MHz. Samples dissolved ± 10 mg of polymer in 0.6 mL of formic acid using toluene capillary as external reference which is introduced into the tube together with the dissolved sample.

2.6. Scanning electron microscopy (SEM)

The morphological observation of samples was carried out using SEM; the samples were cryogenically fractured and coated with silver. Fractured samples were analyzed in a JEOL-JSM-7401F, operated at 15 kV.

3. Results and Discussion

3.1. Anionic polymerization of caprolactam

Table 1 exhibits the effect of starch content on the conversion, molecular weight (Mn) and % of insoluble material in the anionic polymerization of caprolactam. It can be seen that the highest conversion was achieved during the homopolymerization of CM (90.7%). Also, is observed that conversion decreased when the starch content increased. This decrease is attributed to the presence of high concentration of OH groups in the starch, which tend to deactivate the growing CM anionic species. On the other hand, the Mn of the PA6 obtained in the homopolymerization of CM was also higher, than the polymers obtained in the presence of starch. As expected, upon increasing the starch content Mn decreases, which is also attributed to the excess of OH reactive groups of starch acting as terminator chains in the growing PA6 chains.

Table 1
Effect of starch content on the conversion, Mn and % insoluble

Initial Starch (%)	Conversion (%)	Mn g/mol	Insoluble (%)
0	90.7	12,000	0
3	80.3	14,947	2

6	69.3	13,201	9.1
9	40.3	3,500	3.1

Insoluble content reported in Table 1, could correspond to the amount of starch modified with PA6, where in the soluble part (formic acid) just PA6 was recovered. As expected, the percentage of insoluble obtained for PA6 (without addition of starch) was 0%, where for the reactions with starch contents of 3%, 6% and 9% the insoluble content is different compared to the initial content of starch. As can be seen in Table 1, just for the experiment with initial addition of 6%, all the starch could have been recovered in the insoluble material. For reactions with 3% and 9% of initial addition of starch, an apparent loss of 33.3% and 65.5% of starch occurred during the polymerizations, what can be attributed to the loss or extraction of low Mw chains of species contained in the starch particles used. As for the reaction with initial addition of 6% of starch, contrary to the other reactions an increase of insoluble material is evident, where was considered that also the loss of low MW chains of species into the starch should occur, but in this case the polymerization conditions were more favorable for the formation of PA6 onto starch. Is important to mention that starch particles were susceptible to suffer some morphological change on its structure, when were previously treated with heat and vacuum, in order to avoid the deactivation of anionic polymerization of ϵ -caprolactam. This was confirmed by SEM studies on samples of starch applying the same drying process, comparing with SEM of starch undried (Fig 1).

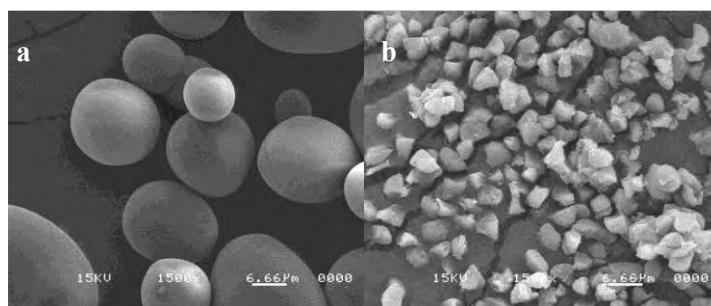


Figure 1. SEM micrographs 1500x of a) undried starch b) dry starch

Figure 1a shows the SEM micrographs of the original starch granules (undried starch), which have oval shape and smooth surface. Figure 1b, shows the same starch particles after drying for 1 hour at 100°C and argon bubbling, which seems to be fragmented into amorphous small pieces. According to the above starch morphology it is probably that: 1) the starch can be solubilized in the molten caprolactam released as smaller molecules from the starch fragments. 2) The solubilized starch passed through the filter pores used due to its size. Based on the above, it can be said that for 3% and 9% reactions, a portion of starch was solubilized in the CM, then it could pass through the filter during the process, and only some starch is retained in the filter (2 and 3.1%, respectively). However, for the reaction with 6% of starch, the amount of solids retained on the filter paper was increased up to 50% more with respect to the initial starch. Although, it is obvious that also there was loss of starch in the drying process, it is also obvious that there PA6 since was achieved to obtain 9.1% of retained solids, likely PA6 grafted onto starch.

3.2. Scanning electron microscopy (SEM)

Figure 2 shows the SEM micrographs obtained for fractured surfaces of a mixture physical of starch and PA6 (made in the Brabender) and the sample of the insoluble part of PA6/6% starch. It can be seen in Figure 2a that the ovals shape of some starch granules, as well as smooth surface in these. Whereas, in Figure 2b can be seen after a cryogenic fracture as the starch granules are of micrometer size and are dispersed only in the PA6 matrix, also have smooth surfaces which indicate that the temperature in the mixing process does not affect the starch granules. Furthermore, shows a fragile fracture confirming that there is no a chemical bond between starch and PA6. On the other hand, for insoluble (6%) part of PA6/6% starch Fig. 2c after a cryogenic fracture is observed a starch granule surrounded by PA6, the starch granule as well as

the polymeric matrix have rough surfaces and very good adhesion between both, which shows a type of fracture ductile suggesting the chemical bond between starch and PA6.

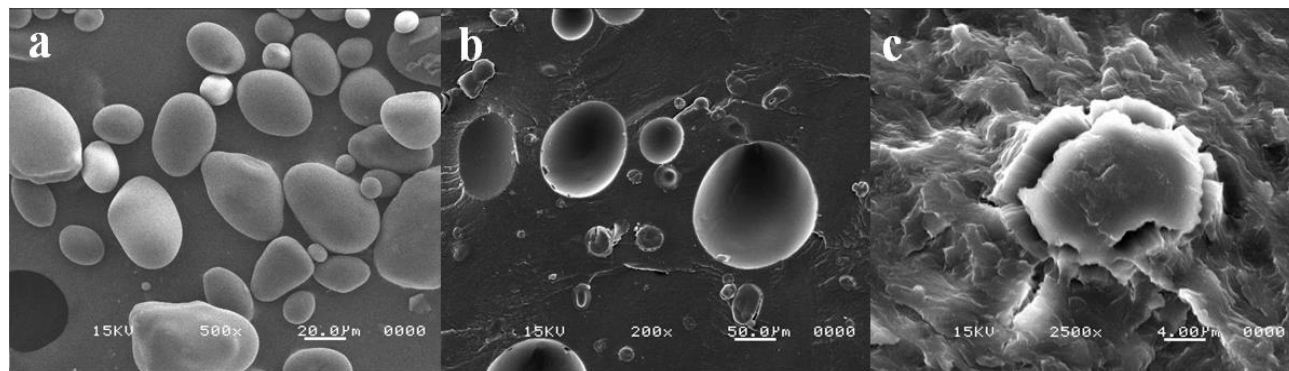


Figure 2. SEM micrographs a) granular starch b) mixture of starch and PA6 and c) solid retained in the filter (the insoluble parts of PA6/6% starch).

3.3. Proton nuclear magnetic resonance (^1H NMR)

Figure 3a and 3b shows the ^1H NMR spectra of PA6 and of the insoluble part of PA6/6% starch, respectively. In Fig. 3a is observed the proton signals for the CH_2 chains of PA6 at 1.8 ppm, 2.2 ppm, 2.4 ppm, 2.8 ppm and 3.8 ppm. While, for the insoluble sample (PA6/6% starch) the corresponding signals for PA6, besides broad signals in the region from 4 to 5.8 ppm corresponding to the starch protons, are observed. The spectra were assigned as reported by Dragunski y Pawlicka[21]. The signal observed at 4.1–4.2 ppm corresponds to methylene protons of the alcohol $\text{CH}_2\text{-OH}$ (6) and ether group $\text{CH}_2\text{-O}$ (7). At 4.2 and 4.3 ppm are observed the signals for the methine protons of CH-O groups (1, 4). The signals at 4.7, 5.0 and 5.2 ppm correspond to the protons of secondary alcohols CH-OH (2, 3, and 5) of the cycles, and at 5.8 ppm is present the signal of primary OH groups of starch.

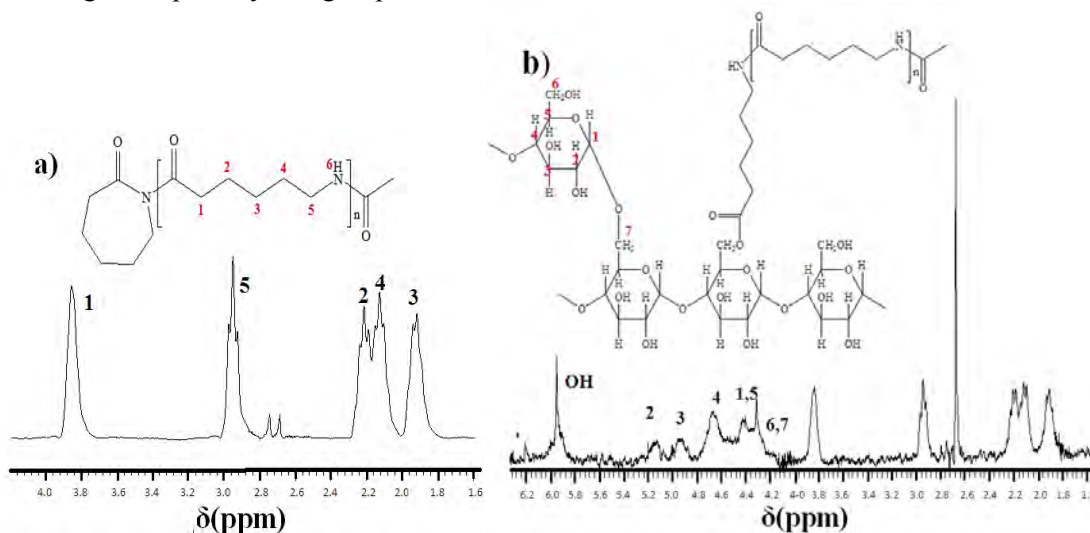


Figure 3. Proton nuclear magnetic resonance (^1H NMR) a) PA6 b) the insoluble part of PA6/6% starch

3.4. Infrared Spectroscopy (ATR)

Figure 4 shows the ATR spectra of starch, PA6 and the insoluble parts of PA6/6% starch and PA6/3% starch. The infrared spectrum of the starch shows the characteristic broad band assigned to OH stretching vibrations in the range of 3000 to 3650cm^{-1} , and the bands at 1650cm^{-1} corresponding to deformation of C-O-C [10]. The broad band from 970 to 1200cm^{-1} with three peaks is the most characteristic band for a polysaccharide and is attributed to stretching C-O [22]. PA6 spectrum presents characteristic bands at

3000 cm^{-1} corresponding to the NH stretching vibrations, at 1640 cm^{-1} stretching band for C=O and 1546 cm^{-1} NH deformations. For insoluble samples of PA6/6% starch and PA6/3% starch, the characteristic signals of PA6 and starch were observed. Furthermore, were found two new bands at 1718 cm^{-1} and 1199 cm^{-1} , corresponding to C=O and C-O groups, respectively, from the ester group formed in the condensation reaction between primary alcohols and carbonyl groups between the PA6 and starch during the polymerization reaction. According to the results obtained by ATR and NMR, the formation of an ester is evidence of the chemical bond between starch and PA6, which confirms the formation of a starch copolymer with grafted PA6 (starch-g-PA6).

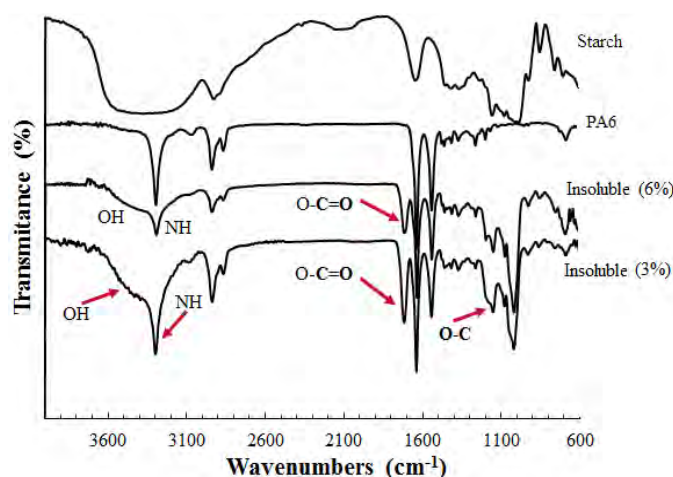


Figure 4. Infrared spectrum (ATR) of starch, PA6 and insoluble part PA6/6% starch and PA6/3% starch

4. Conclusions

The anionic polymerization of ϵ -caprolactam in the presence of different amounts granular starch was carried out. The increment of starch leads to decrease the conversion and the molecular weight in the copolymer. The morphological study of samples demonstrated that the starch granules are broken into small fragments during the drying process. PA6 is grafted onto starch chains during the reaction, which results in the increase of the amount of retained solids (insoluble) as well as improves interfacial adhesion between starch and PA6. It was possible to verify the formation of a starch copolymer with grafted PA6 (starch-g-PA6) by SEM, ^1H NMR and ATR analyses in insoluble samples of 3 and 6% of starch, detecting an ester group resulting from the reaction between starch and PA6, demonstrating for the first time the formation of a starch copolymer grafted with PA6 (starch-g-PA6) obtained by anionic polymerization of caprolactam.

5. References

- [1] K. Ueda, M. Nakai, M. Hosoda, and K. Tai. *Polym. J.*, vol. 29, no. 7, pp. 568–573, 1997.
- [2] G. Rusu. *High Perform. Polym.*, vol. 16, no. 4, pp. 569–584, Dec. 2004.
- [3] S. Ahmadi, J. Morshedien, S. A. Hashemi, P. J. Carreau, and W. Leelapornpisit. *Iran. Polym. J. (English Ed.)*, vol. 19, no. 3, pp. 229–240, 2010.
- [4] J. H. Park, W. N. Kim, H. Kye, S.-S. Lee, M. Park, J. Kim, and S. Lim. *Macromol. Res.*, vol. 13, no. 5, pp. 367–372, Oct. 2005.
- [5] D.-K. Kweon, D.-S. Cha, H.-J. Park, and S.-T. Lim. *J. Appl. Polym. Sci.*, vol. 78, no. 5, pp. 986–993, Oct. 2000.
- [6] Qingxia Gong; Li-Qun Wang; Kehua Tu. *Carbohydr. Polym.*, vol. 64, pp. 501–509, 2006.
- [7] L. Chen, X. Qiu, M. Deng, Z. Hong, R. Luo, X. Chen, and X. Jing. *Polymer (Guildf.)*, vol. 46, no. 15, pp. 5723–5729, Jul. 2005.
- [8] L. Chen, Y. Ni, X. Bian, X. Qiu, X. Zhuang, X. Chen, and X. Jing. *Carbohydr. Polym.*, vol. 60, no. 1, pp. 103–109, Apr. 2005.
- [9] V. D. Athawale and V. Lele. *Starch - Stärke*, vol. 52, no. 6–7, pp. 205–213, Jul. 2000.
- [10] V. Nikolic, S. Velickovic, and A. Popovic. *Carbohydr. Polym.*, vol. 88, no. 4, pp. 1407–1413, May 2012.
- [11] M. Li, Z. Zhu, and E. Jin. *Fibers Polym.*, vol. 11, no. 5, pp. 683–688, Sep. 2010.
- [12] L. Rahman, S. Silong, W. A. N. Zin, M. Z. A. B. Rahman, M. Ahmad, and J. Haron. *J. Appl. Polym. Sci.*, vol. 76, pp. 516–523, 1999.

- [13] V. D. Athawale and V. Lele. *Carbohydr. Polym.*, vol. 35, no. 1–2, pp. 21–27, Jan. 1998.
- [14] V. D. Athawale and V. L. Vidyagauri. *Starch - Stärke*, vol. 50, no. 10, pp. 426–431, Oct. 1998.
- [15] M. W. Meshram, V. V. Patil, S. T. Mhaske, and B. N. Thorat. *Carbohydr. Polym.*, vol. 75, no. 1, pp. 71–78, Jan. 2009.
- [16] V. . Athawale and V. Lele. *Carbohydr. Polym.*, vol. 41, no. 4, pp. 407–416, Apr. 2000.
- [17] D. Lu, P. Duan, R. Guo, L. Yang, and H. Zhang. *Polym. Plast. Technol. Eng.*, vol. 52, no. 2, pp. 200–205, Jan. 2013.
- [18] L. Najemi, T. Jeanmaire, A. Zerroukhi, and M. Raihane. *Starch - Stärke*, vol. 62, no. 3–4, pp. 147–154, Apr. 2010.
- [19] L. Najemi, T. Jeanmaire, A. Zerroukhi, and M. Raihane. *Starch - Stärke*, vol. 62, no. 2, pp. 90–101, Jan. 2010.
- [20] E. Choi, C. Kim, and J. Park. *Macromolecules*, vol. 32, pp. 7402–7408, 1999.
- [21] D. C. Dragunski; and A. Pawlicka. *Mater. Res.*, vol. 4, no. 2, pp. 77–81, 2001.
- [22] J. Aburto, I. Alric, S. Thiebaud, E. Borredon, D. Bikiaris, J. Prinos, and C. Panayiotou. pp. 1440–1451, 1999.

POLYMERIZATION FRONTS OF ACRYLIC MONOMERS IN DEEP EUTECTIC SOLVENTS USING MICROFLUIDICS

Roberto Becerra-Olivares,¹ Mario Zorrilla-Valtierra,¹ Jorge Delgado,¹ Arturo Vega,¹ Birzabith Mendoza-Novelo,¹ Carlos Villaseñor,¹ Irais Quintero-Ortega¹

¹ *Sciences and Engineering Division, Universidad de Guanajuato, Campus León. Loma del Bosque 103 Col. Lomas del Campestre, 37150 León, México*

Abstract

Nowadays, the polymeric industry should become more environment friendly as any other important industry. In such an idea, ethylammonium acrylate, a deep eutectic solvent, can be totally reused in waste-free acrylic polymerization as an ionic liquid where a frontal polymerization at 100°C has been achieved in contrast to 200°C in conventional solvents. This difference allows a better polymerization control and polymers with homogeneous physicochemical properties. Using microfluidics and an infrared sensor, it is possible to study in confined tunable geometries, and under homogeneous conditions of temperature and material income, the polymerization front.

Introduction

Polymers had become one of the most used materials in daily life. Unfortunately polymer production frequently involves the use of organic solvents and the generation of a large amount of waste-fluent. As time goes on, new global policies require a polymer production that respects the environment. As a consequence, the polymer industry, as any other important industry, must become friendlier with the environment, not just with the final product but starting with friendly-environment method of production.

In this context, ionic liquids (IL) emerge as an alternative to organic solvents often used in polymerization processes. Because of their unique characteristics, it had been used in separation processes, as electrolytic material, in the elaboration of porous materials, etc.

Different types of polymerizations had been conducted in these solvents: free radicals [1,2], ionic [3,4], atom transfer radical polymerization, reversible addition fragmentation chain transfer (ATRP, RAFT) [5,6].

The high cost of materials to elaborate an IL and the need of use organic solvents to recover the polymers are some of the drawbacks in the use of IL as solvents in polymerizations.

In 2003, Abbot et al. [7] found that mixing quaternary ammonium salts, such as choline chloride with urea produce eutectics that are liquids at ambient temperature and can be used as solvents with very specific properties (viscosity, conductivity and surface tension) that are similar to IL. This new type of solvent was named "Deep Eutectic Solvent" (DES) [8] and it is consider the third generation of IL. Using DES as a solvent has attracted interest because its low cost, easy-elaboration technique, non-toxic nature and biodegradability [9].

DES can be extended to any mix of a quaternary ammonium salt and a wide variety of hydrogen-bond donors (acids, amines, alcohols), in the proper ratio to produce an eutectic. Properties can be tuned simply by varying the molar ratio or by changing the type of salt and hydrogen donor.

The frontal polymerization of acrylic acid (AA) was achieved using a DES formed by acrylic acid and choline chloride [10]. In this case the AA is part of the DES and the monomer. In this extremely reactive polymerization, a better control of temperature and high conversion was obtained because of the properties of the solvent.

Other types of DES were prepared to act as monomer and solvent in frontal polymerizations [11]

with no further understanding of the process or the reaction mechanism. Because the increasing interest in this type of solvent, it is important to elucidate in the kinetic, reaction mechanism and all the physical phenomena involved in the frontal polymerization. Ethylammonium acrylate (ETAC) is a DES formed by acrylic acid and ethylammonium chloride. Because the special properties of this compound it was chosen as case of study.

Experimental

Ethylammonium acrylate was prepared by mixing acrylic acid (AA, Sigma-Aldrich) and ethylammonium chloride (EMC, Merck) in different molar ratios as detailed in the text. The mixture was heated at 80°C under stirring until a homogeneous and colorless liquid was obtained. EMC was kept at 60°C to prevent hydration.

The polymerization of ETAC was carried out in a glass tube of 5.4 mm in diameter where enough DES was placed to fill the tube approx. 40 mm height (1,1-bis(ter-butylperoxy)-3,3,5-trimethylcyclohexane) (Luperox 231, Sigma-Aldrich) and 90°C in combination were used to initiate the polymerization. Since Luperox and ETAC have an extremely different density and polarity, and because AA contains 180-200 ppm of hydroquinone monoethyl ether as inhibitor, certain amount of Luperox should be available along the tube to keep going the polymerization front. It was possible by using a cotton cord inside the tube, along it, wet with Luperox as it is discussed ahead. Polymerization fronts were monitoring with an infrared camera Xenics Gobi 640 (Leuven, Belgium) sensible at 8 to 14 μm .

Results and Discussion



Figure 1. An infrared imprint of a polymerization front experiment. The white bottom surface is a hotplate at 90°C where a glass tube filled with DES is placed to promote the polymerization. The external diameter of the glass tube is 7 mm. At the top of the tube it is observed the cotton cord wet with the initiator that goes from the bottom of the glass tube to the top.

An infrared radiation (IR) imprint of a typical experiment of polymerization is observed in Figure 1. The contrast is basically result of temperature differences: the hotter it is the brighter it looks. By this way, it is observed the tube filled with DES on a hot whitish surface at 90°C. In contrast, the tube appears darker as well as the end of the cotton cord used for keeping the initiator available to the DES along the tube. The glass tube is opaque to the IR radiation, what avoids the observation of its inner part where the DES and the cord are placed. As a consequence, the elevation of temperature along the tube during the polymerization is going to be “observed” only on the tube surface. Figure 2 shows a sequence of IR imprints in time and a space-time plot (STP) obtained from a single row of pixels along the tube as show by the yellow

line in the middle IR imprint suggests. Imprints and STP suggest the existence of three rough different levels of temperature during polymerization: a “dark” region, where the polymerization has not started, a pale white region, where we can presume that the polymerization is taking place at some extent and a bright white region where the polymerization occurs extensively.

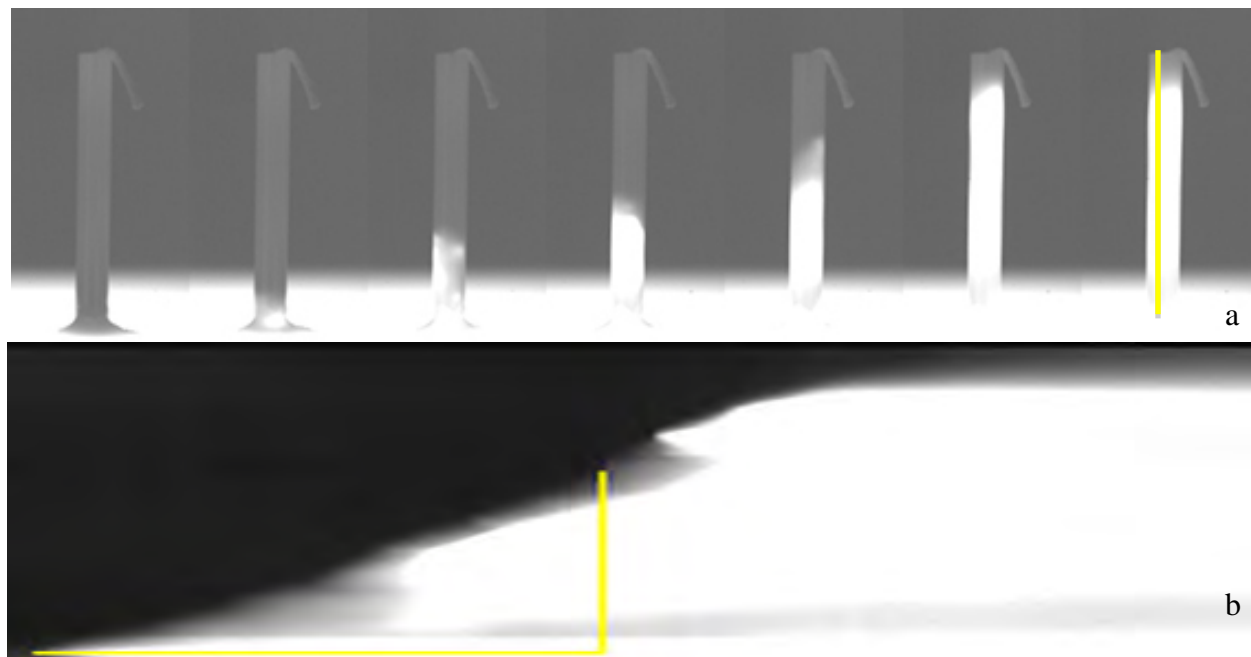


Figure 2. a. A sequence of images that show the local increment of temperature during the polymerization and the formation of the front as time goes on from left to right. b. We took a row of pixels of each image during the advance of the polymerization front as illustrated in the last picture of the sequence of imprints. Using that row of pixels we built a space-time plot (STP) observed here. Using this picture, and assuming that the polymerization front is linear, we can compute the speed.

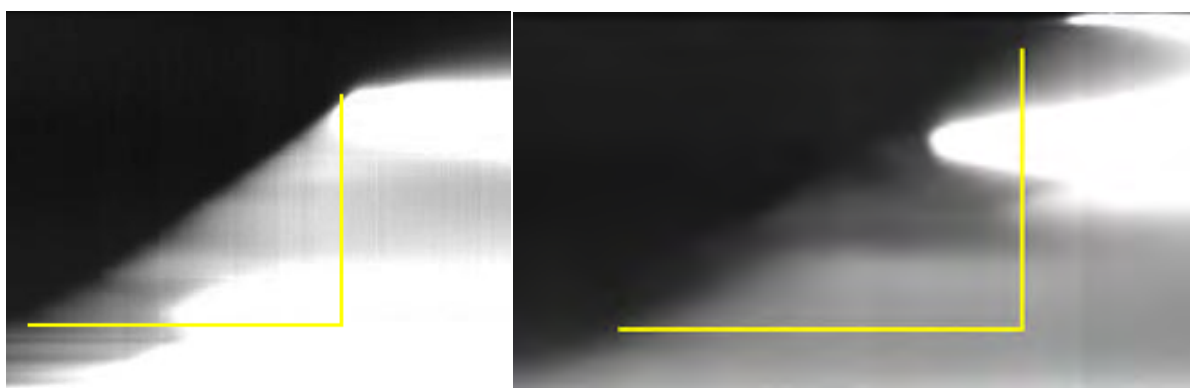


Figure 3. Space-time plots of two different experiments; similar to the one reported in Figure 2.

We can see in the STP that a polymerization front can be defined considering that once the polymerization starts, in the pale white region, a front polymerization is propagating. A second stage, formed by a bright white region, follows the front, in a wave that could or could not be periodic. For DES formed by 1:2 EMC:AA molar ratio, we can compute the speed of the polymerization front as 0.93 mm/s (Figure 2b), 0.64 mm/s (Figure 3a) and 1.12 mm/s (Figure 3b)

in three different experiments. Values are of the same order, but clearly the speed can be doubled in similar experiments. The main difference among these experiments is the amount of initiator locally available: in the range of microliters, we use as much as it is necessary to wet completely the cotton cord from the bottom of the glass tube until the top of the DES. As we previously mention, we use that wet cotton because Luperox 231 does not dissolve extensively in DES, but it is necessary to start the polymerization front. The experiments that confirm it bring an exciting phenomenon: some polymerization fronts start from the top of the tube because of an accumulation of Luperox 231. An example is in Figure 4, where a complete “reversed polymerization front”, starting from the top, is observed. Mixed scenarios, where a polymerization front starts from the bottom and suddenly another front starts at the top of the tube take place more often as the amount of Luperox 231 is increased by using more than one cord at the time as it is illustrated in Figure 5a. Interestingly, if the amount of Luperox 231 is further increased, the polymerization front is so fast and violent, that it avoids the starting of another one as observed in Figure 5b. The previous discussion helps us to understand that we have an excitable media, capable of starting reaction by temperature but also by local amount of initiator and of course, by a combination of both conditions. At the time, we are conducting experiments to determine the role of the geometry (diameter of the tube) in our polymerization fronts, since it appears that they stop easily if the diameter is small.

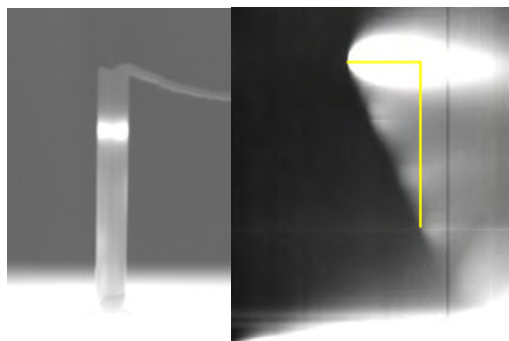


Figure 4. A polymerization front starting from the top of the tube: At left an illustration of the phenomenon is observed. At right, the space-time plot of the experiment, showing the front starting from the top of the tube.



Figure 5. At left, a space-time plot where a polymerization wave starts near the top of the tube. At right, a polymerization front with four cotton cords inside the glass tube, what grants four times the local amount of Luperox 231 with respect to the experiment described in Figure 2. Evidently, the front advances much faster.

Since diffusion of Luperox 231 in the DES and temperature seem to be two important variables to get a good polymerization front in our system, we have also started to conduct experiments in

2D microfluidic chips to have a precise control of diffusion and amount of Luperox available in the DES. In these chips, the DES was injected in a chamber similar to an ice cream cone with its tip open to a channel where initiator can flow inside the chip. In such a way, the surface available to diffusion is fixed. We have succeeded of observing polymerization in these chips, but due to technical difficulties, more work should be done to present the polymerization front in them. For the moment, we present only a picture where we clearly see the advance of the polymerization front inside the cone at right (Figure 6).

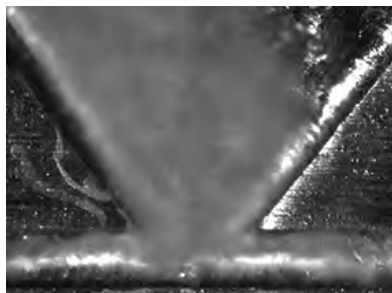


Figure 6. Polymerization of ETAC en a 2D microfluidic chip

Conclusions

Polymerization of acrylic acid using ETAC as solvent was achieved and monitored by an infra red camera. The analysis of the results by space time plots allow us to calculate the polymerization front rate in an accurate way. Further work using a 2D microfluidic chip will give us more information about the phenomena involve in this type of process.

Acknowledgements

Financial support from projects: DAIP 2013 (Jorge Delgado) and PROMEP 2012 (Irais Quintero) are gratefully acknowledged.

References

- [1] H. Zhang, K. Hong, J.W. Mays, *Macromolecules*, 35, 5738 (2002)
- [2] T. Kaneko, A. Noda, M. Watanabe, *J. Am. Chem. Soc.*, 127, 4976 (2005)
- [3] R. Vijayaraghavan, D.R. MacFarlane, *Chem. Commun.*, 700 (2004)
- [4] R. Vijayaraghavan, D.R. MacFarlane, *Macromolecules*, 40, 6515 (2007).
- [5] S. Ding, M. Radosz, Y. Shen, *Macromolecules*, 38,5921 (2005).
- [6] V. Percec, T. Guliashvili, J.S. Ladislaw, A. Wistrand, A. Stjerndahl, M.J. Sienkowska, M.J. Monteiro, S. Sahoo, *J. Am. Chem. Soc.*, 128, 14156 (2006).
- [7] A.P. Abbott, G. Capper, D.L. Davies, R.K. Rasheed, V. Tambyrajah, *Chem. Commu.*,70 (2003).
- [8] A.P. Abbott, G. Capper, D.L. Davies, R.K. Rasheed, V. Tambyrajah, *J. Am. Chem. Soc.*, 126, 9142 (2004).
- [9] M. Domínguez, *Angew. Chem. Int. Ed.*, 47, 6960 (2008).
- [10] J.D. Mota-Morales, M.C. Gutiérrez, I. Sánchez, G. Luna-Bárcenas, F. del Monte, *Chem. Commun.*, 47, 5328 (2011).
- [11] J.D. Mota_morales, M.C. Gutiérrez, M.L. Ferrer, I.C. Sanchez, E.A. Elizalde Peña, J.A. Pojman, F. Del Monte, G. Luna-Bárcenas, *J. Polym. Sci., Part A: Polym. Chem.*, 51, 1767 (2013)

OLIGOMERIC DISPERSANTS BASED ON MALEAMIC ACID COPOLYMERS

Maricela García-Zamora, Mildred Flores-Guerrero, Maria Teresa Córdova-Alonso
Odilia Pérez-Camacho*

Departamento de Síntesis de Polímeros, CIQA, Saltillo, 25250, Coahuila, México,
maricela.garcia@ciqa.edu.mx , odilia.perez@ciqa.edu.mx

Abstract

In this work we report the synthesis of new polymeric surfactants based on maleamic acid copolymers with acrylamide, *bis*-acrylamide and itaconic acid. Polymers and copolymers derived from maleamic acid and acrylated co-monomers are considered friendly environment materials, easier to degrade.¹ The copolymers also contain hydrophilic functional groups such as amides, carboxylic acids, or ester groups and hydrocarbon chains of different sizes, which generate better compatibility or miscibility with various types of hydrocarbon chains or paraffin in mixtures of crude oil. The polar functional groups also can modify waxes leading to stable dispersions. Maleamic polyacid copolymers were synthesized by free radical polymerization, in bulk or solution using ammonium persulfate as initiator. The copolymers were evaluated as dispersants of copper oxide (CuO) nanoparticles, showing high stability for several weeks. Surface properties and drop angle of the different dispersant solutions was compared.

Introduction

Dispersants are chemical agents which consist in solutions formulated with tensoactives and additives, in water or organic solvents. Dispersants have multiple applications, depending on its potential as surface or emulsificant agents, its toxicity and structure, among others.² Its main function is to reduce the surface tension between two phases of different nature, such as water or organic solvents, or water and solid particles (separating the agglomerated particles). Dispersants have many applications in industry food, pharmacy, agrochemical formulations such as fertilizer and pesticides, as additives for detergents and cosmetics, in the manufacture of paints, metal removal in waste water treatments, etc.³ Another type of dispersants consists in functionalized polymers or copolymers, which for many applications have shown better results than dispersants based on monomeric surfactants. For example in dispersion of hydrocarbons in the oil spill in the seas, polymeric dispersants tend to better disperse viscous oil mixtures. In paint industry, polymeric dispersants reduce more efficiently interactions between pigment particles, than the conventional monomeric dispersants.⁴ In nanotechnology the stabilization and dispersion of metal nanoparticles, metal salts or oxides, is one of the most studied issues, for which several methods have been developed.⁵ Polymeric or oligomeric solutions of different types of functionalized polymers, or crosslinked polymers have been used as templates, which are able to disperse nanoparticles of the most utilized metals as Ag, Au, Pd, Pt, Ni, CuO, ZnO, FeO, Fe₂O₃, TiO₂, etc. Ag, Au, Pd, Pt, Ni, CuO, ZnO, FeO, Fe₂O₃, TiO₂, etc. In this work we report the synthesis of oligomeric surfactants based on copolymers of maleamic acids, acrylamide, *bis*-acrylamide and itaconic acid. The surface properties of the copolymers were determined by the method of drop contact angle and by the calculation of critical micelle concentrations from interfacial tension-concentration curves.

Experimental

Maleic anhydride (99%), N-4-carboxybutyric acid (98%), dodecylamine (98%), N,N-methyleneacrylamide (99%), N,N-methylene-*bis*-acrylamide (99%), itaconic acid (99%) and potassium persulfate (99%), were purchased in Sigma-Aldrich and used without further purification. Acetone and methanol were previously distilled. Characterization of monomers and copolymers was carried out by RMN using a Jeol Eclipse 300MHz equipment, and FTIR in a Nicolet Magna 550, using KBr for samples preparation. MW was determined in tetrahydrofuran (THF) solutions of 1mg/ml by GPC in an Alliance 2695 equipment, using poly(vinyl-benzene-styrene) packed columns of 10⁵ Å y 10³ Å with ultraviolet detector model

Third US-Mexico Meeting "Advances in Polymer Science" and XXVII SPM National Congress
Nuevo Vallarta, December 2014

2487 (248 nm). THF (HPLC grade) at 30 °C, and injection volume of 25 μ L. Angel contact of the polymer solutions in water were determined in a Goniometer Fostec equipment, comparing with deionized water using a polyester substratum. Critical micelar concentration (CMC) was determined by interfacial tension-concentration curves in water solution of the copolymers using a bubbled tensiometer SensaDyne PC500-L. Ultrasonic bath (Branson 2800) 40 KHz/110 watts. The dispersion of nanoparticles: in copolymer solutions (0.1 wt.%) was determined by SEM analysis in dried samples at 0.7 kV (JEOL, JSM-7401F)

Maleamic acids synthesis

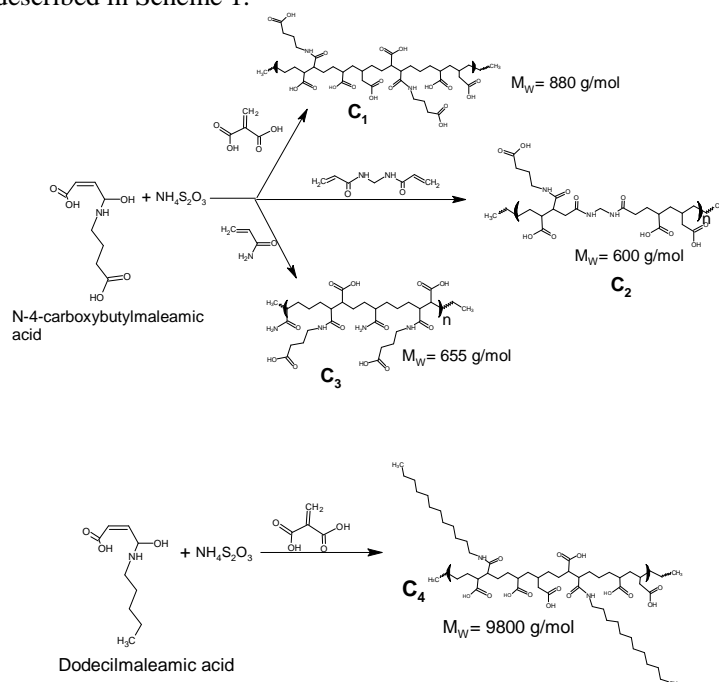
Maleic anhydride (2.0 g, 0.02 mol) was solubilized in 20 ml of methanol or acetone, and this solution was dripped to the corresponding amount of amine or aminoacid solubilized in 20 ml of the used solvent. The mixture was mixed for 15 min, and then heated at 50°C for 3 h. The maleamic acid precipitated as a white powder, which was recrystallized in chloroform/hexane.

Synthesis of maleamic acids copolymers

Maleamic acids and co-monomers (N,N-methylenacrylamide or itaconic acid) were solubilized or suspended in 50 ml of water or 2M NaOH solution using molar ratios of 1:1. When using N,N-methylen-*bis*-acrylamide a 10% mol was utilized, and 1% of initiator $\text{NH}_4\text{S}_2\text{O}_8$ (ammonium persulfate). The solution was bubbled with Ar for 10 min, and then refluxed during 6 h. After this time, the mixture was liofilized for 24 h. The powder obtained was suspended in methanol, precipitated with hexanes, filtered and dried for 6 h in vacuum oven. Then diluted solutions of the copolymers in deionized water were prepared for surface properties characterization.

Results and Discussion

Different copolymerization reactions were carried out with maleamic acids derived of N-4-carboxybutylmaleamic and dodecylmaleamic acids, using acrylamides and itaconic acid as co-monomers, as described in Scheme 1.



Scheme 1

The copolymers based on maleamic acids (C₁-C₄, Scheme 1) were characterized by NMR, FTIR and the molecular weights (MW) were determined by GPC. Oligomers of low MW were obtained for these reactions, where just C₄ showed Mw of 9,800 g/mol, however according to their structures, containing amphiphilic groups, these copolymers can confer interfacial properties, modifying surface tension of heterogeneous mixtures. In order to evaluate surface properties, diluted aqueous solutions of 0.1wt. % of copolymers were prepared, and the contact angle of the solutions was determined over a polyester film (used as substratum) comparing with the contact angle of deionized water under the same substratum. The contact angle of the samples were measured according to the schematically representation (besides Table 1), where all the copolymer solutions showed wettability grades higher than water, indicating stronger interaction with the substratum (polyester film), as expected. The above was attributed to the functional groups (carboxylic, hydroxyl and amide groups) present in the copolymers, which increase the adhesive force with the polyester substratum.

Table 1 Surface property of maleamic acids solutions

Sample	Contact angle(°)	CMC mmol/L
H ₂ O	68	-
C ₁	135	63
C ₂	140	-
C ₃	136	-
C ₄	155	0.65

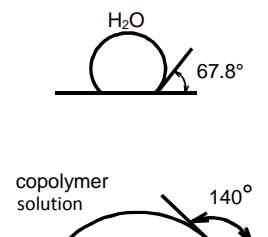


Table 1 also shows critical micelle concentration (CMC) calculated by interfacial tension-concentration curves for two of the copolymer solutions (C₁ and C₄). Comparing to the CMC reported for SDS (6-8 mmol/L), as expected, the higher MW copolymer showed lower CMC than SDS, due to higher contents of functional groups (carboxylic acids or amides) which is also reported as cause of decrease of the CMC in surfactant solutions.⁶

Dispersion properties of C₁ copolymer were evaluated, using copper oxide (CuO) nanoparticles, suspending 40 mg of CuO nanoparticles in 10 ml of 0.1 wt% of the copolymer solution in deionized water. The solution was ultrasonicated for 1 h, where the dispersion in C₁ solution (Fig. 1b) was compared with analogous concentration of CuO in deionized water, without using any copolymer (Fig. 1a). These solutions were analyzed by SEM after two weeks of preparation for observing stability of the nanoparticles in the solutions.

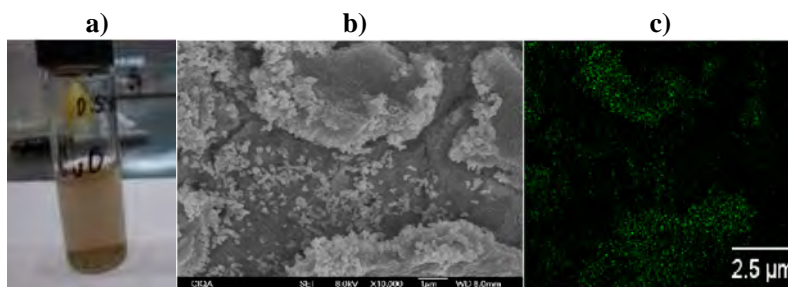


Figure 1 a) Dispersion of CuO nanoparticles in water b) SEM micrograph of dried CuO dispersed without using copolymers c) EDX map of Cu of SEM micrograph.

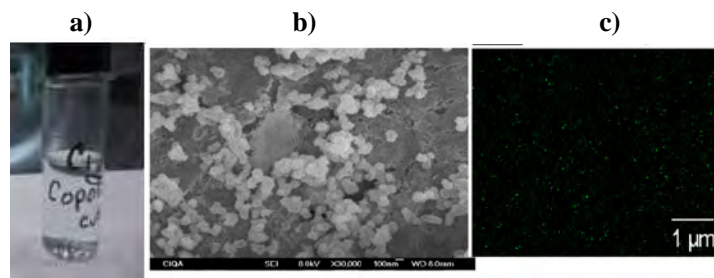


Figure 2 a) Dispersion of CuO nanoparticles in C_1 solution b) SEM micrograph of a dried CuO dispersed in C_1 solution c) EDX map of Cu of SEM micrograph .

Figure 1a, shows a cloudy solution of CuO in water, after sonification for 30 min, its SEM micrograph, after two weeks of preparation (Fig. 1b), exhibits a clear agglomeration of the nanoparticles, as well as its corresponding map of Cu by EDX of the same area (Fig. 1c). Contrary to the observed in figure 2a, where the copolymer solution of C_1 with CuO, is completely transparent, in light blue color. After two weeks of preparation, the solution was analyzed by SEM (Fig. 2b) where dispersed nanoparticles around 100 nm are observed, and the EDX map analysis shows more uniform dispersion of Cu in the sample.

According to the above results, it could be confirmed that maleamic acid copolymers show good surface properties which conduce to stable dispersions of nanoparticles like CuO.

Conclusions

New copolymers based on maleamic acids were synthesized by free radical polymerization in water. The copolymers were characterized by standard spectroscopic methods, showing several functional groups, where some preliminary surface properties were determined by drop angle contact of diluted solutions of the copolymers in substrates of polyester films, as well as critical micelle concentrations, showing comparable properties to commercial monomeric surfactants like SDS.

Acknowledgments

The authors thanks to Beatriz Reyes Vielma, Maria Concepción González Cantú for technical support in surface characterizations, Víctor Eduardo Comparán, for the technical support. Also thanks to Teresa Rodríguez for GPC determinations, Myriam Lozano for SEM micrographs and Josefina Zamora for solution photographs.

References

- [1] M.B. Milovanovic, S.S. Trifunovic, L. Katsikas and I.G. Popovic, *J. Serb. Chem. Soc.*, 72(12) 1507-1514 (2007).
- [2] a) Martin J. Schik, "Non-ionic Surfactants" *Surfactants Science Series, Vol. 1*, Marcel Dekker Inc., 1988 b) D. Jiménez, A. Medina, J.N. Gracida, *Rev. Int. Contam. Ambient.*, 26(1) 65-84, 2010
- [3] a) Dahms, Gerd, H. and Kwetkat, Klaus "Composición de agentes tensoactivos que contienen agentes tensoactivos Gemini y co-anfífilos, su obtención y empleo" *ES Patent* 2, 238, 315 T3, 2001. b) Merv Fingas, "Environmental Technology Center, Environment Canada" www.Pwsrca.org, March 2002 c) M. Larson, W.-C. Huang, M.-H. Hsiao, Y.-J. Wang, M. Nyden, S.-H. Chiou, D.-M. Liu, *Prog. Polym. Sci.*, 2013, 38, 1307-1328.
- [4] a) Deshnuh S., Bharambe D.P., *Fuel Process Technol.*, 2007. b) Machado L.C. André, Lucas F. Elizabete, González Gaspar, *J. Petrol. Sci. And Eng.*, 2001, 32, 150-165.
- [5] a) R. Lupitskyy, and S. Minko, *Soft Matter.*, 2010, 6, 4396-4402 b) F. Müller, W. Peukert, R. Polke, F. Stenger, *Int. J. Miner. Process*, 2004, 74S, S31-S41.
- [6] Ayman M. Atta, Amro, K. F. Dyab, Hamad A. Al-Lohedan *J. Surfact. Deterg.*, 2013, 16, 343-355.

SYNTHESIS OF CROSSLINKED AND FUNCTIONALIZED POLYSTYRENE BY MINIEMULSION POLYMERIZATION: PARTICLE SIZE CONTROL.

Alba Nidia Estrada Ramírez,¹ René Darío Peralta Rodríguez,¹ Odilia Pérez Camacho², Gladys Cortez Mazatán¹

Centro de Investigación en Química Aplicada, Blvd. Enrique Reyna Hermosillo 140 C.P 25294 Saltillo Coahuila, México

¹*Departamento de Procesos de Polimerización.*

²*Departamento de Síntesis de Polímeros.*

Abstract

The synthesis of crosslinked polystyrene P(St-DVB) and crosslinked polystyrene functionalized with acrylic acid P(St-DVB-AA) by miniemulsion polymerization using two polymerizable surfactants (PS) Noigen RN50 (NRN50, non-ionic) and Hitenol BC30 (HBC30, anionic), in addition of two oil-soluble initiators: 2,2'-azobisisobutyronitrile (AIBN) and 2,2'-azobis (2-methylbutyronitrile) (V-59) is reported. The effect of the AA content and the type of polymerizable surfactant on the average particle diameter (Dp) was studied. The particles were characterized by dynamic light scattering, zeta potential, scanning electron microscopy, differential scanning calorimetry and thermal gravimetric analysis. The results indicated that the amount and type of polymerizable surfactant affects the size of the particles. The amounts of NRN50 used were greater than for HBC30 to obtain the same Dp. The incorporation of 3 % AA as comonomer did not change the Dp with each surfactant used. The particles obtained will be used as organic supports for the synthesis of polyolefins like HDPE and LLDPE.

Introduction

Miniemulsion polymerization is used for the synthesis of functionalized polymers. The particles that have surface functional groups (e.g. carboxyl, amino, hydroxyl. etc) have been great of interest as adhesives or supports.[1] It is well know, that in miniemulsion processes, a large droplet's surface area is created by shearing the system which consists of monomer(s), water, surfactant, initiator and hydrophobe (to suppress Ostwald ripening). The monomer droplets obtained by this process have average diameters in the range of 50-500 nm, and act as single nanoreactors for polymerization. In this process droplet nucleation is the dominant initiation mechanism for polymerization. [2] The particle size can be controlled by variation of the amount of surfactant and high shearing ultrasound parameters (power and time). The form to stabilize the monomer droplets obtained in the miniemulsification process is using conventional (non polymerizable) or PS, the difference, is that the PS contain a double bond capable of covalent linking onto the particles, thus preventing its desorption.[3] As it is well known, the increase in the amount of surfactant in miniemulsification processes decreases the average particle diameter (Dp) of the monomer droplets, this allows to obtain more particles with great surface area and more functionalities.[4] It has been established that PS are used to enhance stability or to functionalize the latex particles surface. Acrylic acid as a functional comonomer has been used to synthesize crosslinked polystyrene particles by miniemulsion polymerization. Some years ago Kappler et al. [5], reported the use of PS with propylene oxide units to synthesize crosslinked polystyrene-based particles that were used as organic supports to immobilize methylaluminoxane (MAO) for the synthesis of high density polyethylene (HDPE). This catalytic system showed high activity. In

addition, Kappler indicated that the morphology of the support is an important factor in polymer formation in the slurry process, they observed by scanning electron microscopy (SEM) that the morphology of polyethylene is a replicate of the support used.

In this work, the synthesis of crosslinked and functionalized polystyrene particles with different amounts of acrylic acid as comonomer (1-3 %), via miniemulsion polymerization was studied. Two oil soluble initiators were used in order to avoid the generation of free radicals in the aqueous phase, namely (2,2'-azobis(2-methylbutyronitrile, V-59), which posses a more hydrophobic character compared to 2,2'-azobisisobutyronitrile (AIBN). In addition, two PS were used, both possessing an alkyl phenol ethoxylate backbone: polyoxyethylene 4-nonyl-2-propylene-phenol with 50 ethylene oxide groups, (Noigen RN50, nonionic; NRN50) and polyoxyethylene 4-nonyl-2-propylene-phenol ether ammonium sulfate with 30 ethylene oxide groups, (Hitenol BC30, anionic; HBC30). The latices were characterized by dynamic light scattering, zeta potential, scanning electron microscopy, differential scanning calorimetry and thermogravimetric analysis.

Experimental

Materials

Styrene (St), acrylic acid (AA), hexadecane (HD), divinylbenzene (DVB) and 2,2'-azobisisobutyronitrile were purchased from Sigma-Aldrich, 2,2'-azobis(2-methylbutyronitrile, from Akzo Nobel, PS from Dai-ichi Kogyo Seiyaku (Japan) were generously supplied by Montello, Inc. (Tulsa, OK). Styrene and divinylbenzene were passed through a column packed with cotton and aluminum oxide (Sigma-Aldrich, porous size 58 Å) to remove the inhibitor. Distilled water was acquired from the distillation plant at CIQA.

Miniemulsion Polymerization Procedure.

In this work two types of particles were prepared by miniemulsion polymerization: crosslinked polystyrene and crosslinked and functionalized polystyrene particles with AA. The recipe employed in this work for the preparation of the dispersed phase were 5.7 g of styrene, 0.3 g of DVB, 0.25 g of the HD and 0.1 g of AIBN or 0.12 g of V-59. The continuous phase consisted in 24 g of water and (0.3-0.8 g) of NRN50 or (0.3-0.6 g) of HBC30. The acrylic acid (0.06-0.24 g) was added to the dispersed phase to prepare the crosslinked and functionalized polystyrene particles. Both phases were stirred for 15 min, after the continuous phase was added to the oil phase containing monomer(s), HD and initiator, the mixture was subsequently stirred for 1 h at 1000 rpm. Finally after 1 h of stirring of pre-emulsification, the miniemulsion was prepared by applying ultrasound (Sonics and Materials, Inc., VC 505, Newtown, USA) to the mixture for 3 min at 81 % of power with the aid of a water bath at 0 ° C in order to prevent polymerization. The temperature of polymerization was of 72 °C.

Characterization of Latex Particles.

Particle size was measured by dynamic light scattering (DLS) using a Malvern Zetasizer S90 (Malvern Instruments, UK) at a single scattering angle of 90° and a temperature of 25 °C. Zeta potential was measured in a Nanotracs Wave apparatus equipped with autotitration (Microtracs, USA). SEM was used to analyze the morphology of particles: a diluted colloidal solution (10 % solid content) of the sample was placed in a silica plate and dried at ambient temperature, previous

to SEM analysis at 0.7 kV (JEOL, JSM-7401F). The particle size distribution analysis from the SEM images was done using the ImageJ program (National Institutes of Health, USA). The latices were dialyzed using dialysis membranes (40 x 25 mm of Sigma-Aldrich) pretreated with ethylene diamine tetra acetic acid (EDTA) 0.1 mM, at pH 8 adjusted with a 2 % aqueous solution of sodium bicarbonate, the solution was heated to 90 °C during 10 min. Afterwards, the membranes were washed with distilled water and submerged in a solution of EDTA 0.1 mM at 90 °C during 10 min. Finally the membranes were stored at 0 °C until use. The dialysis time was three weeks to remove the unreacted PS. After this time, the latices were lyophilized. The effect of the incorporation of acrylic acid in each lyophilized latex was analyzed by DSC Discovery series, the analyses were performed on a modulated TA Instrument 2920 (USA), at a heating rate of 10 °C/min under atmosphere of N₂ (50 mL/min) and thermal gravimetric analyses (TGA) were performed on a model Discovery series, (USA) under the same conditions that DSC.

Results and Discussion

To find conditions to prepare particles with $D_p \approx 100$ nm and $D_p \approx 250$ nm, a set of runs were carried out to determine adequate settings of ultrasound power and time, then, changing the concentration of PS to obtain the desired D_p . As expected, [6], with both, HBC30 and NRN50, a decrease in D_p occurs (HBC30: 110 – 86 nm; NRN50: 304 – 102 nm) with increase in the amount of surfactant. The variation of D_p with PS concentration is shown in Fig. 1. The PS concentrations to achieve 100 nm and 250 nm were 0.0141 mol/L and 0.0053 mol/L, respectively.

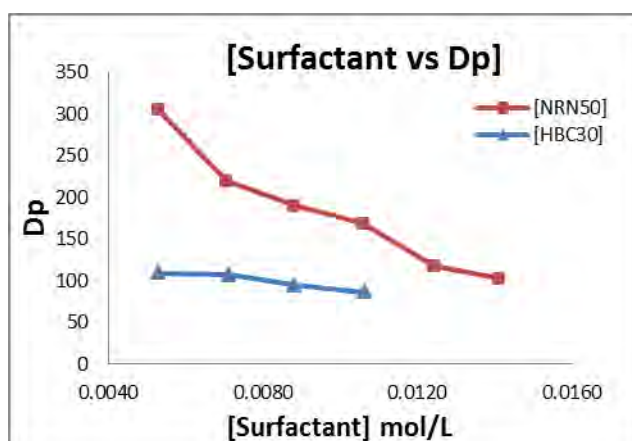


Figure 1.-Average particle diameter (D_p) as a function of PS concentration. $t_{us} = 3$ min al $W_{us} = 81\%$.

These conditions were the basis to prepare the latices using NRN50 with AA and HBC30 with and without AA. The results are presented in Table 1.

Table 1 shows the characterization of the latices obtained by miniemulsion polymerization, using the above condition. As can be seen, the amount of 0.0141 mol/L of NRN50 (Exp.1,2) used were greater than for HBC30 0.0053 mol/L (Exp. 6,7) to obtain the same D_p , this was attributed to the polyethyleneoxide (PEO) chain of NRN50, which has higher polarity than the chain with 30 ethylene oxide units of the HBC30. In addition, the polar parts of the POE chains interact both electrostatically and sterically, and the better packaging of the PEO chain in NRN50, causing an increased demand for surfactant to stabilize the same particles. Experiments 3 and 4 correspond

to the latex prepared without and with 3 % of acrylic acid, respectively. It can be observed that in both cases, the particles have the same Dp even with the incorporation of AA, although the solids content of the functionalized latex is less than the unfunctionalized one. This was attributed to the interactions between the PEO chain and -COOH groups of AA, which causes an increase in viscosity of the latex. The Z potential was measured in the functionalized latices with AA, as can be seen in Table 1, the values are greater than ± 30 mV[7], this indicates that the latices are more stable with AA than the latex without AA.

Table 1.-Characterization of latex particles prepared with non-ionic and anionic PS at 72 °C.

Exp.	% AA	Initiator	Solids Content (%)	Potential Z ξ (mV)	Dp (nm) \pm Std. Dev. SEM	Dp (nm) \pm Std. Dev. DLS	Tg (°C)	TGA Tmax (°C)
Exp 1a	0	V-59	20	-22	114 \pm 11	108 \pm 1.41	113	392
Exp 2a	3	V-59	20	-	108.4 \pm 16	106 \pm 3.54	120	417
Exp 3a	0	AIBN	19.5	-25.2	236 \pm 47.6	253 \pm 3.32	116	420
Exp 4a	3	AIBN	12	-31.4	242.3 \pm 43.6	253 \pm 5.66	121	426
Exp 5a	3	V59	9	-	210 \pm 24.6	242 \pm 1.84		
Exp 6b	0	V59	20	-25.5	99.8 \pm 10	104 \pm 7.10	114	419
Exp 7b	3	V59	20	-33.7	109.8 \pm 12	101 \pm 2.46	121	425

a) Latex prepared with NRN50, 0.0141 mol/L. b) Latex prepared with HBC30, 0.0053 mol/L. Tg of polystyrene = 100°C

According to the results of the glass transition temperature (Tg), all polymers showed an increase of 14 to 20 ° C in Tg, (Tg of polystyrene: 100 °C) [8], due to the presence of the crosslinking agent (DVB) which makes more rigid the polymer chains. Furthermore, copolymers prepared using AA as functional comonomer showed an even greater increase in the Tg of the latex prepared with both surfactants (NRN50 and HBC30). TGA showed the good thermal stability of the particles to high temperatures (up 400 °C), Tmax of functionalized particles is greater (6-15°C) than the non-functionalized particles, attributed to the presence of the AA and DVB.

In this work we used two oil soluble initiators in order to avoid the generation of free radicals in the aqueous phase, namely V-59, which possesses a more hydrophobic character compared to AIBN. The use of V-59 allowed to obtain more uniform particle size distributions, as can be seen in Figure 2 a in comparison with the particles prepared with AIBN, Figure 2b.

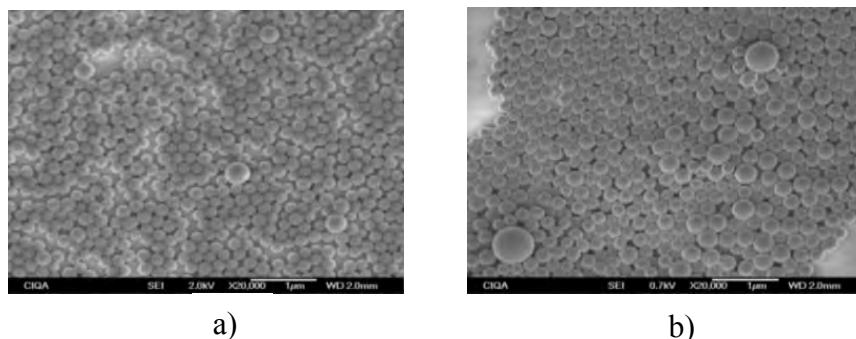


Figure 2.-SEM images of the particles prepared by miniemulsion polymerization using as initiator a) V-59, Exp. 5 and b) AIBN, Exp. 4

Conclusions

Miniemulsion polymerization allowed obtaining functionalized stable latices. Stability was confirmed with the results of the Z potential (± 30 mV) [7]. The amount of NRN50 was greater than for HBC30, and this fact was attributed to the improved stability that provides the sulfate groups of the HBC30 compared with the PEO chain of the nonionic surfactant NRN50. In addition, PEO chains in NRN50 package more tightly than PEO chains in HBC30 increasing a demand for surfactant to stabilize the same particles. SEM analysis of the particles showed spherical particles morphology and particle size distribution was narrower using V-59 than using AIBN as initiator. The Dp of particles of the particles measured by DLS was similar to that obtained by SEM. The presence of acrylic acid as functional comonomer in the particles obtained by miniemulsion polymerization allowed to obtain Tg and Tmax greater than the particles without AA, attributed to the rigidity provided by this comonomer and to the presence of divinylbenzene. The spherical morphology and high glass transition temperature are key features that have the particles obtained by the miniemulsion polymerization process described here. This allows to considering that these polymeric materials can be used as organic support for the synthesis of polyolefins such as HDPE and LLDPE.

Acknowledgements

The authors would like to thanks to CONACYT, Mexico for financial support through Grant CB-2011/168472. Fellowship to ANER from CONACYT for her Ph. D. studies at CIQA. We also thank to Maricela García for technical support, LCQ. Guadalupe Méndez Padilla, QFB. Jesús Angel Cepeda Garza for DSC and SEM characterization respectively.

References

- [1] Musyanovych A, Rossmanith R, Tontsch C, Landfester K., Langmuir, 23(10), 5367-76 (2007).
- [2] Bedri E. Yves S. E.David Sudol, V. L. Dimonie., Langmuir, 16, 4890-4895 (2000).
- [3] H. Matahwa, J. B. Mcleary., J. Polym. Sci. Part A Polym. Chem., 44, 427-442 (2006).
- [4] R. Motokawa, T. Taniguchi., Macromolecules, 45,9435-9444 (2012).
- [5] Jang Y, Nenov N, Klapper M, Miillen K., Polym. Bull. 50, 343-350 (2003).
- [6] K. Landfester, JÖrdis EisenblÄter RR., JCT Res., 1,1 (2004).
- [7] Chern C-S, Sheu J-C., Polymer, 42(6):2349-2357 (2001).
- [8] Asua JM. Book, Polymer Reaction Engineering. Blackwell Publishing, pag. 216 (2007).

PREPARATION AND STUDY OF EPOXY SHAPE MEMORY POLYMERS

Maria Lydia Berlanga Duarte¹, Ricardo Acosta Ortiz,¹ Aida E. Garcia Valdez,¹ Luis A. Reyna Medina,¹ Fernando Aranda Guevara,¹.

¹ *Centro de Investigación en Química Aplicada, Blvd. Enrique Reyna Hermosillo No 140, Saltillo, Coahuila, México, lydia.berlanga@ciqa.edu.mx.**

Abstract

In this work were developed epoxy shape memory polymers (SMPs). To obtain this kind of smart polymers is necessary to add a “soft” polymer to the rigid epoxy polymers. In this study was combined the anionic polymerization of an epoxy monomer, with the thiol-ene photopolymerization. This was achieved by using allyl functionalized tertiary amines as curing agents. The tertiary amine induced the anionic polymerization of the epoxy resin, producing the stiff polyethers. At the same time, the allyl groups of the curing agent reacted with an added multifunctional thiol to produce the soft polythioethers. Parameters like free strain recovery, shape fixity and shape recovery sharpness were determined for each studied formulation.

Introduction

The smart materials have the ability to react reversibly and also can be controlled with physical and chemical stimulation, to modify some of their properties. Some of these smart materials are known as shape memory materials, they have the facility to return from a temporary shape to their original shape, when they are exposed to an external stimulus, such as temperature change, irradiation exposure and it can be induced for a magnetic or electric field. [1-3]

Shape memory polymers (SMPs) are makeup of a soft phase that helps to keep a transient shape, and a stiff phase that retains the original shape of the material [4]. Some SMPs are derivate from epoxy resins and it been found, a scientific and technology interest due to that the epoxy resins shown excellent physical and mechanical properties, in addition to their capability of shape recovery using an appropriate stimulus[5-6]. Also the epoxy resins are economic and able to react with a lot of organic compounds such as: amines, hydroxyl, carboxyl and inorganic acids to give thermo stables polymers [7]. These epoxy resins can be polymerized in anionic form using ternary amines.

The thiol-ene reaction is simply hydrothiolation of a C C bond. This kind of reaction has the advantage of proceed in high yield without formation of byproducts, under mild reaction conditions. It has been found that the thiol groups can react with any kind of double bonds; also these reactions are not inhibited by the presence of humidity as cationic polymerizations do.

Thiol-ene photopolymerization it's carried out by the step-growth mechanism that consists initially in the irradiation treatment of a thiol with photoinitiator, resulting in the formation of a thiyl radical RS; the second step involves the addition of thiyl radical across the double bond C=C yielding an intermediate carbon-centred radical followed by a chain transfer to a second molecule of thiol to give the thiol-ene addition product, with the generation of a new thiyl radical. Thiol-ene systems on the other hand offer a unique combination of properties that are advantageous for shape memory polymer systems, including rapid polymerization, low volume shrinkage and shrinkage stress, the formation of homogeneous networks, and insensitivity to oxygen inhibition [8]

Figure1. Step-growth mechanism of thiol-ene photopolymerization

Experimental

Materials

The epoxy resin used is bisphenol-A-diglycidyl ether (BADGE), thiol monomer is trimethylolpropane tris(3-mercaptopropionate) (TMP) and the photoinitiator is 4-Dimethylaminopyridine all were obtained from Aldrich. The chemical structure of epoxy resin BADGE, TMP and the curing agents as ALA4, ALA5 and TRIS, employed are showed in Figure 2.

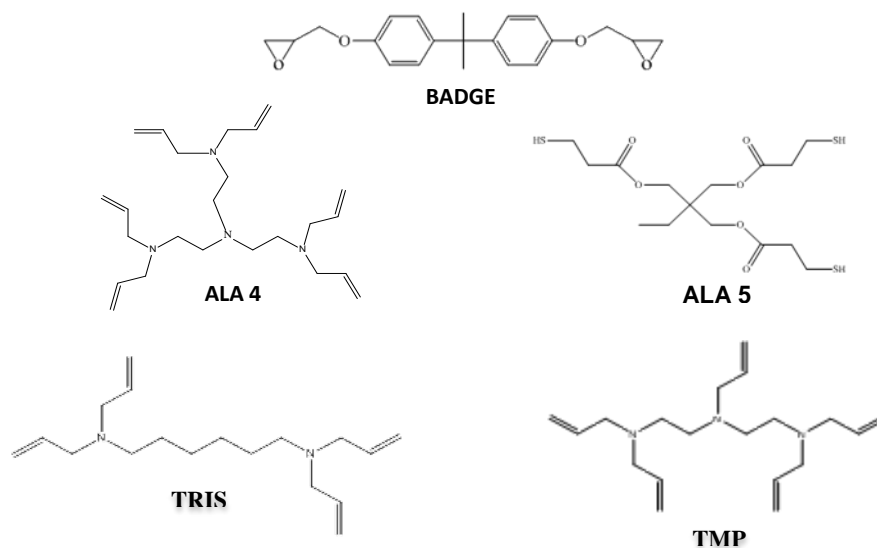


Figure 2. Chemical structures of the compounds used in this study

Synthesis of the different curing agents used in the formulations of epoxy shape memory polymers.

Synthesis of N1,N1,N6,N6-tetraallylhexane-1,6-diamine (ALA 4)

Into a 500ml three neck round-bottomed flask provided with an addition funnel, condenser and magnetic stirring, were added 200ml of saturated solution of KOH. Then were added 36g (0.310

mol) of 1,6-hexane diamine, 0.6g (0.310mol) of KI and 0.6 g (0.310mol) of (Bu)₄N⁺Br⁻ as phase transfer catalyst. Thereafter, were added dropwise 150.18g (1.24mol) of allyl bromide. The reaction mixture was heated at 70°C for 30 h. After this time the reaction mixture was extracted with ether (4 x 100mL) and then washed with a NaCl saturated solution. After drying with anhydrous Na₂SO₄ and evaporation of the solvent the crude product was purified by column chromatography using hexane:ethyl acetate 9:1. The desired product was obtained as slightly yellow liquid at 76 to 80 % yield. The obtained compound was characterized by FTIR and ¹H NMR.

Synthesis of N1,N1,N2—triallyl-N2-(2-diallylamino)ethyl)ethene-1,2-diamine (ALA5) and N1,N1-diallyl-N2,N2-bis(2-(diallylamino)ethyl)ethane-1,2-diamine (TRIS)

A similar method than the one described above was used to prepare these others curing agents, but with their amines corresponding and the relation corresponding of allyl bromide.

Samples Preparation

The mixtures were prepared by adding an equimolar thiol-ene mixture of thiol-ene mixture of curing agents-TMP in the range between 10 and 20 mol% to BADGE resin. First, the photoinitiator was dissolved in the amine and subsequently BADGE and thiol were added in an adequate content with respect to the allylic double bonds. The composition of the evaluated formulations is reported in the Table 1. The composition is added to stainless Steel mold, irradiated under UV lamp (FUION UV F300S INC with intensity of 40mW/cm² for 10 min to 85°C. Where obtained epoxy resin specimens with sample size of 1.5cm X 6cm X 3mm.

Table 1. Formulations in composition equimolar thiol-ene with curing agents used.

#	Formulation	curing agent	%Ala	%thiol (TMP)
1	A410%	Ala 4	10	13.3
2	A420%	Ala 4	20	26.6
3	A510%	Ala 5	10	16.6
4	A520%	Ala 5	20	33.3
5	TRIS10%	Tris 1	10	20
6	TRIS 20%	Tris 2	20	20

Ala= Allyl-amine; TRIS= N1,N1-diallyl-N2,N2-bis(2-(diallylamino)ethyl)ethane-1,2-diamine; TMP= Trimetilolpropan trimercapto propionate

Results and Discussion

The obtained results in the photopolymerizations of the different curing agents used in the formulations of epoxy shape memory polymers showed that the photopolymerizable epoxy systems are highly reactivities when are combined the anionic photopolymerization of epoxy monomers with a thiol-ene system due to the allyl amines ALA4 and ALA5 and TRIS promote high reactivity of the resin epoxy, curing at 85°C when the samples are irradiated under UV lamp with intensity of 40mW/cm². Due that these photopolymerizable systems have a soft phase derived of polythioethers from thiol-ene system that are flexible polymers with low tg and these are inside from rigid polymer that is highly cross-linked due to the polyethers from the BADGE, for all these components is possible the formation of a shape memory polymer.

The polymer systems were examined for shape memory programming and shape retention. The results are given in Table 2, Figure 2, that details the different times in seconds, obtained when the

samples reflect the temporary shape and when return to initial shape by heating to 10°C above T_g. Is possible to modulate the shape retention capacity with modification in concentration of the soft phase in the rigid polymer. To fewer amounts of polythioethers, the SMP return rapidly to the original form.

Table 2. The glass transition temperature (T_g) and different mechanical properties determined in the

System	Strength	Impact resistance (J/mm)	Flexural Strength (MPa)	Storage Modulus (MPa)	Shape recovery time (s)	T _g
A410%	158.3	51	102.4	3567	13	87
A420%	169.4	57.6	93.4	2881	27	72.3
A510%	106.1	53.5	91.5	5204	26	80
A520%	116.5	45.2	100.1	3155	36	64
T10%	109.5	56.3	98.3	3082	20	88.9
T20%	82.6	46	91.7	3536	29	72

Figure 3. Effect of glass transition temperature (T_g) and shape recovery time.

The same behavior for each system of ALA4, ALA5 and TRIS, is observed in the Figure 2, where at T_g higher it will take less time to recovery the original shape of the material, therefore there is less amount of soft phase. In the other hand at lower T_g will take a longer time to recovery the original shape hence there will be a greater amount of soft phase formed by the polythioethers. So the stiff phase from BADGE retains the original shape of the material in the case of each system.

Figure 4. Different systems that show: Temporary shape (a) and recovery shape (b).

All the systems were determined their deformation in the temporary shape and final recovery, this is observed in the Figure 4, which shows some photos of photopolymerizable systems.

Conclusions

The photopolymerizable epoxy systems are highly reactive when combined with the anionic photopolymerization of epoxy monomers with an epoxi-amine-thiol system. Due to these systems it was possible to obtain shape memory polymers, was observed the same behavior for each system of ALA4, ALA5 and TRIS due to when increasing concentration of each system it will decrease time to recover the original shape of the material therefore there is less amount soft phase and T_g will also decrease. In the other hand decreasing the concentration of each system will increase the recovery time to the original shape, hence there will be a greater amount of soft phase at lower T_g. So the stiff phase retains the original shape of the material in the case of each system.

Acknowledgements

The authors thank the CONACYT for funding this project 222230. We also acknowledged for the collaboration in Analysis of samples to Guadalupe Mendez, Ma Concepción Gonzales, Julieta Sánchez, Silvia Torres.

References

- [1] T. Ware, K. Hearon, et al. *Macromolecules* 45, 1062 (2012).
- [2] J.A. Shumaker, et al. *Polymer* 53, 4637 (2012).
- [3] K.M. Lee, H. Koerner, R.A.. *Soft Matter* 7, 4318 (2011).
- [4] Sun L, Huang WM.. *Soft Matter*. 6: 4403–4406 (2010).
- [5] Wei, K.; Zhu, Guangming;., *Journal of Materials Research* 28(20), 2903-2910(2013).
- [6] Ding, J.; Zhu, Y.; Fu, Y.; *Polymer Composites* , 35(2), 412-417(2014).
- [7] Rozenberg, B.A.; *Advances in Polymer Sciences*, , 75, 113-165, (1986).
- [8] Hoyle CE, Lee TY, *Journal of polymer Science. Part A: Polymer Chemistry*, 42(21)5301-38(2004).

PERFORMANCE OF ZINC OXIDE AS CATALYST FOR THE POLYMERIZATION AND GRAFTING REACTIONS IN THE MICROWAVE-ASSISTED SYNTHESIS OF POLY(D,L-LACTIDE)/ZINC OXIDE NANOCOMPOSITES

Heriberto Rodríguez-Tobías,¹ Graciela Morales,^{*1} Javier Enríquez¹ and Daniel Grande²

¹ Centro de Investigación en Química Aplicada, Blvd. Enrique Reyna 140, C.P. 25294, Saltillo, México. *graciela.morales@ciqua.edu.mx

² Systèmes Polymères Complexes, Institut de Chimie et des Matériaux, 2-8 Henri Dunant 94320 Thiais, France

Abstract

Poly(*D,L*-lactide) (PLA) is a biodegradable polymer widely used in medical applications, whose properties have been diversified by the incorporation of nanoparticles, i.e., polymer nanocomposites production. In this communication a simple microwave-assisted method for the one-step synthesis of nanocomposites based on PLA and zinc oxide (ZnO) is disclosed. Through several spectroscopic and thermal analysis techniques the *D,L*-lactide polymerization and simultaneous formation of ZnO-*graft*-PLA were demonstrated. Taking into account the experimental results, different mechanisms for the polymerization and grafting reactions were established. Moreover, a strong dependence of the ZnO catalytic performance and its concentration on the ZnO morphology (or size) was revealed.

Introduction

In recent years biopolymers have raised great interest due to the sustainable development policies. Unfortunately for certain applications, biopolymers cannot be fully competitive with conventional thermoplastics since some of their properties are too weak. Therefore, in order to extend their applications, these materials have been formulated with nano-sized particles, which bring a large range of improved and/or new properties [1]. In the case of PLA, the production of nanocomposites is mainly achieved by melt-mixing, meanwhile *in situ* polymerization, by which nanoparticle-*graft*-PLA species could be formed, has been scarcely explored. Most of the works related to *in situ* lactide polymerization have been published by Takamura et al. (silica) [2], Yang et al. (graphene) [3] and Qiu et al. (hydroxyapatite) [4-6]. Nevertheless, in all the above mentioned cases a multi-step methodology and the use of stannous octoate as the catalyst are required. As a result, a long time-consuming process takes place while the use of stannous octoate leads to the formation of potentially toxic by-products (stannous oxide and hydroxides), both of them undesirable features for a sustainable process.

In this communication, a one-step microwave-assisted technique for the synthesis of PLA/ZnO nanocomposites is attended and mechanisms for the polymerization and grafting reactions are postulated. Moreover, the effect of morphology/size as well as the concentration of particles on the polymerization development are analyzed.

Experimental

The *D,L*-lactide, chloroform and anhydrous toluene were purchased in Sigma-Aldrich, while petroleum ether was supplied by Fermont. The ZnO particles with dimensions in nano- (20-30 nm with a quasi-spherical morphology) and micro-scale (600-1000 nm with a star-like morphology) were synthesized in our laboratory by a previously reported method [7], and the corresponding SEM images are displayed in Figure 1.

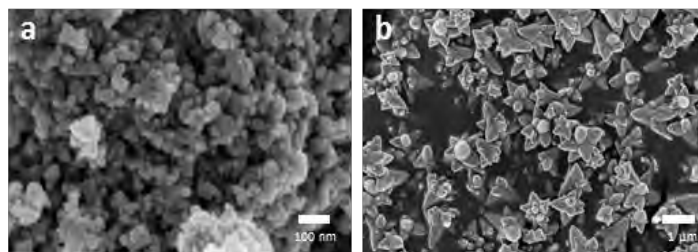


Figure 1. ZnO particles obtained by the precipitation method: (a) quasi-spherical and (b) star-like morphology

Regarding the polymerizations, the D,L-lactide and a certain amount of ZnO were put in a test tube (specially designed to be used in an Anton Paar microwave, Monowave 300) followed by the addition of anhydrous toluene (weight/volume ratio = 1/2) under inert atmosphere. Subsequently, a lyophilization process was applied in order to get rid of water traces in the reaction mixture. Afterwards, anhydrous toluene was added once again (weight/volume ratio = 1/3) and the reaction system was placed into the microwave oven and it was irradiated at 130°C at a stirring rate of 600 rpm. Under the condition previously described, a reference PLA was also synthesized using a conventional catalytic system (benzyl alcohol/stannous octoate molar ratio = 3) which exhibited a number-average molecular weight (\bar{M}_n) of 6,427 g mol⁻¹ and a polydispersity index (\bar{M}_w/\bar{M}_n) of 1.25. The raw product was precipitated in cold petroleum ether, re-dissolved in chloroform and precipitated three times. Reaction mixture, raw or isolated products were characterized by several techniques such as proton nuclear magnetic resonance (¹H NMR), Fourier transform infrared spectroscopy (FTIR), thermo-gravimetric analysis (TGA) and size exclusion chromatography (SEC).

Results

Effect of ZnO morphology/size on the production of PLA. Figure 2a depicts the ¹H NMR spectrum of the reaction product for the microwave-heated of D,L-lactide in the presence of the quasi-spherical ZnO particles (8.7 wt-%). From this spectrum it can be inferred that the ZnO nanoparticles provoked the polymerization of D,L-lactide as the typical chemical shifts corresponding to PLA are observed at 5.1-5.3 ppm for the methine group and at 1.4-1.6 ppm for the methyl group. Regarding monomer conversion, a quadruplet centered at 5 ppm and a doublet at 1.65 ppm indicate the existence of D,L-lactide traces, even though an excellent yield was achieved, ca. 96%. Meanwhile star-like ZnO particles presented a lower catalytic activity since the ¹H NMR exhibited the characteristic signals of D,L-lactide in a higher extent and only traces of the resulting polyester (see Figure 2b), with a monomer conversion ca. 22%. The mechanism of PLA formation can be established as follows: zinc lactate is formed by the release of Zn⁺² ions from the ZnO particles in the presence of water traces, and a subsequent initiation of the polymerization reaction occurs by the mentioned zinc salt. On the other hand, the higher activity of spherical ZnO nanoparticles can be explained in terms of a higher surface area, i.e. higher concentration of Zn⁺² ions released and consequently, a higher production of zinc lactate.

Effect of ZnO nanoparticles concentration on the production of PLA. Due to the fact that ZnO nanoparticles promote the polymerization of D,L-lactide, the effect of quasi-spherical ZnO concentration on the production of PLA was studied. Figure 3 reveals the monomer conversion as a function of reaction time at three different concentrations, in which an optimal ZnO nanoparticles concentration is perceived since an increase from 2.44 wt-% to 4.58 wt-% provoked a higher monomer conversion and then, an increase of it up to 8.68 wt-% diminished the conversion values. This behavior can be explained due to the agglomeration of nanoparticles, which reduces the surface area and consequently the formation of zinc lactate (initiator) is limited.

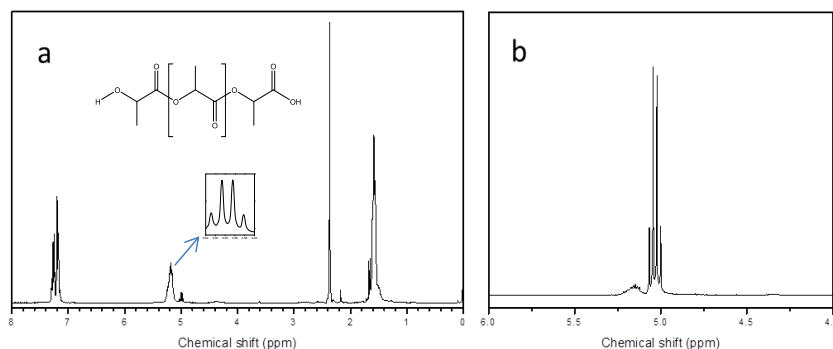


Figure 2. ¹H NMR spectra of the reaction mixture of D,L-lactide polymerization in the presence of (a) *quasi*-spherical ZnO nanoparticles and (b) star-like microparticles (zoom at the methine region)

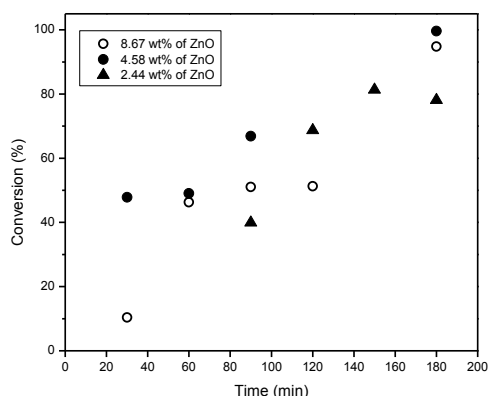


Figure 3. Effect of ZnO nanoparticles concentration on monomer conversion as a function of reaction time

PLA grafting onto ZnO nanoparticles surface. The ZnO nanoparticles were isolated from the polymer after the reaction. Figure 4a shows a series of FTIR spectra, the isolated ZnO exhibits the typical signals of PLA: vibrations C-H from CH₃ at 2994 and 2945 cm⁻¹, C=O stretching at 1750 cm⁻¹, C-O-C vibrations at 1270 and 1185 cm⁻¹. An additional signal in the isolated ZnO spectrum at 1585 cm⁻¹ is observed, which indicates the presence of carboxylate groups in the PLA chains. These groups can be interacting with the ZnO surface and consequently forming a hybrid ZnO-*graft*-PLA. In fact, grafting PLA onto ZnO nanoparticles can be detected by the TGA technique (see Figure 4b), the isolated ZnO nanoparticles exhibit a loss weight at the same temperature range than the reference PLA meanwhile neat nanoparticles do not present this feature. Moreover, the PLA with functional groups strongly attached to nano-metal oxide particles can be corroborated by the presence of a shoulder ca. 200-400°C.

PLA grafting reaction could have taken place by two mechanisms: i) first functionalization of ZnO particles with lactic acid, which along with the zinc lactate forms the catalytic system, followed by the ring opening polymerization of D,L-lactide (*grafting from*), as mentioned by Luo *et al.* [8] for the case of hydroxyapatite and/or ii) transesterification reaction between -OH groups onto the ZnO nanoparticles and free PLA formed (*grafting to*) [9], as it is depicted in Figure 5. These assertions were corroborated by FTIR analysis, by one hand, of the suspended solids (supernatant) and on the other hand, of the sediment isolated from the ZnO/monomer/toluene mixture stirred at room temperature (22-25°C), respectively. Figure 6 displays the corresponding FTIR spectrum of the sediment, which exhibits exclusively the typical signal of the D,L-lactide: C=O stretching at 1750 cm⁻¹, -CH₃ deformation at 1453 cm⁻¹, C-O-C stretching at 1247 cm⁻¹ and -CO-O- of the lactone ring at 930 cm⁻¹, meanwhile the supernatant spectrum shows multiple signals that can be related to the presence of species containing lactate groups such as zinc

lactate (COO^- at 1590 cm^{-1}) and lactate onto ZnO surface (C=O at 1750 cm^{-1} and C-O-C at 1205 cm^{-1}) as well as traces of unreacted D,L-lactide. Moreover, the reference PLA was dissolved in toluene and mixed with ZnO nanoparticles in the same ratio that the reaction of the monomer/ZnO, during 3 hours at 130°C using microwave heating. The FTIR spectrum of the isolated nanoparticles is also shown in Figure 6, where the signal at 1595 cm^{-1} corresponding to the carboxylate group, can be clearly observed.

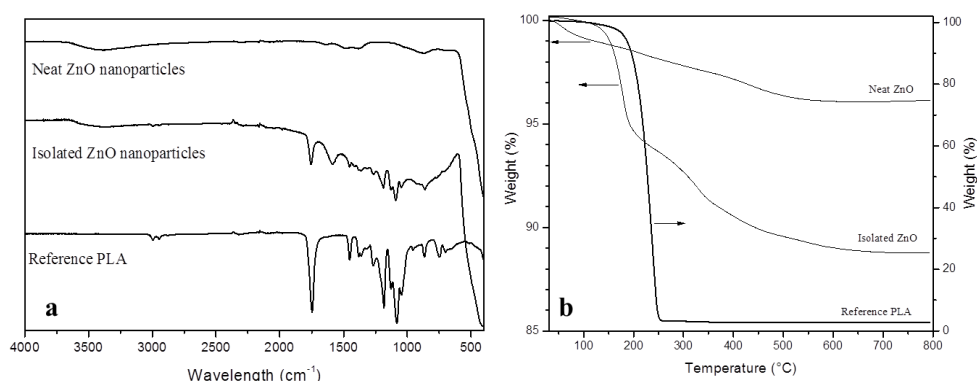


Figure 4. (a) FTIR spectra and (b) thermograms of neat ZnO, isolated *quasi-spherical* ZnO nanoparticles and reference PLA

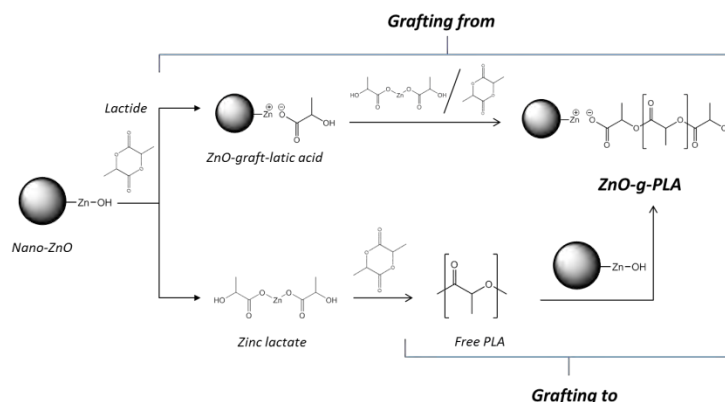


Figure 5. Representative scheme of the possible PLA grafting reactions onto ZnO particles

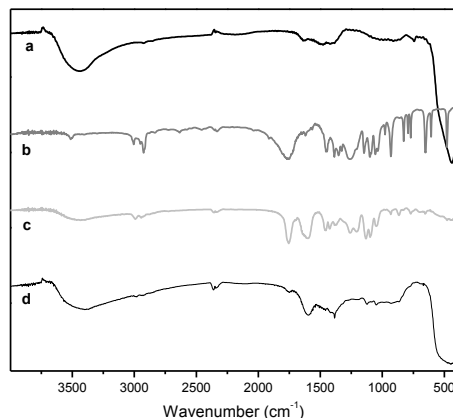


Figure 6. FTIR spectra of (a) neat nano-ZnO, (b) sediment and (c) supernatant derived from the reaction of monomer/ZnO mixture ($\text{ZnO} = 8.68\text{ wt-\%}$) at $22-25^\circ\text{C}$, and (d) nano-ZnO isolated from the reaction between ZnO and reference PLA ($\text{ZnO} = 8.68\text{wt-\%}$) at 130°C

Conclusions

A new green methodology for the microwave-assisted polymerization of *D,L*-lactide has been developed, which is catalyzed by micro- and nano-ZnO particles. Microwave heating has proven to be a highly time-saving technique, since high conversion (96%) has been achieved in 3 hours, meanwhile conventional heating needs 24-172 hours. On the other hand, a strong effect of ZnO morphology/size and concentration on the monomer conversion was evidenced.

Additionally, the existence of a hybrid material, *i.e.*, ZnO-*graft*-PLA was corroborated by TGA and FTIR techniques, whose formation is due to *grafting to* and/or *grafting from* reactions. The ZnO-PLA composite as well as the ZnO-*graft*-PLA hybrid could have a great potential for medical applications due to the combination of the antibacterial properties of ZnO and biocompatibility and biodegradability characteristics of PLA.

Acknowledges

The authors would like to thank the Mexican National Council for Science and Technology (CONACYT) for Heriberto Rodriguez scholarship and to Pablo Acuña for his technical support.

References

- [1]. P. Bordes, E. Pollet and L. Avérous, Progress in Polymer Science, 34, 125 (2009).
- [2]. M. Takamura, T. Yamauchi and N. Tsubokawa, Journal of Applied Polymer Science, 124, 3854 (2012).
- [3]. J.-H. Yang, S.-H. Lin and Y.-D. Lee, Journal of Materials Chemistry, 22, 10805 (2012).
- [4]. X. Qiu, Z. Hong, J. Hu, L. Chen, X. Chen and X. Jing, Biomacromolecules, 6, 1193 (2005).
- [5]. Z. Hong, P. Zhang, C. He, X. Qiu, A. Liu, L. Chen, X. Chen and X. Jing, Biomaterials, 26, 6296 (2005).
- [6]. Z. Hong, X. Qiu, J. Sun, M. Deng, X. Chen and X. Jing, Polymer, 45, 6699 (2004).
- [7]. G. Barreto, G. Morales and M. L. López-Quintanilla, Journal of Materials, 2013,1 (2013).
- [8]. B. H. Luo, C. E. Hsu, J. Yang, J. H. Zhao and C. R. Zhou, Advanced Materials Research, 204-210,1929 (2011).
- [9]. M. Murariu, A. Doumbia, L. Bonnaud, A. L. Dechief, Y. Paint, M. Ferreira, C. Campagne, E. Devaux and P. Dubois, Biomacromolecules, 12, 1762 (2011).

TAKING ADVANTAGES OF THE UNIQUE PROPERTIES AT NANOSCALE OF THE ZINC OXIDE FOR THE DEVELOPMENT OF FUNCTIONAL POLYMER MATERIALS: FROM PARTICLE SYNTHESIS TO FINAL APPLICATIONS

Graciela Morales,^{1*} Carlos Espinoza-González,¹ Oliverio Rodríguez,¹ Adriana García,¹ Heriberto Rodríguez-Tobías,¹ Daniel Grande² and Gastón Barreto³

¹ Centro de Investigación en Química Aplicada, Blvd. Enrique Reyna 140, C.P. 25294, Saltillo, México. *graciela.morales@ciqa.edu.mx

² Complex Polymer Systems Laboratory, Institut de Chimie et des Matériaux, Thiais, France

³ Facultad de Ingeniería, Universidad Nacional del Centro de la Provincia de Buenos Aires. Avda. del Valle 5737, B7400JWI, Olavarría, Buenos Aires, Argentina

Abstract

Nano- and micro-ZnO particles with different morphologies were obtained by means of microwave-assisted technique (MAS), through a complete study that comprised the modification of different variables (precursor reagents, temperature, irradiation time, microwave radiation power, and additives addition). The effects of the morphology of nanoparticles and the nature of a surface coating on UV-protection properties in polyolefins were studied. The UV-protection was improved and the secondary effects due to photocatalytic activity of nanoparticles were almost avoided. Also, the unprecedented use of micro- and nano-ZnO particles with different morphologies were evaluated as catalysts for the ring-opening polymerization of *D,L*-lactide through microwave activation, for the synthesis of PLA-ZnO based composites. Furthermore, the ZnO catalytic effect was extended to the radical polymerization of methyl methacrylate and its ZnO-bases composites. Finally, the effect of ZnO particles on the mechanical and UV properties of ABS and PP based nanocomposites were evaluated for outdoor applications such as automotive parts and greenhouses, respectively.

Introduction

The use of polymeric materials for outdoor applications has a limitation related to their ability to resist the effects of ultraviolet light (UV). The prolonged exposure to UV radiation causes the degradation of the materials, which leads to loss of physical and mechanical properties and thus, to decreasing their life-time. In recent years one of the strategies implemented in order to reduce the effects of UV radiation in different polymer matrices has been the incorporation of zinc oxide (ZnO) nanoparticles, since they absorb at a wavelength between 315-400 nm and they have transparency in the visible light spectrum [1].

In the last decades various methods have been employed, from gas phase processes in solution to synthetic routes for the synthesis of nano-ZnO particles [2], where an alternative to conventional thermostatic control techniques has been the use of microwave radiation through which nanostructures could be obtained with different morphologies including spherical particles, rods, hexagonal rings, wires, hexagonal tubes, among others [3]. In this sense, this paper addresses in a first instance, a comprehensive study on the effect of different variables in the final morphology of the obtained ZnO nanoparticles through microwave assisted technique. However, the UV energy absorbed by ZnO particles is sufficient to initiate their photocatalytic activity, which generates free radicals that can react with the polymer matrix, promoting its photocatalytic degradation.

To prevent and/or reduce the photocatalytic activity of ZnO different methods have been implemented for surface modification of ZnO nanoparticles [4]. However, the possible effects of the method used for surface modification in reducing the photocatalytic activity of ZnO are still unknown. In this work, the dependence of the method of surface modification of ZnO nanoparticles in the coating thickness and its photocatalytic activity is under study. Moreover, the effect of the photocatalytic activity on the final properties of ABS, PP and PE based nanocompounds, are analyzed.

Experimental

ZnO nanoparticles were synthesized by microwave-assisted synthesis, according to the method and conditions described by Barreto et al. [5] and characterized by Transmission Electron Microscopy (TEM) using a FEI TITAN 80-300 equipment, Fourier Transform Infrared Spectroscopy (FTIR), UV-Vis Spectroscopy, and X-ray diffraction (XRD).

For surface modification, (3-aminopropyl) triethoxysilane (APTES) and tetraethoxyorthosilicate (TEOS), both from Sigma Aldrich, were used as precursors. The methods used for surface modification of nano-ZnO are shown in Figure 1, wherein the molar ratio of ZnO/APTES is 2.87 and the molar ZnO/TEOS ratio is 2.66. The study of the morphology and thickness of the coating of ZnO nanoparticles were performed using TEM. Determination of the photocatalytic activity of ZnO nanoparticles with and without surface modification was performed by monitoring the degradation of methylene blue (MB). Figure 2 shows the different methods used for the preparation of polymer-ZnO nanocomposites.

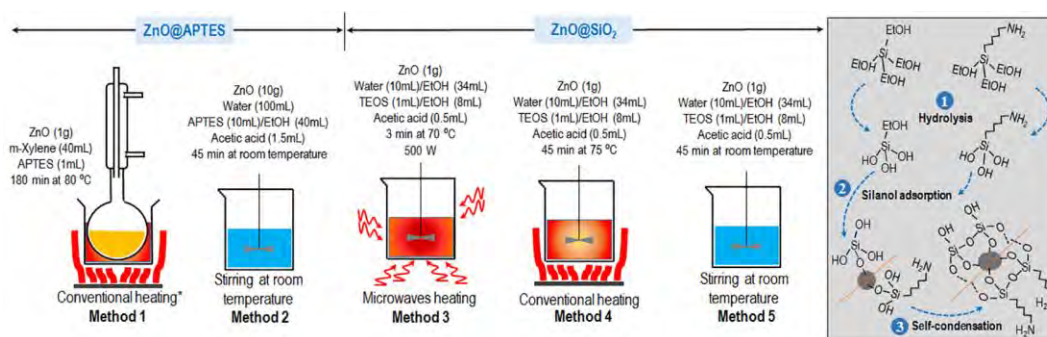


Figure 1. Surface modification methods of ZnO nanoparticles using amino-silane (APTES) and silica (TEOS) as precursors.

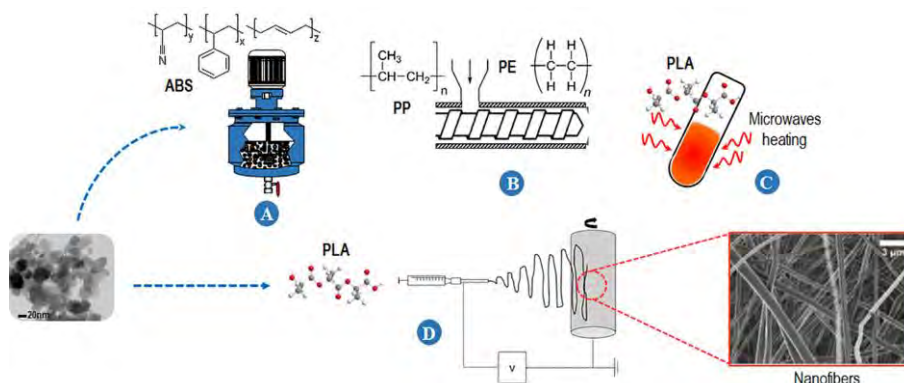


Figure 2. Different methods for preparation of polymer-ZnO nanocomposites. (A) ABS/ZnO prepared in-situ by mass-suspension technique [6]. (B) PE/ZnO, PP/ZnO by extrusion processing [7, 8]. (C) PLA/ZnO prepared by microwaves-assisted in-situ polymerization [9]. (D) PLA/ZnO nanofibers prepared by electrospinning/electrospraying [9].

Results

Effect of different parameters on the morphology of the nano-ZnO in MAS.

By XRD analysis it was demonstrated that when $\text{Zn}(\text{NO}_3)_2$ and $\text{Zn}(\text{CH}_3\text{COO})_2$ were used as the precursors, the diffraction peaks fitted with the hexagonal wurtzite type crystal structure of ZnO. In the first case, a hexagonal bi-prism type morphology (6 microns in length and 2 mm in diameter) was obtained; while in the second, the morphology was of the prismatic type (3–4 μ microns in length and

diameter). For $\text{Zn}(\text{NO}_3)_2$ and $\text{Zn}(\text{CH}_3\text{COO})_2$ as the precursors, larger particles are formed from small primary particles through an oriented aggregate process, in which adjacent nanoparticles self-assemble to share a common crystallographic orientation and are coupled on a flat interface. When ZnCl_2 was used as the precursor salt, the results were completely opposite. The difference in morphology in the three evaluated systems was attributed to the fact that the anion halide is more strongly adsorbed onto the ZnO surface than acetate or nitrate ions. As the absorption increases, the thickening process decreases and the particles have smaller sizes following the order: $\text{NO}_3^- > \text{CH}_3\text{COO}^- > \text{Cl}^-$.

An increase in irradiation time generated more defined structures with a more uniform particle size distribution and morphology; meanwhile, an increase in radiation power favored the formation of agglomerates.

Effect of modification method on the coating thickness of ZnO.

The effect of different modification methods on coating thickness in ZnO nanoparticles is described in Figure 3. TEM analysis demonstrates that greater coating thickness can be reached using modification methods where water is used as solvent/co-solvent. Independently of the surface modification, the coated ZnO nanoparticles presented the same intensity of absorption in the UV spectra.

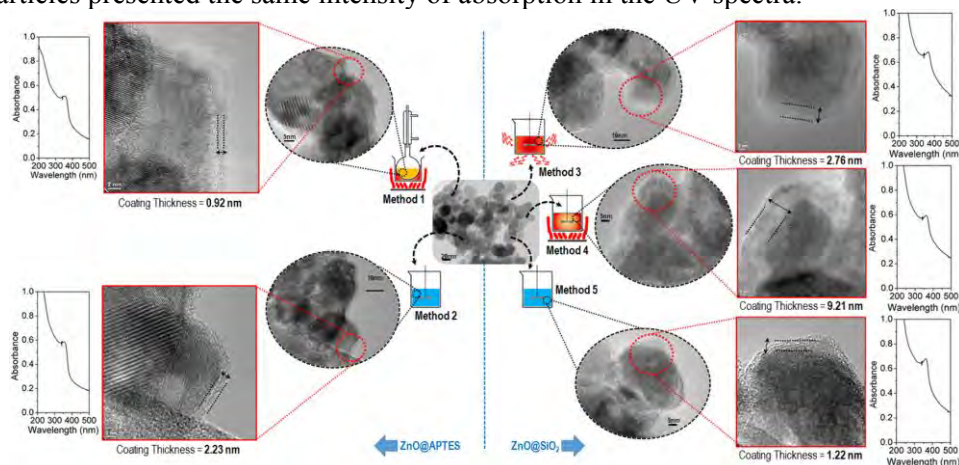


Figure 3. Dependence of the surface modification method of ZnO nanoparticles on coating thickness evidenced by TEM images and conservation of the UV absorption property.

Effect of modification method on Photo-catalytic activity of ZnO.

The photocatalytic activity of modified ZnO nanoparticles is described in Figure 4. Uncoated ZnO nanoparticles showed a degradation of MB up to 92 %. A large coating thickness does not necessary assurance a greater decrease in the photocatalytic activity. A low degradation level is obtained when the coating retards or inhibits the migration of the *electron-hole* pair.

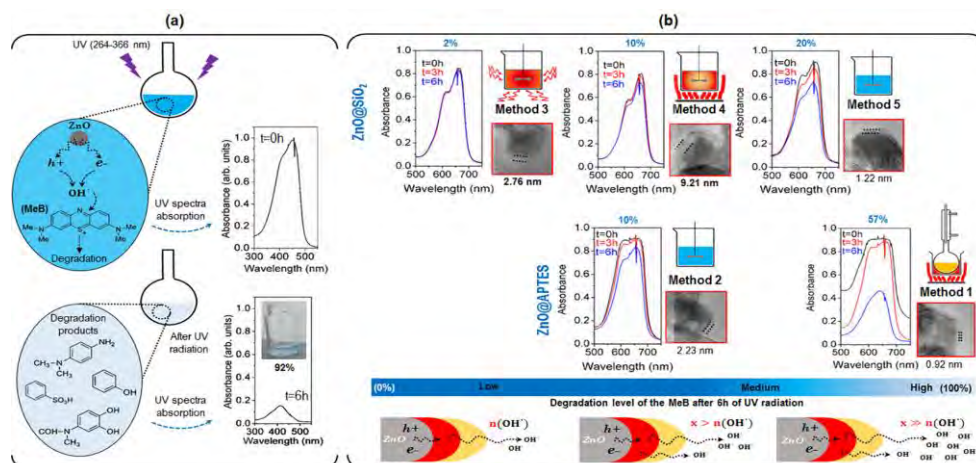


Figure 4. Photodegradation kinetic studies of methylene blue (MB) in the presence of coated ZnO evidence the influence of the modification method and their coating thickness on photocatalytic activity. (a) Scheme of the photo-degradation of MB induced by hydroxyl radicals. (b) The effect of the photocatalytic degradation of MB induced by the coated ZnO nanoparticles is re-organized according to the observed degradation level (from low to high).

Nanocomposites ZnO/polymeric matrix.

➤ ABS and PE based nanocomposites.

When ABS obtained via in situ mass-suspension is submitted to post-extrusion in order to prepare ABS/ZnO nanocomposites, the obtained morphology is similar to the one obtained with an emulsion ABS. The change in the morphology increased the mechanical properties with respect to a blank ABS (108 and 249 J/m, respectively) at a critical content of ZnO (0.05%). On the other hand, the higher the inorganic additive content, the higher the UV protection (Figure 5). The use of ZnO nanoparticles exhibit excellent UV blocking (80%) whereby it is possible to extend the lifetime of the films.

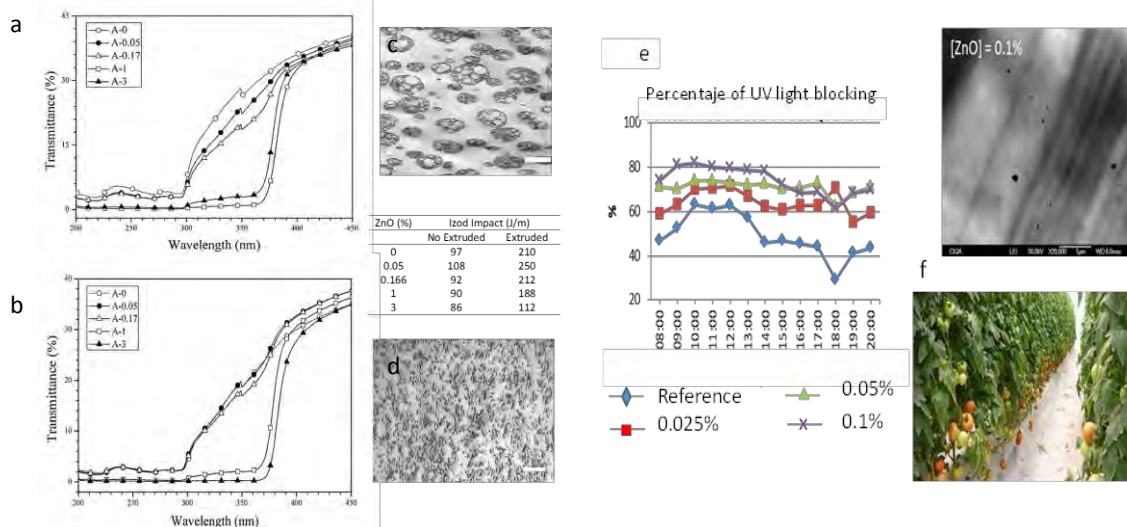


Figure 5. a-d) Properties of ABS/ZnO nanocomposites obtained by post-extrusion of ABS. e-f) PE films containing 0.1 wt% of ZnO. The development and production of the crop can be improved since the films with ZnO presented higher rate of radiation PAR, higher rate of diffuse radiation and lower stomatal resistance to the CO₂ diffusion in comparison with a reference commercial film.

➤ PLA and PP based nanocomposites.

For PLA/ZnO nanofibers, the presence of nanoparticles in any concentration had no significant influence on the morphology of nanofibers. For PP/ZnO nanocomposites, the surface modification of ZnO increases the elongation at break, due to a good interaction nanoparticle/matrix and dispersion. After aging, the nanocomposite ZnO-TEOS (RP-CE-S2) shows a lower elongation loss attributed to a decrease in degradation by UV light, where RP-CE-AS2 and RP-CE-S2 preferably degrade by chain scission; contrary to RP-EC where degradation occurs by the random chain scission according to obtained Chain Scission Distribution Function (CSDF).

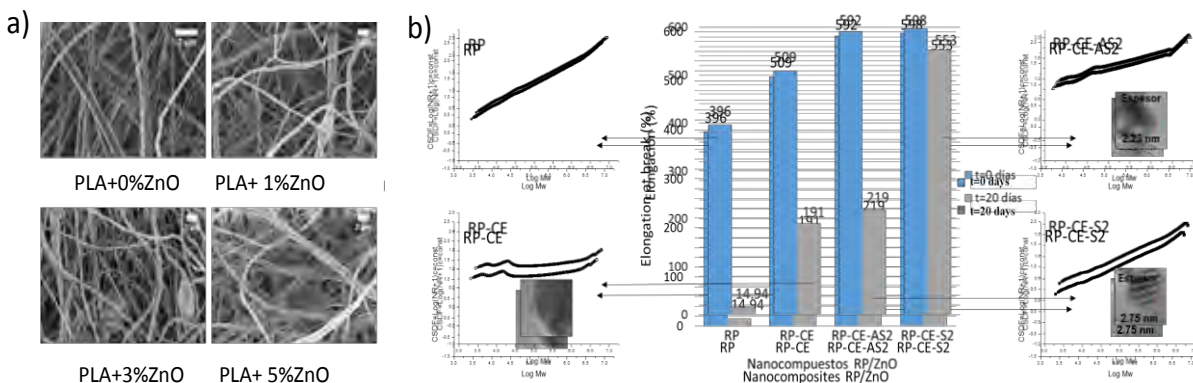


Figure 6. a) SEM micrographs of the fibers obtained by the electrospinning of the PLA/ZnO mixed with different concentrations of nanoparticles. b) Elongation at break of aged RP/ZnO nanocomposites, and the degradation mechanism revealed by the CSDF

Conclusions

The results obtained show that ZnO nanoparticles can be obtained through MAS technique with controlled morphology and the thickness of the surface modification of nano-ZnO depends of the method of modification employed. Remarkably, in ABS/ZnO nanocomposites obtained post-extrusion of ABS, the impact strength doubles the values obtained before extrusion, due to morphological changes and a better dispersion of the nanoparticles into the matrix. For PLA/ZnO nanofibers, the presence of nano-ZnO enhanced the mechanical performance of the materials, exhibiting an optimal concentration of nanoparticles for 3 wt%. In all cases the nano-ZnO improved the mechanical and/or the UV properties of the different nano-compounds where they were incorporated.

References

- [1] Z. Fan and J.G. Lu, Journal of Nanoscience and Nanotechnology, 5(10), 1561 (2005).
- [2] J. Wang and L. Gao, Journal of Materials Chemistry, 13, 2551 (2003).
- [3] J. Huang, C. Xia, L. Cao and X. Zeng, Materials Science and Engineering: B, 150, 187 (2008).
- [4] R. Y. Hong, J. H. Li, L. L. Chen, D. Q. Liu, H. Z. Li, Y. Zheng and J. Ding, Powder Technology, 189(3), 426 (2009).
- [5] G. P. Barreto, G. Morales and M. L. L. Quintanilla, Journal of Materials, ID 478681, 1 (2013).
- [6] H. Rodríguez-Tobías, G. Morales, O. Rodríguez-Fernández and P. Acuña, Journal of Applied Polymer Science, 6(127), 4708 (2013).
- [7] A. C. Contreras, M. A. Arellano, M. R. Quezada, G. Morales, A. Zermeño and J. Munguia, The International CIPA Conference, Tel Aviv, Israel (2012)
- [8] A. García-Hernández, G. Morales, O. Rodríguez-Fernández and C. Espinoza-González, Proceedings IMRC, Cancún, México (2014)
- [9] H. Rodríguez-Tobías, G. Morales, A. Ledezma, J. Romero, D. Grande. Journal of Materials Science 49, 8373 (2014)

NANOCOMPOSITE OF ACICULAR ROD-LIKE ZnO NANOPARTICLES AND SEMICONDUCTING POLYPYRROLE PHOTOACTIVE UNDER VISIBLE LIGHT IRRADIATION FOR DYE PHOTODEGRADATION

Victor M. Ovando-Medina¹, Raúl G. López², Blanca E. Castillo-Reyes³, Jaime E.A. Orozco¹, Hugo Martínez-Gutiérrez⁴, Pedro A. Alonso-Dávila³

¹*Coordinación Académica Región Altiplano (COARA) Universidad Autónoma de San Luis Potosí, Carretera a Cedral KM 5+600, San José de las Trojes, Matehuala, San Luis Potosí 78700, México.*

²*Centro de Investigación en Química Aplicada, Boulevard Enrique Reyna Hermosillo No. 140, Saltillo 25253, Coah, México.*

³*Facultad de Ciencias Químicas, Universidad Autónoma de San Luis Potosí, San Luis Potosí Av. Manuel Nava No. 6, Zona Universitaria, San Luis Potosí, S.L.P. 78290, México.*

⁴*Centro de Nanociencias y Micro y Nanotecnologías, Instituto Politécnico Nacional (IPN), Luis Enrique Erro S/N, D.F. 07738, México.*

Abstract

Nanoparticles of ZnO with acicular rod-like morphology were synthesized using a bi-continuous microemulsion and coated with polypyrrole, by polymerization in the presence of sodium dodecyl sulfate (SDS) surfactant with ammonium persulfate (APS) as oxidizing agent to obtain nanocomposites of ZnO/PPy. The resulting material was characterized by FTIR, Raman spectroscopy, Scanning Electron Microscopy and voltammetry cyclic. The synthesized nanocomposite consisted of ZnO nanoparticles immersed in a polypyrrole matrix with a conductivity of 6.4×10^{-6} S/cm. The synthesized nanocomposite was tested in the photodegradation of methylene blue (MB) dye under visible light irradiation resulting in photodegradation efficiency of 95.2% after 60 min of irradiation using 3.6 g/L of nanocomposite in an aqueous solution of MB at 20 mg/L. Pseudo first-order kinetics were used to describe the photodegradation reactions.

Introduction

ZnO has been considered a promising low-cost photocatalyst with physical and chemical stability, high oxidative capacity, and availability [1]; however, due to its bad gap (*ca.* 3.25 eV [2]) it is photoactive only under UV light irradiation ($265 < \lambda < 370$ nm) which is dangerous and expensive. It has been demonstrated that ZnO particles with morphology in the nanometric scale show improved performance due to its large surface area, short carrier diffusion length, and low reflectivity [3].

In this work, ZnO/PPy nanocomposites were synthesized polymerizing pyrrole monomer by chemical oxidation onto ZnO nanoparticles of acicular rod-like morphology, previously obtained by precipitation from a bi-continuous microemulsion with high yield, and characterized by chemical, electrochemical, and electron microscopy procedures. The nanocomposite was tested as a photocatalyst in the degradation of methylene blue under visible light irradiation. To the best of our knowledge, this is the first time this nanocomposite with the aforementioned morphology is used in photodegradation of a dye in aqueous solutions using visible light irradiation.

Experimental

ZnO nanoparticles were prepared by a precipitation method in a bicontinuous microemulsion system following the methodology reported [4] and briefly described. A bicontinuous microemulsion composed of 40.5 wt.% surfactants (AOT/SDS 2/1 wt./wt.), 32.5 wt.% 0.7 M zinc nitrate aqueous

solution, and 27 wt.% toluene was prepared. A 250 mL jacketed glass reactor was loaded with 100 g of microemulsion, raising the temperature to 70 °C under magnetic stirring. Afterwards, an aqueous NaOH solution (41.6 wt.%) was fed using a calibrated dosing pump. The dosing time of this solution was 15 min. The reaction proceeded for 30 min and acetone was added to precipitate the ZnO nanoparticles. Finally, the precipitate was washed several times with water-acetone mixture (80/20, wt./wt.) and dried at 70 °C to obtain purified ZnO nanoparticles.

Pyrrole polymerization onto ZnO nanoparticles was performed as follows: 30 g of water were mixed with 0.8 g of SDS in a 60 mL vial. Subsequently 250 mg of ZnO nanoparticles were added and ultrasonicated for 10 min, 0.4 g of pyrrole was added and allowed to homogenize under magnetic stirring for 2 h. Then APS was dissolved in 10 mL of water (0.6 M) and added to the reaction mixture to start pyrrole polymerization. The reaction proceeded under magnetic stirring for 1 h. The reaction mixture was poured into an excess of methanol to precipitate the ZnO/PPy nanocomposite. The samples were decanted and dried at 60 °C in an oven for 24 h.

The resulting materials were analyzed by FTIR and by Raman spectroscopy, SEM and XRD. The electrical conductivities of samples were determined by the four-probe method. The cyclic voltammetry measurements were performed in a glass cell using a potentiostat/galvanostat.

The synthesized ZnO/PPy nanocomposite was tested in methylene blue (MB) dye photodegradation in aqueous solutions. The reactor consisted of a glass vessel with two quartz bulbs, the first for water recirculation at constant temperature (20 °C) and the second to insert the visible light source. 0.90, 1.6, and 3.6 mg/L of ZnO/PPy nanocomposite were used in MB photodegradation experiments. The sample, either containing pure ZnO or ZnO/PPy nanocomposite was well dispersed in 150 mL of an aqueous solution of MB dye at 20 mg/L of initial concentration. Samples of 0.5 mL were withdrawn at different times to determine absorbance at a wavelength of 664 nm.

Results and Discussion

Figure 1 shows the SEM micrograph of ZnO nanoparticles synthesized in this work. Acicular rod-like morphology [4] was observed in the ZnO nanoparticles, which demonstrates the reproducibility of their experiments. The size of these nanoparticles was in the range from 8-15 nm in diameter and between 20-35 nm in length. After pyrrole polymerization onto these ZnO nanoparticles, a composite consisting of a semiconducting PPy matrix in which ZnO nanoparticles were totally immersed can be observed (Figure 1).

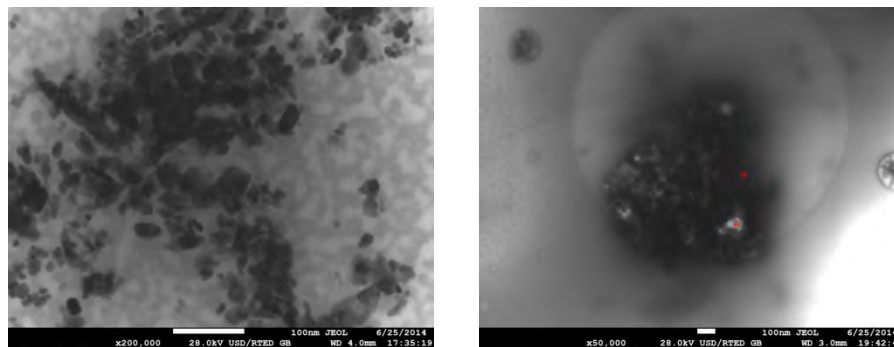


Figure 1 SEM image of pure ZnO nanoparticles synthesized by precipitation in a bicontinuous microemulsion.

Figure 2 shows the Raman spectrum of synthesized ZnO nanoparticles. The main peaks of ZnO at 97, 330, 488, and 555 cm^{-1} can be observed. The signal at 330 cm^{-1} represents second order Raman spectrum due to zone-boundary phonons of hexagonal ZnO, the peak at 488 cm^{-1} is ascribed to non-

polar optical phonon E_2 of wurtzite ZnO, and the signal at 555 cm^{-1} can be attributed to A_1 (LO) mode of hexagonal ZnO [5].

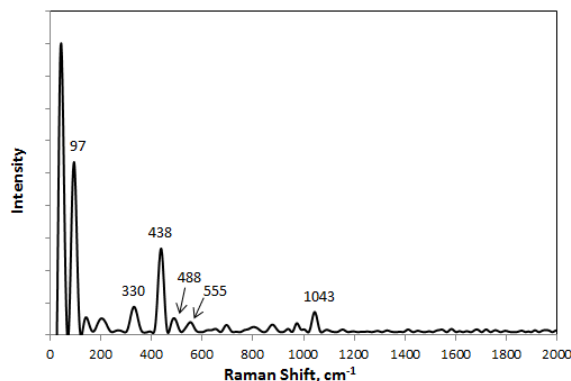


Figure 2 Raman spectrum of ZnO nanoparticles

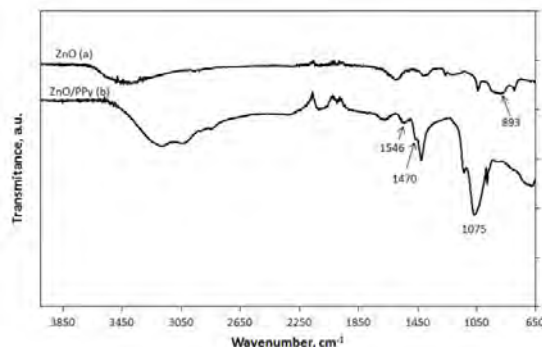


Figure 3 FTIR spectra of ZnO nanoparticles and ZnO/PPy composite.

It was not possible to analyze the ZnO/PPy composite by Raman spectroscopy because the signals were not clear. Therefore, FTIR analyses of both ZnO and ZnO/PPy composite were conducted. Figure 3 shows the FTIR spectra of ZnO nanoparticles (a) and ZnO/PPy composite (b). It can be observed from curve (a) that the typical signal of ZnO interaction in stretching mode was near to 893 cm^{-1} [4,6]. The presence of PPy can be observed in curve (b) where characteristic signals were present: the band at 1560 cm^{-1} and a weak band at 1470 cm^{-1} are assigned to stretching vibration of C=C and C–C in the pyrrole ring while the peak at 1075 cm^{-1} can be ascribed to C–N stretching vibrations. The peak located at 1560 cm^{-1} is considered as a reflection of effective conjugated length. The greater the red shift of this peak, the longer the effective conjugated length of the conducting polymer [7]. The peak corresponding to ZnO in curve (b) is almost absent, indicates that ZnO nanoparticles were well coated with PPy. Figure 4 shows the elemental analysis obtained by EDS run at two zones of the SEM image (shown as triangular and circular areas in Figure 1). It can be seen in Figure 4 that the triangular area corresponds to a zone with a high content of ZnO whereas the circular area corresponds to organic material (PPy rich). With these results it can be concluded that ZnO nanoparticles were well distributed into the PPy matrix. Additionally in both EDS spectra from Figure 4 other elements are observed, such as S and Na, which indicates that some surfactant molecules and oxidizing agents remained even after composite purification.

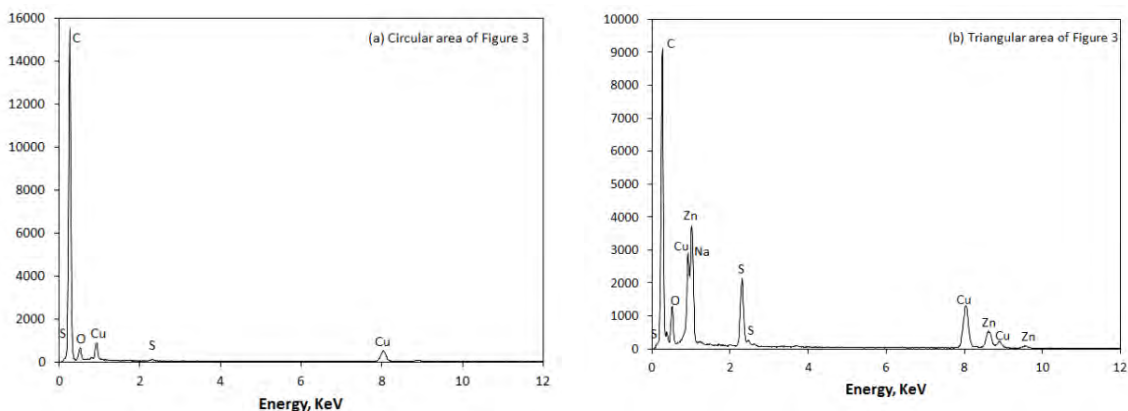


Figure 4 EDS spectra of ZnO/PPy composite: (a) Circular and (b) triangular area of Figure 1, respectively.

In Figure 5 the UV/Vis spectra of ZnO nanoparticles (a) and ZnO/PPy composite (b) are shown. The uncoated ZnO nanoparticles had a strong absorption in the UV region with spectral wavelength between 250 and 400 nm, which is similar to that reported by Wang et al. [8]. On the other hand, the ZnO/PPy composite showed absorption above the uncoated ZnO nanoparticles in the visible region with the absorption edge shifted toward longer wavelength, this behavior can be ascribed mainly to the presence of semiconducting PPy.

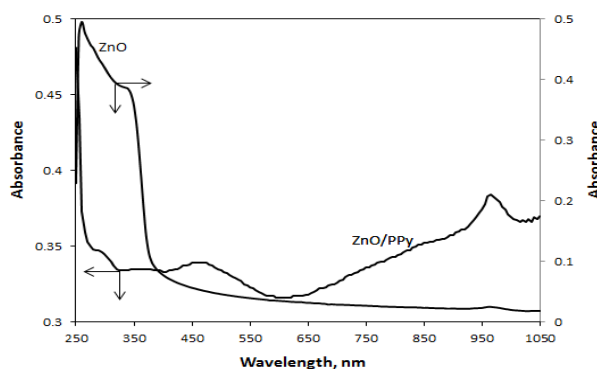


Figure 5 UV/Vis spectra of ZnO nanoparticles and ZnO/PPy composite.

Two absorption bands with maxima at 460 nm and 960 nm were observed in the spectrum of the composite. The first band is attributed to transitions of the valence band to the polaron state, which is directly related to the conductivity of the PPy chain (high degree of π -conjugation, i.e. π - π^* interactions along the polymer chain). The second band is related to the bipolaron state. The bipolaron state is common when some dopant is present in the conducting polymer chain. In this work the bipolaron state can be ascribed to the presence of surfactant molecules used throughout the synthesis, which act as dopants [9]. The conductivity values for pure ZnO and ZnO/PPy were 7.9×10^{-10} S/cm and 6.4×10^{-6} S/cm, respectively; thus the presence of PPy increased not only photoactivity (Figure 8) of the composite but its conductivity.

The electrochemical properties (not shown here) of ZnO nanoparticles showed negligible redox activity compared to ZnO/PPy composite. The cathodic and anodic peaks of ZnO were +1.4 V and +0.85 V, respectively. Here the characteristic redox behavior of PPy was observed, with an oxidation peak (cathodic) around -0.24 V while the reduction peak (anodic) was near to -0.48 V vs. Ag/AgCl for the sample of ZnO/PPy composite. Typical values of potential corresponding to cathodic and anodic peaks for pure PPy are approximately +0.15 V and -0.31 V vs. Ag/AgCl. Thus, the presence of ZnO shifted the potentials of cathodic and anodic peaks of PPy to lower values.

The photocatalytic performance of the ZnO/PPy composite was studied following the MB dye degradation in aqueous solutions under visible light irradiation. Figure 6a shows the ratio of residual to initial MB concentration (C/C_0) as a function of time using the ZnO/PPy composite (540 mg) for different MB initial concentrations. It can be observed that 93.3% of degradation efficiency can be achieved after only 30 minutes of visible light exposition (for the smallest value of MB initial concentration). When the MB initial concentration was increased, maintaining constant the catalyst load fixed to 540 mg, lower degradation efficiencies were observed (71.8% and 55.9% for 50 and 100 mg/L of MB initial concentration, respectively) after 30 minutes of irradiation. Furthermore, only 1 min was needed to achieve 68% of degradation for 20 mg/L of initial MB concentration using 540 mg of ZnO/PPy composite. Thus, a plot of $-\ln(C/C_0)$ vs. time leads to a linear diagram which slope equals the observed pseudo first-order rate constant of photodegradation. Figure 6b shows a plot of $-\ln(C/C_0)$ vs. time in which it can be observed that all photodegradations followed pseudo first-order kinetics, indicating that the photodegradation rate is directly proportional to MB concentration. The k value

using 540 mg of catalyst and 20 mg/L of initial MB concentration for the ZnO/PPy composite was 3 times higher ($k = 0.055 \text{ min}^{-1}$) than that using 100 mg/L of initial MB concentration ($k = 0.0182 \text{ min}^{-1}$).

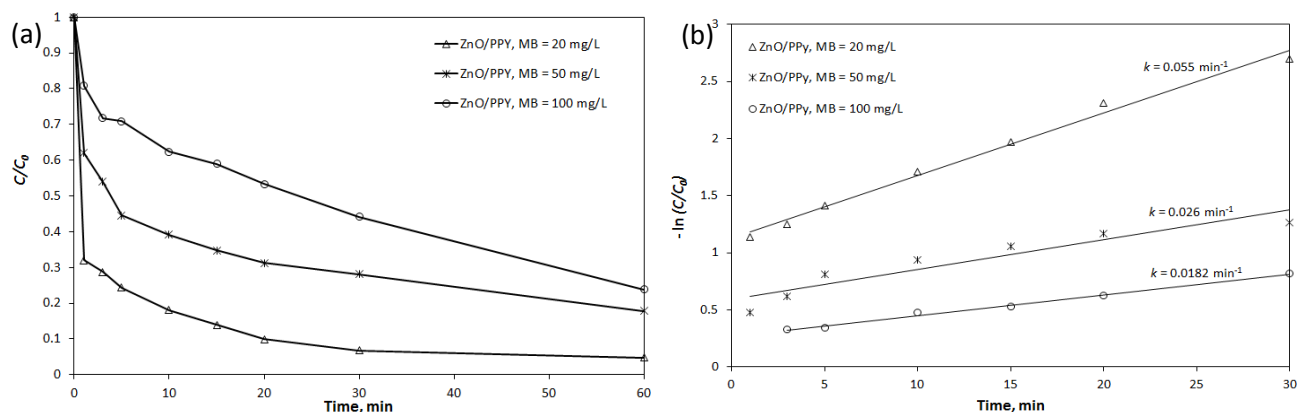


Figure 6 (a) Kinetics of MB dye photodegradation, and (b) $-\ln(C/C_0)$ as a function of time throughout MB dye photodegradation, both under visible light irradiation using ZnO/PPy composite for different MB initial concentrations

Conclusions

ZnO nanoparticles were synthesized with high yield by precipitation from a bicontinuous microemulsion and coated with semiconducting PPy by chemical oxidation to obtain ZnO/PPy nanocomposite. It was observed that ZnO nanoparticles were totally immersed into a PPy matrix and showed photoactivity not only in the wavelength region of the UV light but also in the visible light region with increased conductivity. Photocatalytic performance of the nanocomposite was demonstrated in the MB dye degradation under visible light irradiation, showing efficiencies as high as 95.2% after 60 min of reaction following a pseudo first-order mechanism.

Acknowledgements

V.M.O.M. wants to thank the Consejo Nacional de Ciencia y Tecnología (CONACYT)-México by Grant # SEP-80843. B.E. Castillo-Reyes acknowledges the scholarship from CONACYT-229857.

References

1. Rajbongshi B.M., Ramchiary A., Jha B.M. and Samdarshi S.K. (2014) J Mater Sci: Mater Electron 25:2969-2973.
2. Senadeera G.K.R., Kitamura T., Wada Y. and Yanagida S. (2006) J. Photochem. Photobiol. A 184:234.
3. Zhang M., Li Y.B., Delaunay J.J. (2012) Nanoscale 4:1509.
4. Romo L.E., Saade H., Puente B., López M.L., Betancourt R. and López R.G. (2011) Journal of Nanomaterials. Doi:10.1155/2011/145963.
5. Reddy A.J., Kokila M.K., Nagabhushana H., Rao J.L., Shivakumara C., Nagabhushana B.M. and Chakradhar R.P.S. (2011) Spectrochimica Acta Part A 81:53-58.
6. Batool A., Kanwal F., Imran M., Jamil T. and Siddiqi S.A. (2012) Synthetic Metals, 161: 2753-2758.
7. Ovando-Medina V.M., Peralta R.D., Mendizábal E., Martínez-Gutiérrez H., Lara-Ceniceros T., Ledezma-Rodríguez R. (2011) Colloid Polym Sci 289:759-765
8. Wang Z., Xiao P., Qiao L., Meng X., Zhang Y., Li X. and Yang F. (2013) Physica B 419:51-56.
9. González-Iñiguez J.C., Ovando-Medina V.M., Jasso-Gastinel C.F., González D.A., Puig J.E. and Mendizábal E. (2014) Colloid Polym Sci 292:1269-1275.

SYNTHESIS OF TiO₂/POLYPYRROLE NANOCOMPOSITES PHOTOACTIVE UNDER VISIBLE LIGHT USING ANIONIC AND CATIONIC SURFACTANTS

Blanca E. Castillo-Reyes¹, Víctor M. Ovando-Medina², Pedro A. Alonso-Dávila¹, Elías
Perez³, Hugo Martínez⁴

¹ *Facultad de Ciencias Químicas, Universidad Autónoma de San Luis Potosí, San Luis Potosí Av. Manuel Nava No. 6, Zona Universitaria, San Luis Potosí, S.L.P. 78290, México.*

² *Coordinación Académica Región Altiplano (COARA) Universidad Autónoma de San Luis Potosí, Carretera a Cedral KM 5+600, San José de las Trojes, Matehuala, San Luis Potosí 78700, México.*

³ *Instituto de Física, Universidad Autónoma de San Luis Potosí, Av. Manuel Nava No.6 Zona Universitaria, San Luis Potosí, SLP 78290, México.*

⁴ *Centro de Nanociencias y Micro y Nanotecnologías, Instituto Politécnico Nacional (IPN), Luis Enrique Erro S/N, D.F. 07738, México.*

Abstract

TiO₂/polypyrrole nanocomposites were synthesized by batch (B) and semi-batch (SB) heterophase polymerization of pyrrole onto TiO₂ nanoparticles. Sodium bis-2-ethylhexyl sulfosuccinate (AOT), hexadecyltrimethylammonium bromide (CTAB), and sodium dodecyl sulfate (SDS) were used as surfactants while ammonium persulfate served (APS) as oxidizing agent. The resulting nanocomposites were analyzed by SEM, FTIR, XRD, UV/Vis-NIR, Raman spectroscopy and Voltametry Cyclic. Nanocomposites with conductivities between 1.75×10^{-8} and 4.19×10^{-3} S/cm were obtained. Nanoparticles were tested as photocatalyst under visible light in the degradation of methylene blue. It was concluded that the polymerization mode and the surfactant type, used as a stabilizing agent, have a strong effect on the photocatalytic activity of the materials. The best results were obtained when SDS-SB was used. Percentage of photodegradation under visible light after 15 minutes was 99.3%.

Introduction

Composites of conducting polymer/inorganic materials have been considered as a new class of materials due to their improved properties compared with those of pure conducting polymers or inorganic materials. Inorganic nanoparticles can be introduced into the matrix of a host-conducting polymer either by some suitable chemical route or by an electrochemical incorporation technique [1]. Microemulsion systems are more advantageous because it is possible to obtain polymeric nanoparticles with diameters smaller than 50 nm, polymers with high molar mass, and a variety of microstructures, which influence polymer properties [2]. Particularly, microemulsions are thermodynamically stable systems and formed spontaneously by mixing oil and water in the presence of an appropriate amount of a surfactant with a co-surfactant [3].

In the case of TiO₂/polypyrrole nanoparticles, improvement of the bulk properties as electronic transference have been reported when compared with pure TiO₂; which can be used as a photocatalyst in the degradation of some organic compounds [4]. Polypyrrole (PPy) is easy to prepare by electrochemical techniques and its surface charge characteristics can easily be modified by changing the dopant anion (X⁻) that is incorporated during the synthesis. The objective of this work was the synthesis and characterization of TiO₂/PPy nanoparticles by heterophase polymerization of pyrrole in

the presence of three different surfactants (SDS, CTAB and AOT), and with two polymerization modes: batch and semi-batch. The performance of the synthesized nanocomposites was also studied in the photodegradation of methylene blue under visible light, which is not dangerous and has a lower cost than UV light.

Experimental

In a typical synthesis, 39 g of water were mixed with 0.8 g of surfactant in a 60 mL vial. Subsequently, 250 mg of TiO_2 (Degussa P25) were added and ultrasonicated for 10 min; then 1.36 g of APS was added and homogenized in 1 mL of water. In batch polymerizations (B), 0.4 g of pyrrole was added in one shot. The reaction proceeded under magnetic stirring for 2 h. In semibatch (SB) polymerization mode, pyrrole was loaded into a syringe fixed to an infusion pump at a rate of 0.0133 g/min; the reaction mixture was allowed to react for 2 h after monomer addition. The reaction mixture was poured into an excess of methanol to precipitate the TiO_2/PPy nanoparticles. The samples were decanted and dried at 60 °C in an oven during 24 h.

The resulting materials were analyzed using UV/Vis NIR diffuse reflectance spectroscopy, from these data and using the Kubelka-Munk, the band gap value of each one of the Synthesized materials was calculated. The samples were also analyzed by FTIR and by Raman spectroscopy, SEM and XRD. The electrical conductivities of samples were determined by the four-probe method. The cyclic voltammetry measurements were performed in a glass cell using a potentiostat/galvanostat.

TiO_2 and TiO_2/PPy nanoparticles synthesized through different conditions were tested in methylene blue dye photodegradation in aqueous solutions. Amounts of TiO_2/PPy nanoparticles equivalents to 80 mg of TiO_2 (shown in Table 2) were well dispersed in 50 mL of an aqueous solution of methylene blue dye at 20 mg/L under magnetic stirring in the dark through 30 minutes to achieve physical equilibrium adsorption. Solutions were exposed to a visible light source from a halogen lamp with tungsten filament at 40 cm from solutions to avoid heating or a UV light source consisting of a UV lamp of high intensity (UVP Black-Ray, 100 W and 365 nm wavelength) at room temperature. 0.5 mL samples were withdrawn at different times and centrifuged to determine UV/Vis spectra and absorbance at a wavelength of 664 nm.

Results and Discussion

Reaction mixtures were white and opaque before polymerization of pyrrole, they became dark at the beginning of polymerization and totally black at the end of polymerizations which is typical of PPy formation. Figure 1 shows the corresponding spectra of TiO_2/PPy nanoparticles obtained in the different studied syntheses. Only one absorption band with a maximum at 300 nm is observed in Figure 1, which is characteristic of TiO_2 [5].

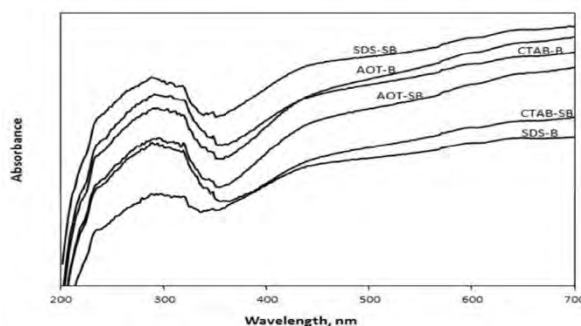


Figure 1 UV/Vis-NIR spectra from nanoparticles of TiO_2/PPy obtained under different conditions.

The first band is observed between 200 and 350 nm, with a maximum around 300 nm, and the second band between 360 and 700 nm. The first band has been attributed to transitions of the valence band to the polaron state [6] and it is directly related to the conductivity of the PPy chain (high degree of π conjugation, i.e. π - π^* interactions along the polymer chain). The second band is related to the bipolaron state of PPy. From the Kubelka-Munk functions of UV/Vis-NIR analysis, the band gap values of materials were calculated and shown in Table 2. It can be seen that band gap values were higher than that for pure TiO_2 . Figure 2 shows the FTIR spectra of materials from different syntheses, the characteristic peaks of PPy chains can be detected. The peak at 1450 cm^{-1} is ascribed to the C-C ring stretching, the peak around 1540 cm^{-1} is due to C=C.

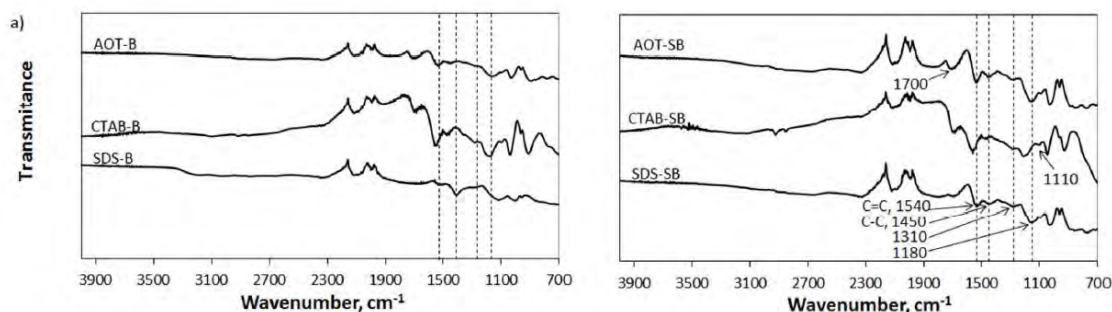


Figure 2 FTIR spectra of TiO_2 /PPy nanoparticles obtained with different surfactants in batch (a), semi-batch (b).

Conductivity values are shown in Table 1. It can be observed that conductivities were in the order: AOT-SB > SDS-B > SDS-SB > AOT-B > CTAB-B > CTAB-SB. In the Raman spectra shown in Figure 3, the signals of TiO_2 can be clearly identified [7] six active raman modes are allowed for anatase TiO_2 which must appear at 144 cm^{-1} (Eg), 197 cm^{-1} (Eg), 399 cm^{-1} (B1g), 513 cm^{-1} (A1g), 519 cm^{-1} (B1g), and 639 cm^{-1} (Eg). In the present work, only five peaks can be observed at 630, 500, 380, 180, and 140 cm^{-1} for pure TiO_2 . However for the TiO_2 /PPy nanoparticles, depending on surfactant type and polymerization mode, these signals are displaced to lower values with enhanced intensities. Moreover some new signals are observed near to 200, 250, and 550 cm^{-1} . These can be ascribed to strong interactions of TiO_2 with PPy and surfactant molecules.

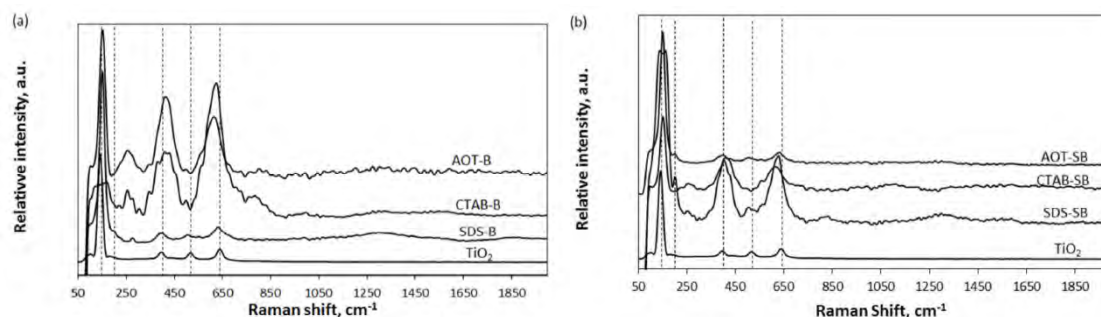


Figure 3 Raman spectra from pure TiO_2 and TiO_2 /PPy nanoparticles obtained with different surfactants in batch (a) and semi-batch (b) polymerizations

Figure 4a shows the X-ray diffractograms of the samples obtained in the different syntheses, the positions of diffraction peaks associated to the tetragonal TiO_2 from the 211276 and 211272 cards of the Powder Diffraction File database are also shown; as it can be seen the peaks presented in the experimental diffractograms are due to the diffraction of the anatase phase and some rutile phase can

also be observed. Absence of signals corresponding to PPy implies that most likely only the amorphous form of polymer was obtained in all syntheses.

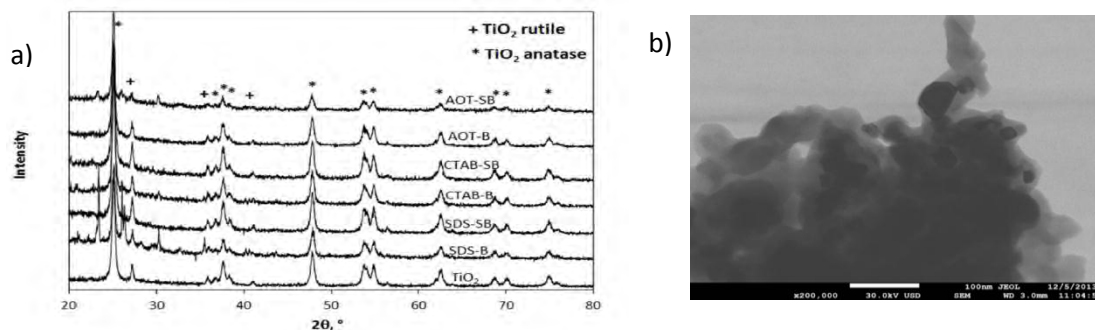


Figure 4 a) XRD spectra from pure TiO_2 and TiO_2 /PPy nanoparticles obtained with different surfactants in batch and semi-batch polymerizations, b) Scanning electron micrograph (SEM) of SDS-SB sample.

Here the characteristic redox behavior of PPy [6], with an oxidation peak (cathodic) around +1.0 V while the reduction peak (anodic) is near to +0.4 V vs. Ag/AgCl for samples obtained with SDS and AOT. The anodic peak for samples with CTAB showed lower redox activity. The cathodic and anodic peaks are resumed in Table 1. It can be seen that pure TiO_2 shows negligible redox activity compared to samples with PPy. The sample with the best redox activity was that synthesized with SDS in SB mode. Redox activity increased from batch to semi-batch polymerization mode when CTAB and SDS were used while it decreased when using AOT.

Table 1 Values of band gap from UV/Vis-NIR analysis, % of PPy in the different materials, Voltage of cathodic and anodic peaks from cyclic voltammetry and conductivities (C) of materials TiO_2 /PPy.

Sample	% of PPy	Band gap, eV	Cathodic, V	Anodic, V	C, S/cm
TiO_2	0	3.30	0.33	0.55	---
SDS-B	58.4	3.42	1.06	0.46	3.32×10^{-3}
SDS-SB	46.5	3.62	1.00	0.46	2.05×10^{-3}
CTAB-B	57.8	3.44	1.10	1.02	5.03×10^{-6}
CTAB-SB	56.3	3.46	1.06	0.92	1.75×10^{-8}
AOT-B	58.3	3.47	1.08	0.42	4.09×10^{-5}
AOT-SB	47.5	3.44	1.04	0.44	4.19×10^{-3}

The ratios of concentrations at a given time/initial concentration (C/C_0) of methylene blue through photodegradation using the synthesized materials and TiO_2 nanoparticles are shown in Figure 5. Under visible light irradiation, CTAB-B samples showed very low photocatalytic activity when compared to pure TiO_2 ; however, both TiO_2 and CTAB-B samples showed poor photocatalytic performance under visible light when compared to the other test samples. Better performance can be observed for the same conditions using CTAB-SB, AOT-SB, SDS-B, and SDS-SB.

On the other hand under UV light irradiation, photodegradation rates were slower (15 minutes were needed to observe considerable changes) resulting in a better photocatalytic behavior for the samples AOT-SB, SDSSB, and AOT-B. For photodegradation under visible light an inhibition was observed after 5 minutes of reaction, excluding the sample of SDS-SB that allowed for practically total degradation. This inhibition in photodegradation was not observed under UV light irradiation and similar results were observed for AOT-B and SDS-SB. Percentage of photodegradation under visible light after 15 minutes were as follows: TiO_2 35 %, CTAB-B 42%, CTAB-SB 62%, AOT-B 79%, SDS-B 87%, AOT-SB 92%, and SDS-SB 99.3%; while under UV light irradiation after 60 minutes the

corresponding percentages were: SDS-B 64%, CTAB-SB 67%, CTAB-B 69%, TiO₂ 71%, AOT-SB 88.2%, AOT-B 95%, and SDS-SB 96.5%.

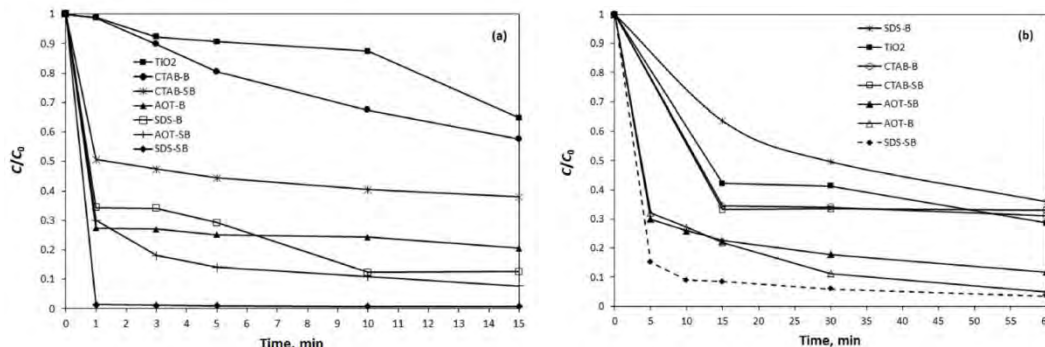


Figure 5 Kinetics of methylene blue photodegradation under visible light (a) and UV light (b) irradiation at different reaction times.

Although samples were washed several times with methanol, some surfactant molecules remained strongly attached to TiO₂/PPy materials. It is clear that better results were observed with anionic (SDS and AOT) than with cationic surfactant (CTAB). This behavior can be ascribed to electrostatic interactions between methylene blue, which is a cationic dye, and the surfactant molecules. When using CTAB as surfactant, methylene blue molecules are repelled thus diminishing the photodegradation rate.

Conclusions

Nanoparticles of TiO₂/PPy were successfully synthesized in the presence of different surfactants by batch and semi-batch polymerization processes. The as-synthesized nanoparticles showed photoactivity under visible light. The surfactant type and polymerization mode strongly affected the nanoparticles morphology, polymer conductivity, and the photocatalytic performance. It was observed that the best photocatalytic activity in methylene blue degradation was that using TiO₂/PPy nanoparticles synthesized in presence of SDS as surfactant and in SB polymerization mode, only 1 minute of photodegradation was needed to achieve more than 99% of photodegradation when compared to TiO₂ (Degussa P25) which achieved only 35% of photodegradation under visible light irradiation. Synthesized materials could be used in photodegradation of some other organic dyes as reactive red 120 under visible light irradiation, which is cheaper than UV light and not dangerous.

Acknowledgements

V.M.O.M. wants to thank the Consejo Nacional de Ciencia y Tecnología—Mexico Grant # SEP-80843. B.E. Castillo-Reyes acknowledges the scholarship No. 229857 from CONACYT.

References

- [1] R. Gangopadhyay and A. De, *Chem. Mater.*, **12**, 608 (2000).
- [2] J.R. Herrera, R.D. Peralta, R.G. Lopez, L.C. Cesteros, E. Mendizabal and J.E. Puig, *Polymer*, **44**, 1795 (2003).
- [3] Y. Shi, Y. Wu, J. Hao and G.J. Li, *Polym. Sci.: Part A: Polym. Chem.*, **43**, 203 (2005).
- [4] A. Oliveira and H. Oliveira, *Polym. Bull.* **70**, 579 (2013).
- [5] R. Vijayalakshmi and V. Rajendran, *Archives of Applied Science Research*, **4**, 1183 (2012).
- [6] P. Saville, Pyrrole formation and use. Defence Research and Development Canada—Atlantic. Technical Memorandum 2005–004, Canada.
- [7] T. Ohsaka, *Journal of the Physical Society of Japan*, **48**, 1661 (1980).

EFFECT OF SYNTHESIS CONDITIONS ON MORPHOLOGY, CRYSTALLINITY AND THERMAL STABILITY OF MAGNESIUM HYDROXIDE PARTICLES SYNTHESIZED THROUGH THE MICROWAVE-ASSISTED TECHNIQUE

H. Ortiz-Vázquez,¹ G. Morales,^{1*} O. Rodríguez-Fernández,¹ C. J. Espinoza-González,¹ D. Grande² and L. G. Valdés-García³

¹ Centro de Investigación en Química Aplicada, Blvd. Enrique Reyna 140, C.P. 25294, Saltillo, México.

*graciela.morales@ciqa.edu.mx

² Systèmes Polymères Complexes, Institut de Chimie et des Matériaux, 2-8 Henri Dunant 94320 Thiais, France

³ Instituto Tecnológico de Saltillo (ITS), Venustiano Carranza 24000, C.P. 25280, Saltillo, México.

Abstract

The influence of synthesis conditions on the morphological characteristics of magnesium hydroxide particles (MDH) obtained by microwave-assisted technique was evaluated varying different reactions parameters. Experimental results showed that among others, the temperature, precipitant agent employed and the order of reactant addition were the most relevant parameters that caused important variations on morphology and crystal array of the particles. Thermo-gravimetric analyses (DTGA) indicated that variations in thermal stability of the MDH particles were more dependent on their crystalline size rather than their particle size and morphology as it was hypothesized. These findings in the thermal behavior could have important implications for the flame retardant performance of MDH particles in different polymers matrices.

Introduction

MDH is commonly used as flame-retardant filler in composite materials due to its ability to undergo endothermic dehydration under fire conditions, ease of synthesis and low cost [1]. Nowadays, many methods have been used to prepare different shapes/morphologies of MDH. In particular, microwave-assisted synthesis technique attracts more interest because it is considered a fast, eco-friendly and easy operating method [2]. With respect to the different morphologies that can be obtained, Ding et al. [3] and Wang et al. [4] reported that the structure of MDH particles can be well controlled by choosing different reaction conditions. It is necessary to emphasize that, it has been hypothesized that changes in morphology of MDH nanoparticles could produce variations on their thermal properties that in turn, could have repercussions on the flame retardant property of polymers [5]. In this work, MDH particles were prepared by microwave-assisted synthesis and the influence of different reactions parameters on their morphology and thermal stability was evaluated.

Experimental

Synthesis of magnesium hydroxide.

The experiments for MDH synthesis were conducted through a Taguchi experimental design, using an orthogonal array (TOA) L27(37) (27 experiments, 7 factors at 3 levels each) (Figure 1), in a multimodal microwave CEM model Mars 6 at 600W and 20 minutes of irradiation. After that, the product was cooled at room temperature for 15 minutes. Then the suspension obtained was centrifuged at 20,000 rpm for 15 min and the precipitate was washed with water and methanol three times each, and dried at 70°C (Figure 2).

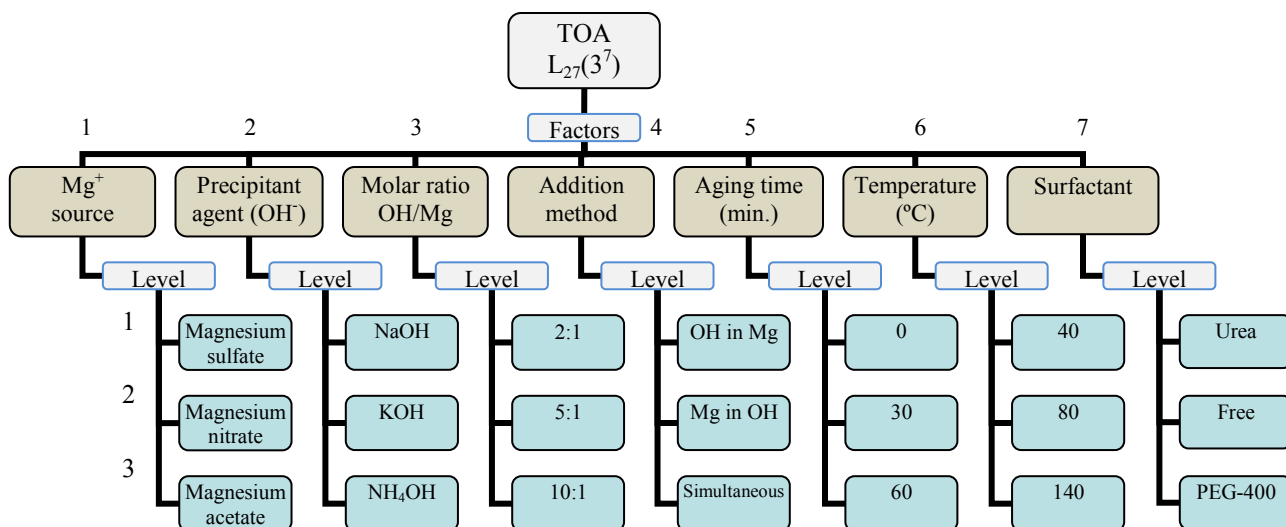


Figure 1. TOA experimental design with the different factors and levels used for this work.

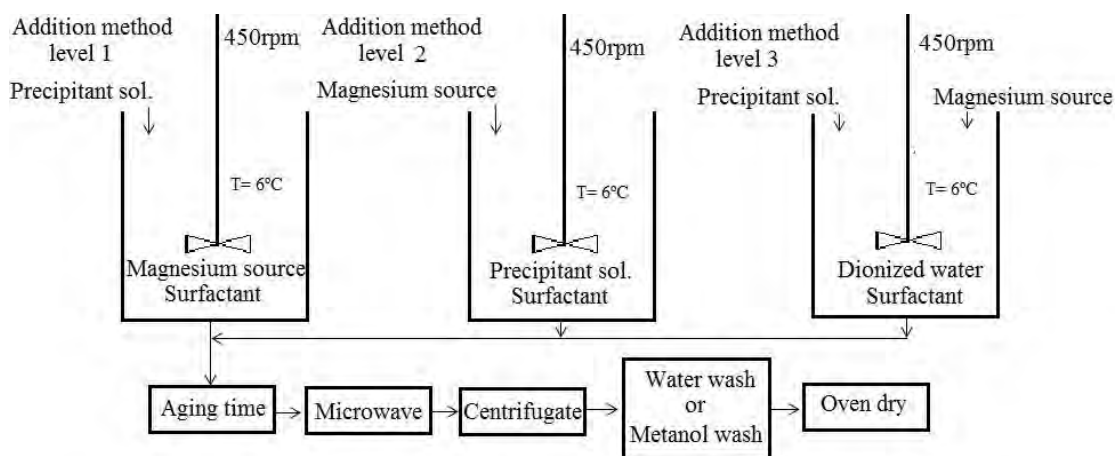


Figure 2. MDH synthesis process depending on the addition method. Reaction temperatures and chemical reagents were used according to the TOA experimental design.

Morphological and thermal characterization of MDH particles.

The morphology of the synthesized MDH was observed with a Transmission Electron Microscope (JEOL JSM-7401F) and the particle size was obtained by direct measurement using an ImageJ software. The X-ray crystallographic patterns were obtained with a XRD SIEMENS, from 2 to 80 in 2θ scale, at 25mA and 35Kv. The crystal size was calculated from the Debye–Scherrer equation. The derivative thermal gravimetric analysis (DTGA) was carried out with a TA instruments TGA Q500 at a scan rate of 10°C/min from 30°C to 800°C.

Results

Variance analysis of TOA and its effect on particle morphology.

The analysis of variance demonstrated that the main factors that influence on particles morphology were the addition method ($F_{\text{exp}}=66$), OH⁻/Mg⁺² molar ratio ($F_{\text{exp}}=63.38$) and reaction temperature ($F_{\text{exp}}=52.75$).

Effect of $\text{OH}^-/\text{Mg}^{+2}$ molar ratio and addition method on particle morphology.

Figures 3 and 4 show that a variation in the molar ratio ($\text{OH}^-/\text{Mg}^{+2}$) from 2:1 to 5:1, reduced the particle size from 129.3 to 47.5nm. On the other hand, when the molar ratio was 10:1, agglomeration of particles took place and the agglomerates presented a size of 109.1nm. This effect was associated to the pH generated by the OH^- ions in the reaction system. When OH^- concentration increases, residual electric charges could be generated onto the particles, producing strong attractions between them [6], and resulting in large particles agglomerates.

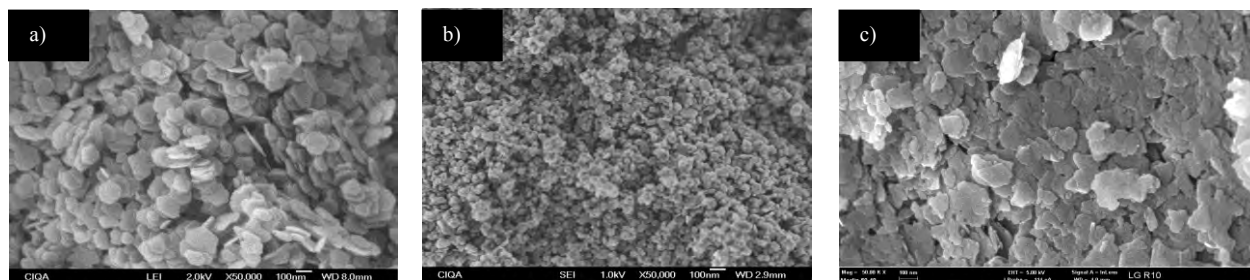


Figure 3. $\text{OH}^-/\text{Mg}^{+2}$ molar ratio effect on MDH particles morphology synthesized at 140°C . a): molar ratio 2:1; b): molar ratio 5:1; c): molar ratio 10:1.

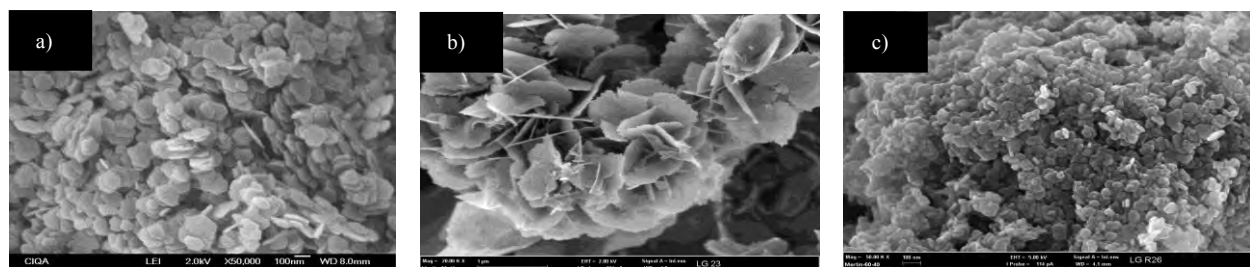


Figure 4. Effect of the addition method on MDH particles morphology synthesized at 140°C . a): OH^- incorporated to Mg^{+2} source; b): Mg^{+2} source incorporated to OH^- , c): simultaneous addition.

Effect of reaction temperature.

Figure 5 shows that particle size increased with the increase in reaction temperature, giving also better defined morphologies. This effect could be attributed to an increase in the system energy, which allows a higher mobility of the ions and increases the number of collisions [7].

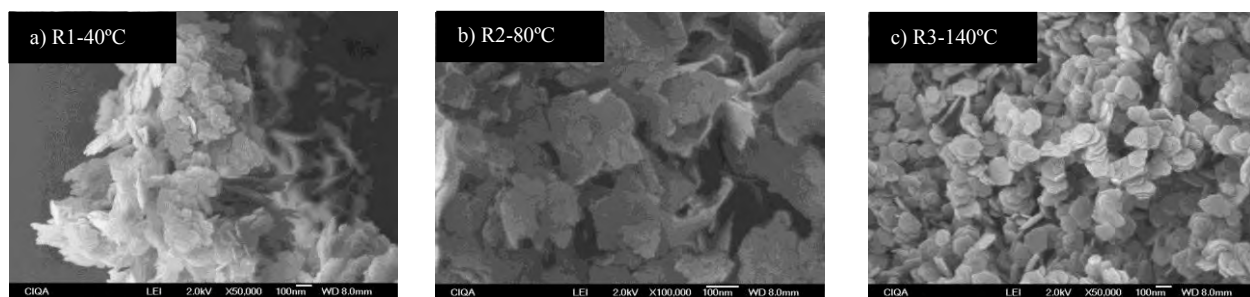
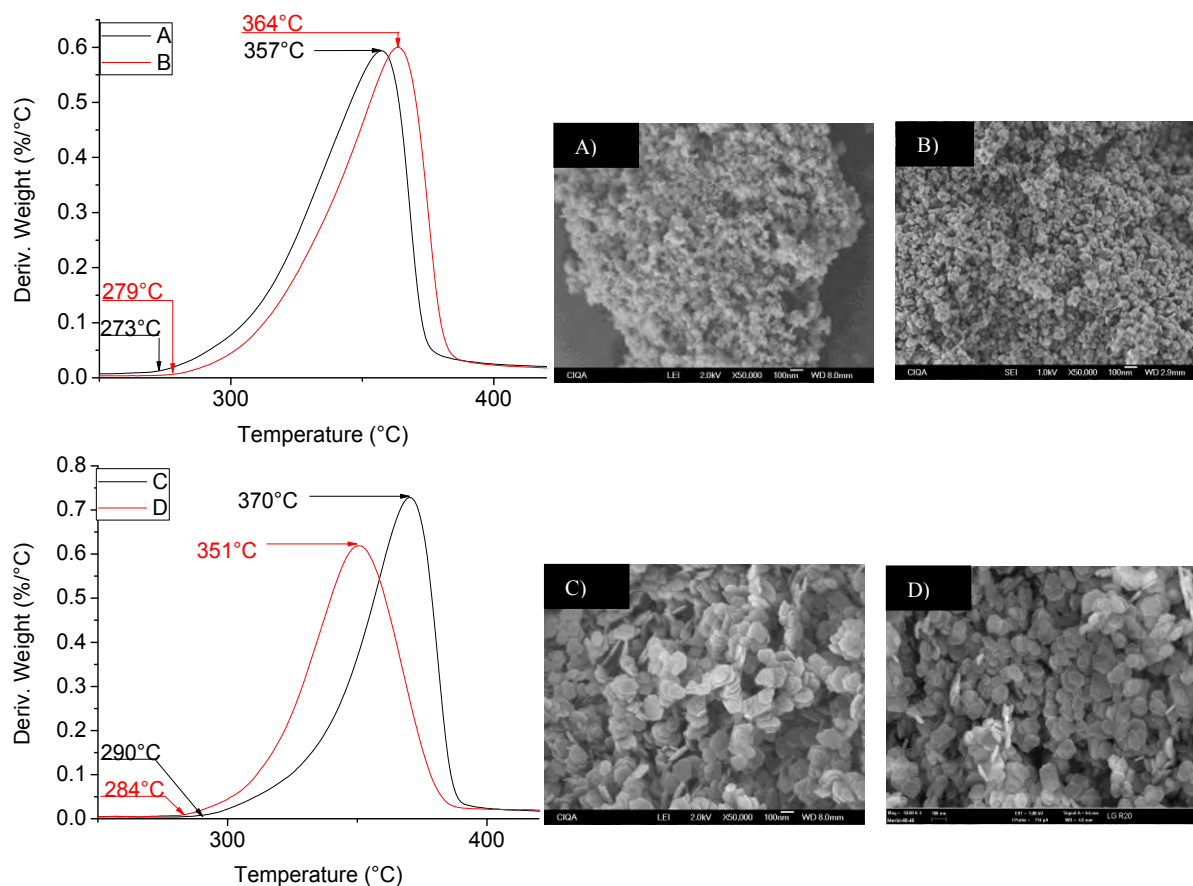


Figure 5. Effect of the temperature on MDH nanoparticles morphologies; a) particle size= not determined, crystal size on plane 101= 5.42nm; b) particle size on plane 101= 92.53nm, crystal size on plane 101= 10.25nm and c) particle size=129.34nm, crystal size on plane 101=14.77nm.

Effect of morphology on MDH thermal stability.

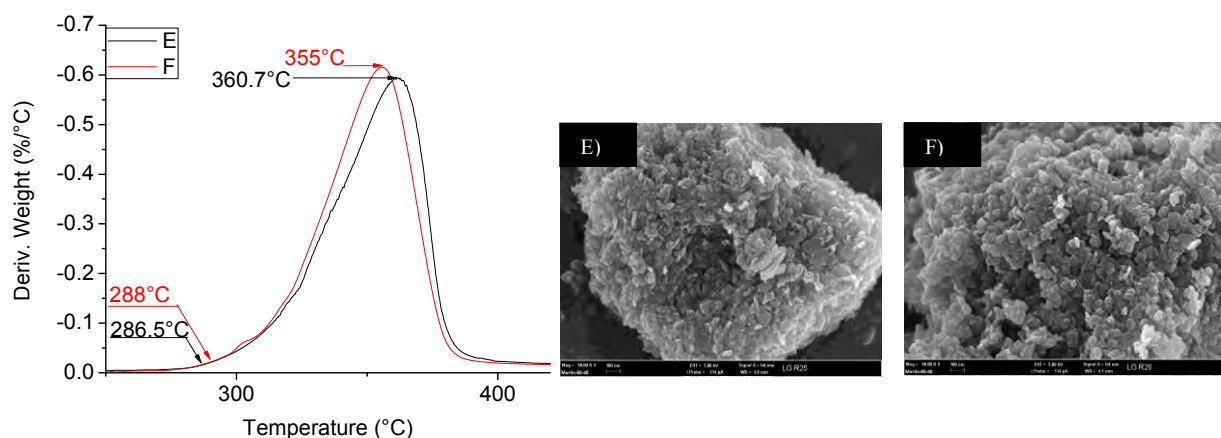
The thermal analysis evidenced a tendency of thermal stability to decrease as average particle size decrease. This decrement in thermal stability is associated to the vibrational degrees of freedom of the surface atoms and to a higher molar surface energy generated by an increase in the aspect ratio of smaller particles [5]. This behavior was in accordance to the results reported by Zixiang *et al.* [8], where mathematical models applied to CaCO_3 nanoparticles exhibited the same behavior.

For particles with the same morphology presenting different crystal size, the derivative thermal analysis (DTGA) showed that particles with larger crystals were degraded in shorter intervals of time than particles with smaller crystal size (Figures 6 and 7). These results suggest that the particles contained big crystals could enhance the flame retardant performance of MDH, due to a higher endothermic degradation could generate faster cooling of the material and a thermal insulating due to fast formation of the oxide layer.



Parameter	A vs B		C vs D	
Particle	A	B	C	D
Area under curve	21.97	22.21	21.59	23.92
Degradation time (min)	11:42	11:30	10:54	10:42
Crystal size (101)	14.57nm	18.31nm	14.77nm	22.56nm
Particle size	31.73	47.54nm	129.34nm	117.53

Figure 6. Comparison of DTGA analyses for MDH nanoparticles; A) particles synthesized from $\text{MgSO}_4 + \text{KOH}$ at 40°C, $\text{OH}^-/\text{Mg}^{+2}$ 5:1, B) $\text{MgSO}_4 + \text{KOH}$ at 140°C, $\text{OH}^-/\text{Mg}^{+2}$ 5:1, C) $\text{MgSO}_4 + \text{NaOH}$ at 140°C, $\text{OH}^-/\text{Mg}^{+2}$ 2:1, D) $\text{Mg}(\text{NO}_3)_2 + \text{KOH}$ at 140°C, $\text{OH}^-/\text{Mg}^{+2}$ 10:1.



Parameter	E vs F	
Particle	E	F
Area under curve	21.32	21.51
Degradation time (min)	11:00	10:24
Cristal size (101)	12.72nm	17.68nm
Particle size	Indeterminate	56.93nm

Figure 7. Comparison of DTGA analyses for MDH nanoparticles; E) particles synthesized from $\text{Mg}(\text{NO}_3)_2 + \text{NaOH}$ at 80°C , $\text{OH}^-/\text{Mg}^{+2}$ 5:1, F) $\text{Mg}(\text{NO}_3)_2 + \text{NaOH}$ at 140°C , $\text{OH}^-/\text{Mg}^{+2}$ 5:1.

Conclusions

Most influential parameters on particle size and morphology of MDH during microwave assisted synthesis are the molar ratio, method of addition and reaction temperature. These variables not only changed the size and morphology of the particle, but also the crystals size, generating significant changes in the thermal behavior of MDH, which in turn could have significant effects on the performance of the flame retardancy of this compound.

References

- [1] J. Ok and K. Matyjaszewski, *Journal of Inorganic and Organometallic Polymers and Materials*, 16, 129 (2006).
- [2] G. W. Beall, E. Z. M. Duraia, F. E. Tantawy, F. Al-Hazmi and A. A. Al-Ghamdi, *Powder Technology*, 234, 26 (2013).
- [3] Y. Ding, G. Zhang, H. Wu, B. Hai, L. Wang, and Y. Qian, *Chemistry of Materials*, 13, 435 (2001).
- [4] P. Wang, C. Li, H. Gong, H. Wang and J. Liu, *Ceramics International*, 37, 3365 (2011).
- [5] V. N. Likhachev, G. A. Vinogradov and M. I. Alymov, *Physics Letters A*, 357, 236 (2006).
- [6] C. Henrist, J.-P. Mathieu, C. Vogelsb, A. Rulmonta, R. Clootsa. *Journal of Crystal Growth*, 249, 321 (2003).
- [7] X. Song, S. Sun, D. Zhang, J. Wang, J. Yu. *Frontiers of Chemical Science and Engineering*, 5, 416 (2011).
- [8] C. Zixiang, X. Yongqiang, X. Libai and W. Tingting, *Journal of Computational and Theoretical Nanoscience*, 10, 569 (2013).

PREPARATION AND CHARACTERIZATION OF POLYETHYLENE WITH NANOMAGNESIUM HYDROXIDE AS FLAME RETARDANT.

Edgar Nazareo Cabrera Álvarez,¹ Luis Francisco Ramos de Valle,¹ Saúl Sánchez Valdés,¹

¹ *Centro de Investigación en Química Aplicada, Blvd. Enrique Reyna 140, Saltillo, Coahuila 25253, México.*

Abstract

In this work, was evaluated the effect caused by compatibilizer, such as maleic anhydride grafted polyethylene (PE-g-MA), on the mechanical properties and the flame retardancy in nanocomposites HDPE / MH modified with silane coupling agent type. We studied the mechanism by which the use of PE-g-MA as a compatibilizer improves the properties of flame retardancy based materials HDPE / MH. TGA-IR showed that when using PE-g-MA in nanocomposites, the properties of flame retardancy are modified, due to the generation of volatile compounds in the thermal decomposition. Nanocomposites was evaluated by cone calorimetric, IR, TGA-IR and STEM.

Introduction

Polyolefins, have a serious limitation when flame resistance is of importance in a given application. To offset this limitation, flame retardants are added into the PE composition. Some efficient halogen-free flame retardants are the hydrated metallic hydroxides, such as magnesium and aluminum hydroxides [1–4]. These metallic hydroxides reduce the flammability of polyolefin compositions, though high hydroxide content has to be used in order to attain acceptable flame retardancy. This high filler content has a negative effect on several mechanical properties, turning the PE into a brittle and fragile composition with very poor tensile properties. This negative effect is mainly due to the lack of interactions and/or compatibility between the polymer matrix and the filler particles. One way to promote these interactions and/or compatibility is through the addition of a coupling agent, such as a silane or a titanate [5–7]. In this respect, the organic silanes of the R-Si-(OR)₃ type have shown to be very effective for the surface modification of the magnesium and aluminum hydroxides, generating -Si-O- metal bonds, which force the inter-actions between the polymer matrix and the metallic hydroxide particles [8]. However, care must be taken in order to find the adequate reaction conditions, when adding a coupling agent, in order to promote the formation of the strong covalent -Si-O- Metal bonds. The reaction between the R-Si- (OR)₃ silane with magnesium hydroxide (MH). The ethoxide groups from the silane react with the MH, producing ethanol via a condensation reaction, plus Mg-O-Si- bonds. The R groups in the silane are the ones responsible for the inter-action and/or compatibility towards the polymer matrix [9]. Several methods have been used for the surface modification of metallic hydroxides, one of which is due to Chen et al. [10, 11] who carried out the MH modification with silanes and titanates, in a high speed powder mixer. They state that the coupling agent is adsorbed on the hydroxide surface, though they do not show any evidence of Si-O-Si bonds. Recently Wan [12] described a patent about a particle surface modification method using ultrasound, which permits the modification in a short period of time. Zhang [13] reported the surface modification of magnesium hydroxide using ultrasound. Kong et al. [14] carried out the surface modification of MH with 5 wt% of a silane, in xylene, at 140° C for 6 h, using dibutyl tin dilaurate as catalyst. Thereafter, they found that PE composites with 50 wt% of modified MH attained a V-0 classification in the UL-94 flame retardancy standard. But they also found, however, that when using less than 5 wt% of silane during the surface modification reaction, resulted in LLDPE composites that attained a V-2 classification. While studying EVA with nano-sized MH composites, Jiao et al. [15] found that fatty acid modified MH nanocomposites produced an increase in mechanical properties as compared to unmodified MH composites. Bahattab et al. [16] found that crosslinked LDPE/EVA composites with surface modified MH produced superior tensile properties. Recently, it was

reported [17] that the silane modified MH nanoparticles markedly improved the mechanical properties of epoxi resin, as compared to the same epoxi resin with an unmodified MH. In general, surface modified metallic hydroxides have shown to produce good mechanical properties such as, tensile strength and elongation, as well as impact resistance. From the above, it can be concluded that the studies on the MH silane modification methods have provided ample information on the matter, but most of these have not been related to the effect on the mechanical properties and flame resistance of the resulting polymer composites. Therefore, the purpose of this work is to study the effect of different MH surface modification methods on the mechanical properties and flame resistance of HDPE/MH nanocomposites.

Experimental

Materials used were: magnesium hydroxide (MH), with nominal particle size of 15 nm, from Nanostructured and Amorphous Materials Inc, USA; Triethoxy Vinyl Silane (TVS), dibutyl tin dilaurate and boric acid, from Aldrich, USA; and the Xylene solvent from CTR Scientific, Mexico. The high density polyethylene used was from Dow Chemical, USA, with MFI of 0.7 g/10 min, density of 0.954 g cm³, and fusion temperature (T_m) of 127° C.

Surface modification of flame retardant

500 g of MH plus 5 wt% with respect to the MH, of a 2:1 TVS:Boric Acid mix were added into a high speed powder mixer. The mixing was started and kept at 1700 rpms, at 30° C, for 30 min. The product (modified MH) was designated as MHMTVS. Another mix, was prepared in the same way, but adding only 3.33 wt% of TVS, without boric acid. This product was designated as MHMTVS (S/B). All modified MH samples were powdered and dried under vacuum, at 60° C, for 12 h. Unmodified magnesium hydroxide was used as reference and is designated as MH.

Preparation of HDPE/MH Nanocomposites

Each nanocomposite sample was prepared as follows: HDPE was mixed with unmodified and modified MH in a Brabender internal mixer, using roller type rotors, at 190° C and 60 rpm, for 10 min. In all cases the unmodified or modified MH concentration was 55 wt%. The resulting nanocomposites were grounded and then compression molded to obtain 150 X 150 X 3 mm³ laminates from which test specimens were taken.

Results and Discussion

Surface Modification of Magnesium Hydroxide (MH)

Figure 1, shows the IR spectra of the method modified MH. Either including (MHMTVS) or not (MHMTVS (S/B)) the boric acid, in both cases the spectrograms show the characteristic peaks of MH, at 1,421 and 1,487 cm⁻¹, due to the Mg-O bonds and at 3,443 and 3,693 cm⁻¹, due to the O-H bonds of the MH [13, 18, 19]. In addition, the signal of TVS, at 1,045 cm⁻¹, due to the Si-O bonds and at 2,900–3,000 cm⁻¹ due to the C-H of the ethoxy groups. When boric acid was included (MHMTVS), a signal at 1,268 cm⁻¹, and due to the acid O-H groups was observed. Deconvolution of the MHMTVS compound IR spectrum between 2,000 and 1,500 cm⁻¹, in Fig. 1A, permits a much clearer view of the vinyl group signal at 1,627 cm⁻¹, which was overlapped with the MH signal. This corroborates the presence of the vinyl group in the modified MH.

Flammability Tests

In Table 1, the results of the materials were evaluated by the UL-94 standard horizontal and vertical position is summarized. It can be seen that all properties of the nanocomposites obtained flame

retardancy by the use of MH or MHMTVS, as a flame retardant and derive a classification in the UL94 HB test horizontally, is that all materials are self-extinguishing when flame is applied for 30 seconds, which burns the material, but dies without spread. For HDPE / MH and HDPE / MHMTVS compounds when evaluated horizontally, 125 mm test specimens are marked with a length of 25 to 100 mm length to measure its rate of burning, but in this case as already mentioned materials swell for a certain time without reaching the mark 25 mm, is a measure of the speed with which the flame is extinguished in the material.

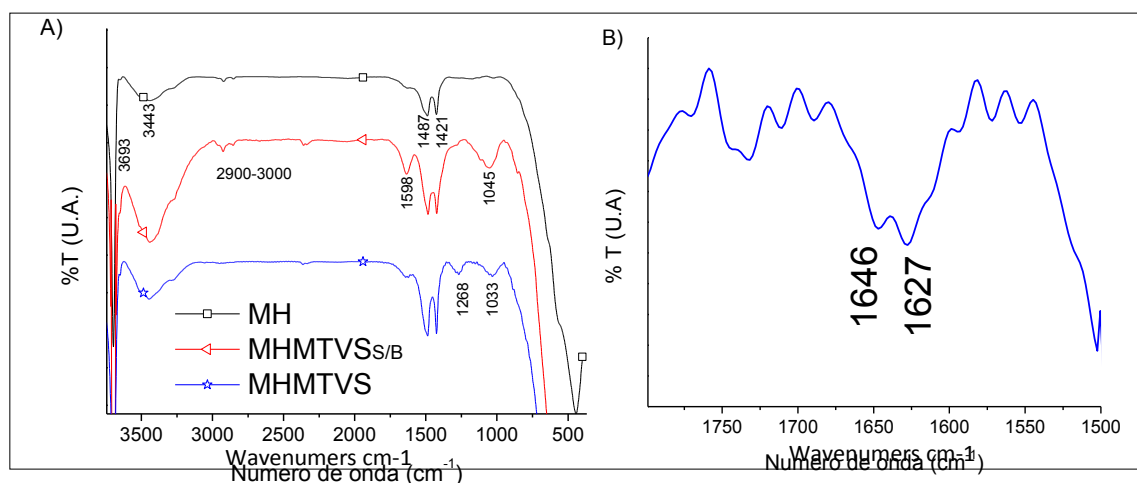


Figure 1. (A) IR spectra of MH and (B) Deconvoluted IR spectra of MHMTVS.

Table 1. Classification of HDPE/MH, HDPE/MHMTVS compounds by UL-94 standard.

Composites	PE-g-MA (% weight)	Classification Horizontal-UL94	Classification Vertical-UL94
HDPE/MH	0	HB	--
	5	HB	V-1
	10	HB	V-1
	20	HB	V-0
HDPE/MHMTVS	0	HB	--
	5	HB	--
	10	HB	V-1
	20	HB	V-1

Quantitative Analysis for Hydrocarbons released from materials.

In Figure 2, profile shown aliphatic hydrocarbon obtained by simultaneous TGA-IR analysis, compounds based on HDPE / MH to different concentrations of PE-g-MA. Can be seen that increasing the temperature of the materials by TGA analysis, they tend to generate volatile substances, which can be analyzed by IR-TGA equipment, in this case the compounds are identified as hydrocarbons and concentration profile (absorbance) is plotted with respect to temperature. Is observed, the generation of hydrocarbons at the same temperature (489 ° C), but it was found that as the content of PE-g-MA is increased materials tend to generate fewer hydrocarbons.

Cone Calorimetry Analysis

As we see in Figure 3, HDPE is a flammable material which takes a time of 39 seconds, when persistent flame arise in the material due to the radiation of the cone, is the time of ignition (Tign) and it can be inferred, in less time that reaches a maximum of 1140 KW/m², heat release rate (PHHR), these values are lower than the present HDPE, so the PE-g-MA tends to have higher flame resistance than HDPE.

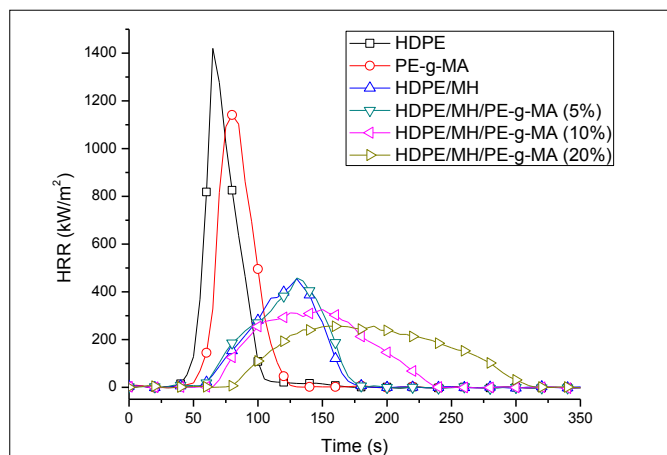


Figure 2. Release of hydrocarbons.

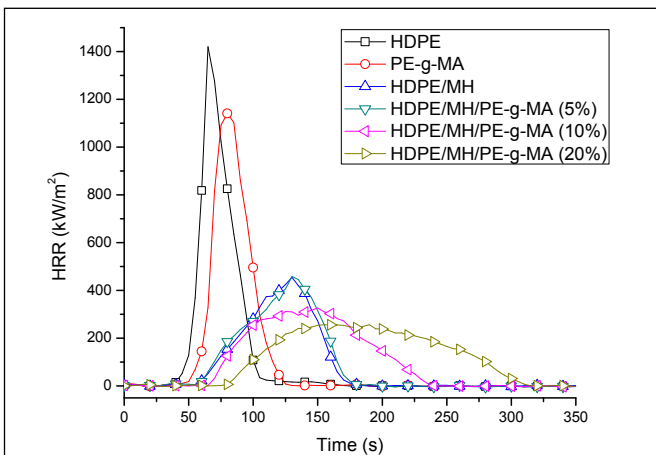


Figure 3. Heat release rate (HRR)

Nanocomposite Structure

In Figure 4, the micrographs of the compounds based on HDPE / MH with 5%, 10% and 20% of PE-g-MA are presented, with a fixed MH unmodified 55% by weight concentration. One can infer that the particles have a morphology MH disc as in all cases, with thicknesses below 100nm with 5% by weight of PE-g-MA, analyzing micrograph agglomerated particles that are distributed and little, leaving no MH polyethylene domains (designated spaces in the micrograph) are observed. Figure 4B, the particles are more distributed, the difference of the dispersion and / or distribution of the particles is due to the increased content of PE-g-MA and 10 wt%. Figure 4C, shows a greater distribution of the particles of MH in the HDPE matrix and agglomerates of smaller size than in the previous cases, is due to 20% of PE-g-MA.

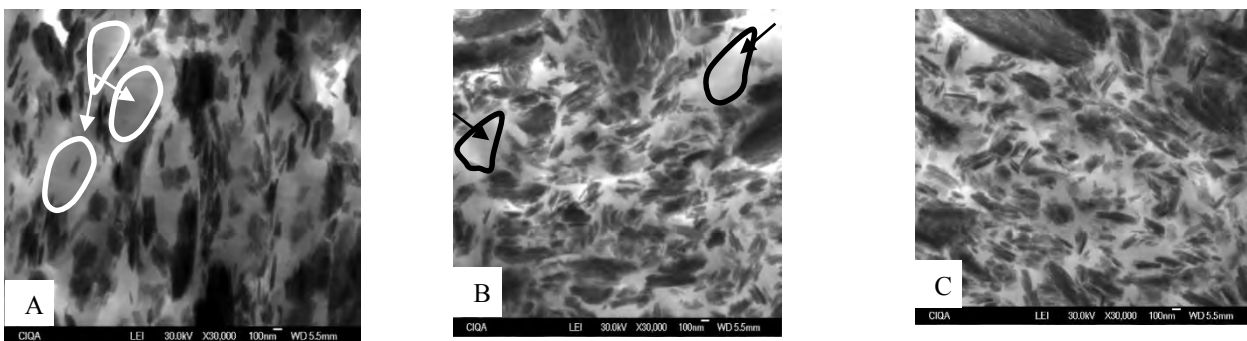


Figure 4. STEM micrographs

Conclusions

Use of a compatibilizing agent such as PE-g-MA improves the mechanical and the flame retardancy of the compounds based on HDPE / HDPE MH / LDH properties. It was found that as the amount PE-g-MA is increased, compounds improve its properties to the flame retardancy

because the amount of volatile hydrocarbons generated in the thermal decomposition of material is decreased. Also with increasing PE-g-MA polymer greater compatibility is observed with the flame retardant, increasing the continuity of phases, causing a good distribution of particles and resulting in an improvement in the mechanical properties of the materials.

Identification by TGA-IR, of volatile compounds generated in the thermal decomposition of materials generation suggests aliphatic hydrocarbons, esters and CO₂ when thermally decomposed in a range of 400 ° C to 600 ° C. Use of a compatibilizing agent such as PE-g-MA, improved mechanical and flame retardancy of the compounds based on HDPE / HDPE MH / LDH properties, because the amount of volatile hydrocarbons generated in the thermal decomposition of the material is decreased.

Acknowledgements

The authors are grateful to staff of the Centre for Research in Applied: Josefina Zamora, Miriam Lozano, Guadalupe Méndez, Jesus Cepeda, Silvia Torres, Concepcion Gonzales, Jesus Rodriguez, Francisco Zendejo, Fabian Chavez, Rodrigo Cedillo, Sergio Zertuche, Adan Herrera, Alejandro Espinosa, Mario Palacios, Jose Lopez, Marcelina Sanchez, Rosario Rangel, Sandra Ramos, Irma Solis, Efraín Alvidrez, Marcelo Ulloa, Javier Borjas, Fabiola Castellanos, Daniel Alvarado, Juan Peña and Jose Luis de la Peña, for their help and technical assistance with this research.

References

- [1] A.K. Sen, B. Mukherjee, A.S. Bhattacharya, L.K. Sanghi, P.P. De, and A.K. Bhowmick, J. Appl. Polym. Sci., 43, 1673 (1991).
- [2] F. Carpentier, S. Bourbigot, R. Delobel, and M. Foulon, Polym. Degrad. Stab., 69, 83 (2000).
- [3] Z. Wang, B. Qu, W. Fan, and P. Huang, J. Appl. Polym. Sci., 81, 206 (2001).
- [4] Z. Li and B. Qu, Polym. Degrad. Stab., 81, 401 (2003).
- [5] C.M. Liauw, Plast. Addit. Compound., 2, 26 (2000).
- [6] B. Haworth, C.L. Raymond, and I. Sutherland, Polym. Eng. Sci., 40, 1953 (2000).
- [7] L. Chen and Y.Z. Wang, Polym. Adv. Technol., 21, 1 (2010).
- [8] T.S. Lin, S.P. Bunker, P.D. Whaley, J.M. Cogen, K.A. Bolz, and M.F. Alsina, Proceedings of the 54th IWCS/ Focus, International Wire and Cable Symposium, 229 (2005).
- [9] K. Yoshinaga, M. Iwasaki, and H. Karakawa, Polym. Polym. Compos., 4, 163 (1996).
- [10] X. Chan, Y. Jie, G. Shaoyun, L. Shengjun, and H. Min, J. Mater. Sci., 44, 1324 (2009).
- [11] X. Chen, J. Yu, and S. Guo, J. Appl. Polym. Sci., 102, 4943 (2006).
- [12] J. Wan, G. Tang, and J. Li, China Patent, 200,710,124,976, (2009).
- [13] F. Zhang, H. Zhang, and Z. Su, Appl. Surf. Sci., 253, 7393 (2007).
- [14] X. Kong, S. Liu, and J. Zhao, J. Central South Univ. Technol., 15, 779 (2008).
- [15] C.M. Jiao, Z.Z. Wang, Z. Ye, Y. Hu, and W.C. Fan, J. Fire Sci., 24, 47 (2006).
- [16] M.A. Bahattab, J. Mosnacek, A.A. Basfar, and T.M. Shukri, Polym. Bull., 64, 569 (2010).
- [17] R. Suihkonen, K. Nevalainen, O. Orell, M. Honkanen, L. Tang, H. Zhang, Z. Zhang, and J. Vuorinen, J. Mater. Sci., 47, 1480 (2012).
- [18] R.A. Nyquist and R.O. Kagel, Infrared Spectra of Inorganic Compounds, Academic Press, p.234, California, USA, (1971).
- [19] B. Smith, Infrared Spectral Interpretation, a Systematic Approach, CRC Press, p.158, Florida, USA, (1999).

PARTICLE SIZE EFFECT OF NANO-CACO₃ ON THERMAL AND MECHANICAL PROPERTIES ON A NANO-CACO₃-PP COMPOSITE.

D. S. Villarreal-Lucio^a, J. L. Rivera-Armenta^a, A. L. Martínez-Hernández^b, C. Velasco-Santos^b, J. Guerrero-Contreras^c, I.A. Estrada-Moreno^a, A.M. Mendoza-Martínez^a

^a*División de Estudios de Posgrado e Investigación del Instituto Tecnológico de Cd. Madero, Cd. Madero, Tams.*

^b*División de Estudios de Posgrado e Investigación-Instituto Tecnológico de Querétaro, Querétaro, Qro.*

^c*Instituto Politécnico Nacional - CICATA Altamira, Altamira, Tamps.*

Abstract

Thermal and mechanical properties of a PP matrix reinforced with three different particle sizes of calcium carbonate (CaCO₃) were evaluated. Compounding was carry out in a single extruder. Nanoparticles were obtained using two mechanical attrition technics and an ultrasonic treatment: the eggshell was ground in a blender, the second grinding was made in ball mill and finally the particles were subjected to an ultrasonic treatment. The particle size diminished in every step resulting in three distinct sizes. The optimal PP-CaCO₃ formulation according to particle size was investigated.

1. Introduction

Nanomaterials production by ultrasonic technology represent an important alternative for development of nanotechnology, by reducing material size new properties can be industrially exploded [1]. Nanoparticle is a material between 1 and 100 nm in at least one dimension, at this size a nanoparticle possesses a large number of surface atoms [2]. Ultrasound emit sound waves up to 20 KHz in liquids, this waves are capable of produce physical phenomena and give suitable conditions to carry out chemical reactions [3]. Ultrasound technology uses involve medical applications [4], biochemical uses, organic compound synthesis, polymerization o just for mixing substances in laboratories [5].

Sonochemistry is the application of ultrasonic frequencies, in order to produce cavitation in liquids, liquid-liquid and liquid-solid systems and can take place reactions of high energy. This occurs due to the passage of ultrasound through a liquid medium cause mechanical vibration and in turn, also an acoustic flow in the medium. Under normal conditions a liquid contain dissolved gas, usually air, the gas will form bubbles that grow, reach a maximum size and finally collapse. This phenomenon of growth and collapse of the bubbles is called acoustic cavitation. The bubbles generated by cavitation generated several physical effects such as: shock waves, microjets, turbulence and shear forces [6].

Eggshell are meanly compose of calcium carbonate (87 – 97 % weight)[7], CaCO₃ has medical and cosmetics applications and it is used in food industry, has been used as reinforcement in polymer industry, improving mechanical properties [8-10]. Eggshell was modified with NaOH and then mixing con polyethylene conferring elasticity to the polymer and showing an enhanced on impact properties [11]. This investigation used a mechanical method and a sonochemical effect to obtain calcium carbonate nanoparticles from eggshell.

2. Experimental

2.1 Materials

Eggshells were collected from household waste and washed. Acetone were analytic grade purchase from Analytyka. N,N-Dimethylformamide (DMF) was used to keep the particles suspended during ultrasonic process. Polypropylene PROFAX 6331 was provided by INDELPRO.

2.2 Size reduction

Eggshells were grinded using a blender, the powder was soaked in acetone for 2 h in order to separate the CaCO₃ from organic compounds. A second size reduction of CaCO₃ particles was performed in a SPEX 8000M high energy ball mill during 1 h in the presence of distillated water. Finally the particles were suspended in DMF and subjected in an ultrasonic Cleaner bath AS10299B, whit a 42 KHz frequency for 5 h for further size reduction[12]

2.3 Composite preparation

Composites were prepared in a Brabender Intellitorque mixer with roller blades, using a speed of 100 rpm, a mix temperature of 190 °C for 10 minutes.

2.4 Characterization

CaCO₃ samples were analyzed in a X ray Bruker Advance D8 (40kV y 40 mA) diffractometer with Cu- α radiation (0.15406 nm). The Fourier transform infrared spectroscopy (FT-IR) was carry out in Spectrum 100 Perkin Elmer, the samples were analyzed in KBr pills. The particles were observed using a field emission gun transmission electron microscope (JEM 2200FS, JEOL Ltd).

Thermo-mechanical properties were investigated in a Dynamic Mechanic Analyzer (DMA 2980, TA Instruments) with a cooling rate of 3 °C/min, whit a 1 Hz frequency, from -50 to 170 °C. The crystallization behavior and melting characteristics of the composites were studied by differential scanning calorimetry (DSC) using a Spectrum 100 Perkin Elmer with a cooling rate of 10 °C/min. In the first heating and cooling scans the samples were heated from 10 to 250 °C, and then cooling from 250 to 10 °C, in order to eliminated the thermal history. The analysis was carry out from -30 to 180 °C.

3. Results

3.1 Crystalline structure and composition of CaCO₃

The results of DRX analysis shows that the crystalline structure of CaCO₃ from eggshell is of calcite kind, whose characteristic diffraction peak appear at $2\theta = 29.4$, it also shows a diminish in the intensity of these peak, suggesting a particle size reduction.

The FT-IR spectra shows no differences in both samples, meaning that the ultrasonic irradiation does not affect the particle composition, the transmission band at 3312 cm⁻¹ can be attributed to OH stretching vibration from residual water. Both spectra shows a weak band at 1801 cm⁻¹ corresponding a carbon-oxygen characteristic carbonates bond (C-O), the well-defined bands at 1473 and 715 cm⁻¹ are characteristic of C-O stretching and bending, respectively. The strong band at 878 cm⁻¹ match with a OCO out of plane of vibration mode. The band at 2516 cm⁻¹ is associated to HCO₃.

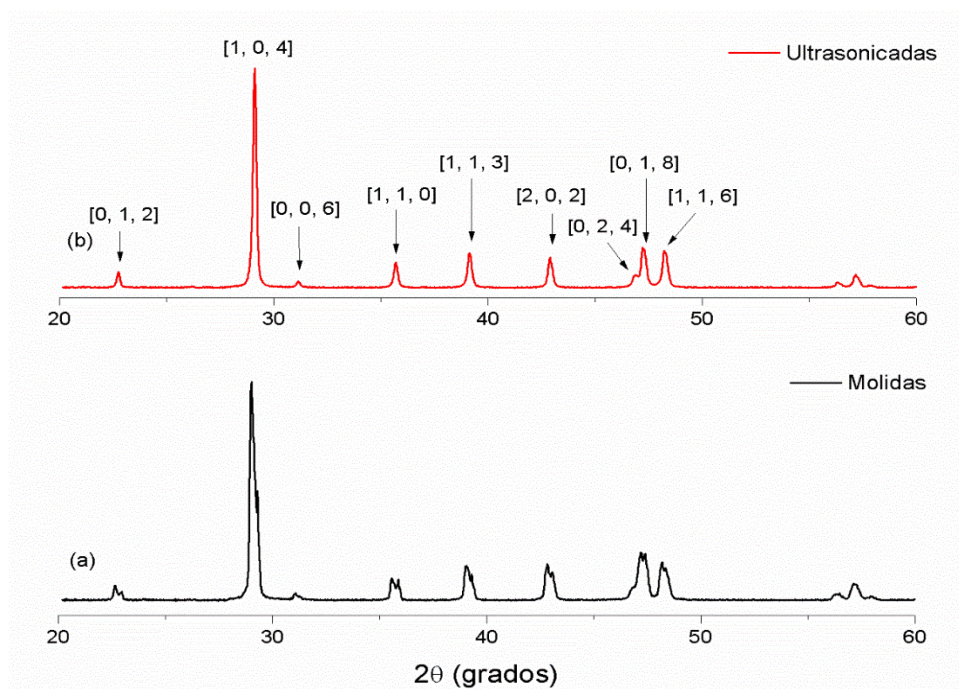


Figure 1. XRD patterns of eggshell a) milling in blender, b) size reduction by ultrasound. Both patterns are associated to the crystallography card JCPDS No. 47-1743.

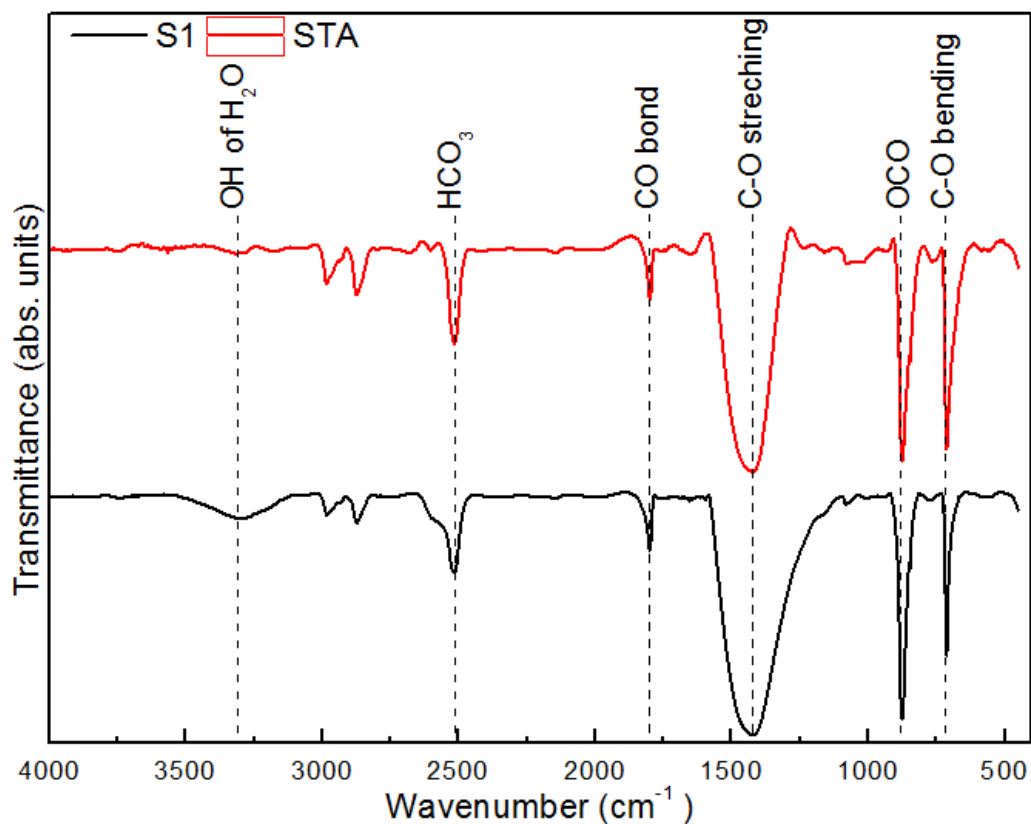


Figure 2. FT-IR spectra of eggshell: S1-sample after sonication, STA-mill sample

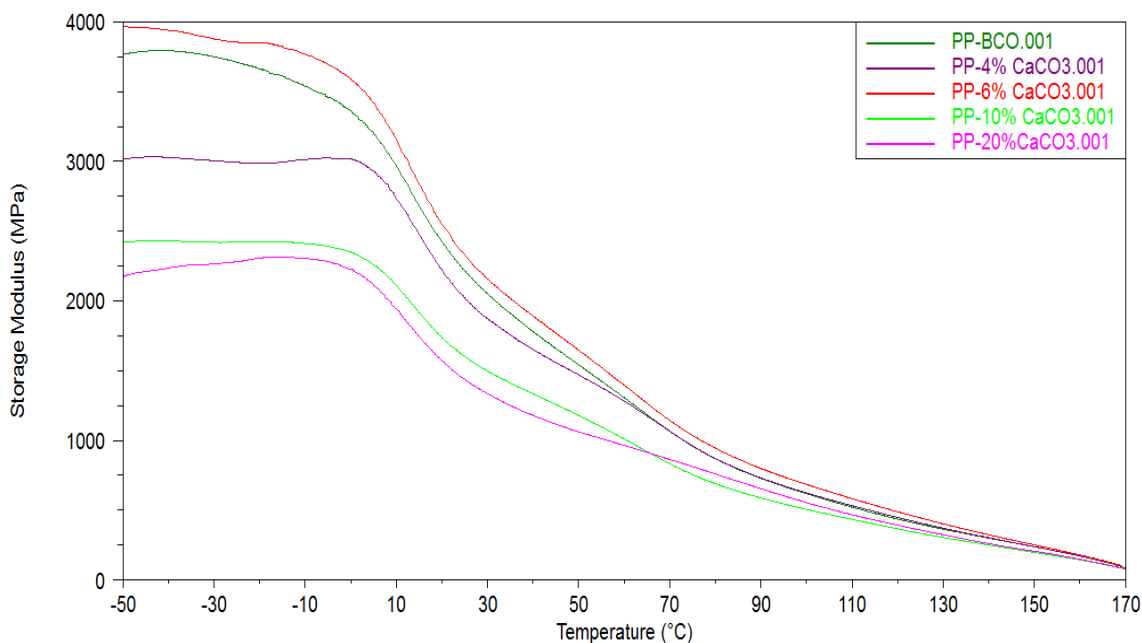


Figure 3. Storage moduli of PP and composites

3.2 Composites thermal behavior

Fig. 3 shows the storage modulus of PP and composites, the composite filled with 6% of CaCO₃ has the highest storage moduli, this means that this content of filler (6%) is immobilizing the PP chain and

increasing the stiffness, by the other hand, the decreasing in the storage moduli in the other three composites could indicated an increased in the elasticity and an enhanced on tensile properties. Despite the increased on the storage moduli in 6% composite, T_g remain under the T_g value for PP (Table 1), and all composites show this behavior. The damping factor for 4, 6 and 10% composites are the lowest comparing whit PP and 20% composite, according to Maries and col.[13] the lowest the damping factor the better the interfacial interaction, then, this composites could have higher values on mechanical properties.

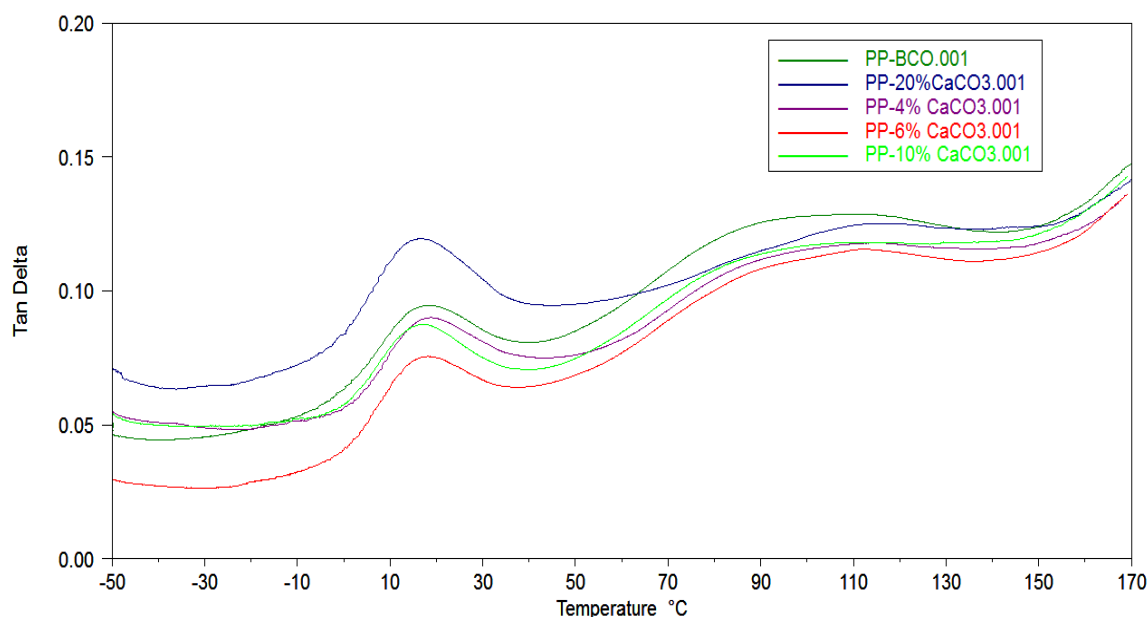


Figure 4. Tan Delta of PP and Composites

Table 1. Melt temperature (T_m), Glass transition temperature (T_g) and Heat of fusion (ΔQ) for PP and composites, from DSC analysis.

Muestra	T_g (°C)	T_m (°C)	ΔQ (J/g)
BCO	19.1	160.80	61.78
CaCO ₃ -PP 4%	18.8	164.90	52.56
CaCO ₃ -PP 6%	18.2	160.56	55.59
CaCO ₃ -PP 10%	17.3	163.06	55.38
CaCO ₃ -PP 20%	16.8	161.40	52.07

DSC results provide information about the crystallinity of composites, changes on enthalpies or heat of fusion (ΔQ) can provide useful indicators on crystallinity changes, an increased in enthalpy leads an increased in crystallinity, and so does melt temperature (T_m), a higher T_m higher crystallinity, this is due to contribution of movement impediment that fillers does to the polymer chains. Table 1 shows no significant variations in T_m , therefore the crystallinity in PP does not change because of the CaCO₃ presence. However the heats of fusion decreased 9 degrees for 4 and 20 % composites and 6 degrees for 6 and 10 % composites. Further analysis must be done in order to know if mechanical properties can be affected by the eggshell milled in blender.

4. Conclusions

It seems that the composite filled whit 6% of CaCO₃ from eggshell could have the best mechanical behavior, since this material showed the lowest value in damping factor and the highest storage moduli.

References

1. Gedanken, A., *Using sonochemistry for the fabrication of nanomaterials*. Ultrasonics Sonochemistry, 2004. **11**(2): p. 47-55.
2. Ju-Nam, Y. and J.R. Lead, *Manufactured nanoparticles: An overview of their chemistry, interactions and potential environmental implications*. Science of The Total Environment, 2008. **400**(1-3): p. 396-414.
3. Suslick, K.S. *Sonoluminescence and sonochemistry*. in *Ultrasonics Symposium, 1997. Proceedings., 1997 IEEE*. 1997.
4. Foley, J.L., S. Vaezy, and L.A. Crum, *Applications of high-intensity focused ultrasound in medicine: Spotlight on neurological applications*. Applied Acoustics, 2007. **68**(3): p. 245-259.
5. Zhao, Y., et al., *Sonochemistry in China between 1997 and 2002*. Ultrasonics Sonochemistry, 2005. **12**(3): p. 173-181.
6. Ashokkumar, M., *The characterization of acoustic cavitation bubbles – An overview*. Ultrasonics Sonochemistry, 2011. **18**(4): p. 864-872.
7. Kang, D.J., et al., *Effect of eggshell and silk fibroin on styrene-ethylene/butylene-styrene as bio-filler*. Materials & Design, 2010. **31**(4): p. 2216-2219.
8. Chen, X., et al., *Hydrophilic CaCO₃ nanoparticles designed for poly (ethylene terephthalate)*. Powder Technology, 2010. **204**(1): p. 21-26.
9. Gao, X., et al., *Synthesis and characterization of well-dispersed polyurethane/CaCO₃ nanocomposites*. Colloids and Surfaces A: Physicochemical and Engineering Aspects, 2010. **371**(1-3): p. 1-7.
10. Xiong, Y., G. Chen, and S. Guo, *The preparation of core-shell CaCO₃ particles and its effect on mechanical property of PVC composites*. Journal of Applied Polymer Science, 2006. **102**(2): p. 1084-1091.
11. Hussein, A.A., R.D. Salim, and A.A. Sultan, *Water absorption and mechanical properties of high density polyethylene/egg shell composite*.
12. Hassan, T.A., et al., *Sonochemical effect on size reduction of CaCO₃ nanoparticles derived from waste eggshells*. Ultrasonics Sonochemistry. **20**(5): p. 1308-1315.
13. Idicula, M., et al., *Dynamic mechanical analysis of randomly oriented intimately mixed short banana/sisal hybrid fibre reinforced polyester composites*. Composites Science and Technology, 2005. **65**(7-8): p. 1077-1087.

PREPARATION AND CHARACTERIZATION OF MODIFIED ASPHALT BLENDS USING SEBS/NANOCLAY

S. Zapién-Castillo¹, M.Y. Chávez-Cinco¹, J.L. Rivera-Armenta¹, M. Mendoza-Martínez¹, B.A. Salazar-Cruz¹

¹ *División de Estudios de Posgrado e Investigación del Instituto Tecnológico de Ciudad Madero, J. Rosas y J. Urueta s/n Col. Los Mangos. Cd. Madero, Tamaulipas, C. P. 89440, México.*

Abstract

SEBS (styrene-ethylene-butylene-styrene) block copolymer and montmorillonite nanoclay composites were prepared through a melt mixing technique at different SEBS/nanoclay mass ratios for asphalt modification. Asphalt binder blends with 3%, 4% and 6% of SEBS/nanoclay modifier were obtained by means of a high shear mixer. There were performed conventional physical tests to the final mixes and it was also evaluated their rheological behavior as well as their thermal storage stability. The modifier effect on the asphalt binder was shown as an enhancement on these properties, which can be related to a better field performance of the asphalt.

Introduction

Almost the worldwide production of asphalt is destined for road pavement construction. Concrete asphalt is basically composed by two constituents: an asphalt binder and an aggregate of mineral particles. The function of the asphalt is to bend the mineral aggregate while protecting it from water and other harmful agents, thus the properties and nature of this binder are closely related to the pavement performance. Initially pure conventional asphalt was good enough for this purpose, but more recently as the traffic load increased and the environmental factors worsened, road pavements prepared just with pure asphalt became useless more rapidly than before. Consequently there were conducted some studies with the aim of finding elements to modify the asphalt behavior in order to promote its durability, to improve its performance in a wider interval of weather conditions and to give it better mechanical resistance^[1]. Polymers were extensively used as modifiers because they are capable of transferring their properties to the asphalt, for example it was observed a greater rutting, fatigue and cracking resistance on the polymer-modified binders, as well as an important reduction of its thermal susceptibility. Although this kind of polymer-modification of asphalts was considered as a great innovation on road pavement technology, it also revealed an important restriction: compatibility between the asphalt and its polymeric modifier must be entirely guaranteed in order to minimize the risk of phase separation during its period of high temperature storage. Recent researches on this area has shown that mineral clays of nanometric scale can be used as fillers to improve both mechanical and physical properties of polymers; furthermore when they are used as part of the modification agents of an asphalt binder, the modified asphalt mixture seemed to improve significantly its high temperature storage stability^[2].

SBS elastomer (styrene-butadiene-styrene) has been the most broadly used polymer for asphalt modification because of its nature and properties. SBS is part of a family of polymers referred as thermoplastic elastomers (TPE), which combine both the elastic behavior of rubbers and the processability characteristics of common thermoplastics. TPE's such as SBS are generally used as asphalt modifiers because of its rigid domains of styrene and its soft matrix of butadiene that simultaneously impart mechanical resistance and elastic behavior to the asphalt which are important for avoiding permanent deformations on pavement roads. Unfortunately, the typical double bond of unsaturated compounds such as butadiene is a very reactive site. Double bonds usually promote degradation reactions when exposed to oxidant agents or UV rays^[3], therefore, asphalts modified with SBS are prone to suffer the effects of aging and degradation processes because they are mandatorily subjected to those and other environmental conditions when used in roads construction. Hence, in this work it is proposed the saturated SEBS copolymer (styrene-ethylene-butylene-styrene) instead of SBS to

be used as asphalt modifier combined with commercial montmorillonite nanoclay. Both SEBS and montmorillonite nanoclay have proved to be efficient asphalt modifiers, either separately or combined with other elements. For example there are studies in which the effects of SEBS modification on the conventional properties and rheological characteristics of pure bitumen were investigated. In those studies it was concluded that polymer modification improves some properties of the base bitumen such as penetration, softening point and temperature susceptibility ^[4]. On the other hand, it has also been investigated the effect of organically modified montmorillonite in asphalt binders modified by SBS and it was observed that the modified binders showed an enhancement of rheological parameters and physical properties as well^[2]. However, there is no record of any study in which SEBS and montmorillonite were both combined together in the same modification process, so this is one of the major contributions of this work.

In this study there were prepared composites formed by SEBS and montmorillonite clay at two mass ratios: 100/10 and 100/30 (SEBS to clay), which were used to modify asphalt by mixing it with 3%, 4% and 6% mass content of the composites. Some tests were performed to describe the physical and rheological properties of the modified asphalt blends, and then they were compared to the original bitumen and the asphalt modified just by SEBS.

Experimental

Materials

Asphalt binder graded as AC-20 was supplied by PEMEX, Refinería Madero. It was also used SEBS copolymer provided by Dynasol Elastomers; this thermoplastic elastomer, which has a linear structure and a total styrene content of 33%. Organically modified montmorillonite nanoclay named Cloisite 15A (C15A) was obtained from Southern Clay Products, Inc.

Ten different samples were obtained and evaluated in this study: pure asphalt (BCO), asphalt modified by 3% of SEBS (300), asphalt modified by 3% of 100/10 composite (310), and asphalt modified by 3% of 100/30 composite (330). The same formulations were made for 4% and 6% modified asphalts: 4% of SEBS (400), 4% of 100/10 nanocomposite (410), 4% of 100/30 composite (430), 6% of SEBS (600), 6% of 100/10 composite (610), and 6% of 100/30 composite (630-n).

Preparation of SEBS/C15A composites

SEBS/C15A composites (100/10 and 100/30 SEBS to C15A ratios) were produced by means of a Brabender mixing machine (Intelli-Torque Plasti-Corder) operated at 190°C/235°C and 150 rpm during 30 minutes.

Preparation of modified asphalt bends

All modified asphalts were prepared using a high shear mixer IKA-WERKE, RW16 basic model. Asphalt was heated and then it was poured into a 500 mL iron can that was placed into a heating system where it was preheated during 1 hr. The melting process was performed at 180°C, and it was used a shearing speed of 1200 rpm for a period of 30 minutes to accomplish the complete distribution of the modifier into the asphalt.

Methods

X-ray diffraction

The potential nanoclay exfoliation in the rubber matrix was estimated from the intensity of the d_{001} peak in the X-ray diffraction analysis (XRD). The XRD patterns were obtained using an Xpert MPD Philips X-ray diffractometer with a copper radiation source of 1.54 Å. The angular region 2θ of 5°-110° was explored at a sweep speed of 0.05°/s and an angular resolution of 0.05°.

Rotational viscosity

Viscosity is a measure of the internal friction of a fluid that causes it some resistance to flow freely. Rotational viscosity, also known as Brookfield viscosity (from the viscosimeter's brand), determines the

torque level needed for maintaining a particular rotation speed of a spindle which is submerged into the fluid. The viscosity test was performed by means of a Brookfield viscosimeter model DV II +Pro, under the ASTM D4402 at 135°C.

Softening point

The softening point test (often known as ring and ball test) aims to determine the temperature at which a material changes from a solid or very viscous state, to a softer or more fluid one. According to ASTM D36 the method is based on the determination of the temperature needed for a steel ball to produce a deformation, under standard conditions on the asphalt sample due to the ball mass as well as the temperature of the system.

Storage stability test

The storage stability test finds out whether the elements of the modified asphalt blend are properly compatible or not and gives a reasonable idea of the modification efficiency. The test requires the asphalt to be poured into an aluminum tube that is then exposed to extreme temperature conditions (heating in an oven at 163°C for 48 hrs. immediately followed by cooling in a freezer at $-7 \pm 6^\circ\text{C}$ for at least 4 hrs.)^[2]. After these operations, pieces of sample have to be taken from the top and bottom sections of the tube to be subjected to the softening point test; the closer the values of the softening temperatures, the better the storage stability of the asphalt binder.

Rheology

From the relationship between the applied stress and the obtained deformation of the material, it can be determined the complex modulus (G^*) that shows the viscoelastic properties of the material and gives a global idea of how resistant it is. It was also estimated the parameter $G^*/\sin(\delta)$ that was used to calculate a particular temperature value stipulated by the Strategic Highway Research Program (SHRP), often named as T_{SHRP} , which is closely related to rutting resistance of asphalts. The test was conducted by means of an Anton Paar Dynamic Shear Rheometer (DSR), Model MSR300, using a parallel plate geometry of 25 mm in diameter and setting a 1 mm gap. The technique was performed under the oscillating mode fixing a deformation value of 10% at which the linear viscoelastic range was encountered. The analysis comprised a frequency sweep test varying between 0.01 rad/s and 250 rad/s within a temperature interval ranging from 52°C to 100°C for asphalt modified by just SEBS and from 52°C to 118°C for asphalt modified by SEBS/C15A composites.

Results and Discussion

X-ray diffraction

The preparation process of the composites was performed using two different temperatures (190°C and 235°C); the rest of the variables involved in the mixing process were fixed as constants. From those two temperatures it was selected as definitive the lower one, not only because of an energy saving issue, but also because of the X-ray diffraction results. Montmorillonite clay has characteristic peaks appearing approximately at 7° and 25° which can be seen on X-ray diffractograms available in scientific literature^[2]. The diffraction pattern shown in Figure 1 corresponds to the crystallographic structure of C15A contained in the studied composites. It can be observed that the peak corresponding to the composite prepared at 235°C is more intense than that of the one obtained at 190°C. This indicates that the crystallographic pattern of the 190°C sample has almost completely collapsed, while the structure of the 235°C composite is less affected. Consequently, the nanoclay in the 190°C composite has been partially exfoliated, leading to the formation of a nanocomposite which is highly desirable because of the special properties that can be conferred to the asphalt when it is modified by a nanomaterial.

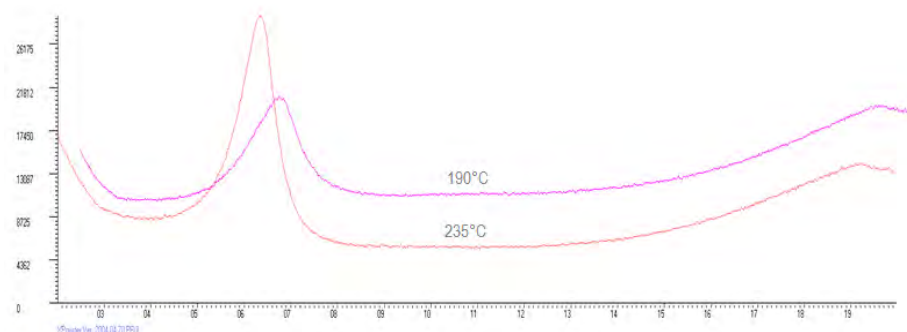


Figure 1. X RayDiffractograms for 100/10 nanocomposite prepared at 190°C and 235°C

Rotational Viscosity

Asphalt mixes showed an increment in viscosity as a result of modification. It is expected that clay incorporation induce a slightly decrease of the sample's viscosity regarding the modification done just by SEBS^[4] but in this study the nanocomposites cause the major increase of the material viscosity as shown in Figure 2. This is not a rare event, because some researchers^[2,3,4,5,6] have encountered that their best preparations of modified asphalt have greater viscosity than asphalt modified just by SEBS in the same proportion. When 4% and 6% of modifier are used, the higher viscosity is reached when the nanocomposite proportion is 100/10 SEBS to C15A. The magnitude of this growth is even higher than the one gotten by the modification with 100/30 nanocomposite; this shows that nanoclay content must be kept low in order to achieve good final characteristics. The results also reveal that it is not convenient to use the higher percentage of nanocomposite (except for 6% X00-n) because using 3% and 4% of nanocomposite implies approximately the same level of viscosity enhancement. The dramatic improvement on viscosity of nanomcomposite-modified asphalts is an evidence of the very special features offered by nanocomposites when used as additives and modifiers.

Softening point

The softening point raised in all modification processes; an increase in the softening point is favorable since asphalt binders with higher values may be less susceptible to permanent deformation^[5]. The softening point behave quite similar to viscosity; actually these two properties are closely related because it is reasonable to find out that asphalts with high softening point are also more viscous than those having low softening point. As it can be seen in Figure 3, the difference between the blends prepared just with SEBS and those with nanocomposites was more significant at low content (3% and 4%) than at high content (6%), which contributes to confirm that it may be more convenient to perform modification of asphalt by adding just few amounts of nanocomposite.

High temperature storage stability

As it is illustrated in Table 1, the softening point of the top and bottom sections of the phase separation tube was determined and compared. The maximum difference in softening point is clearly correspondent to those asphalt binders modified by just polymer; as many researching groups have concluded, incorporating nanoclay into the mixture causes narrowing of the difference between the characteristics of the tube's top and bottom regions^[2,5]. Once again, the test proves to be more efficient for samples prepared with low nanocomposite content, but even at 6% of modifier, the difference value enters within the storage-stable blends range.

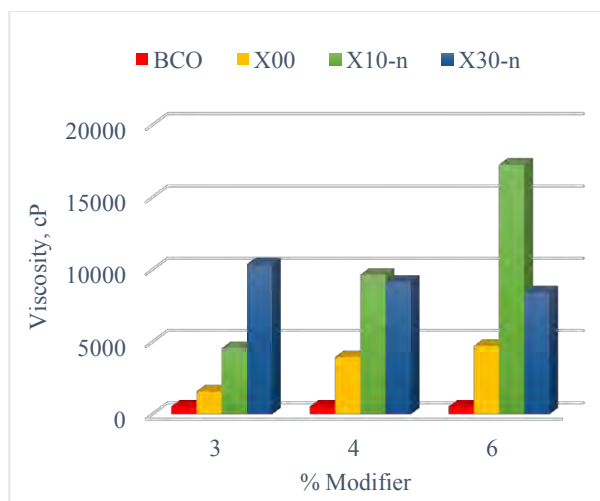


Figure 2. Effect of SEBS/C15A nanocomposite content on the viscosity of modified asphalt blends measured at 135°C.

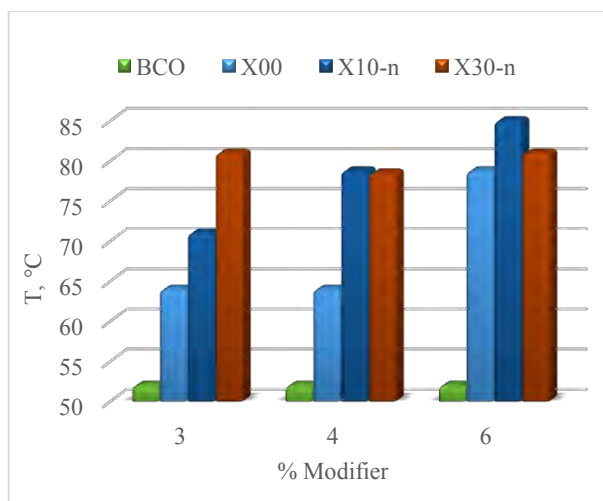


Figure 3. Effect of SEBS/C15A nanocomposite content on the softening temperature of modified asphalt blends.

Table 1. Effect of SEBS/C15A nanocomposite content on high temperature storage stability of modified asphalt

Modifier content (%)	Sample	Softening point (°C)		Difference (°C)
		Top	Bottom	
3	300	101.5	68.5	33
	310-n	71	70	1
	330-n	83	82	1
	400	114	68.75	45.25
4	410-n	78	77	1
	430-n	76	76.5	-0.5
	600	79	61	18
6	610-n	88	85	3
	630-n	78	76.5	1.5

Rheology

The relationship between frequency and complex modulus for the asphalt mixtures is shown in Figure 4, which presents the G^* master curves for 3%, 4% and 6% of modifier content, respectively. It was observed higher values of G^* for all the modified asphalts in comparison with the original asphalt binder. The modification seems to be more significant at low nanocomposite content, provided that for 4% and 6% the values of G^* are similar among the samples containing nanocomposite as modifier and those modified just by SEBS, although it is clear that in all cases, the best values of G^* correspond to nanocomposite-modified asphalts. As former researchers conclude^[2], the effect of G^* rising in this work is also more noticeable at low frequencies, which are equivalent to high temperatures. This behavior is desirable because G^* provides a measure of the total resistance to deformation when the asphalt binder is subjected to shear loading and reflects its total stiffness. Consequently, the nanocomposite-modified asphalts seem to be more resistant to rutting. It is also important to point that at 4% and 6% of modifier, varying SEBS/C15A ratio from 100/10 to 100/30 is not really causing substantial changes on G^* , which confirms what other researchers state about keeping the nanoclay content low in order to generate huge changes on the nanomaterial final properties.

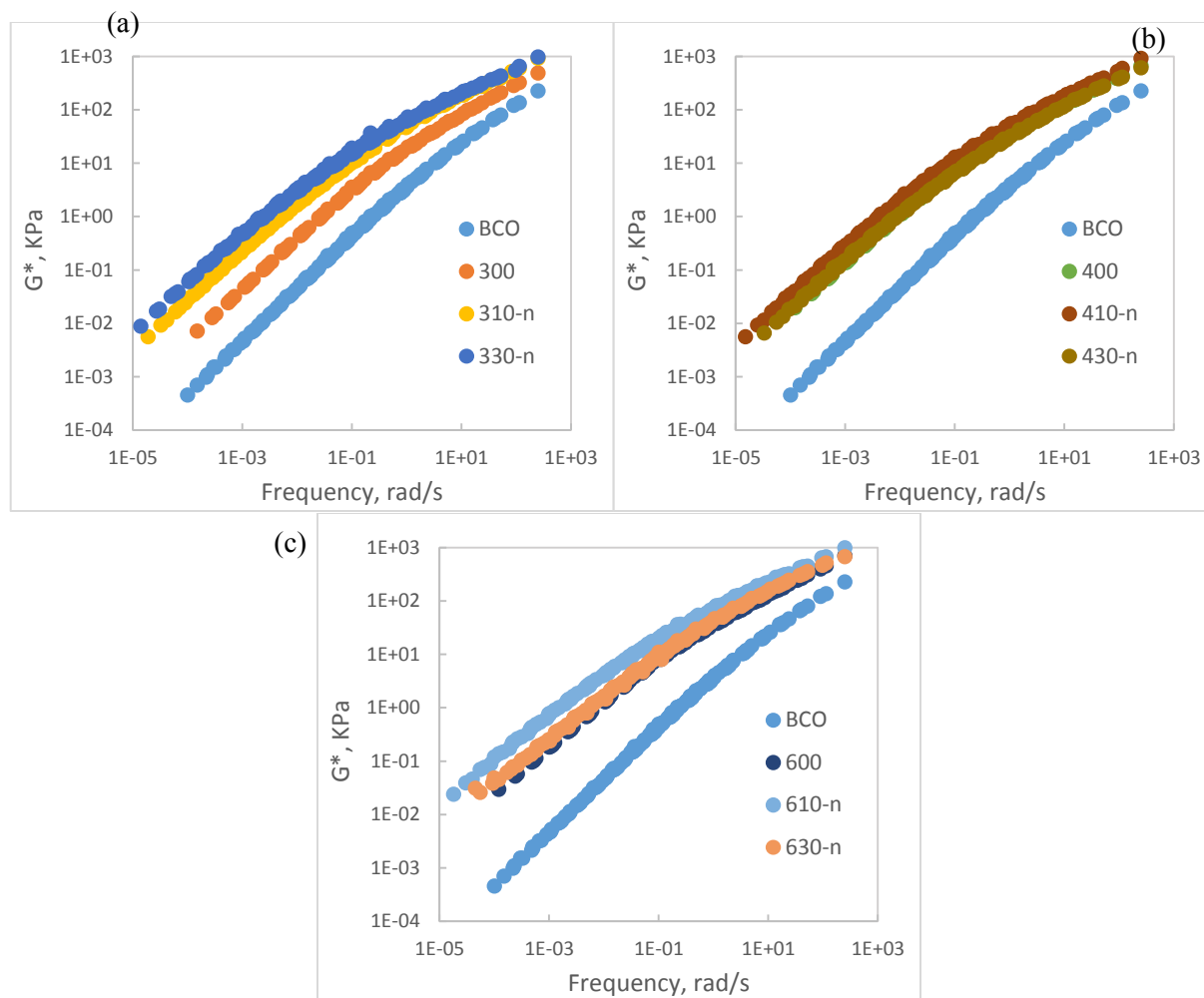


Figure 4. Master curves of complex modulus G^* for pure and modified asphalts at 3% (a), 4% (b) and 6% (c) of modifier content, as function of frequency at a reference temperature of 52°C.

In Table 2 there are presented the values of T_{SHRP} that was calculated by plotting the parameter $G^*/\sin(\delta)$ with respect to temperature, and then it was found out the temperature at which the parameter equals to 1 KPa. T_{SHRP} and softening point describe the binder resistance to permanent deformations at high temperature in the following way: the higher these temperatures, the better the asphalt high temperature properties. It can be appreciated in Table 2 that all modified asphalts have a greater value of T_{SHRP} than that of pure asphalt, but among the modified asphalts, those incorporating nanocomposites achieve better temperatures than those modified just by polymer. This suggests that interaction between nanoclay platelets is efficient enough to affect the thermal and mechanical properties of the asphalt.

Conclusions

Partially exfoliated SEBS/C15A nanocomposites were obtained by means of a melt mixing process; this dispersion pattern was confirmed via X-ray diffraction. The incorporation of nanocomposites as modifying elements of asphalts lead to an improvement of the physical and rheological properties of the original binder, when compared with pure asphalt and versus SEBS-modified asphalt. The viscosity and softening point of these modified binders increased; it indicates an enhancement of the stiffening effect

and the high temperature properties of the asphalt. Nanocomposite-modified asphalts proved to be more storage-stable than their corresponding samples modified just by polymer. In terms of rheological characteristics, the samples in which nanocomposites were present achieved the best values of complex modulus G^* , which means that asphalts modified in that way will be more rutting-resistant. The nanocomposite-modified asphalts also got the best T_{SHRP} values, consequently it was confirmed that this kind of modification enhances considerably the binder's resistance to permanent deformations at high temperatures. The overall results analysis guides to conclude that the effect of nanocomposite modification is more remarkable when little amounts of nanoclay are used as modifying agent, so the most convenient SEBS/C15A ratio is the one set as 100/10 since using 100/30 may not be so worthy in terms of the properties improvement magnitude. The results of this work are a clear evidence of the enormous changes that a material can undertake when it is subjected to a modification process including nanomaterials.

Table 2.. Effect of SEBS/C15A nanocomposite content on the high temperature properties of asphalt.

Modifier content (%)	Sample	T_{SHRP} , °C
0	BCO	80.3
	300	94.6
3	310-n	100.7
	330-n	113.9
	400	102.7
4	410-n	107.7
	430-n	107.9
	600	104.8
6	610-n	119.0
	630-n	113.2

Acknowledgements

Authors thanks to Dynasol Elastomers, Altamira, for providing SEBS and to Instituto Tecnológico de Ciudad Madero and CONACyT for financial support to carry out the present research.

References

- [1]. F. Changqing, Y. Ruien, L. Shaolong, L. Yan., J. Mater. Sci. Technol., 29(7), 589-594 (2013).
- [2]. T. Pamplona, B. Amoni, A. de Alencar, A. Lima, M. Nágila, J. Soares, S. Soares, Journal of the Brazilian Chemical Society, vol. 23, No. 4 (2012).
- [3]. C. Ouyang, S. Wang, Y. Zhang, Y. Zhang, European Polymer Journal 42 446-457 (2006).
- [4]. S. Djaffar, D. Samy, A. Khadidja, International Journal of Engineering Science and Technology, Vol. 5, No. 05, (2013).
- [5]. C. Ouyang, S. Wang, Y. Zhang, Y. Zhang, Polymer Degradation and Stability 87 (2005) 309-317.
- [6]. S. Jahromi, A. Khodaii, Construction and Building Materials 23, 2894-2904 (2009).

MORPHOLOGICAL AND ELECTRICAL PROPERTIES OF PE/CARBON NANOPARTICLES NANOCOMPOSITES FOR THERMAL APPLICATIONS

Janett A. Valdez-Garza,¹ Víctor J. Cruz-Delgado,¹ Juan G. Martínez-Colunga,² Carlos A. Ávila-Orta,¹

¹ *Departamento de Materiales Avanzados, Centro de Investigación en Química Aplicada, Blvd. Enrique Reyna Hermosillo No. 140, Col. San José de los Cerritos. Saltillo, Coahuila. 25294. México.*

² *Departamento de Procesos de Transformación, Centro de Investigación en Química Aplicada, Blvd. Enrique Reyna Hermosillo No. 140, Col. San José de los Cerritos. Saltillo, Coahuila. 25294. México.*

Abstract

Polymer nanocomposites of high density polyethylene (HDPE) and carbon nanotubes (CNT) or carbon black (CB) were prepared by melt extrusion. Carbon nanoparticles were added in contents of 1, 5, 10, 15 and 20 % w/w to the resin. A morphological and electrical study was conducted on polymer nanocomposites. Thermal transitions as a function of nanoparticle content were evaluated by DSC showing high nucleation activity for PE/CNT nanocomposites than PE/CB ones. WAXD analysis has shown a structural change for PE/CNT samples meanwhile for PE/CB this is not detected. Electrical conductivity of PE/CB is higher than PE/CNT nanocomposites for all contents of nanoparticles, values obtained are in the range of electrical conductors.

Introduction

The use of carbon nanoparticles as a reinforcement in polymer matrices has taken increased interest, mainly due to the amazing chemical, mechanical, electrical and thermal properties that these nanoparticles possess [1-3]. The possibility of electrical and thermal conduction in a polymer matrix with very low amounts of the nanoparticles, brings opportunity for high demanding applications such as electrical conductors and heat exchangers [4-6]. In this study, the effect of geometry and content of carbon nanoparticles on electrical conductivity, thermal transitions, morphology and dispersion was investigated. For this purpose, polymer nanocomposites of high density polyethylene (HDPE) and carbon nanotubes (CNT) or carbon black (CB) were prepared by melt extrusion.

Experimental

Materials

High density polyethylene (HDPE) with a MFI = 0.35 g/10 min, pipe grade was used as polymer matrix. Industrial grade CNT with an average O.D. = 40 nm, length 5 – 20 micron, purity \geq 90wt% and SSA \geq 300 m²/g were purchased to AlphaNano Technology Co., Ltd., China. Carbon Black, BP-2000 with an average particle size = 15 nm, SSA \geq 1500 m²/g, purity \geq 95% was acquired from Cabot, USA. Carbon nanoparticles were used without further purification.

Methodology

A twin screw extruder L/D: 40:1 Thermo Scientific 24-MC, was employed to process all the samples, with a plain temperature profile of 220 °C and 300 rpm. Firstly, a masterbatch of 20% wt/wt for each powder was prepared as follow: resin chips and powder, were feeded to the

extruder with the assistance of gravimetric feeders for each one at a rate of 5 and 1 kg/h respectively. Secondly, a proper amount of masterbatch was diluted with pure HDPE to obtain nanocomposites with 0, 1, 5, 10, 15 and 20% wt/wt of carbon nanoparticles.

Characterization

Thermal analysis were carry out in a DSC TA Instruments model Q2000 at a heating/cooling rate of 10 °C/min with a flow of N₂ of 50 ml/min. Four points electrical resistance measurements were recorded with a Keithley SourceMeter 2400, silver paint was used to cover both sides of the samples, 5 specimens were tested and the average value was reported. XRD patterns were collected in a Siemens D5000 X-ray diffractometer with a voltage of 20kV and current intensity of 25 mA were used, within the range of 5 - 40 ° of the 2θ angle. Electron microscopy experiments were done in a JEOL model JSM7401F with a voltage of 15kV, samples of nanocomposites were cryogenically fractured and coated with Au-Pd.

Results and Discussion

Thermal transitions for polymer nanocomposites with different contents of CNT or CB were evaluated by means of differential scanning calorimetry (DSC). The results obtained are presented in Table 1. The melting temperatures (T_m) for nanocomposites with CNT or CB (full symbols) exhibit a tendency to diminish, this behavior is more evident for higher contents of nanoparticles. The crystallization temperatures (T_c) for nanocomposites (empty symbols) with CNT shown a slight increase, which could be associated with the nucleation ability of these nanoparticles [3], meanwhile CB nanoparticles tends to diminish the crystallization temperature for nanocomposites, this behavior could be related with the amorphous nature of these nanoparticles (Figure 1a). On the other hand, the melting enthalpy (ΔH_m) for all nanocomposites decreases as the content of carbon nanoparticles increases, the above could be explained in terms of the hindrance of the crystalline phase development by the presence of nanoparticles.

Table 1. Thermal transitions for polymer nanocomposites with different contents of CNT or CB.

Sample	T _m , (°C)	T _c , (°C)	ΔH _m , (J/g)	Sample	T _m , (°C)	T _c , (°C)	ΔH _m , (J/g)
PE-CNT - 0%	131.85	116.51	229.28	PE-CB - 0%	131.85	116.51	229.28
PE-CNT - 1%	132.13	117.96	221.43	PE-CB - 1%	131.61	117.04	224.15
PE-CNT - 5%	130.04	119.03	222.65	PE-CB - 5%	130.96	116.12	209.77
PE-CNT - 10%	130.72	119.26	209.13	PE-CB - 10%	130.56	116.13	187.39
PE-CNT - 15%	130.91	118.73	190.73	PE-CB - 15%	129.06	116.33	175.29
PE-CNT - 20%	129.73	119.31	181.70	PE-CB - 20%	128.59	114.86	148.74

Electrical properties for polymer nanocomposites with different contents of CNT or CB are illustrated in Figure 1b. Electrical conductivity for nanocomposites with 1 and 5% wt/wt of both carbon nanoparticles are beyond of the limit of the apparatus (2 MOhm) and were no reported. With the addition of 10% wt/wt of CNT the electrical conductivity of the nanocomposites reach a value of 2.03×10^{-4} S/cm, which means 14 orders of magnitude higher than plain PE resin (1.00×10^{-18} S/cm). For nanocomposites with 15 and 20% wt/wt the values obtained are 6.00×10^{-3} and 1.82×10^{-1} S/cm respectively. Surprisingly, nanocomposites with CB nanoparticles shown higher values of electrical conductivity at the same weight content, the values are 6.29×10^{-3} and 3.03×10^{-1} and 1.56×10^0 S/cm for contents of 10, 15 and 20% respectively. The better

response in electrical conductivity for CB nanoparticles would be associated with the size reduction and dispersion of entangled nanoparticles, besides of the higher surface area compared to the one of CNT. The electrical conductivity values for nanocomposites are in the range of electrical conductors and suggest potential use in electronic/electric applications.

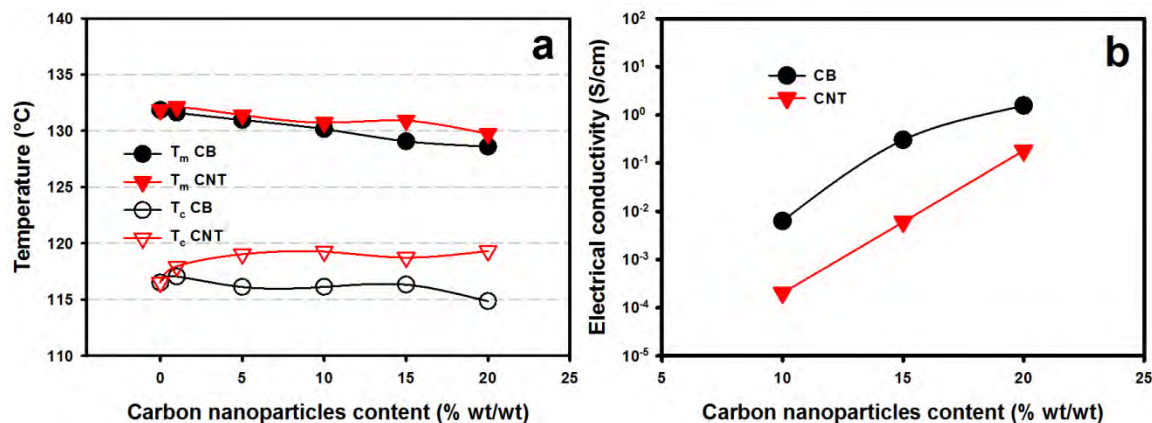


Figure 1. a) Thermal transitions and b) electrical properties for polymer nanocomposites with different contents of CNT or CB.

The crystalline structure of polymer nanocomposites with different contents of CNT or CB is shown in Figure 2. The addition of CNT does not modify the XRD pattern of polyethylene which exhibit a well defined crystal structure, only a slight decrease in intensity is observed for the planes located at 21.5 and 24° in the 2 θ as the content of CNT increase, meanwhile the plane located in 26° which is related to the presence of CNT, increase in intensity as the content increases too. For nanocomposites with CB only the two well defined planes for polyethylene are observed, and the corresponding plane associated with carbon particles is not observed, the above would be related with the amorphous nature of this kind of nanoparticle. A possible explanation is that planar structure of CB could be very well exfoliated and covered for a coating of polymer; this issue will be studied in deep in the future.

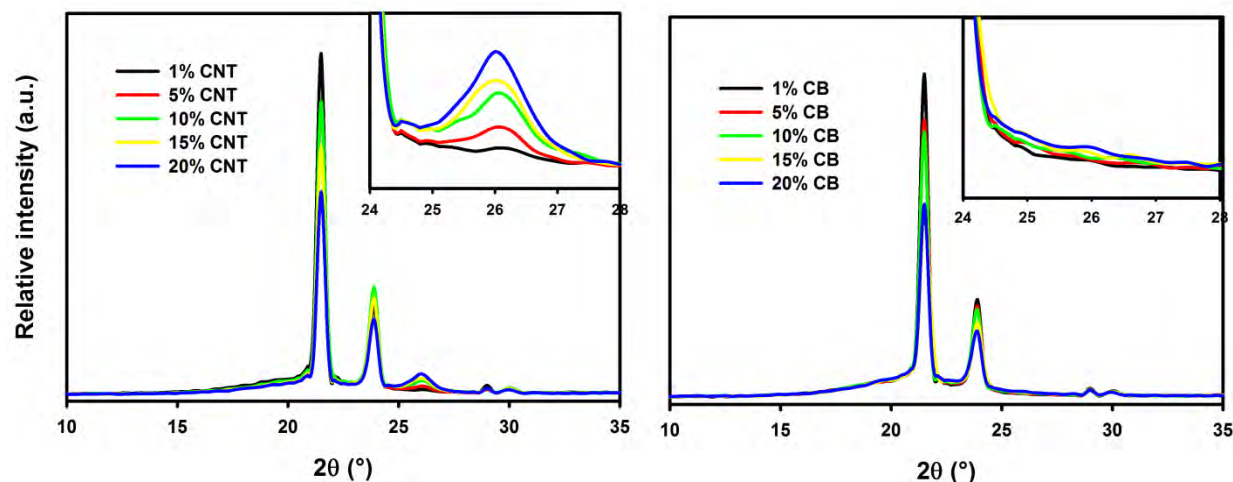


Figure 2. XRD patterns for polymer nanocomposites with different contents of CNT or CB.

Microscope images of cryofractured surfaces for polymer nanocomposites with 10% wt/wt of CNT and CB are shown in Figure 3. Polymer nanocomposites with CNT (left image) show a very well distribution of nanoparticles without agglomeration, besides it is possible to observe isolated carbon nanotubes embedded in the polymer matrix. For nanocomposites with CB (right image) is not evident the observation of aggregates or isolated carbon nanoparticles. It can be observed the formation of web like structure on the surface, which can be related with a higher level of compatibility and associated with the well dispersed and covered nanoparticles as discussed in the above section, besides this web like structure could be responsible for the higher electrical response observed for CB nanocomposites.

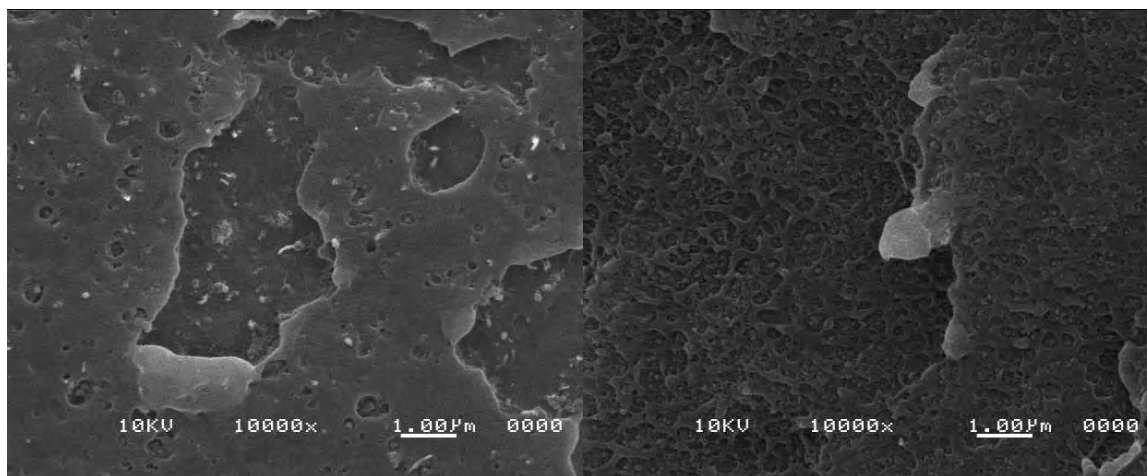


Figure 3. Microscope images of cryofractured surfaces for polymer nanocomposites with 10% wt/wt of CNT (left) and CB (right).

Conclusions

Electrical conductivity in polymer nanocomposites show a great increase with addition of both kind of nanoparticles, being more evident for CB than CNT; values of electrical conductivity are in the range of conductors. Thermal transitions of nanocomposites show a slight decrease in melting temperature, meanwhile crystallization temperature exhibits a slight increase with CNT and no apparent change with CB. Addition of CNT did not modify the crystalline structure of HDPE, only a small peak located around 26° in 2θ due the presence of CNT which increases as contents rises, for CB this peak is absent due the amorphous nature of this nanoparticle. Electron microscopy images have shown a high level of dispersion of nanoparticles even at high contents of 10% wt/wt. The aspect ratio of CB modifies the electrical behavior of nanocomposite in higher extent than CNT. Due the planar geometry of this nanoparticle the mechanical properties are increased up to 60% (not shown in this work) at a loading of 15%, besides the crystalline structure of nanocomposite did not shown an apparent change, this behavior suggest a better compatibility of CB with polymer matrix and the possible use in polymeric heat exchangers.

Acknowledgements

This work was supported by SENER through Centro Mexicano de Innovación en Energía Solar CeMIE-Sol P-12. Authors thank the assistance of Blanca Huerta, Myriam Lozano and Gilberto Hurtado with characterization of polymer nanocomposites.

References

- [1] Z. Spitalski, D. Tasis, K. Papagelis, C. Galiotis. Prog. Polym. Sci, 35 (3), 357-401 (2010).
- [2] T. Kuilla, S. Bhadra, D. Tao, N. Kim, S. Bose, J. Lee. Prog. Polym. Sci. 35 (11), 1350-75 (2010).
- [3] V. Cruz-Delgado, C. Ávila-Orta, A. Espinoza-Martínez, J. Mata-Padilla, S. Solís-Rosales, A. Jalbout, F. Medellín-Rodríguez, B. Hsiao. Polymer, 55 (2), 642-50 (2014).
- [4] Z. Han, A. Fina, Prog. Polym. Sci. 36 (7), 914-44 (2011).
- [5] L. Chen, Z. Li, Z. Guo. Exp. Therm. Fluid Sci. 33 (5), 922-28, (2009).
- [6] Y. Qin, B. Li, S. Wang. Ind. Eng. Chem. Res. 51 (2), 882-90 (2012).

EVALUATION OF PROPERTIES FOR NANOCOMPOSITES (PE/CARBON NANOPARTICLES) FOR HIGH TEMPERATURE APPLICATIONS

Mariela F. Rea Escobedo, Janett A. Valdez Garza, Víctor J. Cruz Delgado, Juan G. Martínez Colunga, Carlos A. Ávila Orta, Fabián Chávez Espinoza, María G. Méndez Padilla

*Centro de Investigación en Química Aplicada, Blvd. Enrique Reyna 140, C.P. 25294, Saltillo, México. *guillermo.martinez@ciqa.edu.mx*

Abstract

Polymer nanocomposites of high density polyethylene (HDPE) and multiple wall carbon nanotubes (MWCNTs) or carbon black (CB) were prepared by melt extrusion. Carbon nanoparticles were added in contents of 1, 5, 10, 15 and 20 % w/w with the resin. Thermal properties were evaluated by means of DSC, TGA and rheological properties by MFI and mechanical properties with a universal testing machine. Thermal transitions were enhanced and thermal decomposition temperature extended for nanocomposites with respect to non loaded HDPE. Viscosity and elastic moduli were also enhanced for nanocomposites.

Introduction

Carbon nanoparticles have excellent electrical, thermal properties, among them MWCNTs have excellent mechanical properties. These make them ideal and attractive reinforcing element to manufacture the next generation materials. They also motivated the researchers to use CNTs in composite materials for several applications. Outstanding properties of MWCNTs have led to their increasing use as fillers for a large variety of polymers [1]. This carbon nanoparticles tend to aggregate into bundles and hence they are difficult to be dispersed homogeneously in polymer matrices, due the polymer-MWCNTs interfacial adhesion is weak, preventing an efficient load transfer from the polymer matrix to MWCNTs. As a result of poor dispersion and inefficient load transfer, the mechanical properties of polymer-MWCNTs composites are often not as good as expected [2]. Moreover, other carbonaceous material is Carbon black (CB), a form of nearly pure, elemental carbon. It differs in molecular structure from the more common forms of elemental carbon, graphite and diamond, and therefore also differs in physical properties. Carbon black is softer than either graphite or diamond and is intensely black in color. Carbon black has many applications in plastics. It is used as a pigment, thermal an electrical conductive filler material, particulate reinforcement, and ultraviolet light (UV) absorber. In this paper, we investigate the effect of carbon nanoparticles (MWCNTs and CB) on properties of the HDPE/ carbon nanoparticles composites using different content of nano-fillers.

Experimental

Materials. High density polyethylene (HDPE) with a MFI = 0.35 g/10 min, pipe grade, was used as polymer matrix. Industrial grade Multiple Wall Carbon Nanotubes (MWCNTs) with an average O.D. = 40 nm, length 5 – 20 micron, purity $\geq 90\text{wt}\%$ and SSA $\geq 300 \text{ m}^2/\text{g}$ were purchased from AlphaNano Technology Co., Ltd., China. Carbon Black (CB), BP-2000 with an average particle size = 15 nm, SSA $\geq 1500 \text{ m}^2/\text{g}$, purity $\geq 95\%$ were acquired from Cabot, USA. Carbon nanoparticles were used without further purification

Methodology. A twin screw extruder L/D: 40:1 Thermo Scientific 40-MC, was employed to process all the samples, with a plain temperature profile of 220 °C and 300 rpm. First, a masterbatch of 20% w/w of each powder was prepared as follows: resin chips and powder were feed to the extruder by separate with the assistance of gravimetric feeders at a rate of 5 and 1 kg/h respectively. A proper amount of masterbatch were diluted with pure HDPE to obtain nanocomposites with 0, 1, 5, 10, 15 and 20% w/w of carbon nanoparticles (CN).

Table 1. Reaction conditions of butadiene polymerizations

Samples	HDPE content (%)	MWCNTs or CB content (%)
1	99	1.0
2	95	5.0
3	90	10.0
4	85	15.0
5	80	20.0

Results

The mechanical properties of nanocomposites are shown in Figure 1. The elastic modulus of the nanocomposite prepared with CB increases more than nanocomposites prepared with MWCNTs (Figure 1a), which is considered as a representative increment due to the better dispersion. In elongation at break behavior (Figure 1b), nanocomposites with MWCNTs showed an increase, comparing with materials containing CB, as corroborated with the elastic modulus behavior. The tensile strength for nanocomposites with MWCNTs and CB decreases due to high nanoparticle content and low interfacial adhesion between nanoparticle and polymer (Figure 1c). Table 2. Results of butadiene polymerizations.

Thermal properties of HDPE/CN composites obtained by DSC are shown in Figure 2. T_m decreases with the CN content (Figure 2a) and T_c increases for the HDPE/MWCNTs nanocomposites but T_c decreases for the HDPE/CB composites (Figure 2b). The crystallinity temperature increases for nanocomposites with MWCNTs and decreases for nanocomposites with CB (Figure 2c). This behavior can be attributed to the MWCNTs surface, which is more homogeneous and more adequate for deposition of polymer chains, enhancing crystallinity and can act as a nucleated agent.

Temperature of weight loss of nanocomposites obtained by TGA are shown in Figure 3. It is clear to observe that such temperature increases with level of carbon nanoparticles content, indicating an effect of thermal stability. The nanocomposites that presented better thermal stability are those with CB (Figure 3b). This behavior can be attributed to major dispersion particles in the polymer matrix.

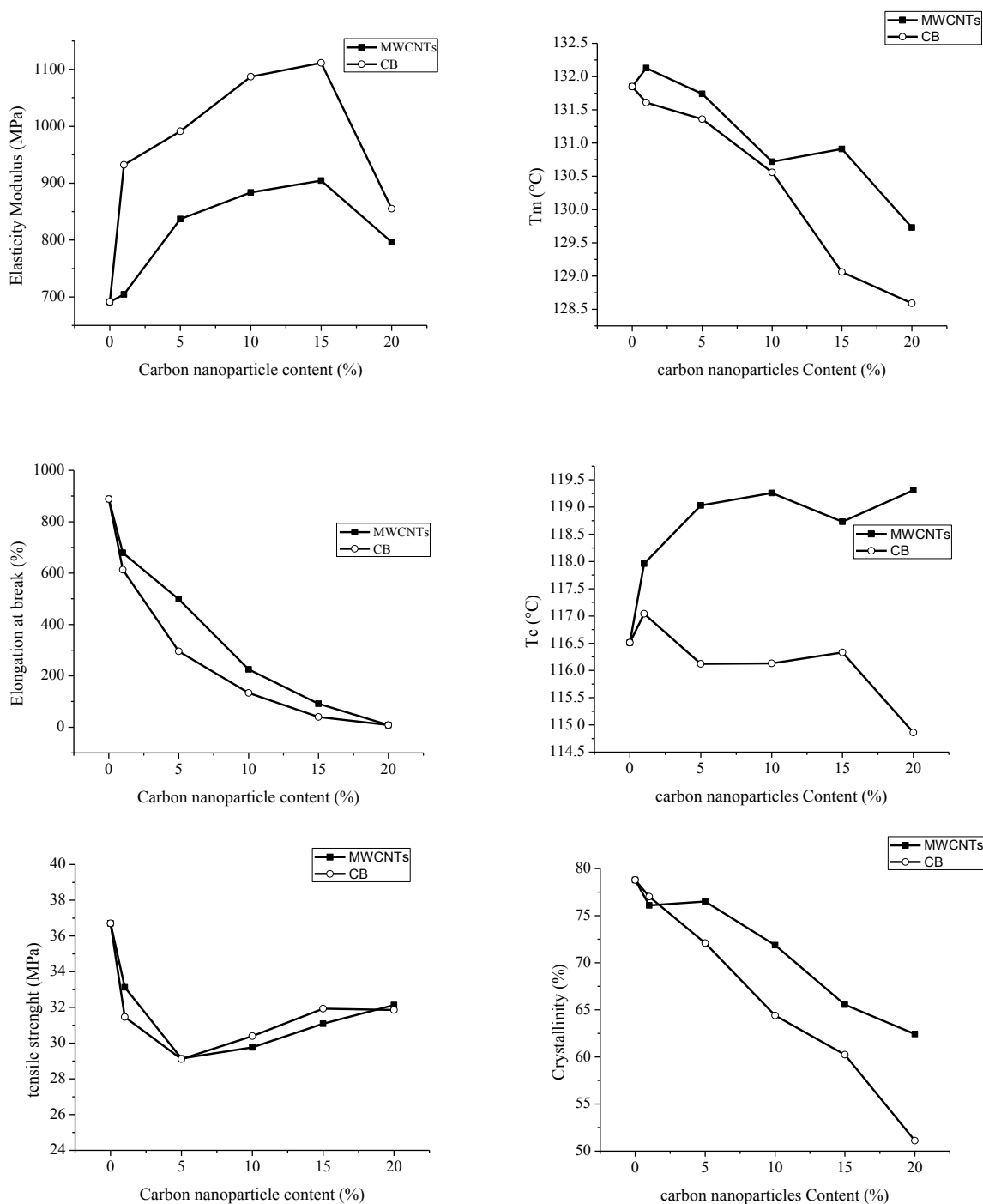


Figure 1. Mechanical properties of HDPE/CN nanocomposites. a) Elastic modulus; b) elongation at break; c) tensile strength.

Figure 2. Thermal properties of HDPE/CN nanocomposites. a) T_m; b) T_c; c) crystallinity.

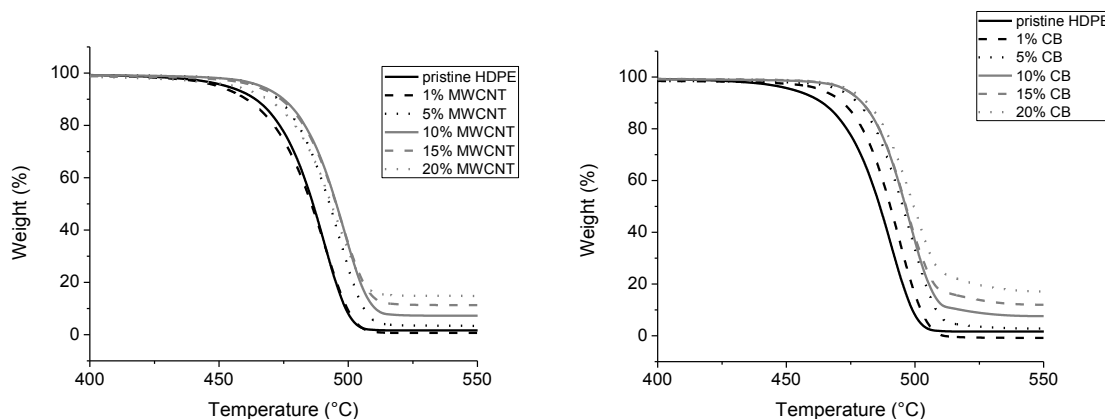


Figure 3. Temperature of Weight loss by TGA.

SEM images show the effect in the structure for the nanocomposites. The MWCNTs-10% have an heterogeneous morphology (figure 4a) while the nanocomposites with CB have homogenous morphology (figure 4b).

(a)

(b)

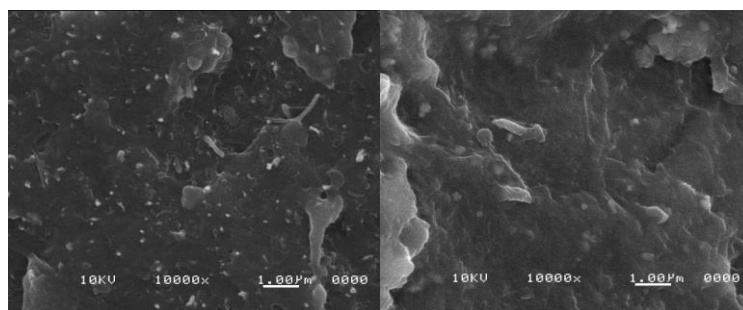


Figure 4. SEM images of nanocomposites: Nanocomposites with MWCNTs-10% (a) and nanocomposites with CB-10% (b).

Conclusions

Carbon nanometric structures enhance rigidity of HDPE. MWCNTs can behave as nucleating agent for HDPE. HDPE crystallinity is reduced by carbon black, even more than MWCNTs. HDPE thermal stability is enhanced significantly by carbon structures. Carbon black has a higher dispersion in HDPE, compared with MWCNTs.

Acknowledgements

The authors thank to CONACYT for the financial support through the project 156366. We also thank to Ricardo Mendoza, Jesús Cepeda, Guadalupe Méndez, Uriel Peña and Francisco Zendejo for their technical

support.

References

- [1] Valentino O., Sarno M., Rainone N. G., Nobile M. R., Ciambelli P., Neitzert H. C., Simon G. P., *Physica E: Low-dimensional Systems and Nanostructures*, Vol 40, (7) (2008), 2440–2445.
- [2] Chao-Xuan Liu and Jin-Woo Choi, *Nanomaterials* 2012, 2, 329-347.
- [3] Fan Y., Zhang X., Ye B., Zhou X., Weng H., Du J., Ham R., Jia Zh., *Chinese J. Polym. Sci.*, Vol 20, No. 3 (2002), 243-252.

THE ROLE OF POLYMER'S NATURE USED AS REDUCING AGENT IN THE SYNTHESIS OF METAL NANOPARTICLES

Alejandra Pérez-Nava^{1*}, Jessica Steffany Pérez-Campos¹, J. Betzabe González-Campos¹, Yliana López-Castro¹, Judit A. Aviña Verduzco¹

¹Instituto de Investigaciones Químico Biológicas, UMSNH, Morelia, Michoacán, México.

*janna0516@hotmail.com

Abstract

Preparation of metal nanoparticles, as gold or silver, is an important sector of scientific research due to their wide range of applications in different industrial areas. Several synthetic strategies have been employed in order to control size and morphology, however chemical reduction of metal salts is the most common procedure; reducing agents and energy sources are required, in the process, polymeric solutions are used as capping agents or stabilizers. In recent years polymeric solutions have been explored as reducing agents in chemical reduction for the synthesis. This strategy is an excellent option to obtain hybrid composites, polymer/metal nanoparticles. In this research, the synthesis of metal nanoparticles using polymeric solutions as reducing agents of metal salts is explored. *AunPs* and *AgnPs* were successfully obtained by an eco-friendly one-pot synthesis; chemical reduction was driven by sunlight exposure as unique energy source and with no additional reducing agents or stabilizers. This approach makes possible the preparation in situ of a nanocomposite conformed by metal nanoparticles embedded into polymer matrix which can be electrospun to obtain nanofibers with potential biomedical applications.

Introduction

The field of nanotechnology has become a major thrust in scientific research since it has adapted to various sectors of science and technology. The use of nanoparticles in the biomedical area is one of the most important fields of nanotechnology because many applications are possible using nanoparticles with low toxicity and biocompatibility.

Metallic colloid solutions have been empirically synthesized since 5th or 4th centuries B.C. by the Egyptian and Chinese civilizations, who used them for medical purposes. Nowadays gold and silver nanoparticles can be useful for medical devices, catalysis, chemical sensing or in construction of devices based on their electronic, magnetic and optical properties [1].

The preparation of noble metal nanoparticles, as gold and silver, has been extensively studied in order to find techniques friendlier with the environment [2]. There are several procedures for preparation of gold and silver nanoparticles, nevertheless chemical reduction of metal salts is still the most common method, this technique made possible the size and morphology control by using stabilizers and different salt concentrations.

It is well known that the preparation of metal nanoparticles embedded into polymeric solution is a good strategy because the polymer acts as a surface capping agent and it is also an excellent host material for nanoparticles. Nowadays there are a number of reports on preparation of silver nanoparticles in polymer solutions with or without using a reducing agent, and several polymers such as Polyacrylamide (PAM), Chitosan (CTS), Polyacrylic acid (PAA), Polyvinyl alcohol (PVA), Polyacrylonitrile (PAN), polyethyleneoxide (PEO) and Polyvinylpyrrolidone (PVP) had been studied in this respect. In the case of the *in situ* preparation of nanoparticles in a polymeric matrix and using the polymer itself as the reducing agent, the chemical nature of the polymer is very important for this objective, since this methodology is a good option for a one-pot preparation of

hybrid nanocomposites in an eco-friendly mechanism; in the green synthetic strategy of nanoscale materials, the usage of nontoxic chemicals, environmental friendly solvents, renewable materials and reduction of the use of chemicals in general have attracted considerable attention due to their advantage in reducing the environmental risks [3].

In this research, we study the influence of the chemical nature of the polymer in the reduction of metallic salts using a natural polymer, Chitosan (CTS), and a synthetic polymer, Polyvinyl alcohol (PVA) since both polymers can act as reducing agents due to they possess hydroxyl and amino groups in their structure. They also can act as capping agents and finally the polymer is the matrix for the composite material obtained.

Furthermore the chemical nature of Chitosan and PVA along with their non-toxic character makes these biopolymers quite interesting to build up hybrid materials based on metallic *nPs* and organic polymers using a green approach by a photo-induced synthesis procedure besides these composite polymeric solutions are suitable for their use in the electrospinning process to obtain nanofibers with potential biomedical and pharmacological applications.

Experimental

Materials

Chitosan with degree of deacetylation >75% and Polyvinyl alcohol with >90% hydrolysis degree, were used in solution as reducing agents and stabilizers, by the other hand chloroauric acid ($\text{HAuCl}_4 \cdot 3\text{H}_2\text{O}$) with molecular weight of 393.83 g/mol and silver nitrate (AgNO_3) with molecular weight of 20.913 g/mol where used as metallic precursors. All reagents where obtained from Sigma Aldrich® and used without further purification.

Synthesis of gold and silver nanoparticles

CTS and PVA powders were dissolved in acetic acid (1wt%) solution and distilled water respectively, to obtain solutions with concentrations of 2wt% for CTS and 8wt% for PVA. CTS solutions were stirred for 12 h at room temperature and the PVA solutions were dissolved at 90°C for 4 h. Metal precursor was added separately in different concentrations (0.001, 0.005, 0.01 and 0.05wt% respect to the dry weight of the corresponding polymer), and no additional reducing agents or stabilizers were used; chemical reduction was driven by sunlight exposure as unique energy source.

The UV-vis spectra of all solutions were obtained by a Genesys 10S spectrophotometer. The scanning wave was in the 200-600 nm range.

Thin film composites were obtained by the solvent evaporation method, while nanofibers composites by the electrospinning technique in an electrospinning unit NaBond Technologies (experimental conditions: rate of spinning 0.5 mL/h, at 40°C and 15 kV). The electrospun nanofibers were collected on aluminum foil at a distance of 15 cm from the syringe needle.

Results and Discussion

Homogenous solutions were exposed directly to sunlight at different periods of time: e.i. 30 minutes for PVA- AgNO_3 and PVA- HAuCl_4 solutions; 120 min for CTS- AgNO_3 and CTS- HAuCl_4 solutions. After this period of time the initial solutions turn from transparent to colored solutions as shown in Figure 1.

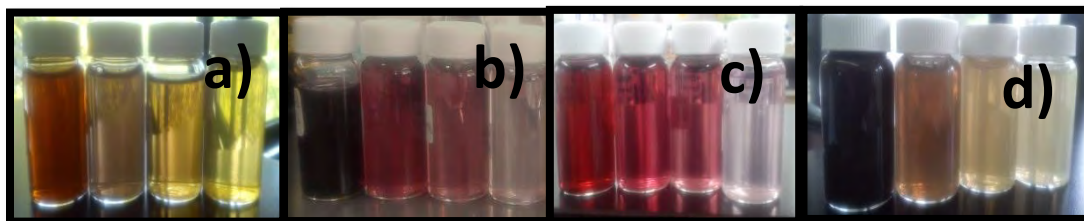


Figure 1. a) PVA-AgnPs, b) PVA-AunPs, c) CTS-AgnPs and d) CTS-AunPs solutions after sunlight exposition, nanoparticles concentration: 0.05, 0.01, 0.005 y 0.001 wt% (right to left).

Nanoscale noble metals display different optical properties than their bulk counterparts. These properties depend on composition, size, shape and surrounding medium of the particles. Surface Plasmon Band (SPB) of gold (AunPs) and silver nanoparticles (AgnPs) comes in the visible region and in the UV-vis spectra is possible the localization of these SPB at 534 nm corresponding to AunPs (Figure 2a) and in 420 nm corresponding to AgnPs (Figure 2b).

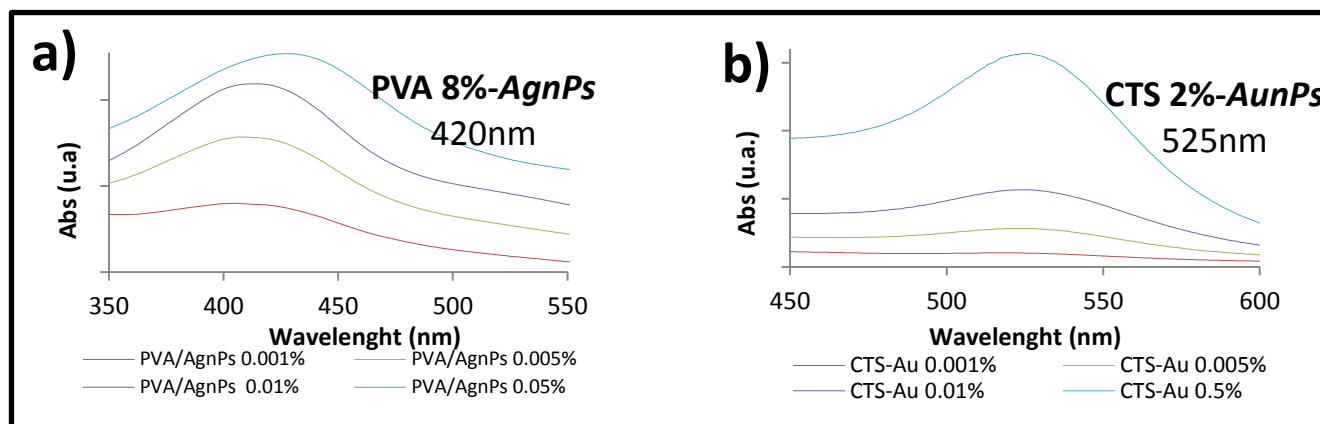


Figure 2. UV-vis spectra after sunlight exposition a) PVA-AgnPs and b) CTS-AunPs different concentrations of metal precursor.

The SPB can be used to monitor shape, size and aggregation of the nanoparticles in order to build reaction kinetic graphics (Figure 3); all the solutions show similar behavior. The surface plasmon band is sensitive to interparticle distance due to the overlapping of dipole resonance from the neighboring nanoparticles.

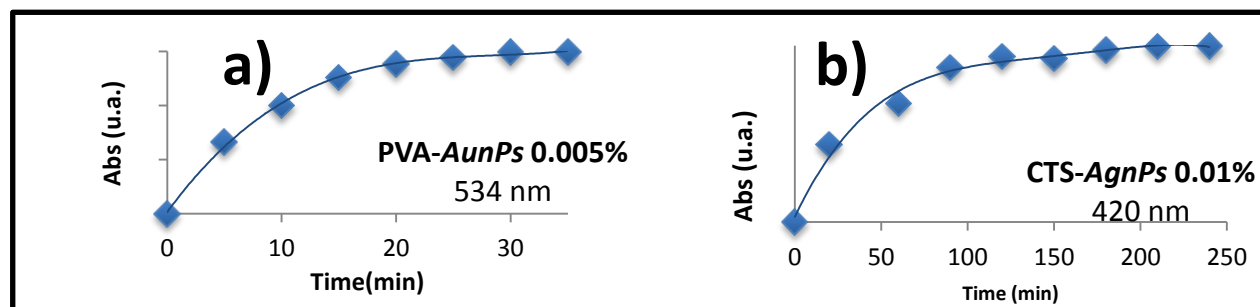


Figure 3. Reaction kinetic a) PVA (8 wt%)-AunPs 0.005% and b) CTS (2 wt%)-AgnPs 0.01%.

To know the effect of the polymeric solution on the chemical reduction process, the polymer concentration was varied, keeping the metal precursors concentration constant (Figure 4 and 5).

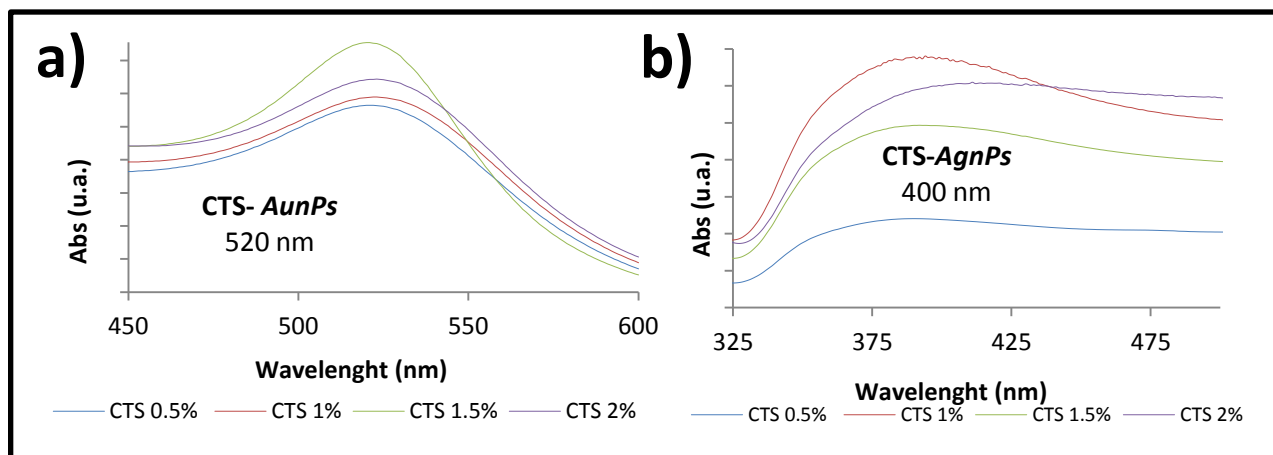


Figure 4. UV-vis spectra after 2 hours sunlight exposure a) CTS-AunPs and b) PVA-AgnPs (precursor metal concentration 4.5% w/v) different concentrations of polymeric solutions.

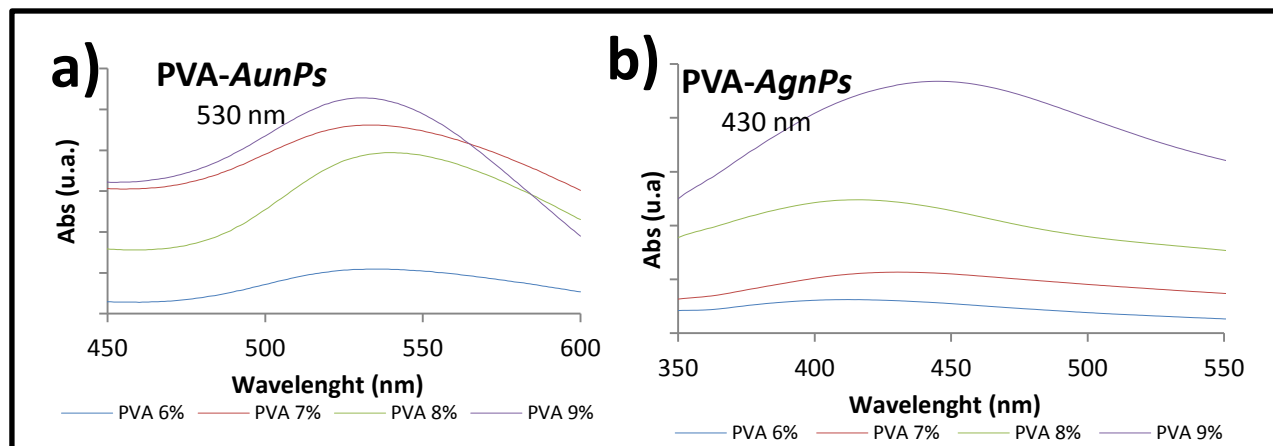


Figure 5. UV-vis spectra after 30 min of sunlight exposure a) PVA-AunPs and b) PVA-AgnPs (precursor metal concentration 0.01% w/v) different concentrations of polymeric solutions.

Due to the nature of PVA-*nPs* and CTS-*nPs* composite solutions, they can be electrospun to obtain nanofibers, therefore PVA solutions were processed in electrospinning unit. The resulting nanofibers have diameters around 120 nm and no defects were present along the fibers (Figure 6).

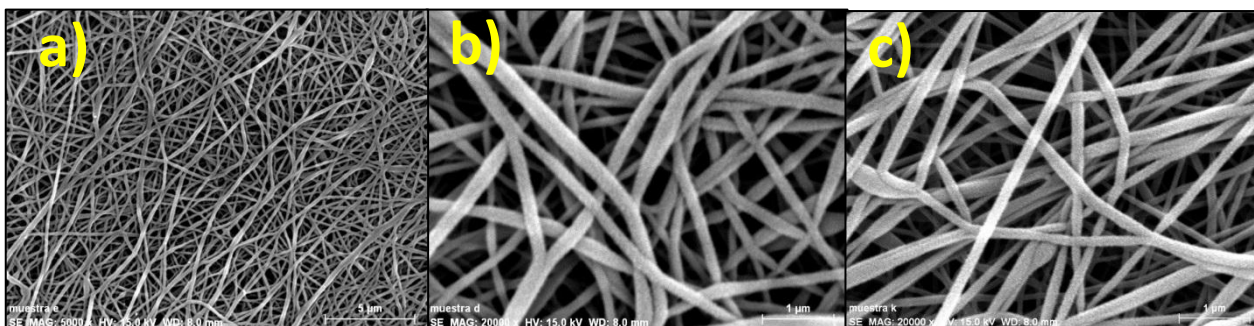


Figure 6. SEM images of nanofibers a) PVA 8%, b) PVA /*AgnPs* and c) PVA/*AunPs*.

Conclusion

AunPs and *AgnPs* were successfully synthesized by an eco-friendly one-pot synthesis using two different polymeric solutions; PVA and CTS, where additional reducing agents or stabilizers were not needed. In this experiment, both polymeric solutions assume the role of reducing agents due to the presence of $-NH_2$ and $-OH$ groups. Also, polymeric solutions act composite matrix and support and they could be processed not only to obtaining films but also nanofibers by the electrospinning process. The resulting nanofibers are defect-free with ideal quality desirable for biomedical applications.

Acknowledgements

Authors thank CIC-UMSNH and CONACyT for the financial support aimed at the project 150767.

References

- [1] S. Boufi, M. Rei Vilar, M.A. Ferraria and A.M. Botelho do Rego. Colloids and Surfaces A: Phy. Eng. Aspects, 151-158 (2013).
- [2] R. Nidhija, G. Archana, J. Aditi, B. Susinjan and R. Vibha. Environmental toxicology and pharmacology, 807-812 (2013).
- [3] H. Ling, Z. Maolin, P. Jing, X. Ling, L. Jiuqiang and W. Genshuan. J. Coll. and Int. Sci. 398-404 (2007).

Silver nanoparticles by in-situ synthesis on a low density polyethylene film and their characterization

L. Muñoz-Jiménez^{1*}, L.F. Ramos-De Valle¹, S. Sanchez-Valdés¹

¹ Centro de Investigación en Química Aplicada, Blvd. Enrique Reyna 140, Saltillo, Coahuila, 25253, México

Abstract: Oxo-degradable PE film was prepared with a thin deposit of silver nanoparticles layer through in situ reaction of nanoparticles on the extruded PE film. Prior to synthesis the film surface was modified by corona discharge. The adhesion of the nanoparticles was performed by polyol, replacing the application temperature in the reaction by sound energy. The surface analysis was performed using STEM, UV-vis and DRX; The nanoparticles showed a size of 41 nm, spherical morphology and changes in the surface tension. The best antimicrobial properties against E. coli bacteria, found within the different reactions performed are present in oxo-degradable film.

Introduction.

Contamination food occurs in postprocessing and in packaging. It occurs by microorganisms. Silver have good antimicrobial properties, it has been used in medicaments and coatings⁽¹⁾. Silver coating is regarded as an important standard treatment of medical devices⁽²⁾. Silver nanoparticles properties are well studied by high surface area provides by its small size combined with its antimicrobial effect.

The mechanism of the antibacterial effect of silver is related to the silver ions (Ag^+). The positively charged silver ions attracted bacteria cells. Silver ions penetrate the cell membrane, acting on DNA preventing bacteria reproduction. The silver ions also interact with the thiol groups of proteins, which induces the inactivation of bacterial proteins⁽³⁾. Microorganisms with resistance to the antimicrobial activity of silver are rare⁽⁴⁾.

Oxo-degradable films increased because provide us a good choice for today's environmental pollution's problems. Polymeric compounds with oxodegradable particles help plastics decompose in several steps by chemical additives (oxodegradable agents) that automatically start degradation. First degradation initiated by UV light reducing the molecular weight due to the breaking of the polymer chains leaving as oligomers which can be biodegraded with time by microorganisms action⁽⁵⁾.

The objective of this work is: development of an antimicrobial coating on a oxo-degradable PE film which could be used for food wraps using silver nanoparticles as antimicrobial agent. The silver nanoparticles were synthesized by polyol method in presence of the ultrasonic waves effect to the reaction initiation and propagation.

Experimental.

Materials.

The silver nanoparticles are synthesized using silver nitrate (AgNO_3) like; ethyleneglycol (EG) anhydride; polyvinylpyrrolidone (PVP) like stabilizer agent with a MW of 10 000 g/mol; the reducing agent was ammonia hydroxide NH_3 at 24 %, deionizer water and nitrogen (N_2).

To obtain the oxo-degradable film we used polyethylene (PE) 20020 like a matrix, the load was a oxo-degradable agent MBO-E11 at two concentrations: 0.9 and 1.8% wt.

Procedure.

The PE was premixed with the oxo-degradable load. The oxo-degradable film was processed by extrusion under the next temperature profile: Zone 1: 160 °C; Zone 2: 175 °C; Zone 3: 190 °C; Zone 4: 190 °C. The concentrations were 0.9 and 1.8 % wt. Previously to the silver nanoparticles synthesis a corona treatment discharge was performed on the PE films premixes with

the oxo-degradable load. The silver nanoparticles were synthesized on the PE film by polyol method, using ultrasound during the reaction. Table 1 shows the conditions of reactions for the samples.

Table 1. Conditions of reaction.

Sample	Corona Treatment (cm)	Temperature (°C)	PVP (mL) at 300 mL	NH ₃ OH: AgNO ₃	Oxo-degradable Load(%)
B-B	1	25	-----	-----	-----
B-1.8	1	25	-----	-----	1.8
RF-03	1	0	-----	2:1	0.9
RF-04	1	25	-----	2:1	0.9
BF-05	1	0	25	2:1	1.8

Results and Discussion.

Fig. 1 presents a UV-vis spectra of the RF-05 sample whit a peak at 450 nm, indicating the presence of spherical silver nanoparticles^(6,7), the results are representative for all samples. The high wavelength peak width reflects the high particle size distribution, and the low wavelength peak reflects the low concentration of silver nanoparticles. This result agrees well with the findings from the STEM images of the nano-sized silver particles

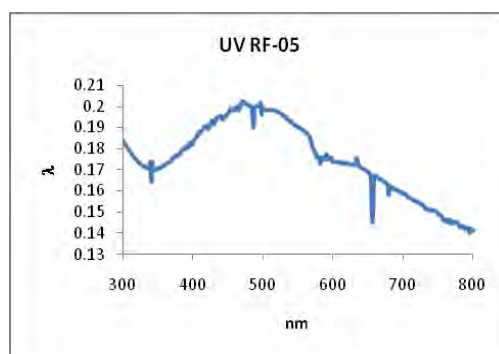


Fig. 1. Graphics UV-vis representative simple RF-05.

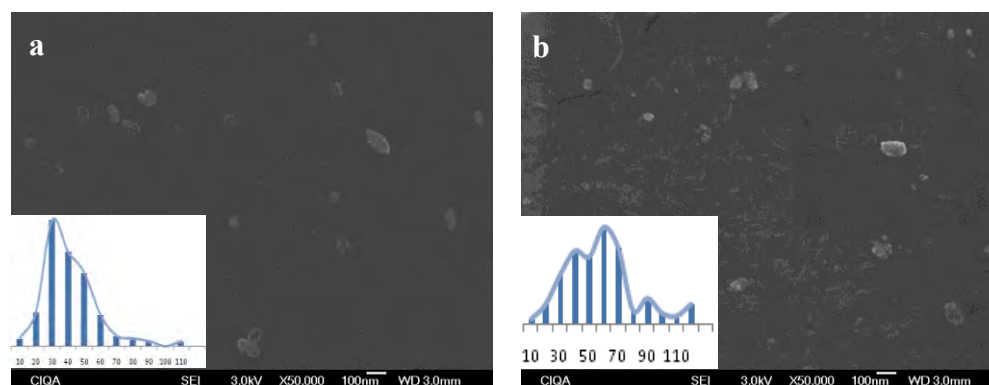


Figura 2. Micrographs and particle size distribution of samples: a) RF-03 y b) RF-04.

The three-dimensional structure of each film was investigated using SEM. The micrographs for samples RF-03 and RF-04 are presented in Fig. 2 (magnification 50x). For the silver nanoparticles the histograms shows a average particle size of 41.13 nm for the RF-03 sample and 58.39 nm for the RF-04 sample. Lows temperatures origins smaller particle size. The reaction conditions provide a spherical geometry to the silver nanoparticles. Like in the UV-vis spectrum we can see spherical particles and high particle size distribution. Also we can see too the agglomerates presence with size of 100 nm⁽⁸⁾.

Sample RF-03 diffractogram, it's show in fig. 3, the peaks 21.72 and 23.79 are characteristic peaks from PE. The peaks from silver nanoparticles cristallinity are: 38.35, 44.56, 65.02, 78.06 and 82.34, this peaks represent the face centered cubic phase. This shows the presence of silver nanoparticles on the surface of PE film samples^(9,10).

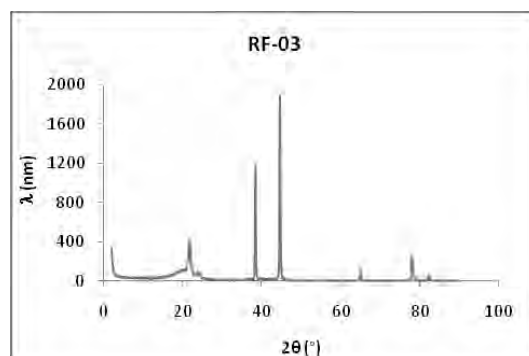


Figura 3. Diffractogram of sample RF-03 in oxo-degradable PE films.

Table 2. γ_1 , γ_{LD} and γ_{LP} values from water and DMF.

	H ₂ O	DMF
$\gamma_1 \left(\frac{mM}{m} \right)$	72.2	37.3
$\gamma_{LD} \left(\frac{mM}{m} \right)$	22	32.4
$\gamma_{LP} \left(\frac{mM}{m} \right)$	50.2	4.9

Table 3. Contact angle with H₂O and DMF.

Sample	Water (°)	DMF (°)
B-B	81.6	56.8
B-1.8	78.8	56
RF-05	51.8	41.6
B-1.8 (degraded)	43.4	30.2

Young's equation provides information about the film wettability. It depends from the system interfacial tensions. The contact angle depends on the changes on the polymer surface, to obtain the polar and dispersion components of surface energy of the films are solved equations (1) and (2).

$$W_A = \gamma_1 (1 + \cos \theta)$$

Ec.1

$$W_A = 2(\gamma_{S,P} \gamma_{L,P})^{1/2} + 2(\gamma_{S,D} \gamma_{L,D})^{1/2}$$

Ec.2

Where:

W_A = Adhesion work

θ = Contact angle at equilibrium.

$\gamma_{S,P}$ $\gamma_{L,P}$ = Surface free energy components in the solid and liquid.

$\gamma_{S,D}$ $\gamma_{L,D}$ = Surface dispersion components for solid and liquid.

Values $\gamma_{S,D}$ and $\gamma_{S,P}$ were calculated by measuring the contact angle with water and dimethylformamide (DMF) on the film. The values are already reported at Table 2. The contact angles measured are presented at table 3.

Table 3 shows that both the contact angles of water and the DMF decreases as the film has a treatment or degrades, suggesting an decrease in polarity to this films by the decreasing molecular weight and corona treatment.

In table 4 we see that the total surface energy increases as the affinity of the phases. While γ_{SD} not vary much between samples, as it degrades and / or is present in the silver nanoparticles, γ_{SP} increases becoming increasingly important this component suggesting an increase in the polarity on the film surface.

Table 4. Polar energy calculations and dispersion of samples.

Sample	Water (°)	DMF (°)	$\gamma_{SP} \left(\frac{mM}{m} \right)$	$\gamma_{SD} \left(\frac{mM}{m} \right)$	Total surface energy $\left(\frac{mM}{m} \right)$
B-B	81.6	56.8	11.18	14.22	25.4
B-1.8	78.8	56	13.25	13.64	26.89
RF-05 (degraded)	51.8	41.6	35.99	11.52	47.51
B-1.8 (degraded)	43.4	30.2	40.98	13.10	54.08

Table 5. Antimicrobial results.

Sample	Inhibition %
100 % oxo	99.98
Blanco oxo-1.8	99.978
Blanco oxo-0.9	98.498
RF-02	96.438
RF-03	95.138
RF-04	95.728
RF-05	97.968
RF-06	93.988
RF-07	92.088

Later elemental analysis test was conducted. It found that the oxo-degradable film have Fe in the formulation, which provides antimicrobial properties to the film. Reports⁽¹⁵⁾ show that silver has an hydrophobic effect and don't inhibit the growth of bacteria. Microorganisms also tend to

evolve to survive and Gram negative bacteria (such E. Coli) tend to have more hydrophobic sites which adhere to the silver nanoparticles⁽¹¹⁾. According to Van Oss⁽¹²⁻¹⁴⁾, hydrophobic interactions are stronger than non-covalent interactions of long range, often the only force aid on the hydrophobic attraction forces are the acid-base forces.

Oxo-degradable bactericidal studies are conducted with E. Coli. Table 5 presents the results of tests. The better antibacterial efficiency were films without silver nanoparticles presence

Conclusion.

The reaction conditions are effective to obtain silver nanoparticles with 40 nm size. The PVP use its useful to keep control about the reaction. But the uses of silver nanoparticles don't help to increase the antimicrobial properties on the films.

Acknowledgements.

CONACYT Project 232753 Laboratorio Nacional de Materiales Grafénicos. Marcelina, Sánchez Adame, Myriam Lozano Estrada, Marcelo Israel Ulloa Pérez, María Luisa López Quintanilla, María Concepción González Cantú, Rodrigo Cedillo García and Juan Francisco Zendejo Rodríguez.

References.

- [1] P. Limjaroen, E. Ryser, H. Lockhart, B. Harte, Journal of Plastic Film & Sheeting, 19, 95 (2003).
- [2] J. M. Schierholz, N. Yucel, A. F. E. Rump, J. Beuth, G. Pulverer, International Journal of Antimicrobial Agents, 19, 511 (2002).
- [3] Q. L. Feng, J. Wu, G. Q. Chen, F. Z. Cui, T. N. Kim, J. O. Kim, Journal of Biomedical Materials Research t A.-52, 4, 662 (2000).
- [4] Won, Ji Ho, Taek Seung, Won Ho, Macromolecular Rapid Communications, 25, 1632 (2004).
- [5] R. Amaud, P. Dabin, J. Lemaire, S. Al-Malaika, S. Chohan, M. Coker, Polymer Degradation and Stability, 46, 211(1994).
- [6] M. Braic, V. Braic, M. Balaceanu, G. Pavelescu, A. Vladescu, Journal of Optoelectronics and Advanced Materials, 5 (5), 1399 (2003).
- [7] M. Mihailova, M. Kreteva, N. Aivazova, V. Kretev and E. Nedkov, Radiation physics and chemistry, 56, 581(1990).
- [8] S. Wizel, R. Prozorov, Y. Cohen, D. Aurbach, S. Margel, A. Gedanken, Journal of Materials Research, 13, 211 (1998).
- [9] N. Perkash, M. Shuster, G. Ambrian, Y. Koltypin, A. Gedanken, Journal of Polymer Science: Polymer Chemistry, 46, 1719 (2008).
- [10] M. Garduño Thesis: Fabricación de nanopartículas metálicas para aplicaciones fotovoltaicas (2011).
- [11] W. C. Duncan-Hewitt, Nature of the hydrophobic effect, in: Microbial Cell Surface Hydrophobicity, ASM Publications Washington, D.C., (1990).
- [12] C. J. Van Oss, M. K. Chaudhury, R. J. Good, Chemical Reviews, 88, 927 (1988).
- [13] C. J. Van Oss, Molecular immunology, 32, 199 (1995).
- [14] C. J. Van Oss, Current Opinion in Colloid & Interface Science, 2, 503 (1997).
- [15] I. Carvalho, M. Henrique, S. Carvalho, Microbial pathogens and strategies for combating them: science, technology and education. Ed.: FORMATEX (2013).

MORPHOLOGICAL, MECHANICAL AND DIELECTRIC PROPERTIES OF PP/COPPER NANOPARTICLES NANOCOMPOSITES FOR THERMAL APPLICATIONS

José A. Velázquez de Jesús,¹ Janett A. Valdez Garza,¹ Víctor J. Cruz-Delgado,¹ Juan G. Martínez Colunga,² Carlos A. Ávila-Orta,¹ Gilberto F. Hurtado López,¹ Jesús G. Rodríguez Velazquez,² María G. Méndez Padilla.³

¹ *Departamento de Materiales Avanzados, Centro de Investigación en Química Aplicada, Blvd. Enrique Reyna Hermosillo No. 140, Col. San José de los Cerritos. Saltillo, Coahuila. 25294. México.*

² *Departamento de Procesos de Transformación, Centro de Investigación en Química Aplicada, Blvd. Enrique Reyna Hermosillo No. 140, Col. San José de los Cerritos. Saltillo, Coahuila. 25294. México.*

³ *Laboratorio Central de Instrumentación Analítica, Centro de Investigación en Química Aplicada, Blvd. Enrique Reyna Hermosillo No. 140, Col. San José de los Cerritos. Saltillo, Coahuila. 25294. México.*

Abstract

Polymer nanocomposites of polypropylene (PP) and copper nanoparticles (nCu) were prepared by melt extrusion. The copper nanoparticles were added in contents of 0, 1, 3 and 5 % w/w within the resin. A morphological, mechanical and dielectric study was conducted on polymer nanocomposites. Thermal properties were evaluated by means of DSC and mechanical properties with a universal testing machine. Thermal transitions were decreased with respect to as received PP. Elongation and elastic moduli were also enhanced for nanocomposites for samples with low copper content. Dielectric constant showed an increase of 100 units as well.

Introduction

Polymer nanocomposites have taken increased interest in both academia and industry, mainly due to the enhanced properties like chemical, mechanical, electrical and thermal, that these materials possess [1-3]. Copper nanoparticles offer the possibility of electrical and thermal conduction when is mixed with a polymer matrix [4], and open a field of application in electrically conductive composites and polymeric heat exchangers [5]. In this study, the effect of size and content of copper nanoparticles on electrical properties, thermal transitions, morphology and dispersion was investigated. For this purpose, polymer nanocomposites of polypropylene (PP) and copper nanoparticles with different sizes were prepared by melt extrusion.

Experimental

Materials

Polypropylene (PP) with a MFI = 35 g/10 min, injection molding grade was used as polymer matrix. Copper nanoparticles (nCu-25) with an average particle size = 25 nm, purity \geq 99.8 wt% were purchased to SkySpring Nanomaterials, Inc. USA. Copper nanoparticles (nCu-50) with an average particle size = 50 nm, purity \geq 99.5 wt% were purchased to Nanostructured & Amorphous Materials, Inc. USA. Paraffin wax was used to coating nCu nanoparticles.

Methodology

Copper nanoparticles were coated with paraffin wax in order to avoid oxidation, for this purpose a controlled atmosphere glove box with N₂ purge was used.

A twin-screw extruder Thermo Scientific Prism TSE 24-MC with L/D: 40:1, was employed to process all the samples with a plain temperature profile of 200 °C and 300 rpm. A masterbatch of 5% wt/wt for each nCu nanoparticles was prepared as follow: PP resin and coated nCu nanoparticles were feed to the extruder with the assistance of volumetric feeder at a rate of 3 kg/h. After that, a proper amount of masterbatch was diluted with pure PP resin to obtain nanocomposites with 0, 1, 3, 5% wt/wt of each copper nanoparticles.

Characterization

Thermal analysis was carried out in a DSC TA Instruments model Q2000 at a heating/cooling rate of 10 °C/min with a flow of N₂ of 50 ml/min. XRD patterns were obtained in a Siemens D5000 X-ray diffractometer with a voltage of 20kV and current intensity of 25 mA were used, within the range of 5 - 40 ° of the 2θ angle. A scanning electron microscope JEOL model JSM7401F with a voltage of 15kV, was used to observe the cryogenically fractured nanocomposites, samples were coated with Au-Pd prior the experiment. Dielectric measurements were recorded with a LCR meter TEGAM model 3550 at a frequency of 1 kHz, silver paint was used to cover both sides of the samples, 5 specimens were tested and the average value was reported. Mechanical properties were evaluated in a universal testing machine Instron model 4220, following the procedure described in ASTM D368 standard, with a deformation rate of 50 mm/min.

Results and Discussion

Thermal transitions and crystallinity percent for polymer nanocomposites with both kinds of copper nanoparticles are presented in Table 1 and Figure 1. The melting and crystallization temperature and crystallinity for polymer nanocomposites with nCu-25 exhibit a tendency to decrease as the content of the nanoparticles increase, the same trend is observed for nanocomposites with nCu-50. The most evident change is observed for nanocomposites with 5% of both copper nanoparticles, for example the crystallinity diminish 13% and 18% for nCu-25 and nCu-50 respectively. It is well known, that the addition of additives such as copper nanoparticles enhance the crystallization rate and nucleation activity for a variety of polymers, nevertheless in our case we observe an apposite behavior. This behavior may obey to the impingement of crystalline growth by the occurrence of copper nanoparticles covered by a layer of paraffin wax.

Table 1. Thermal transitions and crystallinity percentage for polymer nanocomposites with both kind of copper nanoparticles.

Sample	T _m , (°C)	T _c , (°C)	Crysta llinity (%)	Sample	T _m , (°C)	T _c , (°C)	Crysta llinity (%)
PP/nCu-25 0%	148.46	119.54	53	PP/nCu-50 0%	148.46	119.54	53
PP/nCu-25 1%	147.59	117.62	46	PP/nCu-50 1%	146.64	115.31	41
PP/nCu-25 3%	147.6	118.16	46	PP/nCu-50 3%	146.39	116.15	43
PP/nCu-25 5%	146.42	105.40	40	PP/nCu-50 5%	146.15	99.60	35

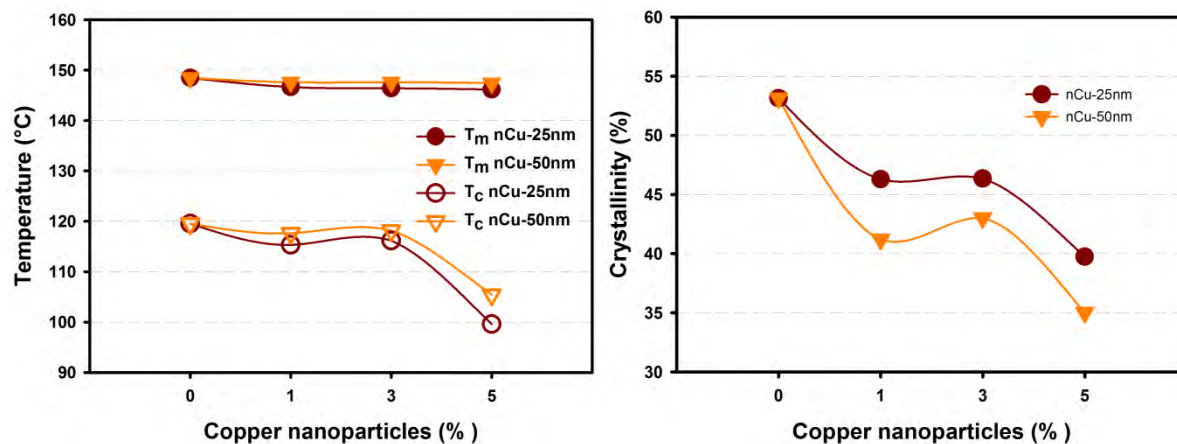


Figure 1. Thermal transitions and crystallinity for polymer nanocomposites with both kind of copper nanoparticles.

The crystalline structure for polymer nanocomposites with both types of copper nanoparticles is shown in Figure 2. Neat polypropylene exhibit a well defined α -phase crystalline structure, with the addition of low contents 1 or 3% of nCu-25 or nCu-50 this structure is preserved. The addition of 5% of nCu-25 promotes the reduction in intensity of the plane (041) located at 21.5° in 2θ . On the other hand nCu-50 causes the disappearance of plane (111) located at 20° in 2θ given place to the appearance of a β -phase. These changes in crystalline structure were discussed in the above section and would affect the final properties of the nanocomposites.

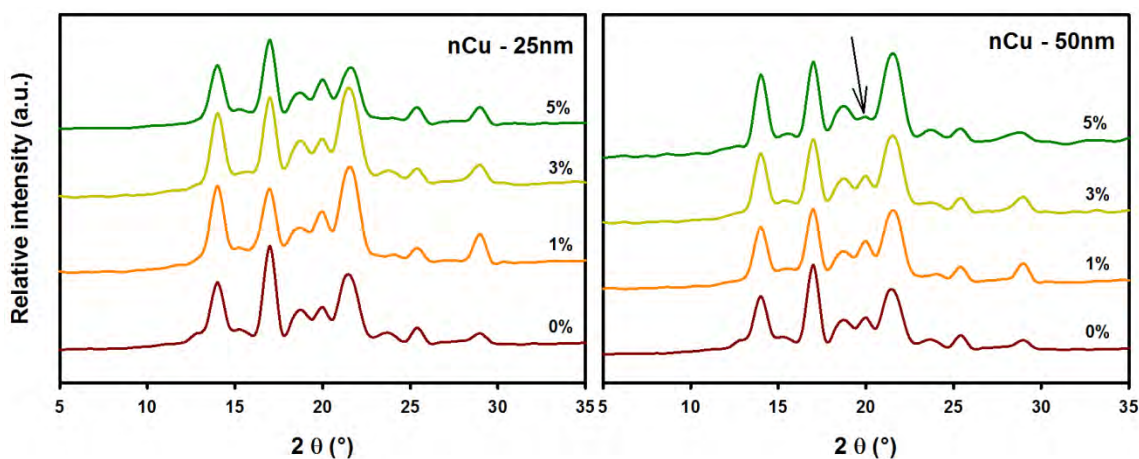


Figure 2. Crystalline structure for polymer nanocomposites with both kind of copper nanoparticles.

Mechanical and dielectric properties for polymer nanocomposites with both types of copper nanoparticles are shown in Figure 3. The increase in tensile strength for nanocomposites with 1 and 3% of nCu-25 are 12 and 19% respectively, meanwhile for nanocomposites with nCu-50 the increase at same content is only 3 and 10% respectively. The addition of 5% of both types of

nanoparticles does not enhance the mechanical response. On the other hand, elongation percent has shown a slight increase for lower contents of nanoparticles, and fall down abruptly for higher contents. The dielectric constant for nanocomposites with nCu-25 is increased by about 100 units for all contents, nevertheless for nanocomposites with nCu-50 only the 1 and 3% show an increase in dielectric constant, the higher content exhibit a small increase of 9 units. The ability of copper nanoparticles for enhancement of the mechanical and dielectric properties is size dependent and shown a better response for small sizes, i.e. 25 nm.

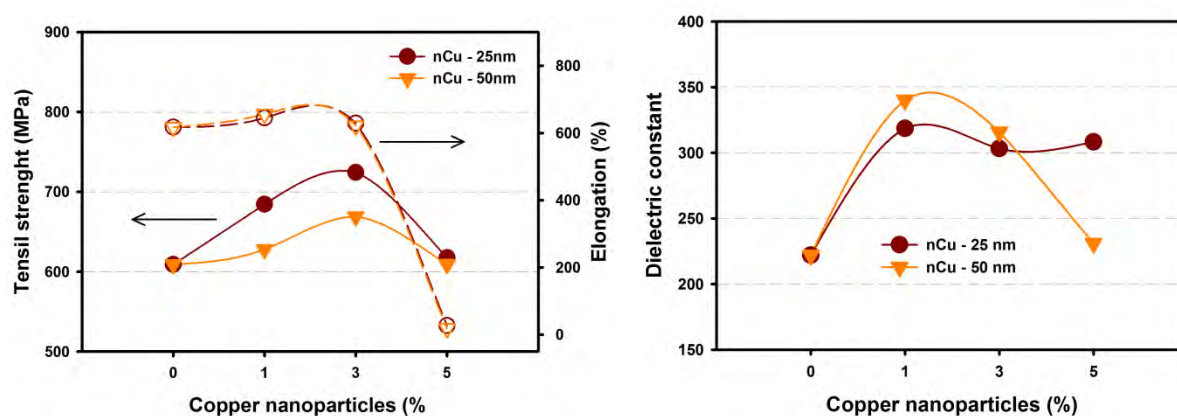


Figure 3. Mechanical and dielectric properties for polymer nanocomposites with both kind of copper nanoparticles.

Electron microscope images of cryofractured nanocomposites with 5% wt/wt of copper nanoparticles are shown in Figure 4. In these images, it is possible to observe that both types of copper nanoparticles tend to form agglomerates and that such agglomerates are well distributed in the whole polymer matrix. The poor dispersion of copper nanoparticles could be related with the treatment to avoid oxidation, which prevents the dispersion during the melt mixing procedure.

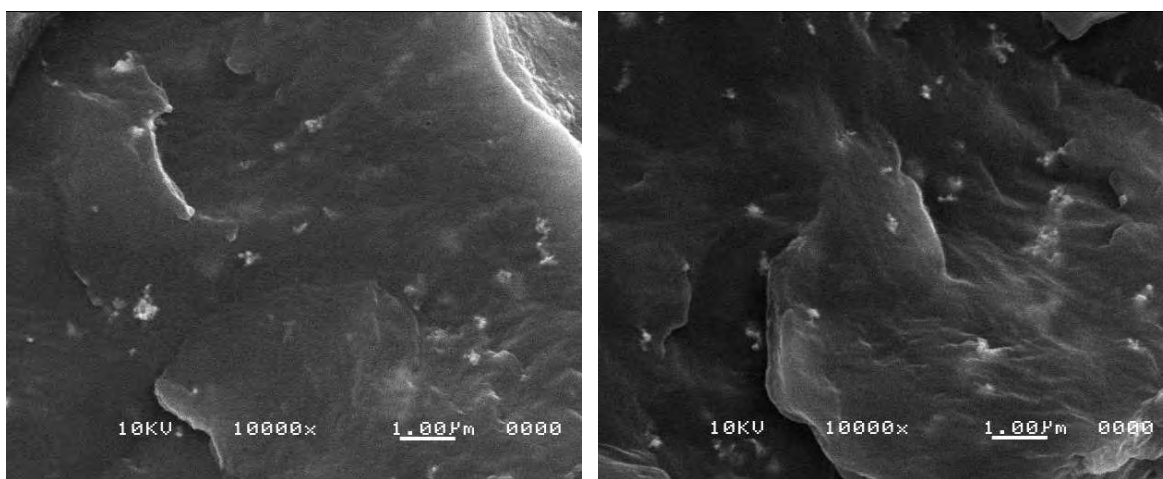


Figure 4. Electron microscope images of cryofractured nanocomposites with 5% wt/wt of nCu-1 (left) and nCu-2 (right).

Conclusions

Thermal transitions and crystallinity of PP/nCu show a slight decrease as content of nCu increase for both sizes of nanoparticles. XRD patterns exhibit a well defined α -phase and no apparent change at low contents of nCu, nevertheless the nanocomposites with 5% of nCu-50nm promote the formation of β -phase. Mechanical properties are enhanced with 1 and 3% of nCu, nanocomposites with 5% exhibit at small increase respect of PP without nCu, this would be due the agglomeration of nanoparticles as shown in SEM images. nCu-25nm nanoparticles promote an increase of dielectric properties of PP at all contents, nevertheless nCu-50nm only does for 1 and 3%. The occurrence of agglomerates in nanocomposites with high content of nanoparticles has a negative impact on the micro-structure of the nanocomposite as revealed by the thermal, mechanical and dielectric properties.

Acknowledgements

This work was supported by SENER through Centro Mexicano de Innovación en Energía Solar CeMIE-Sol P-12. Authors thank the assistance of Blanca Huerta and Myriam Lozano with characterization of polymer nanocomposites.

References

- [1] D. Sundstrom, Y. Lee. J. Appl. Polym. Sci. 16 (12), 3159-3167 (1972).
- [2] Y. Mamunya, V. Davydenko, P. Pissis, E. Lebedev. Eur. Polym. J. 38 (9), 1887-1897 (2002).
- [3] C. Avila-Orta, C. Raudry-López, V. Cruz-Delgado, M. Neira-Velázquez, Int. J. Polym. Mater. 62 (12), 635-641 (2013).
- [4] J. Molefi, A. Luyt, I. Krupa. Exp. Polym. Lett. 3 (10), 639-649 (2009).
- [5] R. Shukla, K. Sumathy, P. Erickson, J. Gong. Renew. Sust. Ener. Rev. 19 (2), 173-190 (2013).

In situ polymerization of ethylene with CNT and/or Cu nanoparticles using zirconocene aluminohydride complexes on heterogeneous phase.

C. Cabrera Miranda¹, O. Pérez Camacho^{*1}, J. G. Martínez Colunga², M. García Zamora¹, C. A. Ávila Orta³.

¹Departamento de Síntesis de Polímeros, Centro de Investigación en Química Aplicada (CIQA), Saltillo, 25250, Coahuila, México. *odilia.perez@ciqa.edu.mx

²Departamento de Procesos de Transformación de Plásticos, CIQA, Saltillo, 25250, Coahuila, México.

³Departamento de Materiales Avanzados, CIQA, Saltillo, 25250, Coahuila, México.

Abstract

In the present work, we have carried out the synthesis and characterization of nanocomposites based on high-density polyethylene (HDPE) with carbon nanotubes and/or copper nanoparticles by *Polymerization Filling Technique*, using as precatalyst a zirconocene aluminohydride supported on modified silica with MAO. The effect of the inclusion of nanoparticles on catalytic activity of the heterogeneous system, crystallization behavior, thermal stability, crystalline structure and electrical conductivity of the final product (PE nanocomposites) was evaluated. It was concluded in this study, that the presence of nanoparticles in the reaction medium led to more stable active species than in the polymerizations without fillers synthesized under similar conditions; furthermore, the nanocomposites that were prepared at a low zirconocene concentration showed better physicochemical properties than those obtained at high catalyst concentrations.

Introduction

Nowadays, the development of new hybrid materials based on polyolefin matrices is a promising research field for various industrial applications or as academic support to understand thermodynamically and kinetically the processes that occur during their synthesis, providing the opportunity to generate many future projects involving non-polar matrices such as polyethylene, polypropylene, among others.¹ In this work is studied the *Polymerization Filling Technique* (PFT) of ethylene in presence of CNT and/or Cu nanoparticles, using aluminohydride bis(*n*-butylcyclopentadienyl) zirconocene [*n*-BuCp₂ZrH(μ-H)₂AlH₂] supported in modified silica with methylaluminoxane (MAO) as the pre-catalyst, this system has not been tested previously in the production of HDPE nanocomposites with these type of nanoparticles.

Experimental

All procedures were performed in vacuum-argon atmosphere (Schlenk technique). Toluene, diethyl ether and iso-octane were reagent grade, all distilled with appropriate drying agents. MAO (10% toluene) and LiAlH₄ (1M, Et₂O) from Sigma-Aldrich were used as purchased. Carboxyl groups-functionalized multi-walled carbon nanotubes 0.5~3% (MWNT-COOH) with outer diameter of 50 to 80 nm, length ~10 μm and purity > 95% by weight were from AlphaNano Technology Co., Ltd. Cu nanoparticles with average diameter < 10 nm were synthesized in CIQA's Advanced Materials Department.

Molecular weights were measured in a Gel Permeation Chromatograph Alliance GPCV 2000 (Waters), using 1,2,4-trichlorobenzene as mobile phase at 140°C. The GPC was calibrated using polystyrene standards with molecular weights ranging 580 to 3,500,000.

Residual aluminum content and Cu were measured in a SpectrAA-250 Plus equipped with an Al or Cu Hollow Cathode Lamp from Varian.

Thermal properties were measured in a DSC of TA Instruments 2920 in a temperature range of 0–160 °C. And in a TGA of TA Instruments model Q500 under N₂ atmosphere from ambient temperature to 600°C and under O₂ atmosphere from 600-800°C. Both, DSC and TGA analysis were performed at a heating rate of 10°C/min.

The crystal structure of nanocomposites was investigated by X-ray Diffraction Spectra (XRD, Siemens), CuK α (25 mA, 35 kV) at ambient temperature in the interval $10^\circ \leq 2\theta \leq 100^\circ$.

The morphology and dispersion of the nanocomposites were analyzed with a Scanning Electron Microscopy JEOL JSM-7401F.

The electrical properties (C_v , S/cm) of the less conductive synthesized materials (resistance > 200 M Ω) were determined with an equipment that contains three amplifiers: Lock-In (Stanford Research Systems) model SR850, TEGAM, Inc. high voltage model 2340 and a converter designed in CIQA. And the more conductive materials (resistance < 200 M Ω) were measured on a Keithley apparatus Model 2400.

Thermal treatment of the nanoparticles. The MWCNT-COOH and Cu nanoparticles were dried in a Linder-Blue muffle at 100 °C by seven days and 24 h, respectively to avoid the premature deactivation of the catalyst.

Polymerization reaction. The preparation of the complex $(n\text{-BuCp})_2\text{ZrH}_3\text{AlH}_2$ and treatment of the support (silica) are described in detail in a previous report.² The in situ polymerizations of semicontinuous operation were carried out at 500 rpm in iso-octane (2,2,4-trimethylpentane), with $\text{P}_{\text{C}_2\text{H}_4}$ (42 psi) and constant T (70 °C) on a 600 mL Parr 5100 reactor, provided with stirring, digital temperature controller, a mass flow controller 0–200 mL/min (AALBORG®). CNTs and/or Cu nanoparticles were previously dispersed in iso-octane for one hour in ultrasonic bath Branson model 3510 and subsequently mixed in the reactor with 5 mL (5.6×10^{-3} mol) of scavenger (MMAO-7 13 wt% Al in ISOPAR-E, AkzoNobel). The pre-catalyst of zirconocene was activated with MAO in a flask, and subsequently introduced with a syringe with lock into the reactor (pre-cured), holding the ethylene pressure to 42 psi. The polymerization is ended by removing ethylene gas from the reaction mixture and adding slowly 20 mL of acidified MeOH (10 vol% HCl). Subsequently, the formed polymer (with or without nanoparticles) is precipitated in 600 mL of MeOH, rinsed with MeOH and finally dried in a vacuum oven at 60 °C for 24 h.

Results and Discussion

In Table 1 are presented the results and conditions of the ethylene polymerization in the presence of nanoparticles, which were carried out at two catalyst concentration levels (~ 40 and 17 mg) corresponding to a molar concentration of 2.98×10^{-5} and 1.26×10^{-5} , respectively. The above conditions were pre-established with the aim of produce nanocomposites with high and low content of nanoparticles to study their interaction with the polymeric matrix of HDPE. Also we synthesized two neat HDPE, without nanoparticles, in order to compare their characteristics and properties with the nanocomposites prepared under identical conditions.

Table 1. Polymerization of ethylene using $(n\text{-BuCp})_2\text{ZrH}_3\text{AlH}_2/\text{SiO}_2/\text{MAO}$ in absence or presence of CNT and/or Cu nanoparticles at Al/Zr (mol/mol) ratio of 1000^a

Exp.	Zr (10^{-6} mol)	Activity ^b	M_w (Da)	\bar{D}	Atomic Absorption		CNT (%) Theoretical ^c	CNT (%) by TGA ^d
					Al (mg/g _{sample})	Cu (mg/g _{sample})		
PE1	6.0	1235.8	14 782	2.2	12.45			
PE2	2.5	1058.2	24 697	2.7	22.09			
NT1	6.2	723.1	19 143	2.5	5.46		18.4	14.7
NT2	2.4	1783.4	31 055	2.5	2.57		19.0	17.0
NTCu1	6.3	415.7	ND	ND	16.09	0.38	31.2	28.1
NTCu2	2.2	905.4	ND	ND	13.31	1.20	41.7	34.8
Cu1	6.0	772.2	23 222	2.3	12.72	0.45		
Cu2	2.6	1625.6	31 639	2.3	10.36	4.23		

^aConditions: iso-octane (200 mL), 5 mL of scavenger (MMAO-7), 500 rpm, 42 psi C_2H_4 , T of 70 °C, 1h. ^bKgPE (mol Zr)⁻¹ h⁻¹.

^c% of incorporation of CNT in HDPE (calculated gravimetrically). ^d% of CNT obtained by TGA. "ND, undetermined"

Aluminum content reported in column six (Table 1) corresponds to co-catalyst or scavenger residuals used in the polymerization reaction. It has been reported³ that alumina residual present in HDPE nanocomposites is inert for the nucleation process and polymer crystallization, therefore, any change

observed in the thermal behavior could be attributed to the incorporation of the nanoparticles into the materials.

In Figure 1a the results of catalytic activity of the system employed in our work, molecular weight (M_w) and index of molar mass dispersity (\bar{D}) for HDPE (pure) and with nanofillers are compared, where we can see how a slight variation due to the presence of CNT and/or Cu nanoparticles is able to disturb considerably during the course of the polymerization. Unfortunately, was not possible to determine the molecular weight for the experiments **NTCu1** and **NTCu2**, since both samples were nearly insoluble under typical conditions of analysis by GPC (1,2,4-triclobenceno at 140 °C) and the experimental data would not be representative or trustworthy. On the other hand, Figure 1b shows the chromatograms for the nanocomposites and HDPE pure prepared with the catalyst in heterogeneous phase (**n-BuCp₂ZrH₃AlH₂/SiO₂/MAO**), where can be observed values of \bar{D} commonly seen for olefin polymerization with supported metallocene catalyst (range of 2–5)⁴. Nevertheless, if we examined in detail the experiments **PE2**, **NT1** and **NT2** we can distinguish a broadening of MWD towards higher molecular weights (shoulder develops). As is well known, occasionally the supported systems generate "leaching" or desorption of catalytic system in the medium of reaction, promoting the formation of polymer both in heterogeneous as homogeneous phase,⁵ which could explain the slight shoulder in the profile of **PE2** that is displayed in Figure 1b. Whereas, the behavior for the **NT1** and **NT2** in the GPC plots is attributed to the desorption of the zirconocene followed by in situ support of the catalytic system on the surface of the CNT, leading to a production of polymer on silica modified with MAO as well as CNT-supported metallocene catalysis, forming different active centers because of that.

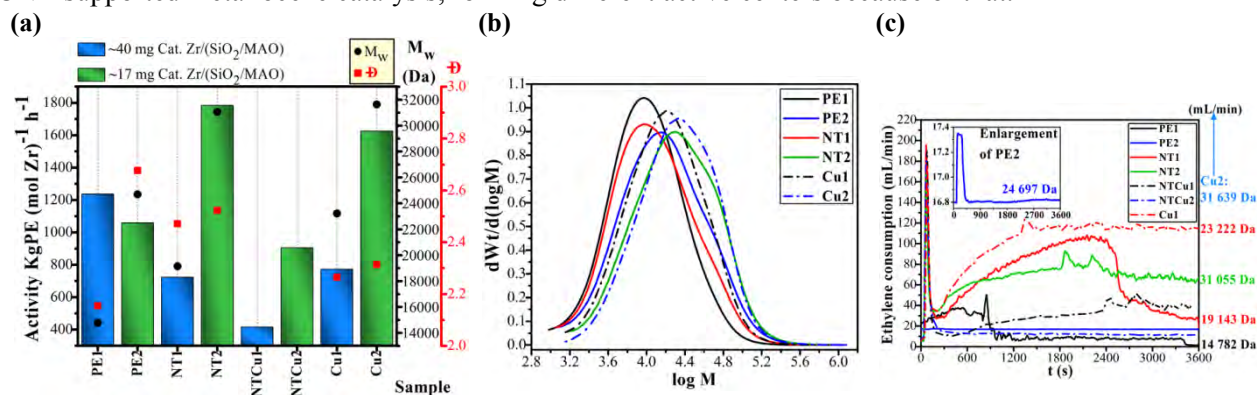


Figure 1. Polyethylenes obtained without and with nanoparticles, using (**n-BuCp₂ZrH₃AlH₂/SiO₂/MAO**) (a) Comparison of activity, M_w and \bar{D} . (b) Molecular weight distribution. (c) Kinetics profiles.

Also, is visible in the Figure 1a that when the concentration of the zirconocene is increased in the samples **PE1** and **PE2** of 1.26×10^{-5} mol (17 mg) to 2.98×10^{-5} mol (40 mg) the molecular weight decreases from 24,697 Da (**PE2**) to 14,782 Da (**PE1**) even though the polymerization reaction of **PE1** shown a higher activity in comparison to **PE2** synthesized under similar conditions (Table 1). This drop of M_w could be caused by chain transfer reactions; to the aluminium from the co-catalyst (MAO) mainly. Moreover, it has also been reported⁶ that the catalytic activity is low or reduced when the quantity of catalyst goes increases because is most likely to happen a bimolecular deactivation as a consequence of the proximity that exists between the active centers and the probability for occur this phenomenon is bigger in a small or confined space by the presence of the nanoparticles themselves. The text previously mentioned supports the reduction in activity around 41–48%, observed when we are comparing the corresponding pairs of experiments (see Table 1) in the presence of CNT and/or Cu nanoparticles. In addition, the activity of **Cu1** is a little higher than **NT1** where the possible explanation are: i) the smaller size of Cu nanoparticles that leaves less hindered the active sites and the coordination of the monomer is favoured and ii) probably when forces and energies of shear are applied in the ultrasonic bath, the agglomerates of Cu nanoparticles are broken, releasing metallic copper and the layer of copper oxides is somewhat diluted, affecting at lesser extent the catalyst activity.

Figure 1c shows the polymerization rate profiles (kinetic behavior) of the experiments indicated in the Table 1. The shape of these curves refers to the instantaneous polymerization rate determined from the

consumption of monomer as a function of the time; it is noteworthy that the profiles will change according to the conditions of each reaction. In polymerizations of gaseous monomers such as ethylene, the slope of the curve shown in the first minutes of reaction is related to the initial rate, after this point the rate continues to climb until a maximum value is reached. Generally in the systems based on aluminohydride zirconocene or classical metallocenes can be observed a steady-state period represented by a constant rate (propagation stage). Subsequently the rate dropped more gradual, evidencing the catalyst decay, which has been pointed out as the termination stage.

The results of the kinetic behavior of **PE1** and **PE2** (polymerizations without nanoparticles) are shown in Figure 1c, on these profiles we can watch that initial rate of these polymerizations (22.74 and 17.35 mL/min, respectively) are inferior with regard to their corresponding nanocomposites. Taking into account the above facts, we assumed that the presence of the nanoparticles in the medium of reaction increases the rate not only in the first minutes of polymerization; these contribute besides to keeping a high rate until the reaction is terminated 60 minutes after catalyst injection. In particular, the experiments marked as **Cu1** and **NT2** showed a consumption of monomer almost constant and high during the time of reaction, this fact suggest that under these conditions are present more stable active sites; in contrast to the behavior for **NTCu1** and **NTCu2**, where their profiles show low rates of initiation and polymerization. It should also be noted that only the **NT1** nanocomposite exhibits a continuous increase on its polymerization rate, reaching the decay step after have elapsed ~42 minutes of reaction, where a slow catalyst deactivation begins. In this regard it is worth noting that **Cu1** and **Cu2** (in situ polymerization with Cu nanoparticles) were the samples with the highest ethylene consumption, where even the consumption of monomer in **Cu2** exceeded the capacity of the mass flow meter (0–200 mL/min), so it was not possible to obtain the kinetic curve. As mentioned above, the variations of the kinetics behaviors are characteristic of each reaction conditions, wherein the concentration, size and type of nanoparticle affect significantly, perhaps because these may interact with the ion-pair of the catalytic system.

In Figure 2a,b are displayed the exothermic (T_c) and endothermic (T_m) transitions ("peaks"), respectively, for HDPE without nanoparticles as with CNT and/or Cu, in some cases is observed a slight increase in the peak melting temperature (T_{mp}) when the nanoparticles are incorporated, this is a positive sign that are melting crystals thermodynamically more stable. Which is directly related to the time it takes for the nucleation of the polymeric chains over the surface of the CNT, according to experimental data reported by Trujillo, *et al.*⁷ It must be mentioned that to date there are only a few reports in the literature about this type of investigations that involve a metallocene catalyst and CNT or Cu nanoparticles.

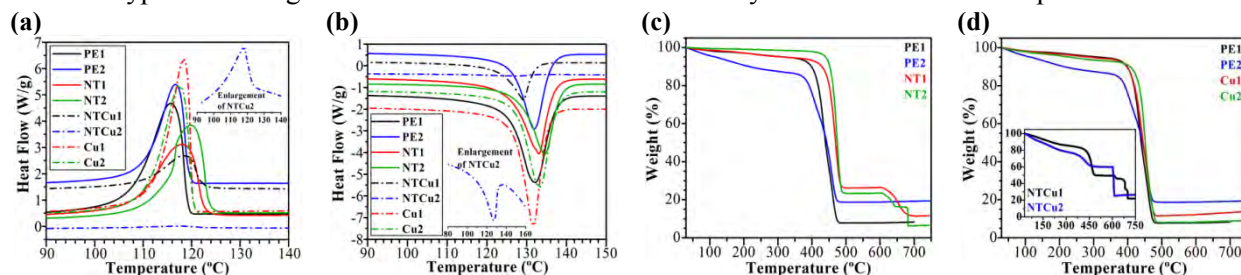


Figure 2. Samples of HDPE without and with nanoparticles obtained using the $(n\text{-BuCp})_2\text{ZrH}_3\text{AlH}_2/\text{SiO}_2/\text{MAO}$ complex (a) Peak crystallization temperature (T_{cp}). (b) Peak melting temperature (T_{mp}). (c, d) Weight loss percent as a function of the temperature for the different experiments carried out in this work.

The effect of the incorporation of CNT and/or Cu nanoparticles in the matrix of HDPE was analyzed by TGA (Figure 2c,d) to measure the degradation of the polymers prepared via in situ polymerizations using two different concentrations of the zirconocene aluminohydride system, in the Figure 2c is clear how independently of CNT concentration in **NT1** and **NT2** (14.71 and 17.02%, respectively), the thermal stability of the final product is enhanced, but when Cu nanoparticles were introduced in the polymeric matrix (Figure 2d) the stability is improved only when we were able to achieve more weight content of Cu nanoparticles in the matrix (**Cu2**) varying the zirconocene concentration in the synthesis of the nanocomposite. The TGA decomposition curves of the samples of the Figure 2d for the nanocomposites of HDPE/CNT/Cu seems like it undergo a premature mass loss

starting at ~ 125 °C and up shortly before 300 °C; however, this multi-step decomposition process observed in the experiments **NTCu1** and **NTCu2** could be attributed to loss of other constituents as coordinated water or compounds of low molecular weight (eg., solvent). The Table 2 resumes the parameters of characterization of HDPE and their nanocomposites studied by TGA and DSC, the values listed indicate that with just modifying the catalyst concentration is possible to get an improvement up to ~ 87 °C in T_{ONSET} by the incorporation of a nanofiller (**NT2**), without decreasing the crystallinity of the material, where on the contrary, it seems that under this reaction condition the CNT play an essential role acting as a nucleating agent; which also is confirmed by the shift in T_{cp} of 116.68 to 119.83 °C. The shift towards higher values in the T_{cp} of Cu nanocomposites in comparison to neat HDPE, as described above, is a sign that the nanofiller acts as effective nucleating agent, this is more evident in the **Cu2** sample; thus, when the concentration of Cu nanoparticles is too low in the matrix (**Cu1**), the crystallinity is reduced $\sim 3\%$, the main reason of this observation can be due to that the polymeric chains with lower molecular weight (**PE1**) crystallize faster than the chains of higher molecular weight (**Cu1**) at the same rate (°C/min set in the measurements by DSC) as a consequence of a restriction in the motion-disentanglement of the polymer chains. On the other hand, the crystallinity for **NT1** decreases $\sim 8\%$ (see Table 2) in comparison with **PE1** this could be due to that when a high loading of CNT is present in the nanocomposite, the mobility and diffusion of the polymeric chains is limited by effects of molecular confinement, because the polymer is not able to be organized building crystals with large thickness due to the reduced space by the presence both CNT and residual alumina and hence, the crystallinity is lower.^{3,8}

Table 2. Information from TGA/DSC of HDPE without and with CNT and/or Cu

Exp.	T_{onset} (°C) ^a	T_{max} (°C) ^b	T_{cp} (°C)	T_{mp} (°C)	ΔH_m (J/g)	χ_{cm} (%) ^c
PE1	408.56	434.34	115.71	132.08	240.9	83.10
PE2	368.88	457.58	116.68	131.89	170.9	58.95
NT1	446.32	469.20	118.06	133.08	195.8	75.06
NT2	455.92	473.43	119.83	134.48	171.3	77.13
NTCu1	—	466.03	118.68	129.14	80.72	31.32
NTCu2	—	425.65	117.80	127.52	5.807	2.69
Cu1	410.48	437.51	118.36	131.64	227.9	79.76
Cu2	427.76	449.61	117.50	133.19	225.9	81.04

^aDecomposition temperature at 5% weight loss (TGA). ^bTemperature at which the decomposition rate is maximum (peak in the DTG plot of derivative weight against temperature). ^cNormalized considering the fraction of CNT and/or Cu nanoparticles and ΔH_m° of 289.9 J/g.⁹ "—, undefined"

The X-ray diffractograms of pure HDPE and its composites filled with CNT and/or Cu nanoparticles corroborated that the thermal behavior of the materials are not attributable to changes in the crystalline structure, since unit cell parameters of these, remain intact and the characteristic peaks for HDPE with orthorhombic crystals appears ~ 21.76 y 24.15° in 2θ scale that belongs to the planes (110) and (200), respectively.¹⁰ Whereas, from 25 – 50° in 2θ the following planes are identified: (002) related to the presence of MWNT; (100) peak assigned to the presence of Fe impurity due to ferrocene used as a carbon source to produce the CNT; peaks like (112) and (006) due to amorphous carbon and impurities caused by the presence of different crystalline species,¹¹ observing in our samples that the intensity of the (002) plane close to 25° in 2θ is related to the amount of CNT that we reached to incorporate by in situ polymerization. During the course of our investigations we discovered that if we tried to compare the diffraction pattern of the nanocomposites HDPE/Cu (**Cu1** and **Cu2**) with the representative peaks of the Cu obtained from a database that has clearly visible peaks corresponding to the reflections from the (111), (200) and (220) planes of the unit cell face-centered cubic (FCC) structure at the angles of 43.3 , 50.4 and 74.1° in 2θ , respectively, the presence of Cu nanoparticles in the composite can be confirmed with certainty only through (220)_{FCC} plane plotting the desired area in our diffractograms (40 – 70°), because between 40 – 50° in 2θ may be that the peaks are overlapped with the amorphous carbon and impurities resulting from the synthesis process of CNT or the alumina present in the materials that according to Tian, *et al.*¹² exhibits its peaks in the range of 35 – 70° in 2θ .

Figure 3 shows the SEM images of all materials synthesized in the absence or presence of nanoparticles (CNT and/or Cu). In the micrographs we can see that **PE1** and **PE2** (Figures 3a,b) exhibit a morphology in layers and flake-like shape with a slightly smooth surface. Meanwhile, micrographs corresponding to the synthesis of **NT1** and **NT2** (Figure 3c,d), it can be appreciated that although the particles used in this work (MWNT-COOH) were considered in a range of 50–80 nm according to the supplier. Figure 3d shows a CNT with a wide diameter ~ 89.80 nm. This may be due to more than one CNT has been wrapped by polymer layer; however, it could be also a variation in the original material. The micrographs 3c,d also can distinguish how CNT are interconnected, to form a network structure in the polymeric matrix. Besides, according to the images of **NT2** (Figure 3d), the growth of the polymeric chains occurred onto the surface of each CNT, serving as a dispersion mechanism, avoiding the agglomerates or bundles of nanotubes during in situ polymerization.

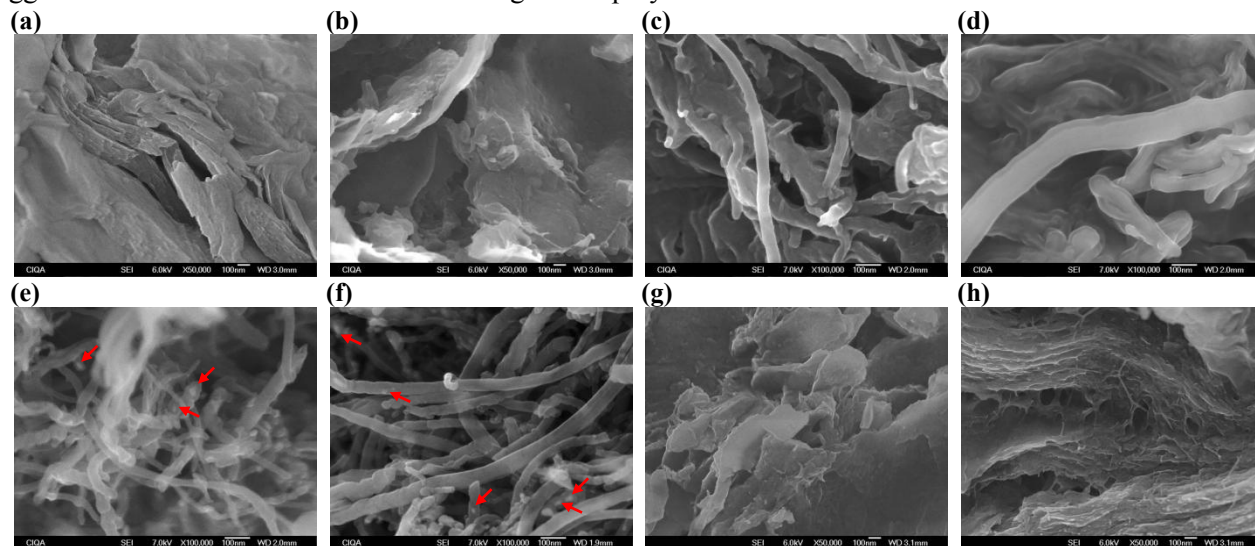


Figure 3. SEM images of (a) **PE1**. (b) **PE2**. (c) **NT1**. (d) **NT2**. (e) **NTCu1**. (f) **NTCu2**. (g) **Cu1**. (h) **Cu2**.

In Figures 3e–3h are shown the micrographs obtained by SEM for the HDPE synthesized in the presence of CNT and/or Cu nanoparticles, using two levels of catalyst concentration (~ 40 and 17 mg). If we compare the Figure 3c with 3e where have been incorporated 18.42 y 31.19% of CNT, respectively is evident that when there are a higher content of nanofiller in the polymeric matrix, the distance between the CNT becomes shorter. In Figures 3e,f the Cu nanoparticles are indicated with a red arrow, which look agglomerated. Unfortunately, was not possible to get a higher magnifications in these micrographs. It is necessary to clarify that in the Figures 3g,h; the tiny spherical particles observed could be attributed to Cu dispersed in HDPE; however, their localization and distribution in the polymeric matrix cannot be confirmed because the volume fraction of Cu nanoparticles are much lower, but different morphology of layers can be observed in micrographs of Figures 3a,b (HDPE without nanoparticles).

One of the improved physical properties in the PE matrices with the addition of nanoparticles like CNT or Cu may be electrical conductivity. Thus, the common HDPE is an insulating material without the presence of nanofillers or conductive particles, but it can modify its value of volumetric conductivity (C_v , S/cm) through networks interconnected when a fraction of an appropriate filler is reached to create a conductive path, which would be proportional to the content of the material used as nanofiller (CNT and/or Cu) and to the way that they are distributed in the polymer domain. The descending order of the C_v measured for the materials synthesized in this work is as follows: **NTCu2** > **NTCu1** > **NT1** > **NT2** > **PE2** > **Cu1** > **PE1** > **Cu2**, and correspond to 1.36 , 1.11 , 2.83×10^{-1} , 6.27×10^{-2} , 2.07×10^{-7} , 3.91×10^{-9} , 1.71×10^{-9} y 1.70×10^{-9} S/cm, respectively. The fact that the polyethylenes without nanoparticles exhibit dissipative characteristics instead of insulating has been attributed to the residual amount of alumina present in the polymeric matrix (HDPE).

Conclusions

Polymerization of ethylene with zirconocene aluminohydride complex in the presence of CNT and/or Cu nanoparticles obtained by PFT technique is a promising process for the production of masterbatch nanocomposites based of HDPE useful with commercial polyethylenes, to improve or modify its thermal and electrical properties. Moreover, it is noteworthy that this study is one of the few where it has carried out the addition of Cu nanoparticles in polyolefin matrices, which could have different applications. Respect to crystallization and melting of HDPE nanocomposites, the DSC results suggest that both CNT and Cu nanoparticles act as nucleating agent, as long as they decrease the density of the polymer molecular entanglements, forbidding the diffusion of the polymer chains that form crystals. XRD studies revealed that the crystalline structure of HDPE matrix with orthorhombic unit cell remains unchanged regardless of the amount of nanoparticles incorporated by in situ polymerizations. Finally, according to the results of C_v measurements, the **NTCu1** and **NTCu2** nanocomposites showed modulable electrical properties, based on the nanoparticles content.

Acknowledgements

The authors are grateful to the project CUVITO (127151) by the needed in this research. In addition, C. Cabrera Miranda acknowledges the financial support of CONACYT for doctoral fellowships. We also appreciate the support in this work to: Q.F.B. Myriam Lozano Estrada, M.C. María Teresa Rodríguez Hernández, L.C.Q. Jesús Alejandro Espinosa Muñoz, L.C.Q. María Guadalupe Méndez Padilla, Q.F.B. Bertha Alicia Puente Urbina and M.C. Gilberto Francisco Hurtado López during the characterization of the samples by SEM, GPC, AA, TGA/DSC, XRD and electrical conductivity tests, respectively. As well as the M. C. Víctor E. Comparán Padilla for his help in adapting the ethylene polymerization reactor and finally, I should like to extend my grateful thanks to Dr. José Ramiro Infante Martínez for his guidance and assist in the implementation, operation and interpretation of the acquisition data system Field Point and supervisory control system (LabVIEW software).

References

- [1] Koval'chuk A. A.; Schegolikhin A. N.; Shevchenko V. G.; Nedorezova P. M.; Klyamkina A. N.; Aladyshev A. M. *Macromolecules* **2008**, *41*, 3149-3156.
- [2] Charles R.; Estrada A. N.; Lugo L.; Revilla J.; García M.; Pérez O. *Macromol. Symp.* **2009**, *285*, 90-100.
- [3] Trujillo M.; Arnal M. L.; Müller A. J.; Bredeau St.; Boundel D.; Dubois Ph.; Hamley I. W.; Castelletto V. *Macromolecules* **2008**, *41*, 2087-2095.
- [4] Odian G. *Principles of Polymerization*, John Wiley & Sons, Inc., 2004.
- [5] Mortara S.; Fregonese D.; Bresadola S.; Boaretto R.; Sostero S. *J. of Polym. Sci. Part A: Polym Chem* **2001**, *39*, 4243-4248.
- [6] Franceschini F. C.; Tavares T. T. da R.; Bianchini D.; do Carmo M.; Lujan M.; dos Santos J. H. *Z. J. Appl. Polym. Sci.* **2009**, *112*, 563-571.
- [7] Trujillo M.; Arnal M. L.; Müller A. J.; Laredo E.; Bredeau St.; Boundel D.; Dubois Ph. *Macromolecules* **2007**, *40*, 6268-6276.
- [8] Fouad H.; Elleithy R.; Al-Zahrani S. M.; Al-haj Ali M.; *Materials and Design* **2011**, *32*, 1974-1980.
- [9] Olmos D.; Domínguez C.; Castrillo P. D.; González J. *Polymer* **2009**, *50*, 1732-1742.
- [10] Chiu F.-C.; Yen H.-Z.; Lee C.-E. *Polym. Test.* **2010**, *29*, 397-406.
- [11] Tripathi G.; Tripathi B.; Sharma M. K.; Vijay Y. K.; Chandra A.; Jain I. P. *Int. J. Hydrogen Energy* **2012**, *37*, 3833-3838.
- [12] Tian F.; He C. N. *Mater. Res. Bull.* **2011**, *46*, 1143-1147.

EFFECT OF DIFFERENT NATURE NANOPARTICLES SURFACE MODIFICATION ON POLYMER NANOCOMPOSITES THERMAL CONDUCTIVITY

Olivares-Maldonado Y.¹, Ramírez-Vargas E.¹, Ramos-deValle L. F.¹, Neira-Velázquez M. G.¹

¹ *Center for Research in Applied Chemistry.*

Abstract

Polymers have very low thermal conductivity, because of this cycle time process become longer and materials can suffer some degradation. This makes necessary to obtain polymers with higher thermal conductivity. In this sense, the addition of particles with high thermal conductivity has become very useful. So in this study, particles of different nature, but all with high thermal conductivities, were modify by cold plasma treatment, and HDPE nanocomposites were obtained. Treated particles and nanocomposites were characterized by different techniques as TEM, TGA, XPS, MDSC, among others. Results showed nanocomposites with higher thermal conductivities, in some cases even 3 times higher than pure resin. Characterization results were associated to nanocomposite final thermal conductivity.

Introduction

Thermal conductivity characterizes de ability of a material to conduct heat. Polymers have very low thermal conductivity (e.g. high density polyethylene HDPE has a conductivity of 0.35 W/m·K, so cycle time during its processing become longer (1), this means more cost and polymer is exposed to higher temperatures for longer, so having polymers with higher thermal conductivity will help to reduce this cycle time. Also, there are various components in electronic devices, where heat dissipation becomes critical not only to maintain the life span of the device, but also to its performance and reliability (2; 3). Polymers reinforced with organic or inorganic fillers with high thermal conductivity are becoming more and more common to increase polymers thermal conductivity (4). One of the most important factors that can affect the final thermal conductivity of the composite is heat resistance at the interphase (5). Modifying the particle surface could improve polymer-particle interactions (6). Plasma is a versatile and clean technique for this purpose. When a polymerizable gas is used, a nanometric film layer is deposited on the particle surface. In this study, the surface of boron nitride nanoparticles, carbon nanofibers and silver nanoparticles was modified by plasma with polyethylene, and the thermal conductivity of final composite was determined.

Experimental

Materials

A high density polyethylene (HDPE) was used with melt flow index of 5g/10 min, density of 0.9665 g/cm³ and melting point of 130°C. Boron nitride was supplied by Lower Friction with hexagonal shape and particle size of 70 nm. Carbon nanofibers were supplied by Pyrograf Products with a diameter average of 150 nm. Silver nanoparticles with flake shape were used with particle size between 20-80 nm.

Plasma treatment

A copper wire was rolled on a round flask with flat bottom to act as inductive electrode. One wire side was connected to a radio frequency generator, which had attached an energy controller. One system entrance was connected to a vacuum pump, while the other one to a valve that control ethylene gas flux. Details are reported elsewhere (7) (8).

Vacuum was applied during 30 min until a pressure of 4.3×10^{-2} mbar was reached. Thereafter ethylene flux was started for 5 min until system pressure was of 7.9×10^{-2} mbar. Treatment was for 20 min with 60 W, constant ethylene flux and continue stirring.

Composites preparation

First, nanoparticles and HDPE were handily mixed; this mixture was then fed into an internal mixer, and processed during 15 min, at 60 rpm. Concentrations are shown on Table I.

Table I. Composites

Particle	Symbol of composite	Concentration (%vol)
Boron nitride	H/BN	3
Modified BN	H/BN-Et	3
Carbon nanofiber	H/CNF	3
Modified CNF	H/CNF-Et	3
Silver	H/Ag	3
Modified Ag	H/Ag-Et	3

H is used to indicate the HDPE and Et to indicate the plasma treated particles

Characterization techniques

Field Emission Scanning Electron Microscopy (FE-SEM) was used to obtain composites micrographs, with a voltage of 15 kV, working distance 6-11 mm and image magnification of 50 000X. SEM (Scanning Electron Microscopy) was used to study magnetite morphology, with a voltage of 15 kV and working distance of 8 mm. TEM studies were done with Transmission Electron Microscope of FEI, TITAN model.

X ray diffraction (XRD) measurements were done with SIEMENS diffractometer, model D-5000, in a 2θ interval of 10 to 70, intensity of 25 mA and voltage of 35 kV. Thermal conductivity was based on E1952-06 standard.

Results and Discussion

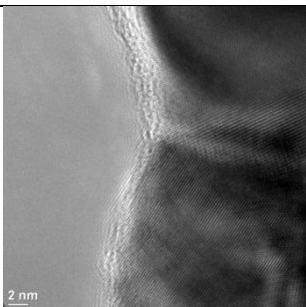
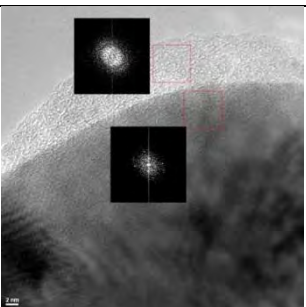
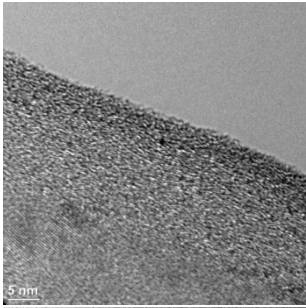
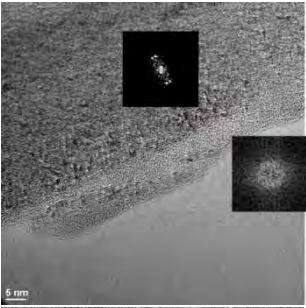
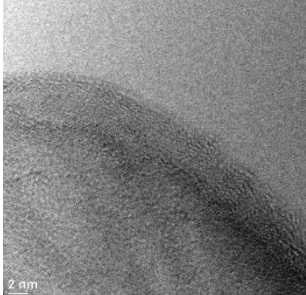
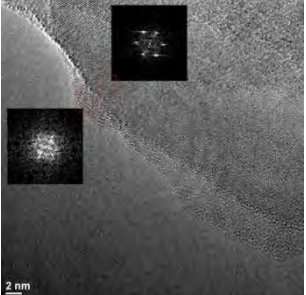
Treated Nanoparticles

Table II shows the difference by TEM micrographs between treated and untreated particles. It was possible to observe the polyethylene film deposited on the surface of the different nanoparticles (Ag, NFC, BN), with a nanometric thickness. On the TEM micrographs of the treated nanoparticles (Table II) nanoparticle phase shows diffraction pattern related to crystalline phase of these materials, while in the deposited layer it cannot be observed any diffraction pattern due to it is an amorphous layer.

Nanocomposites

In order to study the morphology, SEM micrographs were obtained of the different nanocomposites (Table III). In the composites with the nanoparticles before treatment there is no good compatibility, so in this case voids are seen at the interphase. Instead of that, in the SEM micrographs of the composites with treated nanoparticles, it can be seen that there is good wettability of the particle with HDPE, this means that plasma treatment on particles surface promotes nanoparticles/HDPE compatibility.

Table II. TEM micrographs of Ag, NFC and BN, before treatment and with amorphous polyethylene film and its fast Fourier transform (FFT) diffraction pattern.

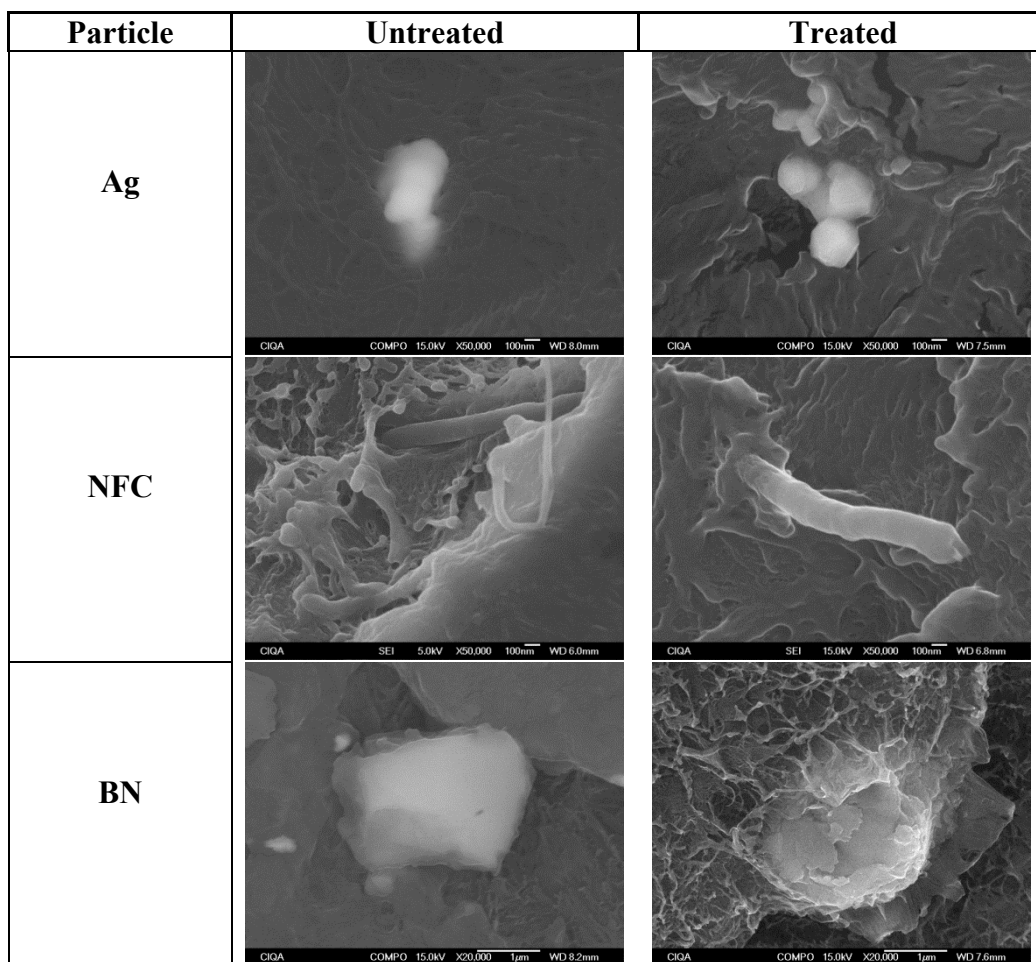
Particle	Untreated	Treated
Ag		
NFC		
BN		

Thermal Conductivity

Composites thermal conductivity was determinate by modulated differential scanning calorimetry MDSC (Table IV). In all cases it can be seen that after treatment, the property is increased. In the case of boron nitride it was found that before treatment the composite even lowered polymer thermal conductivity; this could be attributed to voids between particle and polymer, which promotes phonon dispersion (9).

In the cases of the composites with treated particles were higher thermal conductivity was determinated, it was seen good wettability and no voids were seen at the interphase. This structure could promote the formation of phonon mean free paths that allow heat flux through the interphase (as phonons and electrons). When the interphase doesn't favors heat flux, then dispersion process is promoted and there is thermal energy lose (10).

H/NFC-Et is the composite with highest thermal conductivity, and with the lowest nanoparticle content, this could be attributed to the length of carbon nanotubes, which is in the range of microns. This characteristic favors the formation of a thermal conductivity network between the particles, where heat conduction can be more effective.

Table III. SEM micrographs of nanocomposites with untreated and treated nanoparticles.**Table IV.** Nanocomposites thermal conductivity.

Sample	EM concentration (%vol)	Thermal Conductivity (W/m·K)	Increase (%)
HDPE	0	0.35	0
H/Ag	3	0.46	30
H/Ag-Et	3	0.55	57
H/NFC	1	0.37	5
H/NFC-Et	1	0.67	91
H/BN	3	0.31	-12
H/BN-Et	3	0.42	18

Conclusions

Plasma treatment is a process that let the deposit of a polyethylene thin (3nm) film on particles surface. By TEM technique was possible to identify the deposited film. Composites micrographs showed better compatibility between polymer and nanoparticles when treated nanoparticles were used; this was attributed to interaction between ethylene groups in the deposited film and the polymer.

Composites thermal conductivity was increased with modified nanoparticles because voids between particles and polymer were eliminated, plus phonon mean free paths were increased (removing phonons and/or electrons losing for dispersion).

Using nanoparticles with different characteristics allowed to obtain composites with specific characteristics. In the case of H/BN-ET the composite does not conduct electricity; H/NFC-Et is a composite lighter than the other ones and with higher thermal conductivity; H/Ag-Et is thermal and electrical conductor.

Acknowledgements

The authors would like to thank M. Lozano E., J.A. Cepeda G., E. Díaz B., R. Cedillo G., J. Rodríguez V., B. A. Puente U., S. P. García R., J. F. Zendejo R., M. C. González C., F. Chávez E., A. Herrera G., S. Zertuche R., B. Huerta, M. G. Mendez P., C. G. Hernández R. for their experimental measurements and some suggestions. They would also like to tank to the Proyect CONACYT 232753 Graphene Materials National Laboratory.

References

1. Sarrabi S., Colin X., Tcharkhtchi A. J. Appl. Polym. Sci. Vol. 118, 980-996, (2010).
2. Agrawal A., Satapathy A., Procedia Engineering Vol. 52, 573-578, (2013).
3. Hong J. A., Young J. E., Sung D. P., Eung S. K., Thermochimica Acta, 138-144, (2014).
4. Hashim, Abbass., Nanotechnology and nanomaterials <<Smart nanoparticles technology>>, Chapter 23. (2012).
5. Bagchi A., Nomura S. Composites Science and Technology, Vol. 66, 1703-1712, (2006).
6. M., Stamm. Germany, Springer, 1a Ed. (2008).
7. Neira-Velázquez M.G., Ramos-deValle L.F., Hernández-Hernández E., Zapata-González I., e-Polymers, 162 (2013).
8. Ramos-deValle L.F., Neira-Velázquez M.G., Hernández-Hernández E., J. Appl. Polym. Sci., Vol. 107, 1893 (2008).
9. Shenogin S., Xue L., Ozisik R., Keblinski T., Cahill D.G., J Appl Phys, Vol. 95 (12), 8136-44 (2004).
10. Cahill D.G., Ford W.K., Goodson K.E., Mahan G.D., Majumdar A., J Appl Phys, Vol. 93, 793 (2003).

PINWOOD RESIDUES/RECYCLED HDPE COMPOSITES TO SUBSTITUTE MEDIUM DENSITY FIBERBOARDS: MECHANICAL PROPERTIES EVALUATION

Obed E. Rivero-Be,¹ Ricardo H. Cruz-Estrada*,¹ Carlos V. Cupul-Manzano,¹ José G. Carrillo-Baeza,¹ Emilio Pérez-Pacheco²

¹ *Centro de Investigación Científica de Yucatán, Unidad de Materiales, Mérida, México. rhcruze@cicy.mx*

² *Instituto Tecnológico Superior de Calkiní en el Estado de Campeche, Calkiní, México.*

Abstract

Popularity of wood-plastic composites is growing in many eco-applications (e.g., construction) because recycled thermoplastics, and low-density-natural fillers/reinforcements, which are renewable resources, less abrasive, and biodegradable, are used for producing them. Besides that, they can substitute medium density fiberboards (MDFs). This work reports on the preparation of pinewood residues/recycled HDPE plaques to evaluate their performance under flexion, extraction of nails and screws, and moisture absorption, to assess the possibility to substitute MDFs. The effect of the filler particle size was evaluated, and scanning electron microscopy was conducted to examine the state of the filler-matrix interphase.

Introduction

During the last years, reinforcing thermoplastic matrices with cellulosic fibers has become an attractive topic for the environment, and natural fibers have several advantages among which we can mention their low cost, low density, acceptable properties of specific resistance and their biodegradability [1, 2]. Among other things, composites with wood and plastics are known as wood-polymer composites (WPC), and have had significant growth in their production as they have many applications [3], for example can be used as profiles for windows, doors or panels in the automotive industry. Because wood-plastic products usually have an approximate 50% content of wood, they have a promising potential to replace a variety of wood-made products [4-6], being possible of using them as a replacement for medium density fiberboards (MDFs) [7], which have problems with moisture absorption, causing them to swell and crumble. In this paper the preparation of pinewood/recycled HDPE plates is described. To evaluate the possibility of MDFs replacement, evaluation of the composites performance under bending, removal of nails and screws, and moisture absorption is also described. The effect of the filler's particles size was evaluated, and scanning electron microscopy was used to examine the state of the interphase of the composite materials.

Experimental

Raw materials: Pine residues (from Maderas Bajce, Merida, Mexico) were used as dispersed phase. They were ground, and 3 particles sizes were used (4 mm particles, 30 mesh particles, and flour-like particles retained on the plate collector of a W.S. Tyler RO-TAP sieve shaker). They are referred to as M4mm, R30 and TF, respectively. Recycled HDPE (from Recuperadora de Plásticos Hernández, Merida, Mexico) was used as polymer matrix. Polybond 3009 (MAPE) was used as coupling agent, and Struktol TPW 113 as processing aid.

Control materials: MDFs panels with 15 and 25 mm in thicknesses were purchased from MASISA (Merida, Mexico).

WPCs preparation: HDPE, wood and additives were premixed and dried (105 °C, for 24 hours) prior to extrusion. Three different composites (different wood particle size for each) based on 40% by weight (wt.%) of wood, and 60 wt.% of plastic were prepared. The wt.% content of MAPE and Struktol with respect to wt.% of wood were 5 and 3, respectively. The extrusion was performed with a conical twin-screw extruder (Brabender EPL-V5501 using a extrusion die 2 mm in inner diameter fitted to the extruder. During extrusion the screw speed was 50 rpm and the barrel and die temperatures were set at 140 °C.

Samples for mechanical characterization: Test samples of the composite materials were produced by compression molding with a thickness of 15 (bending, moisture absorption) and 25 (removal of nail and screws) mm, according to ASTM D 1037. Bending test, nail and screw extraction: the plates were cut into 410 x 76 x 15 mm for bending which were tested at a speed of 7.2 mm/min; for nail extraction samples were 76 x 152 x 25 mm (the test was performed using a nail 2.8 mm in diameter with a length of 50.8 mm, at a extraction speed of 6 mm/min); and for screw extraction samples were 76 x 102 x 25 mm, using extraction speed of 15 mm/min.

Moisture absorption: The test was performed following ASTM D 1037 standard.

Results and Discussion

The results of the mechanical characterization are presented in Figure 1.

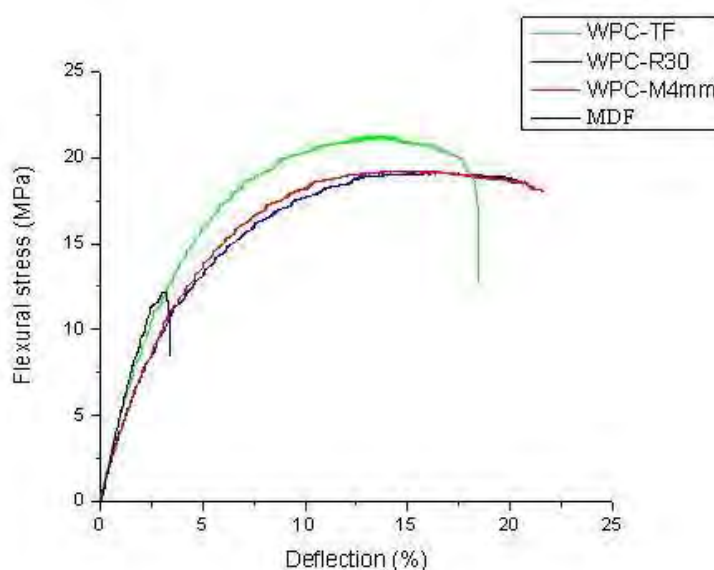


Figure 1. Flexural stress vs. deflection.

Composites exhibited better resistance compared to the MDF; the flexural strength of the composites was higher in all cases, the MDFs are more rigid at their deformation is therefore lower compared to the composite materials. The WPC-TF exhibited better flexural strength because particles' smaller sizes provide larger interphase area per unit volume, which improves resistance to bending, and deformation rate decreases compared to the other two WPC formulations (M4mm and R30), which had similar behavior. Chaharmahali et al. [7] developed

panels from scrap of MDFs and chipboard exhibiting similar behavior to that observed in this research.

Figure 2 shows the comparison of the flexural modules of the different tested materials, showing that the MDFs are more rigid.

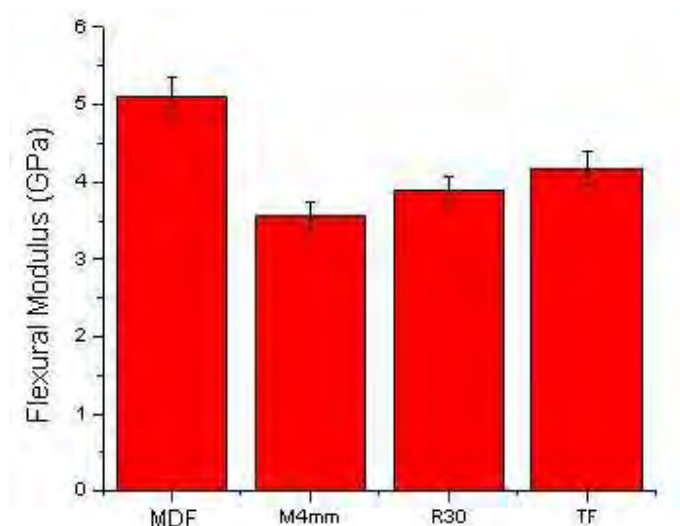


Figure 2. Flexural Modulus of WPCs and MDFs.

Nail and screw extraction force are presented in Figures 3(a) and (b), respectively.

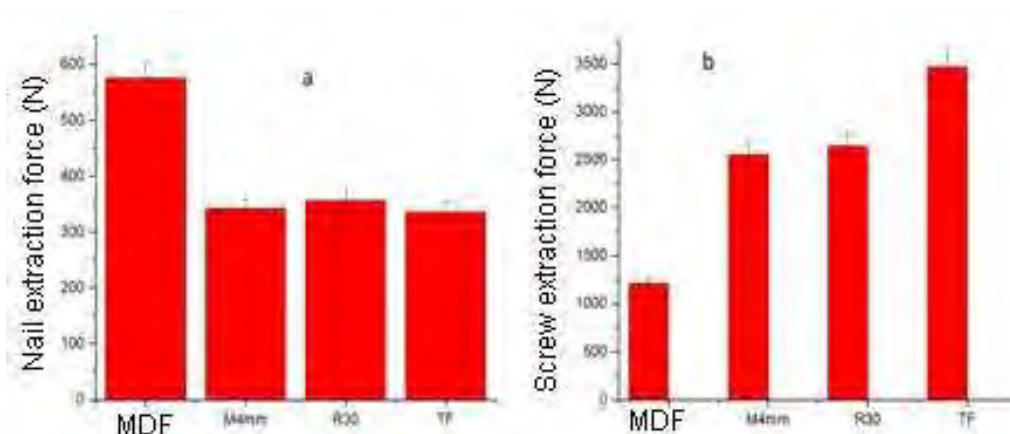


Figure 3. Comparison of nail (a) and screw (b) extraction force for WPCs and MDFs.

Nails and screws are common mechanisms used for assemblies in wooden buildings; and knowing the resistance to remove them is important. So, it can be seen in Figure 3(a), a poor resistance to nail extraction for the WPCs compared with that for the MDF. We think that happens because, contrasting with what occurs from MDFs, the WPCs have no anchor or fixed points, thus making nails sliding out the WPCs easier. The opposite happens regarding screw extraction, WPCs are more dense than MDFs, hence the pullout strength is higher, being that the best result was obtained for the WPC with the smaller wood particle size.

Figure 4 shows the results of moisture absorption at 2 and 24 hours after being submerged in water.

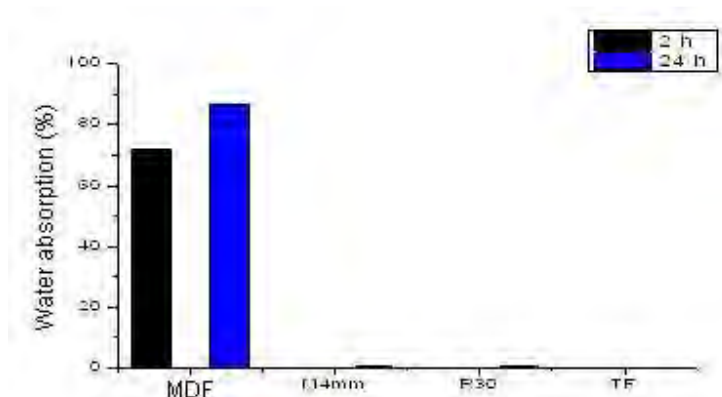


Figure 4. Water absorption after 2 and 24 hours.

Water intake results show that the MDFs are highly hydrophilic, at 2 hours absorbed 72%, and at 24 hours the absorption was 86.83%; while WPCs have absorption % lower than 1% after 24 hours, this because the highly hydrophobic matrix contributes to generate a barrier that prevents access of moisture, so it can be assumed that the WPCs have much better fiber-matrix interphases than that of the MDFs where this practically do not exists. This was evidenced through the SEM analyses performed on the materials (Fig. 5). For the three tested WPCs it was observed a strong bond between the polar wood and nonpolar HDPE matrix due to the use of a coupling agent. As reported in other studies [8, 9], the wood particles are encapsulated by the HDPE, which contributed to a better resistance to water absorption and improved mechanical properties in the WPCs.

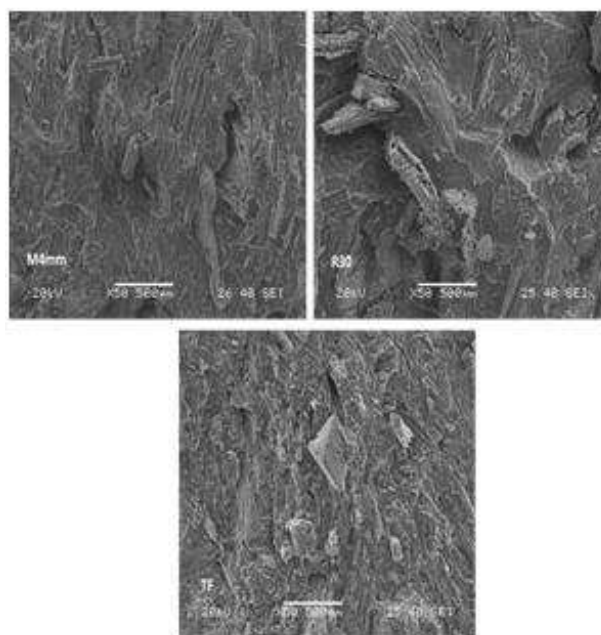


Figure 5. SEM micrograph of the fracture surface of the WPC.

Conclusions

The results have demonstrated the possibility of producing WPC panels with thicknesses of 15 and 25 mm that showed best resistance to bending than MDFs. The WPC with the smallest wood particle size have better resistance. For the WPC is recommended to use screws because they showed to have better extraction resistance. The moisture absorption for the WPCs was much lower than that for the MDFs.

Acknowledgements

Project YUC-2008-C06-107327 ("FoMix CONACyT-Gobierno del Estado de Yucatán").

References

- [1] J.P. López, J. Gironès, J.A. Mendez, M.A. Pèlach, F. Vilaseca and P. Mutjé, *Polymer Composites*, 34(6), 842-848 (2013).
- [2] S. Zhang, Y. Zhang, M. Bousmina, M. Sain and P. Choi, *Polym. Eng. Sci.*, 47(10), 1678-1687 (2007).
- [3] A.K. Mohanty, M. Misra and L.T. Drzal, *Natural Fibers, Biopolymers, and Biocomposites*, Taylor & Francis, pp. 361-403 (2005).
- [4] D.W. Thompson, E.N. Hansen, C. Knowles and L. Muszynski, *BioResources*, 5(3), 1336-1552 (2010).
- [5] C. Clemons, *Forest Prod. J.*, 52(6), 10-18 (2002).
- [6] J.H. Schut, *Plastics technology*, 51(9), 62-69 (2005).
- [7] M. Chaharmahali, M. Tajvidi and S.K. Najafi, *Polymer Composites*, 29(6), 606-610 (2008).
- [8] Y. Zhang, S. Zhang and P. Choi, *Holz als Roh-und Werkstoff*, 66(4), 267-274 (2008).
- [9] S.M. Lai, F.C. Yeh, Y. Wang, H.C. Chan and H.F. Shen, *J. Appl. Polym. Sci.*, 87(3), 487-496 (2003).

EFFECT OF UV STABILIZERS ON THE MECHANICAL PROPERTIES OF A PINEWOOD RESIDUES/RECYCLED HDPE COMPOSITE

Jhonny M. Peraza-Góngora,¹ Ricardo H. Cruz-Estrada*,¹ Carlos V. Cupul-Manzano,¹ Javier Guillén-Mallete,¹ Miguel A. Rivero-Ayala,¹ Javier Reyes-Trujeque²

¹ Centro de Investigación Científica de Yucatán, Unidad de Materiales, Mérida, México. rhcruze@cicy.mx

² Universidad Autónoma de Campeche, Centro de Investigación en Corrosión, Campeche, México.

Abstract

During outdoor applications the surface of wood-polymer composites is affected. Although the observed damage is superficial, it fosters occurrence of different types of degradation. This work deals with the preparation of polymer composites with recycled HDPE and pinewood residues (40 % by weight), with and without UV stabilizers (UVS). One of them had different weight % of a 50/50 blend of a pair of UVS (i.e., 0.5, 1 and 1.5) to assess the effect on the composites' mechanical performance after exposure to UV-light accelerated weathering. After that, mechanical properties were evaluated; and FTIR spectroscopy and SEM analyses were conducted.

Introduction

Wood-plastic composites (WPCs) are promoted as low-maintenance, high-durability products [1]. However, after exterior use for larger periods, questions arise regarding durability, which are based on documented evidence of polymer degradation [2], wood decay [3], and susceptibility to mold, which negatively affect the aesthetic qualities of the product. Environmental, biological, chemical, mechanical, photo(light)-induced, and/or thermal modes of degradation all contribute to the degradation of WPCs. Outdoor use, exposes WPCs to degradation modes that can act synergistically. Accelerated weathering is a technique used to compare performance by subjecting samples to cycles that are repeatable and reproducible. WPCs exposed to weathering may experience color change, which affects their aesthetic appeal, as well as mechanical property loss, which limits their performance. Although photodegradation of both polymers and wood has been extensively examined, the understanding of WPCs weathering should continue to comprehend fully the changes that occur. Photostabilizers are often used to protect WPCs against the attack of weather. They are compounds that protect polymers and combat UV degradation. A relatively new class of materials, hindered amine light stabilizers (HALS), has been extensively examined for polyolefin protection [4, 5].

Experimental

Materials: Pinewood residues (from Maderas Bajce, Merida, Mexico), screened in a Tyler nest of sieves (W.S. Tyler RO-TAP, model RX-29). Residues retained on mesh 40 were used (particle size > 0.43 mm). Injection grade recycled HDPE with a MFI = 4.56 g/10 min from Recuperadora de Plásticos Hernández (Merida, Mexico) was used as polymer matrix. The as-received flake-shaped material was ground with a Brabender granulating machine (model TI 880804) fitted with a screen plate drilled with holes of 1 mm in diameter. Maleic anhydride grafted-high density polyethylene (Polybond 3009) supplied by Brenntag México, S.A de C.V. was used as coupling agent (CA). A blend of modified fatty acid esters (Struktol TPW 113, from Struktol Company of America) was used as processing aid (PA). Both CA and PA were ground using the instrument previously described. Different wt% of a 50/50 blend of a pair of UV stabilizers (UVS) was used (i.e., 0.5, 1 and 1.5). They are a 62 and a 65 HALS, respectively (from GRUPO ALBE, S.A. DE C.V., Jalisco, Mexico).

WPCs Preparation: HDPE, pinewood and additives were premixed using a horizontal mixer with a helical agitator (Intertécnica Co., model ML-5), and dried in a convection oven (Fisher Scientific) at 105°C for 24 hours before extrusion. A pinewood-HDPE formulation with 40 wt.% content of wood was prepared. Details of it are shown in Table 1. Compounding was carried out in a conical twin-screw extruder (Brabender EPI-V5501) using a 4 cm long extrusion die of 2 mm in internal diameter fitted to the extruder to obtain rods of approximately 3 mm in diameter that were pelleted (Brabender, type 12-72-000). During extrusion, the screw speed was 50 rpm and the barrel and die temperatures were set at 180°C.

Table 1. Formulation of tested WPCs based on pinewood residues, recycled HDPE, and UVS.

Material	Wood (wt.%)	HDPE (wt.%)	CA (wt.%)*	PA (wt.%)*	UVS (wt.%)*
WPC0.0	40	60	5	3	0
WPC0.5	40	60	5	3	0.5
WPC1.0	40	60	5	3	1.0
WPC1.5	40	60	5	3	1.5

Notes: *wt.% with respect to wood content. UVS is a 50/50 blend of 62 and 65 HALS, respectively

Preparation of Flexural Test Specimens: Pellets were hot-pressed using a Carver automatic hydraulic press (model 3819) at 140°C for 5 minutes using a compression force of about 26,690 N (6,000 lbf) to obtain 3 mm thickness flat plaques, from which compression molded samples were cut. The test specimens' dimensions are the specified in ASTM D 790 standard test method (i.e., 3.2 x 12.7 x 127 mm).

Accelerated Weathering Tests: Experiments were performed using a QUV-Accelerated Weathering Tester. Samples were exposed to 24 hours of UV light irradiation cycles at 60°C with UVB-313 type fluorescent lamps, using ASTM D 4329 and ASTM G 154 methods as reference. Prior to their exposure, samples (10 replicates per material) were conditioned according to ASTM D 618 standard (105°C, for 24 hours). Samples were subjected to weathering cycles for 0, 384, 576 y 1000 hours, and will be referred to throughout the text as 0AW, 384AW, 576AW and 1000AW, respectively. The experiments were performed on samples with and without UVS.

Mechanical Characterization: Flexural tests were carried out using an Instron 5500R (1125) universal tester machine according to ASTM D 790 method. The three-point loading system was used, employing a crosshead speed of 10 mm min⁻¹ and a 500 kg load cell. In each case 10 specimens were tested to obtain the flexural strength. All samples were conditioned at 23 ±2°C and 50 ±5% relative humidity during at least 40 hrs, before testing according to ASTM D 618. The tests were performed on specimens with and without UVS.

FTIR spectroscopy: Experiments were conducted on a Nicolet Protégé 460 spectrophotometer to identify the evolution of the functional groups present at the surface of the samples as a result of exposing them to weathering. A photo-acoustic detector was used for the experiments. Scans were run at a resolution of 8 cm⁻¹. For each sample 100 scans were recorded from 4000 to 400 cm⁻¹. The peak intensities were normalized using the peak at 2912 cm⁻¹ that corresponds to alkane CH stretching vibrations of the methylene groups. This peak was chosen as reference because it

changed the least due to weathering. Three replicate specimens were analyzed for each type of material exposed to 0AW, 384AW, 576AW and 1000AW. Samples were analyzed on the exposed side of all specimens with and without UVS.

SEM: Morphological analysis was performed on the samples surfaces. WPCs specimens were cut into small sections using a razor blade, and then mounted onto stubs and gold-coated employing a sputter coater (Denton Vacuum Desk II). The samples were examined with a JEOL JSM-6360 LV electron microscope at a working distance of approximately 10 mm and a voltage of 10 kV. The analysis was performed on samples 0AW, 384AW, 576AW and 1000AW, with and without UVS.

Results and Discussion

Mechanical Characterization: The results of the flexural strength evaluation are presented in Table 2.

Table 2. Effect of weathering cycles and content of UVS on the flexural strength.

MATERIALS	Flexural strength (MPa)			
	WEATHERING CYCLES			
	0AW	384AW	576AW	1000AW
WPC0.0	14.52	13.87	12.48	11.87
WPC0.5	14.47	14.04	13.52	12.91
WPC1.0	14.24	14.41	13.49	13.20
WPC1.5	14.47	14.56	13.48	13.33

The flexural strength decreased as AW was increased. It can be clearly observed however, that the WPC without UVS, exposed to the largest period of AW (1000 hours) was mostly affected. The diminishment of the flexural strength with increasing the exposure time to AW is attributed to the damage that the UV irradiation caused on the materials surface (appearance of cracks) which originated from chain scissions in the HDPE. Therefore, this occurred to a different extent, depending on the formulation of the material, which affects the surface appearance and the state of the interphase.

FTIR spectroscopy: Figure 1 shows the shape and location of the carbonyl and hydroxyl bands for WPCs samples after various exposure times to accelerated weathering. For simplicity only selected spectra are presented (specimens WPC1.5, weathered and 0AW). The main absorption peaks, characteristic of HDPE are observed at 2919 and 2850 cm^{-1} . However, special interest was focused on the carbonyl region and hydroxyl region, which are indicators of WPCs oxidation (damage caused because of UV irradiation). In the carbonyl region (1750-1700 cm^{-1}) a sharp peak formed at 1715 cm^{-1} and a shoulder peak at 1735 cm^{-1} , corresponding to carboxylic acid and ester groups respectively, can be observed. The increase in the carbonyl group concentration due to weathering is known to be proportional to the number of chain scissions that occur in the polyethylene matrix. Then, these results indicate that chain scission increased as the exposure time to accelerated weathering also increased. Similar results have been reported previously by Stark et al. [6]. On the other hand, the hydroxyl region (3080-3500 cm^{-1}) assigned to the presence of wood components clearly shows a decrement in its concentration upon exposing the samples to accelerated weathering, meaning that wood was lost in all composites. The carbonyl region is observed better in Fig. 2. For materials with UVS, the carbonyl increase is observed in materials exposed to 0AW in the region 1750-1700 cm^{-1} as the content of UVS is

increased (i.e., the bands corresponding to ester and ketone groups, containing the UVS, are increased). It was observed that as the weathering time was increasing the peak between 1750 cm^{-1} and 1700 cm^{-1} was decreasing as more UVS is added. This is attributed to the UVS functional groups that are reacting with free radicals present in the material and those that could be produced because of the weathering. Summarizing, accelerated weathering seems to have affected materials WPC1.0 and WPC1.5 to a lesser extent. Firstly, those materials presented the highest increase on the intensity of bands corresponding to carbonyl groups, contrasting with the observed for materials WPC0.0 and WPC0.5. Thus, it could be inferred that in the latter pair of materials occurred a highest number of chain scissions in the HDPE matrix. As a result, the interphase was damaged to a greatest extent. Additionally, even in the most extreme case (i.e., 1000 hours of AW), laminar separation from the HDPE on the materials WPC1.0 and WPC1.5 was inferior than that occurred on the other two materials. This indicates that the UVS are protecting the HDPE, preventing damage of the wood particles/polymer matrix interphase.

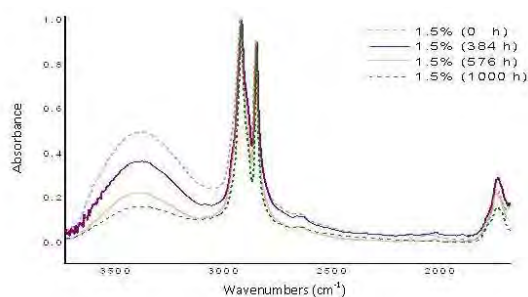


Figure 1. FTIR spectra for specimens WPC1.5, weathered and 0AW.

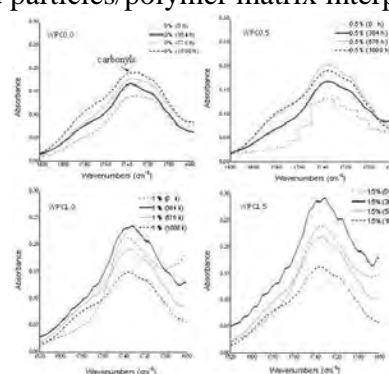


Figure 2. FTIR spectra showing the carbonyl region for all WPCs, weathered and 0AW.

SEM: Micrographs corresponding to Figs. 3 and 4 show the surface of the materials examined. It can be observed that for the non-weathered materials the samples' surface is relatively smooth, and that the polymer matrix apparently encapsulated well the wood particles. When the materials were exposed to 384 hours of AW, cracks and holes appeared on those with 0% of UVS, whereas the materials with 0.5% of UVS were affected to a lesser extent. In contrast, the materials with 1.0 and 1.5 % of UVS practically did not show damaged on their surfaces. Upon exposure to 576 hours of AW, specimens without UVS showed larger cracks exposing wood particles to the environment. The contrary happened on specimens with higher contents of UVS (i.e., the cracks on their surfaces were smaller). Exposure to 1000 hours of AW caused laminar separation of the HDPE, exposing and detaching in this way particles of the composites' disperse phase. Materials WPC0.5, exposed to 1000 hours of AW did not show considerable damage that could lead to detachment of wood particles from the materials' surface. Materials with content of UVS of 1.0 and 1.5 % presented surface damage to a lesser extent.

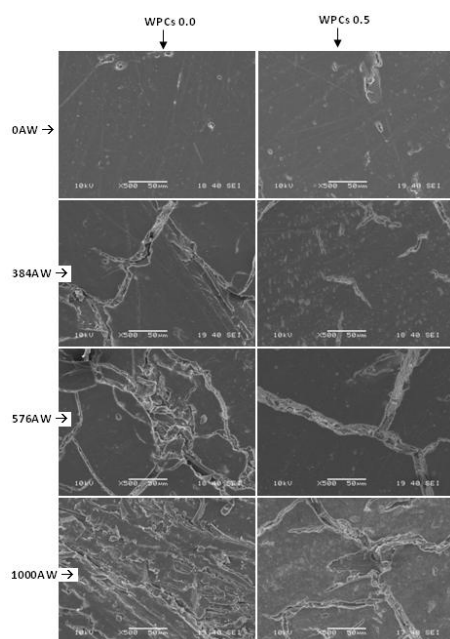


Figure 3. SEM micrographs corresponding to WPCs0.0 and WPCs0.5, weathered and 0AW.

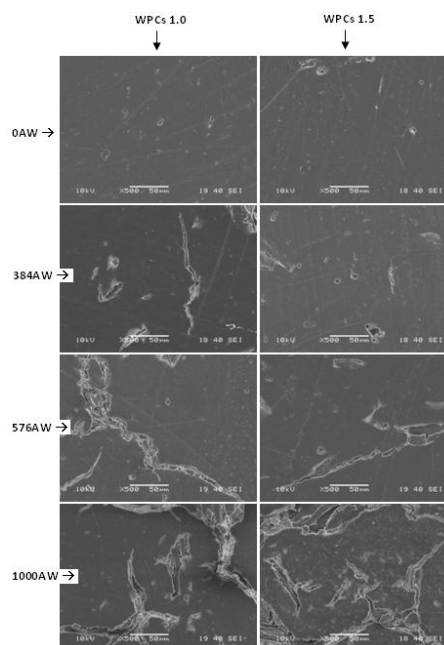


Figure 4. SEM micrographs corresponding to WPCs1.0 and WPCs1.5, weathered and 0AW.

Conclusions

The flexural strength decreased as AW was increased. WPCs without UVS, exposed to the largest period of AW were mostly affected. Increasing the exposure time to AW caused appearance of cracks on the materials surface, originated from chain scissions in the HDPE. Accelerated weathering affected materials WPC1.0 and WPC1.5 to a lesser extent. They presented the highest increase on the intensity of FTIR bands corresponding to carbonyl groups, contrasting with the observed for materials WPC0.0 and WPC0.5 for which occurred a highest number of chain scissions in the HDPE matrix, damaging the interphase to a greatest extent. For the most extreme case (i.e., 1000 hours of AW), laminar separation from the HDPE on the materials WPC1.0 and WPC1.5 was inferior, indicating that the UVS are preventing damage of the wood particles/polymer matrix interphase.

Acknowledgements

Project YUC-2008-C06-107327 ("FoMix CONACyT-Gobierno del Estado de Yucatán").

References

- [1] C. Clemons, Forest Prod. J., 52 (6), 10-18 (2002).
- [2] A.A. Klysov, Proceedings of The Global Outlook for Natural Fiber & Wood Composites 2005, November 15-16, Orlando, FL.
- [3] P.I. Morris and P. Cooper, Forest Prod. J., 48(I), 86-88 (1998).
- [4] P. Gijssman, J. Hennekens and D. Tummers, Polymer Degrad. Stabil., 39(2), 225-233 (1993).
- [5] F. Gugumus, Polymer Degrad. Stabil., 40(2), 167-215 (1993).
- [6] N.M. Stark and L.M. Matuana, Polymer Degrad. Stabil., 86, 1-9 (2004).

STRUCTURAL SISAL FIBER-POLYESTER COMPOSITE LAMINATE CHARACTERIZATION

U Ramirez-Barragán¹, J. P. Dominguez-Cruz¹, F. Estrada-De los Santos², M. Talavera-Ortega¹,
O.A. Jiménez-Arévalo^{1*}

¹ Universidad Aeronáutica en Querétaro, Carretera estatal 200 Querétaro-Tequisquiapan No 22154, Colón, Querétaro, C.P. 76270; e-mail: omar.jimenez@unaq.edu.mx.

² Facultad de Química, Universidad Nacional Autónoma de México, Ciudad Universitaria, C.P. 04510, Méx., D. F.

Abstract

The characterization of the mechanical behavior of reinforced orthophthalic polyester matrix-orthogonal sisal fiber fabric laminated composites has been performed. The influence of the volume fraction and the configuration of the reinforcement on the mechanical properties of the materials have been studied using optical microscopy, vibration analysis and tensile testing. The material obtained has volume fractions of fiber, resin and voids of 21.9%, 77.1% and 0.9% respectively with an elastic modulus of 2.5 GPa. Based on the results found the quality of the manufacturing process was determined and discusses the implications of the material behavior in the development of applications.

Introduction

The use of natural fibers has been largely studied to develop polymer matrix composite used in automotive components [1], in order to being more friendly with the environment, replacing or complementing the glass fiber in order to obtain a more competitive composite [2], avoiding the problems refereed to the final disposal or decreasing the energy amount and cost to obtain it.

The natural fibers are renewable resource, having lower price, but their mechanical properties are also lower than synthetic fibers. Although, there are some good performance natural fibers that has been used in the past in industrial appliances like Henequen or Sisal fiber. Now a day, it has been extendedly studied [3, 4]. This fiber is obtained from the foils of the Henequen agave, having large cellulose fraction that allow a higher properties compared with others vegetable fibers [5], and recently a high damping coefficient has been founded, allowing the material to damp vibration produced by external forces [6]. Some properties of sisal fiber is show in table 1.

Sisal fiber	
Property	Value
Diameter	170 μm (+/-5 μm)
Density	1.49 g/cm ³
Elastic Moduli	12 GPa
Tensile Strength	560 MPa

Table 1. Sisal fiber properties [7].

This work is focused in the mechanical characterization of polyester matrix-sisal wave fiber laminate composites, being produced by infusion process. Determining the composite properties, it will determine the feasibility use in high performance in structural parts or components.

Experimental

3.1 Material manufacture

Orthophthalic polyester resin cured with 4% mass MEKP (Peroxide Methyl Ethyl Ketone) catalyzer and orthogonal plain wave 1x1 Yucatan sisal fiber has been used to obtain a 4 layer 30x30 cm laminate using a resin infusion process over an aluminum mold to dissipate heat and get

an slower polymerization reaction in order to improve the mechanical compliance and avoid over cured cracks. The four layers were placed and cover with peel ply and a distribution mesh to improve the resin flux, avoiding the adherence between the composite and the resin distribution elements. 800 gr of polyester resin has been prepared and infused using a central point disposable inlet port as show in figure 1. When the resin had fill the whole part, the inlet port has been closed applying the vacuum until gel time has been reached, being the part released from the mold after 20 hour cure time. From the laminated obtained Figure 2, samples for mechanical test, modal analysis and optic microscopy has been obtained using a diamond cutting dish.

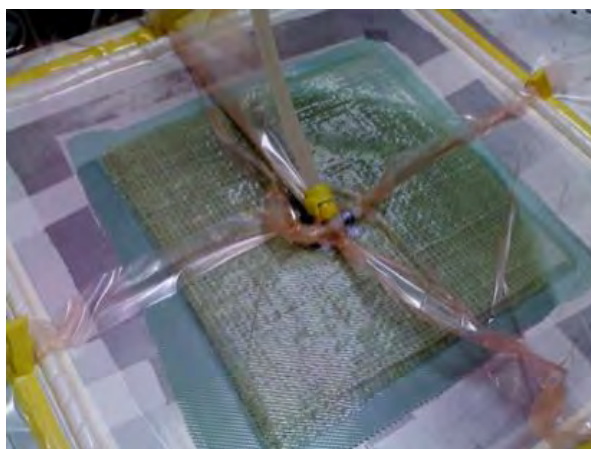


Figure 1. Sisal FRP laminate Infusion process



Figure 2. Sisal fibers on polyester matrix

3.2 Optical Microscopy

Microscopy samples were prepared in a non-permanent fixture. The observation Surface was cut along one of the principal directions of the composite in order to observe the fibers in the transversal direction using a Carl Zeiss Axio Observer D1M optical microscope, scanning the surface sample to do a fiber count win 50x objective. Using AxioVisio software, fiber number, size and area were determinate to calculate volume fiber fraction and porosity.

3.3 Modal Analysis

In order to determinate the composite dynamic properties, 30x30 cm plate have been used. 25 points net has been drawing over the sample surface. These point were used to hit the composite with an impact instrumented harmer an then its behavior has been registered using a digital laser Dooper vibrometer PDV-100. The experiment has been done by suspend the sample with 4 wires attached to a frame structure in order to avoid external noise and register only the material response in the center of the plate when each point was hit. The data registered in the harmer sensor and the vibrometer have been archived and processed using VibSoft-desk-3 software. By adjusting the response signal of the vibrometer and the harmer the frequency and amplitude of the vibration waves generate by the material due the impact. The analysis of the signals has been done using a Matlab program to obtain the data mean and give the representative vibration mode graphic for the sisal-polyester plate.

3.4 Tensile test

Tensile samples have been cut from the sisal-polyester plates according to ASTM-D3039-08 standard [8] having dimensions of 25x200x8 mm due the span limitation of the test machine. The specimens have been tested after four weeks from their manufacture to assure the cure process

finish. The tensile test was carryout in universal test servo hydraulic machine Instron model 8874 with 25 kN load cell. The effective test area was of 150mm long, using sanding paper to avoid the specimen slip in the clamps. Six specimens has been tested with 2 mm/mm deformation rate, registering the load-displacement curve to obtain stress-strain graph and then evaluate yield stress, stress at break and elastic moduli

Results and Discussion

4.1 Microscopy

In figure 3, a part of the surface scanning of one of the specimens is showed. The sisal fiber is composed by small fibers, and it confirms that the manufacture process fill completely the space between the fibers with resin, improved the material quality compared with other manufacture process like wet preg.

Using the equations (1) and (2) table 2 data, the volumetric fiber and resin fractions have been calculated.

$$v_f = \frac{\frac{\% wf}{\rho f}}{\frac{\% wf}{\rho f} + \frac{\% wr}{\rho r}} \text{Ec. (1)} \quad v_r = \frac{\frac{\% wr}{\rho r}}{\frac{\% wf}{\rho f} + \frac{\% wr}{\rho r}} \text{Ec. (2)}$$

Fiber volumetric fraction result in 23.3% and the resin fraction 76.7%, mainly produced by the fiber cloth used, having larges spaces between strands. It's possible to improve the fiber fraction using a closer wave or unidirectional fibers laminates.

Sisal-polyester composite laminate		
	Fiber	Resin
Density (g/cm ³)	1.49	1.16
Weight (%)	0.28	0.72

Table 2. Fiber and matrix density and weight fraction for the samples.



Figure 3. Micrography of fibers in sisal-polyester composite (50X).

From the microscope analysis, it's possible to determinate the fiber, resin and porous area occupied by each one. Due the fact that:

$$A_T = A_f + A_r + A_p \quad \text{Ec. (3)}$$

And also:

$$v_f = \frac{A_f}{A_T} ; v_r = \frac{A_r}{A_T} ; v_p = \frac{A_p}{A_T} \quad \text{Ec. (4)}$$

The mean area for each composite component has been obtained troughs the analysis of the scan surface micrograph and show in table 3. Using equation 4 the volumetric fractions the values in the table were obtained and compared with those of the first method, follow in both case the same tendency, but the last one give lower fraction for the fiber due the presence of porous (near 1%). Also the first method doesn't take in account the existence of parts with low content of

resin in the borders of the sample that can be discriminate by the second method. Finally, the microscope characterization led to know that the infusion process give a material with good quality, kipping low porous content and in general a goof resin distribution excluding the borders of the plate. The fiber has been covered properly and the porous content was lower than others process used previously.

	Mean area μm^2	Volumetric fraction
Fiber	561064.75	0.2192
Resin	1975998.65	0.7719
Porous	22936.6	0.0090

Table 3. Volumetric fractions obtained from the microscope analysis. Total area 2560000 μm^2

4.2 Modal Analysis

From the vibration data, after post processing, a mean frequency vs amplitude vibration graph is obtained (Figure 4), where the highest peaks represent the natural frequencies of the sisal-polyester plate. As show in the graph, the natural frequencies are 170.43; 374.38, 866.11 and 1181.82 Hz for a frequencies range from 0 to 1500 Hz, being the damping coefficients in these frequencies: 0.0162; 0.0185; 0.0074 y 0.0008 respectively.

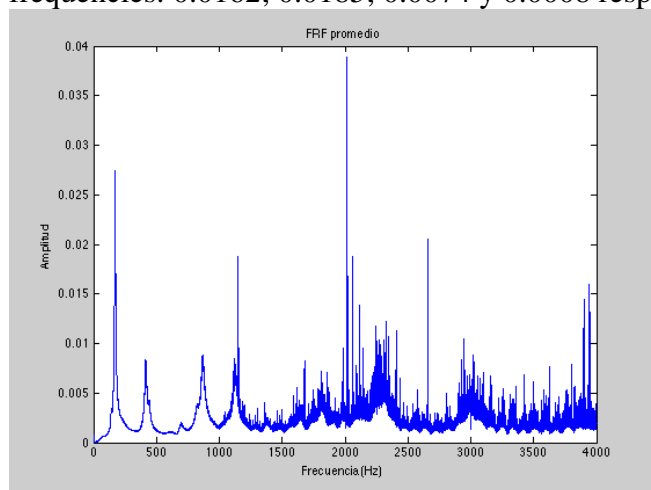


Figure 4. Response function vs amplitude graph at until 4000Hz for the composite specimen.

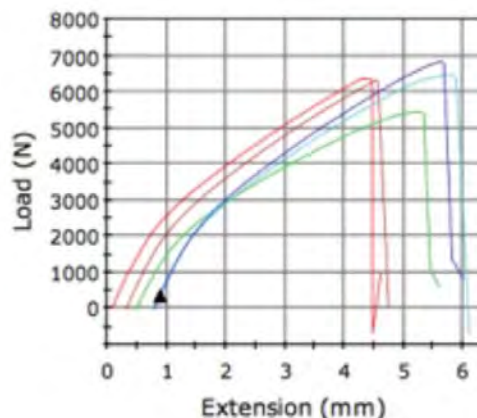


Figure 5. Load extension curves for sisal-polyester composite laminate samples.

The experiment over the sisal-polyester plate, denote that the first natural frequency occurred at 170.43 Hz. In this frequency, the higher amplitude occurs, and then the maximum induced stresses are produced. Then, it's necessary to keep the system far from the natural frequency to avoid the premature fail of the material. The result are similar to those obtained in previous works [3], exiting a small difference that ca be attributed to the specimen support, being in the reference supported by bubble wrap rather than suspended in a frame. From the results of both works the good performance of the composite to damping vibrations caused by external events can be confirm.

4.3 Tensile Test

Graph 5 shows the load-extension curves from the tensile test for all the specimens. The behaviors presented in all cases are not linear, and it's consistent along the set of samples. Non

lineal behavior is related with the polymeric origin of the fibers and matrix as expected in this kind of composites. The consistency of the moduli behavior can be assumed as result of the material homogeneity produced by the manufacture process.

From graphic, the mean elastic modulus is 2.6 GPa calculated in the first third of the curves. The yield stress calculated by the intersection of a 0.02% deformation parallel line is 21.7 MPa, near the half of the break stress of 41.36 MPa whit deformations of 0.037 mm/mm. The high matrix volume fraction yields lower properties, but it can be increased if fiber volumetric fraction is increases by the use of closer wave in the cloth.

Conclusions

The volume fractions show that the material has a high percentage of matrix, prevailing the resin properties. This is caused by a low compaction of the process but mainly by a too open wave fabric leading a fiber configuration with large space where the matrix concentration has been increased. In the other hand, the low porous concentration indicates that the process has a good air control, being inside the acceptable range according with standard. This is important because less porous, less fracture nucleation points, and then, the improvement in the quality over the results with standard manufacture methods can be concluded.

Vibration test shows better damping properties comparing with common glass fiber-polyester plates like mentioned in reference [8], leading a better behavior in order to damping vibration. In order to corroborate this result it's necessary to design a better fixture to execute the test.

The mean stress at break of 41 MPa and mean elastic modulus of are lower comparing with some composite material used in aerospace application, having a good challenge to improve the material performance changing the sisal fiber configuration and adding others components that help to reach the goal of a structural material based in natural fibers.

References

- [1]B. Mano, J. Araújo, N. Spinacé y M. de Paoi, "Polyolefin composites with curaua fibres: Effect of the processing conditions on mechanical properties, morphology and fibres dimensions", *Journal of Composites Science and Technology*, No.70, pp. 29-35, 2010.
- [2]A. K. Mohanty, M. Misra y L. Drzal, "Natural fibers, biopolymers, and biocomposites", Taylor y Francis, Michigan, 2005.
- [3] Sangthong S,(2009) "Mechanical property improvement of unsaturated polyester composite reinforced with admicellar-treated sisal fibers", *composite Part A: applied science and manufacturing*, 40(6-7) july, pages 687-694.
- [4] Canché, G. (2010) *Los materiales compuestos y la unidad de materiales*, Centro de Investigación Científica de Yucatán, A.C. México.
- [5] Chilquillo, Francisco Adriano (2009) "el sisal", *Universidad Nacional De Ingenieria* <http://es.scribd.com/doc/30102443/Monografia-de-Sisal>.
- [6] Análisis de vibración en un compuesto laminado de fibra de henequen-poliéster, Hugo E. Vega, Omar Jiménez Arevalo, Sergio Rojas Ramírez. Congreso Cycyta 2013.
- [7] Cruz, C. (2010) *Química aplicada y la división de química*, Centro de Investigación Científica de Yucatán, A.C. México.
- [8] ASTM (2008) D3039 / D3039M - 08 Standard Test Method for Tensile Properties of Polymer Matrix Composite Materials.

WATER ABSORPTION AND MECHANODYNAMIC PROPERTIES OF COMPOSITES BASED ON THERMOPLASTIC STARCH/POLY(LACTIC ACID)/AGAVE FIBER

Aranda-García F.J.¹, Gonzalez-Nuñez R.¹, Jasso-Gastinel C.F.¹, Mendizabal E.¹✉

¹Universidad de Guadalajara, Centro Universitario de Ciencias Exactas e Ingenierías,
Departamento de Ingeniería Química, Blvd Marcelino García Barragán 1421.Gdl, Jal.,
Méx.

✉lalomendizabal@hotmail.com

Abstract

Water absorption and mechanodynamic properties are presented in this work for composites based on thermoplastic starch (TPS), wherein the concentration of agave fiber (0-15 wt %) and poly(lactic acid) (PLA, 0-30 wt %) is varied. Glycerol (G) is used as plasticizer of corn starch (S) as polymer matrix (70/30 w/w, S/G). Hgrosopicity of plasticized TPS decreases as PLA and fiber content increases. Mechanodynamic results show that storage moduli and relaxation temperature depend on fiber and PLA content.

Introduction

Starch (S) is a biopolymer which occurs abundantly; it is economical and it can be used to produce plastic materials¹. Starch has a melting temperature (T_m) around 240°C²⁻⁴ and it is mainly composed of two molecules, amylose and amylopectin which have very different physical and chemical properties. Unfortunately, materials based on starch have low mechanical properties because of its hydrophilic character;^{5,6} to overcome such problem, polymer mixtures, plasticizers and compatibilizers in different proportions, or reinforcing agents (i.e. natural or synthetic fibers¹⁻³ have been used). By adding a plasticizer (water, glycerol, sorbitol, sugars, or amino acids) to the starch, thermoplastic starch (TPS) can be prepared; in that way, there is a decrease in the glass transition temperature (T_g) and its molding becomes feasible under the action of temperature and pressure^{7,8}. Glycerol (G) is the plasticizer most commonly used in proportions ranging from 20 to 50 % by weight of starch (S/G, % w/w). Among the advantages of natural fibers as reinforcing material, the following may be considered: mechanical properties improvement of the thermoplastic matrix, minimization of environmental pollution^{6,9} and lower production costs; however, the fibers have some limitations because processing temperatures are restricted to $\leq 200^\circ\text{C}$, and they have poor resistance to microorganisms^{6,9}.

Dufresne *et al.* in an early report on starch/fiber composites showed that films made of potato starch mixed with cellulose nanofibers presented thermomechanical properties improvement, with a decrease in moisture sensitivity and maintaining biodegradability; they also found that by increasing glycerol content the equilibrium moisture increased, and increasing fiber content the equilibrium water content decreased.¹⁰

It has also been reported that by mixing a biodegradable polymer such as the poly(lactic acid) (PLA) with TPS, a polymer blend with an increase in Young's modulus and ultimate strength with respect to TPS, is formed^{11,12}.

Although there are several studies on the effect of PLA or fiber over moisture absorption and mechanical properties, there are no reports on the effect of the simultaneous addition of both materials to the TPS. In this work, the effects of PLA and/or agave fiber addition on moisture absorption and mechanodynamic properties of TPS are reported.

Experimental

Materials. The materials used in this work were: corn starch (IMSA) with 10% humidity, Glycerol QP (Reagents Golden Bell), agave bagasse tequilana Weber blue var., PLA (Ingeo Biopolymer 3521D Industries Leben) and Magnesium Nitrate (Fermont.). To obtain TPS, starch was dried for 24 h at 60 °C; then it was manually mixed with glycerol (30 % w/w). The TPS was then mixed with different amounts of PLA and fiber (Table 1), in a co-rotating twin screw extruder (Leistritz Micro 27 equipment GL / GG 32D) and pelletized after extrusion. The pellets of the different composites were molded by thermal compression in a Schwabenthan Polystat 200T compression equipment at 180 °C and 200 bar.

Table 1. Formulation of TPS Composites.

S, g	G, g	TPS*, g	PLA, g	A. Fiber, g	PLA % in polymer blend	A. Fiber % in composite
70	30	100	0	0	0	0
63	27	90	10	0	10	0
56	24	80	20	0	20	0
49	21	70	30	0	30	0
70	30	100	0	11.11	0	10
63	27	90	10	11.11	10	10
56	24	80	20	11.11	20	10
49	21	70	30	11.11	30	10
70	30	100	0	17.65	0	15
63	27	90	10	17.65	10	15
56	24	80	20	17.65	20	15
49	21	70	30	17.65	30	15

* TPS represents the addition of S and G.

Equilibrium Moisture. First, composites were dried at 60° C for 24 h; then the material was weighed and placed at 25 °C in a closed chamber maintained at a relative humidity of 53% (saturated solution of magnesium nitrate). The composites weight was recorded at different times until a constant weight was reached.

Mechanodynamic tests. Mechanodynamic tests were carried out following ASTM D5023-01, using a thermomechanical analyzer (TA Q800 DMA) and the following conditions:

Temperature range: -85 °C to 150 °C, heating rate: 2 °C/min in three-point bending mode and frequency of 1 Hz. Before a test, composite samples were dried in an oven at 60 °C for 30 days.

Results

Figure 1 shows typical moisture absorption curves for the studied composites. Such figure indicates that the rate of moisture absorption decreases as the fiber content increases, and that equilibrium is reached in approximately two weeks. The reduction in the equilibrium moisture content as the fiber amount increases, can be seen in Figure 2 for all formulations; that can be explained by the lower hydrophilic character of the fiber compared to the TPS. It has been reported that composites of bagasse fibers and TPS showed a decrease in moisture equilibrium as fiber content increased¹³. Because PLA is a material less hydrophilic than

TPS, independently of fiber content, an increase in PLA concentration causes a decrease in the moisture absorption capacity of the composite (Figure 2).

Figure 3 shows the storage modulus as a function of temperature for the composite containing 20% of PLA. The composites containing fiber maintain the modulus plateau about 10 °C more than the polymer blend without fiber; this indicates that the fiber acts as a reinforcing material due to fiber rigidity and hydrogen bonding between TPS and fiber. Similar storage modulus behavior was obtained for the other composites.

The storage modulus at 25 °C of the studied composites is shown in Figure 4. This figure indicates that higher storage moduli are obtained with the inclusion of fiber and/or PLA and such increase is larger as more PLA and/or fiber are added. Such reinforcement effect is due to the PLA and fiber rigidity and that they can interact with TPS by hydrogen bonding.

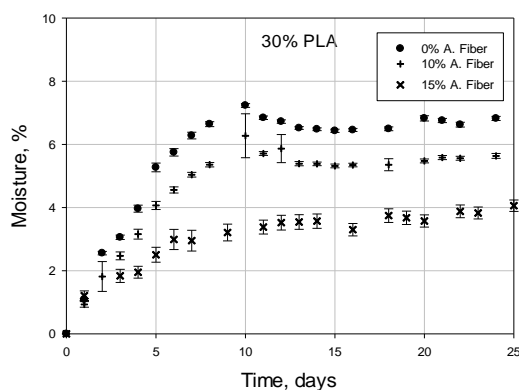


Figure 1. Moisture absorption of composites vs. time for composites containing 30 wt % PLA.

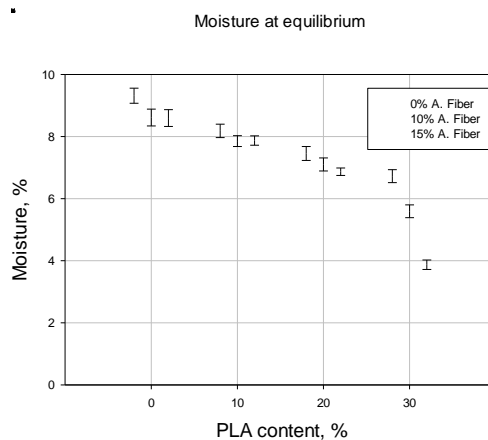


Figure 2. Equilibrium moisture for TPS composites.

Figure 5 shows the dissipation factor ($\tan \delta$) versus temperature for the composite containing 20% of PLA. This figure shows that peaks appear in three regions; one around -55 °C (T_g of glycerol), another one at 60 °C, which is attributed to T_g of PLA and a third one at 115 °C that corresponds to the TPS.

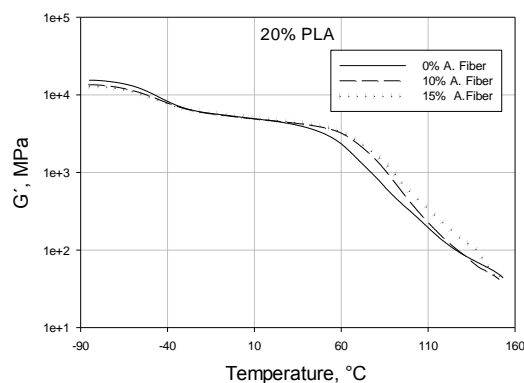


Figure 3. Storage modulus as a function of temperature for composites containing 20% of PLA.

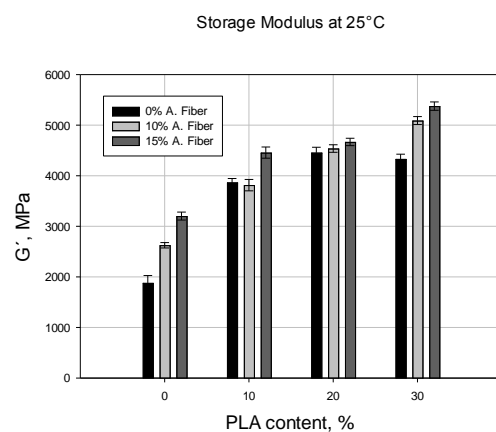


Figure 4. Storage modulus of the composites at 25 °C.

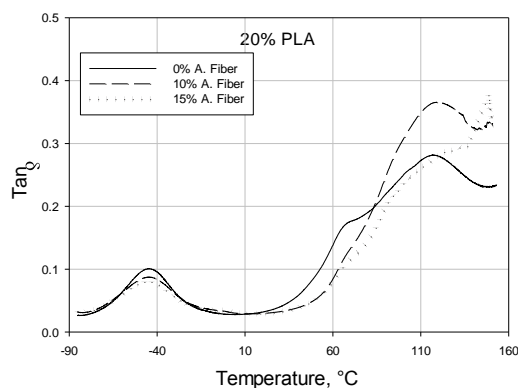


Figure 5. Tan δ Vs temperature for composites containing 20% PLA;

Table 2 indicates that increasing PLA content lowers the T_g of the composite; that can be explained by the lower T_g value of PLA compared to that of the starch ($T_g = 220\text{ }^\circ\text{C}$)⁴. In table 2, it can also be noticed that for constant PLA content, there is an increase in T_g as fiber content increases; the T_g displacement can be attributed to the decrease of starch chains mobility and the interaction of fibers and TPS.¹⁴

Table 2. T_g of the composites.

Polymer Blend	T_g °C		
	0% A. Fiber	10% A. Fiber	15% A. Fiber
10	120	124	132
20	115	120	130
30	111	114	127

Conclusions

For the studied composites, PLA and agave fibers contribute to a decrease in water absorption, and an increase in storage modulus. Glass transition temperature increases with increasing agave fiber content, and decreases with PLA content.

Acknowledgements

Francisco José Aranda García thanks CONACYT for his graduate studies scholarship.

References

1. J.L. Guimarães, F. Wypych, C.K. Saul, L.P. Ramos and K.G. Satyanarayana, K. G. *Carbohydr. Polym.* **80**, 130–138 (2010).
2. P. Sarazin, G. Li, W.J. Orts and B.D. Favis, *Polymer (Guildf)*. **49**, 599–609 (2008).
3. H. Wang, X. Sun and P. Seib, P. *J. Polym. Environ.* **10**, 133–138 (2002).
4. A. Dufresne, *J. Appl. Polym. Sci.* **676**, 2080–2092 (1999).
5. R.L. Shogren, *J. Polym. Environ.* **3**, 75–80 (1995).
6. L. Yu, K. Dean and L. Li, L. *Prog. Polym. Sci.* **31**, 576–602 (2006).
7. H. Liu, F. Xie, L. Yu, L. Chen and L. Li, *Prog. Polym. Sci.* **34**, 1348–1368 (2009).
8. P.M. Forssell, J.M. Mikkilä, G.K. Moates and R. Parker, R. *Carbohydr. Polym.* **34**, 275–282 (1997).
9. M.J. John and S. Thomas, *Carbohydr. Polym.* **71**, 343–364 (2008).
10. A. Dufresne and M.R. Vignon, *Macromolecules* **31**, 2693–2696 (1998).
11. M. Huneault and H. Li, *Polymer (Guildf)*. **48**, 270–280 (2007).
12. L. Jiang, B. Liu and J. Zhang, J. *Macromol. Mater. Eng.* **294**, 301–305 (2009).
13. M.E. Vallejos, A.A.S. Curvelo, E.M. Teixeira, F.M. Mendes, A.J.F. Carvalho, F.E. Felissia, and C.A. Area, *Ind. Crops Prod.* **33**, 739–746 (2011).
14. L. Averous, C. Fringant, and L. Moro, L. *Polymer (Guildf)*. **42**, 6565–6572 (2001).

GRAPHITIC STRUCTURES EFFECT ON THE THERMAL CONDUCTIVITY OF HDPE COMPOUNDS

Esperanza Elizabeth Martínez Segovia*, Luis F. Ramos de Valle, Saúl Sánchez Valdés.

*Transformation Processes Department, Center for Research in Applied Chemistry, Blvd. Enrique Reyna Hermosillo 140
C.P. 25294, Saltillo, Coahuila, México.*

Abstrac.- The high thermal conductivity graphite having thermally conductive compounds can develop. Work in this part of the method of melt-mixing is employed to disperse the graphite (a 3 to 5 wt%) in high density polyethylene (HDPE). Additionally graphite pretreated with ultrasound for observing gas phase fraction distribution in commercial graphite agglomerates present before being added to the HDPE matrix was performed. The characterization of the HDPE / Graphite systems was by the technique of differential scanning calorimetry mode modulated (MDSC), optical microscopy (POM), ray diffraction -X (WAXD and cryogenic fracture SEM and light scattering (DLS). The thermal conductivity of the polymeric compounds from graphite shows increased using a 3% by weight of graphite at 185°C. However, pretreatment with ultrasound graphite particles shows improved particle size distribution before being incorporated into the polymer melt to improve the thermal conductivity of the final composite.

Introduction.

Polymeric materials are limited in certain applications due to their inherent low thermal conductivity, low thermal stability and high electrical resistivity as a result of a low concentration of free conduction electrons so they are considered as non-conductive or insulating materials. For this reason, they are not suitable for applications where its use requires good heat dissipation and transport. There are processes that require high temperatures for the manufacture of conductive adhesives or the reduction of cycle times in large parts¹, so the utility of conducting polymers arise from a low resistivity of about $1 \times 10^4 \Omega/\text{cm}$ and a thermal conductivity value of at least $1 \text{ W/m}\cdot\text{K}^2$. Despite this, the polymers remain attractive because they can support large loads at the macroscopic level ($> 20\% \text{ vol}$), besides being inexpensive materials and easy to process³. Such drawbacks have led to the development of conductive polymers, wherein the combination of conductive plastic materials improves the thermal conductivity and their multifunctionality commercially. This is achieved by including graphitic structures⁴, carbon black⁵ or metallic particles^{6,7} in low amounts ($< 3\% \text{ vol}$) and nanometer size, which has been of great scientific interest. Graphene is the basic structure of the graphite materials as the OD fullerene, carbon nanotube or several stacked sheets 1D 3D graphite. Graphene is formed from a layer and even a few layers (2-10 layers) to form several stacked layers (graphite)^{8,9}. Since the discovery of graphene by A. Geim and K. Novoselov in 2010 to preserve the outstanding thermal properties ($5300 \text{ W/m}\cdot\text{K}$)¹⁰⁻¹⁵, electrical³ and mechanical¹⁶. This ideal is to reduce to a single layer structure. Its chemical properties such as surface area, mesoporous surface and geometry allow it to be chemically modified through processes of pre-oxidation and oxidation¹⁷⁻¹⁹, which makes it a potential candidate for use in the development of polymeric materials based on graphene. However, incorporation into polymer matrices is still being studied today however, the problem of dispersion is the inability to incorporate graphene sheets in polymer matrices without problem.

Methodology

The graphite was mixed with the HDPE used a Brabender Plasticorder model k07-176/A, at 175 to 185 °C, 60 rpm and a mixing time of 15 min using concentrations of 3 and 5% wt. Additionally the synthesis of graphite oxide (GO) is performed by performing a pre-oxidación¹⁷ followed by an oxidation process using Hummers¹⁸ method, using as precursor graphite with particle size of $< 75 \mu\text{m}$.

Third US-Mexico Meeting "Advances in Polymer Science" and XXVII SPM National Congress Nuevo Vallarta December 2014.

GO particles were used to be incorporated into the HDPE matrix (at concentrations of 0.25, 0.5, 0.75 1.0% wt).

Characterization.

Techniques were used as Differential Scanning Calorimetry Modulated (MDSC) (TA Instruments) mode to measure the thermal conductivity of the compounds developed, analysis of dispersion and distribution of the particles in the polymer matrix for Optical Microscopy (MOP) using a Olympus BX-60 microscope using polarized light and scanning electron microscopy (TEM) in a scanning microscope JOEL JMS-741F field (Field Emission scanning electron microscope) using secondary electron detector SEI and a working distance between the lens sample target and 6.0 mm. The technique of spectroscopy, Fourier transform infrared (FTIR) was performed on a Nicolet 550 device, the chemical and structural information of the synthesized GO was obtained by the Raman spectroscopy technique, the distance between GO sheets once joined HDPE matrix was determined by diffraction (XRD) X-ray equipment using a SIEMENS model D-5000 with Cu Ka radiation with a Ni filter at 25 mA current and an accelerating voltage of 35 kV, Thermo gravimetric Analysis (TGA) was used to evaluate the thermal behavior of GO prepared from graphite powder.

Results.

From the micrograph obtained (Fig 1), one can observe that the particles have a flaked or flakes with a size that is on the order of microns.

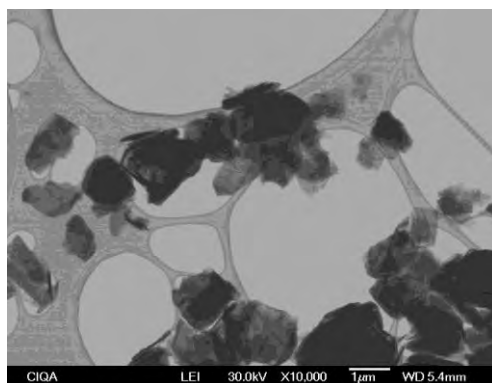


Figure 1. SEM micrograph of graphite powder a 10 000 magnifications with average particle size of the order of microns.

The results for light scattering (DLS) to the graphite particles without sonication are shown in the graph of Figure 2a, the analysis indicates that one has a particle size distribution in the range of $6\mu\text{m}$ to 2.87nm , recording a greater amount of particles with sizes of approximately $1.5\mu\text{m}$. For particles previously treated with ultrasound for a period of 30min, the results by DLS (Fig 2b) show that the particle size is reduced from $6\mu\text{m}$ to $1.3\mu\text{m}$ in addition to a greater amount of particles having sizes of approximately present with 800nm . By increasing the time of ultrasound graphite particles 1h, the analysis result (Fig 2c) shows a bimodal distribution in the particle size, whose maximum is located at $1\mu\text{m}$ and well quantified 700nm reaching sizes of up 4.5nm .

For compounds obtained from melt mixing a statistical analysis from optical micrographs, which takes into account an amount of approximately 1624 items per micrograph, at a total area per micrograph was performed $70599.56\mu\text{m}^2$.

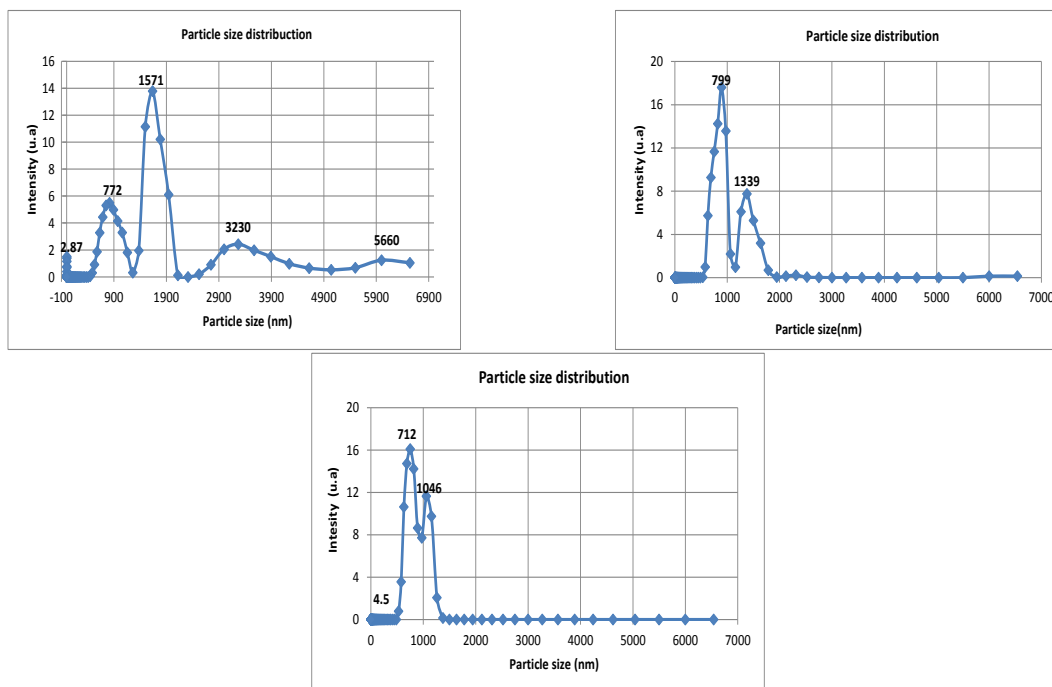


Figure 2. a). Graph of particle size distribution of graphite by Light Scattering without ultrasound treatment, b). Graph of particle size distribution by light scattering with ultrasound treatment for 30 min, c). Graph of particle size distribution by light scattering with ultrasonic treatment for 1 hr.

For these same systems can be observed qualitatively from the photomicrographs of Figure 3, a better particle distribution for HDPE/graphite system with a concentration of 3% wt at 175 °C which is attributed to that for melt blending cutting forces generated between the polymer and the particles helped improve the distribution and/or dispersion of particles in HDPE matrix with a size between 10 μm and 480 nm.

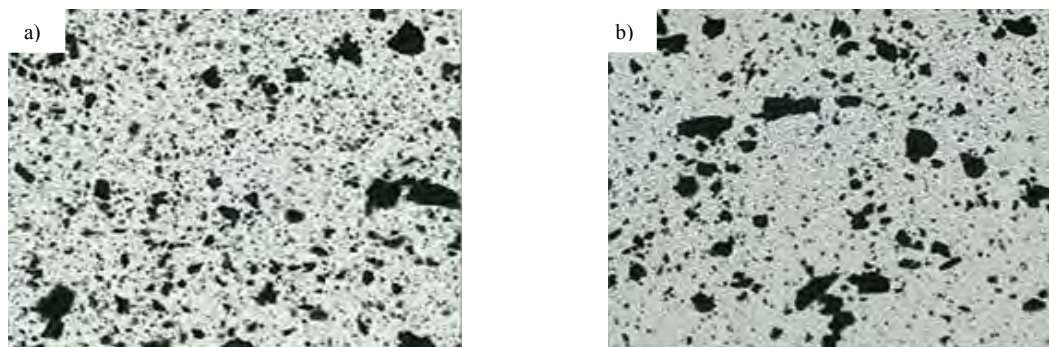


Figure 3. Micrographs obtained by light microscopy for HDPE/Graphite systems with 3 wt% a) at 175, b) at 185°C.

For HDPE/graphite system with 5% wt at 175 °C a 20 μm and 480 nm was obtained, obtained a minority of particles with sizes above 20 μm , qualitatively micrographs you can see only those particles which could not be dispersed in the matrix, that is the larger, which may affect the value of the thermal conductivity of the final compound (Fig 4).

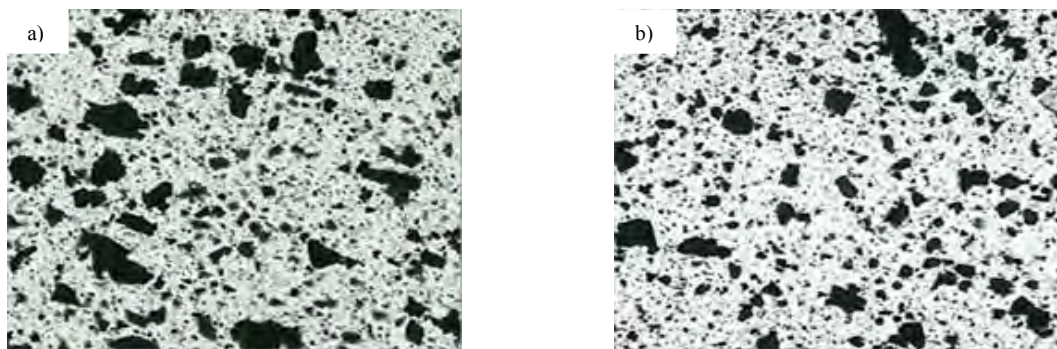


Figure 4. Micrographs obtained by light microscopy for HDPE / Graphite systems with 5% wt a) at 175 ° C b) at 185C.

Micrographs of the samples of HDPE/graphite compounds with 3 to 5% wt of graphite and 185 to 175°C in Figure 5, can be seen taken kind of graphite flakes in the mixture, noting that most micrographs a possible separation of the sheets forming the graphite occurs. In the images, only I could see fragmented parts of the particles with certain porosity, possibly the result of cutting forces generated during melt mixing, this can be attributed in part to the porosity of the particles prevents the chains HDPE freely penetrate between the sheets, making it difficult to increase the separation thereof by causing the polymer is at most around limiting particles that can carry out the intercalation of the compound and in turn to obtain a better dispersion of particulate HDPE matrix.

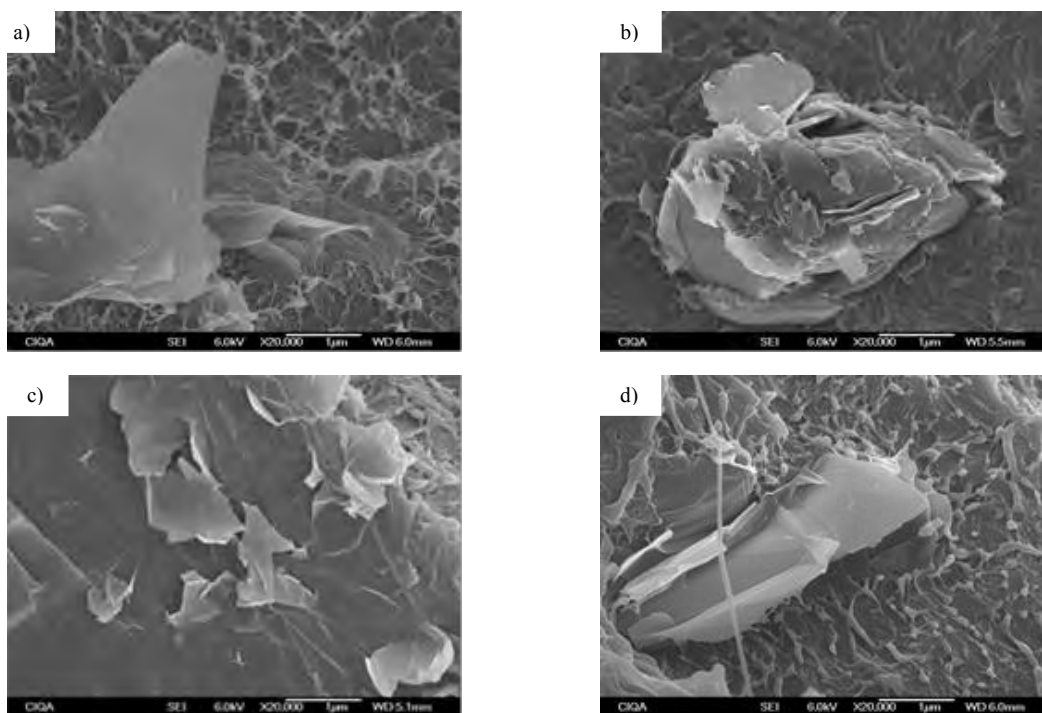


Figure 5. Micrographs obtained by scanning electron microscopy for HDPE / graphite system a) 3% wt at 175 ° C, b) 3% wt at 185 ° C, c) 5% wt at 175, d) 5% wt at 185.

In the diffractogram (Fig 6) shows that the graphite has a peak at $2\theta = 27.7^\circ$ which corresponds to approximately interlaminar spacing of the plane (002)²⁰. While for the pure PE two signals are observed at $2\theta = 21.49^\circ$ and $2\theta = 23.89^\circ$ which correspond to the planes (110) and (200), the signals that are recorded in all compound²¹. In the case of compounds HDPE/graphite to % wt at 175 and

185°C in Figure 8 shows that the intensity in the (002) plane which corresponds to PE shifts slightly to lower angles, This is attributed to the presence of graphite affects the crystalline structure of HDPE an increased graphitic sheets between the system being 3 wt% at 185°C (3.39Å) showing the greater spacing between the blades is shown. This is attributed to that at a higher temperature, the mechanical stresses generated during melt blending is best transmitted in the system, causing the polymer chains to penetrate between the layers of graphite causing interlaminar distance between particles increases. Graphite showed a broader signal (002) indicating that the crystal size is smaller in graphite²².

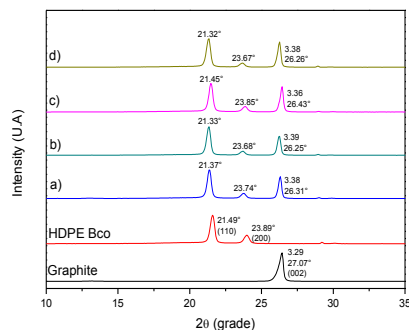


Figure 6. Diffraction patterns for the graphite powder and composite HDPE / graphite X-ray untreated graphite ultrasound; a) 3% wt at 175°C b) 3% wt at 185°C c) 5 wt% at 175°C and d) 5 wt% at 185°C. The values in the signals from the graphite powder

From an analysis of Differential Scanning Calorimetry modulated mode, in which the heat capacity were obtained, the thermal conductivity (k) was calculated in units of $W/(m \cdot K)$ of the polymeric compounds. In the graph of Figure 7, shows that the pure HDPE records a value of thermal conductivity of $0.357 W/(m \cdot K)$, which value was taken as a reference to see if a change occurs with respect to HDPE systems / graphite (a 3 to 5% wt). The graph shows for the composite processed at 185°C (blue line) the value of the thermal conductivity was increased to $0.597 W/(m \cdot K)$ using 5% wt of graphite, this indicates that the handle a higher temperature during mixing, allows the viscosity of the system decreases and the shear stresses are transmitted better helping the polymer is sandwiched between the sheets of graphite contributing to these distributed and dispersed throughout the polymer matrix, as a result obtains a higher thermal conductivity of the compound. Based on these results the HDPE / Graphite analyzed system (3% wt and 185°C), by subjecting graphite to a previous treatment with ultrasound for 1h and 30 min before being added to the molten polymer. The results show that increasing the time of ultrasound in graphite (purple line) the thermal conductivity with the system increases slightly to $0.693 W/(m \cdot K)$ HDPE which used a time of 30min ultrasound system, which has a thermal conductivity value of $0.664 W/(m \cdot K)$ (green line). From these results emerged that the handle 185°C temperature during melt mixing, causes HDPE molecules begin their molecular movement at a temperature between 125 and 130°C¹, temperature at which the polymer chains acquire more fluid, this causes the polymer chains are intercalated between the blades generating frictional graphite, helping to increase the interlaminar space, thereby improving the distribution and/or dispersion along the polymer matrix, increasing the thermal conductivity of the compound. In addition to that, the use of ultrasound long times graphite particles before being incorporated into the molten polymer allows a size distribution of smaller particle sizes, due to this the particles can generate a conductive network throughout the matrix²³, increasing the thermal conductivity of the final composite.

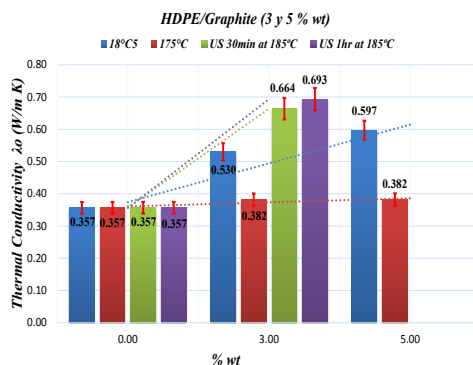


Figure 7. Analysis thermogram of thermal conductivity (MDSC) of HDPE / Graphite systems (3 and 5% wt of graphite and 185 to 175°C) with and without pretreatment gas phase to ultrasound for 30 min and graphite 1h.

Conclusions.

DLS results conducted by the graphite particles before being incorporated into the polymer melt show a reduction in size with increasing time of ultrasound. The micrographs of HDPE/graphite composites, show qualitatively that the graphite particles with untreated ultrasound, are distributed throughout the HDPE matrix, obtaining an increase in the thermal conductivity of the final compound. Statistical analysis from optical micrographs made to the HDPE / graphite composites developed with graphite pretreated with ultrasonic gas phase suggests that increasing time ultrasound particle size is reduced, which causes changes in the order of the graphite structure and thus a better distribution and/or dispersion of the particles in the HDPE matrix, reflected in an increase in the resulting thermal conductivity. With previous studies is possible to select the mixing conditions and the concentration of graphite which better dispersion and / or distribution is obtained for the particles to generate a conductive network throughout the HDPE matrix and obtain a thermally conductive compound.

References.

1. A.J.Peacock and M. Dekker, Distribution EH. Handbook of Polyethylene.; 2000:537.
2. R.Strumpler and J.G.Reichenbach. J. Electroceramics 1999;3(4):329-346.
3. K.Sever and H. Tavman. Compos. Part B Eng. 2013;53:226-233.
4. C. Sun and, W. Zhao Intersci. WILEY 2008;107:4000-4004.
5. S. Agarwal and M. Khan. Polym. Enginner ans Sci. 2008;48(12).
6. Sperling LH. INTRODUCTION TO PHYSICAL POLYMER. Wile-Inter.; 2006.
7. K. Chrissafis and K.M. Paraskevopoulos J. Appl. Polym. Sci. 2009;114:1606-1618.
8. Z. Sun and James DK, J. Phys. Chem. Lett. 2011;2(19):2425-2432.
9. M. B. Krishna and N. Venkatramaiah, J. Mater. Chem. 2012;22(7):3059.
10. A. Balandin and S. Ghosh Nano Lett. 2008;8(3):902-907.
11. H. Shioyama, Synth. Met. 2000;114(1):1-15.
12. H. Fouad and R. Elleithy , Mater. Des. 2011;32(4):1974-1980.
13. D.D.L.Chung, J. Mater. Sci. 1987;22:4190-4198.
14. G. Furdin, Fuel 1998;77(6):479-485.
15. A. Balandin and S. Ghosh, Carbon Nanostructures 2010;18(4-6):474-486.
16. B. Mortazavi and S. Ahzi, Carbon N. Y. 2013;63:460-470.
17. N. I. Kovtyukhova and P.J. Ollivier, Chem. Mater. 1999;11(3):771-778.
18. W. S. Hummers, J. Am. Chem. Soc. 1957;208(6):1937.
19. J. Chen and B. Yao, Carbon N. Y. 2013;64:225-229.
20. S. Cheng and X. Chen, Macromolecules 2012;45(2):993-1000.
21. T. Furukawa and H. Sato, Polym. J. 2006;38(11):1127-1136.
22. G. H. Chen and D. J. Wu, J. Appl. Polym. Sci. 2001;82(10):2506-2513.
23. Y. Li and D.Wu, J. Appl. Polym. Sci. 2007;106(5):3119-3124.

COMPARATIVE STUDY OF PLASTIC FILMS BONDED TO CELLULOSE AS A BILAYER MATERIALS

Magdalena Trujillo¹, Alejandro Vargas¹,
Alfredo Maciel², Marissa Morales²

¹ *Universidad Nacional Autónoma de México, Facultad de Ingeniería, México.*

² *Universidad Nacional Autónoma de México, Instituto de Investigaciones en Materiales, México*

Abstract

A comparative study between films made of polyethylene/cellulose trilayer material and polylactic acid/cellulose bilayer material was done in this work. Both materials were studied using a peeling test to evaluate and compare the mechanical properties and the required force to separate the layers. Bilayer material polylactic acid/cellulose was manufactured by rolling. The rolling process was designed with variations of pressure, temperature and speed for this new polylactic acid/cellulose material previously prepared. Furthermore, an analysis by scanning electron microscopy was performed to determine the morphological, bonding and geometrical characteristics of bilayer materials studied.

Introduction

The consumption of non-biodegradable plastics can hardly be recycled and has increased over the past years. Thus, the accumulation of conventional plastics has become a potential risk to contamination the environment. Biodegradable plastics, which are derived from renewable sources like polylactic acid (PLA), are being investigated to prevent this situation [1][2]. The aim of this work was to prepare and characterize a bilayer film of cellulose/PLA, as a probable solution to decrease the use of non-renewable materials.

Experimental

Materials. Polylactic acid (PLA) 2003D was purchased from Natureworks. The previous characterization of this polymer show a molecular weight (Mw) of 225 670 g/mol with a polydispersity index of 1.77, the determination of these values were made by Gel Permeation Chromatography (GPC). The melting temperature (Tm) and the glass transition temperature (Tg) were determined with Modulated Differential Scanning Calorimetry (MDSC) and the values were 61 °C and 154.05 °C, respectively. The decomposition temperature was 366.4 °C and was determined by Thermogravimetric Analysis. The Young's modulus was 901 ± 123 MPa with an ultimate deformation of 158%, these values were determined by the ASTM D-1708 Standard test method for tensile properties of plastics by use of microtensile specimens.

Scanning Electronic Microscopy. A cross section of the layers were characterized with scanning electron microscopy (SEM) using Jeol JSM-7600F. Specimens were sputtered with gold.

Peel resistance test. The bonded materials were tested in order to determine the resistance of the adhesive. The test conditions were used as the ASTM D-1876-95 Standard test method for peel resistance of adhesives (T-peel test). The strain rate was 254 mm/min, the room temperature was 23 °C and the relative moisture was 50%. The figure 1 shows the dimensions of the specimens.

For the PLA/paper the width of the specimens was 19.06 ± 0.58 mm.

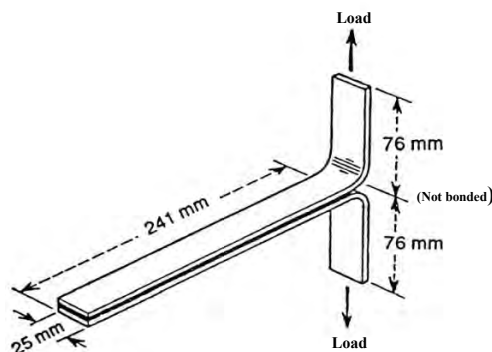


Figure 1. Specimens for T-peel test.

Results and Discussion

SEM micrograph of the film polyethylene/paper shows two well-defined layers, one that corresponds to the cellulose layer of paper and the other one to the plastic film of polyethylene (Figure 2). By the same technique the cross section of the polyethylene film (Figure 3) was seen, which is composed by two layers one is polyethylene and the other one the adhesive that is the copolymer ethylene-vinyl acetate. The adhesive layer is used to bond polyethylene and the paper surface.

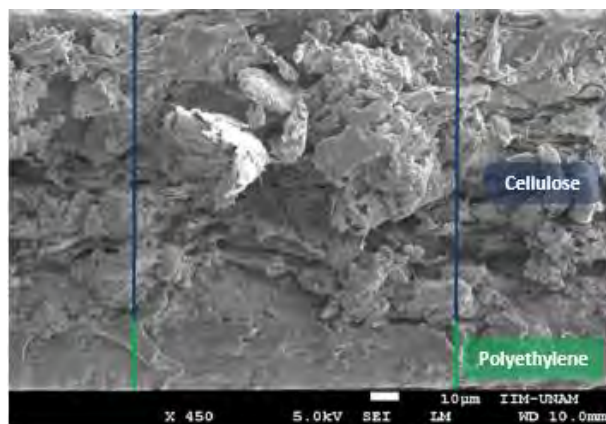


Figure 2. SEM of reference material.

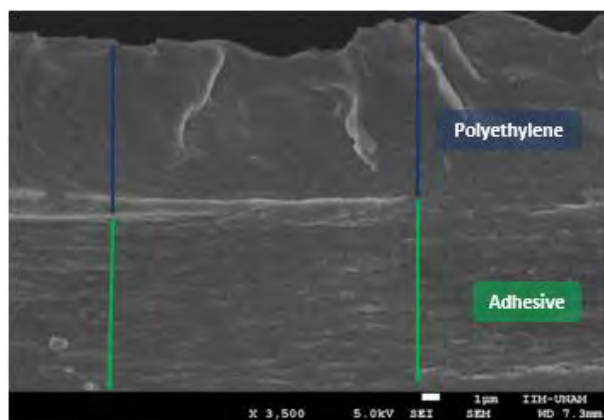


Figure 3. SEM of the plastic film of polyethylene.

The adhesive strength between the flexible layers (Polyethylene/paper), was performed in a peel test, where it was observed three different failures, which are shown below (figure 4).

In the first case (figure 4a) it can be seen a substrate failure of the polyethylene. At the start of test, the polyethylene film removed the paper pigments. By the middle of the specimen, the

adhesion was so strong that the polyethylene layer remained bonded to the paper layer until it broke in a diagonal way. The frequency of this type of failure was 10% and the recorded peel strength was 3.33 ± 0.22 N/cm.

The second case (figure 4b) showed a substrate failure of the paper layer. In the beginning of the test, it was observed that the polyethylene layer removed paper pigments, in the second stage of the test the cellulose fibers were detached until the paper was broke. The frequency of this type of failure was 70% and the recorded peel strength was 2.11 ± 0.26 N/cm.

In the third case (figure 4c) it was observed an intermediate failure, in the first stage the paper substrate failed and subsequently the adhesive failed, because all the polyethylene layer was separated from the paper layer. The adhesive was not strong enough to retain the paper pigments in the final zone. The frequency of this type of failure was 20% and the recorded peel strength was 3.93 ± 0.16 N/cm.

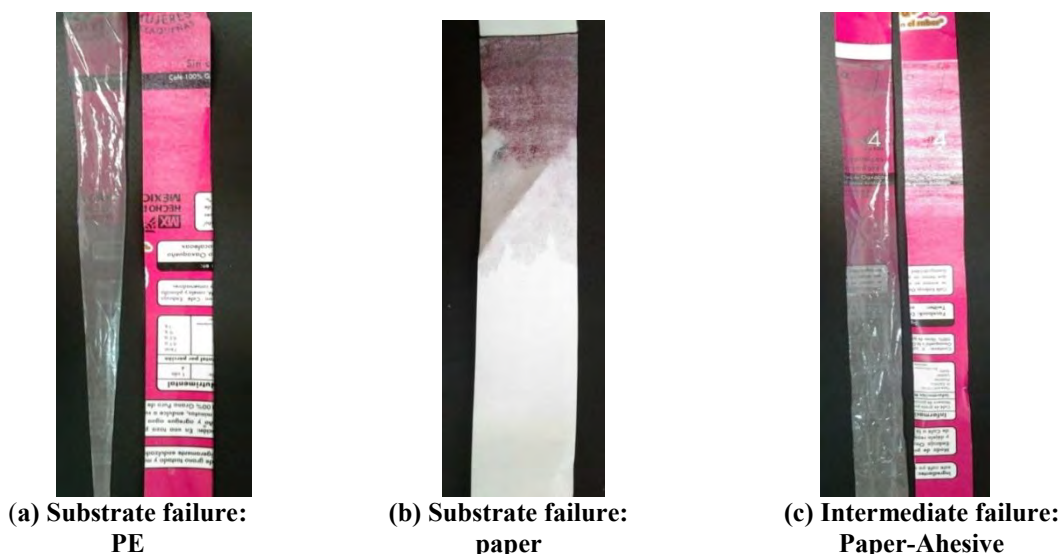


Figure 4. Adhesion failure types in the reference material

A biodegradable polymer, polylactic acid (PLA), was used to replace the polyethylene film. A PLA film was obtained through the process of film extrusion, the thickness of the film was 0.33 ± 0.025 mm and the width was 19.06 ± 0.58 mm.



Figure 5. PLA film obtained.

In order to obtain a bonded material (PLA/paper) these two materials were adhered through a thermal laminate process with constant pressure. The variation of bonding temperature was

analyzed and once the PLA-paper bilayer material was joined, a peel test was done with the purpose of measure the adherence between the layers of the new bilayer material. The effect of rising the adhesion temperature resulted in a curve, where it can be seen that the peel strength growth with the temperature until it reached a peak and then sharply decreased (Figure 6).

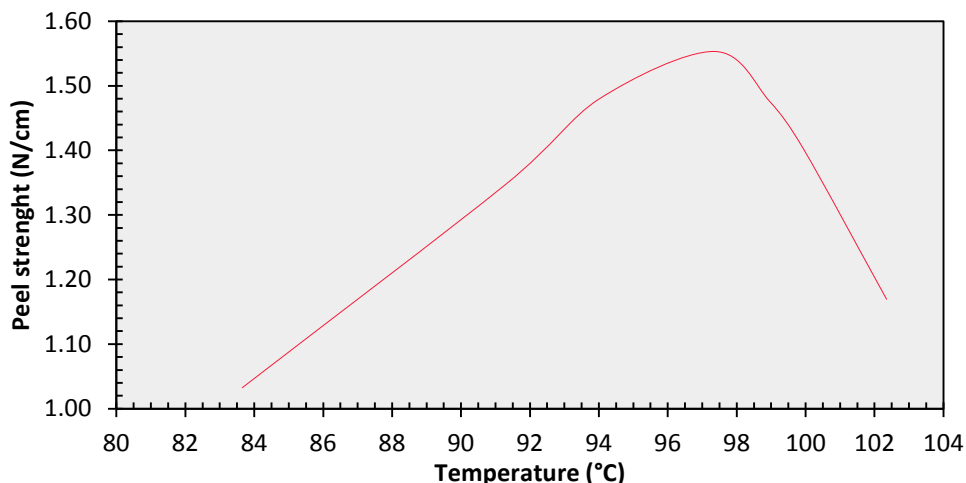


Figure 6a. First peel strength due to the increment of the adhesion temperature.

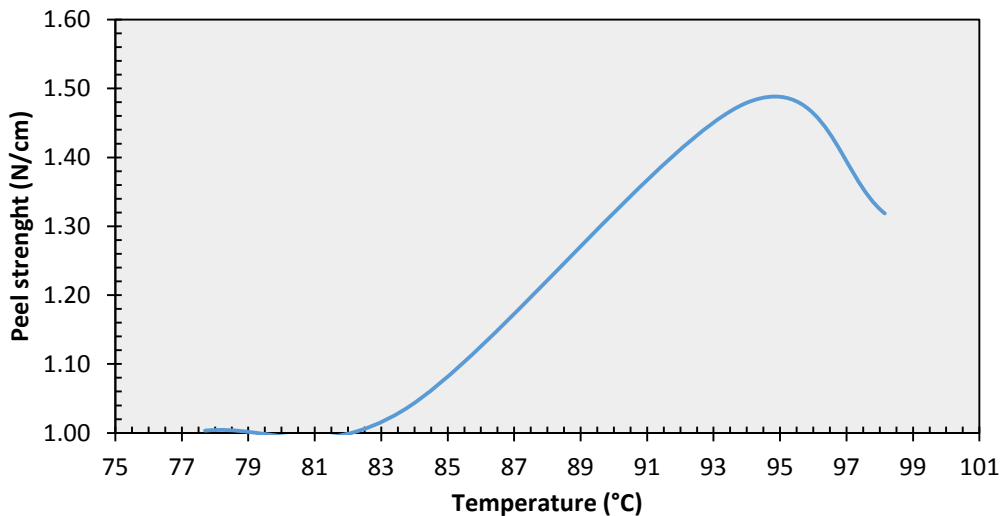


Figure 6b. Second peel strength due to the increment of the adhesion temperature.

The maximum adhesive strength registered between the flexible layers (PLA/paper), was 1.55 N/cm, and it was observed a failure due to the paper substrate.

Conclusions

The SEM micrographs showed that the polyethylene film bonded with paper is composed of three layers. The mean thickness of the paper layer is $109.25 \pm 1.32 \mu\text{m}$ and the polyethylene film (EVA-PE) is $19.32 \pm 1.01 \mu\text{m}$, where the PE has a thickness of $9.41 \pm 0.72 \mu\text{m}$ and the adhesive (EVA) is $10.04 \pm 0.36 \mu\text{m}$. The most frequent adhesive failure was when the paper substrate fails with a peel strength of $2.11 \pm 0.26 \text{ N/cm}$.

A successful adhesion between the paper and the biodegradable PLA film was attached, through a laminate process under conditions of pressure and temperature. The peel test of the bilayer material PLA-paper, showed that the rising bonding temperature increased its adhesion, until a maximum point, where after the peak the peel strength decreases due to a film shrinkage causing folds in the paper layer.

Acknowledgements

This work was performed with support of Consejo Nacional de Ciencia y Tecnologia (CONACYT), project 199132

By the support given to characterization of materials: I.Q. Ernesto Sanchez Colin, Dr. Omar Novelo Peralta, Q.F.B. Damaris Cabrero Palomino, M.C Salvador Lopez Morales.

References

- [1]R. Tharanathan, «Biodegradable films and composite coatings: past, present and future,» Trends in food science and technology, n° 14, pp. 71-78, 2003.
- [2]M. K. Nampoothiri, N. R. Nair y R. P. John, «An overview of the recent developments in polylactide (PLA) research,» Bioresource Technology, n° 101, pp. 8493-8501, 2010.
- [3]M. J. Kirwan, Handbook of paper and paperboard packaging technology, London: Wiley-Blackwell, 2013.
- [4]G. L. Robertson, Food packaging. Principles and practice., 3 ed., United States: Taylor & Francis Group, LLC, 2013.
- [5]S. Ebnesajjad, Handbook of biopolymers and biodegradable plastics: properties, processing and applications, United States: ELSEVIER, 2013.

OPTIMIZATION OF A POLYMER BLEND BASED ON RECYCLED POLYSTYRENE AND STYRENE-BUTADIENE RUBBER

Justine Veilleux,¹ Denis Rodrigue,¹

¹ *Université Laval, Department of Chemical Engineering, Quebec City, Quebec, Canada, G1V 0A6.*

Abstract

In this work, polymer blends based on recycled polystyrene (PS) and styrene-butadiene rubber (SBR) are produced by twin-screw extrusion over a wide range of SBR concentration (0-62% wt.). In particular, a solution treatment of SBR particles is proposed to improve compatibility and mechanical properties of the recycled PS/SBR blends. From the compounds produced, a complete morphological, physical (density and hardness) and mechanical (tension and impact) characterization is performed to determine the level of interaction between both polymers. The results indicate that the proposed treatment can substantially improve the quality of the blends.

Keywords: polystyrene, styrene-butadiene rubber, recycling, extrusion.

Introduction

Today, several polymers are still unfortunately discarded (landfill or incinerated) after their use due to difficulty in recycling them or to find economical applications. Since most of them do not decompose under standard conditions, this causes some environmental problems because of accumulation [1]. Two good examples are expanded polystyrene (PS) from packaging and styrene-butadiene rubber (SBR) mainly encountered in waste tires. PS is actually a good candidate for recycling, but the main drawback is low density leading to high transport costs; i.e. high amount of space [2]. For SBR, the crosslinked structure giving rubber its elasticity and stability substantially decreases its recyclability in other applications. The best recycling way would be to devulcanize the rubber (at least partially), but the process is energy intensive and produces wastes. It is also expensive to run [1]. It is thus interesting to find other alternatives being faster and cheaper to perform at industrial scale. One way to recycle both polymers would be to blend them and produced a thermoplastic elastomer (TPE). These resins have both the characteristics of thermoplastic processing, while having the mechanical properties of a vulcanized material [3].

In the literature, a limited number of articles have been published on TPE made from PS and SBR, but most of them used virgin polystyrene [1, 4-5]. Nevertheless, some of them used recycled PS [6-7]. These works clearly showed that poor miscibility between both materials led to very low mechanical properties. To improve on these results, additives were added while blending [4-5], or chemical rubber modifications were proposed [1]. So, the objective of this study is to propose methods to improve the compatibility between both recycled materials (expanded PS and SBR) using two different processes. First, optimization of the blending step is performed based on a similar work done on recycled ethylene-propylene-diene monomer (EPDM)/polypropylene (PP) blends [8]. In this case, introduction of the SBR particles in the first zone of a twin-screw extruder will apply some thermo-mechanical energy to partially devulcanize the surface of the particles leading to more chain mobility and possible entanglement with the matrix molecules. The second method is to perform a solution treatment of the SBR particles before going to the extrusion step [9]. In this case, the idea is to swell SBR particles with a solvent to force the diffusion of dissolve PS molecules to penetrate the crosslinked structure.

Experimental

The polystyrene used was recycled expanded polystyrene from packaging applications with an average molecular weight of 217 kg/mole, a density of 90 kg/m³ and melt flow index of 20 g/10 min (200°C and 5 kg) and supplied by Ameublement Tanguay (Canada). The material was grounded to reduce particle size below 5 mm. The SBR rubber powder was provided by Royal Mat (Canada) and sieved to keep only particles below 710 microns (fine powder). For the solution treatment, toluene (ACS reagent grade from Anachemia) was selected after previous trials in terms of SBR swelling potential and PS solubility.

Extrusion was done on a co-rotating 27 mm twin-screw extruder from Leistritz USA (ZSE-27). This extruder as a L/D ratio of 40 with 10 heating zones and coupled with a circular die (3 mm diameter). As described in a previous study [8], the SBR powder was fed to the first zone (main feeder) of the extruder, while polystyrene was added through a side-stuffer in zone 4. The screw speed was fixed at 100 RPM and the temperature profile was increased from 160 to 175°C from the main feed to the die exit.

The extruded compounds were then cooled in a water bath and pelletized. Finally, the compounds were injection molded in a laboratory machine Nissei PS60E9ASE (Japan). The injection temperature profile in the screw was set between 190°C and 200°C with a mold temperature of 30°C. The mold dimensions were selected to produce directly the geometries needed for all the characterization.

For the solution treatment step, the recycled polystyrene was first dissolved in toluene under mixing (mechanical stirrer) at a concentration of 10% w/v and 25°C. Then, the SBR powder was added to get a solid concentration of 20% w/v. Mixing was left overnight to get maximum swelling and PS penetration into SBR particles. The solution was filtered in a Buchner with a coffee paper filter. Finally, the filtered solid was dried in an oven at 60°C before use.

Scanning electron microscopy (SEM) was used to study the morphology of the blends in terms of particle dispersion and adhesion. Each sample was fractured in liquid nitrogen and the exposed surfaces were coated with a gold/palladium alloy. Then, a JEOL model JSM-840A scanning electron microscope was used to take micrographs at a voltage of 15 kV. Density measurements were performed using a nitrogen gas pycnometer model Ultrapyc 1200e from Quantachrome Instruments (USA). For each sample, the test was repeated 5 times and the averages are given with standard deviations of less than 1%. Hardness was measured according to the shore D scale (thermoplastics) with a model 307L durometer. The reported values are the average of twenty-five measurements. Tensile tests were performed on an Instron model 5565 universal testing machine with a 500 N load cell. Type V dog bone samples were used as described in ASTM D638. Testing was done at 1 mm/min and room temperature. At least five specimens were used to report the average with standard deviation for Young's modulus, tensile stress at break, and tensile elongation at break. Charpy impact strength was obtained with a pendulum weight of 242 g (1.22 J) on a Tinius Olsen testing machine model Impact 104. The arm length was 279 mm leading to an impact speed of 3.3 m/s. Rectangular samples (60 x 10.15 x 3 mm³) were notched by an automatic sample notcher model ASN (Dynisco, USA) at least 24 hours before testing (ASTM D6110). All the tests were performed at room temperature and the results are the average of at least ten measurements.

Results and Discussion

Figure 1 presented typical SEM micrographs of two selected compounds. First, from the picture at 250X, is possible to observe the contact between SBR particles and the PS matrix. Also, no void or defect can be seen. The images on the left (mechanical treatment) seem to indicate that good contact between the SBR particles and the PS matrix was obtained, but while producing the samples via cryogenic fracture, poor adhesion led to some detachment between both phases and crazing in PS occurred. On the other hand, the images on the right (solution treatment) show that good contact and good adhesion was obtained via the solution treatment since a blurred interphase seems to have been created between both phases.

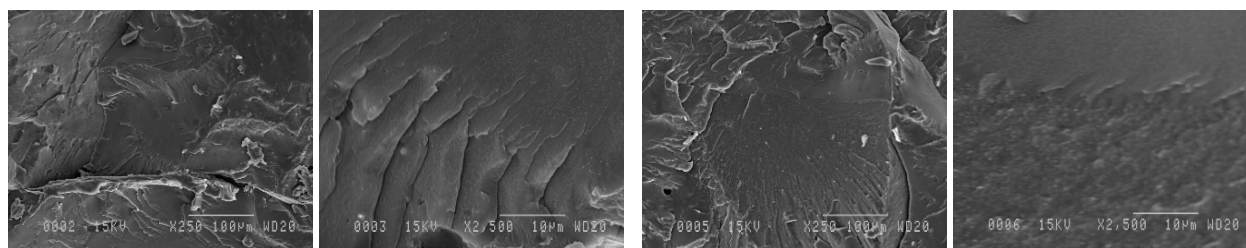


Figure 1: SEM micrographs at different magnifications for 23% SBR produced by a mechanical treatment (left ones) and 24% SBR produced by a solution treatment (right ones).

Figure 2 presents the density of the compound as a function of SBR content. As expected, density increases with SBR content since the density of SBR is higher than the density of compact PS ($1060 \pm 8 \text{ kg/m}^3$). There is a slight difference between both treatments because the density of the neat SBR particles ($1252 \pm 11 \text{ kg/m}^3$) is higher than SBR particles after the solution treatment ($1229 \pm 11 \text{ kg/m}^3$). This might be related to some materials (additives and low molecular weight compounds) that were extracted during the solution treatment and/or swelling of the rubber which increased in volume and was filled with a lower density material; i.e. PS. Finally, Figure 2 shows that hardness decreases with increasing SBR content. As expected, the addition of more elastomer particles in the hard PS matrix will decrease the hardness of the resulting blends. Again, the results show that the solution treatment gives harder materials, probably because of hard PS molecules that were introduced inside the SBR particles, thus increasing the hardness of the dispersed phase.

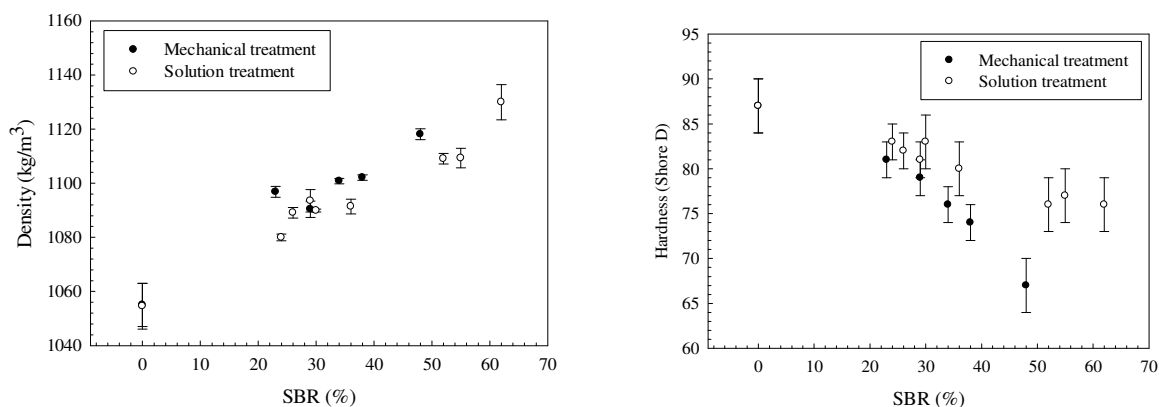


Figure 2: Density (left) and hardness (right) as a function of SBR content.

Tensile results as a function of SBR content are presented in Fig. 3. It can be seen that adding an elastomer phase (SBR) decreases both rigidity (modulus) and strength (stress) since SBR is an elastomer compared to the rigid PS matrix. In all cases, the solution treatment increased substantially the values compared to simple mechanical blending alone. This indicates that better stress transfer at the PS-SBR interface can be associated to the presence of PS molecules acting as mechanical anchoring points between both phases and improving compatibility. Without the solution step, the crosslink rubber particles have limited compatibility with the matrix as reported by Higazy et al [4]. In general, the values of Young's modulus are 20% higher when the solution treatment was applied. Similar trends for tensile stress at break are observed. On the other hand, a complex behavior was observed for the tensile elongation at break. The results obtained seem to indicate a possible maximum at low SBR concentrations (not tested due to time limitations). This can be explained by increasing elasticity of the material at low SBR content resulting from the replacement of brittle PS by more elastic SBR. But as SBR content increases, there is probably not enough matrix to get good dispersion and since the matrix is very brittle, elongation at break decreases. Nevertheless, more work would be needed to fully understand this behavior.

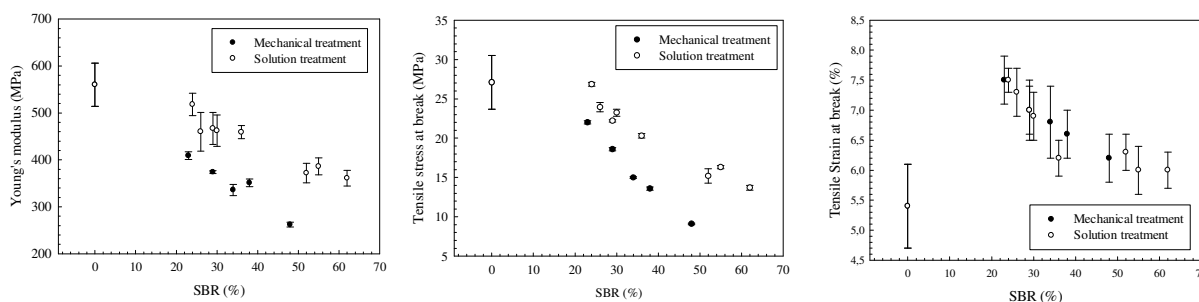


Figure 3: Young's modulus (left), tensile stress at break (middle), and tensile strain at break (right) as a function of SBR content.

Figure 4 shows that Charpy impact strength increases with the introduction of an elastomer phase (SBR) in the brittle PS matrix. In this case, it can be seen that higher impact strength was obtained without the preliminary solution treatment. This again can be related to stress transfer between the phases. The solution treatment produces more rigid compounds (see Figure 2) being more brittle. The presence of PS in the rubber particles reduced their ability to absorb the impact energy leading to less resilient compounds compared to the ones produced by the mechanical treatment.

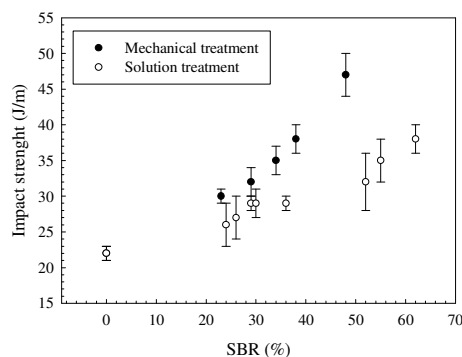


Figure 4: Impact strength as a function of SBR content.

Conclusions

In this study, the effect of recycled styrene-butadiene rubber (SBR) concentration (0-62% wt.) on the properties of recycled polystyrene (PS) was studied. In particular, two different treatments were used to produce the compounds by twin-screw extrusion and injection molding. First, the SBR particles were directly fed in the first zone of the extruder, while PS was introduced in the fourth zone via a side stuffer. Second, the SBR particles were first treated in a PS/toluene solution to introduced PS molecules inside the crosslink rubber structure to improve compatibility when mixed with a PS matrix. In this case, the same blending procedure was applied to produce the compounds as for untreated SBR particles. For each SBR concentration, a complete morphological, physical (density and hardness) and mechanical (tension and impact) characterization was done. From the results obtained, the following conclusions can be made:

- Young's modulus, tensile stress at break, and hardness decreased with increasing rubber content, while impact strength and density increased with SBR addition. This is related to the introduction of an elastomer phase in a rigid matrix.
- Although good contact can be seen in SEM micrographs (no defect or void), good adhesion and compatibility was only obtained for SBR particles treated in solution. This can be inferred from the differences observed in terms of mechanical and physical properties.
- From the results obtained, a wide range of properties can be produced by careful selection of the blend composition (SBR/PS), as well as the dispersed phase surface treatment.

Acknowledgements

Financial support was obtained from the Natural Sciences and Engineering Research Council of Canada (NSERC), while PS and SBR were kindly provided by Ameublement Tanguay and Royal Mat, respectively. Finally, technical help from Mr. Yann Giroux, CERMA, CQMF and CREPEC is acknowledged.

References

- [1] J. Karger-Kocsis, L. Meszaros, T.J. Barany, Mater. Sci., 48(1), 1-38 (2013).
- [2] S. Acierno, C. Carotenuto, M. Pecce, Polym.-Plast. Technol., 49(1), 13-19 (2010).
- [3] O.P. Grigoryeva, A.M. Fainleib, A.L. Tolstov, O.M. Starostenko, E. Lievana, J. Karger-Kocsis, J. Appl. Polym. Sci., 95(3), 659-671, (2005).
- [4] A.A. Higazy, H. Afifi, A.H. Khafagy, M.A. El-Shahawy, A.M. Mansour, Ultrasonics 44, E1439-E1445 (2006).
- [5] J.L. Zhang, H.X. Chen, Y. Zhou, C.M. Ke, H.Z. Lu, Polym. Bull., 70(10), 2829-2841 (2013).
- [6] D. Ciesielska, P. Liu, Jaut. Gummi. Kunstst, 53(5), 273-276 (2000).
- [7] M. Tasdemir, E. Ulug, Polym.-Plast. Technol., 51(2), 164-169 (2012).
- [8] P. Mahallati, D. Rodrigue, Int. Polym. Proc., 29(2), 280-286 (2014).
- [9] A. Macsiniuc, A. Rochette, J. Brisson, D. Rodrigue, Prog. Rubber Plast. Recyc., accepted (2014).

MESOMORPHIC AND OPTICAL PROPERTIES OF IONIC LIQUID-CRYSTALLINE COPOLYMERS

Rosa Julia Rodríguez-González,¹ Christyan de Santiago-Solís,¹ Olga Lidia Torres-Rocha,¹
Leticia Larios-López,¹ Geminiano Martínez-Ponce,³ Dámaso Navarro-Rodríguez,¹

¹ Centro de Investigación en Química Aplicada, Blvd. Enrique Reyna H. 140, 25253 Saltillo Coahuila, México.

² Centro de Investigaciones en Óptica A. C. Apdo. Postal 1-948, 37000 León Guanajuato, México

Abstract

Ionic liquid-crystalline copolymers were synthesized through a partial quaternization of P4VP with a highly anisotropic azomesogen (CN12,6). The thermal stability was determined by TGA and was above 250°C. The thermotropic behavior was evaluated by DSC, POM and XRD. DSC and POM results were not conclusive; however XRD showed that these copolymers develop a smectic type mesophase. On the other hand, optical properties were induced with a 460nm excitation laser beam, using a 633nm laser beam as a probe. Despite of the low light-induced birefringence, it was possible to register a regular surface relief grating with an average depth of 100nm.

Introduction

Solid materials can exhibit liquid-crystalline properties by the effect of changes in temperature or temperature/concentration. The first case corresponds to thermotropic liquid crystals, which have attracted great attention due to their numerous technological applications in optics and optoelectronics. The other kind of liquid crystals is named lyotropic, and they are mainly applied in biotechnological and biomedical areas. Molecules showing both behaviors have attracted the attention of scientists because, combined with nanoscale particles, allow new potential applications in different fields (optics, optoelectronics, biomedical, and others). Ionic liquid crystals are amphiphilic molecules that can develop both lyotropic and thermotropic liquid crystal order. Pyridine and Poly(vinylpyridine) (PVP) quaternized with mesogenic groups are good examples of thermotropic/lyotropic liquid crystals. PVP is capable to electrostatically interact in quaternized or protonated forms with charged surfaces, and also is able to undergo hydrogen bonding with polar species [1-5]. PVP modified with azobenzene groups (mesogens) can show liquid crystal properties and photo-induced alignment. The combination of these two properties in one material is interesting for many applications such as photomechanical actuators, optical data storage, and holographic recording. Recently, poly(4-vinylpyridine) (P4VP) substituted with azobenzene groups have been irradiated to obtain surface relief gratings (SRG). In most cases, P4VP-azobenzene are complexes formed through hydrogen bonding interactions, and in few cases they are covalently linked P4VP- azobenzene materials, having ionic pyridinium groups [6-8]. In this work we present and discuss results on the liquid-crystalline properties and light-induction of SRGs of partially quaternized P4VP with azobenzene groups. These copolymers are potential materials for holographic data recording.

Experimental

All reagents were purchased from Aldrich Co. and/or J. T. Baker and used as received unless otherwise specified. THF was dried over a sodium/benzophenone complex. The azomesogen and P4VP were synthesized according to reported procedures [9-10]. P4VP was synthesized by free-radical polymerization (azobisisobutyronitrile as initiator) to further partially quaternized with

azocompound in concentrations of 30 and 50wt% of azomesogen (CN12,6). The thermal stability of copolymers was determined in vacuum dried samples using a TGA 951 thermal analyzer from DuPont Instruments. Differential scanning calorimetry (DSC) traces were obtained in a MDSC 2920 from TA Instruments. The structure of the mesophases was determined from X-ray diffraction analysis obtained with an SWAXS from Anton Paar equipped with a sample holder unit, an image plate detector, and a temperature control unit. Each sample was sealed in a Lindeman glass capillary. X-ray patterns were captured at different temperatures upon cooling from the isotropization temperature. Thin films (300-450 nm) were prepared by spin-coating as follows: 90 μL of a polymer solution (40 mg/mL in chloroform) was deposited onto a clean glass substrate at a spinning rate of 500-2000 rpm. Films were irradiated with an interference pattern employing a Lloyd arrangement to record a SRG. A 460 nm laser beam was split into two equal intensity beams but with a different polarization state (right/ left circularly polarized light). The irradiation time for all samples was 60 seconds. SRGs were analyzed by polarized optical microscopy (POM) with an Olympus BX53 microscope.

Results and Discussion

Thermal Stability

The thermal stability of copolymers was analyzed by TGA in the temperature range of 30 to 800. Results were compared with that of pure P4VP (figure 1a). In both polymers a first weight loss before 100 °C was observed. This weight loss was attributed to traces of moisture because of the high hydrophilic character of pyridinium groups [8]. More relevant is the lower thermal stability of copolymers as compared to the pure P4VP. Despite the important decrease in thermal stability, degradation occurred at a still relatively high temperature (around 250 °C) to perform the thermotropic characterization.

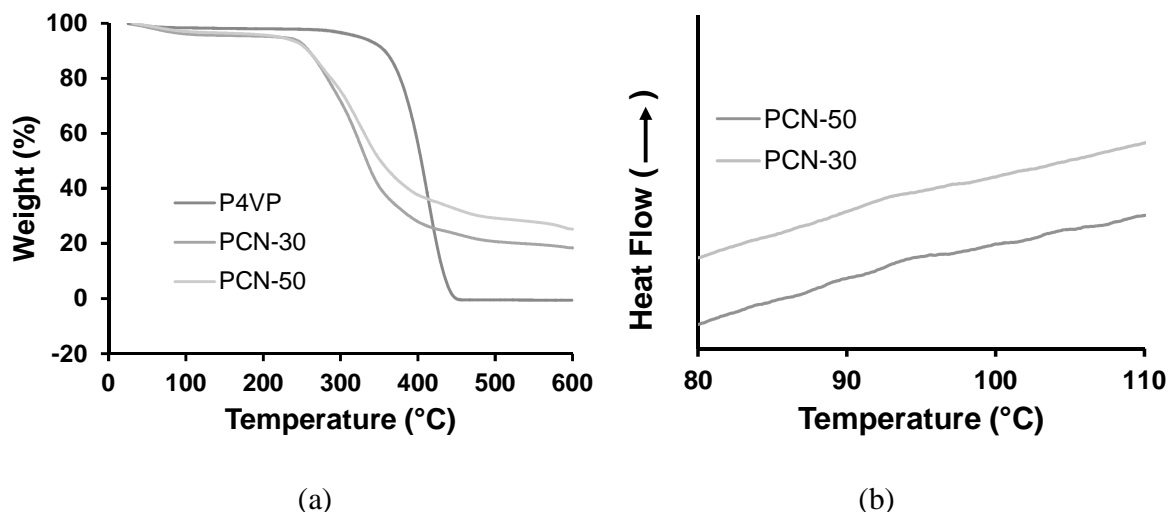


Figure 1. (a) TGA curves for pure P4VP and the copolymers PCN-30 and PCN-50, recorded at a rate of 10 °C min⁻¹ under N₂ atmosphere. (b) DSC traces (80 to 125 °C interval) corresponding to the second heating (10 °C/min) of PCN-50 and PCN-30.

Thermotropic behavior

Thermal transitions of copolymers were determined by differential scanning calorimetry (DSC). The azomesogen (CN12,6) here employed was reported [12] as a liquid crystal azocompound with an isotropic-smectic A (SmA) phase transition at 151°C (labeled as Mes12 in the published manuscript). We used a previously synthesized low molecular weight P4VP (22,000 g/mol determined by solution viscosimetry in ethanol at 25°C [10] showing a glass transition temperature (T_g) around 130°C. Normally, a high molecular weight P4VP is amorphous and shows a T_g around 140°C [8]. The P4VP partially functionalized with azomesogens shows a transition around 95°C, which can be attributed to a T_g (figure 1), taking into account that the azomesogen can act as a plasticizer [8]. Contrary to what was expected for a P4VP modified with liquid-crystalline precursors (CN12,6), no other transitions were perceived in the DSC traces. To determine if copolymers exhibit liquid crystalline order, they were analyzed by X-ray diffraction (XRD) analysis. This characterization revealed that copolymers showed lamellar order typical of smectic type phases. At low angles, diffraction patterns showed a sharp Bragg peak associated to the lamellar spacing, whereas at wide angles they displayed a single broad diffraction peak, indicating non-order within the smectic layers. To determine if molecules are parallel or tilted with respect to the normal of the smectic plane, the lamellar spacing (d_{001}) was compared to the theoretical length of the molecule (L) in its most extended conformation (calculated by modeling software from SPARTAN 2010) [9]. Calculated d_{001}/L ratios seem indicate a double layer stacking with molecules tilted with respect to the smectic plane (SmC), however, there exist a possibility that mesogens are parallel to the normal to the smectic plane (SmA) but interdigitated from one chain to the other as proposed in a previous work [9]. Results are presented in table 1.

Table 1. Structural parameters calculated from the XRD spectra obtained at different temperatures.

Copolymer	L (Å)	d (Å)	d/L
PCN-30	45.655	66.07	1.45
PCN-50	45.655	69.44	1.52

Surface relief gratings

Holography data storage is one of the most important applications of this kind of materials. To test if these polymers are candidates for this application several SRGs were recorded by using an arrangement of two laser beams ($\lambda = 460$ nm and circularly polarized) as described in a previous work [13]. In both copolymers, it was possible to record SRGs, as shown in POM images of figure 2. These stripe-like images show a more regular grating for PCN-30 than for PCN-50. The high concentration of mesogens in PCN-50 is favorable to the formation of aggregates that may affect the optical response. PCN-30 may be a good candidate for holography data storage.

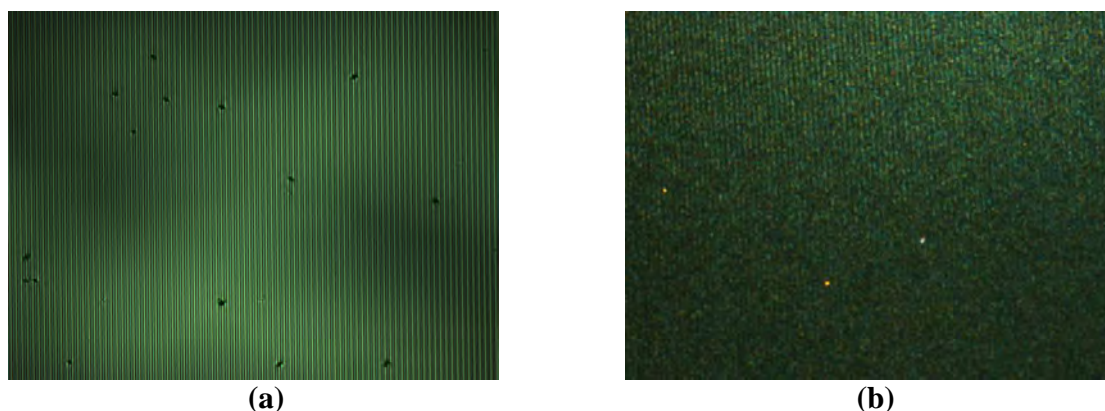


Figure 2. POM images of surface relief gratings of (a) PCN 30, and (b) PCN-50.

Conclusions

Ionic copolymers were synthesized through the quaternization reaction of P4VP with azomesogens at 30 and 50wt%. These materials presented good thermal stability and displayed a liquid crystalline behavior of the smectic A type, as demonstrated by X-ray diffraction. Finally, PCN-30 developed good quality SRGs with minimum of aggregates. Results showed that these materials are promising for holography data storages.

Acknowledgements:

This work was supported by CONACYT, México (Projects 130902 and 157652). Authors thank to Guadalupe Méndez Padilla for her technical assistance.

References

- [1] K.V. Axenov and S. Laschat, *Materials*, 4, 206 (2011).
- [2] F. Camerel, B. Donnio, C. Bourgogne, M. Schmutz, D. Guillon, P. Davidson and R. Ziessel, *Chem. Eur. J.*, 12, 4261 – 4274 (2006).
- [3] A. Bubnov, M. Kaspar, V. Hamplová, U. Dawin and F. Giesselmann, *Beilstein J. Org. Chem.*, 9, 425–436 (2013).
- [4] S. Malynych, I. Luzinov and G. Chumanov, *J. Phys. Chem. B*, 106, 1280–1285 (2002).
- [5] H. Dong, E. Fey, A. Gandelman and W. E. Jones Jr., *Chem. Mater.*, 18, 2008–2011 (2006).
- [6] A. Priimagi, J. Vapaavuori, F.J. Rodriguez, C.F.J. Faul, M.T. Heino, O. Ikkala, M. Kauranen and M. Kaivola, *Chem. Mater.* 20, 6358–6363 (2008).
- [7] J. Vapaavuori, V. Valtavirta, T. Alasaarela, J. Mamiya, A. Priimagi, A. Shishido and M. Kaivola, *J. Mater. Chem.* 21, 15437–15441 (2011)
- [8] J. del Barrio, E. Blasco, L. Oriol, R. Alcalá and C. Sánchez-Somolinos, *J. Polym. Sci., Part A: Polym. Chem.*, 51, 1716–1725 (2013)
- [9] T. García, L. Larios-López, R.J. Rodríguez-González, G. Martínez-Ponce, C. Solano, D. Navarro-Rodríguez, *Polymer*, 53, 2049–2061 (2012).
- [10] R.G. Santos-Martell, L. Larios-López, R.J. Rodríguez-González, B. Donnio, D. Guillon, D. Navarro-Rodríguez, *J. Appl. Polym. Sci.*, 120, 2074–2081 (2011)
- [11] Y. Liu, F. Meng, S. Zheng, *Macromol. Rapid Commun.*, 26, 920–925 (2005).

- [12] T. García, L. Larios-López, R.J. Rodríguez-González, J.R. Torres-Lubián, D. Navarro-Rodríguez, *ChemPhysChem*, 13, 3937–3944 (2012).
- [13] O.L. Torres-Rocha, R.J. Rodríguez-González, L. Larios-López, G. Martínez-Ponce, C. Solano and D. Navarro-Rodríguez, *Polym Int*, 63, 652–659 (2014).

MORPHOLOGY AND CONDUCTIVITY TUNING OF POLYANILINE USING SHORT-CHAIN ALCOHOLS BY HETEROPHASE POLYMERIZATION

Miguel A. Corona-Rivera,¹ Víctor M. Ovando-Medina,¹ Hugo Martínez-Gutiérrez,²
Francisca E. Silva-Aguilar,¹ Elías Pérez, Iveth D,³ Iveth D. Antonio-Carmona,⁴

¹ Departamento de Ingeniería Química, Coordinación Académica Región Altiplano (COARA) –Universidad Autónoma de San Luis Potosí, Carretera a Cedral KM 5+600, San José de las Trojes, Matehuala, SLP, México 78700. e-mail: coronamiguelangel@yahoo.com.mx.

² Centro de Nanociencias y micro y nanotecnologías, Instituto Politécnico Nacional, Luis Enrique Erro S/N, D.F., México 07738.

³ Instituto de Física – Universidad Autónoma de San Luis Potosí, Av. Dr. Manuel Nava No. 6 Zona Universitaria, San Luis Potosí, S.L.P., México 78210.

⁴ Departamento de Botánica, Universidad Autónoma Agraria Antonio Narro. Calzada Antonio Narro 1923, Buenavista, Saltillo, Coah., 25315, México.

Abstract

Conducting polyaniline (PANI) nanostructures were obtained by heterophase polymerization of aniline monomer using sodium dodecyl sulfate (SDS) as surfactant in presence of the short-chain alcohols: ethanol, propanol, butanol, pentanol, and hexanol as co-surfactants, and ammonium persulfate (APS) as oxidizing agent. Were obtained when polymerizing without alcohol and in presence of ethanol, while very big agglomerates were obtained in presence of propanol and butanol; using pentanol as co-surfactant well defined and spherical nanoparticles were obtained, the presence of hexanol through polymerization gives both spherical agglomerated and needle-like nanostructures. Conductivities were in the range of 0.81 to 1.1 S/m with the higher value for that synthesized in presence of pentanol.

Introduction

PANI is attracting by its chemical and physical properties, like: high electrical conductivity, environmental stability, stable redox activity, and ease preparation, as well as low cost [1-5], which allow some applications in areas as: electrostatic dissipation, fuel cells, batteries, anion exchanger, biochemistry, inhibition of steel corrosion, sensors, anticorrosion coatings, etc. [6]. PANI can be synthesized by oxidizing aniline either electrochemically or chemically. The latter is of particular importance because this is the most practical route for the production of conducting polymers on large scale [7].

Experimental

In a typical reaction 17.3 mmol of SDS were dissolved in 150 g of water. Then, 21 mmol of alcohol was added to the solution, for each of the different reactions and homogenized. After that, 21 mmol of aniline were added. The mixture was bubbled with argon through 20 minutes. 21 mmol of APS was added to start polymerization. Reaction proceeded throughout 6 h. At the onset of polymerization a brown color was observed and a dark green solid precipitated was formed at the end of polymerizations. The reaction mixture was poured into an excess of methanol to precipitate the PANI nanoparticles and to remove impurities. The resulting materials were analyzed using UV/Vis spectroscopy. For the morphology and particle size determination and distribution, a 1:1,000 water dilution of the latex without purification was used. A drop of the diluted latex was poured onto a copper grid coated with Formvar™ resin and carbon film, and then, it was allowed to dry overnight at room temperature. The samples were analyzed by scanning electron microscopy in SEM (at 2 or 1 kV of acceleration voltage with secondary electron detector) and STEM (a 30 kV of acceleration voltage with a bright field transmitted

electron detector) modes using a Field Emission High Resolution SEM (JEOL, JSM 7800F). The electrical conductivities of samples were determined by the four-probe method (SP4 probe head Lucas/Signatone with 0.04 inches of spacing between tips) coupled to a Keithley (2400 SourceMeter) instrument.

Results and Discussion

Figure 1 shows the scanning electron micrographs in STEM mode (a) and (c) of PANI synthesized without alcohol and with ethanol, respectively; and the corresponding SEM image (b) and (d). It can be observed that well defined fibrillar nanostructures were obtained in these two cases. However, nanostructures with ethanol tend to deform fibrillar morphology as a result of interaction of ethanol tail with aniline monomer through polymerization. In Figure 1, very large fibers (approx. 5 μm in large) and between 60 and 90 nm of width are observed for aniline polymerization without alcohol, while 50 and 85 nm of width were observed for polymerization in presence of ethanol. Also, some agglomerates were formed in presence of ethanol, losing some of the fibrillar morphology.

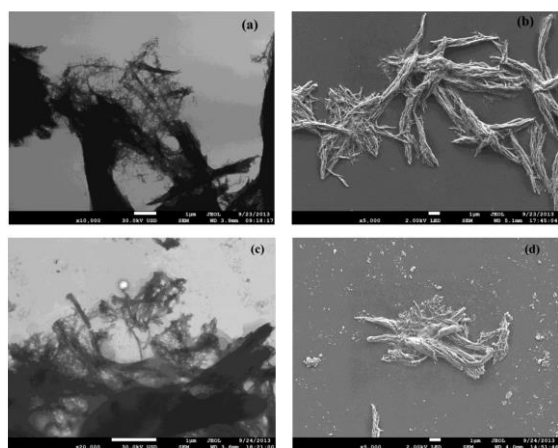


Figure 1 Scanning electron micrographs in STEM mode (a) and (c) of PANI synthesized without alcohol and with ethanol, respectively; and the corresponding SEM image (b) and (d).

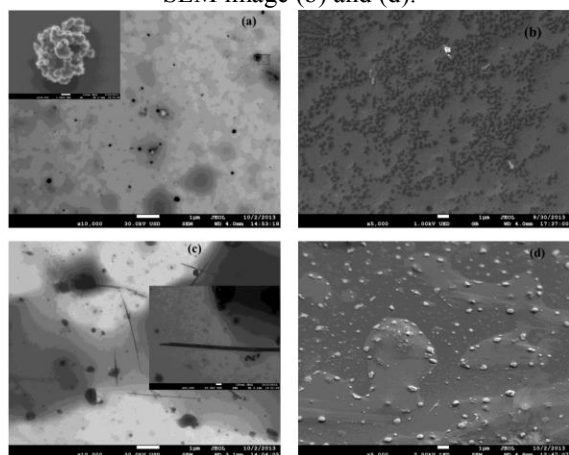


Figure 3 Scanning electron micrographs in STEM mode (a) and (c) of PANI synthesized with pentanol and with hexanol, respectively; and the corresponding SEM image (b) and (d).

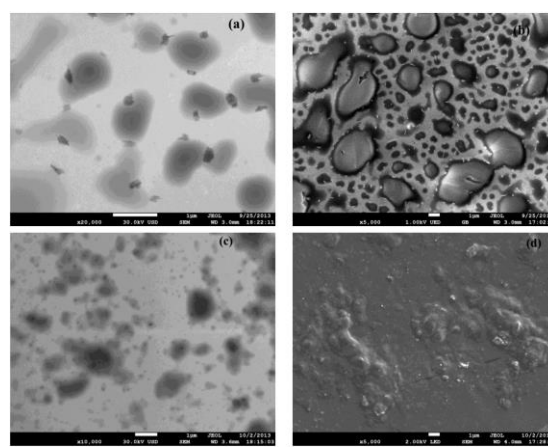


Figure 2 Scanning electron micrographs in STEM mode (a) and (c) of PANI synthesized with propanol and with butanol, respectively; and the corresponding SEM image (b) and (d).

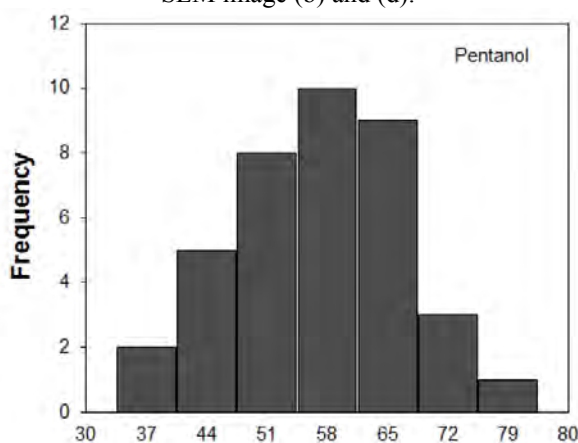


Figure 4 Particle size distribution of spherical nanoparticles of PANI obtained polymerizing in presence of pentanol as co-surfactant.

PANI morphologies were strongly affected by increasing the alcohol tail. Figure 2 shows the scanning electron micrographs in STEM mode (2a) and (2c) of PANI synthesized in presence of propanol and butanol, respectively; and the corresponding SEM image (2b) and (2d). It can be seen that fibrillar structures were not present with very big PANI agglomerates in both cases. By increasing the alcohol chain length used through aniline polymerization from butanol to pentanol and hexanol, new defined structures were obtained, as can be observed in Figure 3. For example by using pentanol as co-surfactant, small agglomerates consisting of well-defined spherical nanoparticles were observed.

The number- and weight-average particle diameters (D_n , and D_w) and polydispersity index in sizes (PDI) of the PANI nanoparticles synthesized using pentanol as co-surfactant were calculated using the following equations:

$$D_n = \sum n_i D_i / \sum n_i \quad (1)$$

$$D_w = \sum n_i D_i^4 / \sum n_i D_i^3 \quad (2)$$

$$PDI = D_w / D_n \quad (3)$$

where n_i is the number of particles with diameter D_i .

Changing to hexanol as co-surfactant, needle-like structures were obtained, as can be observed in Figure 3c, with diameters between 25 and 40 nm and 4 μ m in length. Also spherical nanoparticles near to 50 nm of diameters were formed.

The calculated values of D_n and D_w were 56 nm and 61 nm, thus giving a PDI of 1.1, which imply that narrow and monomodal particle size distribution can be synthesized by using pentanol, as can be seen in Figure 4.

Figure 5 shows the FTIR spectra of PANI nanoparticles obtained without and with different alcohols. It can be seen the characteristic peaks of the PANI base, which are at 1572, 1496, 1448, 1299, 1128, 1040, 823, 758 and 697 cm^{-1} . The band at 1448 cm^{-1} is related to mixed C–C stretching, and C–H and C–N bending vibrations observed in the spectra of the aromatic oligomers. Peaks at 1572 and 1128 cm^{-1} can be ascribed to C=C stretching of quinoid rings (Q), peak at 823 cm^{-1} is due to C–H aromatic out of plane bending of 1,4-ring. Signal at 1299 cm^{-1} is characteristic of C–N stretching in the Q/cis-benzenoid (Bc)/Q, Q/benzenoid ring (B)/B, and B/B/Q of PANI. Peak at 1496 cm^{-1} is due to PANI base, as is consistent with quinone and benzene ring stretching deformations.

As shown in Table 1, conductivity of PANI increased about 15% when using ethanol and 30% using pentanol as co-surfactants, respectively compared to PANI synthesized without any alcohol. This behavior can be explained as a function of doping degree. In all cases, initial pH values are near to 3.2 and decreases at the end of polymerizations to values between 2.1 for that obtained without alcohol and 2.8 for that synthesized in presence of propanol and hexanol. These results suggest that acids are produced through polymerizations. Thus, acids derived from reactions between alcohols and APS can be doping PANI, increasing its conductivity.

Figure 6 shows the UV/Vis spectra of PANI obtained in the different polymerizations. The absorption spectra of PANI show bands around 300 nm and 540 nm corresponding to π - π^* transition within the benzenoid moieties and due to the formation of a doping level owing to the ‘exciton’ transition, caused by inter-band charge transfer from benzenoid to quinoid moieties, respectively. The maximum absorbance of the first peak for PANI synthesized without alcohol is centered at 440 nm, whereas in the presence of alcohols, the maximum absorbance is shifted to 405 nm, except for PANI obtained in presence of pentanol, which was near to 440 nm.

In order to demonstrate the effect of pentanol on electrical properties of PANI, reactions were carried out varying pentanol concentration, and the UV/Vis spectra are shown in Figure 7. It

can be observed that intensity of band corresponding to π - π^* transitions increases with pentanol amount, thus more conductive PANI can be formed, which is in agree with conductivity values: 0.9, 1.1 and 1.9 S/m for molar ratios of pentanol/aniline of 0.5, 1.0 and 1.5, respectively. This behavior was also observed for propanol with PANI conductivities of 0.83, 0.90 and 0.92 S/m for the same molar ratio of alcohol/aniline. For the other alcohols used, conductivities were not strongly affected by the alcohol concentration.

Alcohol used	Conductivity S/m	Conversion %	Initial pH; final pH
Without alcohol	0.840	50	3.1; 2.1
Ethanol	0.965	63	3.3; 2.2
Propanol	0.901	61	3.2; 2.8
Butanol	0.956	67	3.4; 2.7
Pentanol	1.094	73	3.2; 2.6
Hexanol	0.808	73	3.1; 2.8

Table 1 Conductivity values of synthesized PANI and pH of latexes.

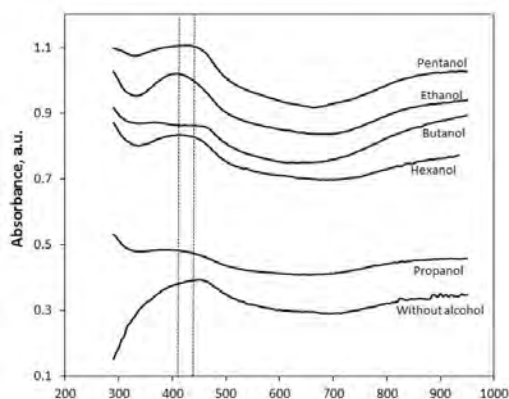


Figure 6 UV/Vis spectra of final PANI obtained in presence of different alcohols.

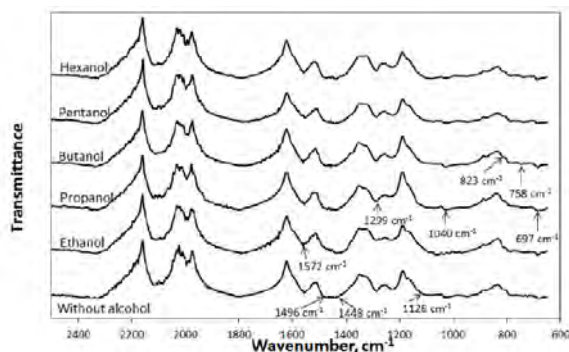


Figure 5 Infrared spectra of PANI obtained in the different syntheses.

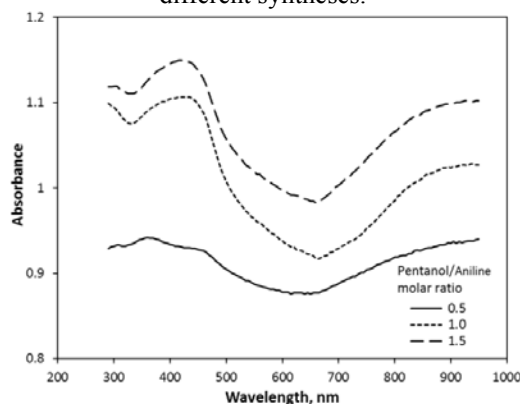


Figure 7 UV/Vis spectra of final PANI obtained at different pentanol to aniline molar ratios.

A proposed mechanism of PANI nanostructures obtained in our work is shown in Figure 8. When SDS is dissolved in water, globular micelles are present, because we are using a concentration of 115 mM of SDS (the critical micellar concentration of SDS is 8 mM), and when alcohols were added, alcohol molecules are placed between the polar heads of SDS molecules. The main function of alcohol was to increase particle stability throughout polymerization. Then, when no alcohol was used, micelles are not spherical at all, and upon polymerization particle coagulation was verified (Figure 8, part a), polymerizing in both: inside the micelles and at the micelle-water interface forming fibers, consisting of diameters among 60 and 90 nm (Figure 1b). For polymerizations in presence of ethanol, particles are more stable and fibers diameters decreased to values between 55 and 85 nm (Figure 1d); by increasing the alcohol chain length, to propanol and butanol, fiber structure are not present any more, and particles consist of very big agglomerated globular structures, and when pentanol was used particles are so stable that only globular structures are formed (Figure 8, part b). For alcohol chain length as long as hexanol, particles become unstable again due to high separation of polar heads of SDS molecules, resulting in particle coagulation but not as

unstable as polymerization without alcohol, thus both needle-like and globular structures were observed.

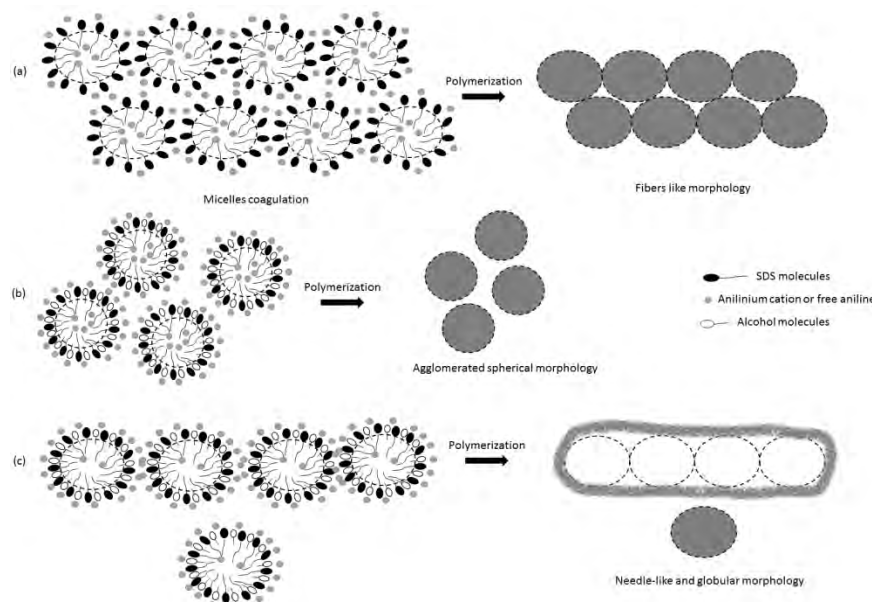


Figure 8 Proposed mechanisms for the different nanostructures of PANI obtained changing the alcohol type.

Conclusions

Conductivity and morphology of PANI were tuned by polymerizing in the presence of different short chain alcohols. Fibrillar nanostructures were observed without alcohol and in presence of ethanol, respectively. In the presence of propanol and butanol, very large PANI agglomerates were obtained, and by increasing the alcohol chain length to pentanol, structures consisting of well-defined spherical nanoparticles between 56 and 61 nm were formed with monomodal and narrow PSD, while the presence of hexanol resulted in needle-like structures. The higher conductivity of PANI was that synthesized using pentanol (1.9 S/m for a molar ratio of pentanol to aniline of 1.5), which was ascribed to formation of acids and aldehydes derived from reactions between alcohol and APS thus doping PANI, increasing its conductivity.

Acknowledgements

M.A.C.R. wants to thank to the Consejo Nacional de Ciencia y Tecnología (CONACyT – México) by Grant # CB-169444. Especial thanks are given to José A. Andraca-Adame by his help in XRD analysis and to the Centro de Nanociencias y micro y nanotecnologías-IPN by the facilities in SEM characterization.

References

- [1] C.J. Pérez-Martínez, T. del Castillo-Castro, M.M. Castillo-Ortega, D.E. Rodríguez-Félix, P.J. Herrera-Franco, V.M. Ovando-Medina, *J. Synth Met* 184, 41–47 (2013).
- [2] J. Chen, B. Winther-Jensen, Y. Pornputtkul, K. West, L. Kane-Maquire, and G.G. Wallace, *Electrochem Solid-State Lett* 9 (2006).
- [3] N.V. Blinova, J. Stejskal, M. Trchová and J. Prokes, *Polym Int*, 57, 66–69 (2008).
- [4] S. Bhadra, D. Khastgir, N.K. Singha and J.H. Lee, *Prog Polym Sci* 34, 783–810 (2009).

Graphene oxides modification with poly(phenyleneethynylene)s by microwave-assist for solar cell applications

Gleb Turlakov, E. Arias, I. Moggio, R.F. Ziolo, R.M. Jiménez, P. González Morones

Centro de Investigación en Química Aplicada (CIQA), Blvd. Enrique Reyna 140, 25294, Saltillo, México. Tel: 00528444389830, Fax: 00528444389839, e-mail: eduardo.arias@ciqa.edu.mx

Abstract

The functionalization of graphene oxide (GO) with a series of conjugated copolymers of phenyleneethynylene type (PPE) bearing different electron-donating and withdrawing groups was obtained by microwave-assisted esterification or amidation reactions with the GO. Copolymers and the GO-PPEs nanocomposites were characterized by UV-Vis, fluorescence and Raman XPS spectroscopies. Effective interaction of the copolymers with the GO is evidenced by a strong quenching of the fluorescence quantum yield (ϕ), which suggests an energy transfer process from polymer to GO. The presence of GO in the copolymers allows for band gap reduction of the active layer as determined by UV-Vis spectroscopy, which is a requisite for development of solar cells devices.

Introduction.

PPE copolymers and G/GO have received an enormous amount of attention in the literature because of their important photovoltaic properties [1] and unique electronic and optical properties, respectively [2, 3]. The key parameters of organic photovoltaic devices are fast and efficient charge separation and transport to the electrodes due to the crucial importance of the interpenetrating donor-acceptor phase. Generally, the active layer of organic photovoltaics is composed of a bulk heterojunction formed by a polymer (electron donor) and an electron acceptor such as a fullerene, a carbon nanotube or graphene. There are many reports where G or GO were used as an electron acceptor for solar cells applications. Typically, two bonding schemes are used to explain G/GO interactions with the polymers. The first consists of π - π interactions between the pi bonds of the G with those of the polymer backbone. The second relies on covalent linkage[4] of the functionalized polymers to the GO surface using, for example, esterification, amidation, click, or nitrene chemistry, radical addition, etc. Although there are many reports describing these functionalization methods, the esterification reaction provides a facile way of attaching a polymer molecule to GO. Previously, microwave irradiation (MWI) was used as a suitable and rapid heating method for preparing exfoliated graphite from many graphite intercalation compounds [5-7]. Recently, MWI was used for GO exfoliation and reduction [8, 9], including the heating of its suspensions in aqueous or organic media [10]. The advantage of MW-assist is in lower reaction times (from 6 days by traditional reactions to 90 minutes by MW-assist) and the complete activation of the GO surface for esterification and amidation reactions with polymers.

Experimental

GO powder was prepared from purified natural graphite powder using a modified Hummers'-method [11]. The derivatives of the PPE-conjugated copolymers were previously synthesized by a Sonogashira [12] cross-coupling reaction. The typical procedure for the functionalization of GO with the copolymers, (**Fig 1**), using MW-assist is as follows: 1 weight ratio of GO was suspended in

DMF in a microwave vial. The suspension was then subjected to ultrasound bath for 30 min and a sonicated solution of the copolymer (4 weight ratio) in dichlorobenzene (DCB) was added and stirred for 15 min. A second solution containing dicyclohexylcarbodiimide DCC (4 weight ratio), 4-(dimethylamino)pyridinium toluene-4-sulfonate DPTS (1.5 eq. with respect to DCC) and 4-pyrrolidinopyridine (4PPy) (0.5 eq. with respect to DCC) in DMF was later added to the first mixture. The final reaction mixture was then re-dispersed in chloroform by ultrasound for 15 min and irradiated at 4.75 GHz and a constant power of 300 W, while stirring at 600 rpm for 90 min at 150 ° C. The mixture was centrifuged and the precipitate washed with toluene, ethanol and chloroform at least twice to eliminate the catalyst and unreacted copolymers, filtrated, and dried under reduced pressure. All experiments were carried out at an ambient pressure of 84.5 kPa.

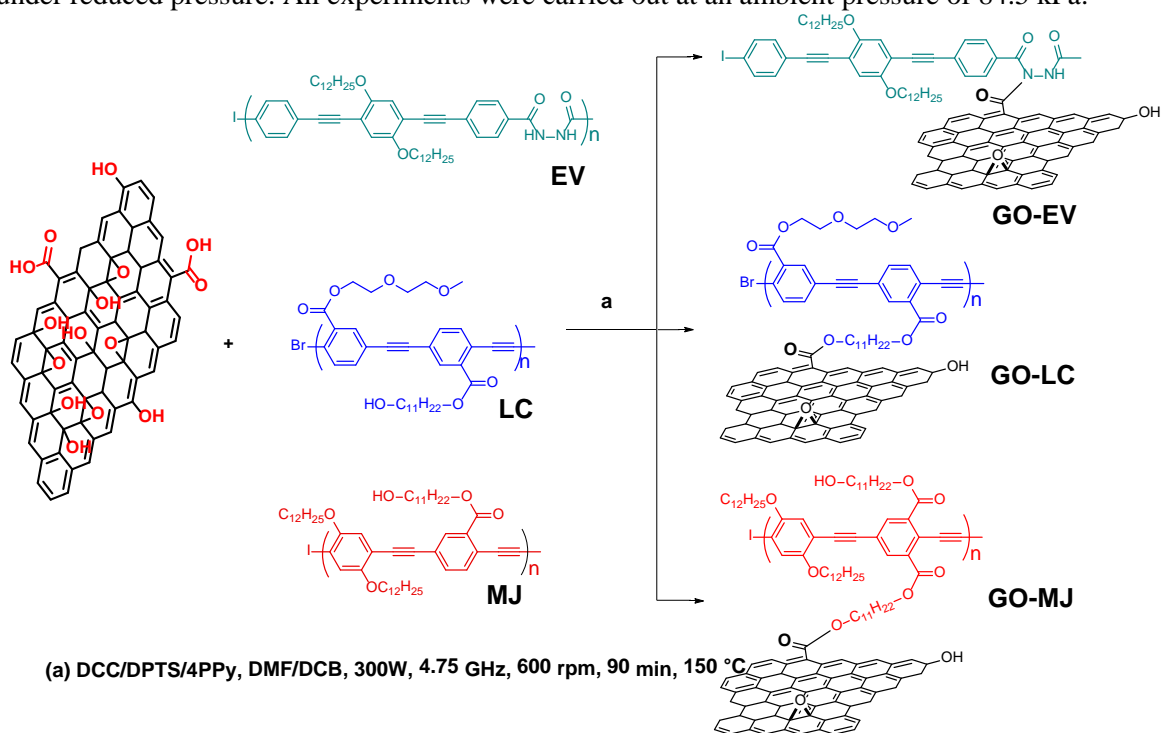


Fig.1 General pathway to functionalize graphene oxide with conjugated polymers via microwave

Results and Discussion.

GO was successfully modified by MW-assisted functionalization with poly(phenylethynylene)s by esterification and amidation to form new GO-PPE nanocomposites (NCs).

Vibrational properties. Raman spectra of the copolymers are shown in **Fig.2**. Spectra in the left are for excitation at 785 nm to avoid the strong fluorescence of these materials in the visible region. The bands around 2200 cm^{-1} are associated with the $\text{C}\equiv\text{C}$ stretching and provide evidence of the π -electron delocalization along the conjugated backbone, MJ is the most conjugated of the materials due to the electron donor character of the 2,5-bis(dodecanoxy) chains and shows a slightly higher intensity for this band. Notice that the band at 1590 cm^{-1} associated with the vibrational modes of the double bonds of the phenyls is not affected by the type of electron donor- or acceptor-aryl.

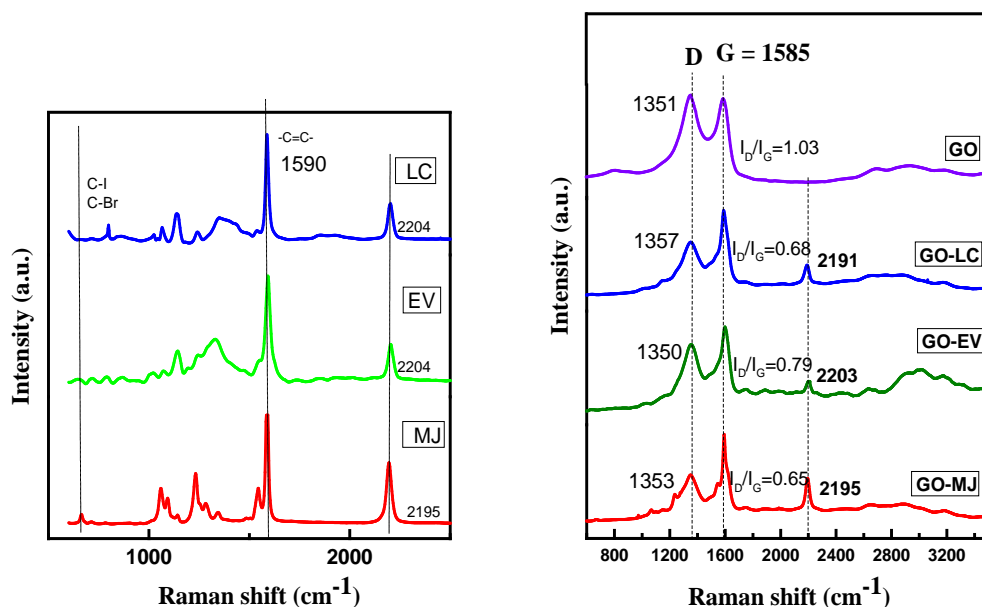


Fig. 2 Raman spectra of: the conjugated copolymers (left) and the GO-PPE' NCS (right).

The Raman spectra of GO and the NCs are shown on the right side of **Fig. 2**. The peaks at about 2200 cm^{-1} for the NCs associated with the $\text{-C}\equiv\text{C-}$ stretching band support the functionalization of the GO. The two main GO bands, the D band ($\sim 1345 \text{ cm}^{-1}$, breathing mode of A_{1g}) and G band (the in-plane bond-stretching motion of pairs of C sp^2 atoms, E_{2g} mode), practically coexist with the shifts observed for the copolymers. The relative intensities of the D and G peaks, as expressed by the I_D/I_G ratio, which is an indication of the ratio of the sp^3/sp^2 carbons[13], is a measure of the relative disorder in the GO structure. The data show that functionalizing GO with the copolymers clearly affects the structural nature of the GO.

Optical properties. Copolymers were characterized by absorption and fluorescence spectroscopy with results presented in the **Table 1**. Each copolymer exhibits two distinct absorption bands with a maximum at around 350–400 nm, which is attributed to $\pi\text{-}\pi^*$ transitions of the aromatic ring (HOMO-1/LUMO electronic transition) and at 418 nm (MJ), 386 nm (LC) and 385 nm (EV) which are attributed to the $\pi\text{-}\pi^*$ transitions of the copolymer conjugated backbone (HOMO/LUMO electronic transition). Upon excitation of the copolymers in solution, all of the exhibit an excitonic band with a well-structured vibronic band having a typical shoulder at the lower energy side of λ_{abs} - which may be considered as evidence of a higher molecular order of the polymeric chains in the excited state and that the excited-state geometry of the copolymers is more planar compared to that in the ground state.

Table 1. Optical properties of the polymers and corresponding composites.

Compound	λ_{abs} [nm]	λ_{em} [nm]	ϕ_r	t [ns]
GO-MJ	454	470	0.014	0.39
MJ	418	465	0.47	0.72
GO-LC	368	421	0.041	0.70
LC	386	429	0.31	0.45
GO-EV	310	476	0.050	0.79
EV	385	476	0.63	1.18

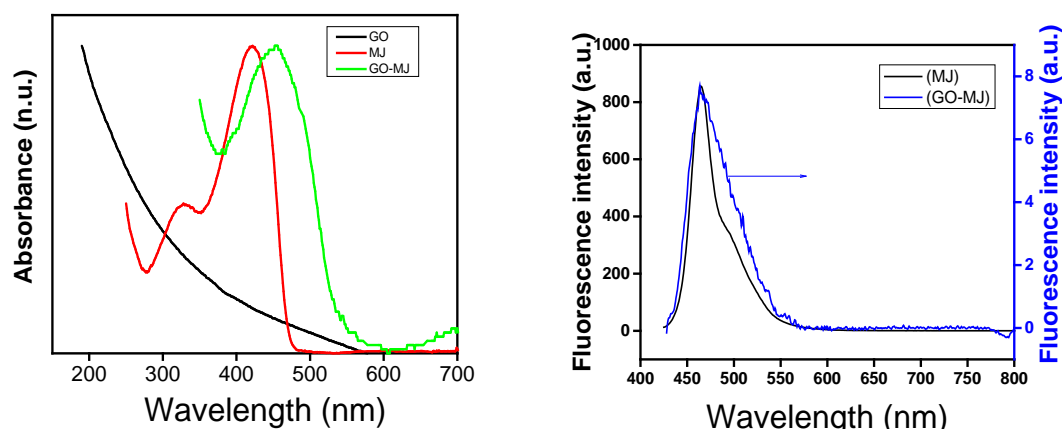


Fig. 3 Absorbance and fluorescence spectra of GO, MJ and GO-MJ; note the two orders of magnitude difference in the fluorescence spectra.

The quantum yield (**Table 1**) is in the same range as for other PPEs[14]. After functionalization with GO, the NCs show the absorption features of the polymer superimposed on a strongly inclined baseline due to light dispersion by the GO. On the contrary, the emission spectra of the NCs are the same as those of the copolymers, at all excitation wavelengths, but show a two-order decrease in the quantum yield (and in general of the lifetimes, τ) suggesting photoinduced electron transference (**Table 1**). This result is promising in view of the possible application of these composites in solar cells. **Fig. 3** shows the UV-Vis and fluorescence spectra of MJ and its composite in DMF as example for the optical properties of the copolymers and GO-PPEs materials.

Conclusions

GO was successfully modified by MW-assisted functionalization with poly(phenylethynylene)s by esterification and amidation to form new GO-PPE nanocomposites (NCs). The functionalizations were confirmed by Raman, UV-Vis and fluorescence spectroscopies. The addition of the copolymers significantly improved the solvent dispersibility of the GO-PPE NCs, which themselves showed fluorescence quenching, likely indicating a photoinduced electron transfer process.

AKNOWLEDGEMENTS

This work was supported by CONACYT through project 232753 Laboratorio Nacional de Materiales Gráficos

References

1. Robertson, N., *Organic Photovoltaics. Mechanisms, Materials and Devices*. Edited by Sam-Shajing Sun and Niyazi Serdar Sariciftci. Angewandte Chemie International Edition, 2006. **45**(44): p. 7321-7321.

2. Harker, A.H., *Graphene: A New Paradigm in Condensed Matter and Device Physics*, by E.L. Wolf. Contemporary Physics, 2014. **55**(4): p. 355-355.
3. Zhao, J., L. Liu, and F. Li, *Graphene Oxide: Physics and Applications*. 2015, Springer Berlin Heidelberg.
4. Layek, R.K. and A.K. Nandi, *A review on synthesis and properties of polymer functionalized graphene*. Polymer, 2013. **54**(19): p. 5087-5103.
5. Tryba, B., A.W. Morawski, and M. Inagaki, *Preparation of exfoliated graphite by microwave irradiation*. Carbon, 2005. **43**(11): p. 2417-2419.
6. Falcao, E.H.L., et al., *Microwave exfoliation of a graphite intercalation compound*. Carbon, 2007. **45**(6): p. 1367-1369.
7. Wei, T., et al., *A rapid and efficient method to prepare exfoliated graphite by microwave irradiation*. Carbon, 2009. **47**(1): p. 337-339.
8. Zhu, Y., et al., *Microwave assisted exfoliation and reduction of graphite oxide for ultracapacitors*. Carbon, 2010. **48**(7): p. 2118-2122.
9. Chen, W., L. Yan, and P.R. Bangal, *Preparation of graphene by the rapid and mild thermal reduction of graphene oxide induced by microwaves*. Carbon, 2010. **48**(4): p. 1146-1152.
10. Hassan, H.M.A., et al., *Microwave synthesis of graphene sheets supporting metal nanocrystals in aqueous and organic media*. Journal of Materials Chemistry, 2009. **19**(23): p. 3832-3837.
11. Hummers, W.S. and R.E. Offeman, *Preparation of Graphitic Oxide*. Journal of the American Chemical Society, 1958. **80**(6): p. 1339-1339.
12. Sonogashira, K., Y. Tohda, and N. Hagihara, *A convenient synthesis of acetylenes: catalytic substitutions of acetylenic hydrogen with bromoalkenes, iodoarenes and bromopyridines*. Tetrahedron Letters, 1975. **16**(50): p. 4467-4470.
13. Gómez-Navarro, C., et al., *Electronic Transport Properties of Individual Chemically Reduced Graphene Oxide Sheets*. Nano Letters, 2007. **7**(11): p. 3499-3503.
14. Huang, W.Y., et al., *Synthesis and Characterization of Poly(alkyl-substituted p-phenylene ethynylene)s*. Macromolecules, 2001. **34**(6): p. 1570-1578.

SYNTHESIS AND THERMAL PROPERTIES OF METHACRYLIC POLIMERS WITH A PENDANT ZWITTERIONIC MOIETY

Gregorio Guzmán¹, Judith Cardoso¹, Dora Nava¹ and Ignacio González²

¹ Polymer Area, Physics Department, CBI, UAMI Av. San Rafael Atlixco 186, Col. Vicentina, C.P. 09340, México, D.F. México. e-mail: jcam@xanum.uam.mx.

² Chemical Department, CBI, UAMI.

Abstract

The development of polymer electrolytes (PE) has recently reached its highest point, mainly by its application in ion lithium batteries (LB). This paper presents the synthesis of two polymers with different degree of functionalization derivatives of poly(ethyleneglycol)methacrylate. The synthesis of materials was carried out via radical polymerization. Polymers were characterized by NMR, FT-IR, TGA and DSC. The formation of PE is also showed A polymer fully functionalization with 1,3-propanesultone (5a) showed a Tg -49°C, compared to a polymer without functionalize which showed a Tg -52°C. A polymer with 80% of functionalization (5b) showed a Tg -44°C. Decomposition temperatures decreased according to the degree of functionalization.

Introduction

Research and application of polymer electrolytes (PE) is a subject of academic and industrial interest. The main application of PE is in the automotive industry, electric and hybrid cars, mobile devices and in the emergency energy supply. It was demonstrated that modified poly(oxyethylene) (PEO) electrolytes, operating at 40 to 80°C, allowed the harnessing of the electrochemical ion lithium batteries with maximum energy per unit weight [1]. Many PEs have been studied but they did not shown enough conductivity for a commercial application. Meanwhile, Cardoso et al. [2] have shown that the zwitterionic groups are able to interact with different types of inorganic salts in a 1:1 molar ratio, i.e. $LiClO_4$, lithium triflate (CF_3LiO_3S) and $LiClO_4$, without compromising the phase separation.

The aim of this work is to illustrate the synthesis of three polymer electrolytes which contain into their structure derivatives of poly(ethylene glycol)methacrylate (PEGMA), their functionalization with zwitterionic groups and their formulation as polymer electrolytes. Finally, their physicochemical characterization and thermal properties are also shown.

Experimental

PEGMA, 4,4'-azobis(4-cyanovaleric acid) (ACVA), 1,3-propanesultone (PS), 1-butyl-1-methylpyrrolidinium-bis(trifluoromethylsulfonyl)imide, ($PYR_{11}TFSI$), lithium-ion salt ($LiPF_6$) were obtained from Sigma-Aldrich and were used as received, except the monomer which was purified by vacuum distillation.

The thermal polymerization of Poly(ethylene glycol)methacrylate (PEGMA) was conducted up to almost total monomer conversion, at a temperature of 70° C for 16 h, using a vacuum oven (50 mm Hg). The polymer was washed with acetone and dried in vacuum for 24 hours.

A synthetic pathway of three stages is carried out for precursor monomers (see Figure 1). The first one was a substitution reaction with thionyl chloride in ($CHCl_3$) for 3 h at 0 °C to obtain (1). After that, a second substitution reaction with dimethylaminethanol in THF under nitrogen atmosphere, using trimethylamine as catalyst for 3h at room temperature yielded (2). Later, a quaternization

reaction was obtained using 1,3-propanesultone in DMF at 100 °C for 20 h to get the 4 product. To obtain the functionalized polymers (3 and 5a), 2 and 4 were polymerized by radical polymerization using ACVA as initiator. Finally, aminated polymer (3) was quaternized with 1,3-propanesultone in [monomer]/[PS]=1:1.1 ratio to get 5b. All the intermediated products were purified and characterized by AE, NMR, FTIR, NMR, confirmed the structure proposed. The preparation of polymer electrolytes was made from three types of polymer electrolytes, their formulation with a lithium salt as a binary system with molar ratio of [polymer]/[LiPF₆] = 1:1 and one ternary system adding an ionic liquid with a molar ratio of [polymer]/[LiPF₆]/[IL] = 1:1:1. 5a, the lithium salt and the IL were dissolved separately in dioxane. They were then mixed with stirring until a homogeneous solution was obtained. They poured into a container of teflon and left to slowly evaporate the solvent and dried in an oven at 50 °C for 24 h. It was kept in a desiccator until further use.

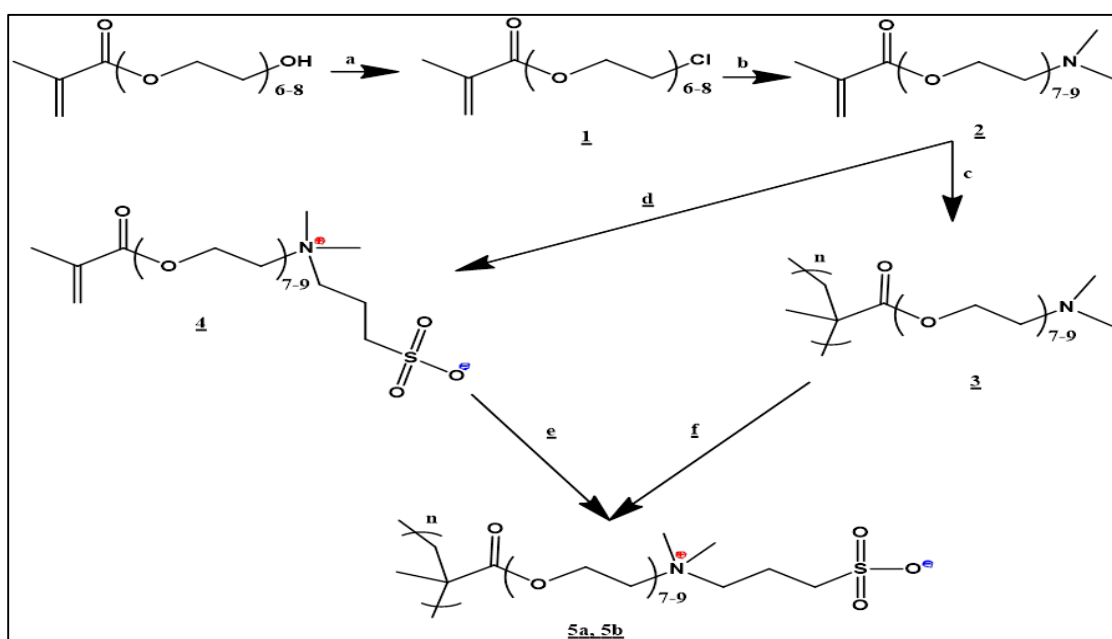


Figure 1. Synthetic pathway to get the zwitterionic polymers where 5a is fully and 5b is partially functionalized polymers (80%). a) CHCl₃, SOCl₂, 0 °C, 3h; b) THF, N₂, DMAE, (Et)₃N, rt; c) thermal polymerization 60 °C, 60 mmHg; d) and f) 1,3- propanesultone, DMF, 100°C, 20h; e) bulk polymerization N₂, 70 °C, 60 mmHg, ACVA.

Physicochemical and thermal characterization. Physicochemical and thermal characterization. Elemental analysis was used to verify the chemical structure of the polymers. The FTIR spectra were collected in a Perkin Elmer 1500 unit with 2 cm⁻¹ resolution and sample was dispersed and measured in dry KBr discs. Thermogravimetric analysis was performed with a PYRIS Perkin Elmer with a nitrogen flow of 50 mL/min in the range of 30 °C to 800 °C. Differential Scanning Calorimetry was carried out in a stream of nitrogen (50 cm³/min) in a MDSC-2920 manufactured by TA Instruments (Newcastle, Delaware, USA), with a heating rate of 10 °C/min with amplitude of ± 1.06 °C and a period of ±40 seconds in the range of -50 to 200 °C with a flow of 50 mL/min under nitrogen atmosphere. The glass transition temperature (T_g), was obtained from the second scan; the samples were previously heated at 100° C for 120 minutes to remove the residual water in the sample.

Results and Discussion

In Figure 2 is shown the FTIR spectra from 5a and 5b. At 1735 cm^{-1} is associated with C=O stretch vibration for ester groups. A strong band at $1070\text{--}1150\text{ cm}^{-1}$ region consists overlapping of two functional groups C-O-C v stretch and S=O v stretch symmetric and other band for S=O at 1345 cm^{-1} for stretch asymmetric vibration. A strong band at 3490 cm^{-1} (-OH v str) showed that the polymers are hydroscopic.

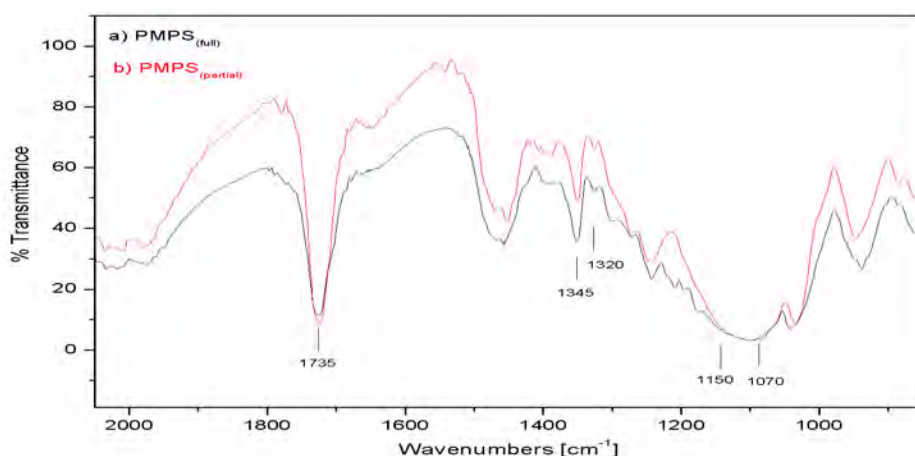


Figure 2. Infrared spectroscopy spectra of 5a: fully functionalized polymer and 5b: partially functionalized.

In Figures 3A y 3B are shown the ^1H -NMR and ^{13}C -NMR spectra, respectively, from zwitterionic monomer 4, according to the assignation of the monomers confirmed the structure proposed.

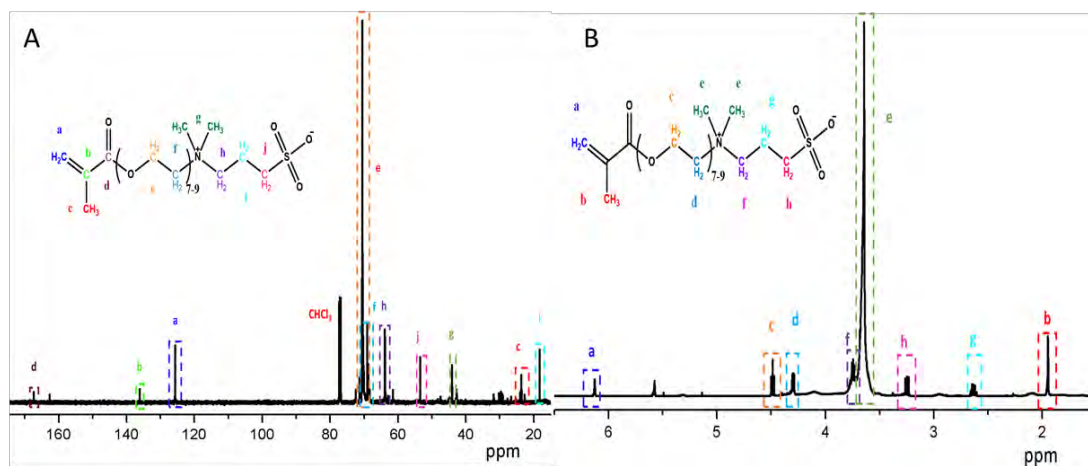


Figure 3. NMR spectrum from compound 4. A) ^1H -NMR and B) ^{13}C -NMR.

Elemental analysis results confirmed the structure of the polymers as is shown in Table I, where 5a polymer is the fully functionalized and 5b is only functionalized 82% with sulfobetaine groups. The $\%S_{\text{experimental}}/\%S_{\text{theoretical}}$ and $\%N_{\text{experimental}}/\%N_{\text{theoretical}}$ proportions confirms this result.

Table I. Elemental Analysis for PMPS8 5a and 5b polymers

PMPS8	%C	%H	%N	%O	%S	%Chemical modification
Theorist	51.1	8.4	2.38	32.7	5.46	100
Experimental 5a	48.3	8.71	2.28	**	**	98
Experimental 5b	50.7	8.34	2.22	**	4.65	82

Thermal properties. Figures 4A and 4B show the thermal behavior for pPEGM, 5a, 5b and their binary and ternary systems. The glass temperatures (T_g) for all the studied systems are shown in Figure 4A. All binaries systems (polymer/) display an increases in their T_g . In contrast, for all ternaries systems (polymer/ $LiPF_6$ / $PYR_{11}TFSI$). Decomposition temperatures at 10% ($T_{d10\%}$) were 220 °C, 230 °C and 270 °C for pPEGM, 5a and 5b, respectively (figure 4B). All binaries systems (polymer/ $LiPF_6$) display a decrease in their $T_{d10\%}$. In contrast, for all ternaries systems (polymer/ $LiPF_6$ / $PYR_{11}TFSI$), $T_{d10\%}$ show an intermediate temperature as is exhibited in Figure 4B.

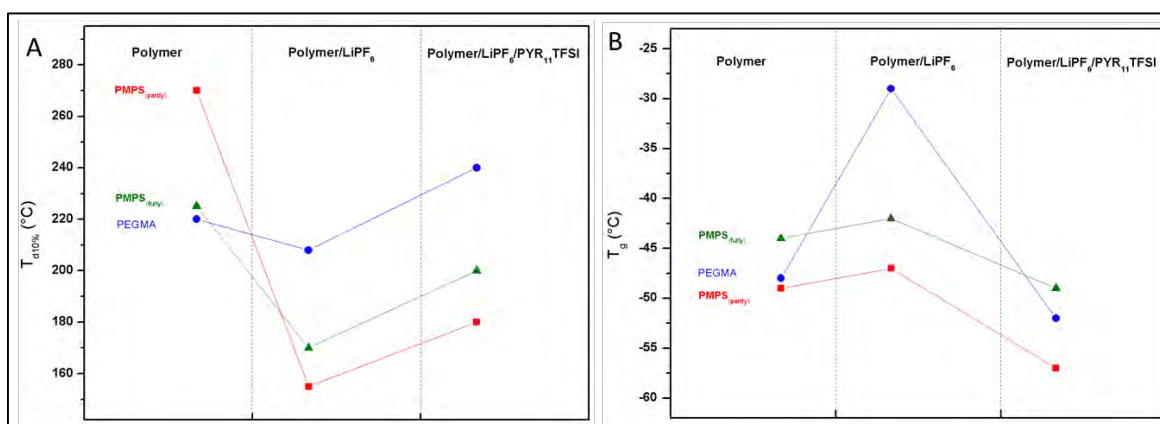


Figure 4. Thermal behavior: A) T_g from DSC and B) $T_{d10\%}$ from TGA for PEGM, 5a: fully functionalized polymer and 5b: partially functionalized.

Taking into consideration the thermal properties in these kinds of zwitterionic polymers and the number of ethoxy groups in the lateral chains, it is possible to predict the T_g of a series homologue with sulfobetaine groups and different number of carbon atoms in their structure, according to results published in this work and by Cardoso and coworkers [2-4]. In Figures 5 is displayed the structure of zwitterionic polymer (Figure 5A) and the T_g as a function of carbon atoms in the polymers structure (Figure 5B).

The possible interaction among ion lithium (Li^+) and the different groups in the polymer structure is displayed in Figure 6 for pPEGMA and 5a polymer. The different positions where ion lithium interacted in ethoxy groups in pPEGMA as is shown is Figure 5A, and these groups increased in functionalized polymer because of sulfobetaine groups. That could be the reason that 5a dissolve a high amount of lithium salts.

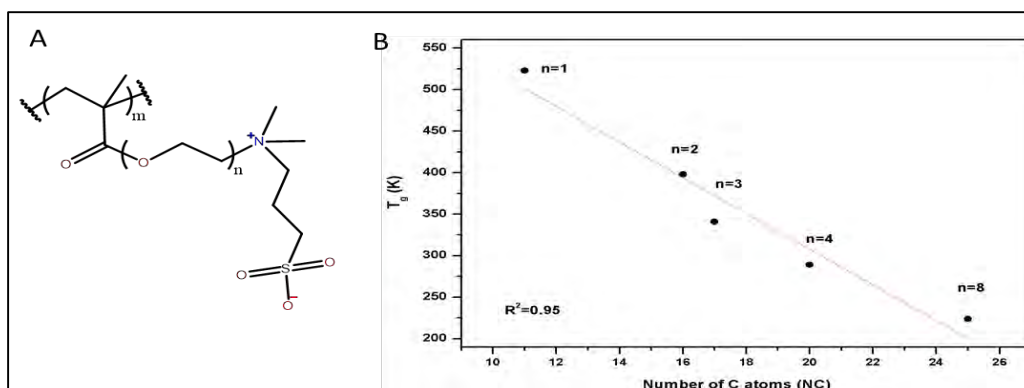


Figure 5. A) Zwitterionic polymer structure with different number of ethoxy groups. B) T_g as a function of number of carbon atoms of structure A. Data obtained from [2-4].

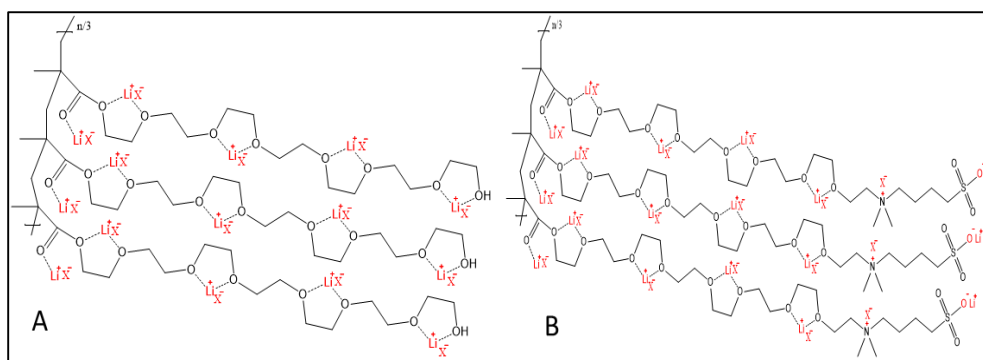


Figure 6. Possible interaction among ion lithium and groups in the polymer structure of A) pPEGMA and B) 5a polymer

Conclusions

This work shows that it is possible to predict the T_g of a series of homologues with sulfobetaine groups and different number of carbon atoms in the structure of zwitterionic Poly(ethylene glycol)methacrylate. The polar properties of sulfobetaine groups help to dissociate lithium salt, and their ethoxy groups interact with lithium ions.

Acknowledgements

References

- [1] P.V. Wright, *British Polymer Journal*, 7 (1975), p. 319
- [2] J. Cardoso, O. Soria-Arteche, G. Vázquez, O. Solorza, I. González. *J Phys Chem C*, 114 (2010) 14261.
- [3] J. Cardoso, O. Manero, *Macromolecules*, 24, 2890 (1991)
- [4] J. Cardoso, R. Manrique, M. Albores-Velasco, and A. Huanosta. *J. Polym. Sci. Part B: Polym. Phys.* V. 35, 479-488 (1997)

MORPHOLOGICAL AND ELECTROCHEMISTRY PROPERTIES OF POLYMER ELECTROLYTES

Dora Nava,¹ Gregorio Guzmán,¹ Judith Cardoso¹, and Ignacio González²

¹ Polymer Area, Physics Departments. DCBI, UAMI. Av. San Rafael Atlixco 186, Col. Vicentina CP 09340, México.

² Chemistry Departments. DCBI, UAMI. Av. San Rafael Atlixco 186, Col. Vicentina CP 09340, México

Abstract

Polymer electrolytes (PE) play a very important role in the development of lithium ion batteries (LB). This paper presents morphological evaluation and ionic conduction properties of three polymer electrolytes derived from poly(ethylene glycol) methacrylate (PEGMA) and its blends with LiPF_6 (binary system) and ionic liquid (ternary system). The materials are amorphous and they did not shown phase separation among their components by WAXS. Conductivity properties were carried out by electrochemical impedance spectroscopy in the range of 25-100°C, whose values in binary system is 10^{-5} - 10^{-4} S/cm and the ternary blends 10^{-4} - 10^{-3} S/cm, showing its feasibility to be used as PE in LB.

Introduction

Renewable energy and sustainable energy are one of the great challenges of today's society due to the limitation of fossil fuels [1]. The energy obtained by these means is not fully available, due to variants undergoing natural, such as: the wind speed on wind turbines, solar radiation on photovoltaic sources, among others. Energy storage has a vital role in the effort to combine the provision of sustainable energy services technical standard. To meet this requirement, batteries, which are rechargeable secondary cells, acting in accordance with a reversible principle. Lithium ion batteries are the most promising because they possess an intrinsic discharging voltage with a relatively light weight. This type of batteries contains flammable organic electrolytes, so it is put at risk the security of the system during its operation. For this reason has been proposed to replace this type of electrolyte for non-flammable polymer electrolytes. In lithium ion batteries is required a polymer with selective conductivity, i.e., exclusively cationic. That is, a polymer electrolyte with a large cationic conductivity and no anionic conductivity would be ideal. One approach to design single ion conductive systems is with polyelectrolyte, which anionic groups are covalently bound to the polymer backbones [2]. For example, poly(ethylene oxide) is a host polymer, its ethoxy groups interact with ions lithium, given solvation capabilities. However, it is important to consider the low relative permittivity of the host, ion association leading to the formation of long-lived ion pairs occur. Also, PEO is semi-crystalline, so it has been proposed several alternatives to avoid the crystallization phenomenon. By the above, this study proposes to improve mechanical properties and avoid ion association pairs using poly(ethylene glycol) methacrylate functionalized with sulfobetaine pendants. The polar properties of sulfobetaine groups help to dissociate lithium salt [3]. The conductivity of polymer electrolytes derived from poly(poly(ethylene glycol) methacrylate) (pPEGM) and its sulfobetaine derivative (PMPS8) (Figure 1) and formulated with an ionic liquid and LiPF_6 are determined.

Experimental

Preparation of the samples. The polymer electrolytes were prepared according to Cardoso et al. [3] It was made two types of polymer electrolytes: binary system with molar ratio of $[\text{Polymer}]/[\text{LiPF}_6]=1:1$ and one ternary system adding an ionic liquid (1-butyl-1-

methylpyrrolidinium-bis(trifluoromethylsulfonyl)imide, $\text{PYR}_{11}\text{TFSI}$) with a molar ratio of $[\text{Polymer}]/[\text{LiPF}_6]/[\text{PYR}_{11}\text{TFSI}] = 1:1:1$. The binary and ternary systems were prepared by separately dissolving polymer, $\text{PYR}_{11}\text{TFSI}$ and LiPF_6 in 1,4-dioxane and then, mixed with stirring until a homogeneous solution was obtained. They were poured into a teflon container and left to slowly evaporate the solvent and dried in an oven at 50°C for 24 h. It was kept in a desiccator until further use.

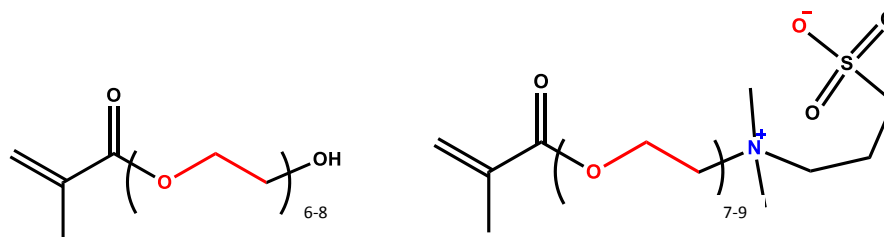


Figure 1. Structures of A) PEGMA and B) PMPS8

Physicochemical and electrochemical characterization of polymer electrolytes: After the synthesis and purification of samples, they were put to dry overnight in a vacuum oven at 50°C and stored in a desiccator hermetic vacuum, using drierite as a desiccating agent, for its further use. Impedance measurements were made with two electrodes (of parallel plates) electrochemical device placed in a box of gloves with atmosphere of argon. The cell temperature was controlled within a range of temperatures of $25\text{--}100^\circ\text{C}$. The impedance spectra were performed over a range of frequencies of 1.0 MHz to 0.1 Hz with amplitude of potential AC of 50 mV in a Potentiostat/Galvanostat BioLogic VMP3-Multi attached to a PC with a Software (FRA) frequency response Analyzer. Patterns of diffraction of X rays for samples were obtained from an advanced X-ray diffractometer (Bruker D-8 with geometry Bragg-Brentano), using radiation $\text{CuK}\alpha$, through the accomplishment of sweeps at $1^\circ/\text{min}$ from 2θ from 2 to 70° .

Results and Discussion

Morphology of the samples

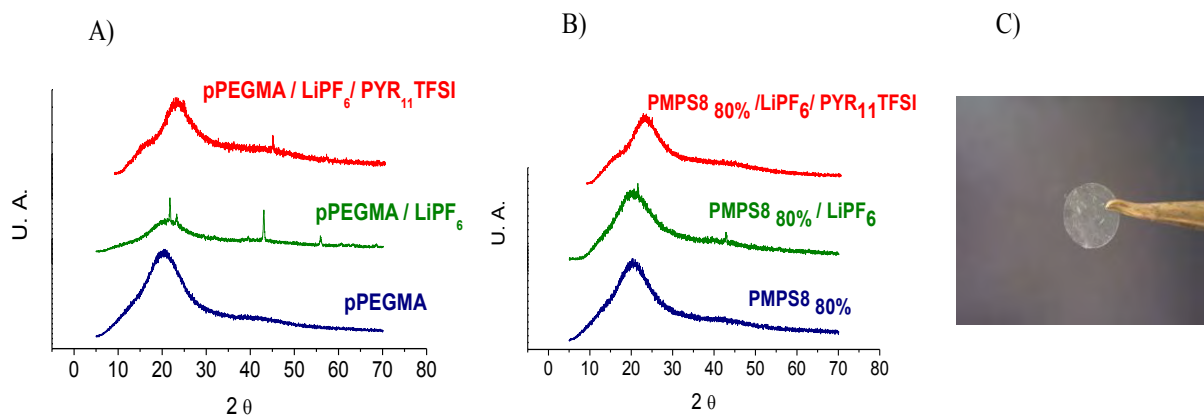


Figure 2. X-ray Diffraction patterns: A) PEGMA B) PMPS8 80% functionalized and their mixtures with lithium salt and ionic liquid: C) film of $\text{PMPS8}/\text{LiPF}_6/\text{PYR}_{11}\text{TFSI}$.

X-ray Diffraction patterns (figure 2 A y B) show a characteristic amorphous phase of the pPEGMA and PMPS8, but in binary system pPEGMA/ $LiPF_6$, there are separation phases. Meanwhile the systems PMPS8/ $LiPF_6$, there is a good solubility of lithium salt. This proves that the presence of sulfobetaine groups help to dissociate lithium salt. When the IL is added in PMPS8, the salt is completely solubilized, due IL has good solvent properties.

Determination of ionic conductivity by EIS

The samples were analyzed by Electrochemical Impedance Spectroscopy (EIS). The ionic conductivity value was obtained according to following equation:

$$\sigma = \frac{l}{R_b A}$$

Where A is the area of the electrodes, l is the length of the current passage between them and R_b represents the resistance of Polymers electrolytes.

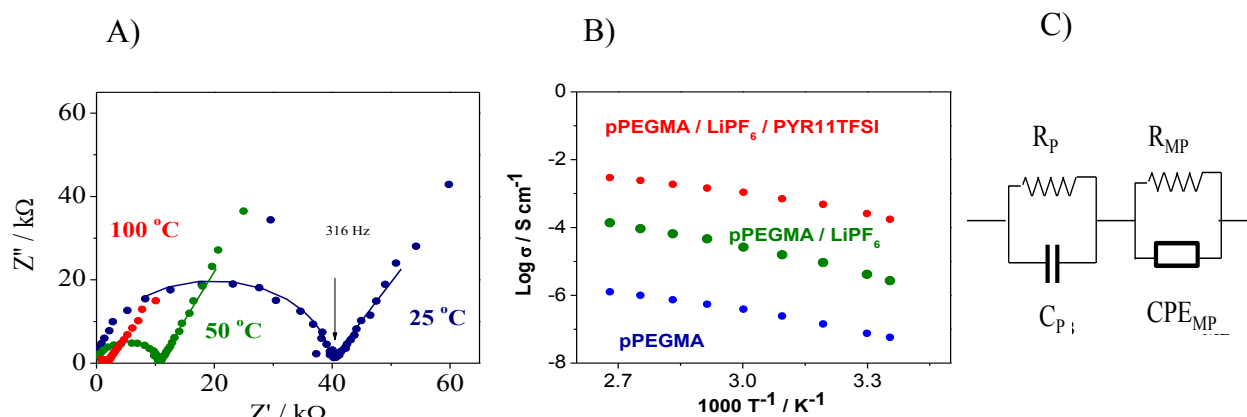


Figure 3. A) Cole-Cole diagrams of the pPEGMA three-temperature 25 °C, 50 °C and 100 °C; B) Arrhenius plots: for pPEGMA, pPEGMA/ $LiPF_6$, and pPEGMA/ $LiPF_6$ /PYR11TFSI; C) Equivalent circuit representing the polymer electrolyte.

In this work was to carry out a preliminary study of the conductivity as a function of the temperature (25 to 100 °C) of the polymer without functionalize (pPEGMA), the binary system pPEGMA/ $LiPF_6$ and the ternary system pPEGMA/ $LiPF_6$ / PYR₁₁TFSI (Figure 3). Table 1 shows that the presence of salt in the binary system (pPEGMA/ $LiPF_6$) the conductivity value increase two orders of magnitude, 10^{-8} at 10^{-6} Scm^{-1} with respect to the pPEGM, because the ion lithium transport is carried out, through the interaction of the ethoxy groups. Salt concentration in molar ratio (EO/Li = 5) indicates 5 ethoxy groups available for ion lithium. It is important to mention that the intrinsic conductivity of the pPEGMA is greater than the polymers that are reported by other authors [4] this is due to the synthesis method used in this work. The presence of the PYR₁₁TFSI improvement the transport properties, reaching a conductivity value of 10^{-4} Scm^{-1} at 25 °C (Table1) but is important to note that there is still phase separation (figure 2A).

In binary systems, PMPS8/ $LiPF_6$ (Table 2) the conductivity increased three orders of magnitude (10^{-5} Scm^{-1}) at room temperature compared to unfunctionalized. In ternary system, only PMPS8

partially functionalized, 80% (Table 2) reaches a value 10^{-4} Scm^{-1} at 25 °C and 10^{-3} at 50 °C, which is more higher than the values reported for other composite polymer electrolyte. This latter is temperature value at which batteries usually operate [5].

Table 1

Sample	σ / Scm^{-1} 25 °C	σ / Scm^{-1} 50 °C	Tg
pPEGMA	7.54×10^{-8}	2.76×10^{-7}	-48
pPEGMA / LiPF ₆	2.69×10^{-6}	1.57×10^{-5}	-32
pPEGMA / LiPF ₆ /PYR ₁₁ TFSI	1.91×10^{-4}	7.04×10^{-4}	-52

Table 2

Polymer Electrolyte	σ / Scm^{-1} 25 °C	σ / Scm^{-1} 50 °C	Tg
PMPBS8	2.29×10^{-5}	7.96×10^{-5}	-44
PMPBS8/LiPF ₆	2.26×10^{-5}	1.52×10^{-4}	-42
PMPBS8/LiPF ₆ /PYR ₁₁ TFSI	4.07×10^{-4}	1.55×10^{-3}	-49

Table 1 and 2. Conductivity and glass temperature values for pPEGMA and PMPS8 systems at 25 and 50 °C.

The temperature dependence of the ionic conductivity (figure 4) was well-described by the following Vogel-Tamman-Fulcher (VTF) equation in the temperature range of 25 - 100 °C:

$$\sigma T^{1/2} = \sigma_{\infty} \exp \left[\frac{-E_a}{R(T - T_0)} \right]$$

Where σ_{∞} is the fitting parameter, E_a is the activation energy, R the gas constant, and T_0 is often related to the glass transition temperature (T_g). The VTF expression implies that the main mechanism of ion conduction can be related to the free volume theory.

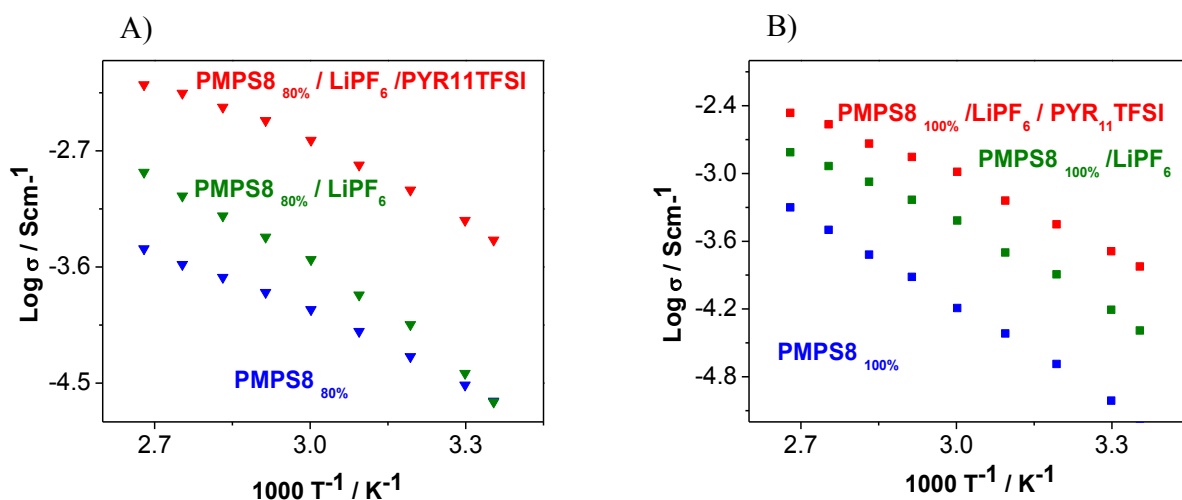


Figure 4. Arrhenius plots for: A) PMPS8-80, PMPS-8-80/LiPF₆ and PMPS8-80/LiPF₆/PYR11TFSI; B) PMPS8, PMPS8/LiPF₆ and PMPS8/LiPF₆/PYR11TFSI.

Conclusions

It was presented morphology and electrochemistry properties for three different polymers and their mixture with lithium salt and ionic liquid. To make measurements of ionic conductivity a film from a solution of polymer and $LiPF_6$ was generated in the ratio of 1:1 in mol in 1,4-dioxane. Measurements were performed with a strict control of moisture ($<0.2\%$) in the range of 25-100 °C. The intrinsic conductivity of the pPEGMA is greater than the polymers that are reported by other authors, this is due to the synthesis method used in this work. Systems PMPS8/ $LiPF_6$ show amorphous phase, their proving that the presence of sulfobetaine groups help to dissociate lithium salt, also their conductivity increased three orders of magnitude (10^{-5} Scm^{-1}) at room temperature compared to binary unfunctionalized system. In ternary systems, the presence of ionic liquid improve the conductivity in all cases, whose values are 10^{-4} Scm^{-1} at room temperature, but only PMPS8 partially functionalized (80%) reaching values to 10^{-3} Scm^{-1} at 50 °C, due to structure allows more free movement of ionic liquid.

Acknowledgements

The authors want to thank the financial support of the Ministry of Science and Technology and Innovation through the project PICCO11-22. Also special thanks to LDRX (T-128) UMI-I for XRD measurements.

References

- [1] D. Bisquert, S. Cahen, G. Rühle, C. Hodes, and A. Zaban, "Physical chemical principles of photovoltaic conversion with nanoparticulate, mesoporous dye- sensitized solar cells.," J. Phys. Chem. B 108, 8106 (2004)
- [2] K. Hatada, T. Kitayama, O. Vogl. Macromolecular design of polymeric materials. Plastics Engineering; 40. 1997.
- [3] G. Guzmán, D. Nava, J. Cardoso, I. González. Macromex 2014 (in edition)
- [4]. G. B. Appetecchi, G. T. Kim, M. Montanino, M. Carewska, R. Marcilla. Journal of Power of Sources 195 (2010) 3668-3675.
- [5] D. Linden, T. B. Reddy, 2002, "Handbook of Batteries", 3a Ed, McGraw- Hill, USA.

Au NANOPARTICLES SUPPORTED ON AMINOPROPYL FUNCTIONALIZED SILICA PARTICLES AS CATALYST FOR THE SELECTIVE OXIDATION OF STYRENE

Martínez-Lejía, Dalia Carolina;^{1,2} Moggio, Ivana;¹ Romero-García, Jorge;¹ Gallardo-Vega, Carlos Alberto;¹ Arias, Eduardo;¹ Torres-Lubián, José Román.²

¹ Departamento de Materiales Avanzados. ² Departamento de Síntesis de Polímeros, Centro de Investigación en Química Aplicada, Blvd. Enrique Reyna 140, Saltillo Coah., C.P. 25294, México.

Abstract

Au nanoparticles (AuNPs) of 7.5 ± 1.4 nm were synthesized by reduction of the hydrogen tetrachloroaurate (III) hydrate with boron hydride in the presence of commercial aminopropyl silica particles (size 40–63 μ m). The content of gold of the AuNPs on the Si surface particles was determined by atomic absorption spectroscopy, while their morphology was studied by SEM, TEM and EFM. The Si/AuNPs were used as catalysts in the oxidation of styrene to form the corresponding epoxide by using peroxide as oxidant. It was found that both the yield and selectivity of the products formed during the oxidation were very sensitive to the experimental conditions; for instance, if the reaction was carried out under vacuum, the styrene consumption was of 50%. In contrast, if the reaction was achieved under air, this was of around 90%, while the selectivity to generate the epoxide group was of 62 %.

Introduction

In the epoxidation of styrene, the selectivity to epoxide it is an important fact as byproducts are obtained from oxidation. An oxidant agent is needed for reaction, the most common ones at industrial level being peracids as peracetic acid¹, hydroperoxides as *t*-butyl hydroperoxide (TBHP)^{2,3} or ethylbenzene hydroperoxide⁴; H₂O₂⁵ and molecular oxygen⁶. A catalyst that promotes the conversion of olefin into epoxide group is also necessary, some useful catalysts are metal complexes as molybdenum^{7–9}, titanium¹⁰, magnesium¹, ruthenium¹¹, cobalt¹², organometallic compounds or coordination complexes with salen¹³, porfirins¹¹, Schiff⁸ bases, metallic oxides³ ligands, zeolites¹² and gold nanoparticles^{2,6,14–17}.

Gold catalytic activity in organic compounds oxidations has been studied in recent decades, particularly gold nanoparticles (AuNPs) with 1–42 nm in size present an interesting catalytic activity in aerobic oxidations and are able to activate oxygen molecules in their surface. Selective epoxidation of terminal olefins is important in synthetic industrial processes to obtain precursors from other reactions as valuable epoxides. Haruta *et al.* discovered the activity of supported AuNPs (AuTiO₂) as catalyst in propylene oxide OP synthesis and with H₂/O₂ as oxidant. These authors also compared the results with Pt, Pd and Ag NPs and they concluded that AuNPs are more selective.¹⁸ After that the interest in AuNPs heterogeneous catalysis increased, many works for different preparation methods have been published: homogeneous deposition precipitation, impregnation, post-synthesis and post-modification. The nature of the support, synthesis method and AuNPs size are important factors in catalytical activity.¹⁹ The most common oxidant used in the selective epoxidation of styrene assisted by AuNPs is TBHP. In this work we report the selectivity of AuNPs prepared in situ on commercial aminopropyl silica particles in the catalysis of the epoxydation of styrene.

Experimental

Synthesis of supported gold nanoparticles. 100 mg of functionalized silica were dispersed in 10 mL of ethanol with an ultrasonic bath for 5 min. The corresponding milligrams of gold(III) chloride (HAuCl₄) to prepare 3, 5 and 7% p/p Au charge were dissolved in 1 mL of ethanol, and slowly added into the dispersion of silica under vigorous stirring, the dispersion turned into pale yellow. It was kept under stirring for 1 h

and then 1 mL of a freshly prepared solution of NaBH_4 (concentration adjusted at a relationship of 4:1 mol/mol with HAuCl_4) in ultrapure water was slowly added. The color turned into dark purple. It was kept under stirring for 3 h and finally the silica with AuNP's was washed three times with ethanol and dried under vacuum.

Epoxydation reaction with supported AuNP's catalyst.

2.5 mmol of styrene (0.29 mL), 10 mg of $\text{AuSiO}_2(\text{CH}_2)_3\text{NH}_2$ and 3.75 mmol of TBHP (0.625 mL), were reacted in a flask under reflux, heated at 85 °C with an oil bath and provided with a CaCl_2 tramp for 3 h (figure 1).

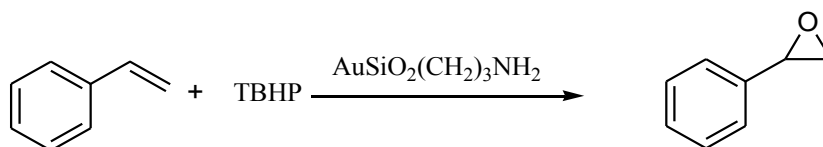


Figure 1. Styrene epoxydation with AuNPs as catalyst and TBHP as oxidant agent.

Characterization. ^1H (300 MHz) spectra were obtained at room temperature with a Jeol Eclipse spectrometer using CDCl_3 as solvent and internal reference. Transmission electron microscopy (TEM) studies have been carried out in a FEI-TITAN-300 kV field emission gun microscope, which has a symmetrical condenser-objective lens S-TWIN type (with a spherical aberration $C_s = 1.25$ mm). Images were acquired in a CCD camera. The nanoparticles were deposited by casting a dilution of the reactions suspension on copper grids. AFM morphological characterization was performed on a Nanoscope III DimensionTM 3100 from Digital Instruments with a Pt-coated Si tip (20 nm nominal radius) in tapping and Electrical Force Mode (EFM) at a scanning rate (256 lines) of 0.2 Hz. For EFM studies, a voltage of 12V was applied to the tip and the separation distance was 100 nm.

Results and Discussion.

The AuNP's supported on commercial 3-aminopropyl silica were obtained in two loadings: $3.6 \pm 0.3\%$ p/p and $6.9 \pm 0.5\%$ p/p Au, as determined by atomic absorption. A change in color from white to purple as compared with $\text{SiO}_2(\text{CH}_2)_3\text{NH}_2$ was observed by optical microscopy. Morphological and structural NP's characterization was accomplished by TEM. The AuNPs with 3.6% p/p of loading are spherical with an average size of 7.6 ± 1.4 nm (figure 2) while the higher loading presents polyhedral particles with 15.1 ± 4.6 nm. $\text{AuSiO}_2(\text{CH}_2)_3\text{NH}_2$ with 3.6% p/p Au has the most appropriate morphology and size distribution for catalysis and the results with those particles (hereafter called just AuNPs) will be considered for the following.

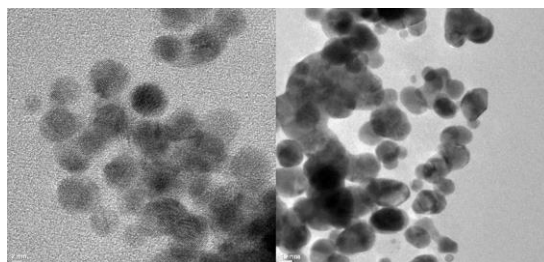


Figure 2. TEM from supported AuNPs on $\text{AuSiO}_2(\text{CH}_2)_3\text{NH}_2$ with different loadings. Left: 3.6 wt% Au, right: $7,6 \pm 1,4$ nm.

The distribution of the gold nanoparticles on the silica was investigated by electrical force microscopy (EFM). In figure 3, the EFM images (right images) of AuNPs and of silica (bottom) reveal the presence of the gold nanoparticles as conductive regions. By comparing those images with the topographic ones (left images), it can be observed that the particles are on the surface as expected.

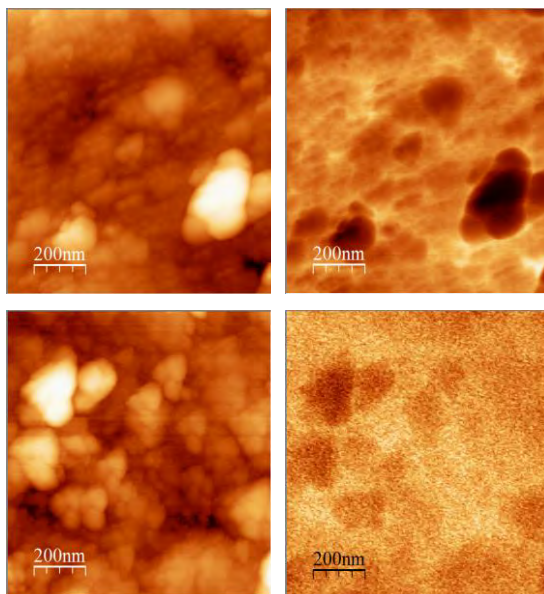


Figure 3. AFM Tapping images (left images) and EFM (right images) of AuNPs (top) and silica (bottom).

Catalytic Studies. The AuNPs were tested in the epoxidation of styrene using TBHP as oxidant agent. Two reaction blanks (figure 4) were first performed and the chemical structure of the products was determined by RMN ^1H . In the reaction 1 carried out in inert atmosphere (table 1), styrene conversion was 75% and phenylformate ($\text{H}(\text{CO})\text{OPh}$) and others (scheme a, figure 4) were obtained as byproducts. In the reaction 2, table 1, the second blank experiment, gave 69% of styrene conversion and 21.4% of styrene oxide (SO) selectivity. 1-phenylethane-1,2-diol, benzaldehyde, 2-2-hydroxy-1-phenylethanone (HPE), and others (scheme b, figure 4) were obtained as by-products. Only TBHP has no selectivity to SO, instead the bi-alcohol is in mayor proportion due the humidity present in the system.

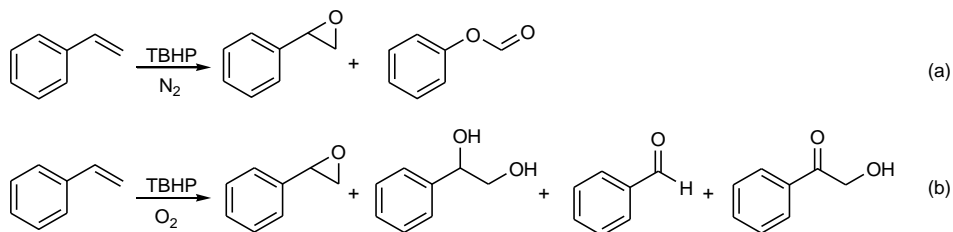


Figure 4. Products of the oxidation of styrene with TBHP.

When AuNPs were used as catalysts and in inert atmosphere (reaction 3, table 2) the SO selectivity increased comparing with the blank. Reaction 4, performed in O_2 atmosphere, presents also an increase in SO selectivity and styrene conversion percent. Reaction 5 that was accomplished in an aerobic system, gives the highest yield of 57,9% and selectivity of 64.6%. Comparing with reaction 3 and 4, it can be inferred the participation of water or molecular oxygen as a possible proton acceptor in the epoxidation mechanism.

The AuNPs catalyst has been used 2 more times in reaction 5, filtered and washed several times with chloroform, and then dried under vacuum, after that it was used again (reactions 6 and 7). It can be noted that the St conversion and SO selectivity, even if lower, is still quite good indicating a good re-usability of the catalyst.

Table 1. Styrene epoxidation reaction with TBHP^a.

	% Yield			% Selectivity					
	Au % Mol	St % Conversion	SO	SO	Benzaldehyde	Bi-alcohol	HPE	Others	TOF (h ⁻¹) ^d
1	-	75.1	16.1	13.8	-	-	-	86.2	-
2	-	69.1	9.52	21.4	5.19	39.8	9.32	24.2	-
3	0.0704	51.9	31.1	59.9	-	20.0	-	20.0	147
4	0.0704	91.1	26.3	28.9	9.89	35.3	19.6	6.27	124
5	0.0704	89.6	57.9	64.6	0.76	18.6	8.53	7.34	274
6 ^b	0.0704	97.4	53.2	52.4	5.86	17.7	15.7	8.23	252
7 ^c	0.0704	85.2	44.8	52.6	1.48	11.7	22.4	12.2	212

^a 3.75 mmol TBHP, 80 °C, 3 h. ^b 2^o reuse. ^c 3^o reuse ^d TOF= SO mol/Au mol per h.

In table 2, we finally compare the catalytic performance of AuNPs with literature works which also used supported AuNPs for styrene epoxidation, using TBHP as oxidant, and temperatures from 80 to 85 °C for all cases. It can be observed that the NP's size, the support's nature and NP's preparation method have an influence in the catalyst activity. This work has the highest TOF (the number of revolutions of the catalytic cycle per unit). Also it can be deduced that the combination between nanoparticle size, Au wt% and preparation method are directly related with the NP's size and catalytic activity in the present reaction.

Table 2. Comparison from AuNPs based catalyst styrene epoxidation.^a

Catalyst	Preparation method ^b	Au wt%	AuNPs Diameter (nm)	St % Conv.	SO % Sel.	TOF ^c (h ⁻¹)	Ref.
Au/MgO	HDP	7.5	7.9±0.3	62.6	54.3	29.8	3
Au/Al ₂ O ₃	HDP	6.4	4.1±2.3	44.0	28.0	11.4	20
Au/PMO-SBA-15	Postsintesis	2.0	1.8	94.8	75	58.4	21
Au/LDH	HDP	5.5	5.8±1.5	61	53	47.8	17
Au/TiO ₂	HDP	6.0	2.8±0.8	61	53	34.4	22
Au/HPA	IM	0.5	1.4±0.6	100	92	114	2
Au/SiO ₂	HDP	4.0	6.4	98.5	82.8	66.9	17
AuSiO ₂ (CH ₂) ₃ N H ₂	HDP	3.6	7.6 ± 1,4	89.6	64.6	274	This work

^a The reactions were run using TBHP and 80-85°C. ^b HDP: homogenous deposition-precipitation, IM: impregnation. ^c TOF: St mol/Au mol per h.

Conclusions

Gold nanoparticles supported on 3-aminopropyl functionalized silica synthesized by direct reduction of the gold salt in presence of the silica support and with two different charge percentage, 3.6 and 6.9 wt%, giving a diameter of 7.6 and 15.1nm respectively. 3.6 wt% AuNPs have an average diameter less than 10 nm, and

also have a narrow size distribution and spherical morphology observed by TEM. Agglomeration of gold nanoparticulas is also observed, however an uniform distribution over $\text{SiO}_2(\text{CH}_2)_3\text{NH}_2$ was determined by EFM, likely due to the presence of aminopropyl groups which are electron donors and can work as stabilizers of gold nanoparticles. In catalytic studies, styrene oxide was obtained from styrene with TBHP as oxidant agent and $\text{AuSiO}_2(\text{CH}_2)_3\text{NH}_2$ (3.6 Au wt%), the styrene oxidation occur with a conversion of 90%, styrene oxide is obtain with 58% of selectivity and final yield of 64%, and a $\text{TOF}=274\text{h}^{-1}$. The catalyst is very active still after three uses even if a decrease in selectivity is observed after each reuse. The reaction is accomplished more efficiently in aerobic atmosphere comparing with inert atmosphere (N_2) and oxidant atmosphere (O_2), which are water free. This results suggests that water or molecular oxygen participate in the epoxidation reaction.

Acknowledgements:

Gabriela Padrón Gamboa y Josefina Zamora Rodríguez, Jesús Alejandro Espinoza Muñoz, Ma. Luisa López Quintanilla, Ma. de Lourdes Guillén Cisneros. for technical help. CONACyT and SEP for the financial support on the following projects: SEP-CONACyT CB-2009-131103 and SEP-CONACyT 98513R.

References:

- [1] Garcia-Bosch, I.; Company, A.; Fontrodona, X.; Ribas, X.; Costas, M. *Org. Lett.*, 10, 2095–8 (2008).
- [2] Liu, Y.; Tsunoyama, H.; Akita, T.; Tsukuda, T. *Chem. Commun.*, 46, 550–2 (2008).
- [3] Patil, N. J. *Catal.*, 223, 236–239 (2004).
- [4] Vassilev, K.; Turmanova, S.; Dimitrova, M.; Boneva, S. *Eur. Polym. J.*, 45, 2269–2278 (2009).
- [5] Grigoropoulou, G.; Clark, J. H.; Elings, J. a. *Green Chem.*, 5, 1–7 (2003).
- [6] Ren, Y.; Xu, L.; Zhang, L.; Wang, J.; Liu, Y., 84, 561–578 (2012).
- [7] Abrantes, M.; Neves, P.; Antunes, M. M.; Gago, S.; Almeida Paz, F. a.; Rodrigues, A. E.; Pillinger, M.; Gonçalves, I. S.; Silva, C. M.; Valente, A. a. *J. Mol. Catal. A Chem.*, 320, 19–26 (2010).
- [8] Tangestaninejad, S.; Moghadam, M.; Mirkhani, V.; Mohammadpoorbaltork, I.; Ghani, K. *Catal. Commun.*, 10, 853–858 (2009).
- [9] Barrio, L.; Campos-Martín, J. M.; de Frutos, M. P.; Fierro, J. L. G. *Ind. Eng. Chem. Res.*, 47, 8016–8024 (2008).
- [10] Matsumoto, K.; Oguma, T.; Katsuki, T. *Angew. Chemie*, 121, 7568–7571 (2009).
- [11] Chatterjee, D. *Coord. Chem. Rev.*, 252, 176–198 (2008).
- [12] Sebastian, J.; Jinka, K.; Jasra, R. J. *Catal.*, 244, 208–218 (2006).
- [13] Silva, A.; Freire, C.; Castro, B. *De New J. Chem.*, 28, 253–260 (2004).
- [14] Chang, C.-R.; Wang, Y.-G.; Li, J. *Nano Res.*, 4, 131–142 (2010).
- [15] Zhu, K.; Hu, J.; Richards, R. *Catal. Letters*, 100, 195–199 (2005).
- [16] Sun, J.; Fujita, S.; Zhao, F.; Hasegawa, M.; Arai, M. *J. Catal.*, 230, 398–405 (2005).
- [17] Liu, J.; Wang, F.; Qi, S.; Gu, Z.; Wu, G. *New J. Chem.*, 37, 769 (2013).
- [18] Sinha, A. K.; Seelan, S.; Tsubota, S.; Haruta, M. *Top. Catal.*, 29, 95–102 (2004).
- [19] Ma, Z.; Dai, S. *Nano Res.*, 4, 3–32 (2010).
- [20] Patil, N. S.; Jha, R.; Uphade, B. S.; Bhargava, S. K.; Choudhary, V. R. *Appl. Catal. A Gen.*, 275, 87–93(2004).
- [21] Jin, Y.; Wang, P.; Yin, D.; Liu, J.; Qiu, H.; Yu, N. *Microporous Mesoporous Mater.*, 111, 569–576 (2008).
- [22] Patil, N. S.; Uphade, B. S.; Jana, P.; Sonawane, R. S.; Bhargava, S. K.; Choudhary, V. R. *Catal. Letters*, 94, 89–93(2004).

NANOPARTICLES OF POLYMERS SYNTHESIZED BY PLASMA POLYMERIZATION.

M. VASQUEZ-ORTEGA¹, M. ORTEGA-LOPEZ¹, J. MORALES-CORONA², R. OLAYO².

1. Departamento de Ingeniería Eléctrica, Sección de Electrónica del Estado Sólido, Centro de Investigación y Estudios Avanzados del Instituto Politécnico Nacional, Av. Instituto Politécnico Nacional 2508, Col, San Pedro Zacatenco, CP 07360, DF, México

2. Departamento de Física, Área de Polímeros, Universidad Autónoma Metropolitana, Unidad Iztapalapa, Av. San Rafael Atlixco 186, Col, Vicentina, CP 09340, DF, México

ABSTRACT

Plasma polymerization is a method to produce nanoparticles with different monomers, at low or atmospheric pressure. Polymers produced by plasma polymerization are not chemically regular as conventional polymers; they are complex polymers rich in functional groups, some of these groups may not be present in the original monomer, and the concentration of these groups on the surface can be tuned by changing plasma polymerization variables.

In this work, we report the synthesis of several polymeric nanoparticles using monomers as ethylenglicol, hexametildisilixane, pyrrole, and pyrrole doped in situ with iodine. The nanoparticles were studied by FTIR in ATR mode, SEM and TEM, and average size was determined, potential uses are also discussed.

INTRODUCTION.

Today, nanoparticles are used in different fields of science and technology, can be used in controlled drug delivery, electronics, nonlinear optics, cancerous tumors control as well as cell markers in RMI contrast. There are different ways to synthesize nanoparticles, using traditional chemical techniques like sol-gel, electrochemical, etc. Sometimes, generating metal precursor nanoparticles is the star step and than polymer grows, the result is a core-shell type structure. One way of synthesizing solid nanoparticles and polymer core-shell structure is through the plasma polymerization technique under vacuum or atmospheric pressure [1,2]. In this work, plasma polymerization under vacuum and atmospheric pressure of nanoparticles from different monomers is studied.

EXPERIMENTAL

For the nanoparticles synthesis two types of plasma, vacuum and atmospheric pressure reactors are used. The scheme of the reactor used is shown in Fig. 1. Fig. 1(a) shows the reactor operating under vacuum and in Fig (b) the reactor operating at

atmospheric pressure. A detailed description of this operation can be found in [1,2]. The monomers used were: In a vacuum reactor polyethylene glycol, PEG, Polypyrrole, PPy, and a copolymer of Polypyrrole and polyethylene glycol, PEG-PPy, these materials have applications in the reconnection of the spinal cord of rats. In the atmospheric pressure reactor polyhexamethyldisiloxane, PHDMS-ATM, the PPy-ATM and a core-shell PPy-ATM. The conditions of synthesis for these materials are shown in Table 1.

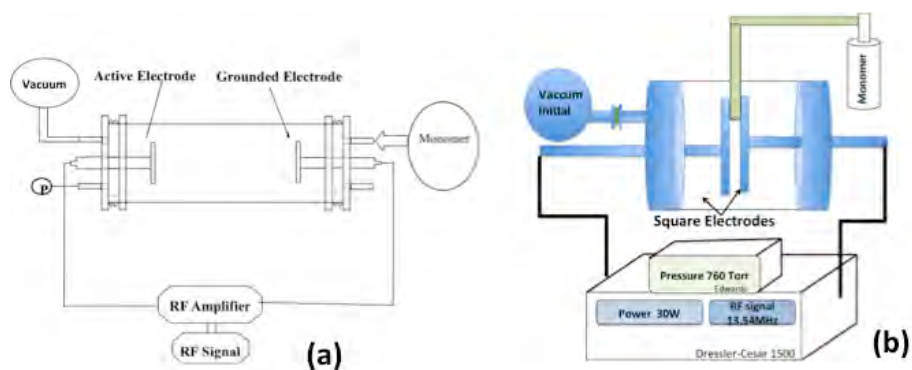


Fig.1 Plasma reactors, (a) to vacuum, (b) atmospheric pressure.

Table 1. Experimental conditions to synthesis of several nanoparticles.

Polymer	Reactor	Pressure (Torr)	Power (W)	Synthesis time (min)	Distance between electrodes (mm)
PEG	Vaccum	2×10^{-2}	100	30	50
PPY	Vaccum	2×10^{-2}	120	30	50
PPy-PEG	Vaccum	2×10^{-2}	100	30	50
PPy-ATM	Atmospheric pressure	760	20	60	7
PHDMS-ATM	Atmospheric pressure	760	20	60	7
PPy-ATM-CS	Atmospheric pressure	760	18	60	7

RESULTS.

PEG-Nanoparticles

In Fig. 2 shows PEG nanoparticles synthesized in the plasma reactor under vacuum, dispersed spherical particles are on the surface, it also shows the size distribution, the average particle size was 70nm with a standard deviation of 31nm. Finally it shows the infrared spectrum in absorption mode. The absorption band at 3437 cm^{-1} is due to the O-H stretching band, 2932 cm^{-1} is due to the aliphatic group C-H in mode stretching, 1366 is due to C-H bending vibrations, and also the combination of O-C-H and C-O-H deformation bands. The vibration in the plane of C-H and O-H groups appears in 1166

cm^{-1} can be observed. In the region 571 cm^{-1} , the C–O and C–C groups vibration modes are present.

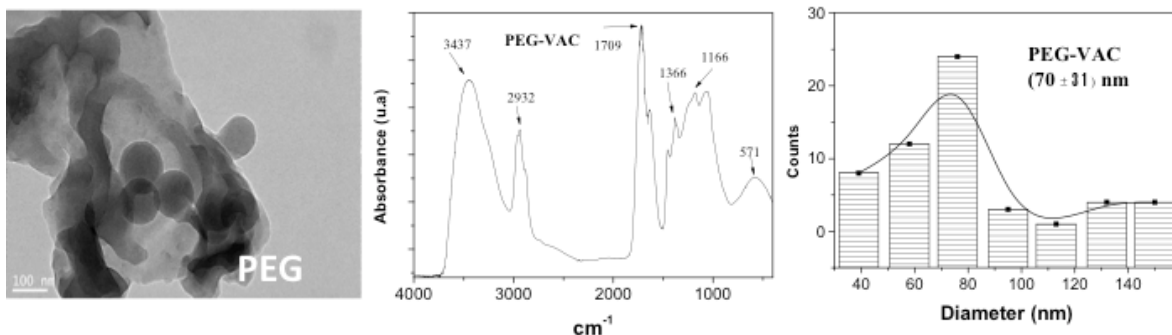


Fig. 2 PEG nanoparticles synthesized under vacuum.

PPy-Nanoparticles

Fig. 3, shows PPy solid clusters of nanoparticles, particles are of different sizes. It also shows the size distribution in the range from 70 nm to 140 nm with an average of 95 nm and a standard deviation of 18 nm and the infrared spectrum in absorption mode. It has broad and complex bands characteristic of plasma polymers. At 3353 cm^{-1} the vibration of the amine groups is shown, while in 2951 cm^{-1} the vibration of aliphatic carbons is present. The peak in 2188 cm^{-1} is an indication of rupture of some pyrrole rings.

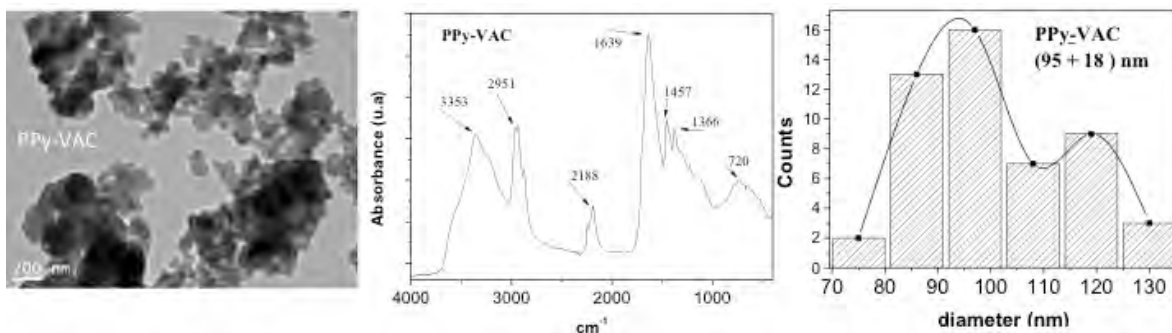


Fig. 3 PPy nanoparticles synthesized in vacuum.

Copolymer of PPy-PEG.

In order to increase the PPy biocompatibility, the polypyrrole and polyethylene glycol copolymerization is performed by plasma polymerization in vacuum. In Fig. 4 nanoparticles of this copolymerization are shown. The histogram of distribution shows a particle distribution ranging from 70 to 220 nm with two modes at 70 nm and 146 nm. It also shows the IR spectra, compared with previous spectra the disappearance of the aliphatic carbons peak in 2951 cm^{-1} can be appreciate and the peak at 3136 cm^{-1} is a combination of vibration of the -OH and -NH₂, including a shoulder near to 3400 cm^{-1} .

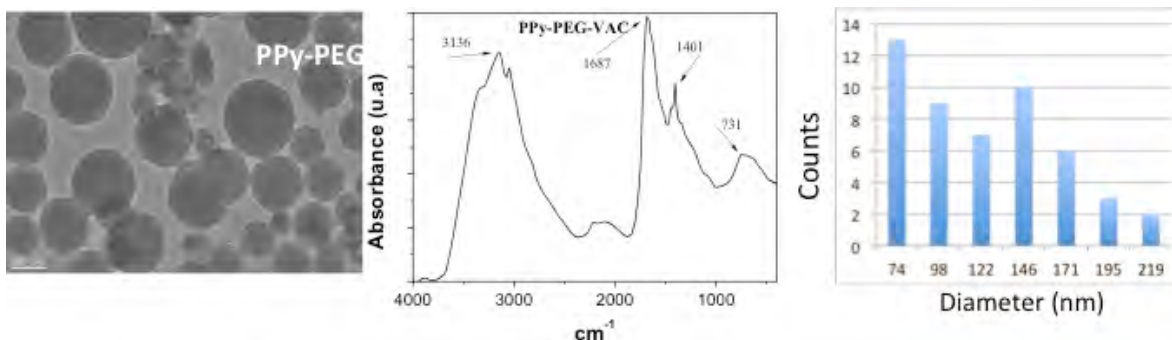


Fig 4. PPy-PEG Copolymer.

PHDMS nanoparticles.

In Fig 5. a TEM micrograph of nanoparticles of poly-hexamethyldisiloxane, PHDMS, synthesized by atmospheric pressure plasma is displayed. Spherical particles formed as a bunch of grapes are appreciated. They have a diameter distribution not very disperse, it is on a range of 40 to 70nm, with an average size of 52nm and a standard deviation of 7nm. Figure also shows the FT-IR spectrum of the PHDMS nanoparticles in absorption mode. In 3347cm^{-1} vibration of Si-CH₃ group is appreciated. The vibration of the aliphatic carbons are centered at 2964cm^{-1} , CH₂ and CH₃. The group associated with the symmetric deformation vibration of Si-CH₃ has its peak at 1263cm^{-1} . The most intense peak in the spectrum, which corresponds to silicon oxide, SiO_x, is centered on the 1063cm^{-1} . The peak at 791cm^{-1} is assigned to the vibration of the CH₃ bond. This material was also synthesized in a vacuum plasma reactor [3] and IR spectra show that there is no difference in the material.

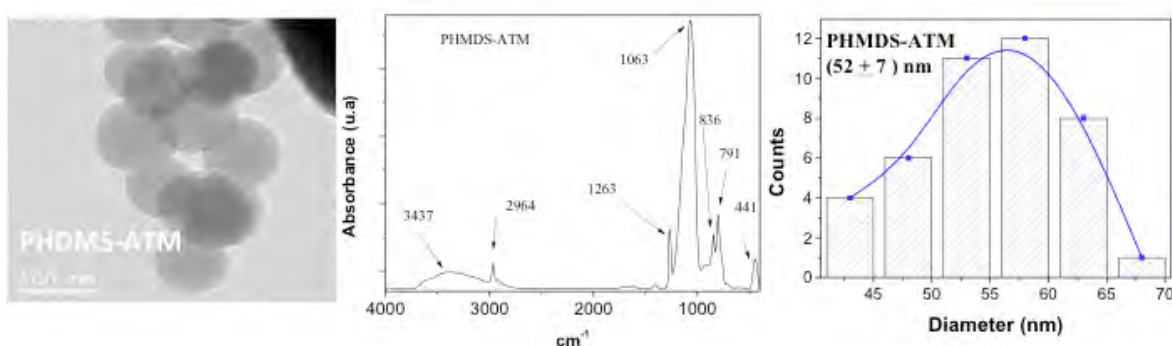


Fig. 5 PHDMS nanoparticles synthesized to atmospheric pressure.

PPy nanoparticles at atmospheric pressure.

Nanoparticles of Pyrrole synthesized at atmospheric pressure, are shown in Fig. 6, a TEM micrograph of these nanoparticles is shown with an average size of (230 ± 40) nm. These particles have a core-shell structure as can be seen, a detailed discussion of their synthesis and their characterization is shown in the ref [2]. IR shows broad bands and complex characteristics of the materials synthesized by plasma. At 3329

cm^{-1} a strong vibration is associated with aromatic amines of pyrrole, during the polymerization tertiary, secondary and primary amines can be originate. At 2956 cm^{-1} the vibration of the aliphatic carbons of pyrrole is reported. The absorption found at 2191 cm^{-1} corresponds to the vibration of the $\text{C}\equiv\text{N}$ bond. At 1633 cm^{-1} is the $\text{C}=\text{C}$ and at 1456 cm^{-1} the $\text{C}-\text{C}$ bond.

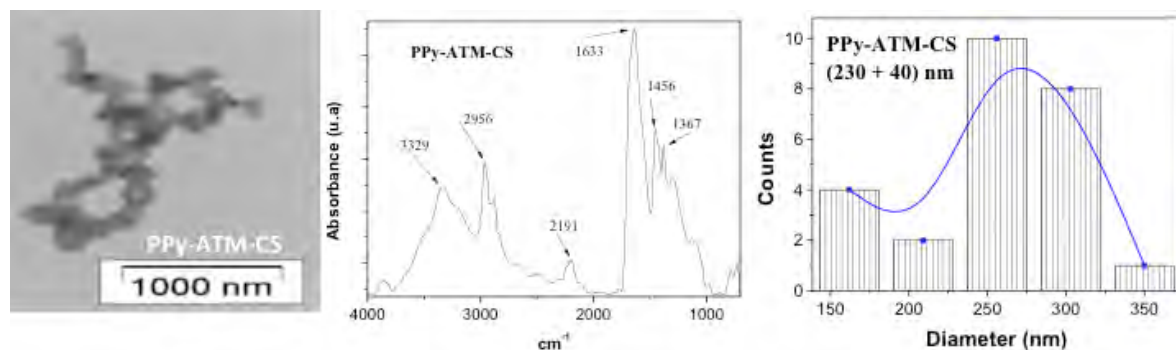


Fig. 6 nanoparticles PPY core-shell type.

Conclusions.

Polymer nanoparticles can be synthesized from various monomers by the plasma polymerization technique under vacuum and atmospheric pressure. FTIR shows that polymers generated by vacuum or atmospheric pressure have the same functional groups that the bulk plasma polymers. These materials have shown a good response when interacting with biological systems, since they allow the cell anchor growth and differentiation while maintaining viable and functional. Nanoparticles PPY-ATM-CS is hollow and may be employed in controlled drug delivery.

Acknowledgements

The authors wish to thank: Consejo Nacional de Ciencia y Tecnología for partial support for the realization of this work through project CONACYT-15523 respectively and the Laboratorio de Microscopía de la UAM Iztapalapa.

References.

1. G.J. Cruz, M.G. Olayo, O.G. López, L.M. Gómez, J. Morales, R. Olayo, Nanospherical particles of polypyrrole synthesized and doped by plasma, *Polymer* 51 (2010) 4314-4318. ISSN: 0032-3861.
2. VASQUEZ-ORTEGA MIGUELINA; ORTEGA-LOPEZ MAURICIO; MORALES-CORONA JUAN; Olayo-Gonzalez GUADALUPE; CRUZ-CRUZ, GUILLERMO J.; Olayo, Roberto; Core-shell polypyrrole nanoparticles obtained by atmospheric pressure plasma., *Polymer International* (2014) ISSN: 1097-0126, DOI 10.1002/pi.4756
3. López-Barrea J. Antonio, Pimentel-Tinoco O.G., Roberto Olayo-Valles, Morales-Corona J. and Olayo R. Water permeability of quarry stone superficially modified by plasma polymerization of hexamethyldisiloxane at atmospheric pressure. *J. Coat. Technol. Res.* (2014) DOI 10.1007/s11998-014-9585-8.

PREPARATION OF ZINC OXIDE NANOSTRUCTURES AND HYBRID GRAPHENE/ZINC OXIDE NANOMATERIALS BY A POLYSACCHARIDE AQUEOUS-BASED METHOD

Maira B. Moreno-Trejo¹, Yolanda Agapito-Navarro^{1,2}, Uriel Márquez-Lamas¹, Tania Lara-Ceniceros¹, José Bonilla-Cruz^{1*}, Margarita Sánchez-Domínguez^{1,*}

¹ Centro de Investigación en Materiales Avanzados, S.C.-Unidad Monterrey. Alianza Norte 202, Parque de Investigación e Innovación Tecnológica, C.P. 66600, Apodaca, Nuevo León, México. Email: margarita.sanchez@cimav.edu.mx; jose.bonilla@cimav.edu.mx

² Universidad Tecnológica General Mariano Escobedo, Libramiento Noreste Km. 33.5, C.P. 66050, Escobedo, Nuevo León, México.

Abstract

In this investigation, nanostructured ZnO as well as novel graphene/ZnO nanocomposites were developed and characterized. Nanostructured ZnO was prepared by an aqueous co-precipitation method assisted by a polysaccharide. The synthesis were carried out using three different ZnO:Polysaccharide ratios (1:0.5, 1:1, 1:3). Three different morphologies and sizes were obtained: nanoflowers, nanoalmonds and nanocrosses. XRD results showed that the materials present hexagonal wurtzite structure, with a crystallite size between 12 and 40 nm. The hybrid graphene/ZnO nanomaterials were prepared at three different concentrations of ZnO. The formation of hybrid nanomaterial was confirmed by XRD and SEM.

Introduction

Because of its diverse advantages such as its interesting characteristics, low price, to the numerous practical applications, ZnO has received exceptional attention among numerous semiconducting oxide materials. ZnO is a functional material exhibiting near ultra violet emission, transparent conductivity, semiconducting, magnetic, and piezoelectric properties [1]. Zinc oxide materials and differently shaped ZnO nanocrystals have attracted considerable attention due to their unique properties that strongly depend on their size and morphologies [2]. ZnO occurs naturally in the Earth's crust, and it exists in two main crystalline forms: wurtzite and zinc-blende. The wurtzite structure is the most common and stable form [3]. Therefore, numerous strategies have been attempted to design and fabricate ZnO nanostructures endowed with the suitability to fulfill each purpose for particular applications. Several methods for the fabrication of ZnO nanostructures have been reported, including hydrothermal synthesis [4,5], vapor-liquid-solid (VLS), vapor-solid (VS) [6] processes, metal-organic chemical vapor deposition (MOCVD) [7], chemical vapor deposition [8], solution-liquid-solid growth inorganic solvents [9], and template based methods [10–13]. Most reported synthesis techniques are complicated, time and energy consuming, and not environmentally friendly. In particular, when organometallic precursors are used, complex procedures, high temperatures and sophisticated equipment to control the growth process are involved.

On the other hand, as a new carbonaceous material, graphene has attracted tremendous attention in the past years, due to its unique electronic properties, excellent mobility of charge carriers (200,000 cm² V⁻¹ s⁻¹), and extremely high theoretical specific surface area (~2600 m² g⁻¹) [14]. It was reported that these features can be employed to improve electronic, optoelectronic, electrocatalytic and photocatalytic performance of semiconductor materials [15] as ZnO. Some investigations in graphene/ZnO were also attempted [16–18].

Furthermore, graphene is an important building block in nanotechnology, so that hybrid strategy of graphene with ZnO has provided us with the opportunities for enhancing the intrinsic properties of ZnO in diverse manners. Synergistic effects in photocatalytic,[19-21] electrochemical, [22-24] and optical properties[25-27] have been successfully demonstrated in ZnO-graphene hybrid nanostructures. Because most of the multifunctional properties of ZnO are critically influenced by the behavior of its electrons, understanding the behavior of electrons in the ZnO-graphene hybrid system is of great significance to expand the opportunities in relevant applications.

A simple, inexpensive and green synthesis process is required. Here, we report a novel synthesis route for the preparation of ZnO nanostructures and ZnO-graphene hybrid nanostructures. The growth of shape-controlled ZnO nanostructures in large scale is achieved using a zinc nitrate aqueous solution by adjusting composition, concentration of the polysaccharide and growth temperature.

Experimental

Synthesis of ZnO NPs. First, a certain amount of zinc nitrate hexahydrate (Sigma Aldrich, 98%) and polysaccharide gum (purified in the lab) were dissolved in deionized water at room temperature under constant stirring for 3 h. Then, a certain amount of NaOH was added to the solution under constant stirring in order to raise the pH up to 10-12. After stirring for a few hours, the precipitate was recovered by centrifugation and washing cycles, and the solid was dried at room temperature.

Preparation of Graphene Dispersion. The raw materials are graphite, polysaccharide gum and deionized water. The mixture is processed with a high energy homogenizer (ultraturrax). Turbulent flow helps to delaminate sheets of graphite structure and the polysaccharide gum helps to prevent aggregation or agglomeration of the sheets.

Synthesis of Graphene@ZnO. Graphene nanosheets were used to load ZnO NPs for the production of G@ZnO hybrids via a simple route at room temperature. Briefly, the obtained ZnO powder was added to graphene colloidal suspension in 3 different ZnO concentrations (0.001 M, 0.0001 M, and 0.0005 M) with an identical proportion of polysaccharide gum. The suspension was vigorously stirred for 2 h, sonicated for 10 min and subsequently heated at 80° C to obtain the hybridized ZnO/graphene after evaporation the water.

Characterization. X-ray diffraction (XRD) data were obtained on a Panalytical Empyrean Power X-ray Diffraction (40 kV) with Cu-K α radiation. The morphologies and structures of the samples were investigated by scanning electron microscopy (SEM) Nova Nano 200 FEI and the thermal analyses were with the equipment SDT Q600 from TA Instruments.

Results and Discussion

ZnO NP Results

ZnO nanoparticles produced by the method of precipitation assisted by a natural polysaccharide gum were analyzed by SEM. Figure 1 shows micrographs of the different morphologies obtained. In Figure 1 A) it can be observed that with a 1:1 ratio of zinc nitrate:natural polysaccharide gum, the morphology of nano-flower or nano-star is obtained, but if the concentration of polysaccharide gum is reduced as in the case of B) the size is increased and the morphology is modified to almond shape; when an excess of polysaccharide gum is added as in C) 0.5 micron size particles are obtained and a morphology of nano-cross is obtained.

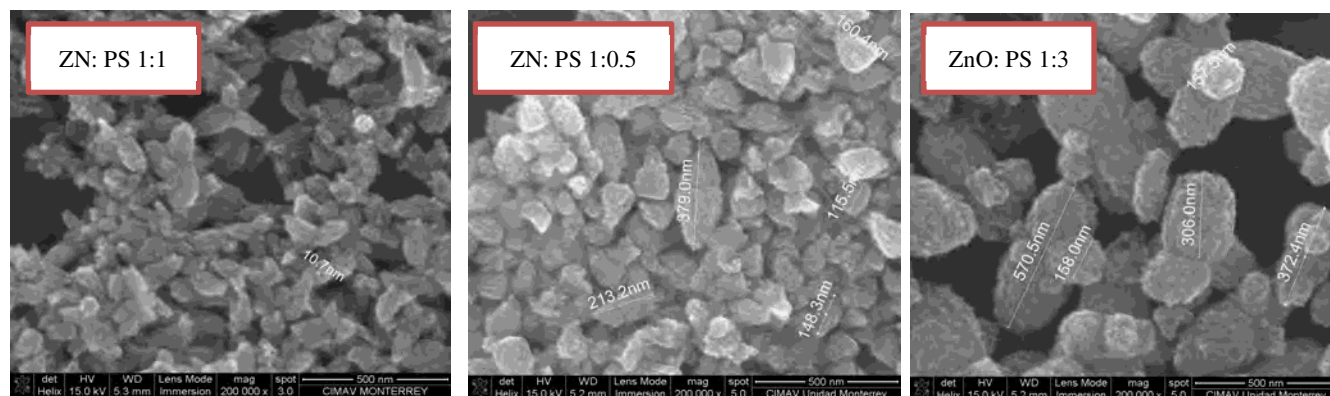


Figure 1.- SEM Micrographs of ZnO nanoparticles obtained at different Zinc Precursor:Polysaccharide gum ratios: A)1:1; B) 1:0.5; and C) 1:3.

Graphene@ZnO Results

X-ray Diffraction

In figure 2 a diffractogram of the nanocomposite graphene@ZnO is shown; the main signals of hexagonal ZnO were evident, and these can be seen from 30°-38°; the wide signals from 0-30° were attributed to graphene natural structure.

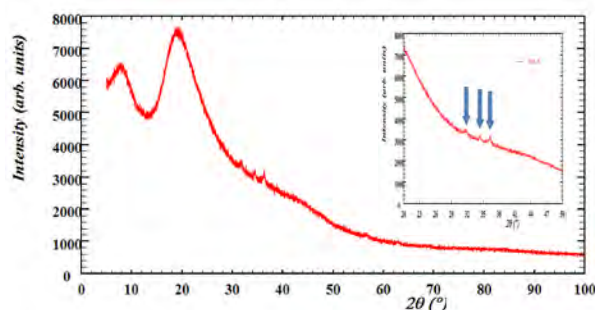


Figure 2.- X-ray diffractogram of Graphene@ZnO nanocomposite.

SEM and EDS Results.

A SEM micrograph of the hybrid material Graphene@ZnO is shown in figure 3; in A) a cluster is observed, however when analyzed at higher magnifications (B) it is possible to distinguish that the cluster is composed of smaller ZnO nanoflowers. Moreover the smoother areas are also distinguished, this layer is graphene.

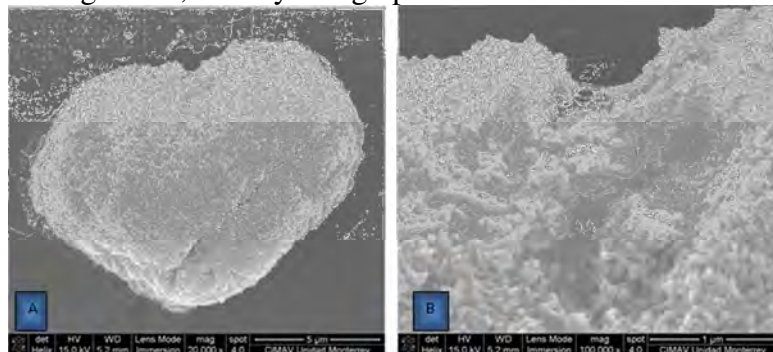


Figure 3.- Graphene@ZnO SEM micrograph: A) Cluster B) ZnO nanoflowers coating a Graphene layer.

In the elemental analysis by EDS, it was found that as predicted, the smooth area is mainly graphene (figure 4, left) but ZnO is also present; and the rough area is ZnO nanoparticles (figure 4, right), but carbon is also detected.

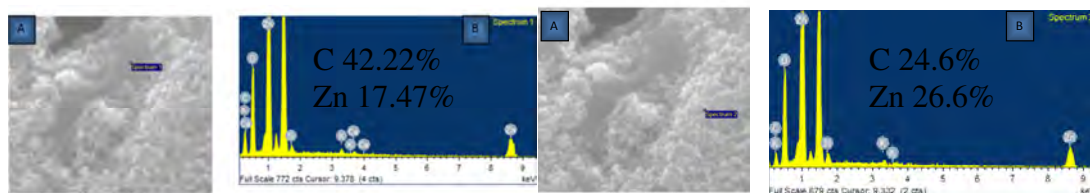


Figure 4.- Left.- Spectrum Analysis 1 “Smooth Area”, Right.- Spectrum Analysis 2 “Rough Area”.

TGA-DTA Results.

Three graphene-ZnO composite samples in different concentrations of the latter (0.001 M, 0.0001 M, 0.0005 M) were analyzed, and a similar behavior could be observed for the different samples due to the low concentration of ZnO nanoparticles in graphene, which is described below. The first mass loss is 5%, around 100 °C, which can be assigned to water molecules trapped within the structure of the graphene or in the samples. The rapid mass loss of about 40% occurring around 300 °C can be attributed to the pyrolysis of the groups containing oxygen in unstable forms of CO and CO₂. This differs from graphene oxide found in the literature [28-31]), this displacement of approximately 50 °C and it is attributed to the presence of the ZnO nanoparticles in graphene (figure 5). At the end of this characterization the remanent is about 20 % ash, the average amount of product testing with graphene.

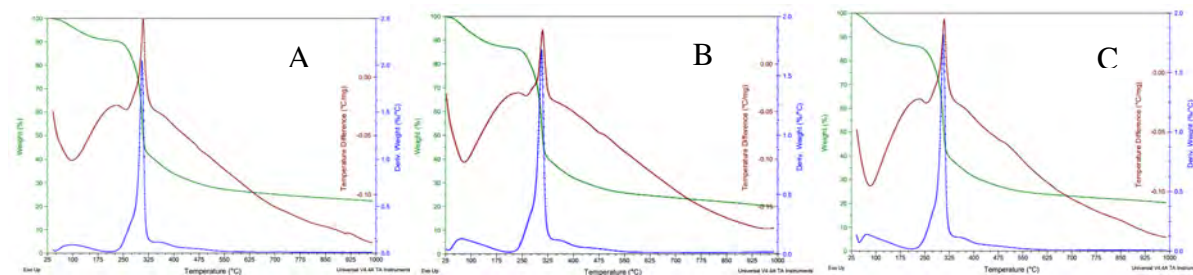


Figure 5.- TGA-DTA curves for Graphene@ZnO nanocomposite: A) ZnO concentration 0.001 M, B) ZnO concentration 0.0005 M, C) ZnO concentration 0.001 M.

Conclusions

It is possible to produce high quality ZnO nanoparticles by a co-precipitation method assisted by a natural polysaccharide gum. The concentration of this polysaccharide affects the morphology of the ZnO nanoparticles. It is possible to produce a composite of graphene@ZnO by the same method.

Acknowledgements

We are Grateful to CONACYT for Financial Support (Proyecto de Redes Temáticas Number 194451).

References

- [1] O. Lupan, L. Chow, Materials Science and Engineering B, 145, 57–66 (2007).
- [2] J. Chen, T. Herricks, Y. Xia, Chem., Int. Ed., 44, 2589 (2005).

- [3] G. Threes, P. Stanislav, Nanotechnology, Science and Applications ,4, 95–112 (2011).
- [4] T. Ma, M. Guo, M. Zhang, Y. Zhang, X. Wang, Nanotechnology, 18, 035605 (2007).
- [5] J. X. Wang, X.W. Sun, Y. Yang, H. Huang, Y.C. Lee, O.K. Tan, L. Vayssieres, Nanotechnology, 17, 4995 (2006).
- [6] G.C. Yi, C. Wang, W. Park, Semicond. Sci. Technol. 20, S22 (2005).
- [7] E. Galoppini, J. Rochford, H. Chen, G. Saraf, Y. Lu, A. Hagfeldt, G. Boschloo, J. Phys. Chem. B, 110, 16159 (2006).
- [8] J.J. Wu, S.C. Liu, Adv. Mater., 14, 215 (2003).
- [9] W.T. Yao, S.H. Yu, Int. J. Nanotechnol., 4, 129 (2007).
- [10] Y. Li, G.W. Meng, L.D. Zhang, Appl. Phys. Lett., 76, 2011 (2000).
- [11] C.L. Hsu, S.J. Chang, H.C. Hung, Y.R. Lin, C.J. Huang, Y.K. Tseng, I.C. Chen, IEEE Trans. Nanotechnol., 4, 649 (2005).
- [12] Y. Li, G.W. Meng, L.D. Zhang, F. Phillipp, Appl. Phys. Lett., 76, 2011 (2000).
- [13] S.H. Park, S.H. Kim, S.W. Han, Nanotechnology, 18, 055608 (2007).
- [14] M.J. Allen, V.C. Tung, R.B. Kaner, Chemical Reviews, 110, 132–145 (2010).
- [15] W.G. Wang, J.G. Yu, Q.J. Xiang, B. Cheng, Applied Catalysis B – Environmental, 119, 109–116 (2012).
- [16] Y. Liu, Y. Hu, M.J. Zhou, H.S. Qian, X. Hu, Applied Catalysis B – Environmental, 125, 425–431 (2012).
- [17] T.G. Xu, L.W. Zhang, H.Y. Cheng, Y.F. Zhu, Applied Catalysis B – Environmental, 101, 382–387 (2011).
- [18] J.F. Wang, T. Tsuzuki, B. Tang, X.L. Hou, L. Sun, X.G. Wang, ACS Applied Materials & Interfaces, 4, 3084–3090 (2012).
- [19] Xu, T.; Zhang, L.; Cheng, H.; Zhu, Y. Appl. Catal., B., 101 (3-4), 382–387 (2011).
- [20] Li, B.; Liu, T.; Wang, Y.; Wang, Z. J. Colloid Interface Sci., 377 (1), 114–121 (2012).
- [21] Kavitha, T.; Gopalan, A. I.; Lee, K.-P.; Park, S.-Y. Carbon, 50 (8), 2994–3000 (2012).
- [22] Lu, T.; Pan, L.; Li, H.; Zhu, G.; Lv, T.; Liu, X.; Sun, Z.; Chen, T.; Chua, D. H. C. J. Alloys Compd., 509 (18), 5488–5492 (2011).
- [23] Wang, J.; Gao, Z.; Li, Z.; Wang, B.; Yan, Y.; Liu, Q.; Mann, T.; Zhang, M.; Jiang, Z. J. Solid State Chem., 184 (6), 1421–1427 (2011).
- [24] Chen, Y.-L.; Hu, Z.-A.; Chang, Y.-Q.; Wang, H.-W.; Zhang, Z.-Y.; Yang, Y.-Y.; Wu, H.-Y. J. Phys. Chem. C, 115 (5), 2563–2571 (2011).
- [25] Williams, G.; Kamat, P. V. Langmuir, 25 (24), 13869–13873 (2009).
- [26] Ye, Y.; Gan, L.; Dai, L.; Meng, H.; Wei, F.; Dai, Y.; Shi, Z.; Yu, B.; Guo, X.; Qin, G. J. Mater. Chem., 21 (32), 11760 (2011).
- [27] Son, D. I.; Kwon, B. W.; Park, D. H.; Seo, W. S.; Yi, Y.; Angadi, B.; Lee, C. L.; Choi, W. K. Nat. Nanotechnol., 7 (7), 465–471 (2012).
- [28] Zhang, Y., Ma, H., et al. J. Mater. Chem., 22, 13064 (2012)
- [29] Liu, C., Hao, F., et al. Low temperature reduction of free-standing graphene oxide papers with metal iodides for ultrahigh bulk conductivity. Sci. Rep., 4, 3965 (2014)
- [30] Liu, J., Ruijie, D., et al. J. Mater. Chem., 22, 13619–13624 (2012)
- [31] Fang, M., Kaigang, W., et al. Mater. Chem., 19, 7098–7105 (2009)

SULFONATION OF COMMERCIAL POLYSULFONES UDEL AND RADEL FOR MEMBRANES OF REVERSE OSMOSIS

M.A. Yam-Cervantes,¹ M.I. Loría-Bastarrachea,¹ J.L. J.L. Santiago-García,¹ M.J. Aguilar-Vega.¹

¹ Materials Unit. Scientific Research Center of Yucatán, AC Calle 43 number 130. Colonia Chuburná de Hidalgo. Mérida, Yucatán, México. Zip: 97200. emails: mjav@cicy.mx. marcial.yam@cicy.mx

Abstract

Keywords: Polysulfone, Fouling, morphology, membranes.

Reverse osmosis membranes are widely used for seawater desalination, due to good performance and low cost. However, membrane fouling and concentration polarization are common problems. Introduction of ionic groups enhance the performance of the membranes with reduction or delay of the boundary layer formation. Modified commercial polysulfones Udel and Radel with sulfonic groups to the main chain varying the ratio of sulfonation were prepared and characterized by FTIR and TGA. Asymmetric membranes from Udel and Radel were formed by the phase inversion method using solutions of N-methylpyrrolidinone (NMP). Morphology of the obtained membranes with different degrees of sulfonation was assessed by SEM. The membranes will be tested for their ability to salts reject and resistance to polarization.

Introduction

Steady growth of the population and economic development is one of the biggest problems increasing the demand of drinking water for human consumption. The oceans water is an alternative to solve scarcity of freshwater¹. Today, membrane based separation processes are the most used technologies for desalination, in particular reverse osmosis (RO). However, a common problem that presents in this kind of membranes is fouling, reducing long time operation, due to flux decline and increased energy consumption and cost operation². Introduction of sulfonic acid groups (SO₃H) in the main chain of polymers such as polysulfones could help to eliminate or reduce the problem. The sulfonation is a way used to increase the hydrophilicity of a polymer, enhance flux and water permeability in RO membranes. In this study the introduction of sulfonic groups in the backbone chain of commercial polysulfones (Udel and Radel) was tested to enhance antifouling properties of the membranes using trimethylsilyl chlorosulfonic acid (CSTMS). The sulfonated polysulfones were used to fabricate asymmetric membranes by linearized cloud point curves. Through a phase inversion process porous membranes of both polysulfones, Udel and Radel were prepared based on the ternary phase diagrams.

Experimental

Materials: commercial Polysulfones Udel, Radel were provided by Amoco. They were dried at 100°C under vacuum (30mmHg) for 24 h before sulfonation. Both are soluble in 1, 2-dichloromethane (Sigma-Aldrich, 99.8% anhydrous) and 1,1,2,2, Tetrachloroethane (Aldrich, 97%). Trimethylsilyl chlorosulfonate ((CH₃)₃SiSO₃Cl, Aldrich 99 %), 2-Isopropanol (JT Baker, 99.8%), Acetone (JT Baker, 99.7%), Absolute Ethylic Alcohol (Fermont, 99.9%), 1-Methyl-2-pyrrolidone anhydrous (NMP), Sigma-Aldrich, 99.5%). N,N-Dimethylformamide (Sigma-

Aldrich, 99.8%), Sodium Hydroxide (JT Baker.99.3%), phenolphthaleine (RICCA, Chemical company).

Polysulfones Sulfonation

Sulfonated polysulfones with various sulfonation levels were prepared via direct electrophilic substitution as reported previously by Lufrano et al, 1999. Udel and Radel samples were treated with trimethylsilyl chlorosulfonate to produce a silyl sulfonate polysulfone. The amount of product formed was controlled by varying the mole ratio between sulfonating agent/polymer repeat units and the reaction time 48 h, figure 1. After this time the sulfonated polymer was added dropwise to isopropanol to obtain the product. The product was dried in an oven for at least 48 h at 110°C to remove all solvent.

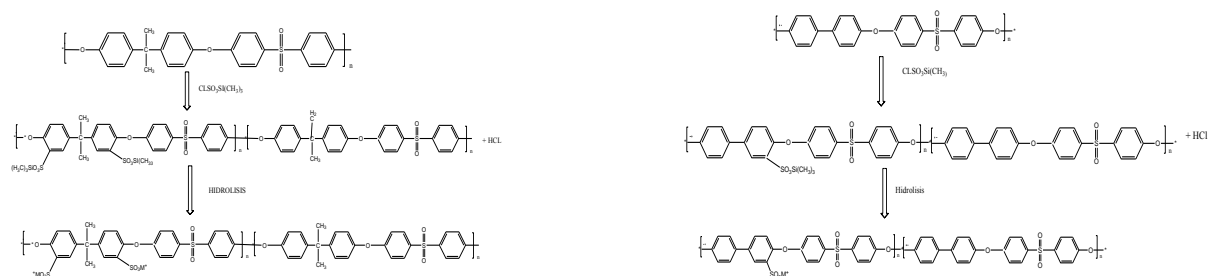


Figure 1. Synthesis of the reaction of polysulfones a) Udel, b) Radel. M^+ could be Na^+ or H^+

Sulfonation Degree

Sulfonation degree was determined by titration of 0.5 g of sulfonated polymer dissolved in 10 ml of N-N Dimethylformamide, and neutralized with NaOH 0.01 M solution using phenolphthalein as indicator. The NaOH consumption value was registered to calculate polymer sulfonation degree by the following equation:

$$SD = \frac{WM(\text{NaOH } M)(\text{NaOH } v_{\text{consumption}})}{w_{\text{Sample}} \times 1000 - (81(\text{NaOH } M)(\text{NaOH } v_{\text{consumption}}))} \quad (1)$$

Where WM the molecular weight in g of polyphenylsulfones repeating unit, $\text{NaOH } v_{\text{consumption}}$ the NaOH solution volume used to neutralize in ml, w_{sample} the sample mass in g and 81 the molecular weight of $-\text{SO}_3\text{H}$ group.

Membrane Preparation

Asymmetric membranes from sulfonated and non-sulfonated polysulfones were prepared in NMP solutions 20% (w/v). The polymeric solution was poured and casted on a glass support after a time period, the support is immersed in a coagulating bath of non-solvent for 24h to conduct the solvent/non-solvent exchange. To release the membrane from the glass support, the membrane was soaked on deionized water. After that the membrane is immersed into deionized water for a day, dried at 50°C for two hours and keep in plastic bag before used.

Phase diagrams from Linearized Cloud Point

The phase diagrams for sulfonated and non-sulfonated Udel and Radel were determined experimentally through of cloud point method by titration-precipitation method. The relation of

non-solvent/polymer and solvent/polymer for both polysulfones in the ternary diagrams representing the binodal for phase separation were developed to determine the concentrations for membrane formation.

Results and Discussion

The ternary phase diagrams Udel/NMP/NS, UdelSu/NMP/NS, Radel/NMP/NS, RadelSu/NMP/NS with different sulfonation degrees show solution-precipitation binodal curves according to the sulfonation degree; there is a tendency to move towards the right of the binodal curves with an increase in sulfonation of the polysulfones. This is due to the affinity of the OH groups to absorb water in the sulfonated materials used to prepare the asymmetric membranes (Figure 2)

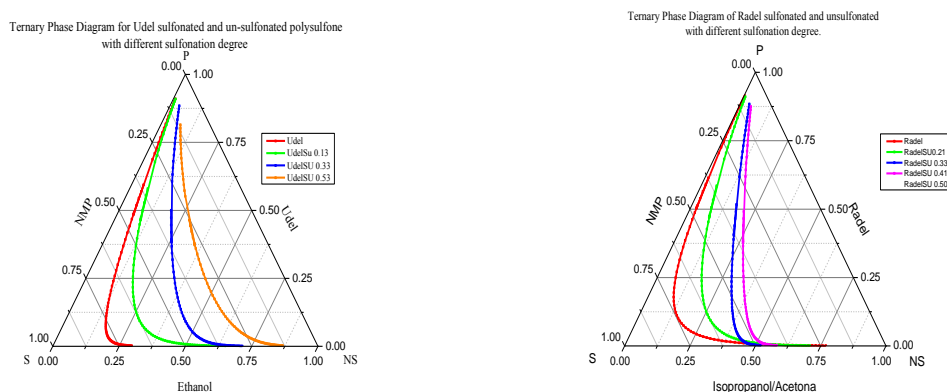


Figure 2. Schematic representation of the phase diagrams and the determination of the bimodal curve obtained by cloud point measurements.

FTIR ANALYSIS

FTIR spectra were performed on Udel, Radel and UdelSU, RadelSU polymers to confirm changes in the chemical structures of the polysulfones. As shown in the figure 3, the presence of two absorption peaks at 1024 cm⁻¹ and 1081 cm⁻¹ for UdelSU and two absorption peaks at 1024 cm⁻¹ and 1088 cm⁻¹ in RadelSU, were assigned to the symmetric and asymmetric stretching vibrations of O=S=O groups, respectively. These bands were in close agreement with the results reported in the literature 5,6 (figure 3).

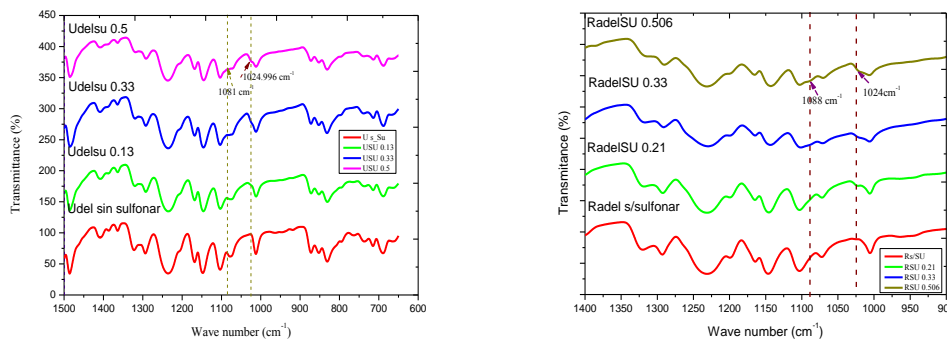


Figure 3. FTIR spectra of a) Udel sulfonated and un-sulfonated b) Radel sulfonated and non-sulfonated, both at different sulfonation degrees.

TGA ANALYSIS

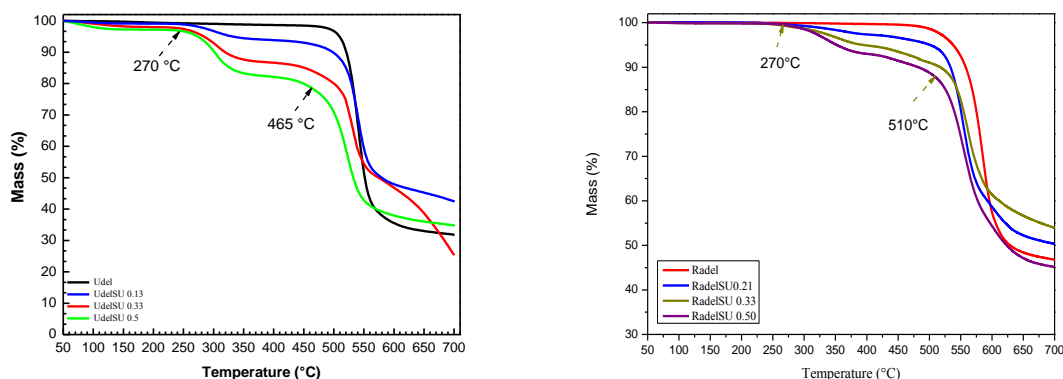


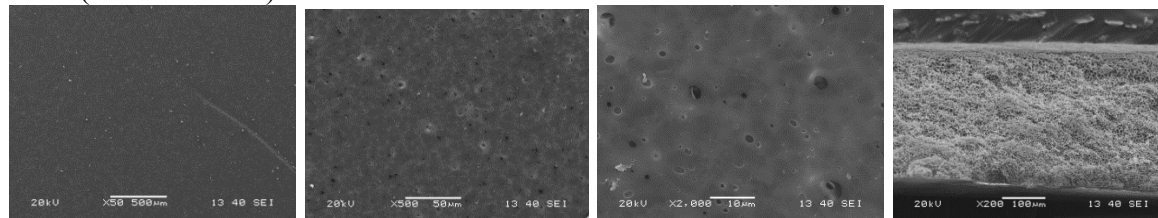
Figure 4. TGA thermograms of Udel and Radel without sulfonation and sulfonated.

TGA analysis shows that the degradation temperature for sulfonic groups starts at 270°C for both polysulfones, with an onset of decomposition temperature for the main backbone chain in 465 °C and percentage of residual mass of ~ 42, 34 and 25 % respectively for Udel. In Radel polysulfone, the degradation temperature was 270°C for sulfonic groups and 510°C for the main backbone. The percentage of residual mass was ~ 54, 50 and 45 %, in sulfonated membranes respectively.

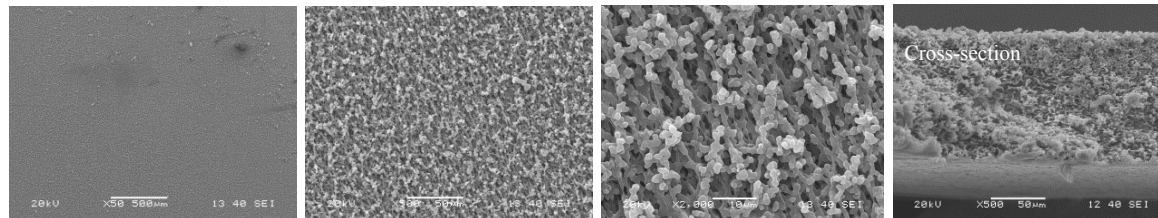
MORPHOLGY AND STRUCTURE

Asymmetric membranes formation from sulfonated and non-sulfonated polysulfones was performed by immersion and precipitation using additives and low temperatures to control the precipitation rate. This combination tends to slow down demixing by diffusion avoiding macrovoids formation due to instantaneous demixing and facilitates the formation of sponge-like structures. SEM images of membranes cast from non sulfonated and sulfonated materials are shown as follow in figure 5.

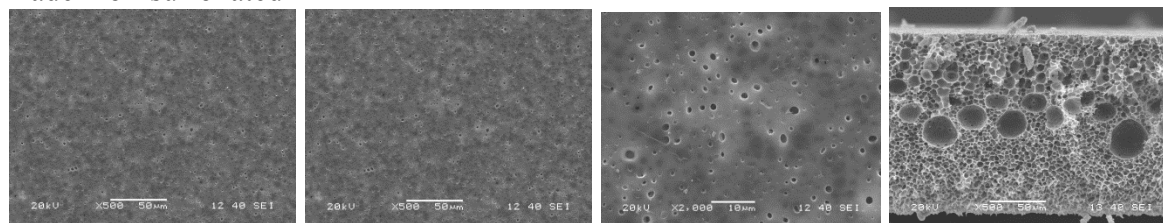
Udel (un-sulfonated)



Udel sulfonated



Radel non-sulfonated



Radel sulfonated

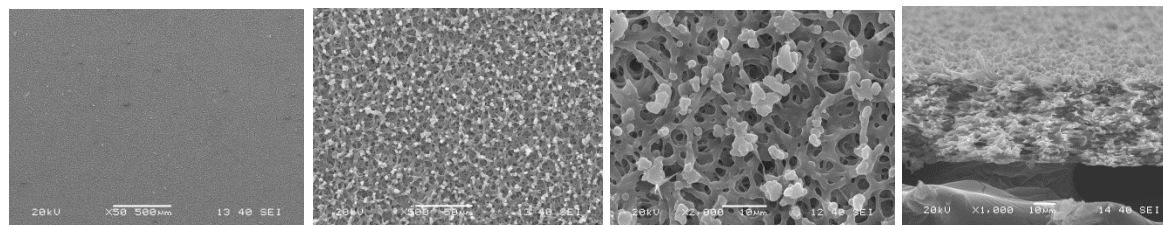


Figure 5. Membranes morphology for non-sulfonated and sulfonated polysulfones. Top face and cross-section with and without sulfonation degree to, a) Udel and b) Radel.

Conclusions

Different sulfonation degrees for Udel and Radel were achieved as expected by controlling the molar ratios of sulfonation agent used. FTIR characterization tests show the presence of sulfonic acid groups, TGA degradation temperatures of sulfonic acid groups in the polysulfones at 270°C are obtained. Through the use of ternary phase diagram developed by the cloud point method the preparation of asymmetric membranes was successfully carried out obtaining ultrafiltration membranes that will be used as support for reverse osmosis membranes preparation.

Acknowledgements

Wish to thank CONACYT for the scholarship, the CICY for allowing me to make a PhD studies and specially Dr. Manuel de Jesús Aguilar Vega for give me the opportunity to be his student.

References

- [1] R. Ibañez, A. Pérez-González, P. Gómez, A.M. Urtiaga, I. Ortiz. Desal. 309, 165-170 (2013).
- [2] R. Guan, H. Zou, D. Lu, C. Gong, Y. Liu. J. Europ. Pol. 41, 1554-560 (2005).
- [3] R.M. Boom, Th. Van den Boomgaard, J.W.A. van den Berg and, C.A. Smolders. Pol. 11 (34), 2348-2356 (1993).
- [4] F. Lufrano, G. Squadrito, A. Patti, E. Passalacqua. J. of App. Pol. Sci. 77, 1250-1257 (2000).
- [5] J. Jaafar, A.F. Ismail, A. Mustafa, Mater. Sci. Eng., A 460-461, 475-484 (2007).
- [6] W/J. Lau, A.F. Ismail, Desal. 249, 996-1005 (2009).

CROSSLINKED PVA AND PAAC MEMBRANES CONTAINING SULFONIC ACID GROUPS: EFFECT OF CROSS-LINKING ON THE SWELLING DEGREE AND ION EXCHANGE CAPACITY.

M. G. Aca-Aca,¹ Loría-Bastarrachea,¹ M. I., J.L. Santiago-García,¹ M. J. Aguilar-Vega¹

¹ *Membrane Laboratory, Materials Unit. Yucatán Scientific Research Center, AC, Calle 43 No 130. Chuburná de Hidalgo. Mérida, Yucatán México. Zip: 97200. emails: mjav@cicy.mx; acagloria15@gmail.com*

Abstract

Membranes were prepared from an 88% hydrolyzed polyvinyl alcohol (PVA-88) and fully hydrolyzed (PVA-99) using sulfosuccinic acid (SSA) as crosslinking agent. Also poly(acrylic acid) (PAAc) membranes were prepared using 4,4'-diaminobiphenyl 2,2' disulphonic acid (BDSA) as crosslinking agent. Membranes were crosslinked at different temperatures and with different amounts of crosslinker SSA (5% and 10% mol) or 5% mol BDSA respectively. Effect of crosslinking on swelling degree in methanol, soybean oil and water of these membranes and their ion exchange capacity (IEC) was studied. They were also characterized through infrared spectroscopy. It was observed for all membranes that acidity increased and swelling degree decreased with crosslinking temperature and SSA content. PAAc-BDSA has IEC values and swelling degree greater than PVA-SSA membranes because BDSA bears two sulfonic acid groups.

Introduction

There has been an increasing interest in polymer catalytically active membranes in biodiesel obtention. A catalytically active membrane combines reaction and separation in a single step, and the catalyst is immobilised in a polymeric matrix [1]. Catalysts that have been embedded in a polymeric matrix are poly (styrene sulfonic acid), sulfated zirconia ($Zr(SO_4)_2$), sulfosuccinic acid (SSA), hydrotalcite, usually, in a hydrophilic polymer matrix like polyethersulfone (PES), polyacrylonitrile (PAN) and polyvinyl alcohol (PVA). One of the advantages of these membranes is the combination of the selectivity of the polymer matrix to hydrophilic solvents such as methanol, water and glycerol, while the incorporated catalysts catalyses esterification and transesterification reactions in biodiesel production [2, 3]. Poly(vinyl alcohol) (PVA) membranes have been tested in biodiesel production [3,4] because of their high hydrophilicity, good thermal properties and good chemical resistance [5]. The most active catalytic membrane (PVA-SSA40) has archived almost 90% equilibrium conversion after 2 h [6].

According to Huang et al., 1989, materials for dense membranes, including water-soluble polymers, should be chosen on the basis of maintaining a proper hydrophilic/ hydrophobic balance criterion for a given separation system. In order to adjust and control the hydrophilic/hydrophobic balance properties of a membrane, several techniques have been tried, such as polymer crosslinking [7]. Sulfosuccinic acid [4], succinic acid [9], fumaric acid [5], maleic acid [8] and glutaraldehyde (GA) can be used as the membrane crosslinking agents for biodiesel.

A high crosslinking can enhance thermal stability of the membrane [5], but it can also cause the membrane to be less hydrophilic and more brittle [10]. In biodiesel production, increased crosslinking can reduce the degree of membrane swelling in oil and methanol, thereby reducing the biodiesel yield because oil and methanol are prohibited from diffusion into the membrane in the catalytic reaction [4].

In the present study membranes were prepared from two different grades of poly (vinyl alcohol) PVA-88, 88% mol hydrolysis, and PVA-99, 99% mol hydrolysis, using SSA as crosslinking agent. In the same fashion poly (acrylic acid) (PAAc) membranes were prepared using 4,4'-diamino sulfonic acid, BDSA, as crosslinking agent at different crosslinking temperatures and two different amounts of crosslinking agent. The effect of cross-linking on swelling degree of these polymers and their ion exchange capacity (IEC) of their membranes was studied. The membranes were also characterized through infrared spectroscopy

Experimental

Membrane preparation of PVA

Aqueous 4.5 wt. % PVA-99 (molecular weight of 89,000–98,000) or PVA-88 (molecular weight of 85,000-124,000) solutions were prepared by dissolving a pre-weighed amount of PVA in water at 90°C, using a magnetic stirrer during 6 h. The PVA solutions were mixed with SSA (70 wt. % solution in water) at 5 and 10 mol %) and then the mixtures were stirred at room temperature for 17 h. Next the solution was sonicated for 4.5 h. After that, the homogeneous solutions were poured and cast onto a metallic ring with a teflon base. The cast membranes were allowed to dry at 60°C during 24 h. In order to complete the esterification reaction the dried membranes were heated at 80, 100, 120 y 130°C, during 1 h, under vacuum. The acronym PVA-SSA-99-x% or PVA-SSA-88-x% means a membrane with x% crosslinking degree.

Membrane preparation of PAAc

The solution of PAAc (M_v= 450,000) at 3.5 wt. % in 8 vol % aqueous triethylamine was prepared using a magnetic stirrer during 2 h. The PAAc solutions were mixed with 5 mol/mol % PAAc and BDSA (Acros) which was previously purified by recrystallization. The solution was vigorously stirred at room temperature for 17 h. In the next step the solution was sonicated for 3 h. The solution was cast in a polystyrene petri dish and dried with a protocol of temperatures as follows: 25°C for 2 h, 15°C for 1 h, 30°C for 17 h and 45°C for 6 h. The cast membranes were allowed to dry at 60°C during 24 h. In order to complete the amidation reaction the dried membranes were heated at 150, 170, 180 y 190°C, during 4 h, under vacuum. The acronym PAAcBDSA-x% means a membrane with x% crosslinking. All membranes have a thickness of between 60 and 130 μm.

Analyses and calculations

Infrared spectroscopy

The FT-IR spectra of the PVA-SSA and PAAc-BDSA membranes were recorded in a Nicolet 8700 FTIR instrument (Thermo Scientific) in the range of 4000–400 cm⁻¹.

Swelling degree and weight loss

The swelling degree of the polymers was measured by immersing the samples in the pure solvent (methanol, soybean oil or water), at 60 °C and left until equilibrium was reached. The samples were weighed at different time intervals until constant weight was reached. This was attained usually after an immersion time of about 5 days. Once the swelling ended, the surface of the polymeric samples was dried with a teflon cloth and the weight gain was measured. Then the swollen polymer samples were allowed to dry at 60°C during 24 h and weighted. The swelling degree (Q), and weight loss (WL) were calculated by:

$$Q = \frac{m_{sh} - m_h}{m_{sh}}; \quad WL = \frac{m_s - m_{sh}}{m_s} \times 100$$

where m_h is the mass of swollen sample, m_s is the mass of the dry sample without swelling and m_{sh} is the mass of the dry sample after swelling.

Ion exchange capacity (IEC)

The amount of sulfonic acid groups in all membranes were measured by classic ion exchange capacity, IEC, acid-base titration. An amount of 0.1 g of each sample was immersed in 5 ml of water at 60°C for 24 h, after in 5 ml 1M HCl solution at 60°C for 24 h, finally in 5 ml of 1M NaCl solution a room temperature for 24 h and subsequently titrated with 0.01N NaOH. The IEC value (mmol/g) of the membrane was calculated by

$$IEC(\text{mmol} / \text{g}) = \frac{M_{\text{NaOH}} V_{\text{NaOH}}}{W_s}$$

where V_{NaOH} is the volume of NaOH consumed in the titration and W_s is the dry weight of the membrane sample and M_{NaOH} is the molarity of NaOH solution.

Results and Discussion

FT-IR spectra

Figure 1 shows The FT-IR spectra for PVA-SSA-99 membranes with 10 mol % SSA treated for 1 h at several reaction temperatures. When the temperature reaction increased, several changes in spectra occur. First, the intensity of the carbonyl band, $-\text{COO}-$, in the ester group appeared at 1726 cm^{-1} increased and it displaces to the right as the temperature increase from 80°C to 130°C. The increase in the characteristic peak of the ester group means that there is a reaction between the carboxylic acid in the SSA and the hydroxyl group in the PVA. Also, the absorption bands at 1043 and 1240 cm^{-1} indicate the presence of sulfonic acid group by the introduction of SSA. Furthermore, the intensity of the O-H group band that appears at 3300 cm^{-1} is decreased and is displaced to the right as the temperature increases.

In a similar way Figure 1b shows the FT-IR spectra of the PVA-SSA-88 membranes with 10 mol % SSA for 1 h at several reaction temperatures. It was reported that the absorption band of ester ($-\text{COO}-$) appeared at 1735 cm^{-1} (Rhim et al., 1998). The intensity of the $-\text{COO}-$ in the ester bond increase as temperature increases from 80°C to 130°C, hence the crosslinking reaction occurs mainly between the hydroxyl group and the carboxylic group. The absorption bands at 1043 and 1240 cm^{-1} indicate the presence of sulfonic acid group by the introduction of SSA.

Figure 1c shows the FT-IR spectra of PAAc-BDSA membranes with 5 mol % BDSA for 4 h at several reaction temperatures (150, 170, 180 and 190°C). The characteristic peaks of BDSA are located at 3300 cm^{-1} of N-H group and 1620-1560 cm^{-1} for the primary amine, while those of PAAc appeared at around ~3000 cm^{-1} for OH of carboxylic acid group, 1716 cm^{-1} and 1270-1160 cm^{-1} characteristic of peaks of C=O. The absorption bands at 1025 cm^{-1} indicate the presence of the sulfonic acid group due to the introduction of BDSA. FT-IRs spectra clearly shows the presence of BDSA and PAAc in all PAAc-BDSA membranes, however there was no clear evidence that amidation has been carried out. When detailed analysis of the range absorptions of 1800 to 1500 cm^{-1} for all crosslinking membranes was applied (because in this area is located amide band) we found by the spectrum deconvolution in this area for PAAcBDSA-5%-150°C the presence of three peaks in 1568, 1622 and 1723 cm^{-1} attributed to the NH_2 groups of primary amine to the carbonyl group ($-\text{C}=\text{O}$) of the amide and carboxylic acid, respectively. Indicating that there was carried out the amidation reaction.

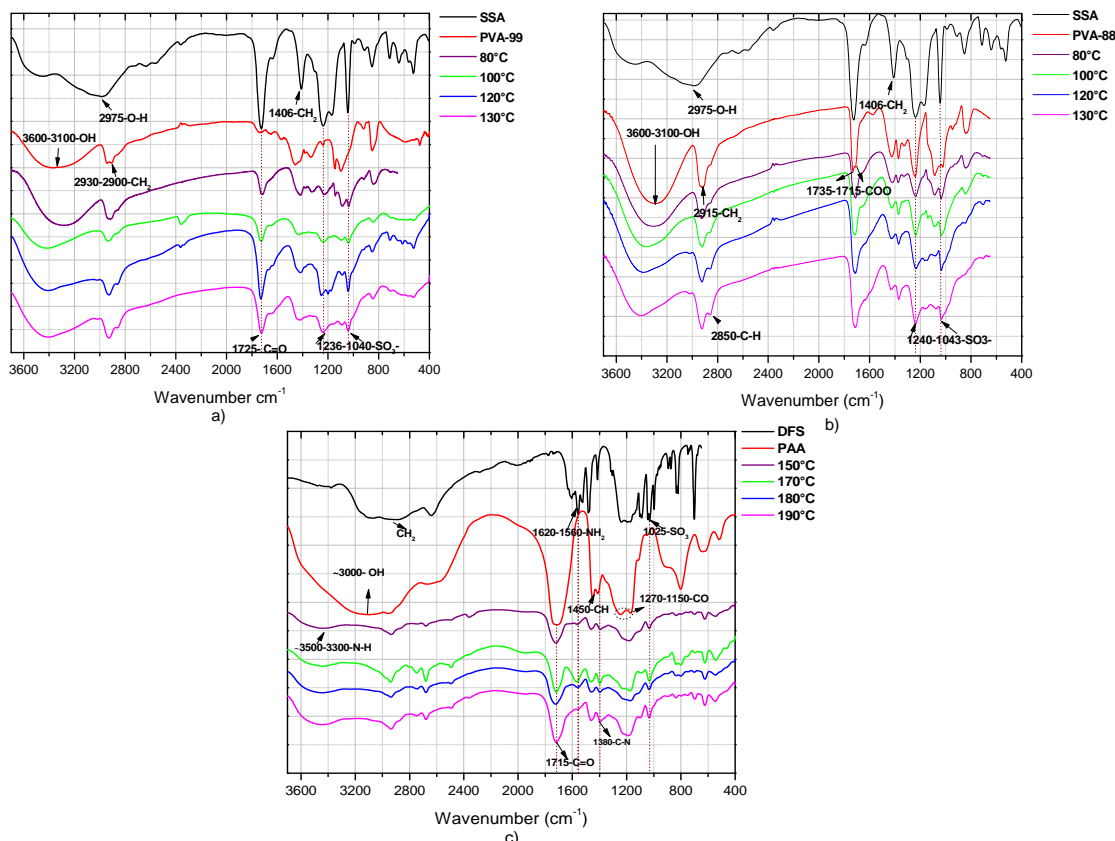


Figure 1. FT-IRs spectra of crosslinked PVA-SSA and PAAc-BDSA membranes at several reaction temperatures. a) PVA-SSA-99; b) PVA-SSA-88 and c) PAAc-BDSA

Swelling degree and weight loss

Figure 2 shows swelling degree the PVASSA-99 and PVASSA-88 membranes in oil (Fig. 2a), methanol (Fig. 2b) and pure water (Fig. 2c). The swelling degree decrease as the crosslinking temperature and SSA content increases. These results indicate that a higher degree of crosslinking in the PVA-SSA membranes might lead to more rigid and compact polymer structure. In the case of the membranes PVASSA-99 the swelling degree in pure oil increases as crosslinking temperature and SSA concentration increases, due to fact that the membranes are more hydrophilic.

Swelling degree in water, methanol and oil in PAAc-BDSA membrane increases in both directions from 170°C when the crosslinking temperature increases. PAAc-BDSA-5%-150°C have the highest value of swelling degree: this is probably due to the fact that the polymeric matrix contains more hydrophilic functional groups (-SO₃H).

One way of qualitatively measure the degree of crosslinking of the polymer, is to determine the percentage of soluble material (percentage weight loss) which indicates the amount of crosslinked polymer. The weight loss in PVASSA-99 and PVASSA-88 decreases when the crosslinking temperature increases but the crosslinking degree increases when SSA content increases at temperatures above 100°C. The weight lost by PVASSA-99 membranes was between 20 and 13% and for PVASSA-88 between 33 and 10%. The weight loss in PAAcBDSA increase as crosslinking temperature increases.

Ion exchange capacity (IEC)

The IEC values of the PVA-SSA membranes are plotted as a function of crosslinking temperatures in Fig. 3a. The PVA-SSA membranes prepared in this study possess IEC values in the range of 0.1-0.6 mmol/g. The IEC values (80, 100, 120 and 130°C) of the crosslinked membranes, increase with SSA amount and crosslinking temperature. This behaviour is ascribed to an increase of sulfonic acid groups anchoring that also increased the esterification reaction on PVA-SSA membranes. However, when the temperature treatment increases from 120 to 130°C the IEC value decreases. This behavior is ascribed to a more compact polymer structure and could become a mass transfer limitation for its use as catalytic membranes.

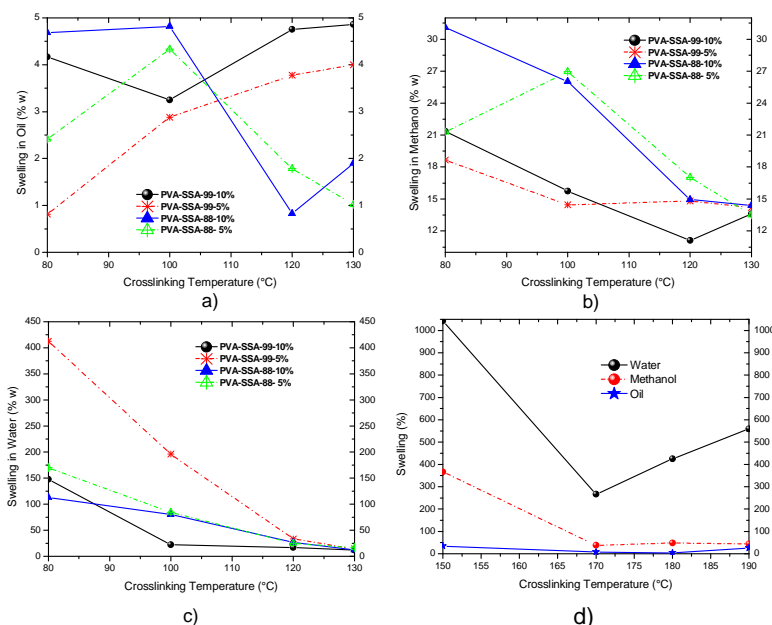


Figure 2. Swelling degree of all polymer membranes. a) PVA-SSA-99 and PVA-SSA-88 in oil; b) PVA-SSA-99 and PVA-SSA-88 in methanol and PVA-SSA-99; PVA-SSA-88 in water and PAAc-BDSA in water, methanol and oil.

The PAAc-BDSA membranes prepared in this study possess IEC values in the range of 0.3-0.95 mmol/g as shown in Figure 3b. PAAc-BDSA-5%-150°C has a higher IEC value. This is attributed to the fact that the membrane treated at relatively low temperature has higher amidation reaction, which could present a larger number of cation-exchange sites, due to the number of sulfonic acid groups introduced. However the stability of these membranes is not as good as that of PVA-SSA membranes yet, since they are too soft to handle.

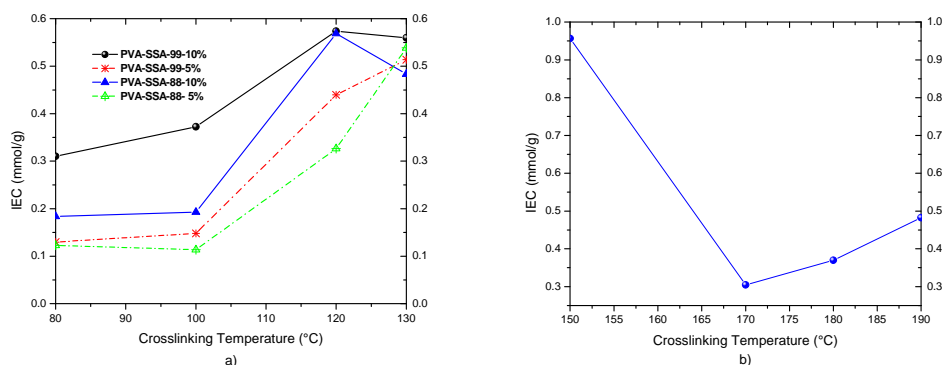


Figure 3. IEC values in crosslinked membranes dependence on crosslinked agent amount and crosslinking temperature. a) PVA-SSA-99 and PVA-SSA-88 and b) PAAc-BDSA

Conclusions

In the FTIR spectra of PVA-SSA-99, PVA-88 and PAAC-BDSA were found bands that indicated the presence of SO₃H groups available. The esterification reaction was successfully carried out between the carboxylic acid in the SSA and the hydroxyl group in the PVA, and the amidation reaction were carried out between amine group in BDSA and carboxylic acid in the PAAC the latter was low.

The increased hydrophilicity of the polymer (PVA-SSA-99, and PVA-SSA-88 and PAAC-BDSA) increases the swelling degree of the membrane.

PAAC-BDSA membranes have higher weight loss than those prepared from PVA. This result may indicate that the amount of polymer crosslinking is low or they are not able to form covalent amide bonds with PAAC.

Acknowledgements

This work was primarily supported by Yucatán Scientific Research Center (CICY) and CONACyT.

References

- [1] M. G. Buonomenna, S. H. Choi, A-P J. Chem. Eng. 5(1), 26-34. (2010)
- [2] W. Shi, B. He, Bioresource Technol., 101, 1501-1505 (2010).
- [3] M. Zhu, B. He, Fuel, 89, 2299-2304 (2010).
- [4] L. Guerreiro, J.E. Castanheiro, Catal. Today, 118, 166-171 (2006).
- [5] H.-M. Guan, T.-S. Chung, J. of Membrane Sci., 268, 113-122 (2006).
- [6] C.S. Caetano, L. Guerreiro, Appl. Catal. A: General, 359, 41-46 (2009).
- [7] J.-W. Rhim, C.-K. Yeom, J. of Appl. Polym. Sci., 68, 1717-1723 (1998)
- [8] K.C.d.S. Figueiredo, V.M.M. Salim, Catal. Today, 133–135, 809-814 (2008).
- [9] J.E. Castanheiro, A.M. Ramos, Appl. Catal. A: General, 311, 17-23 (2006).
- [10] K.-J. Kim, S.-B. Lee, Kor. J. of Chem. Eng., 11, 41-47 (1994).

Control of preparation process to form a sol-gel membrane deposited in plastic fiber optic for pH detection

D. A. Razo-Medina,¹ O. Ortiz-Jimenez,² E. Alvarado-Méndez,¹ and M. Trejo-Durán,²

¹*División de Ingenierías, Campus Irapuato-Salamanca (DICIS), Universidad de Guanajuato, Com. Palo Blanco s/n 36885, Salamanca, Gto. México.*

²*Departamento de Estudios Multidisciplinarios (DEM), Universidad de Guanajuato, Yuriria, Gto. México.*

Abstract

In this work it is showed the results obtained by using Dip-Coater to develop a sol-gel membrane or film mixed with pH indicators, which will be used as recognition component. The pH concentration in the sample was determinate and quantified by the use of absorbance. It is clearly explained the process development step by step to prepare a membrane as well as the parameters to be controlled for the preparation and membrane thickness.

Introduction

The sol-gel technique was developed as an alternative technology for the preparation of glasses and ceramics at low temperatures. It is an easy, inexpensive and highly flexible method to manufacture, study and work. The possibility of starting from molecular precursors and elementary building blocks allows structures at the molecular level, and create new materials with increased performance; Focused for area of integrated optics.

The process depending of its parameters and stages manufacture. It is applied in coatings, new ceramic fibers, ceramic powders with properties (optical, piezoelectric, etc.), new glass and materials HOIM (Organic-Inorganic Hybrid Materials). The latest studies has been about biomaterials, preparation of optical materials, sensors and fabricated thin films [1-9].

In this project present control parameters for production of a sol-gel film and his deposition process on a plastic optical fiber (optrode) for pH detection. The pH is important for his applications in the area of health, food industry, growth of bacteria, treatment of water, agriculture, pharmaceutical and cosmetic industry, petrochemical, metallurgy, etc.

In this work were showed diverse experiments for creating optrodes. It was split into two stages; first to obtain proper consistency of sol-gel mixture and second to produce a film thin by Dip-Coater device.

Experimental

The objective of sol-gel process is the control of surfaces and interfaces of materials. This technique was used for encapsulates the indicators which react with the pH. The reagents used to create the sol-gel, they were Tetra ethyl ortho silicate (TEOS), ethanol and water, at a ratio of 40: 40: 1. There are several factors affect the rate of chemical reaction, especially temperature, humidity, mole ratios between reactants, agitation and solvent. To prevent the sol-gel solution to solidify. The quantity of moles, agitation and temperature were controlled. The figure 1 showed some results of the final process of the sol-gel technique.



Figure 1. Results sol-gel technique, a) spherical silica powder, using hydroxide and b) silica glass, using nitric acid.

Thin films can be deposited through a variety of techniques; this can be classified according to phase of the medium with the solute, some they are related to deposition techniques in solid form, a liquid or gas medium. In this case was using the dip coater, it has an accurately in the controlled of immersion and extraction for any substrate in a liquid (solvent) [10, 11]. A detailed description can be found in the Nima Dip-Coating Manual DC-mono, see figure 2.



Figure 2. Nima Dip-Coating DC-mono device.

With the help of Dip-Coater different films were obtained, which showed various layers, due to the actions or forces acting on them, for example, gravity, viscosity, temperature, capillary force, evaporation of the solvent, speed immersion and submersion of the film, etc. To have better control were performed several tests, to determine the best results and apply the same conditions, to achieve repeatability of film. The deposition system of films by a Dip-Coater is show in figure 3.

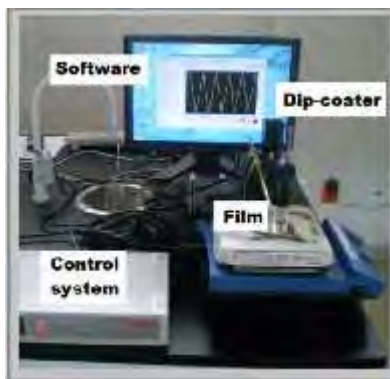


Figure 3. Performing a film with Dip-Coater.

In Figure 4, there are several samples with different film preparation parameters and appreciate as were formed different layers. Due to factors involved in its preparation. Observing that end layer has uniform surface and this increases.



Figure 4. Sol-gel films, there observed a progress of left to right.

To obtain best results, we designed a dome for the control of environment, since the sol-gel solution was kept outside and viscosity was increased rapidly, see figure 5. In this dome is put ethanol at 70°C to saturate the environment and delay the gelling process.



Figure 5. Workspace for preparation of films.

To optimize resources. The deposition proofs were performed in glasses and once was obtained the appropriate methodology, this is applied to the fibers, due a similar deposition was observed on both substrates, see figure 6.

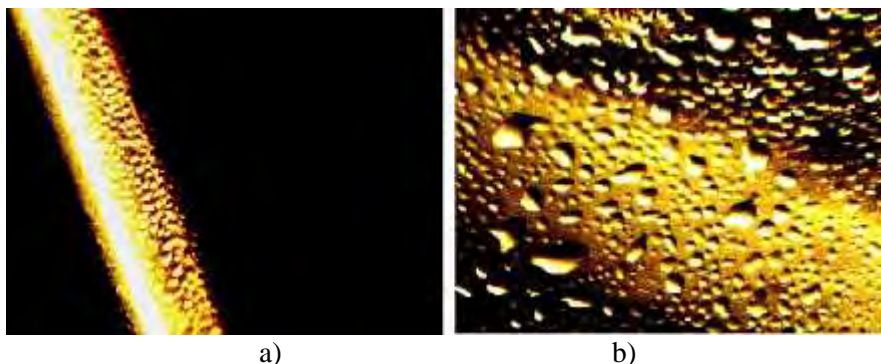


Figure 6. Sol-gel film, a) deposited in fiber b) deposited on glass.

Results and Discussion

Once obtained the control of preparation optrodo, were performed characteristics curves of optrodes, for measuring the pH concentration found in the samples. The measurement system provides a relationship between the amount of light passing through the optrodo and pH unit.

To ensure that the results were repetitive and efficient, were used microscopy techniques such as FTIR, to check or assist that indicators are confined within the sol-gel film and OSA, to determine the light source should be used for best results in the measurement of pH.

With the help of optical microscope, it can clearly see the structure of the films deposited on glass and plastic fibers. In Figure 7 were appreciated the different layers that formed in the early films.

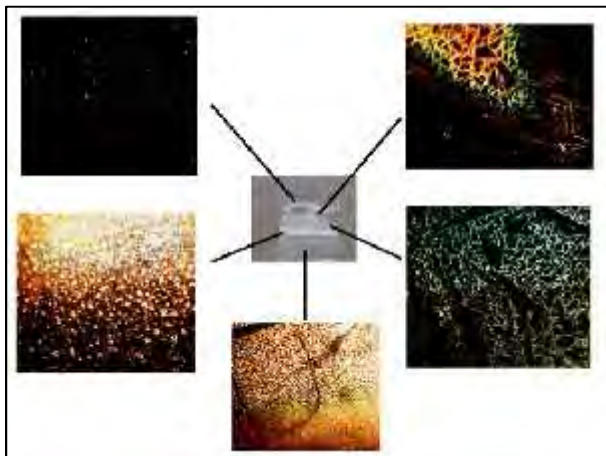


Figure 7. Layers of a film deposited on a glass

The methodology obtain with the development of the experiments and analysis of the manufacturing process of the sol-gel, the control viscosity were obtained, by using a speed of 1.5 for magnetic stirrer to 55°C. The manufacture of films with the Dip-Coater, by using a depth of submergence and elevation about one centimeter, a speed of elevation and Submersion of 5 mm/min, dwell time at the bottom and top of 60sec and number of submersions, remained at 40 cycles. Thus increasing the area where the film presented a uniform structure.

The characteristic curve of pH detector is showed in figure 8, there is observe that the behavior of pH concentration vs voltage is linear and growing in a range of 3 to 9 pH units.

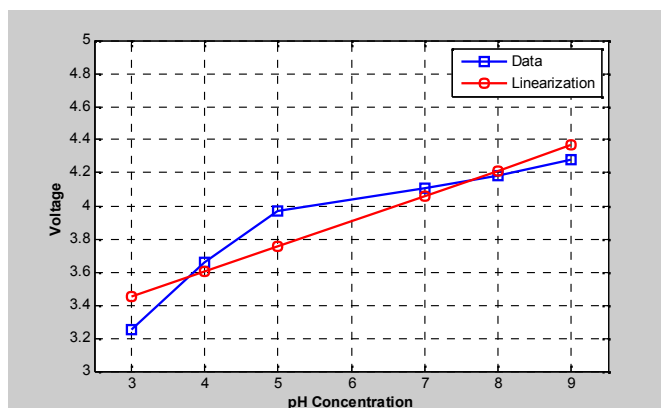


Figure 8. Characteristic curve for pH detector.

Conclusion

In this work focuses on the manufacturing process and deposition of sol-gel films on fiber, due it is important to determine concentration of pH in sample. The molecular structures of optrodes were analyzed qualitatively by using spectroscopic techniques. This to obtain repeatability in experiments, since the results of the characteristic curve, presented a good linearization to determine pH units.

Acknowledgements

This project was supported by a scholarship 213921/206655 from CONACYT and by Guanajuato University-DAIP No. 223/2013, 288/ 2013 and PIFI-2013.

References

- [1] A. Chiappini, A. Chiasera, S. Berneschi, et al., J Sol-Gel Sci Technol, 60, 408–425 (2011).
- [2] C. Jeffrey, G.W. Scherer, Academic Press, INC., (1990).
- [3] S. Sakka, Kluwer academic publishers, (2005).
- [4] L.C. Klein, New Jersey, USA, Noyes publications. (1998).
- [5] Z.N. Kayani, A.Afzal, F. Saleemi, et al., Transactions on magnetics, 50 (8), 2401104 (2014).
- [6] Z.N. Kayani, E.S. Khan, F. Saleemi, et al., Transactions on magnetics, 50 (8), 2200304 (2014).
- [7] B. Wang, J.Huang, M. Li, et al., Proc. of SPIE, 7278, 72780Q-1 (2008).
- [8] M. Messori, M. Toselli, F. Pilati, et al. Surface coatings international Part B, 86(3), 181-186 (2003).
- [9] L. L. Hench and J.K. West, Chem. Rev, 90, 33-72 (1990).
- [10] H. Nguyen, L. Miao, S. mura, Journal of Crystal Growth, 271, 245–251(2004).
- [11] R. Ashiri, A.Nemati, M.S. Ghamsari, Ceramics International, 40, 8613–8619 (2014).

PURE GAS PERMEATION OF MEMBRANES OBTAINED FROM A NOVEL POLYIMIDE (PI BTD-MIMA) /POLIBENZIMIDAZOLE BLENDS

José Manuel Pérez-Francisco*, María Isabel Loría-Bastarrachea, Jose Luis Santiago-García,
Manuel Aguilar-Vega

*Unidad de Materiales. Centro de Investigación Científica de Yucatán, A.C. Calle 43 No. 130, Colonia Chuburná de Hidalgo. Mérida, Yucatán
C.P. CP 97200. Correspondencia a: jmpf20@hotmail.com*

Abstract

In the present work the synthesis and characterization of a novel polyimide [PI BTD-MIMA] derived from bicyclo[2.2.2]oct-7-ene-2,3,5,6 tetracarboxylic dianhydride [BTD] and the diamine 4,4'-methylenebis(2-isopropyl-6-methyl aniline) [MIMA] is reported. The as obtained polyimide was blended with polybenzimidazole [PBI] at three different concentrations (50/50, 75/25 87.5/12.5wt%). The effect of PBI concentration on microstructure was evaluated. The pure gas permeability and ideal selectivity to He, O₂, N₂, CH₄ and CO₂, was determined. Analysis of the microstructure of membranes confirms a variation in d-spacing with PBI concentration in the blend. It was found that the high permeability of the PI BTD-MIMA increase at low PBI concentrations and decreases towards the value of PBI as the concentration of PBI increases in the blend.

Introduction

Membrane technology for gas separation is an alternative to traditional processes such as cryogenic distillation or pressure swing adsorption in the petrochemical industry [1]. The advantageous properties of polymeric membranes such as ease of processing and robustness may help to increase the market of gases separation by membrane technology.

Polyimides (PI) have attracted considerable attention over the last two decades for preparing gas separation membranes. Their high gas selectivity for gas pairs such as CO₂/CH₄ and O₂/N₂ among others and their high chemical resistance, thermal stability and mechanical strength, have made PI promising materials for various gas separation applications [2]. On the other hand, there are interesting advantages offered by blending technology into the area of polymeric gas separation membranes. One of these advantages is to combine the properties of two different polymers such as the high permeability of one and the high selectivity factor of another one.

In this study, dense flat membranes were cast by employing the solution blending technique using a polyimide synthesized in our laboratory (PI BTD-MIMA) and a commercial polymer (PBI). PI BTD-MIMA is a polyimide with high gas permeability and selectivity, high thermal stability, while polibenzimidazole (PBI) is a high performance polymer possessing high glass transition temperature, outstanding thermal stability and chemical resistance but low permeability and high selectivity for several gas pairs [3]. The gas transport characteristics of blends at different concentration of PI BTD-MIMA/polybenzimidazole (PBI) membranes are evaluated. The effects of composition, microstructure and gas separation performance of membranes are also investigated.

Experimental

Materials

Bicyclo[2.2.2]oct-7ene-2,3,5,6-tetracarboxylic dianhydride (BTD), nitrobenzene, pyridine, benzoic acid and 1-methyl-2-pyrrolidone (NMP) were purchased from Aldrich chemical Co. and were used as received. Polibenzimidazole (PBI) was purchased from PBI Performance products Inc. and was dissolved in NMP and poured into ethanol with stirring. 4,4'-methylenebis(2-isopropyl-6-methylaniline) (MIMA) was supplied by 3B Scientific co. and was purified by recrystallization

from hexane.

Synthesis of polyimide PI BTD-MIMA

A one-step method was applied for preparation of the PI BTD-MIMA. In a 50 mL three-necked round-bottomed flask equipped with a nitrogen gas flow and a mechanical stirrer, 2 mmol (620.96 mg) diamine MIMA and 5 mL of nitrobenzene were added. After the diamine was completely dissolved, 2 mmol (496.38 mg) dianhydride BTD and 5 mL of nitrobenzene was added to the stirred solution and the mixture was heated and kept at 80°C during 1 h. Then, pyridine (4 mmol) was added and the solution was heated slowly to 120°C. Afterward, benzoic acid (4.0 mmol) was added, and the mixture was stirred at 150 °C for 3 h. Finally, the temperature was increased and kept to 200°C for 24 h. The solution was poured into ethanol. The obtained polymer was washed thoroughly with ethanol and dried in a vacuum oven at 200 °C overnight.

Preparation of dense flat membranes

Polymer solutions (4 wt.% polymer/96 v% NMP) with various compositions of 50/50, 75/25, 87.5/12.5 wt.% were prepared from PI BTD-MIMA and PBI according to the following steps. Firstly, PBI in the desired quantity was dissolved in NMP at 150 °C using a magnetic stirrer for 24 h. Subsequently, the PI BTD-MIMA was added and stirring was continued for 24 h. The polymer solution was filtered using a 0.45 µm filter and poured onto an aluminum plate. The plate was heated at 100°C and an inverted glass funnel was placed over the solution to minimize the evaporation rate of the solvent. The solution was allowed to evaporate for 24 h. The film was then removed and dried in a vacuum oven at 260 °C for 24 h.

Characterization

Fourier Transform Infrared (FTIR) measurements were performed on all polymers and polymer blends in a Nicolet 8700 FT-IR (Thermo Scientific Co.). Thermo gravimetric analysis (TGA) data for polymers and blends were performed on a TGA-7 (Perkin Elmer Co.) at a heating rate of 10°C/min between 50 and 800°C under N₂ atmosphere. Glass transition temperature (T_g) was determined on a DSC-7 (Perkin Elmer) in the second run.

Gel permeation chromatography (GPC) analysis of the polyimide PI BTD-MIMA was performed on a HP Agilent 1100 HPLC system using a Zorbax column and PS standar 103 to 106 Daltons. Wide angle X-ray diffraction (XDR) measurements were performed on polymeric films using a SIEMENS 5000 X-ray diffractometer between 4 and 60° 2θ.

Permeation measurements of dense films

The gas permeation properties of membranes were determined by following the changes in pressure by the constant-volume method as reported elsewhere [4] at 35°C and 2 atm upstream pressure for He, O₂, N₂, CH₄ and CO₂.

Results and Discussion

Synthesis of polyimide PI BTD-MIMA

Polyimide PI BTD-MIMA was synthesized by the one step polycondensation reaction [5] as shown in the

Figure 1. The IR spectrum shows the characteristic bands at 1776 cm⁻¹ (imide C=O asymmetrical stretching), 1702 cm⁻¹ (imide C=O symmetrical stretching), and 1370 cm⁻¹ (imide CNC axial), confirming the complete imidization.

The solubility of polyimide PI BTD-MIMA was studied in different solvents at room temperature. The polyimide was soluble in aprotic polar solvents and even in chlorinated solvents such 1,2 dichloroethane (DCE) and 1,1,2,2- tetrachloroethane (TCE).

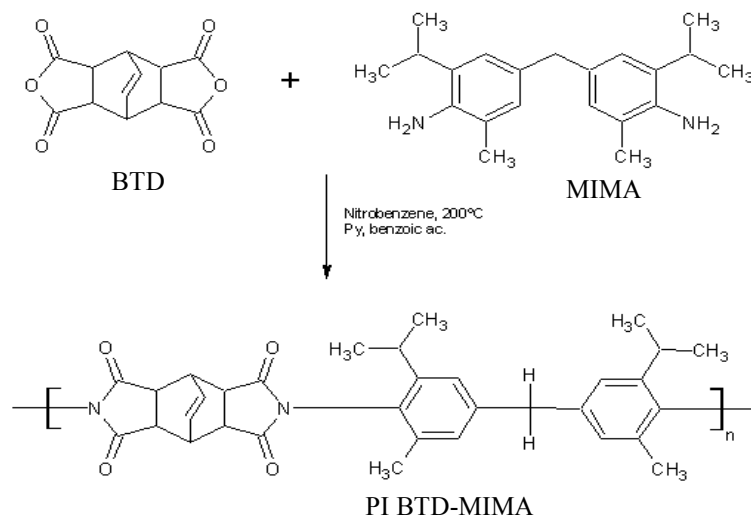


Figure 1. Synthesis of polyimide PI BTM-MIMA

Characterization of membranes from PI BTM-MIMA/PBI

In the IR spectrum obtained for the dense membranes (Figure 2a) the characteristic bands for polyimides and polybenzimidazole can be observed. It is also seen that for the blends there is not a shift in the carbonyls bands (1702 and 1776 cm^{-1}) for polyimide or in the NH band (3281 cm^{-1}) for PBI, the shift was expected as characteristic of hydrogen bonding that correspond to miscible blends. Wide angle X-ray diffraction (XRD) patterns of polyimide PI BTM-MIMA, PBI and their blends are shown in the Figure 2b. The resulting pattern indicates that all polymers and their blends are amorphous. The XRD pattern for PI BTM-MIMA shows a broad peak centered at 13° while PBI has a halo with a 2θ maximum at 23° . The diffraction pattern of blends shows an amorphous halo with a 2θ maximum at 13° and a small shoulder at around 22° that increases with PBI concentration.

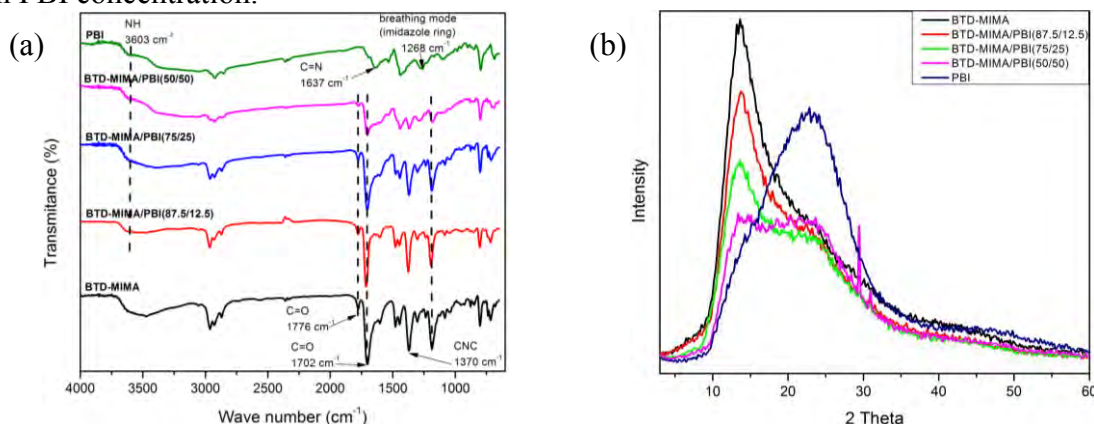


Figure 2. (a) FTIR spectrum and (b) Wide-angle X-ray scattering patterns of PI BTM-MIMA, PBI and blends

The thermal properties of pure polymers and blends were evaluated by DSC and TGA. DSC curves in Figure 3a exhibit high glass transition temperature (T_g) for polyimide PI BTM-MIMA (306 $^\circ\text{C}$) and PBI (362 $^\circ\text{C}$). The T_g 's of the blends are between the T_g 's of the pure polymers for the blend 75/25 wt% while it is not clear for 50/50 wt%. The thermal stabilities of the polymers were evaluated by TGA measurement (Figure 3b) in nitrogen atmosphere.

All polymers were stable up to 375°C. PBI has the lowest weight loss (20 %). This can be attributed to the high content of aromatic rings in the molecular chain. PBI, also has the lowest onset thermal degradation (377°C). PI BTd-MIMA, has the highest onset of degradation temperature (455°C) but the residual material at the end of TGA measurement is about 15 %. For the blends, the onset temperature decreases (449 → 448 → 382 °C) with the increase on PBI content, while the residual increases (20 → 32 → 58 %) as the presences of PBI that has an initial mass loss between 377 and 520 °C. The second mass loss is at 575 to 800 °C.

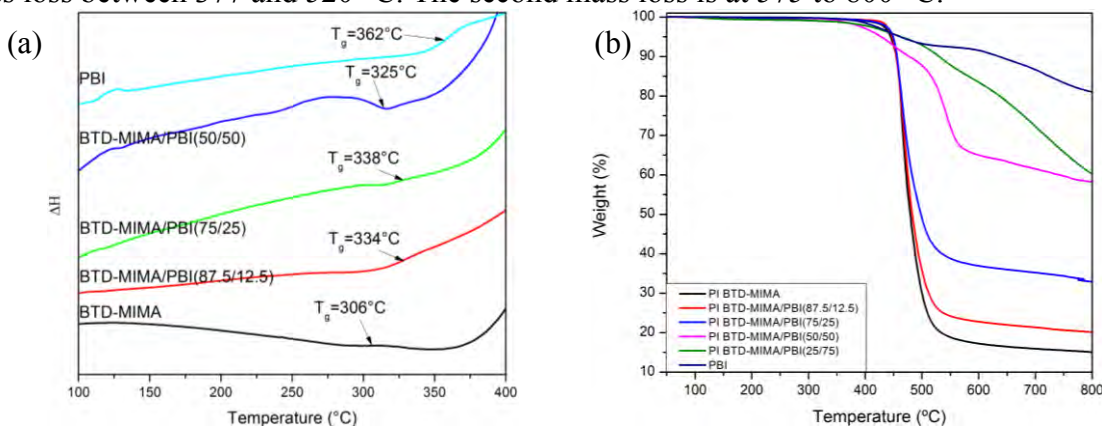


Figure 3. (a) DSC and (b) TGA thermograms for PI BTd-MIMA, PBI and blends

Gas transport properties

Gas permeability coefficients, P , at 2 atm and 35 °C are presented in Table 1. The polyimide and the blend with a low concentration of PBI (12.5 wt%) have the general trend that gas permeability coefficients follow the order $PCO_2 > PHe > PO_2 > PCH_4 > PN_2$. As the concentration of PBI increase in the membrane it is observed that the PCO_2 is drastically diminished, showing a sharp decrease indicating an order related to gas kinetic diameter ($PHe > PCO_2 > PO_2 > PCH_4 > PN_2$). It is also seen that separation factors for gas pairs CO_2/CH_4 , O_2/N_2 and CO_2/N_2 are not improved by blending.

Table 1. Permeability coefficients of PI BTd-MIMA, PBI and their blend membranes with severals compositions

Membrane constituents	Permeability (Barrer)					Ideal Selectivity		
	He	O ₂	N ₂	CH ₄	CO ₂	α_{O_2/N_2}	α_{CO_2/CH_4}	α_{CO_2/N_2}
PI BTd-MIMA	161.7	38.07	9.03	11.11	196.7	4.22	17.70	21.79
BTd-MIMA/PBI (87.5/12.5)	141.1	38.80	10.08	13.64	207.7	3.85	15.23	20.60
BTd-MIMA/PBI (75/25)	59.81	11.15	2.86	3.38	55.85	3.90	16.50	19.51
BTd-MIMA/PBI (50/50)	12.79	0.39	0.30	0.36	0.90	1.28	2.52	2.97
PBIa	0.6	0.015	0.004	0.002	0.16	3.13	88.89	33.33

a From ref. [6]

Apparent gas diffusion, D , and solubility coefficients, S , are given in Table 2 for membranes with several PI BTd-MIMA/PBI compositions at 2 atm upstream pressure and 35 °C. The apparent solubility for PI BTd-MIMA follows the order $SCO_2 > SO_2 > SN_2 > SCH_4$ where the CO_2 is the most soluble gas in the polymer even when the PBI is introduced to the system. In the case of the apparent gas diffusion, O_2 has the largest diffusion coefficient. For O_2 and CO_2 , the

diffusion coefficient increases at low PBI concentration and decreases as the PBI increase in the blend.

Table 2. Apparent Gas Diffusion and Solubility Coefficients of polymer blend membranes with various compositions

Membrane constituents	Diffusion coefficient (10 ⁻⁸ cm ² /s)				Solubility coefficient 10 ⁻² cm ³ (STP)/cm ³ cm Hg			
	O ₂	N ₂	CH ₄	CO ₂	O ₂	N ₂	CH ₄	CO ₂
PI BTD-MIMA	45.04	14.25	32.09	7.32	0.85	0.63	0.35	26.87
BTM-MIMA/PBI (87.5/12.5)	54.67	---	3.20	11.05	0.72	---	4.27	18.81
BTM-MIMA/PBI (75/25)	42.53	0.24	0.57	2.72	0.26	11.89	5.93	20.51
BTM-MIMA/PBI (50/50)	0.23	0.03	0.02	0.06	1.71	10.38	21.92	15.22
PBIa	0.03	0.009	0.003	0.085	0.50	0.53	0.60	1.88

a From ref. [6]

Conclusions

A novel polyimide PI BTM-MIMA was successfully synthesized in our laboratory. Thermal analysis show that it has high thermal resistance (Tonset = 445°C) and Tg = 306°C. The blends of PI BTM-MIMA with PBI were characterized and their permeability coefficient was determined. The results show that PI BTM-MIMA has a high permeability coefficient for all gases evaluated. The ideal selectivity for the gas pairs CO₂/N₂ and CO₂/CH₄ were the largest found of all the membranes evaluated. It was found that with low concentration of PBI (12.5 wt%) the permeability coefficient for all the gases increase while the ideal selectivity decrease, following the usual trade off.

Acknowledgements

The authors would like to acknowledge Dr. Patricia Quintana for allowing to access at The National laboratory of Nano and Biomaterials (LANNBIO) from CINVESTAV-IPN, Merida Unit, in which X-ray diffraction analysis was carried out with technical assistance of M.C. Daniel Aguilar-Treviño.

References

- [1] M. I. Loria-Bastarrachea and M. Aguilar-Vega, Ind. Eng. Chem. Res., 49 (23), 12060–12066 (2010)
- [2] M. L. Cecopieri-Gómez, J. Palacios-Alquisira and J. Domínguez, J. Memb. Sci., 293, 53-65 (2007)
- [3] S. S. Hosseini, M. M. Teoh and T. S. Chung, Polymer, 49, 1594-1603 (2008)
- [4] M. I. Loria-Bastarrachea and M. Aguilar-Vega, J. of Memb. Sci., 369 (1-2), 40-48 (2011)
- [5] M. Calle, A. E. Lozano, J. G. de La Campa and J. de Abajo, Macromolecules, 43 (5), 2268–2275 (2010)
- [6] S. C. Kumbharkar, P. B. Karadkar and U. K. Kharul, J. Memb. Sci., 286 (1-2), 161–169 (2006)
- [7] R. W. Baker, Ind. Eng. Chem. Res., 41 (6), 1393-1411 (2002)

MINIMUM PARAMETERS NECESSARY FOR GROW A THIN FILM WITH A SOL-GEL METHOD

O. Ortiz-Jimenez,^{1*} D. A. Razo-Medina,² M. Trejo-Durán,¹ E. Alvarado-Méndez,² R. I. Mata-Chávez¹, Martínez Rosales M.³

¹ *Departamento de Estudios Multidisciplinarios (DEM), Universidad de Guanajuato, Yuriria, Gto. México.*

² *División de Ingenierías, Campus Irapuato-Salamanca (DICIS), Universidad de Guanajuato, Com. Palo Blanco s/n 36885, Salamanca, Gto. México*

³ *División de Ciencias Naturales y Exactas, Campus Guanajuato, Universidad de Guanajuato.*

Noria alta s/n 36050, Guanajuato, Gto. México.

* o.ortizjimenez@ugto.mx

Abstract

In this work is presented the result of the conditions for grow a thin film with a sol-gel method and with the aid of a dip-coater. The conditions are like preparation of sol-gel, temperature, atmosphere, cycles of immersion, drying of the film, etc., of which here show only the principal variables that is relatively easy to controlled in the section of methodology. Finally, in the section of results we perform the final thin film and the first studies.

Introduction

In the literature there are different techniques for growing films for example sputtering, pulsed laser deposition, and more. When compared with others techniques, the sol-gel presents some advantages such as possibility of depositing in complex-shaped substrates as well as it requires considerably less equipment and is potentially less expensive [1,2].

This technique is useful for example to make a WO₃ and W-Ti-O thin-film gas sensors [3], preparation, characterization and gas-sensing property of thin-film of ZnO [4].

Dip coating by sol-gel process is versatile and low-cost techniques strategies to prepare thin films of particles. In general form, the sol-gel coating consists in dip a substrate in a fluid gel: solvent evaporation and gravitational draining, more condensation reactions, result in the deposition of a solid film [5].

Methodology

For this work, many different experiments are performed for creating a thin film over glass substrate. The project was divided into two stages, the first stage is the sol-gel mixture, different tests are made to modify parameters of the mixture. The second stage of the film is made with the dip-coater device.

The chemicals used in the sol-gel were Tetraethyl Orthosilicate (TEOS), Ethanol and Water, at a ratio of 4:4:1 respectively. The rates were obtained from a previous work [japs2006]. The next step was to determine the ideal viscosity for the mixture. As we know, there are different factors that affect the chemical reaction, for example temperature, humidity, mole ratios between reactants, and others. In order to determine the viscosity of the mixture, it was left to evaporate at room temperature. After that, we started to make a film and we observed the behavior of the mixture with the substrate.

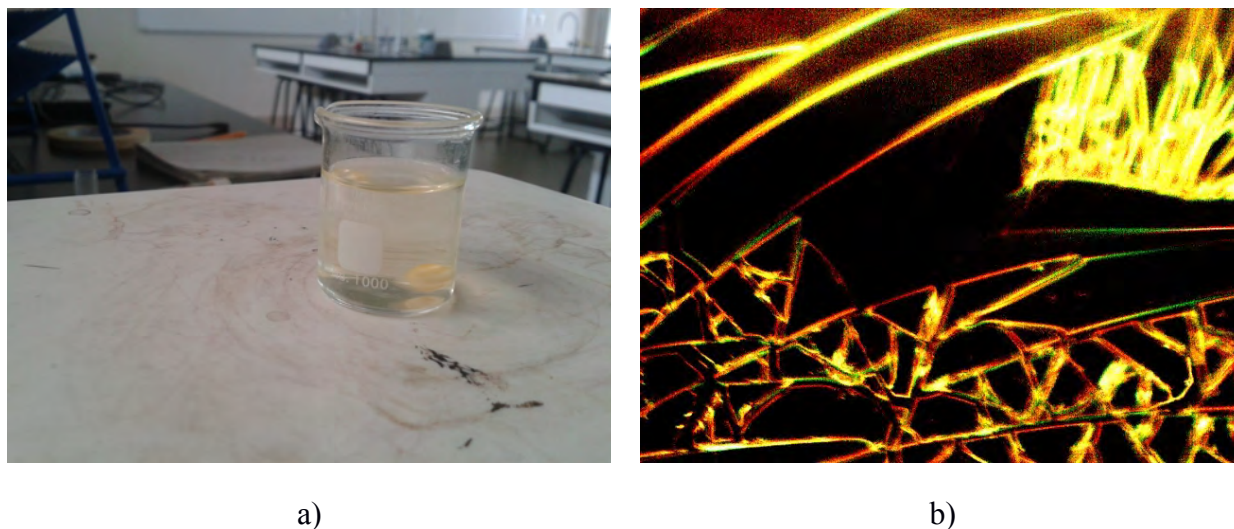


Figure 1. a)Mixture after 24 hours of environmental evaporation. b)Film obtain with the previous mixture

With the help of a dip-coater, which was encapsulated in a glass chamber, the immersion of the substrate was controlled over the mixture. Due the evaporation of the mix, it was necessary to control it; we saturated the chamber environment with ethanol at 70 °C.

The next step was to determine the appropriate speed for the dip-coater. The dip coater is like the one in figure 2. With this variable, we tried with low speed, but in the literature we find that it is better to use fast speed [2]. The fastest speed the dip coater could offer was 61.14 mm/min, so it was the fastest speed to work with and it was also the best.



Figure 2. Dip coater mono.

The next step is to determine the appropriate number of cycles of immersion of the substrate in the mixture. We started with 15 and 30 cycles, but the thickness was not appropriate. We obtained an acceptable homogeneous film at 100 cycles. With the 100 cycles as a starting point, the next step was to create a thicker film. This was obtained when we increased the number of cycles to 150 and 200 cycles.

Once we had the film, the next challenge was the drying process. We found out that the films needed to remain almost three days in the chamber to be completely dried. With this time, it is possible to obtain a film that will not break when exposed in environmental conditions, without having to give any heat treatment.

Results

In the figure 3 we show the evolution of the film when we increase the number of cycles. In each case we keep the same mixture and speed.

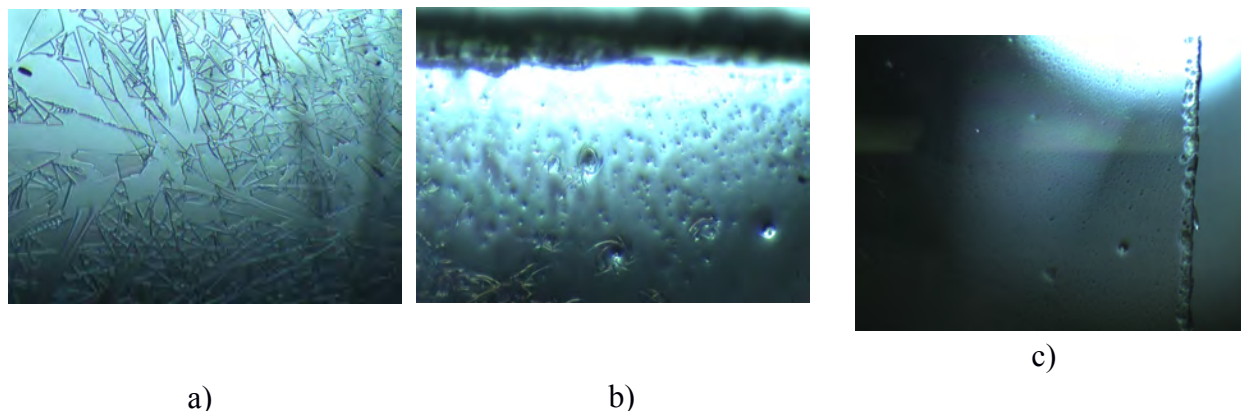


Figure 3. Evolution of the film. a) 30 cycles b) 100 cycles c) 200 cycles

Once we had the film, we took photos of the film with an optical microscope and we found the existence of a little pore. The reason for the existence of the pores is due to the fact that the solvent needed to find a way to leave the film.

Once the speed was determined, the next step was to start increasing the number of cycles, such as is shown in figure 3 with more cycles. The film is more homogeneous and presents less pores or fractures, but when we increasing the cycles, the time in the chamber increases too.

Conclusions

In this work we focused on the manufacturing process and deposition of sol-gel film on glass substrate. The films were analyzed using optical microscopy. We determined the minimum parameters necessary to manufacture good thin films with other components like nanoparticles, coordinate compounds, among others using the sol-gel method.

Acknowledgements

This work was supported partially by Guanajuato University-DAIP No. 223/2013, 288/ 2013 and PIFI-2013.

References

- [1] C. J. Brinker, G. C. Fryem A. J. Hurd and C. S. Ashley, Thin Solid Films, 201, 97-108 (1991).
- [2] M.H. Habibi and M. Khaledi Sardashti (2007), Structure and Morphology of Nanostructured Zinc Oxide Thin Films Prepared by Dip-vs. Spin-Coating MethodsJ. Iran. Chem. Soc., Vol. 5, No. 4, December 2008, pp. 603-609.
- [3] J. Shieh, H.M. Feng, M.H. Hon, H.Y. Juang (2002), WO₃ and W-Ti-O thin-film gas sensors prepared by sol-gel dip-coating, Sensors and Actuators B 86 (2002) 75-80
- [4] X.L. Cheng, H. Zhao, L.H. Huo, S. Gao, J.G. Zhao (2004), ZnO nanoparticulate thin film: preparation, characterization and gas-sensing property, Sensors and Actuators B 102 (2004) 248–252.
- [5] N. V. Kaneva, C. D. Dushkin (2011). Preparation of nanocrystalline thin films of ZnO by sol-gel dip coating. Bulgarian Chemical Communications s, Volume 43, Number 2 (pp. 259–263).

POLYSTYRENE PICKERING POLYMERIZATION: MECHANISTIC EVENTS

L. I. García Damián¹, A. Rosas-Aburto¹, B. Fouconnier², A. Román-Guerrero³, F. López-Serrano^{1*}

¹ Departamento de Ingeniería Química, Facultad de Química, Universidad Nacional de México, D. F., 04510, México. *Email: lopezserrano@unam.mx

² Facultad de Ciencias Químicas, Universidad Veracruzana, Av. Universidad Km. 7.5, Col. Santa Isabel, Coatzacoalcas, Veracruz, 96535, México.

³ Departamento de Biotecnología, Universidad Autónoma Metropolitana – Iztapalapa, San Rafael Atlixco 186, Col. Vicentina, 09340 México, D. F., México.

Abstract

Polymerizations of styrene in Pickering emulsions stabilized by CTAB-SiO₂ aggregates were investigated. 15 wt% of styrene was polymerized at 78°C using ammonium persulfate (APS) as initiator at 3 different concentrations (0.5, 1 and 2 wt% relative to styrene). Styrene conversions higher than 95% were obtained and an auto-acceleration of the reaction occurred at approximately 60% of conversion in all experiments. Nucleation occurred throughout the reaction for the 1 and 2 wt% APS contents. No coagulation was observed nevertheless, a glass effect prevented the total conversion of styrene. Particles of about 150-200 nm were obtained, being of smaller size the higher the APS content.

Introduction

Pickering emulsions are surfactant-free dispersed systems, stabilized by solid particles anchored at the water-oil interface, differing from conventional emulsions due to their very high stability against coalescence [1, 2].

During radical polymerization, in conventional emulsions, the micellar, homogeneous and coagulative nucleation is proposed as possible mechanisms along the reaction [3]. Nevertheless, when functionalized nanoparticles or hydrophobic modified nanoparticles with very low concentration of surfactant are used, as a route for synthesizing organic-inorganic nanocomposite particles, the mechanisms of micellar nucleation can be excluded. Therefore, the most probable nucleation mechanisms involved in Pickering emulsions are homogeneous nucleation and coagulation. The ultimate would be the predominant mechanism involved in the preparation of submicron polymer particles [4]. Although there are many works dealing with the synthesis of organic-inorganic particles by surfactant-free emulsion polymerization, the proposed mechanisms are only described schematically.

In this work we investigated the mechanism of polymer particles nucleation, the effect of silica nanoparticles on the radical absorption and the coagulative of the aggregate to form the nascent nanocomposite particles.

Experimental

Preparation of the CTAB-SiO₂ aggregates.

The Cetyltrimethylammonium Bromide (CTAB) and SiO₂ colloidal (Bendzil 830 CC, 30 wt% SiO₂), aggregates were obtained by mixing 0.29g of CTAB, 75g a SiO₂ Colloidal solution and 0.13g of NaCl in a volumetric flask completed with distilled water until 250 mL were mixed together to form a solution. The solution was placed under magnetic agitation during 12 h and the sonicated using an ultrasonic bath (Branson 5510) for 10 minutes, before preparing the emulsions.

Emulsion Pickering styrene polymerization

A typical preparation procedure is detailed as follows: distilled water, CTAB-SiO₂ solution and styrene (Sigma Aldrich 99% purity), were prepared with the recipe depicted in table 1, followed by emulsification by an homogenizer Ultra-Turrax T18 (IKA®-Werke Works Inc., Wilmington, NC, USA) at 20,000 rpm during 10 min at 25 °C.

Batch polymerization were carried at 78 °C in a 500 mL reactor equipped with jacket, under continuous stirring at 250 rpm using ammonium persulfate (APS, Baker 99% purity) as initiator at 0.5 wt%, 1 wt% and 2 wt% relative to styrene.

Latex samples, were short stopped by a small amount of hydroquinone (Sigma Aldrich 99% purity), and taken during the polymerization for the kinetic study. Finally, kinetics measurements were performed using a Raman spectrophotometer (λ Solutions) and by gravimetry. In this last procedure, the final latex product was dried and weighed for determine the conversion. Conversion was also determined by Raman spectroscopy, using the formula, $X = 1 - (I_t / I_0)$; here I_t represents the intensity ratio between the peak at 1630 cm⁻¹ and the peak at 620 cm⁻¹ at time t and I_0 the intensity ratio at time $t=0$ [4]

Table1. Recipe for synthesis of latex in Pickering emulsion.

Ingredients	Quantity (g)
Water	187.724
Styrene	42.441
CTAB-SiO ₂ solution	55.113

Results and Discussion

Applying the models of conventional emulsion polymerization to styrene polymerization in emulsions stabilized by SiO₂-CTAB aggregates, the reaction rate is given by the eq (1):

$$\frac{dx}{dt} = \frac{k_p M_p n N_T V}{M_T N_{av}} \quad (1)$$

where x is the conversion, t the time (min), k_p is the constant polymerization (L mol⁻¹ min⁻¹), M_p the monomer concentration within the particles (mol L⁻¹), n the average number of radicals, N_T the total number of particles (L⁻¹), V the volume of the reactor (L), M_T the moles of monomer charged (mol) and N_{av} the Avogadro number (mol⁻¹).

The total number of particles can be obtained from a mass balance as shown in eq (2):

$$N_T = \frac{6M_T M_m x}{\pi \rho_p D_p^3} \quad (2)$$

Where M_m is the molar mass of the monomer (g mol⁻¹), ρ_p the polymer density (g cm⁻³) and D_p the particle diameter (nm).

Analyzing eq (1) it is possible to know all the variables except n . If we calculate the derivative of the experimental conversion, eq (1) can be rewritten as eq (3) and thus the average radicals number n_e can be estimated as followed [6]:

$$n_e = \frac{M_T N_{av} \frac{dx}{dt}}{k_p M_p N_T V} \quad (3)$$

Figure 1 shows the values and derivative conversion against time obtained for the three different concentrations of initiator used. It can be observed that for all experiments, there was a rapid conversion of styrene from about 60% due to an auto-acceleration of the reaction. This

phenomena, known as gel or Trommsdorff effect [3], was accentuated with the initiator concentration. This effect can also be depicted by the presence of a maximum on each derivative curve of conversion plotted at the bottom of the figure.

Figure 2 shows the evolution of the particle size for each reaction. At 1 and 2wt% of APS, the particle size remains approximately constant. Nevertheless, in all experiments, the particle size decreased as the initiator concentration increased. At 0.5 wt% APS, the particle size grew up throughout the reaction, indicating that a constant number of particles was achieved or the particles were coalescing.

Figure 3 shows the evolution of the number of NT particles obtained with Eq. (3) by knowing the conversion (Fig. 1) and the particle size (Fig. 2). At 1 and 2wt% APS, the number of particles increased, as the reaction was progressing, indicating that the mechanism of nucleation occurred throughout the reaction.

However, at 0.5 wt% APS the number of particles remained constant at ca. 20% of conversion. It is noteworthy that there is no coagulation, since N_T did not decrease. Therefore, it can be emphasized that under these conditions coagulation did not occur.

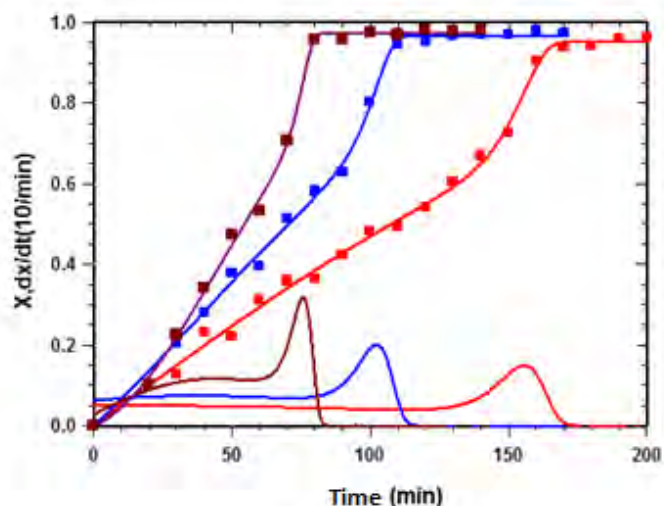


Figure 1. Conversion time versus time for a 15wt% styrene emulsions and various concentrations of initiator (red: 0.5% APS; blue: 1% APS; brown: 3% APS). The bell-shaped curves show the derivative of conversion.

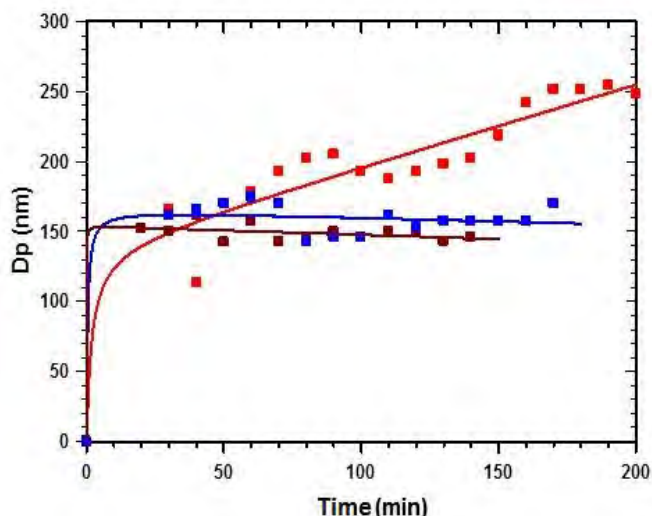


Figure 2. Particle diameter versus the reaction time (red: 0.5% APS; blue: 1% APS; brown: 3% APS)

Analyzing figures 2 and 3, it can be mentioned that the nucleation process changed when the initiator concentration was above 0.5% APS. This indicates that if small particles of about 150 nm were to be synthesized therefore, higher concentrations of initiator would be required.

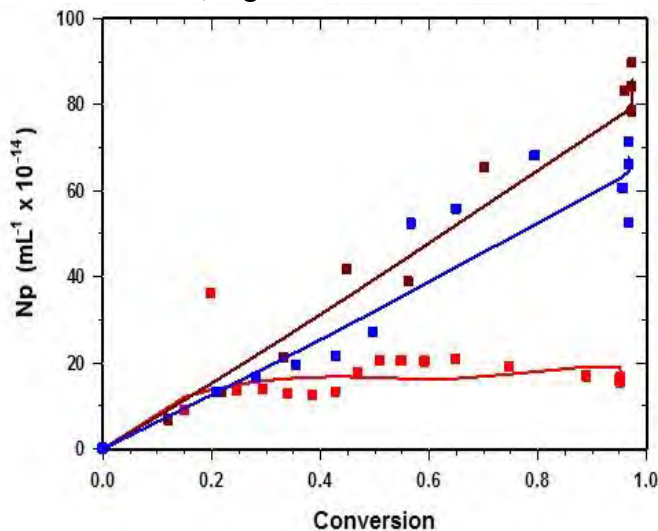


Figure 3. Particle density versus styrene conversion (red: 0.5% APS; blue: 1% APS; brown: 3% APS)

Finally, applying eq. (3), the average number of radicals estimated (n_e) is presented in Figure 4. One can see that at low conversions the average numbers of radicals estimated are not reliable, since Eq. (3) is undetermined when N_T approaches zero. Consequently n_e goes to infinity, which is physically impossible.

Analyzing figure 4, it can be observed that the average number of radicals is approximately three for all experiments. This number is higher than the one obtained in a classical system 0-1, i.e., in which there is zero or one radical within the particles, where the termination is supposed to occur instantaneously when another radical enters the particle, leading to $n = 0.5$. This indicates that within the particles, prepared in these experiments, coexists more than one radical per particle. Figure 4, also corroborates that the gel effect occurred at ca. 60% conversion in all experiments, showing an increase in number of radicals within the particles, getting values between 7 and 14.

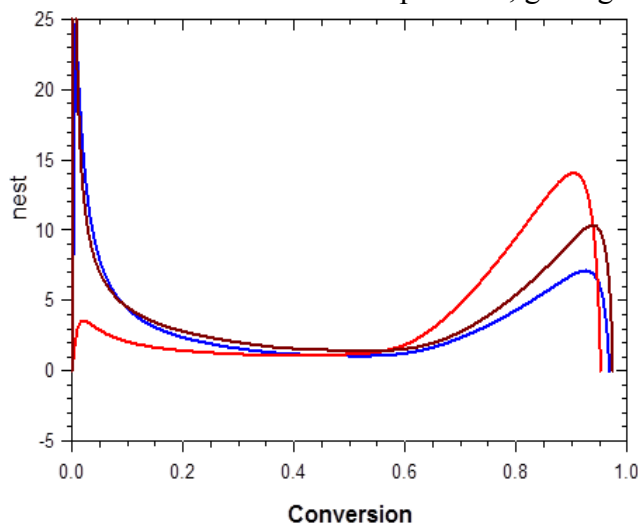


Figure 4. Number average radicals estimated (n_{est}) as a function of conversion (red: 0.5% APS; blue: 1% APS; brown: 3% APS)

It can also be noticed that there is a decrease in the number of radicals within the particles between 90 and 95% of conversion. Actually, in order to generate n_e , k_p was assumed constant, and it is likely that the decrease of n_e is not related to the radicals but due to the appearance of the glass effect, showing that the temperature of the system is getting close to the glass transition temperature of the mixture and k_p is responsible of this effect. The glass transition temperature (T_g) of polystyrene is about 100°C [3]. Therefore, to achieve high conversions, the reaction should be operated above this threshold. In this work, all reactions were investigated at 80°C and explain the reason why any reaction achieved 100% of conversion.

Conclusions

By using Pickering emulsion polymerization route it was possible to synthesize with high conversion higher than 95%, styrene particles of about 150-250 nm and even smaller when 2 wt% APS was used. It has been observed that a gel effect occurred at approximately 60 % conversion independently of the concentration of initiator. In the experiment containing 1wt% APS the nucleation process stopped at about 20% conversion and consequently larger particles were obtained. In this study, coagulation did not occur indicating that Pickering emulsions offer high stability. The emulsified system used for styrene polymerization does not belong to the typical system 0-1 as reported in traditional emulsion polymerization. Nevertheless, it was observed a glass effect between 90 and 95% conversion, we attribute to this effect the reason for the reactions not reaching 100% of conversion.

Acknowledgements

Funds provided by UNAM (PAPIIT IN114212), PROMEP UV-PTC-665, the interchange program between UNAM and U Veracruzana-Coatzacoalcos, as well as a scholarship for one of us (LIGD); are gratefully acknowledged.

References

- [1] Y. Chevalier and M. Bolzinger, Colloids and Surfaces A: Physicochem. Eng. Aspects, 439, 23-34 (2013).
- [2] R. Aveyard, B.P. Binks, J.H. Clint, Adv. Colloid Interface Sci. 100-102, 503-546 (2003).
- [3] G. Odian, Principles of Polymerization, 4th Edition, 2004.
- [4] H. Ma, M. Luo, S. Sanay, K. Rege, L. Dai, Materials, 3, 1186-1202 (2010).
- [5] R. Hardis, J. L.P. Jessop, F. E. Peters, M. R. Kessler, Composites Part A, 49, 100-108, 2013
- [6] F. López-Serrano, Mendizábal E., Puig J.E., Álvarez J., Macromol. Symp. 283-284, 18-26 (2009).

SYNTHESIS OF CORE-SHELL RESINS FOR HEAVY-METAL REMOVAL BY SEEDED SUSPENSION COPOLYMERIZATION

Tlilayatzí-Muñoz Adriana,¹ Carro Shirley,¹ Cardoso Judith²

¹ *Facultad de Ciencias Básicas, Ingeniería y Tecnología, Universidad Autónoma de Tlaxcala, Calzada Apizaquito S/N, Apizaco, Tlax C.P. 90300*

² *Departamento de Física, División De Ciencias Básicas e Ingeniería, Universidad Autónoma Metropolitana-Iztapalapa, C.P. 55-534, México, D.F. 09340, México*

Abstract

Seeded suspension copolymerization was used to synthesize core-shell beads. A two stage copolymerization technique was used. The seed particles for polystyrene or polystyrene-divinylbenzene (Sty-DVB) were synthesized first in an aqueous medium using poly(vinyl alcohol) as suspension agent and 2,2-Azobisisobutyronitrile, AIBN, as initiator. These beads were swollen in a 4-vinylpyridine-DVB-AIBN and polymerized in aqueous phase to produce 4VP-DVB shell. Different conditions to enlarge core size were tested. The aim of this work was the synthesis of resins with a improved mechanical resistance to a post-functionalization, which is performed to increase the sorption capability of the beads with high selectivity and fast adsorption kinetics to eliminate Cr+6

Introduction

Ion-exchange resins are suitable for metal-ion complexation because of their hydrophobicity and high selectivity.[1,2] They are characterized by a permanent porous structure even when they are dried, and they swell less than gel-type resins.[3] The synthesis of a polymer for these applications, therefore, requires specific functionalization to improve the sorption capabilities of the resin. Synthetic ion exchangers have become widely used in both industry and academia for separation operations of inorganic and organic ions. Among the most popular precursor copolymers for obtaining ion exchangers with different functionalities and morphologies are styrene (St)-divinylbenzene (DVB) copolymers. [4] Functional copolymers, linear and crosslinked, bearing primary amine groups are of great interest because of their high reactivity, which allows the incorporation of numerous additional moieties. It is well known that polymers based on vinyl pyridine (VP) can form polymer-metal complexes. [5-7]. However, ion exchangers with primary amine groups are difficult to obtain by chemical reactions with St-DVB copolymers. Ortiz-Palacios et al.[4,8] synthesized macroporous resins with specific surface areas produced by suspension polymerization with 4VP and DVB as comonomers and various proportions of porogens (e.g., toluene and hexane). In this study, three ion-exchange resins based on 4-vinylpyridine and divinylbenzene functionalized with N-oxide groups were obtained. The chromium ions with HCl was observed to increase after the protonation of the N-oxide groups. However, the resins obtained were too sensitive to functionalization and lost their spherical form, besides particle size obtained was too small to be used in other applications, such as electro-deionization columns. In this work core-shell beads were synthesized in order to increase mechanical resistance and bead size.

Experimental

DVB (crosslinking agent; Aldrich), a 55% isomeric mixture, by vacuum distillation. The purification of 4VP included a 5% NaOH washing stage to eliminate the red color and a second stage with distilled water. Poly(vinyl alcohol) (PVA; Aldrich; 80–87% hydrolyzed) had a molecular weight of 8500–12,400 was used as suspension agent and 2,2-Azobisisobutyronitrile

(Aldrich) as initiator.

The ST or ST-DVB copolymer beads were obtained by suspension polymerization. A four-necked, 0.50-L reaction vessel equipped with a thermostat, a stirrer, a water condenser, and a nitrogen inlet was used. The continuous phase (deionized water and a 2 wt % PVA solution) was placed in a reactor vessel, under stirring, at 70°C. At this temperature, the organic phase (monomers and initiator) was added. The mixture was heated to 80°C. The beads were then isolated for filtration. The particles were washed with a methanol– water mixture to eliminate the residual monomer and PVA. The mixture was washed several times until turbidity disappeared. The material was filtered and dried in a vacuum oven at 50°C for 24 h.

The core beads were swollen with a mixture of initiator and 4VP-DVB (1/0.1 %mol) dissolved in methanol (50 wt%) for several hours and subsequently dispersed in an 2% wt PVA aqueous solution and polymerized during 12 hr at 180 rpm. Polymer core-shell beads were washed and dried as it was explained before.

FTIR- ATR spectra were collected on a 1500 Perkin Elmer apparatus with 1 cm⁻¹ resolution and 30 scans. Thermogravimetric measurements were performed with a PIRYS Perkin Elmer under a 50 cm³/min nitrogen flow within the range of 30 °C to 800°C. Differential scanning calorimetry was carried out under a nitrogen flow (50 cm³/min) by a MDSC2920 Modulated Differential Scanning Calorimeter manufactured by TA Instruments (Newcastle, Delaware, USA). Modulated DSC scans were carried out at a heating rate of 10 °C/min with amplitude of $\pm 0.769^\circ\text{C}$ and a period of 30 seconds within the range of 15 to 200°C under 50 mL/min of nitrogen. T_g was obtained from the second or third scan

Results and Discussion

In order to increase core size different condition were tested. It is well known that hydrodynamic conditions play an important role in monomer droplets rupture. In this way, monomer volume, impeller kind and agitation velocity was varied. Monomer droplet size was analyzed by optical microscopy to determine polymerization conditions. Low agitation velocity (150 rpm) and half-moon impeller form gave the best results. The monomer droplet size obtained range from 0.003-0.009 mm.[sniqba14]

Different polymerizations conditions were tested to obtain core size above 0.5 mm (see Table 1). PST beads are easily swollen, however, they tend to stick. To overcome this problem a double volume of 4VP-DVB mixture must be used. In order to increase structural rigidity DVB was added. Two different relations were tested. It was found that when a 10% of DVB is used, the size of beads is reduced in contrast to ST homopolymer beads, however, bead size distribution is narrower. Besides, yield is diminished and beads time swelling is too slow. It is attributed to a fast and excessive chain cross-link that avoids monomer diffusion through beads. If DVB contents is decreased better results are obtained. Larger bead size and narrow particle size distribution are achieved. Figure 1 shows a photograph for these materials. Also typical resins obtained by 4VP-DVB copolymerization are shown. As it can be seen particle size for the resins synthesized in this work are larger in all cases. Unfortunately shell thickness could not be measured.

Table 1. Formulation employed to synthesize core beads

Experiment	ST %wt	DVB %wt	Average core size (mm)	Swollen time (hr)
ST	100	0	0.40	8
ST-DVB1	90	10	0.08	182
ST-DVB2	97	3	0.80	24

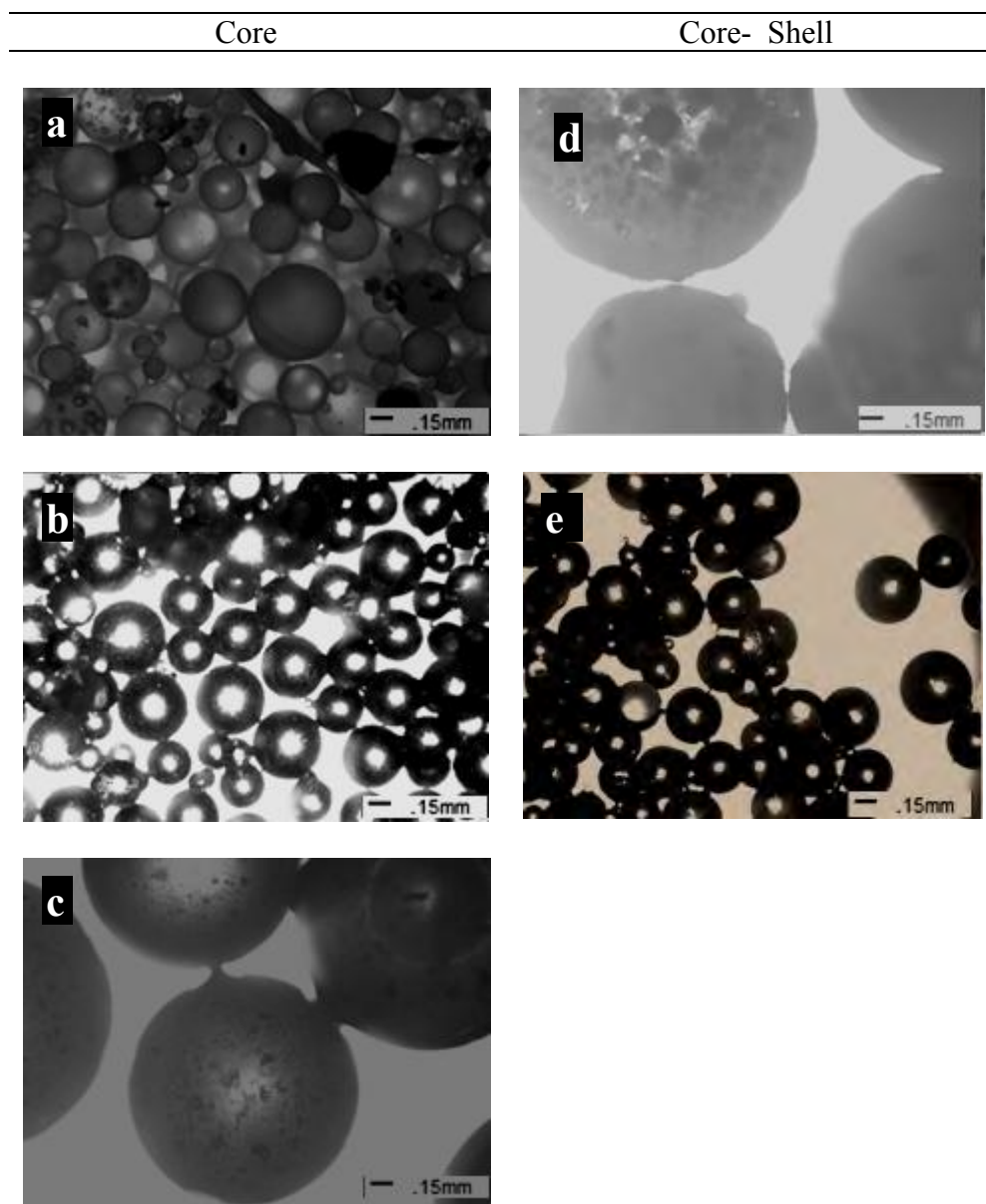


Figure 1. Photographs of suspension polymerized beads a) ST b)ST/DVB (10%) c) ST/DVB (3%) d) core-shell resins e) 4VP-DVB resins.

In Figure 2 it is shown the TGA thermograms for the resins, after and before shell polymerization. Core-shell resins had decomposition temperatures of 10% loss weight (Td10%) lightly higher than the core material in all the cases. Notice that for ST core loss weight at high temperatures is higher than ST/DVB core.

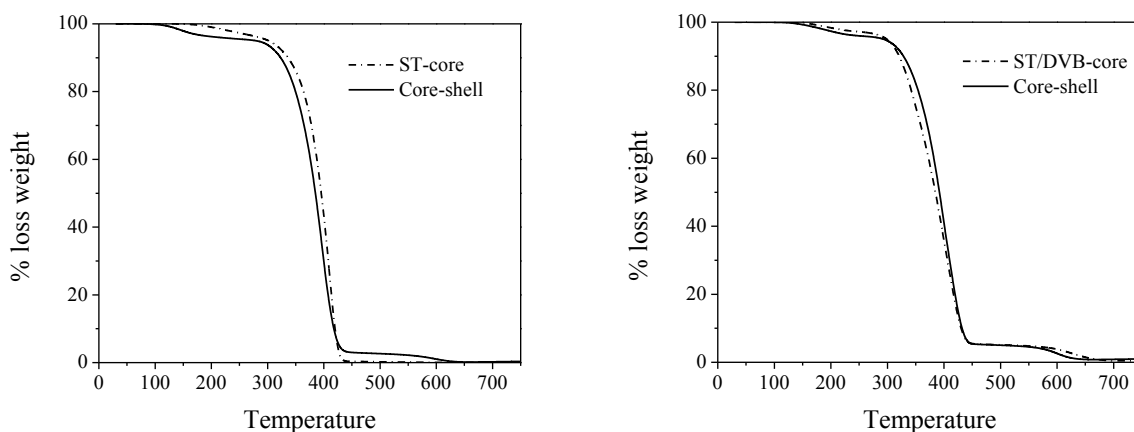


Figure 2. TGA thermograms for polymerized beads a) ST core and core-shell b) ST/DVB core and core-shell

In Figure 3 the DSC thermograms of the resins are shown. The styrene beads had the lower glass temperature (T_g), 83°C, and the core-shell resins with a copolymer of 4VP-DVB had a T_g of 121 °C. In all the cases, the samples exhibited only one T_g . In Table 2 it is summarized the results or their thermal properties.

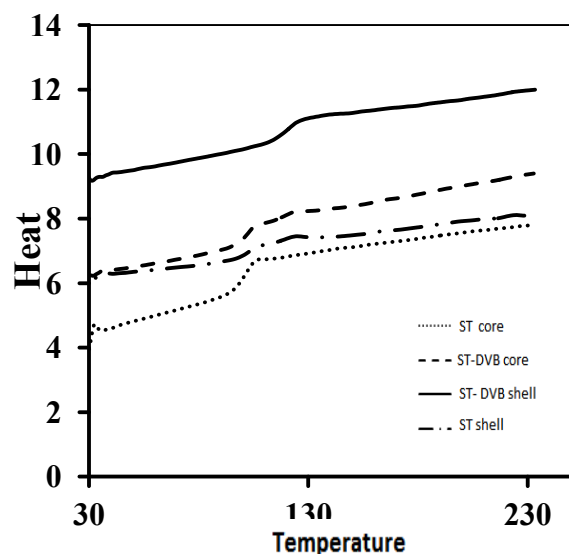


Figure 3. DSC thermograms for polymerized beads.

Table 2. Glass temperatura (T_g), Decomposition temperature at 10 % loss weight ($T_{d10\%}$), Temperature of decomposition maximum (T_p) and residual water (% H₂O)

Sample	T_g (°C)	$T_{d10\%}$ (°C)	T_p (°C)	%H ₂ O
ST core	100	345	411	2
ST- DVB core	101	332	398	3
ST-DVB shell	101	331	394	3
ST-DVB shell	121	341	402	4

Conclusions

Seeded suspension copolymerization was used successfully to synthesize core-shell beads with large spherical size (up to 1 mm). A two stage copolymerization technique was used. Resins obtained by this method are larger than those obtained from direct 4VP-DVB copolymerization. ST/DVB core gave narrower particle size distribution. The effect of crosslinker contents for core beads is reflected in swelling time employed before shell copolymerization. Thermal properties show better resistance and adequate formation of shell structure. The beads reported here are potentially useful as Ion-exchange functionalized resins.

Acknowledgements

Authors thank to CONACyT for financial support to project 220232 and Universidad Autónoma de Tlaxcala for facilities granted to A. Tlilayatzi

References

- [1] S.Ecatina., A. Ecatina, D. Axente, C. Marcu. J Polym Sci Part A: Polym Chem 2004, 42, 2451.
- [2] D. Ratna, V. Dalvi, P. C. Deb, B. C. Chakraborty. J Polym Sci Part A: Polym Chem 2003, 41, 2166.
- [3] D. C. Sherrington. Chem Commun 1998, 2275.
- [4] J. Ortiz-Palacios, J. Cardoso, O. Manero. J Appl Polym Sci, 2008, 2203-2210.
- [5] B. L. Gutanu, H. A. Maturana, M. Luna. J Appl Polym Sci, 1999, 74, 1557.
- [6] B. L. Rivas, H. A. Maturana, M. Luna. J Appl Polym Sci 1999, 74, 1557.
- [7] M. P. McCurdie, L. A. Belfiore. Polymer 1999, 40, 2889.
- [8] J. Cardoso, J. Ortiz-Palacios, O. Manero. J Appl Polym Sci, 2008, 3644-3653.

SYNTHESIS AND CHARACTERIZATION OF MACROPOROUS RESINS FROM POLY(4-VINYLPYRIDINE) AND DIVINYLBENZENE FUNCTIONALIZED BY AMPHOLYTE GROUPS

José Antonio Arcos,¹ Judith Cardoso^{2*}

¹ *División de Ingeniería Química y Bioquímica, Tecnológico de Estudios Superiores de Ecatepec, Av. Tecnológico S/N, Col. Valle de Anáhuac, Ecatepec, Edo. de México, CP 55210.*

² *Physics Department, DCBI, UAMI. Av. San Rafael Atlixco 188, Col. Vicentina, México, D.F. C.P. 09340.*

Abstract

Macroporous resins have been shown to be highly efficient in elimination of toxic metals, such as chromium VI, due to their high surface area. This paper presents the synthesis and characterization of a macroporous resin of P4VP-DVB (60:40 and 75:25 ratio) by suspension technique using toluene and toluene-dodecane as agent porogens and its functionalization with 1,3-propanesultone. It was obtained resins ampholytes and their characterization was performed by FTIR, TGA, DSC and SEM. It was studied its efficiency to eliminate to the Cr (VI) in solutions of 4-100 ppm, showing that sulfobetaine groups are efficient in the elimination of the oxy-metal.

Introduction

The pollution of water bodies due to the indiscriminate elimination of heavy metals has been a concern for a long time [1]. Heavy metals are inorganic contaminants of greatest physiological interest, due to its toxicity to aquatic life, human beings and environment [2]. As an environmental threat, heavy metals are becoming environmental contaminants priority (Fu and Wang, 2011). Industries which work with heavy metals like chrome, causing a large amount of contaminated water from sales both of hexavalent chromium, Cr (VI), as well as trivalent chromium, Cr (III) this last is not a toxic pollutant, however, found that the chrome Cr (VI) is highly soluble in water and 100 times more toxic and harmful than Cr (III).

Due to the toxicity of the Cr (VI), has been implemented several techniques for the removal of this material from industrial waste water such as ion exchange, precipitation with pearls of iron and the most widely used in different countries, includes reduction of chromium to the trivalent form and its subsequent precipitation with alkalis.

The use of ion exchange materials are feasible alternatives that allows the separation or purification of metal ions and due to they can be regenerated and thus be used again in the process [4-6]. The aim this work is developed new ion exchange resins to be used in the elimination of Cr (VI) derived of 4-vinyl pyridine (4VP) and divinylbenzene (DVB) using organic solvents as agent porogens.

Experimental

Synthesis of resins

Materials: poly(vinyl alcohol) (PVA), 4-vinylpyridine (4VP), divinylbenzene (DVB) (55%), 1,5-difenilcarbazonaheptane, and toluene were purchased from Sigma-Aldrich Co, and azobisisobutyronitrile (AIBN) were used as received, except the monomers which were purified by vacuum distillation: 4VP (Tb= 35-37 °C) and DVB (Tb= 55-56 °C)

General Procedure. The reactor with the deionized water and the porogens were warmed up to 80 °C with at a stirring speed chosen. 4VP and DVB were added as is presented in Table 1. 20 mg of AIBN dissolved in toluene was added and stirring speed is adjusted and the reaction was carried out at 70 °C for 20 hours. The resins obtained were rinsed with deionized water repeatedly until washes were transparent. The resins were dried in a vacuum oven at 60 °C for 3 days

Table 1. Experimental condition for the precursor resins

Resin	4VP/DVB molar ratio	Poly(vinyl alcohol) (g)	Porogen Agent (ml)	Stirring speed
R4	60/40	2.0	80:80 heptane:toluene	150
R6	75/25	17.3	80:80	250

Functionalization of resins.. In a round flask, which contained a coolant and a bar magnet, was added deionized water and the resin and 1, 3-propanesultone in 1:1 molar ratio. The reaction mixture is kept with constant magnetic stirring and temperature of 60° C for 72 h. Later the system was cooled to room temperature and it was purified by some washes of acetone that allowed removing the excess of 1,3-propanesultone. The sulfobetaine resin (RS) was dried in a vacuum oven at 60 °C for 24 h.

Characterization. FTIR spectra were collected in a Perkin Elmer 1500 unit with 2 cm⁻¹ resolution and sample was dispersed and measured in dry KBr discs. Thermogravimetric analysis was performed with a PYRIS Perkin Elmer with a nitrogen flow of 50 mL/min in the range of 30 °C to 800 °C. Differential Scanning Calorimetry was carried out in a stream of nitrogen (50 cm³/min) in a MDSC-2920 manufactured by TA Instruments (Newcastle, Delaware, USA), with a heating rate of 10 ° C/min with amplitude of ± 1.06 ° C and a period of ± 40 seconds in the range of 25 to 200 ° C with a flow of 50 mL/min under nitrogen atmosphere. The glass transition temperature (T_g), was obtained from the second scan; the samples were previously heated at 100° C for 120 minutes to remove the residual water in the sample.

Results and Discussion

In Figure 1 is shown the spectra of the precursor and functionalized resins with the sulfobetaine groups. The precursor resin displayed at 3050 cm⁻¹ associated a ν C-H aromatic signal and 1600 cm⁻¹ and 1500 cm⁻¹ for ν C=C; two weak bands in 780 cm⁻¹ and at 810 cm⁻¹ for δ C-H out of plane for mono- and di-substituted. On the other hand, in the case of the functionalized additional two strong bands appeared at 1070 cm⁻¹ is for S=O ν stretch symmetric and other band for S=O at 1345 cm⁻¹ for stretch asymmetric vibration. A strong band at 3490 cm⁻¹ (-OH ν str) showed that the resins are hydroscopic.

Figure 2A showed the thermograms obtained by TGA for synthesized materials. Precursor polymer suffered a loss of 3 ± 1 % of water and about 8 % for functionalized resins. Initial decomposition temperature was lower for functionalized resins than precursor resins. The precursor resins presented two stages: the first started around 300 °C and ended at 350 and the second stage started at 350 °C and ended at 600 °C. Both of them describe the decomposition of the aromatic structures. In the case of the sulfonated resins exhibit a second stage that involved

the decomposition of the sulfonated pendant groups and started at 220 °C and ended at 300 °C. This result is in close agreement with Tsai [7].

DSC analysis was carried out for all the samples glass temperatures (T_g) was only obtained for R4 resin at 156 °C. The other samples did not show any thermal transition in the range studied as is seen in Figure 2B.

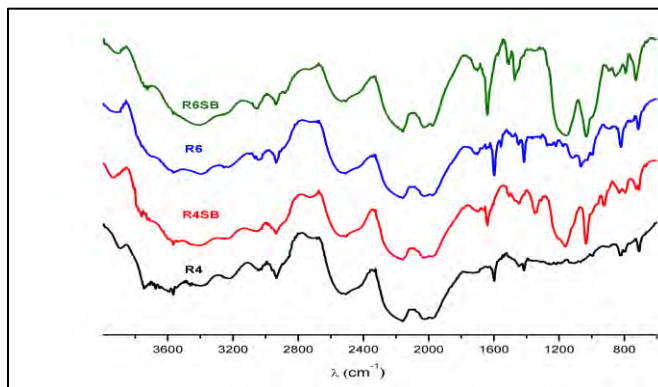


Figure 1. FTIR spectra for precursor resins (R4- R6) and sulfobetaine resins (R4SB - R6SB)

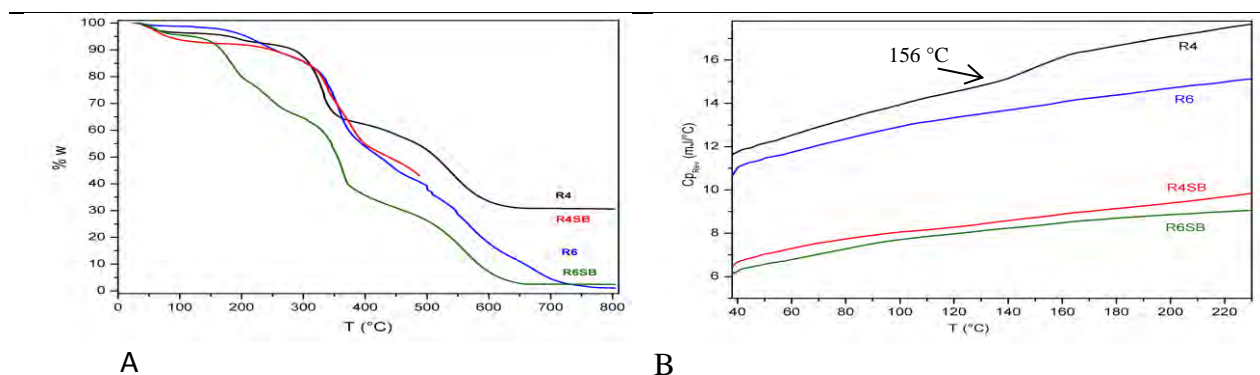


Figure 2. Thermograms obtained by TGA for precursor resins (R4 and R6) and sulfobetaine resins (R4SB and R6SB)

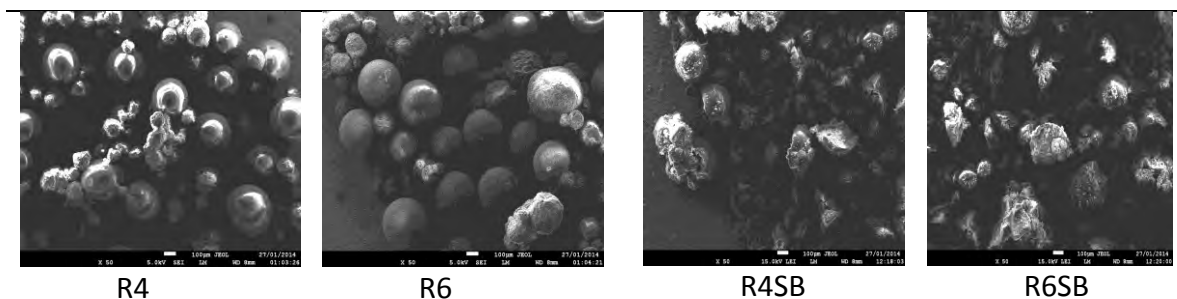


Figure 3. SEM images for precursor and functionalized resins.

Figure 3 exhibits the SEM images for precursor resins R4(A), R6 (B) which had mainly spherical shape with a diameter of 250-300 μm . When the resins were functionalized, the shape of the resins was destroyed as is shown for R4SB (C) and R6SB (D).

Evaluation of Cr (VI). To evaluate the capacity of ion exchange resin experiments were carried out in batch, in order to study the ionic exchange of Cr (VI). For this, it was necessary to prepare

K₂CrO₇ solutions at different concentrations. The chromium was determined by the colorimetric method of diphenylcarbazide. This method is based on a reaction of oxide reduction where the Cr (VI) reacts with 1, 5-diphenylcarbazide in an acid medium to give Cr (III) and 1,5-diphenylcarbazone which displayed a violet color that is read with the spectrophotometer at 540 nm. The calibration curve to evaluate the Cr (VI) was obtained according to Mexican standards [8] (see Figure 4). In order to know the maximum capacity of polymer adsorption proceeded to perform the Langmuir isotherm, according to the plot $\frac{1}{C_s}$ vs $\frac{1}{C_m}$, where C_s , is the chromium adsorbed mass (mg Cr/g resin) and, C_m , is the chromium concentration in the liquid phase (ppm Cr). K , is the equilibrium constant for adsorption and, b chromium adsorption maximum capacity.

$$\frac{1}{C_s} = \frac{1}{bK} \frac{1}{C_m} + \frac{1}{b}.$$

The results are presented in Figure 5 and the capacity to absorb Cr(VI) is summarized in Table 2.

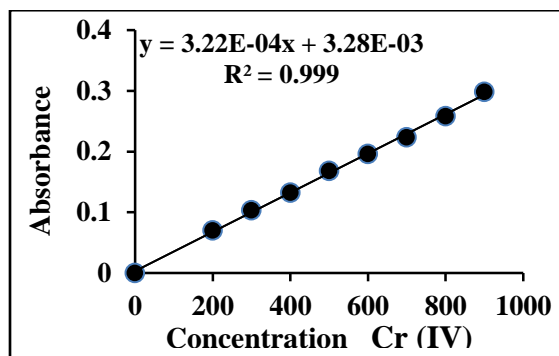


Figure 4. Calibration curve to evaluate the Cr (VI)

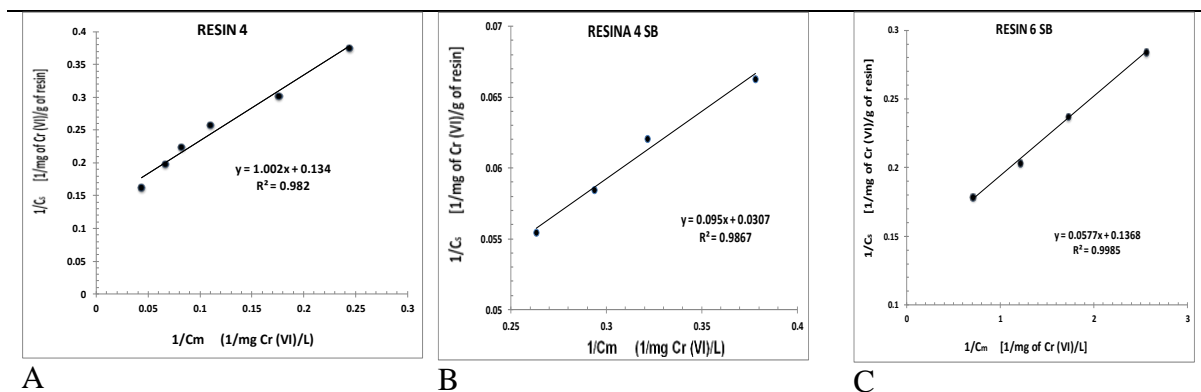


Figure 5. In order to know the maximum capacity of polymer adsorption proceeded to perform the Langmuir, isotherm. A) resin no functionalized, B) and C) functionalized.

Table 2. Determination of the maximum capacity of resin adsorption

Resin	slope	Y intercept	R2	K [L/mg Cr(VI)]	b [mg Cr(VI)/g resin]
R4	1.002	0.134	0.982	0.134	7.46
R4SB	0.095	0.0307	0.987	0.323	32.6
R6 SB	0.0577	0.1368	0.998	2.37	7.31

Column method. Additionally, continuous experiments were also performed; feed stream consisted in 80 ppm of a $K_2Cr_2O_7$ solution (pH 6.0) dosed by means of a peristaltic pump with a flow rate equal to 1.88 ± 0.07 g min⁻¹. The results in figure 6 show the Cr (VI) adsorption rate of the functionalized resin R4SB. The chromium rate of adsorption decreases rapidly during the first ten minutes, then becomes almost constant and, it goes asymptotic to zero. The sorption capability of the R4SB resin is shown in Figure 7. During the first ten minutes, the sorption capability increases steeply with time until saturation for times longer than 120 minutes.

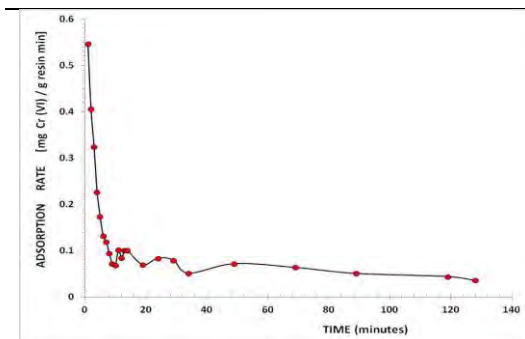


Figure 6. Cr(VI) adsorption rate in the fixed-bed column for the R4SB resin (pH=6.0, at RT).

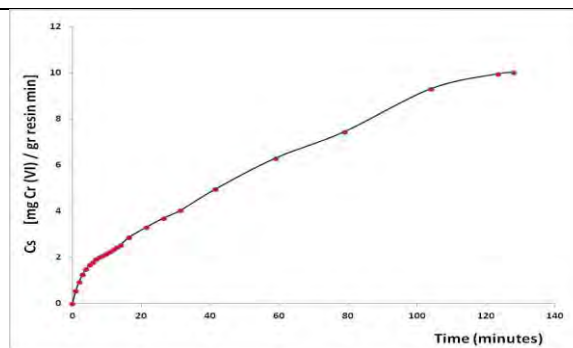


Figure 7. Adsorption time and adsorbed amount Cr (VI) with resin R4SB fixed-bed column (pH=6.0, at RT).

Conclusions

Two different precursor resins were obtained from 4-vinylpyridine and DVB with toluene/heptane as porogens. They were functionalized with 1,3-propanesultone. The morphology of precursor resin had an almost spherical shape but the functionalization destroyed it. Using the adsorption isotherm results, they showed that sulfobetaine groups are efficient in the elimination of Cr (VI).

Acknowledgements

The authors are thankful for the support from CONACYT through the project No. 220232 Investigación Científica Básica 2013-2014

References

- 1] F- I. Khan, T. Husain, R. Hejazi. J. Environmental Management 71, 95–122 (2004).
- [2] S.K. Auki, R.D Neufeld, Chemical Technology. Byotechnology, 80,892 (2005)
- [3] F. Fu, Q. Wang. Journal of Environmental Management, 407–418. (2011)
- [4] S.T. Senevirathna, S. Tanaka, S. Fujii, C. Kunacheva, H. Harada, B.R. Shivakoti, R. Okamoto. Chemosphere. 80, 647–651 (2010).
- [5] J. Ortiz-Palacios, J. Cardoso, O. Manero. J. Appl Polym Sci, 107 (2008) 3644–3653,
- [6] J. Cardoso, J. Ortiz-Palacios, O. Manero, J. Appl Polym Sci.107, (2008)3644–3653,
- [7] H. S. Tsai, Y. Z. Wang, J. J. Lin, W. F. Lien. J. Appl Polym Sci. . 116, 1686–1693 (2010)
- [8] NMX-AA-044-SCFI-2001. Análisis de aguas. Determinación de cromo hexavalente en aguas naturales, potables y residuales tratadas

SYNTHESIS OF POLYMERIC MICROCAPSULES FOR COATINGS APPLICATIONS

A. Ortega Carrizo,¹ M. E. Velázquez Sánchez,¹ J. P. Acosta Ramírez,¹ and I. Sáenz de Buruaga Yurramendi¹

¹ *Centro de Investigación en Polímeros, S. A. de C. V.*

Abstract

In this work, a route for synthesizing polymeric capsules containing hydrophobic core is presented. The capsules were made using in-situ polymerization. With this technique it is possible to obtain capsules with thermally stable shells. Different variables were studied as: the pre-polymer addition rate, the shell polymer composition, the core-shell ratio, the number of layers forming the capsule wall and the electrolyte used. The capsules morphology was followed by optic and electronic microscopy, and their thermal stability was determined by TGA. Finally, some optimized prototypes were obtained and their performance in coatings was studied for different applications as anti-corrosion or energy saving materials; some examples are given.

Introduction

Microencapsulation is an interesting technology, because it has a wide range of applications in architectural, industrial and marine coatings, usually this technology is used as an additive in a coating, and it can impart different type of properties such as: thermal isolation, self-healing, anti-corrosion, anti-fouling, intumescence, insect repellency, controlled release of volatile materials, etc., depending on the composition of the core shell microcapsule. In this paper microcapsules that can be use in architectural and industrial coatings were made using in situ-polymerization, the focus was to obtain capsules with thermally stable shells. From all the different microencapsulation techniques tested: simple coacervation, complex coacervation, interfacial polymerization and in situ polymerization, it was this last technique the one that gave the best results in thermal resistance for the microcapsules shell.

It is possible to prepare microcapsules via in situ polymerization using as materials for the shell resorcinol-formaldehyde, [1] urea-formaldehyde [2] and melamine formaldehyde, [3] the choice of the shell materials will depend on the characteristics of the substance to encapsulate (core). It is almost impossible to affirm beforehand, which is the best shell for a given core, experimentation is required to find the best conditions to optimize a process every time that the core is changed. In this paper it will be presented the experimental variables that affect microcapsules thermal stability and morphology. Some possible applications for the developed prototypes will be mentioned.

Experimental

The microcapsules shell was made using a homemade pre-polymer melamine-formaldehyde, prepared with Aldrich melamine (99%) and industrial grade formaldehyde solution (36%). Different hydrophobic cores were used, such as fatty alcohols and a blend containing anticorrosion materials. To stabilize the emulsion a series of commercial polyelectrolytes (hydrophobic and poly acid) and homemade hydrophobic and hydrophilic copolymers were used; in all cases also a commercial surfactant NP (EO) was added. The experimental variables explored in the synthesis were: the shell polymer composition, pre-polymer addition rate, the core-shell ratio, the number of

layers forming the capsule wall and the electrolyte used. Microcapsules morphology was followed by optic microscopy (OM) and SEM and their thermal resistance by TGA.

Results and Discussion

Shell polymer composition.

Melamine can accept from 3 to 6 formaldehyde molecules to form a methylol melamine compound under basic conditions. It was observed that when a melamine formaldehyde ratio 1:5 is used, precipitation of the pre-polymer takes place, and then lower ratios should be used.

Effect of pre-polymer addition rate.

To have a better control of the capsule wall conformation and the morphology it is necessary to control the pre-polymer addition rate, in this work rates from 0.5 to 3 mL/min were tested, in Figure 1, the microcapsules obtained with the lowest and highest rates are shown. Higher addition rates give as a result microcapsules with a better shell conformation; therefore a better thermal resistance, as it is shown in the TGA results in Figure 1.

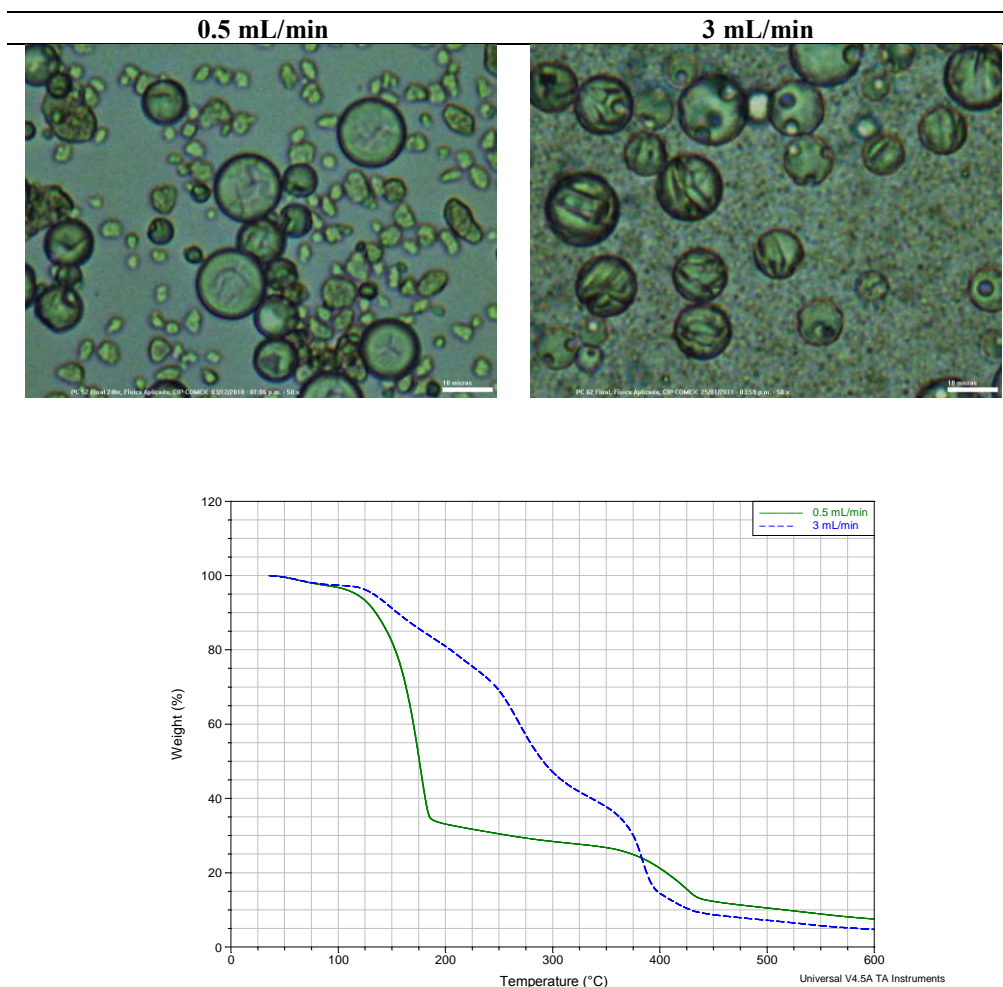


Figure 1. Different pre-polymer addition rates, morphology and thermal stability.

Effect of core shell ratio and number of layers forming the microcapsule wall.

Another variable that affect the shell formation and its thermal stability is the core-shell ratio and the number of layers added to form the microcapsule wall. In Figure 2, microcapsules obtained using core-shell ratios of 1:0.5 and 1:0.75, added in one step (1 layer) and in two steps (2 layers), respectively, are shown. There is not any advantage in making the process in two steps, even the TGA and OM results suggest that a better thermal stability is obtained for the capsules made in a one step process.

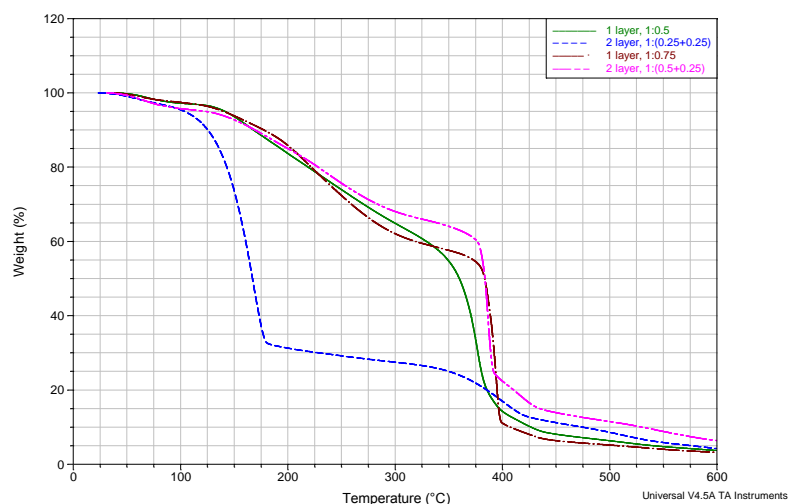
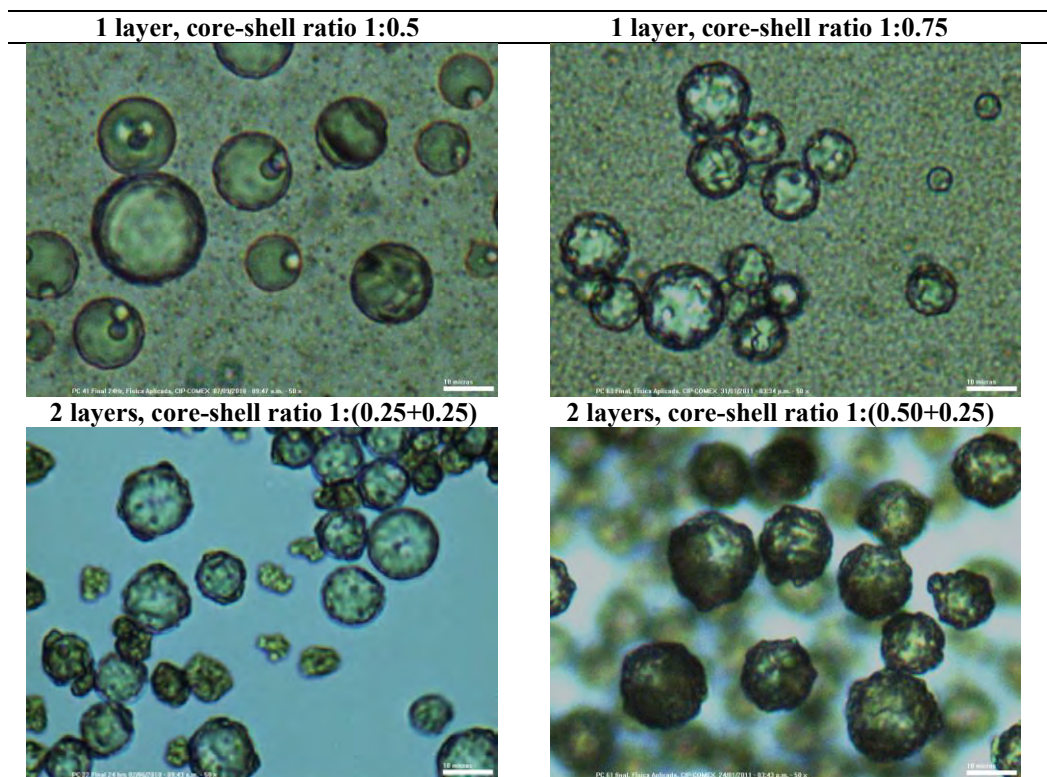


Figure 2. Core-shell ratio and number of layers forming the capsule wall.

Effect of poly electrolyte type.

The microcapsules morphology is very sensitive to the type of poly electrolyte used, see Figure 3, the best result in terms of thermal stability, agglomeration and polydispersity was obtained with the hydrophobic copolymer made at CIP, followed by the ones synthesized with the commercial hydrophobic copolymer. The microcapsules synthesized with the hydrophilic copolymer and the poly acid had very weak walls.

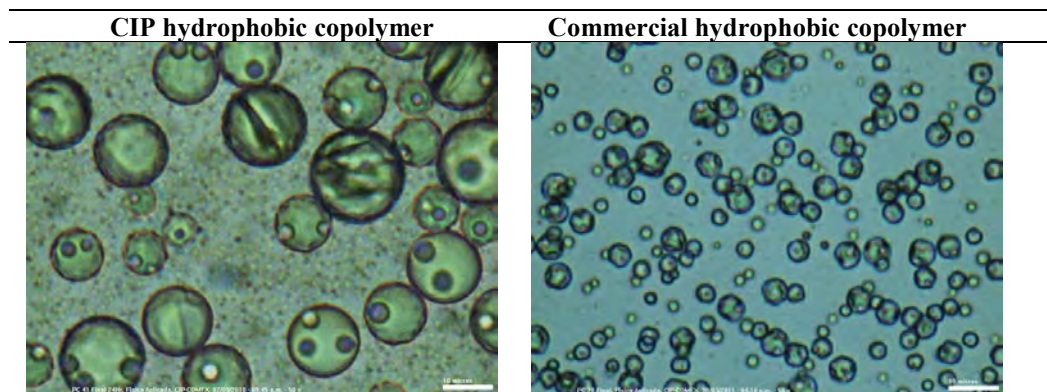


Figure 3. Effect of poly electrolyte on microcapsules morphology and thermal resistance.

The fatty alcohol core microcapsules have been used for energy saving coatings application in wallboards, [4] to get an insulator effect of these materials they must be used in high concentrations and in a thick coating. It must be mentioned that the release mechanism of the core in the microcapsules synthesized is mechanical; this means that it is necessary to apply a mechanical stress to break the microcapsules wall.

The results previously shown correspond to the encapsulation of a fatty alcohol; but also a blend containing anticorrosion materials was encapsulated using the same in situ polymerization process, the results obtained for this last type of microcapsules is shown in Figure 4. These microcapsules presented also a good thermal stability, as shown in the TGA profile, Figure 5. Prototypes of these microcapsules were added to a solvent and to a water based industrial coating, they were very stable in both systems, they did not break during the airless application on metal, but their anti-corrosion performance was not very good, because after the coating exposure in a salt spray chamber there was no difference detected between the let downs containing microcapsules, compared to the standard with no microcapsules inside.

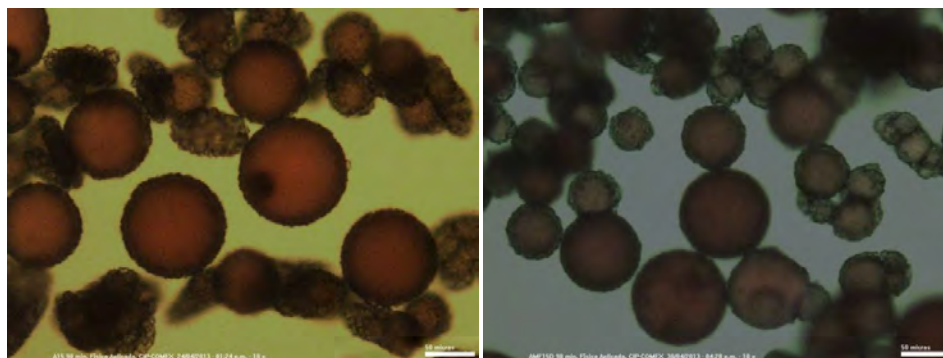


Figure 4. Morphology of microcapsules with anti-corrosion core.

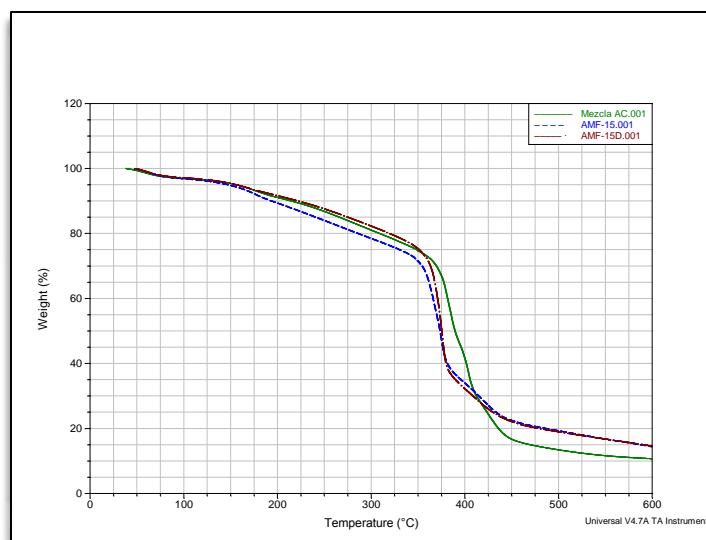


Figure 5. Thermal profiles of microcapsules with anti-corrosion core.

Conclusions

It was shown the effect that the pre-polymer addition rate, the shell polymer composition, the core-shell ratio, the number of layers forming the capsule wall and the electrolyte used; have on the morphology and thermal stability of microcapsules.

It was shown that in situ polymerization can be used to encapsulate a hydrophobic core, preferably using a hydrophobic poly electrolyte.

It was shown that the process used for preparing these microcapsules could be extended to encapsulate other type of hydrophobic materials, but always it will be necessary to play with the variables discussed in this paper.

A brief discussion on two potential applications of these materials was made, one is for saving energy applications and the other, that must be still improved, is for anti-corrosion applications.

Acknowledgements

We want to acknowledge to Centro de Investigación en Polímeros, a member of Comex Group, for the economical support of this project, to Prof. C. Thies for his contributions to the microencapsulation of anticorrosion materials, to Rosalinda Cruz for her participation in the synthesis of these materials and to Fernando Zaldo and Juan Luis Camacho for their guidance.

References

- [1] R. L. Hart et al. U. S. Patent 3,755,190 (1973).
- [2] S. Sarangapani et al. U. S. Patent 7,192,993 B1, (2007).
- [3] J. F. Su et al. Journal of Applied Polymer Science, 101, 1522–1528 (2006).
- [4] S. H. Lee, et al. Korean J. Chem. Eng., 28 (11), 2206-2210 (2011).

SYNTHESIS OF CIS-1,4 POLY(BUTADIENE) IN SOLUTION WITH STYRENE AND THEIR USE AS PRECURSOR RUBBER IN HIGH IMPACT POLYSTYRENE BY “IN SITU BULK” POLYMERIZATION PROCESS

G. Bosques Ibarra, F. Soriano Corral, F. J. Enríquez, R. E. Díaz de León and J. F. Hernández Gámez

*Centro de Investigación en Química Aplicada, Blvd. Enrique Reyna 140, C.P. 25294, Saltillo, México. *ramon.diazdeleon @ciqa.edu.mx*

Abstract

In a first step, cis-1,4-poly(butadiene) (cis-1,4-PB) was synthesized through a ternary catalytic system (neodymium versate/diisobutylaluminum hydride/ethylaluminum sesquichloride) and styrene as solvent. Different molar ratios of Al/Nd and Cl/Nd were evaluated to establish the optimal reaction conditions to produce high cis-1,4-PB with a small polystyrene content. Cis-1,4 microstructure was higher than 94% for all cases, meanwhile the polystyrene content in the rubber was approximately 10%, both percentages were calculated by nuclear magnetic resonance. In a second step, the styrene in the resulting solutions (rubber + styrene) was polymerized by the free radical polymerization technique to produce high impact polystyrene by the "in situ bulk" polymerization, adding an organic peroxide as initiator and pellets of polystyrene in some samples. The obtained results are discussed in terms of morphology and mechanical properties.

Introduction

The reinforcing of thermoplastic materials using a rubber as the toughening agent is one of the most used techniques in the industry for improve mechanical properties in frail plastics [1]. An example of these materials is the high-impact polystyrene (HIPS), which present a broad field of applications due to its combination of high stiffness with a good toughness [2]. HIPS is a heterogeneous material composed for a continuous phase of polystyrene (PS) homopolymer and a dispersed rubber phase. According to the literature reports, the toughness is related with the particle diameter (Dp) and the morphology of the rubber phase, which can be modified by the rubber type employed [3].

The precursor, commonly used, in the synthesis of HIPS is the poly(butadiene) (PB) or copolymers styrene-co-butadiene (SBR) [4]. PB can be obtained through the coordination polymerization using Neodymium-based Ziegler-Natta catalysts [5], resulting in PB with high cis-1,4 units (~98%).

The catalyst systems are classified in binary and ternary [6], where the latter is conformed by a catalyst type carboxylate (NdOCOR), a co-catalyst (AlR₃) and a halogenated compound (Al₂Et₃Cl₃). The polymerization of 1,3-butadiene using a catalyst based ternary neodymium consists in four stages: i) activation of the catalyst system (the catalyst is activated by means of alkylation and halogenation, producing different active species); ii) initiation (the active species are coordinated by bidentate mode with the 1,3 butadiene, which via a bond change is inserted at coordination complex); iii) propagation and iv) termination [7].

There are several factors related to the catalyst system that affect the final microstructure of PB, these factors are: the Al/Nd and Cl/Nd ratios, time and aging temperature, order of addition and the nature of the solvent used [8].

In this work it is reported the selective polymerizations of 1,3-butadiene using the neodymium versate/diisobutylaluminum hydride/ethylaluminum sesquichloride as catalyst system and styrene as solvent. After that, the resulting products (PB + styrene) were polymerized by a free radical process to produce different grades of HIPS.

Experimental

Catalyst system. The synthesis recipes are shown in Table I. All reactants were previously purified and the aging process (Nd activation) was prepared at 25°C with continuous stirring.

Synthesis and characterization of cis-1,4-PB. In a 1L stainless reactor, provided of a duplex turbine stirring system, the butadiene monomer and the styrene were added. When the temperature fixed 60°C the catalyst system (previously aged) was incorporated and the polymerization was followed for 3.5 hours. The PB microstructure was determined by ^1H and ^{13}C NMR techniques, the molecular weight distribution (MWD) was determined by size exclusion chromatography (SEC), finally, the glass transition temperature (T_g) was calculated by differential scanning calorimetry (DSC). Two PB samples with a high cis-1,4 content and different molecular weights were selected to produce the HIPS type materials.

Table 1. Catalyst systems conditions

PB	Addition Order	Aging time (min)	Molar ratio	
			Al/Nd	Cl/Nd
PB ₁	DIBAH/ NdV/EASC	9	30	0.625
PB ₂	EASC/ NdV/DIBAH	3	30	0.625
PB ₃	DIBAH/ NdV/EASC	3	30	0.625
PB ₄	EASC/NdV/ IBAH	9	30	0.625
PB ₅	DIBAH/NdV/EASC	3	20	0.625
PB ₆	EASC/NdV/DIBAH	3	20	0.625
PB ₇	DIBAH/NdV/EASC	3	30	0.445
PB ₈	EASC/NdV/DIBAH	3	30	0.445

Synthesis and characterization of HIPS. Adding benzoyl peroxide (BPO) to the obtained rubber/styrene solution, the styrene monomer was polymerized under free radical polymerization conditions [9]. A small amount of polystyrene homopolymer was added in some reactions at the beginning of the heating as modifiers of the morphology. Resulting materials were characterized in function of the gel content (GC), grafting degree (GD), impact strength (IS), Young's modulus (E'), melt flow index (MFI) and morphology.

Results

Synthesis of cis-1,4-PB

Table 2 shows the characterization results corresponding to the several PB synthesized following the different catalyst systems reported.

Table 2. Characterization of PB synthesized from different catalyst system conditions

Recipe	Conversion (%)	Microstructure		Molecular Weighth		\bar{D}	T_g (°C)
		Cis (%)	PS (%)	Mn (g/mol)	Mw (g/mol)		
PB ₁	94	94	9	38,000	166,000	4.3	-103
PB ₂	73	94	11	27,000	230,000	8.4	-104
PB ₃	88	94	9	40,000	194,000	4.7	-102
PB ₄	91	96	10	37,000	150,000	4.2	-104
PB ₅	84	96	9	88,000	360,000	4.0	-104
PB ₆	81	96	14	86,000	480,000	5.6	-105
PB ₇	80	96	9	53,000	240,000	4.5	-103
PB ₈	81	96	10	63,000	240,000	3.9	-101

The highest content of *cis*-1,4 units (~96%) was calculated by the PB₄-PB₈. There is an interaction of the styrene aromatic ring and the vinyl bond with the coordination site, and this fact provokes a slightly decrease in the butadiene conversion and also a small amount of styrene randomly polymerized in the PB chains. The polystyrene content in the PB chains was around 9-10% for the DIBAH/NdV₃/EASC addition order, while for the EASC/NdV₃/DIBAH addition order it was calculated around 14%. The order of addition EASC/NdV₃/DIBAH resulted in the formation of a heterogeneous system with a low catalytic activity promoting a decrease in the conversion values (see Figure 1), also observing an increase in the PS content. The conversion below 90% for all reactions was attributed to the fact of using styrene as the solvent, justified because aromatic solvents compete with the monomer by the coordination reactions inhibiting in a certain way the polymerization and decreasing the catalyst activity [10].

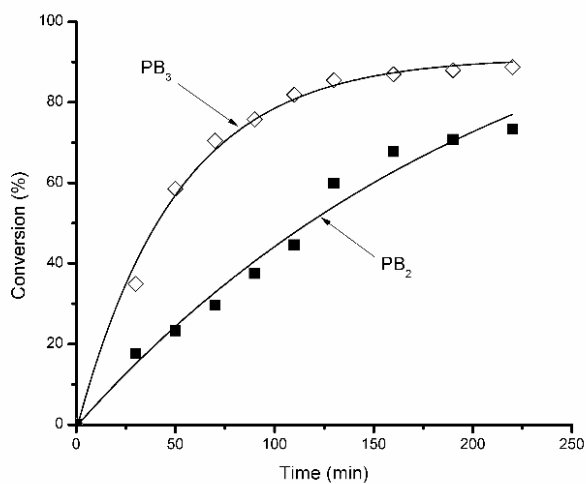


Figure 1. Conversion evolution by using different order of addition DIBAH/NdV₃/EASC (PB₃) and EASC/NdV₃/DIBAH (PB₂) catalyst systems

For the PB synthesized with the molar ratios Al/Nd=30 and Cl/Nd=0.625 (PB₁-PB₄), a high conversion was obtained, due mainly to the high ratios of Al and Cl utilized, which originates an increment of active species. Contrarily, the lower molar ratios such as Al/Nd=20 (PB₅ and PB₆) and Cl/Nd=0.445 (PB₇ and PB₈) originated a slightly decrement on conversion evaluation (See Figure 2).

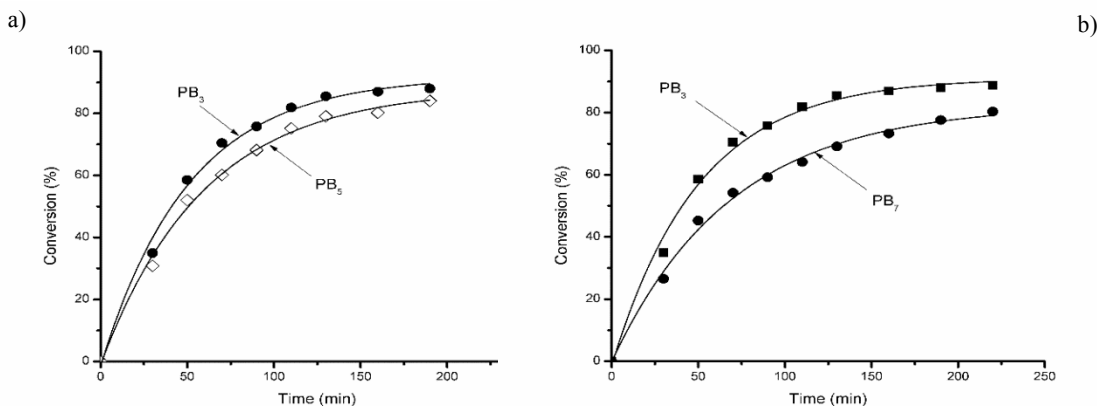


Figure 2. Effect of (a) Al/Nd ratio on the conversion for PB₃ and PB₅, and (b) Cl/Nd ratio on the conversion for PB₃ and PB₇

The molecular weight distributions (MWD) was influenced by the Al/Nd ratio, according to Friebe *et al*, the co-catalysts acts as alkylating agent and at certain concentrations acts as chain transfer agent. At highest Al concentrations more alkylated species are produced, increasing the number of polymeric chains and decreasing the molecular weight (such in PB₁-PB₄). Low Al/Nd ratios results in high molecular weights. According to Quirk [11], the Cl/Nd ratio affects the nature of the active sites. It has been reported the presence of two active sites, from the beginning of the reaction. One site has a short life-time, and its growth occurs on the surface of the catalyst particles. The other site has a slower chain propagation of “quasi-living” manner. Evidence for the formation of these two active sites is shown in the Figure 3, where a bimodal SEC plot can be observed for the PB₇, meanwhile PB₁ presents a monomodal plot.

According to the literature reports, the higher stereo-regularity promotes a displacement of the T_g toward lower temperatures (~ 105 °C) [12]. The T_g of several PB obtained is influenced by the content of cis-1,4 units and also by the polystyrene content, it was found at -104 °C, approximately.

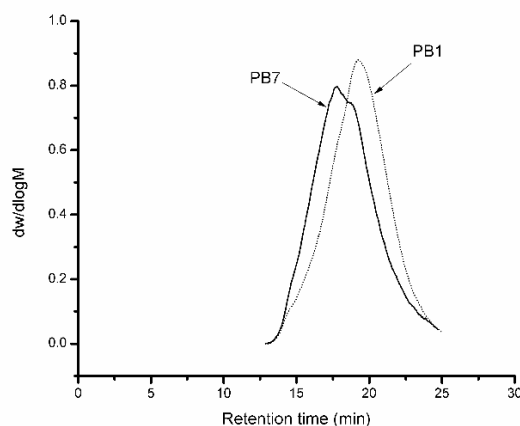


Figure 3. Molecular weight distributions for PB₁ and PB₇

Synthesis of HIPS

In all cases, small values in GC and GD were observed, this behavior can be attributed to the poor ability of these PB to generate grafts (due to the high content of the cis-1,4 structure) and thus diminishes the possibility to be crosslinked. A slight decrease of molecular weights on HIPS synthesized with a 5 wt-% of polystyrene at the beginning of the polymerization was observed (HIPS 2 and HIPS 4) and it is justified because the utilized polystyrene was of low molecular weight ($M_n = 66,000$ g/mol), which is considerably less than that generated in the PS matrix.

Figure 4 shows the micrographs of HIPS 1 and HIPS 3 synthesized in absence of initial polystyrene and they show core-shell and lamellar type morphologies. The increase in the particle diameter of HIPS 1 in relation with HIPS 3 is due to the decrease in the viscosities ratio of the phases ($\eta_{St-PS}/\eta_{St-PB}$), which strongly depends on the molecular weight of the corresponding PB [3]. Thus, if the molecular weight of the PB increases the $\eta_{St-PS}/\eta_{St-PB}$ diminishes and the average particle diameter increases.

The micrographs corresponding to the reinforced HIPS 2 and HIPS 4 (containing 5 % of polystyrene from the beginning of the reaction) are shown in Figure 5. Morphologies core-shell and labyrinth type are observed. The change in the morphology of these HIPS samples in comparison with those showed in Figure 4 was associated to the inclusion of polystyrene from the start of the polymerization, decreasing the viscosity ratio and increasing in the particle diameter.

Respect to the mechanical properties, for all cases it was observed that as the particle size increases the impact strength also increased. Moreover, the Young's modulus (E) is greater in cases where polystyrene is added initially (HIPS 2 and HIPS4), this fact was attributed to a good dispersion of small particles. The MFI was higher for HIPS 2 and HIPS 4, due also to the initial addition of polystyrene.

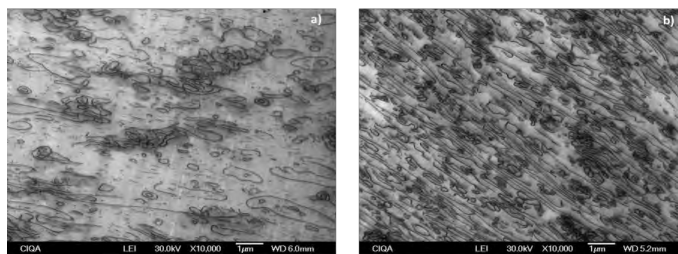


Figure 4. (a) HIPS 1 (PB Mw=138,000 g/mol): GD=69.1; GC=10.5 (%); IS=17 (J/m); E=654.3 (MPa); MFI=10.68 (g/10min). (b) HIPS 3 (PB Mw=250,000 g/mol): GD=72.85; GC=11.8 (%); IS=20 (J/mol); E=588.3 (MPa); MFI=6.74 (g/10min).

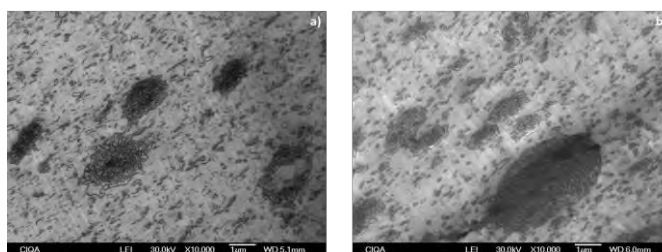


Figure 5. (a) HIPS 2 (PB Mw=138,000 g/mol): GD=64.8; GC=11.4 (%); IS=11 (J/m); E=764.5 (MPa); MFI=20.33 (g/10min). (b) HIPS 4 (PB Mw=250,000 g/mol): GD=81.8; GC=12.3 (%); IS=38 (J/mol); E=625.2 (MPa); MFI=21.17 (g/10min).

Conclusions

PB with a high content of *cis*-1,4 units (96%) was successfully synthesized from 1,3-butadiene in the presence of styrene as solvent using the ternary catalyst system DIBAH/NdV₃/EASC. PB samples with different characteristics were obtained by varying the preparation conditions of the catalyst system. It was possible to produce HIPS through the "in situ bulk polymerization" method, starting from homogeneous HIPS and heterogeneous solutions, using high *cis* PB of low and high molecular weights with a concentration by weight of 7 %, and adding 5% by weight of polystyrene homopolymer in two cases.

Acknowledges

The authors thank to CONACYT for the financial support through the project 156366. They also thank to Ricardo Mendoza, Marcelina Sánchez, Ángel Sánchez, Jesús Cepeda, Guadalupe Méndez, Uriel Peña and Francisco Zendejo for their technical support.

References

- [1] J. P. Dear, Journal of Materials Science, 38, 891 (2003).
- [2] F. Haaf, H. Breuer, A. Echte, B. J. Schmitt, Journal of Scientific and Industrial Reserch, 659 (1981).
- [3] M. Baer, Journal of Applied Polymer Science, 16, 1109 (1972).
- [4] I. Hattori, K. Yasuda, M. Sakakibara, Polymer Advanced Technology, 4, 450 (1993).
- [5] L. Friebe, O. Nuyken, W. Obrecht, Advanced Polymer Science, 1, 154 (2006).
- [6] Y. B. Monakov, N. G. Marina, Z. M. Sabirov, Polymer Science, 10, 1404 (1994).
- [7] N. M. T. Pires, A. A. Ferreira, C. H. Lira, P. L. A. Coutinho, L. F. Nicolini, B. G. Soares, F. M. B. Coutinho, Journal of Applied Polymer Science, 99, 88 (2006).
- [8] L. I. Mello, M. F. B. Coutinho, G. B. Soares, Quim. Nova, 27, 277 (2004).
- [9] H. Yanming, J. Zhongming, L. Yang, C. Li, W. Yurong, Mat. Sci. and Eng, 528, 6667 (2011).
- [10] L. Friebe, J. M. Muller, O. Nuyken, W. Obrecht, J. of Macromol. Sci. Part A: 43, 841 (2006).
- [11] R. P. Quirk, R. P. Kells, K. Yunlu, J. P. Cuif, Polymer, 41, 5903 (2000).
- [12] R. Díaz de León, M. T. Alonso, F. J. Enríquez, J. Díaz, O. Pérez. A. Romo, R. I. Narro, A. Castañeda, Macromol Sym, 325-326, 194 (2003).

POLYMERIZATION OF 1,3 BUTADIENE IN PRESENCE OF STYRENE USING NEODYMIUM VERSATATE CATALYST AND SYNTHESIS OF ABS BY “*IN SITU* BULK” PROCESS

P. A. de León Martínez, F. Soriano Corral, R. E. Díaz de León Gómez, F. J. Enríquez Medrano and J. F. Hernández Gámez

*Centro de Investigación en Química Aplicada, Blvd. Enrique Reyna 140, C.P. 25294, Saltillo, México.*florentino.soriano@ciqa.edu.mx*

Abstract

1,3-butadiene was selectively polymerized in presence of styrene as solvent using a ternary catalyst system constituted by: neodymium versatate/diisobutylaluminium hydride/ethylaluminium sesquichloride (NdV/DIBAH/EASC). Different molar ratios Al/Nd and Cl/Nd were studied, as well as the styrene concentration, the aging time of the catalyst system and the addition order of the reactants. High butadiene conversions were achieved resulting in polybutadienes with a high content of the *cis*-1,4 isomer (> 95%, calculated by NMR). Styrene polymerized in low proportion reaching a maximum of 15 %-wt in the obtained rubbers (polybutadiene-*co*-polystyrene). After that, an appropriate amount of acrylonitrile was added to the reaction medium (rubber/styrene) and the polymerization reactions were carried out by an *in situ* bulk free radicals process to produce poly(acrylonitrile-butadiene-styrene) (ABS) resins which were properly characterized.

Introduction

Styrenic resins reinforced with rubbers such as the poly(acrylonitrile-butadiene-styrene) (ABS) have been widely used in several applications due to their excellent mechanical properties, high thermal stability, high chemical resistance and good processability [1,2]. The ABS is constituted of an elastomeric phase, generally a grafted and cross-linked polybutadiene (PB) dispersed in a poly(styrene-*co*-acrylonitrile) (SAN) matrix. The presence of grafted SAN segments in the PB chains allows a better interaction with the SAN matrix, which produces an ABS with high impact properties [3]. In recent years the *in situ* polymerization of high impact styrenic resins by a single stage process (*In Situ* bulk) has taken great interest [4]. The "*In Situ* Bulk" process consists essentially in the selective polymerization of butadiene (Bt), using styrene (St) as solvent. This selective polymerization can be carried out using a Neodymium-based Ziegler-Natta ternary catalyst [1], leading to a high-*cis*-PB/St solution as resulting product. Subsequently, acrylonitrile monomer (AN) can be incorporated into the high-*cis*-PB/St solution and through a free radical polymerization of both monomers the ABS is obtained. There are some factors related to the catalyst system that can affect the characteristics of the final PB, these parameters are: a) the Al/Nd and Cl/Nd molar ratios, b) the addition order, c) the type of solvent, d) the temperature, e) the aging time of the catalyst system, among others [1,5-6]. The PB microstructure affects directly to the ABS impact properties.

In this work it is reported the selective polymerizations of 1,3-butadiene using the neodymium versatate/diisobutylaluminium hydride/ethylaluminium sesquicloride as catalyst system and styrene as solvent. After that, acrylonitrile was added to the resulting reaction product (PB/St) and the new solution was polymerized by a free radical process to produce different grades of ABS type resins.

Experimental

Catalyst System. The synthesis strategies (addition order, aging time and molar ratios) are shown in Table 1. The reactants used were previously purified and all the catalyst systems were prepared at 25°C with a continuous stirring.

Synthesis and Characterization of *cis*-1,4-PB. The monomer of St was added into a Parr stainless steel

reactor of 1L of capacity provided of an agitator turbine type. Then, the temperature was increased to 50°C and the 1,3-butadiene was added, when the temperature reached the 60°C, the catalytic system was incorporated and the polymerization was carried out during 3.5 hours. Resulting PB were characterized; microstructure was evaluated by ^1H and ^{13}C NMR, the molecular weight distribution was determined by size exclusion chromatography (SEC) and the glass transition temperature (T_g) was determined by DSC.

Table 1. Reaction conditions of butadiene polymerizations

Recipe	[Al] mol*10 ⁻⁴	[Nd] mol*10 ⁻⁴	[Cl] mol*10 ⁻⁴	[St] g	Addition order
R1	60	2	1.25	272.7	St+Bt+Al+Nd+Cl
R2	40	2	1.25	272.7	St+Bt+Al+Nd+Cl
R3	40	2	1.25	181.8	St+Bt+Al+Nd+Cl
R4	40	2	1.25	181.8	St+Bt+CSA
R5	40	2	0.95	181.8	St+Bt+Al+Nd+Cl
R6	40	2	1.25	181.8	St+Al+Nd+Cl+Bt

CSA=catalyst system aged

ABS synthesis by the “In Situ Bulk” process. To describe the reaction to produce the ABS type resins the St/PB solution R6 (Table 1) was selected. In the solution St/PB the monomer of AN was added in a St/AN azeotropic ratio of 3.4/1 and resulting in a new solution of St/AN/PB with St=71.3, AN=20.7 and PB=8 wt-%. Some additives were incorporated, such as the free radical initiation system consisted of Luperox 256 at 0.022 wt-% and 0.11 wt-% of ter-dodecanediol (TDD) used as chain transfer agent (CTA). Additionally, 5 pphr of mineral oil were added. The polymerization of St and AN was carried out at a stirring speed of 60 rpm and a temperature of 90 °C. When the conversion fraction reached a 0.25 value (at this conversion values the morphology was already established) 0.1 wt-% of tert-butyl perbenzoate (TBPB) as radical initiator was added and mixed by 4 min. This reaction mass was transferred to glass tubes to continue the polymerization by 15 h at 150 °C. The final ABS was characterized in function of gel content (GC), grafting degree (GD), impact strength (IS), Young’s modulus (E’), melt flow index (MFI) and morphology.

Results

Synthesis of *cis*-1,4-PB. The co-catalyst (Al) and the halide (Cl) concentrations, as well as the order of addition and the aging time affect the reaction kinetics, the microstructure and the molecular weight distribution.

Table 2. Results of butadiene polymerizations

Recipe	Conversion (%)	<i>cis</i> -1,4 (%)	Mn (g/mol)	Mw (g/mol)	Đ
R1	66.38	96.15	38000	217000	5.7
R2	83.26	95.82	60000	250000	4.1
R3	88.53	96.45	18000	141000	6.5
R4	76.82	96.29	116000	357000	3.0
R5	83.93	96.22	58000	192000	3.3
R6	92.44	96.40	173000	496000	2.8

To establish the effect of the Al/Nd ratio R1 (Al/Nd=30) and R2 (Al/Nd=20) were compared. Figure 1 shows an increase in the conversion at the initial stages of the polymerization, which is expected, however, after one hour of reaction, the behavior changes, the polymerization rate for the system with higher amount of alkyl aluminum (R1) tends to be lower gradually until the end of the reaction. This behavior indicates the presence of active species with lower catalytic activity, which might be formed for about 60 minutes of

reaction. The active species are generated throughout the reaction depending on the alkylation degree and chlorination reached.

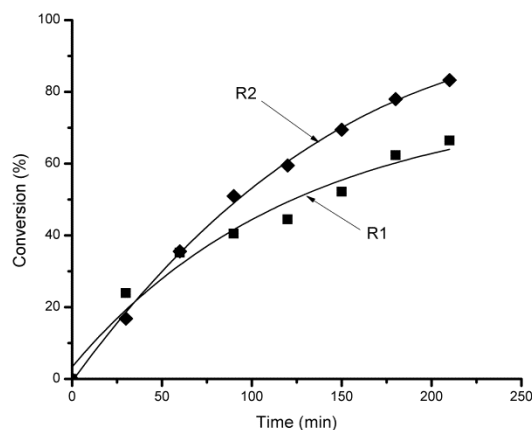


Figure 1. Conversion evolution as a function of polymerization time for R1 and R2

Figure 2a shows the comparison between R3 and R5 with Nd/Cl ratios of 1.6 and 2.1, respectively. In R5 a lower monomer conversion is observed, and this is explained due to a reduction in the number of active sites as a consequence of a lower Nd/Cl ratio (insufficient chlorination) [7]. Therefore, the higher Nd/Cl ratio (R3) provokes a higher conversion. Figure 2b shows the effect of aging the catalyst system (R4), in this reaction the catalyst system was aged for 9 minutes at 30 °C and conversion results are compared with those of reaction R3. A lower conversion observed in R4 suggests that it was not achieved an effective activation due to the formation of several active and non-active species (mono, di, and tri-alkylates) [7]. Therefore, the catalytic activity was lower which results in a higher molecular weight (see Table 2) due to a greater amount of butadiene molecules available per each active neodymium atom. The microstructure was not affected by the aging time.

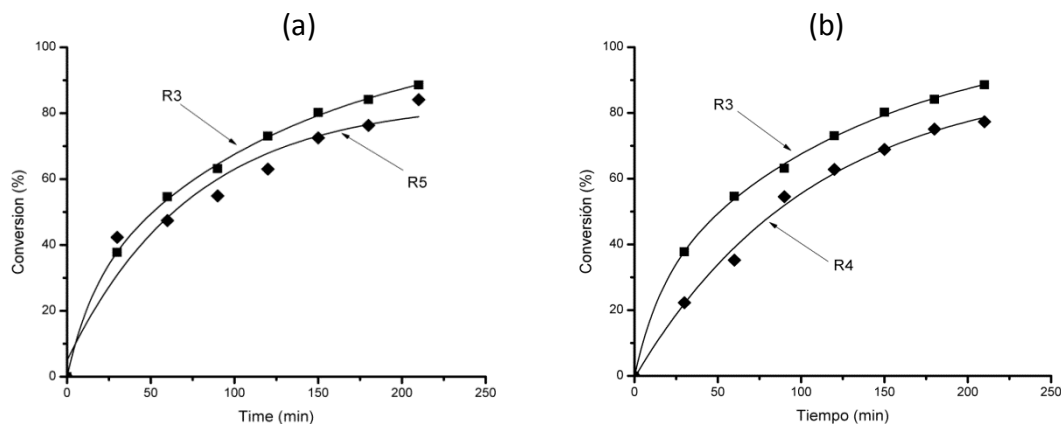


Figure 2. Conversion evolution as a function of polymerization time for a) R3 and R5, b) R3 and R4. Two different addition orders were studied (see Table 1). The addition order used in R6 (St+Al+Nd+Cl+Bt), resulted in a PB with the highest conversion (92.44%) and the highest molecular weight ($M_n=173000$ g/mol), besides the *cis*-1,4 units content remained around 96% and a low incorporation of St units is observed. The low incorporation of styrene suggests that the initial active species did not interact with the St monomer in absence of Bt coordinated.

At higher styrene volumes employed the conversion decreased and the molecular weight increased. These results are justified by the coordination competence of the active sites between the aromatic hydrocarbon and the monomer [8]. According to literature reports this occurs with nucleophilic solvents, the solvent is coordinated with the active site presenting a decrease in the catalytic activity [9-10]. Thus, a higher solvent amount (St), promotes an increase in the coordination competence.

ABS synthesis by the “*In Situ Bulk*” process. The values of some properties such as impact resistance (IR), tensile strength (RT), Young's modulus (E) and melt flow index (MFI) of the produced ABS are shown in Table 3. In this heterogeneous systems, it is well known that an increase in the concentration of initiator, [I], promotes a decrease in the reaction time, size of disperse rubber phase as well as a decrease in the molecular weight of SAN chains [11], expected results for here presented ABS were obtained (Mw of ABS1=136000 and Mw of ABS2=98000 g/mol) in this study. Rubber from experiment R6 was used as precursor of both ABS type reins.

Table 3. Morphological and mechanical properties of synthesized ABS

ABS	[I] (wt-%)	GD	Dp (μm)	Φ	IR (J/m)	RT (MPa)	E (MPa)	MFI (g/10 min)
1	0.022	320	-	-	36	5.7	2081	15
2	0.066	365	3.7	0.38	23	9.5	1855	45

Furthermore, a drastic increase in the MFI of ABS2 compared with ABS1 was observed, this fact can be attributed to a decrease in the Mw or also to the fact that the ABS1 did not properly reach the establishment of the morphology, i.e. the elastomeric phase is the continuous phase (crosslinked) having greater difficulty to flow. In this sense, ABS1 and ABS2 were evaluated by DMA (see Figure 3). Both materials present a signal in $\text{Tan } \delta$, corresponding to the T_g of the *cis*-1,4-PB at a temperature of -74°C ; however, a second relaxation is observed at 36°C for ABS1 and 28°C for ABS2 and this is associated with SAN grafted in the elastomeric phase [12]. The shift of the second relaxation ($T\beta$) in the ABS2 is due to the higher grafting degree (GD) as is observed in Table 3 data.

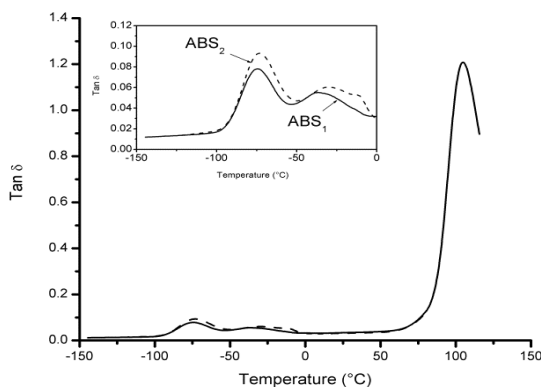


Figure 3. Tan delta versus temperature for ABS1 and ABS2

TEM images corresponding to the morphologies obtained in ABS1 and ABS2 are shown in Figures 4a and 4b, respectively. It can be observed that for ABS1 the morphology is not defined, i.e. a co-continuous phase transition is observed. However, Figure 4b shows a morphology well established with a $D_p=3.7\ \mu\text{m}$

and $\Phi=0.38$. For ABS 1 is observed a type of co-continuous phase, which causes a low MFI value. The higher values of impact strength for ABS1 are due to a co-continuous phase of PB.

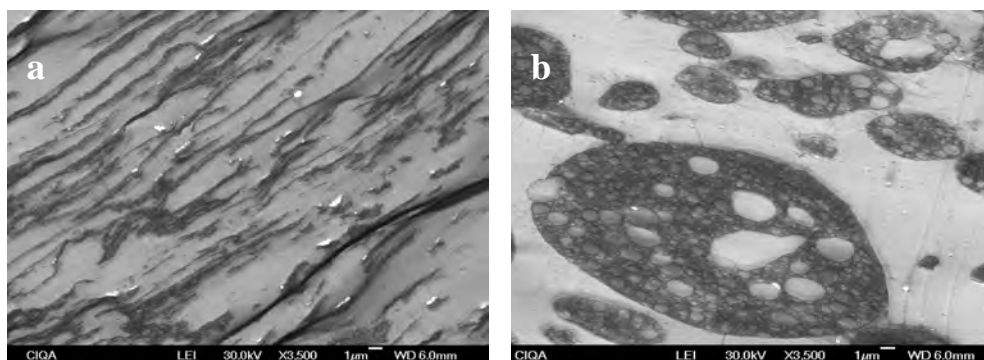


Figure 4. TEM images corresponding to morphologies of: a) ABS1, b) ABS2.

Conclusions

Several polybutadienes were obtained in the presence of styrene as solvent by modifying the Al/Nd ratio, the Cl/Nd ratio, varying the aging time, the ratio of solvent and finally changing the order of addition of the components. A lower percentage of styrene in polybutadiene was founded when the addition order of components is changed. The use of the catalyst system NdV/DIBAH/EASC resulted in a high *cis*-PB (96%). Using the *cis*-PB to produce ABS a morphology salami type was obtained; however, the impact resistance presented a low value.

Acknowledges

The authors thank to CONACYT for the financial support through the project 156366. We also thank to Ricardo Mendoza, Jesús Cepeda, Guadalupe Méndez, Uriel Peña and Francisco Zendejo for their technical support

References

- [1] Y. Hu, Z. Jia, Y. Li, L. Chang, Y. Wang, *Mat. Sci. and Eng. A*, 528(22-23), 6667 (2011).
- [2] Z. Yu, Y. Li, Z. Zhao, C. Wang, J. Yang, Ch. Zhang, Z. Li, Y. Wang, *Polym. Eng. And Sci.* 49(11), 2249 (2009).
- [3] X. F. Xu, H. D. Yang, H. X. Zhang, *J. of Appl. Polym. Sci.*, 98(5), 2165 (2005).
- [4] Z. Shen, *Frontiers in Chemistry China* 3, 247 (2006).
- [5] L. Friebe, H. Windisch, O. Nuyken, W. Obrecht, *J. of Macromol Sci.*, 41(3), 245 (2004).
- [6] R. Díaz de León-Gómez, F. Soriano-Corral, P. de León, G. Bosques MX/a/2013/015219, 2013.
- [7] I. L. Mello, F. M. B. Coutinho, D. S. S. Nunes, M. A. S. Costa, C. de Santa, *Quimica Nova*, 27, 277 (2004).
- [8] L. Friebe, J. M. Müller, O. Nuyken, W. Obrecht, *J. of Macromol. Sci.*, 43, 841 (2006).
- [9] I. L. Mello, F. M. B. Coutinho, D. S. S. Nunes, B. G. Soares, M. A. S. Costa, L. C. de Santa Maria, *European Polymer Journal*, 40(3), 635 (2004).
- [10] H. L. Hsieh, H. C. Yeh, *Rubber Chemistry and Technology*, 58(1), 117 (1984).
- [11] J. Scheirs, D. Priddy, *Modern Styrenic Polymers: Polystyrenes and Styrenic Copolymers*, Wiley Series in Polymer Science; p. 792 (2003).
- [12] Z. Yu, Y. Li, Y. Wang, L. Yang, Y. Liu, *Polym. Eng. and Sci.*, 49(11), 2249 (2009).

SOLUTION POLYMERIZATION OF METHYL METHACRYLATE IN AN IONIC LIQUID EMPLOYING CYCLIC MULTIFUNCTIONAL INITIATORS

Karla Delgado Rodríguez¹, Graciela Morales^{*1}, Pablo Acuña¹, Javier Enríquez¹ and Gastón P. Barreto²

¹ *Síntesis de Polímeros. Centro de Investigación en Química Aplicada, Blvd. Enrique Reyna 140, C.P. 25294, Saltillo, México. *graciela.morales@ciqa.edu.mx*

² *Facultad de Ingeniería, Universidad Nacional del Centro de la Provincia de Buenos Aires. Avda. del Valle 5737, B7400JWI, Olavarría, Buenos Aires, Argentina*

Abstract

1-butyl-3-methylimidazolium tetrafluoroborate ([BMIM⁺][BF₄⁻]) was used as a solvent during the methyl methacrylate (MMA) polymerization, at 120 and 130°C, employing two multifunctional cyclic peroxides as initiators, the pinacolone diperoxide (PDP) and the diethyl ketone triperoxide (DEKTP), and results were compared with those obtained in DMF as a solvent under the same reaction conditions. The polymerization rate was approximately four times faster in [BMIM⁺][BF₄⁻] than in DMF, and this is supported by the higher decomposition rate constants (k_d) calculated for both initiators in pure ionic liquid in comparison with the DMF. The average molecular weights were nearly three times higher in the presence of the ionic liquid, and this is due to transfer reactions in the presence of DMF.

Introduction

Organic solvents are mostly employed in solution polymerizations due to their affinity with monomers/polymers, notwithstanding the environmental concerns of this fact. The study of alternative less harmful solvents to be used in solution polymerizations has gained attention in the last years, for example the use of water, supercritical carbon dioxide or ionic liquids (ILs). Last mentioned solvents have been explored in different chemical processes such as organic synthesis, catalysis and in extraction practices [1]. In radical polymerization reactions, the presence of ILs as the solvents has been scarcely studied due to several factors like their more elevated costs in comparison with typical organic solvents. However, reported results evidenced some advantages such as increments in polymerization rates and molecular weights where both behaviors are related with the increase in the k_p/k_t (propagation and termination rate constants) ratio due the presence of the ILs as the reaction medium [2]. In this sense, Benton and Brazel employed 1-butyl-3-methylimidazolium hexafluorophosphate [BMIM⁺][PF₆⁻] as a solvent during the MMA polymerization initiated with AIBN, and they reported a polymerization rate five times faster and an average molecular weight around four times higher in the presence of the ionic liquid than the corresponding results in benzene [3].

An increase in the k_p values has been also reported in radical polymerizations when ILs are used as solvents instead of bulk polymerizations. For example, Harrison *et al.* reported a k_p value 2.5 times higher in relation with the bulk reaction for the MMA polymerization initiated with AIBN in the presence of [BMIM⁺][PF₆⁻] [4,5]. Schmidt-Naake *et al.* studied several ILs during the MMA and GMA polymerizations using AIBN or BPO as the initiator and they reported higher k_p values (around 4 times higher for MMA and 2 times for GMA) when ILs were used in comparison with the corresponding bulk polymerizations. The ILs studied were the [BMIM⁺][PF₆⁻], [BMIM⁺][BF₄⁻], [EMIM⁺][EtSO₄⁻] and [EMIM⁺][HexSO₄⁻] [6]. In this kind of systems, the increase on the overall polymerization rates is explained by the diminution of the propagation activation energy (E_{ap}) due to the presence of the ILs. The bulk polymerization requires an $E_{ap} = 22.4$ kJ mol⁻¹, while it decreases to 18.1 kJ mol⁻¹ in the presence of 80% v/v of the [BMIM⁺][PF₆⁻] or [BMIM⁺][BF₄⁻] [7].

Cyclic multifunctional initiators have not been reported in solution polymerizations carried out in ionic liquids, thus, in this study it is reported the use of the cyclic initiators pinacolone diperoxide (PDP) and diethyl ketone triperoxide (DEKTP) during MMA polymerizations using $[\text{BMIM}^+][\text{BF}_4^-]$ as a solvent and results are compared with those obtained when DMF is used as the reaction medium.

Experimental

$[\text{BMIM}^+][\text{BF}_4^-]$ was used as received, whereas DMF and MMA were distilled before use. All reactants were acquired from Aldrich.

PDP and DEKTP were synthesized according to methods reported in the literature [8, 9]. PDP synthesis involves the reaction between 3,3-dimethyl-2-butanone and hydrogen peroxide (30% v/v) in sulfuric acid (70% v/v) at -15 to -20°C. DEKTP was obtained by the reaction between 3-pentanone and hydrogen peroxide at the same reaction conditions mentioned for PDP. The purity of the peroxides was confirmed by nuclear magnetic resonance analysis.

Regarding the polymerization reactions, a stock solution of PDP (or DEKTP) in MMA was prepared followed by the addition of $[\text{BMIM}^+][\text{BF}_4^-]$ or DMF 0.01 M of the initiator in the monomer-solvent (20-80 % v/v) mixture was the concentration established. The prepared solution was distributed in glass ampoules to be thoroughly degassed by three freeze-pump-thaw cycles and then sealed with a flame torch. The ampoules were immersed in a thermostatic oil bath stabilized at the selected temperature and they were withdrawn after predetermined times. The polymeric products were dissolved in THF, precipitated adding drop-wise over methanol, filtered and dried under vacuum at room temperature until constant weight. Monomer conversion was determined by gravimetric procedures and the molecular weights were determined by size exclusion chromatography in a Hewlett-Packard instrument (HPLC series 1100) equipped with a refractive index detector and using poly(methyl methacrylate) standards to build up the calibration curve.

Results and Discussion

Solution polymerization reactions of MMA employing PDP and DEKTP as initiators were carried out in $[\text{BMIM}^+][\text{BF}_4^-]$ and DMF, at 120 and 130°C. Figure 1 shows the monomer conversion evolution as a function of the reaction time for polymerizations carried out in both studied solvents at two different temperatures. Figures 1a and 1b correspond to results with PDP and DEKTP, respectively.

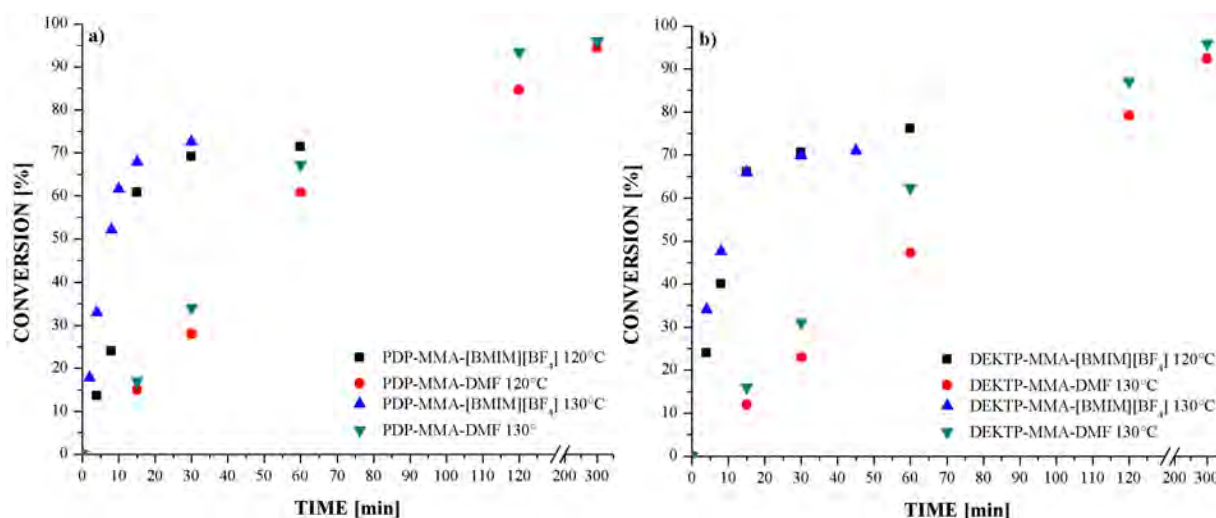


Figure 1. Monomer conversion evolution as a function of reaction time for MMA polymerizations in $[\text{BMIM}^+][\text{BF}_4^-]$ and DMF, at 120 and 130°C, initiated with a) PDP, and b) DEKTP

For both initiators, and independently the temperature employed, the polymerization rate was approximately four times higher in $[\text{BMIM}^+][\text{BF}_4^-]$ than in DMF. The increase in monomer conversion rate in $[\text{BMIM}^+][\text{BF}_4^-]$ was attributed, in part, to the high viscosity of the IL relative to DMF. The high solution viscosity limited the diffusion rates of large polymer chains within the solution. This inability to manoeuvre limited the termination step, increasing the ratio of propagation rate to termination rate.

On the other hand, when $[\text{BMIM}^+][\text{BF}_4^-]$ is used as the solvent, a maximum value of conversion of 75% is reached, in 30 min for PDP and 60 min for DEKTP, and then this value remains without changes through the polymerization. Moreover, in the case of PDP and using the ionic liquid a conversion close to 75% was observed in only 15 minutes meanwhile with DMF it was necessary 60 minutes to reach a similar conversion value.

This maximum conversion value reached with IL was explained by the presence of bimolecular termination reactions as a consequence by one hand, of the high viscosity of the reaction medium in the presence of the IL and on the other hand, to an increase in the termination reaction as a consequence of a high concentration of radicals. This last statement is sustained by the higher decomposition rate constants (k_d) reported for both initiators in pure ionic liquid in comparison with the DMF [10], shown in Table 1.

Table 1. k_d values for PDP and DEKTP, in $[\text{BMIM}^+][\text{BF}_4^-]$ and DMF, at 120 and 130°C

Temperature [°C]	$k_{d,\text{PDP}} \times 10^4$ [s ⁻¹] [BMIM ⁺][BF ₄ ⁻]	$k_{d,\text{PDP}} \times 10^4$ [s ⁻¹] DMF	$k_{d,\text{DEKTP}} \times 10^4$ [s ⁻¹] [BMIM ⁺][BF ₄ ⁻]	$k_{d,\text{DEKTP}} \times 10^4$ [s ⁻¹] DMF
120	3.05	0.54	1.66	0.15
130	8.94	1.44	3.11	0.42

Also, the differences in k_d values reported in Table 1 can be explained, taking as an example the case of the system DEKTP/DMF, due to a higher solvation of the *initial initiator molecular state* (at room temperature) conducting to its stabilization and requiring a higher energetic barrier in order to generate the intermediate bi-radical (transition state). On the contrary, in the case of DEKTP/ $[\text{BMIM}^+][\text{BF}_4^-]$, the *transition state* is mostly solvated as a consequence of a rapid orientation of the solvent molecules, stabilizing the transition state (due to higher interactions initiators-solvent), that causes a reduction in the activation enthalpy (ΔH^\ddagger) and consequently, the products formation is favored. This explanation is supported by the reaction coordinate diagram (Figure 2) where a lower activation energy (E_a) value for $[\text{BMIM}^+][\text{BF}_4^-]$ (22.2 kcal mol⁻¹) can be observed when it is compared with DMF (34.4 kcal mol⁻¹).

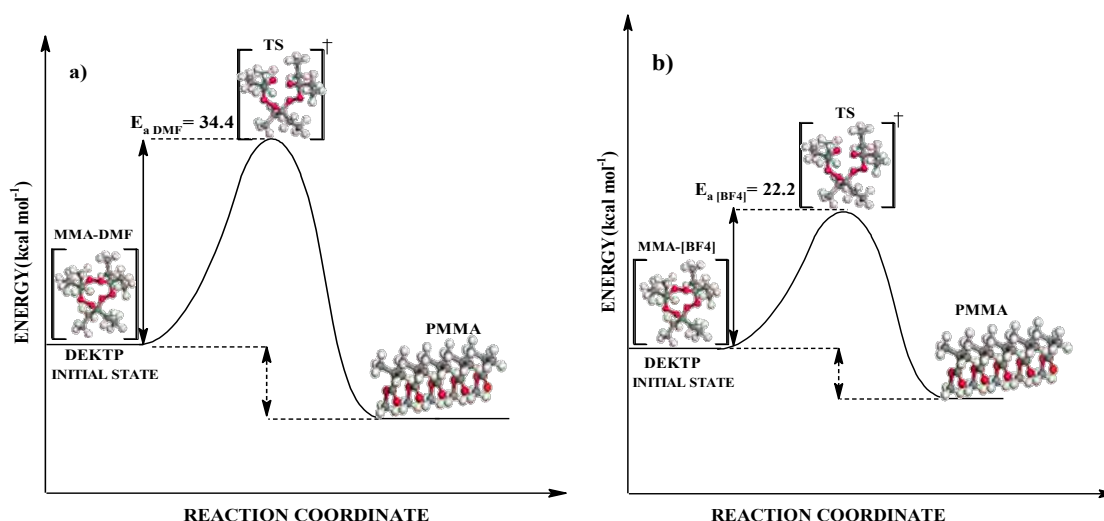


Figure 2. Scheme of energy as a function of reaction coordinate for DEKTP initiator in a) DMF and b) $[\text{BMIM}^+][\text{BF}_4^-]$

Figure 3 shows the effect of initiator, solvent and temperature for the corresponding polymerizations on the average molecular weight (Mw). The temperature effect on the average molecular weight for both solvents (independently of the initiator) shows an expected behavior for a classical radical polymerization, where an increase in the reaction temperature yields a reduction of molecular weights.

In turn, the kinetic chain length (Equation [1]) increases, accounting for the higher PMMA molecular weight found in reactions using $[\text{BMIM}^+][\text{BF}_4^-]$. The kinetic chain length, ν , is proportional to the propagation rate constant, k_p , and monomer concentration $[\text{M}]$, as follows:

$$\nu = \frac{k_p[\text{M}]}{2(fk_dk_t[\text{I}])^{\frac{1}{2}}} \quad \text{Eq. [1]}$$

where f is the initiator efficiency, k_d is the rate constant for initiator decomposition, k_t is the rate constant for termination and $[\text{I}]$ is the initiator concentration. The kinetic chain length is, in turn, directly related to the degree of polymerization (depending upon the mode of termination- in this case predominantly disproportionation). For the reactions in $[\text{BMIM}^+][\text{BF}_4^-]$ and DMF, $[\text{M}]$ and $[\text{I}]$ were held constant, hence meaning that the difference in kinetic chain length was due to a change in a rate constant, initiator efficiency or a decreased radical chain transfer to the solvent. Our results seemed to be consistent with the situation of a probable decrease in the initiator efficiency as well as a decrease in transfer reaction.

On the other hand, comparing both initiators in $[\text{BMIM}^+][\text{BF}_4^-]$ higher molecular weights (around two times higher) were produced with PDP than with DEKTP. This can be justified considering the E_a of DEKTP ($22.2 \text{ kcal mol}^{-1}$) once the initiator has decomposed, which is lower than that for PDP ($28.3 \text{ kcal mol}^{-1}$), making it more susceptible the cleavage of the O-O bonds. This situation together with a lower value of ΔH^\ddagger , yields a higher radical concentration, higher R_p (as it was previously demonstrated) and lower Mw.

On the contrary, in the case of DMF as a solvent, higher molecular weights were produced with DEKTP than with PDP which can also be justified with the E_a values calculated in this solvent ($32.6 \text{ kcal mol}^{-1}$ for PDP and $34.4 \text{ kcal mol}^{-1}$ for DEKTP).

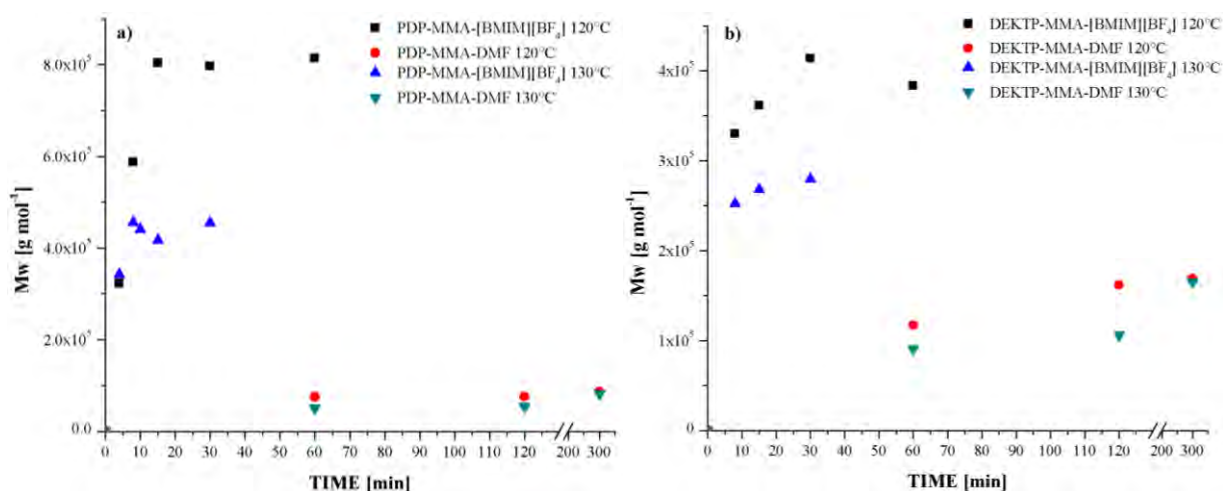


Figure 3. Molecular weight evolution as a function of reaction time for MMA polymerizations in $[\text{BMIM}^+][\text{BF}_4^-]$ and DMF, at 120 and 130 °C, initiated with a) PDP, and b) DEKTP

Conclusions

The MMA polymerization initiated with PDP and DEKTP using [BMIM⁺][BF₄⁻] as a solvent presented a polymerization rate around 4 times faster in comparison with the use of DMF, attributed to a considerable difference on their decomposition rate constants values calculated in both solvents.

The temperature, the type of initiator and the solvent used during the polymerization process affect the molecular weights of resulting samples. Higher molecular weights were obtained in the presence of IL in comparison with DMF attributed to a decrease in initiator efficiency and/or decrease in transfer reactions, and with PDP in comparison with DEKTP which was explained in terms of the *E_a* values.

Acknowledgements

The authors would like to thank the Mexican National Council for Science and Technology (CONACYT) for Karla Delgado's scholarship granted 293911 and for the bilateral Cooperation México-Argentina Program through the Project N°190268.

Barreto is member of the Career of Scientific and Technological Research Council of the National Scientific and Technical Research (CONICET).

References

- [1]. Shadpour Mallakpour, Mohammad Dinari, *Ionic Liquids as Green Solvents: Progress and Prospects*. New York, London: Springer, pp 1-32 (2012).
- [2] G. Schmidt-Naake, A. Schmalfuß and I. Woecht, *Chemical Engineering Research and Design*, 86 (7), 765 (2008).
- [3] M. G. Benton and C. S. Brazel, *Polymer International*, 53(8), 1113 (2004).
- [4] S. Harisson, S. R. Mackenzie and D. M. Haddleton, *Chemical Communications*, (23), 2850 (2002).
- [5] S. Harisson, S. R. Mackenzie and D. M. Haddleton, *Macromolecules*, 36, 5072 (2003).
- [6] G. Schmidt-Naake, I. Woecht, a. Schmalfuß and T. Glück, *Macromolecular Symposia*, 275–276(1), 204 (2009).
- [7] G. I. Woecht, G. Schmidt-Naake, S. Beuermann and M. Buback, *Journal of Polymer Science Part A Polymer Chemistry*, 4(46), 1460 (2007).
- [8] L. F. R. Cafferata, G. N. Eyler, A. I. Cañizo and E. E. Alvarez, *Tetrahedron Letters*, 34, (1993).
- [9] G. N. Eyler and A. I. Cañizo, *Quimica Nova*, 25(3), 364 (2002).
- [10] K. Delgado, Ph. D. Dissertation (First Report), CIQA, México (2013).

COMPUTATIONAL CHEMISTRY APPLIED IN THE STUDY OF THE STRUCTURAL PROPERTIES IN PEHD/WHEAT HUSK/ BENZOPHENONE COMPOSITES

Norma-Aurea Rangel-Vázquez, Alejandra-Ibeth García-Castañón

Departamento de Metalmecánica del Instituto Tecnológico de Aguascalientes. Ave. López Mateos
#1801 Ote Fracc. Bona Gens CP. 20256 Aguascalientes, Ags. norma_rangel79@yahoo.com.mx

Abstract

Molecular mechanics is a part of molecular modeling, since it involves the use of Newtonian mechanics/classical mechanics to describe the physical basis behind the models. Molecular models typically describe atoms (nuclei and electrons together) as point loads with an associated mass. The interactions between neighboring atoms are described by interactions type harmonic oscillator, "springs", which (representing chemical bonds) and forces of van der Waals. In this research the models AMBER and MM+ were used in order to calculate the structural properties (DG, QSAR, length and angle of bond, FTIR and electrostatic potential) for the absorption of benzophenone and a subsequent implementation in the electricity sector.

Introduction

Computational chemistry is a branch of chemistry that uses computer simulation to assist in solving chemical problems. It uses methods of theoretical chemistry, incorporated into efficient computer programs, to calculate the structures and properties of molecules and solids. While computational results normally complement the information obtained by chemical experiments, it can in some cases predict hitherto unobserved chemical phenomena. It is widely used in the design of new drugs and materials. Examples of such properties are structure (i.e. the expected positions of the constituent atoms), absolute and relative (interaction) energies, electronic charge distributions, dipoles and higher multipole moments, vibrational frequencies, reactivity or other spectroscopic quantities, and cross sections for collision with other particles.

The methods employed cover both static and dynamic situations. In all cases the computer time and other resources (such as memory and disk space) increase rapidly with the size of the system being studied. That system can be a single molecule, a group of molecules, or a solid. Computational chemistry methods range from highly accurate to very approximate; highly accurate methods are typically feasible only for small system. In many cases, large molecular systems can be modeled successfully while avoiding quantum mechanical calculations entirely. Molecular mechanics simulations, for example, use a single classical expression for the energy of a compound, for instance the harmonic oscillator. All constants appearing in the equations must be obtained beforehand from experimental data or *ab initio* calculations [1].

The use of natural fiber for the reinforcement of the composites has received increasing attention both by the academic sector and the industry. Natural fibers have many significant advantages over synthetic fibers. Currently, many types of natural fibers have been investigated for use in plastics including flax, hemp, jute straw, wood, rice husk, wheat, barley, oats, rye, cane (sugar and bamboo), grass, reeds, kenaf, ramie, oil palm empty fruit bunch, sisal, coir, water, hyacinth, pennywort, kapok, paper mulberry, raphia, banana fiber, pineapple leaf fiber and papyrus [2].

Third US-Mexico Meeting "Advances in Polymer Science" and XXVII SPM National Congress
Nuevo Vallarta, December 2014

Composites can be tailored to have the desired properties by incorporating particulate fillers into a polymer matrix to suit different applications. For economic and environmental reasons, there is an increasing use of polymer composites filled with lignocellulosic materials such as wood flour, rice husk, wheat husk, jute, and sisal [3]. Wheat gluten is a complex protein that has been investigated for its potential use in food and non-food applications such as food coatings, paints, adhesives, paper coatings, and cardboard or other biopackaging materials. Among these, plastic films are of especial interest because they are so widely used. Because wheat gluten is a low-cost, renewable, and biodegradable resource, using it to make films offers an environmentally friendly alternative to petroleum-based products. However, wheat-gluten-based materials are also quite brittle and suffer from high water sensitivity [4-5].

Experimental

The optimizing process of structures used in this work was started using the AM1 method, because it generates a lower-energy structure even when the initial structure is far away from the minimum structure. The Polak-Ribiere algorithm was used for mapping the energy barriers of the conformational transitions. For each structure, were made 5715 iterations, a level convergence of 0.001kcal/mol/Å and a line search of 0.1 were carried out. The infrared spectrum is commonly obtained by passing infrared electromagnetic radiation through a sample that possesses a permanent or induced dipole moment and determining what fraction of the incident radiation is absorbed at a particular energy. After obtaining a free energy of Gibbs or optimization geometry using AM1 methods, we can plot two-dimensional contour diagrams of the electrostatic potential surrounding a molecule, the total electronic density, the spin density, one or more molecular orbitals, and the electron densities of individual orbitals. HyperChem software displays the electrostatic potential as a contour plot when you select the appropriate option in the Contour Plot dialog box. Choose the values for the starting contour and the contour increment so that you can observe the minimum (typically about -0.5 for polar organic molecules) and so that the zero potential line appears [6].

Results and Discussion

Table 1 shows the DG and log P results, in where in all cases the DG was negative value, indicated the spontaneous nature of the adsorption process of benzophenone. Other property was calculated, log P- in both cases determined that the materials tend to be more negative which found that tend to absorb water (polar solvents) because of its hydrophilic character characteristic of cellulose [7-8].

Table 1 Properties calculated for wheat husk/PE/benzophenone using mechanics molecular.

Propertie	AMBER	AMBER	MM+	MM+
DG (kcal/mol)	-24.89	-93.8	-23.17	-89.6
Log P	-19.09	-17.0	-19.09	-17.0

FTIR results with AMBER method can be observed in table 2, where the characteristic peaks appear at, 4140 cm⁻¹ was assigned at NH₂ (wheat husk), at 2398 cm⁻¹ attributed at C-O-H (wheat husk) and finally was observed at 870 cm⁻¹ the bonds: NH, CH and CO in the composite. Table 3 shows the MM+ results, in where can be appreciated the exits of changes in the wave numbers by means at type of method using in the simulation.

Table 2 FTIR results using AMBER method. Table 3 FTIR results applied MM+ method.

Wave number (cm ⁻¹)	Assignments
4071	CH (Polyethylene)
4140	NH ₂ (Wheat)
3665	CH (Benzophenone-tensión)
3418	Symmetric stretching CH (Polyethylene)
3011	CH (Polyethylene)
2702	CN (Wheat)
2398	C-O-H (Wheat)
2099, 1682	C-C (Benzophenone)
1454	CH (Polyethylene torsion)
1127	C-O, C-C y C-N (Wheat tensión)
870	NH balanceo, CH balanceo, CO tensión

Wave number (cm ⁻¹)	Assignments
3941	CH (Polyethylene)
4140, 3515	NH ₂ (Wheat)
4035-4022	CH (Wheat)
3469	CH (Benzophenone tensión)
3390-3421	C-C rings (Wheat)
3013	NH (Wheat)
2910, 2375	CC y CO (Benzophenone)
2702	CN (Wheat)
2558, 1557	C-O-H (Wheat)
2108, 1369	C-C (Benzophenone)
1454	CN, CO (Wheat)
1264	C-O, C-C y C-N tension (Wheat)
798	NH balanceo, CH balanceo, C-O tensión

The electrostatic potential of rice husk (figure 1a and 2a) with benzophenone (figure 1b and 2a) using AMBER and MM+ methods show that the negative regions (red) are mainly localized on the C=O bond. Also, a negative electrostatic potential region is observed around the OH groups (oxygen atom). Finally, the neutral potential was observed in the different rings of composite.

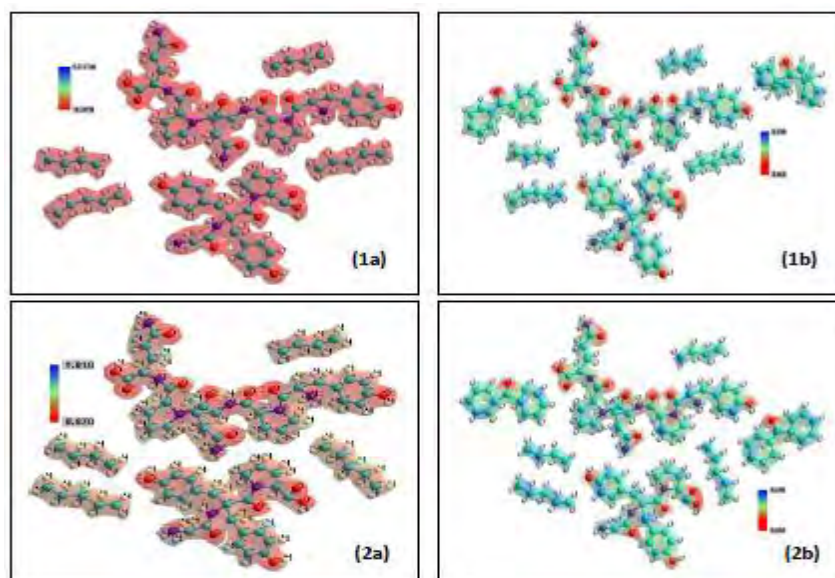


Figure 1 Electrostatic potential of rice husk and rice husk/PE/benzophenone using AMBER and MM+ method, respectively.

Conclusions

The composites are often associated with agglomeration as a result of insufficient dispersion, caused by the tendency of fillers to also form hydrogen bonds with each other during processing. Moreover, the polar hydroxyl groups on the surface of the lignocellulosic materials have difficulty in forming a well-bonded interface with a nonpolar matrix, as the hydrogen bonds tend to prevent the wetting of the filler surfaces.

References

- [1]. R. Lester, R. J. Zauhar, R. G. Lanzara. *J. Mol Grap Mod*, 25, 396–409 (2006).
- [2]. R. S. Shankar, S.A. Srinivasan, S. Shankar, R. Rajasekar, R. N. Kumar, P. S. Kumar. *Inter J Sci Res Pub*, 4, 4-5 (2014)
- [3]. M. S. Sobhy, M. T. Tammam. *Inter J Polym Sci*, 2010, 1-8 (2010)
- [4]. M. Pommet, A. Redl, M. H. Morel, S. Domenek and S. Guilbert, *Macromol. Symp.* 197, 207 (2003).
- [5]. S. Hemsri, K. Grieco, A. D. Asandei and R. S. Parnas, *Compos. Part A-Appl. S.* 43, 1160 (2012).
- [6]. Hyperchem® Computational Chemistry, Canada, 1996
- [7]. S. M. Leal-Rosa, E. Fonseca-Santos, C. A. Ferreira, S. M. Bohrz Nachtigall, *Materials Research*, 12, 333-338, (2009).
- [8]. K. Hardinnawirda and I. Sitirabiatull Aisha, *J Mech Eng Sci*, 2, 181-186 (2012).

ANALYSIS OF THE ABSORPTION PROCESS OF BENZOPHENONE IN RICE HUSK/POLYETHYLENE COMPOSITES DUE AMBER AND MM+ MODELS

Norma-Aurea Rangel-Vázquez, Alejandra-Ibeth García-Castañón

Departamento de Metalmeccánica del Instituto Tecnológico de Aguascalientes. Ave. López Mateos #1801 Ote Fracc. Bona Gens CP. 20256 Aguascalientes, Ags. norma_rangel79@yahoo.com.mx

Abstract

In this research, rice husk was analyzed. The analysis techniques used were, FTIR to study this effect and an option to justify the obtained results is using theoretical calculations by means of the computational chemistry tools. Using QSAR properties, we can obtain an estimate of the activity of a chemical from its molecular structure only. The molecular electrostatic potential (MESP) was calculated using AMBER and MM+ models. These methods give information about the proper region by which compounds have intermolecular interactions between their units.

Introduction

In recent years concern for environmental protection has increased, leading man in the search for solutions through manufacture of materials that are not harmful to it, as in the case of composite materials, which can be made from polymers, whose usage has increased due to the advantages of its properties. One of these is the polyethylene, belongs to the family of thermoplastics, has the characteristic of heat from its solid state to the viscous liquid, once cooled goes back to a solid state, without it being degraded, which is due to their linear macromolecules (branching) is not chained transversely when its temperature is raised [1].

Moreover, the benzophenone is an aromatic ketone. Its properties are located within an important class of organic UV filters and are widely used in sunscreen products because presents the ability to absorb radiation in the UV and UVB ranges, and dissipates it as heat. It can be used in the manufacture of insecticides, agricultural chemicals, drugs, and other antihistamines. According to studies conducted, it was found that benzophenone influences the photodegradation of polyethylene, constituting the consumption of free radicals by Norrish I reaction, leading to the formation of double bonds, which promotes the formation of double bonds in the material [2-3].

Organic fibers can be used as reinforcing materials, example of it is rice husk, it has a percentage of organic matter ranging from 75 to 90%, among which include cellulose, lignin, between others. Likewise, it is formed of silica, alkali and trace elements. The contents of each component vary with the type of rice, soil chemistry and the geographical location. By combining polyethylene and rice husk is possible to create materials that offer greater flexibility and increased strength and hardness [4]. Electrostatics plays an integral part in the study of structure and function of proteins at physiological conditions. Theoretical considerations of the electrostatics in proteins are usually based on solutions to the Poisson-Boltzmann (PB).

All these theoretical descriptions will involve a certain type of charge assignment to the atoms of the protein. Since the result of the PB calculation will inevitably depend on the particular choice made for the charges, it might be of interest to study the influence and variation resulting from different charge assignments.

Of particular interest will be the comparison between a set of classic charges, ie from force fields commonly employed in the simulation of biomolecules, and charges derived from ab-initio calculations performed at a certain level of Quantum Mechanical (QM) theory [5].

Experimental

The optimizing process of structures used in this work was started using the AM1 method, because it generates a lower-energy structure even when the initial structure is far away from the minimum structure. The Polak-Ribiere algorithm was used for mapping the energy barriers of the conformational transitions. For each structure, 5715 iterations, a level convergence of 0.001kcal/mol/Å and a line search of 0.1 were carried out. The infrared spectrum is commonly obtained by passing infrared electromagnetic radiation through a sample that possesses a permanent or induced dipole moment and determining what fraction of the incident radiation is absorbed at a particular energy.

The energy of each peak in an absorption spectrum corresponds to the frequency of the vibration of a molecule part, thus allowing qualitative identification of certain bond types in the sample. After obtaining a free energy of Gibbs or optimization geometry using AM1 methods, we can plot two-dimensional contour diagrams of the electrostatic potential surrounding a molecule, the total electronic density, the spin density, one or more molecular orbitals, and the electron densities of individual orbitals. HyperChem software displays the electrostatic potential as a contour plot when you select the appropriate option in the Contour Plot dialog box. Choose the values for the starting contour and the contour increment so that you can observe the minimum (typically about -0.5 for polar organic molecules) and so that the zero potential line appears [6].

Results and Discussion

Negative values of ΔG indicated the spontaneous nature of the adsorption process of benzophenone (see table 1). Negative values of ΔG indicated the spontaneous nature of the adsorption process of benzophenone [7]. One can see that the properties change with the addition of benzophenone, for example the Log P values in both cases determined that the materials tend to be more negative which found that tend to absorb water (polar solvents) because of its hydrophilic character characteristic of cellulose [7-8].

Table 1 Properties of Rice husk using AMBER method

Property	Rice husk	Rice husk/benzophenone	Rice husk	Rice husk/benzophenone
DG (kcal/mol)	-243.67	-658	-315.56	-712
Log P	-22.24	-16.39	-22.24	-16.39

The FTIR bands of rice husk/benzophenone where the characteristic peaks associated with absorption process are calculated, in where the shifts in the peaks of rice husk attributed to the absorption of benzophenone, so the existence of one or more aromatic rings in a structure is normally readily determined from the CH and C=C-C ring related vibrations. The characteristic infrared absorption frequencies of carbonyl group in cyclic ketones are normally strong in intensity and found in the region 1543–1572 cm⁻¹. The interaction of carbonyl group with other groups present in the system did not produce such a drastic and characteristic change in the frequency of C=O stretch as did by interaction of NH stretch.

The carbon–oxygen double bond is formed by $p\pi$ – $p\pi$ between carbon and oxygen. Because of the different electronegativities of carbon and oxygen atoms, the bonding electrons are not equally distributed between the two atoms. The position of the C=O stretching vibration is very sensitive to various factors such as the physical state, electronic effects by substituents, ring strains. Normally carbonyl group vibrations occur in the region 1728 and 1618 cm^{-1} respectively. The electrostatic potential of rice husk (figure 1a and 2a) with benzophenone (figure 1b and 2b) using AMBER and MM+ methods show that the negative (red) regions are mainly localized on the C=O bond. Also, a negative electrostatic potential region is observed around the OH groups (oxygen atom).

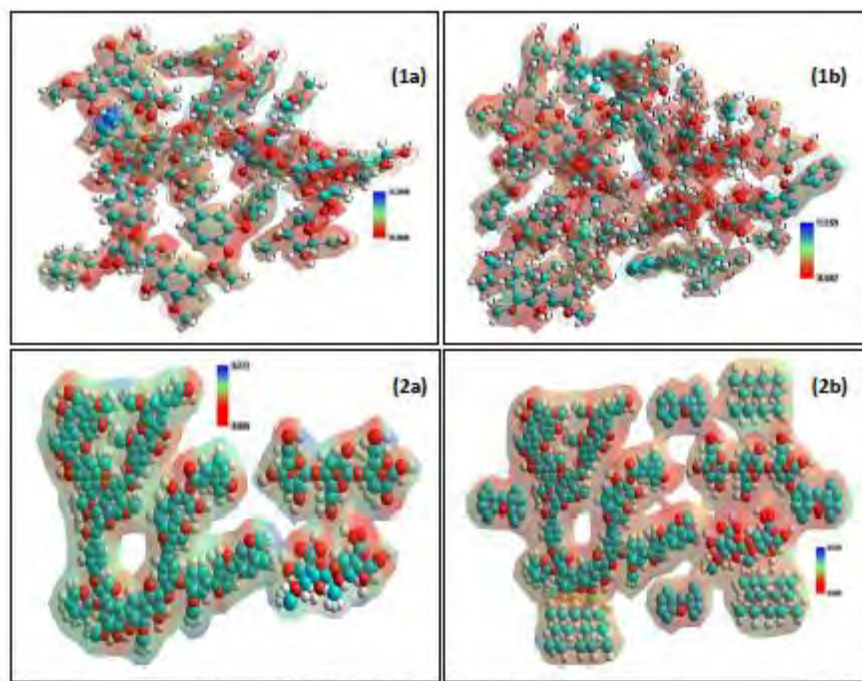


Figure 1 Electrostatic potential of rice husk and rice husk/PE/benzophenone using AMBER and MM+ method

Conclusions

The rice husks on an individual basis and such as benzophenone absorption systems were analyzed to determine the applications of lignocellulosic materials. It was determined that the negative value of the ΔG verifies that the absorption process is carried out in a way spontaneous.

References

- [1]. R. H. Cruz-Estrada, Revista Mex Ing Quím, 5, 29-34 (2006)
- [2]. B. A. Corrêa, A. Gonçalves, T. De Souza, C. Freitas, L. Cabral, M. Albuquerque, C. Castro, E Dos Santos, R Rodrigues, J Phy Chem, 12927-10933 (2012)
- [3]. M. Ramos, L. Cantú, F. Avalos, Dep Inv Polím, (2012).
- [4]. A. Kumar, K. Mohanta, D. Kumar and O. Parkash, Intern J Emer Techn Adv Eng, 2, 86-90 (2012)
- [5]. P. Kar, M. Seel, U. H. E. Hansmann, S. Hofinger. Proc NIC Work, 155-158 (2007)
- [6]. Hyperchem® Computational Chemistry, Canada, 1996

- [7]. S. M. Leal, E. Fonseca-Santos, C. A. Ferreira, S. M. Bohrz Nachtigall, Mat Res, 12, 333-338, (2009).
- [8]. K. Hardinnawirda and I. Sitirabiatull Aisha, J Mech Eng Sci, 2,181-186, (2012)

A DFT STUDY AMONG INTERACTION SITES: NH_3^+ OF POLYMERIC CHITOSAN AND SO_3^- OF AZOIC COLORANT RED 2

Juan Horacio Pacheco Sánchez,¹ Beatriz García Gaitán,¹ Rosa Elvira Zavala Arce¹

¹ División de Estudios de Posgrado e Investigación. Instituto Tecnológico de Toluca. Av. Tecnológico s/n, Metepec, Edo. de México, México, C.P. 52149, Tel. +52 722 208 7224, hpacheco@ittoluca.edu.mx

Abstract

In this DFT study we will calculate optimization geometry to figure out both equilibriums distance and energy of the interaction among the groups NH_3^+ as part of the polymeric chitosan molecule (adsorbent) and the SO_3^- as part of an azoic red 2 colorant molecule (adsorbate), when they are in acid conditions. Then we infer either physisorption or chemisorption among these molecules using also the Gauss law of electrostatics. In addition, the reaction path of the ground state system is obtained, where we recognize the distance on which the adsorbent strength begins influence over the adsorbate

Introduction

The colorants, especially synthetic origin that are present in wastewater, are responsible for many harmful effects to the environment, flora and aquatic fauna. Among the most important effects are the reduction of dissolved oxygen, eutrophication, the formation of recalcitrant and toxic compounds to cells and obstructing the passage of light to the water bodies and aesthetic impairment [1,2]. Red 2 is an azo colorant that may cause intolerance in people who are affected by salicylates. Moreover, it is a histamine liberator, and may intensify symptoms of asthma. It is also involved in cases of hyperactivity in children when used in combination with benzoates. Many countries like the United States have limited their use [3] because it creates problems requiring medical treatment. When azo-type colorants also called Reagent, are dumped into the water bodies produce amines as consequence of the rupture of azo bond, which cause many effects in some human organs such as the brain, liver, kidney, central nervous and reproductive systems [4,5]. Figure 1 shows the chemical structure of red 2 or amaranth red E-123 (trisodium 2-hydroxy-1-(4-sulfonato-1-naphthylazo)naphthalene-3,6-disulfonate, molecular weight 604.5 g/mol, and formula $C_{20}H_{11}N_2O_{10}S_3Na_3$ [1].



Figure 1 Chemical structure of Red 2 or amaranth red.

Effluent discharges of colorant have triggered a great concern for human health and marine life [6]. By this reason, it has been tremendous growth in both the set-up of equipment, corrective facilities, and the development of alternative technologies that respect the environment. Many of these technologies are based on the retention of a contaminant in a solid medium that makes it easy to handle and / or the possible recovery of the material, such as adsorption [7].

Chitosan can be obtained from the partial deacetylation of chitin. At present the chitosan product applications lies primarily in: nutraceuticals, food protectors generally, formulations for cosmetics, medical applications, agricultural uses, feed, flocculation, textiles, pulp and paper. Additionally,

application to water purification has being looked for.

Chitosan repeating units are observed in Figure 2 a) and b). The two molecules are β -(1-4)-2-acetamide-2-deoxy-D-glucopyranose (Figure 2a) with a molecular weight of 162.17, $C_6H_{12}NO_4$ formula, composition: C 44.44%, H 7.46 %, N 8.64, O 39.46%; and β -(1-4)-2-amino-2-deoxy-D-glucopyranose (Figure 2b) with a molecular weight of 205.21, $C_6H_{15}NO_5$ formula, composition: C 46.82%, H 7.37%, N 6.83 and O 38.98%. The valence is somewhat free to these molecules, so that when joined (Figure 2c) the chitosan molecule stays with a molecular weight of 377.37, the formula $C_{15}H_{25}N_2O_9$ composition is: C 47.74%, H 6.68%, N 7.42, O 38.16%. Also the chitosan molecule has exceeded valence which allows them to join colorants and metals as an example.

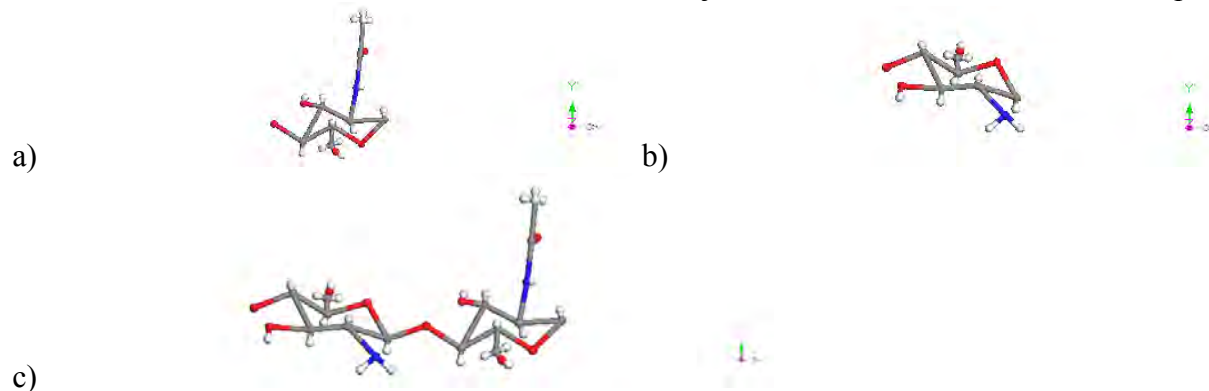


Figure 2. Chemical structure of chitosan repeating units. a) β -(1-4)-2-acetamide-2-deoxy-D-glucopyranose b) β -(1-4)-2-amino-2-deoxy-D-glucopyranose. c) A molecular unit chitosan
Our aim is to apply DFT to the interaction between chitosan and Red 2, right in their reaction sites NH_3^+ y^-O_3 respectively to infer the type of existing adsorption.

Methodology

The DFT method is based on the Hohenberg-Kohn theorems, which allow us to write the total energy of the system in terms of the charge density; however, the practical applications of this are only possible by means of the Kohn-Sham equations, which map the many-body problem to a problem of independent particles, where all the information of the quantum system of interacting electrons is included in the term of correlation and exchange. Thus the exchange-correlation functional contains all electron quantum interactions. As a first approximation the exchange-correlation functional approaches making use of a homogeneous electron gas, this is known as the local density approximation (LDA). The next level is the generalized gradient approximation (GGA), which considers density variations through the derivatives of this amount.

The calculations in this case are accomplished using DMol³ computer program proposed by Delley [8]. DMol³ was used to non-periodic structures with a generalized gradient approximation (GGA) to calculate the exchange-correlation potential and local potential gradient-corrected PW91. In this case, using the DFT method DMol³ with a set of DND numerical radial basis functions to calculate the intermolecular interaction between the reaction sites of chitosan and azoic colorants [8,9]. Non-restricted orbital spin were used, such program achieve simulations with boundary conditions and pseudopotentials to solve Kohn-Sham equations

Results and Discussion

A geometry optimization is independently carried out for each molecule, then these molecules are aggregated into the same system until an initial approach of 1.912 Å among sulfur and

nitrogen, with the geometry observed in Figure 5 corresponding to the Input. Initially, in the O_3S^- molecule, both the sulfur atom and the three oxygen atoms are in the same plane, the bond length of SO is 1.46\AA , and OSO angles are $120^\circ \pm 0.4^\circ$; while the molecule NH_3^+ has a pyramidal shape with the three hydrogen atoms in the same plane at an angle of $37.2^\circ \pm 0.1^\circ$, the angle HNH is $105.55^\circ \pm 0.15^\circ$, and the size of NH bond is 1.027\AA .

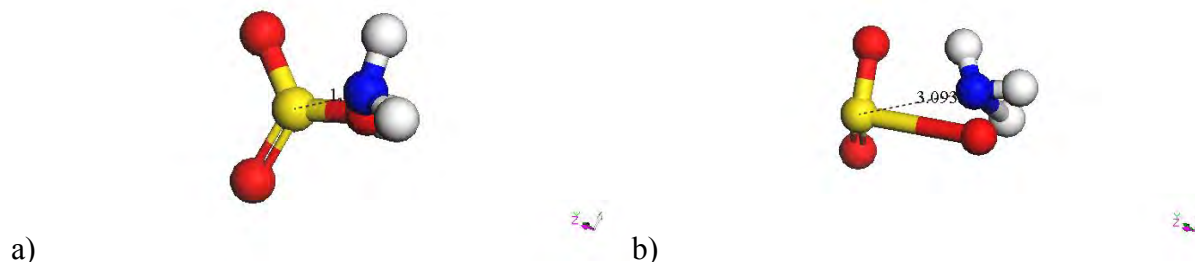


Figure 5. a) Input: Distance 1.912\AA among O_3S^- sulfur oxide and NH_3^+ ammonia ions in plane and pyramid geometry, respectively. b) Output: After the geometry optimization, growth of one OS bond and one NH bond is observed.

The geometry observed in Figure 5 corresponding to Output exhibits repulsion and insertion after the geometry optimization, the distance between sulfur and nitrogen increased to 3.093\AA , an increment of 62%. Also, an increment of 83% of the SO bond to 2.667\AA and 94% of the NH bond to 1.989\AA . The other two SO bonds in the O_3S^- molecule, now in a pyramid shape, have a length of 1.48\AA , and the sulfur atom making SOO angles of 26.413° , 28.776° and 30.955° with the plane in which the three oxygen atoms are located, while the OSO angles are 117.923° , 100.302° and 91.536° . The molecule NH_3^+ has pyramid shape with three hydrogens in a plane making NHH angles of 27.836° , 36.047° and 26.863° , while HNH angles are 107.848° , 88.026° and 92.444° respectively. The size of the NH bonds are 1.032\AA , 1.031\AA and 1.989\AA .

A geometry optimization of 29 steps was applied, in which a distance of 0.6816\AA between H^+ and O^- ions for an equilibrium energy of -654.471 kcal/mol or -28.33998 eV , and for an equilibrium distance of 3.093\AA between nucleus N of NH_3^+ and nucleus S of O_3S^- was obtained. A natural elongation of the bonds corresponding to the ions of each molecule is seen. C_1 symmetry is applied. The energy of the highest occupied molecular orbital (HOMO) is 6681 eV . Orbital number is 50-HOMO and 51-LUMO, with orbital occupation: 25 α (1) and 25 β (1), for a total number of electrons 50.

Assuming a nuclear N-S equilibrium separation $R = 3.093\text{\AA}$ for NH_3SO_3 molecule, the NH_3^+ and O_3S^- ions possess spherically symmetric charge distributions, which up to that point no overlap has occurred, even if an elongation of the corresponding bonds to ions of each molecule is appreciated, where the spacing among such H^+ and O^- ions is about 0.6816\AA . This value is obtained by measuring the distances of the bonds: O^- to H^+ , H^+ to N, and N to O^- of a triangle of sides 0.987\AA , 1.989\AA and 1.446\AA respectively, with OH^+N angle 43.676° . We applied law of sines to get the closest distance between H^+ and O^- ions.

Taking into account the above assumptions, the Gauss law of electrostatics allows evaluation of potential binding energy of Coulomb of the ions with unit charge, from the expression:

$$V = -\frac{1}{4\pi\epsilon_0} \frac{e^2}{R}. \quad \text{Then,} \quad V = -\frac{9 \times 10^9 \frac{\text{Nm}^2}{\text{coul}^2} \times (1.6 \times 10^{-19} \text{ coul})^2}{6.816 \times 10^{-11}} = -3.3803 \times 10^{-18} \text{ joule} = -21.1268 \text{ eV}.$$

Which corresponds to 25.4% deviation of that value calculated with DFT.

Slightly varying the starting position of the interacting molecules, the following results are obtained: $E = 651.640 \text{ kcal/mol} = -28.25723 \text{ eV}$. The spacing between cores is 3.586 \AA . The geometry optimization was carried out in 21 steps. The separation between the H^+ and ^-O ions is 0.6726 \AA . Then Gauss law of electrostatics provides the potential energy $V = -21.41 \text{ eV}$. The deviation from the energy calculated by simulation is 24.2%.

Considering the deviation as the error about 25%, then it is not reliable; however, we note that Gauss law is applied only to the H^+ and ^-O ions, while DFT has been applied to molecular NH_3^+ and ^-O_3S ions, so it is expected a greater potential energy. For the latter case, a connectivity calculation with 0.6 to 1.0 \AA tolerance for the size of the bond (strictly to 0.985 \AA , which is where the minimum $r > 0$ of the potential path shown) the resulting products are: H_2NOH and SO_2 ; as shown in Figure 7a.

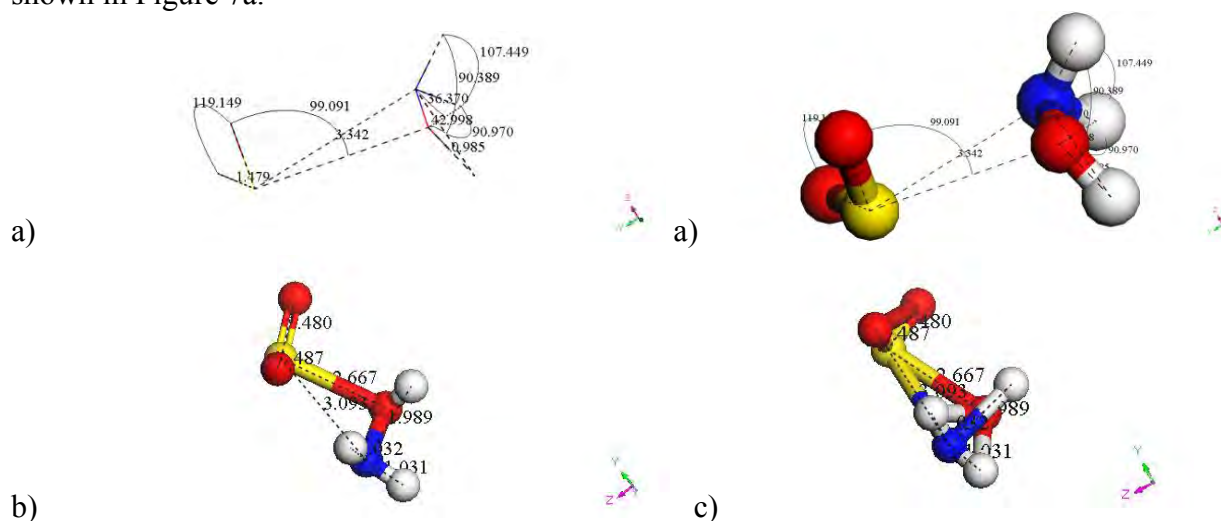


Figure 7. a) Chitosan-colorant (red 2) reaction products H_2NOH and SO_2 given a connectivity 0.6 - 1.0 \AA . b) Product H_2NOHSO_2 given a connectivity 0.6 - 1.51 \AA . c) Product H_2NOHSO_2 mostly linked of this reaction due to a connectivity between 0.6 to 1.91 \AA .

However, since the size of SO bond, originally (before geometry optimization) is 1.46 \AA , when making a connectivity calculation with a tolerance of 0.6 to 1.507 \AA for the size of the bond, we see an oxygen of ^-O_3S molecular ion is inserted into a bond NH ammonia molecule without breaking molecules, therefore one H_2NOHSO_2 molecule is obtained as shown in Figure 7b. That is, the entire colorant molecule is adsorbed to the chitosan molecule without altering the distances at which they grew as much a SO 3.093 \AA bond of the colorant as a NH 1.989 \AA bond of chitosan molecules after a geometry optimization, evidently the NH bond becomes NO 1.446 \AA and OH 0.987 \AA bonds with a NOH angle 108.2° , i.e. no oxygen is inserted between the NH bond in order to make a NOH linear molecule. Note that 1.5 \AA is still part of the potential well. So by making a connectivity calculation with a tolerance of 0.6 to 1.91 \AA for the bond size a molecule with the greatest number of bonds is obtained, as shown in Figure 7c. Since only after optimization an NH bond 1.989 \AA was obtained, this is not the actual molecule formed when the colorant molecule is added to chitosan.

The graph of the reaction path corresponds to the potential energy curve shown in Figure 8a. In this graph two minima occurred when moving ^-O_3S along the y-axis from infinity to an NH bond in the NH_3^+ molecule corresponding to cross the x-axis from positive values to negative values as observed Figure 8b.

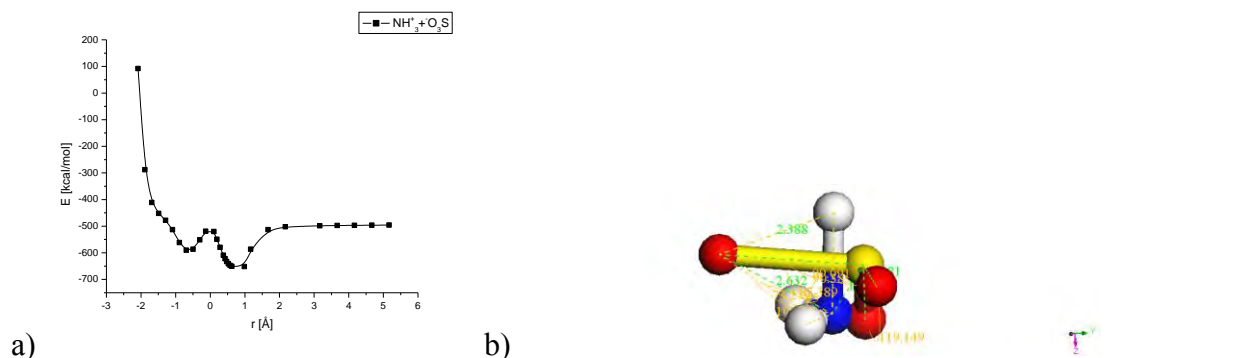


Figure 8. a) Potential energy curve of the NH_3^+ and ^-O_3S molecular interaction. b) Y-axis along which molecules move.

The minimum in r positive side corresponds to a equilibrium distance $R_e = -0.74\text{\AA}$, equilibrium energy $E_e = -650.4\text{ kcal/mol} = -28.2\text{ eV}$, and potential binding energy $V = 151\text{ kcal/mol}$. The other minimum, on the negative side of r corresponds to $R_e = -0.62\text{\AA}$, $E_e = -594.28\text{ kcal/mol} = -25.77\text{ eV}$ and $V = 99.05\text{ kcal/mol}$. The energy tends to infinity for $r < -2\text{ \AA}$ is evidently due to an interaction of one or more other atoms of the molecules, which are oxygen and nitrogen, as their nuclei are approaching directly in this orientation (see Figure 8b).

Conclusions

Analysis of the reaction sites with DFT shows a double potential well, which are two possible adsorption equilibria. In one of them, we observe a connectivity (or insertion) near to the size of the bond 1.5\AA larger than the original system $NH_3^+ + ^-O_3S$ to which corresponds colorant adsorption in chitosan; that is, the colorant achieve to break ammonia molecule to be inserted into an NH bond of the same. We evaluated this directly with DFT and Gauss's law of electrostatics, we obtained an error of about 25%. This comparison indicates that this is a physisorption. It is known that the Langmuir adsorption isotherms are usually best applied to chemisorption, however Bet or Kelvin adsorption isotherms work best for physisorption on microporous surfaces. In this paper a preliminary estimate of the pore diameter about 4 \AA was found. It is preliminary as this is an interaction of one ion with another different ion.

References

- [1] Á. Arango Ruíz, , & L.F. Garcés Giraldo, 2009. Remoción del colorante azoico amaranto de soluciones acuosas mediante electrocoagulación. *Lasallista de Investigación*, 6(2), pp. 31-38
- [2] C.I. Pearce, J.R. Lloyd, & J.T. Guthrie, (2003). The removal of color from textile wastewater using whole bacterial cells: a review. *ELSEVIER*, 58, pp. 179-196
- [3] S.L. Rodríguez Amézquita, (2008). Identificación y cuantificación de colorantes artificiales en refrescos en polvo elaborados y/o distribuidos en Guatemala. Tesis de Licenciatura Universidad de San Carlos, Guatemala
- [4] N. Sánchez, M. Vázquez y R. Torres (2010), “Degradación y adsorción del colorante AZO RR239 en solución acuosa, por partículas de hierro zero-valente a nanoescala, inmovilizadas sobre aserrín”, *Revista de la Facultad de Ing. de la Universidad de Antioquia*, No. 55, pp. 18-25.

- [5] A. Mittal, J. Mittal and L. Kurup (2006), “Adsorption isotherms, kinetics and column operations for the removal of hazardous dye, Tartrazine from aqueous solutions using waste materials—Bottom Ash and De-Oiled Soya, as adsorbents”, Department of Applied Chemistry, Maulana Azad National Institute of Technology, Bhopal 462 007, India
- [6] Wan Ngah, W.S., Teong, L.C. & Hanafiah, M.A.K.M. (2011). Adsorption of dyes and heavy metal ions by chitosan composites: A review. ELSEVIER. 83, pp. 1446-1456.
- [7] E.G. Tuesta, Vivas M., R. Sun, A. Gutarra (2005). “Modificación química de arcillas y su aplicación en la retención de colorantes”. Revista Sociedad Química de Perú; Vol. 71, No. 1, pp. 26-36.
- [8] B. Delley, J. Chem. Phys. 92 (1990) 508; J. Chem. Phys. 113 (2000) 7756
- [9] Quitina y Quitosano: obtención, caracterización y aplicaciones. Editado por Ana Pastor de Abram. Pontificia Universidad Católica del Perú / Fondo Editorial 2004.

RHEOLOGICAL CHARACTERIZATION AND MODELING OF A WATER BASED PERFORATION FLUID

A. Renteria¹, L. Medina-Torres¹, F. Calderas², O. Manero³, Antonio Sánchez-Solís³,
C. Lira-Galeana⁴

¹ *Departamento de Ingeniería Química, Facultad de Química, Universidad Nacional Autónoma de México, México D. F., 04510, MÉXICO*

² *Departamento de Ingeniería Química, Facultad de Estudios Superiores Zaragoza, Campus II: Batalla del 5 de mayo s/n, Col. Ejército de Oriente, Iztapalapa, Ciudad de México, D.F, 09230., MÉXICO*

³ *Departamento de Reología y Mecánica de Materiales Instituto de Investigaciones en Materiales, México D. F., 04510, MÉXICO.*

⁴ *Instituto Mexicano del Petróleo, Eje Central Lázaro Cárdenas 152, San Bartolo Atepehuacan, 07730 Ciudad de México, Distrito Federal*

Abstract

The rheological study of perforating fluids has been an issue of great interest because of their wide application in the petroleum industry such drilling, enhanced oil recovery, well completions, well workover and intervention. Characterization and prediction of the behavior of such fluid systems at the extreme conditions used in petroleum extraction is of paramount importance to optimize and prepare such systems for each type of well. In this study, a perforating fluid based on guar gum and sand was prepared and characterized using rheometric techniques at different temperatures. Master curves in oscillation and continuous flow were prepared from rheometric data. Results indicate that this complex fluid follows time-superposition principles in a reduced concentration range.

Introduction

Hydraulic fracturing is a stimulation treatment performed to restore or enhance the productivity of a well, especially on oil and gas wells in low-permeability reservoirs [1]. The treatment goal consists on create a highly conductive flow path between the reservoir and the wellbore by causing a vertical fracture to open. Perforation fluids are pumped at high pressure and rate into the reservoir interval to be treated. Fracturing fluids consists on a fluid base, and a small amount of a polymer designed to reduce friction pressure and improve the results of the stimulation. In order to keep the fracture opened, a proppant, such as grains of sand of a particular size, is added with the treatment fluid when the operation is complete [2].

Despite of the extensive use of this fracturing fluids, there is slight comprehension of their rheological behavior, mainly due to their complex nature and the particularities of the well to stimulate. In order to be able to modify their rheological properties for accomplish a better function and results of their use, first it is necessary to make a general characterization of their response under different flow situations.

In the present work, a common perforating fluid based on guar gum and sand were prepared and characterized in oscillation and flow tests at different temperatures.

Experimental

i) Perforating fluid preparation. The fluid base was set of a mixture of water, guar gum and reticular solution, and then it was mixed in a concentration of 1lbm sand/gal.

ii) Rheometric characterization. A strain sweep was made to identify the linear viscoelasticity interval. As well, a temperature ramp from 25°C to 80°C was performed in order to determine the fluid stability through temperature changes. Based on the previous tests result's, oscillation flow curves were obtained at 25°C, 35°C, 45°C and 55°C.

iii) Data manipulate. A master oscillation flow curve was constructed by taking account time temperature superposition principles.

Results and Discussion

Figure 1 shows the storage and loss modulus as a temperature function. Storage modulus G' decreases with an increase in temperature and loss modulus G'' follows the opposite fashion. As it was expected, the viscous behavior becomes predominant as the temperature growths. From this test, it is concluded that the fluid has a satisfactory stability between 20°C and 80°C.

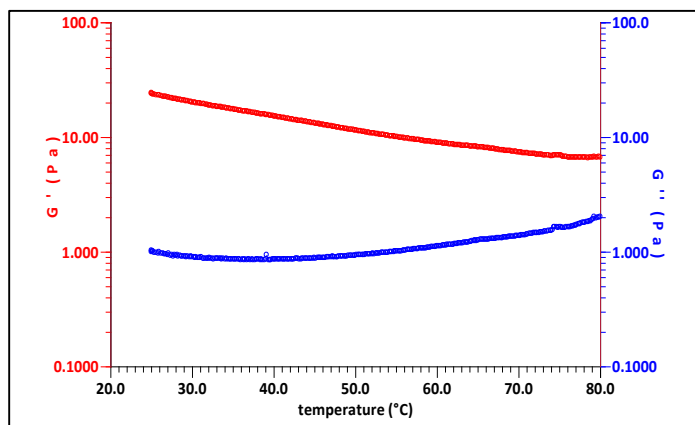


Figure 1. Storage and loss modulus vs temperature. Angular frequency = 5 rad/s and 3% strain.

According to the results on Fig. 1, temperatures selected to carry out oscillation flow curves were 25°C, 35°C, 45°C and 55°C. From these four curves, the master curve in Fig. 2 was constructed, obtaining the fluid viscoelastic behavior in an observation window from 100 to 10000 rad/s.

It is clear that the system elastic modulus is dominant over the loss modulus. This shows solid like behavior.

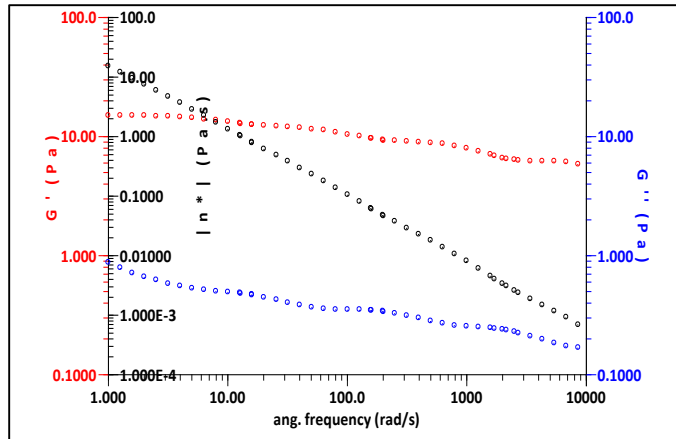


Figure 2. Master curve. Reference curve at 25°C and 3% strain.

Conclusions

A based water perforation fluid was characterized by rheometric techniques. Experimental rheometric data results at 25°C, 35°C, 45°C and 55°C were used to generate a master curve in oscillation flow; which, will be later modeled with a constitutive model for gel like behavior in a further work.

References

- [1] Schlumberger, "Oilfield Glossary," 2014. [Online]. Available: http://www.glossary.oilfield.slb.com/es/Terms/h/hydraulic_fracturing.aspx. [Accessed 08 2014].
- [2] Schlumberger, "Oilfield Glossary," 2014. [Online]. Available: http://www.glossary.oilfield.slb.com/es/Terms/f/frac_fluid.aspx. [Accessed 08 2014].

RHEOLOGICAL AND STRUCTURAL CHARACTERIZATION OF HYDROFOBICALLY MODIFIED POLYACRYLAMIDE SOLUTION OBTAINED BY EMULSION POLYMERIZATION

Valeria Jordana González Coronel,¹ Shirley Carro Sánchez,² Nancy Tepale Ochoa,¹ Judith Cabello Romero,³ José Victor Amador Noya,² Emmanuel Hench Cabrera¹

¹ *Facultad de Ingeniería Química, Benemérita Universidad Autónoma de Puebla, Puebla México, valeria.gonzalez@correo.buap.mx*

² *Facultad de Ciencias Básicas e Ingeniería, Universidad Autónoma de Tlaxcala*

³ *Departamento de Síntesis de Polímeros, Centro de Investigación en Química Aplicada, Coahuila, México.*

Abstract

Abstract: Previously synthesized polymeric structures, of the type water-soluble hydrophobically modified polyacrylamides with low amounts and N-alkylacrylamides. They have been synthesized using two initiators derived from hydrophobic 4'-azobis (4-cyanopentanoic acid) (ACVA), one of which contains linear chains of 12 and 16 carbon atoms. The synthesis was carried out via free radical in emulsion polymerization. Of such syntheses are polyacrylamides with hydrophobic groups both within the chain and to the ends of the water-soluble chain. Such structures have been called as "combined associative polymers", which have been studied and compared with multisticker associative polymers (with hydrophobic groups distributed along the chain) which were prepared with hexadecylacrylamide and dodecylacrylamide; and the (with hydrophobic groups on the chain ends) telechelic associative polymers prepared with the hydrophobically modified initiators. The viscoelastic properties of these three different associative polymers were investigated using steady-state experiments. The effect of the location and concentration of the groups in the viscosity of these associative polymers in solution was analyzed. All curves show three regimes depending on the concentration of two regimes in the semi-dilute range, the first unentangled, where the viscosity increases moderately and second entangled regime where the viscosity varies according to the power law.

Introduction

The hydrophobically modified polyacrylamides are widely used for their thickening power in aqueous media. Because of their outstanding rheological properties, these polymers have many industrial applications such as stabilizers, flocculants and absorbers in tertiary oil recovery, paint formulations, cosmetics, food, paper, drag reduction, controllers in drug delivery, biological / medical agents and superabsorbents.[1] Solutions of polyacrylamides tend to behave as pseudoplastic fluids in viscometric flows.[2] Unfortunately, conventional water-soluble polymers often suffer from a loss of efficiency in many industrial applications, which can involve drastic conditions such as: mechanical degradation of high molecular weight polymers under high shear rates [3]. Some of these disadvantages can be avoided using water-soluble polymers hydrophobically modified, also known as associative polymers.[4]. Associative polymers contain segments that have a tendency to associate in selective solvents. The segments may be randomly distributed along the chain (multisticker) or in the end (telechelic), Jimenez et al. [5] presented a new class of polymer with hydrophobic parts on the chain ends as well as along the macromolecular chain, called combined.

The association of such polymers in solutions has been studied extensively, which come from the hydrophobic interactions. These may be adjusted according to desired effects also depend on many parameters such as polymer concentration, the type and number of hydrophobic units, the location of the hydrophobic parts, molecular weight, temperature, influence of additives, the applied shear stress, etc. These associative polymers form clusters in aqueous solution according to the location

of the hydrophobic groups. If the polymers contain more than one associating block, these blocks may assemble either into the same core forming loops or into different cores forming bridges between the multiplets. The simplest case is that of telechelic polymers that contain associating blocks situated at the ends of the chains. The multiplets can derive from both intra and intermolecular interactions and their respective contribution is a function of the polymer concentration. REF

In this work, we describe a detailed study of the rheological properties in aqueous solutions of three different structures of hydrophobically modified polyacrylamides (telechelic, multisticker and combined) prepared by emulsion polymerization using two different hydrophobic groups linear, of 12 and 16 carbon atoms.

Experimental

Polymerizations

Batch inverse emulsion copolymerization were carried out at 80°C, using a thermostated water bath, in a 500 ml glass reactor equipped with thermometer and mechanical stirrer. Emulsion polymerizations continuous phase (51 wt%) was prepared dissolving in toluene the hydrophobic comonomer and surfactant (4.5% wt relative to monomer feed). Dispersed phase, 49 wt%, was prepared dissolving AM in water and added to organic phase. Total monomer concentration was varied, 1.5 or 4 wt%. Molar monomer relation was maintained as in solution polymerizations. Stirrer was adjusted at 600 rpm. After homogenization, once reached temperature reaction, the mixture was purged with nitrogen, at least 20 minutes before adding initiator, which had been previously dissolved in the continuous phase, 0.002 mol/L of toluene or acetonitrile, and heated to the temperature reaction. The reactions was carried out for 1 h.

The sample code of the copolymers refers to the hydrophilic monomers, hydrophobic monomers and the length of the hydrophobic initiator. For example, PAM-co-DAM/12 stands for a poly(acrylamide-co-dodecylacrylamide) using a linear initiator hydrophobically modified with a 12 carbons chain (C12). The characteristics of the samples investigated are given in Table 1. The chemical structure of the synthesized polymers is presented in the Fig. 1, are shown structures with hydrophobic groups, as modifications of hydrocarbon chains of 12 carbon atoms, for the other group of polymer chains 16C.

Table 1. Polymer Characteristics

Type	Polymer	[H](%mol)	Mv (g/mol)
Homopolymer	PAM		500000
Multisticker	PAM-co-DAM	0.80	530000
	PAM-co-HDAM	0.85	670000
Telechelic	PAM/12		590000
	PAM/16		ND
Combined	PAM-co-DAM/12	0.85	530000
	PAM-co-HDAM/16	0.82	ND

Results and Discussion

Steady Shear Flow Measurements. Figure 1 shows steady-shear viscosities of homopolymer PAM at various concentrations in water as a function of the shear stress. It is apparent that the viscosity increases with an increase of homopolymer concentration. All curves exhibit behavior predominantly Newtonian.

In the Figures 2 and 3 below a some polymer concentration ,the solution behaves as a Newtonian fluid, which means the associations of copolymer are mainly intramolecular. This is due to the chain contraction resulting from intramolecular associations. However, the flow curves exhibit non-Linear rheology behavior above a concentration of 1 wt %. These curves are distinctly separated into two parts, a high viscosity zone at low stress and a low viscosity zone at high shear rate.

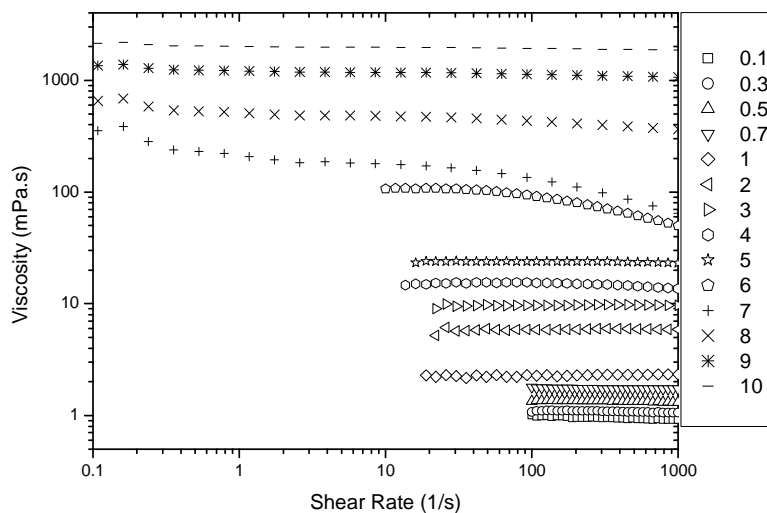


Figure 1. Variation of the viscosity as a function the shear rate for various Concentrations of PAM

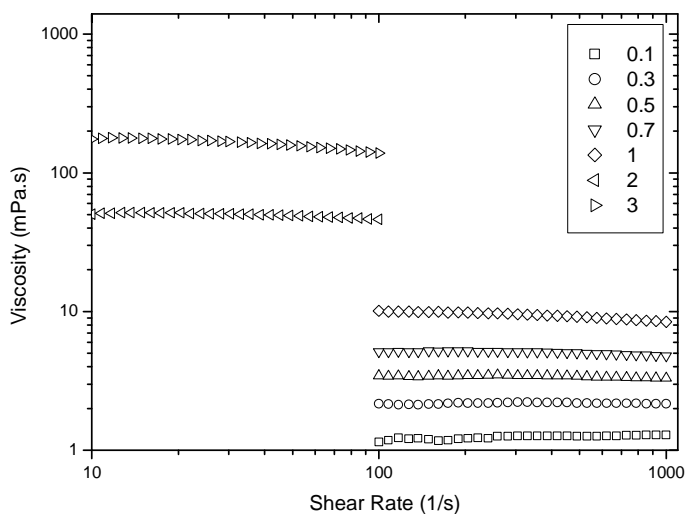


Figure2. Variation of the viscosity as a function the shear rate for various Concentrations of PAM-co-HDAM

Telechelic polymers do not show the a shear thickening behavior like is reported for this type of structure, see figure 3.

In the case of combined polymers have a shear thickening behavior very strong even at low concentrations, see Figure 4.

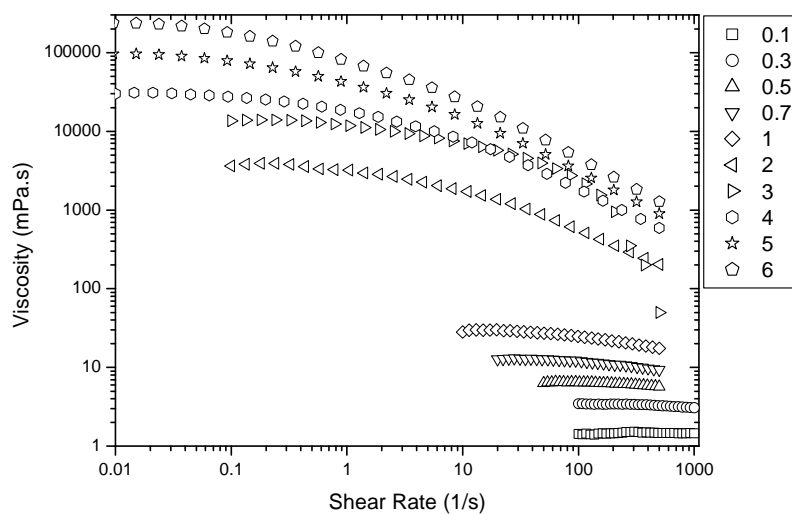


Figure 3. Variation of the viscosity as a function the shear rate for various Concentrations of PAM/16

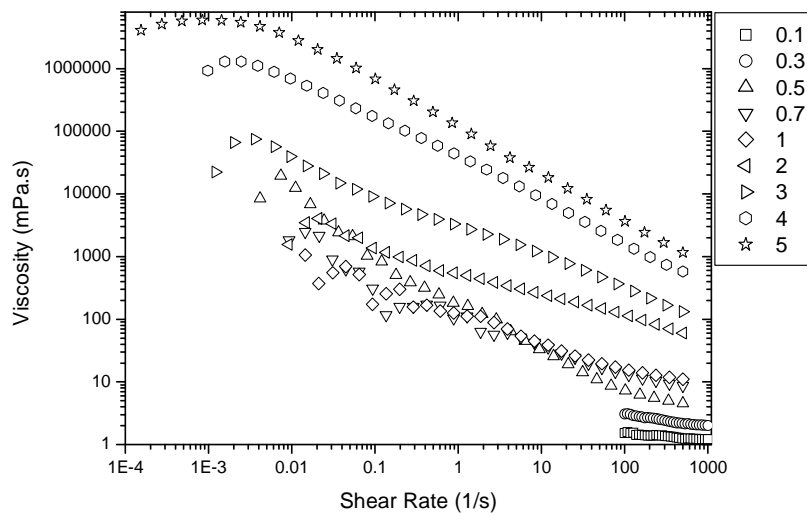


Figure 4. Variation of the viscosity as a function the shear rate for various Concentrations of PAM-co-HDAM/16

Conclusions

By this method of synthesis are obtained high molecular weight polymers. The incorporation of hydrophobic comonomers is high compared with other synthesis. These polymeric materials exhibiting high viscosities according to their molecular weight and concentration of hydrophobic groups. Regarding the location of hydrophobic groups results are consistent with those reported before.

Acknowledgements

At PRODEP for financial support to the Complex Fluids Thematic Network

References

Third US-Mexico Meeting "Advances in Polymer Science" and XXVII SPM National Congress
Nuevo Vallarta, December 2014

1. C. Lu, W.L., Y. Tan, C. Liu, P. Li, K. Xu, P. Wang, *Synthesis and Aqueous Solution Properties of Hydrophobically Modified Polyacrylamide*. J. Appl. Polym. Sci., 2014: p. 40754-40761.
2. Y. Y. Chieng, S.B.C., *Rheological study of hydrophobically modified hydroxyethyl cellulose and phospholipid vesicles*. J. Coll. Inter. Sci., 2010. 349: p. 236-245.
3. S. Hietala, P.M., S. Strandman , P. Jarvi , M. Torkkeli , and S.H. K. Jankova , H. Tenhu, *Synthesis and rheological properties of an associative star polymer in aqueous solutions*. Polymer, 2007. 48: p. 4087-4096.
4. C. Chassenieux, T.N., L. Benyahia, *Rheology of associative polymer solutions*. Current Opinion Coll. Interf. Sci., 2011. 16: p. 18-26.
5. V. J. González-Coronel , E.J.J.-R., *Synthesis, characterization and rheological properties of three different microstructures of water-soluble polymers prepared by solution polymerization*. Polym. Bull., 2009. 62: p. 727–736.

KINETIC STUDY OF THE THERMAL AND THERMO-OXIDATIVE DEGRADATION OF ETHYLENE-NORBORNENE COPOLYMERS

Helia Bibiana León-Molina, Mario Gutierrez-Villarreal, Ricardo Acosta

Centro de Investigación en Química Avanzada CIQA, Boulevard Enrique Reyna Hermosillo N° 140. C.P. 25253. Saltillo – Coahuila, México

Abstract

Thermal degradation and thermo-oxidation of ethylene-norbornene copolymers with cyclic structure contents of 30, 38 and 55 mol %, were studied. The kinetic parameters, thermodegradation order (n), activation energy (E_a), and pre-exponential factor (A) were determined using non-isothermal thermogravimetric analysis (TGA) and derivative thermogravimetric analysis (DTG). Flynn - Wall - Ozawa (FWO), Kissinger-Akahira- Sunose (KAS) and Friedman isoconversional methods were employed. The thermodegradation order was calculated using the Kissinger and Friedman methodologies, and was close to 1 for the copolymers tested. The E_a increased from 230 kJmol⁻¹ to 260 kJmol⁻¹, when the content of cyclic units was diminished from 55 to 30 mol %. DTG curves of the thermal degradation in nitrogen atmosphere shows a one step reaction, in contrast to the behavior of the thermo-oxidation. The presence of several peaks in thermo-oxidation evidenced a complex reaction mechanism, where more than one reaction or step occurred.

Key words: cyclic olefin copolymers, degradation kinetics, activation energy (E_a), pre exponential factor (A), reaction order (n).

1. Introduction

The cyclic olefin copolymers (COC) are synthesized using ethylene and norbornene monomers. The result is a material with cyclic units in the structural chain, which have transparency and low moisture absorption that make it interesting for packaging applications, so it is important to know its degradation behavior. Degradation of polymers can be characterized through its kinetic parameters and its reaction mechanism. The kinetic parameters are activation energy (E_a), pre-exponential factor (A) and reaction order (n). The techniques commonly used to study the kinetic parameters of a decomposition reaction are thermogravimetry (TGA) and differential thermogravimetry (DTGA). All the methods are based in the general equation for reactions in solid state.

$$\frac{d(\alpha)}{dt} = k(T)f(\alpha) \quad (1)$$

Where $\frac{d\alpha}{dt}$ is the decomposition rate [min⁻¹], $k(T)$ is the rate constant, α is the weight loss fraction and $f(\alpha)$ is a decomposition rate function. Using the Arrhenius equation to express $k(T)$. The equation 2 is obtained. Where A is the pre-exponential factor [min⁻¹], E_a is the apparent activation energy [Jmol⁻¹], T is the absolute temperature [K] and R is the ideal gas constant [8.314 JK⁻¹mol⁻¹]^[1, 2].

$$\frac{d\alpha}{dt} = A \times \exp\left(-\frac{E_a}{RT}\right)f(\alpha) \quad (2)$$

Separating the variables, rearranging and integrating expression 2, result in equation 3, where $g(\alpha)$ is the integral form of $f(\alpha)$, β is the heating rate, and T_0 is the temperature at the beginning of the non – isothermal experiment. The right side of the equation 3 is a series of infinite gamma functions, which cannot be exactly calculated, so different approximations have been used to express it^[1, 3].

$$g(\alpha) = \int_0^\alpha \frac{d\alpha}{f(\alpha)} = \frac{A}{\beta} \int_{T_0}^T \exp\left(-\frac{E_a}{RT}\right) dT \quad (3)$$

Some of the approximations used in the current research report are described in table 1

Table 1. Methods to calculate kinetic degradation parameters using DTG data.

Method	Mathematical expression	Considerations
Flynn – Wall – Ozawa (FWO)	$\log(\beta) = \log \left[\frac{AE_a}{g(\alpha)R} \right] - 2.315 - \frac{0.457E_a}{RT}$ (4)	Using Doyle approximation for the right side of (3) ^[4] .
Coats - Redfern	$\ln \frac{g(\alpha)}{T^2} = \ln \frac{AR}{\beta E} \left(1 - \frac{2RT}{E_a} \right) - \frac{E_a}{RT}$ (5)	Asymptotic approximation to the equation (3). Require the knowledge of the degradation reaction mechanism ^[1] .
Kissinger – Akahira – Sunose (KAS)	$\ln \left(\frac{\beta}{T^2} \right) = \ln \left(\frac{AR}{g(\alpha)E_a} \right) - \frac{E_a}{RT}$ (6)	Using the Coats – Redfern approximation and considering $\frac{2RT}{E_a} \ll 1$. ^[3]
Friedman	$\ln \left(\frac{d\alpha}{dt} \right) = \ln(Af(\alpha)) - \frac{E_a}{RT}$ (7)	Using the differential logarithmic expression (7) ^[3, 5] .
Pseudo First Order	$\ln \left(\frac{dW/dt}{W} \right) = E_a \left(-\frac{1}{RT} \right) + \ln A$ (8)	Differential logarithmic expression in which E_a is related to the weight loss rate ^[4] .

The described tools have been employed to determine degradation kinetic parameters of different polymers in nitrogen and oxygen atmospheres. The aim of the present work is to determine the kinetic parameters of the decomposition reaction of ethylene – norbornene copolymers, using TGA and DTG in nitrogen atmosphere and to contrast qualitatively the degradation behavior observed both in nitrogen atmosphere and in oxygen atmosphere.

2. Experimental

2.1. Materials

Ethylene Norbornene copolymers were purchased from TOPAS Advanced Polymers GmbH with 55%mol (COC55), 38%mol (COC38) and 30%mol (COC30) of cyclic units in the main chain and glass transition temperatures of 140 °C, 80 °C and 65 °C respectively, were employed.

2.2. Poly cyclic olefins Characterization

The cyclic structure content of the copolymers was determined by ¹³C NMR that was carried out on a Jeol 300 MHz JNM - ECO 300 Nuclear Magnetic Resonance apparatus, using CDCl₃ as solvent. A differential scanning calorimeter (DSC) TA Instruments Q200, was employed to determine the glass transition temperature. A heating rate of 10 °Cmin⁻¹ was used to heat the 9.0 x 10⁻³ g samples from 0 to 300 °C.

2.3. Thermogravimetric Analysis

The TGA and DTG and DTG analysis were performed in a TA Instruments TGA Q500. The 6.0 x 10⁻³ g samples were heated from 30 °C to 600°C at heating rates of β= 5, 7 10 and 15 °Cmin⁻¹ using nitrogen and oxygen as atmospheres and flows of 50 mLmin⁻¹ in each case. Tests were performed in duplicate to ensure repeatability. The kinetic parameters were calculated using as a base the DTG data and the methods FWO, KAS, Friedman, Coats - Redfern and Pseudo first order. In oxygen atmosphere, the DTG curves exhibited more than one peak, because of that data deconvolution was made using Origin 8.1 © and Peak fit 4.12 © software.

3. Results and Discussion

3.1. Thermal and structure characterization Ethylene – Norbornene Copolymers

The T_g of copolymers studied are shown in figure 1. As can be seen, T_g increase with the increment of cyclic units portion in the copolymer. This could be explained by the rigidity that cyclic units confer to the polymeric chain [6]. Shin and co-workers as well as Richie et al. [7], found similar tendency in T_g of ethylene – norbornene copolymers of the different compositions.

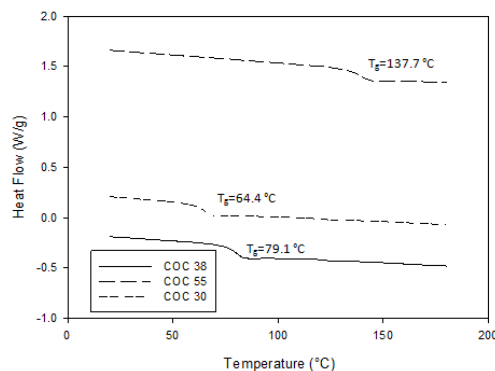


Figure 1. DSC of the Copolymers Ethylene Norbornene studied.

Figure 2 presents ^{13}C NMR spectra of the copolymers COC30, COC38 and COC55. Signal between 28 and 32 ppm correspond to C5 and C6 and overlap with those of the ethylene units. Signals that appear from 32 to 34 ppm are related to C7, while those between 40 and 42 ppm can be associated with C1 and C4. Finally, signals above 45 are assigned to C2 and C3 and give us more information about molecular microstructure. Signal between 46 and 47 ppm proportion of cyclic units decrease. Also, signals around 48 ppm increase when there are sequences of two or three cyclic units joined to ethylene sequences [4, 7, 8]. The ratio between the integrals of C1 and C4 signals and the signals related to the ethylene, make it possible to determine that the content of cyclic units in COC30, COC38 and COC55, were 29.1%mol, 37.6%mol and 54.8% mol respectively.

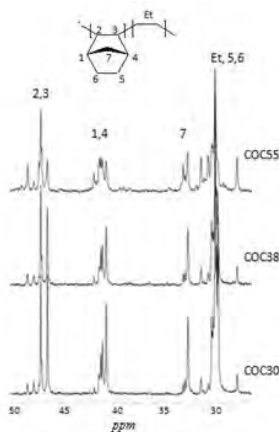


Figure 2. ^{13}C MNR of the Copolymers Ethylene Norbornene studied

3.2. Kinetic Parameters

The reaction orders obtained from the Kissinger and Friedman methods are presented in Table 2. It can be seen, considering the different heating rates, that all the copolymers tested, have n values close to one. As a consequence,

the dependent conversion function, $g(\alpha)$, can be taken as $-\ln(1-\alpha)^{[1]}$. The above was considered when analyzing the degradation reaction of the polymeric materials studied and to calculate the kinetic parameters E_a and A .

Table 2. Reaction orders of the COC30 COC38 y COC55 calculated using the Friedman and Kissinger methods.

Copolymer	β (°C/min)	Kissinger	Friedman
COC30	5	1.09	0.89
	7	1.05	0.99
	10	0.99	0.92
	15	-	-
COC38	5	1.07	0.95
	7	0.98	0.99
	10	0.94	0.84
	15	1.00	0.95
COC55	5	0.98	1.09
	7	0.96	0.96
	10	0.93	0.95
	15	1.01	0.90

Table 3 presents the E_a and A obtained from the processed DTG data through FWO, KAS, Friedman, Coats Redfern and Pseudo First Order methods (4 – 8). It can be noticed that the E_a increases with the decreases of norbornene content. The explanation of this behavior could be the effect of the tertiary carbons in the polymer structure, which are found in greater amount in copolymers with higher concentrations of norbornene. The hydrogens of tertiary carbons are more easily abstracted.

Another issue is related to the obtained values of E_a of the studied copolymers. It was found that by using the different methods, values of the same order of magnitude were achieved, however those obtained from isoconversional methodologies (FWO, KAS and Friedman) are almost half of those calculated by Coats Redfern and Pseudo first order. This phenomenon was observed for the PP and EPDM degradation and was associated with a large weight loss with high temperatures and a high degree of chain scission^[9]. It is important to notice that all correlation coefficients are above 0.97 so the mathematical models employed fit the studied behavior and the reported results are reliable.

Table 3. E_a and $\ln A$ of the decomposition of COC30, COC38 and COC55, calculated by FWO, Friedman, KAS, Coats - Redfern (CR) and Pseudo First Order (PFO) methods. For FWO, KAS and Friedman, average values are presented and for CR and PFO the heating rate was 5 °Cmin⁻¹

Method	COC30			COC 38			COC 55		
	E_a (kJ/mol)	$\ln A$ (min ⁻¹)	R ²	E_a (kJ/mol)	$\ln A$ (min ⁻¹)	R ²	E_a (kJ/mol)	$\ln A$ (min ⁻¹)	R ²
FWO	260.9	41.0	>0.98	247.6	39.1	>0.98	233.3	36.8	>0.99
Friedman	257.1	43.1	>0.90	249.1	44.7	>0.97	233.3	41.8	>0.97
KAS	262.7	41.2	>0.98	249.3	39.4	>0.98	231.6	36.8	>0.99
CR	490.8	81.2	>0.99	486.7	81.2	>0.99	438.6	73.3	>0.99
PFO	521.5	84.4	>0.99	490.3	80.1	>0.99	455.8	74.5	>0.99

3.3. Thermoxidation of Cyclic Olefin copolymers

Figure 3 depicts the weight loss rate versus the temperature during the decomposition of the COC55. In panel a, is displayed the behavior of the reaction in nitrogen atmosphere, while in panel b, is observed the degradative behavior in oxygen. The single peak curve in Figure 3a for the thermal degradation would correspond with a single step reaction while the multi peak curve of Figure 3b, evidenced a very complex degradation process with more than one

reaction occurring simultaneously. It can be seen that Peak 3 represents the predominant reaction that probably occurs during almost all the process and simultaneously with the rest of reactions taking place. With this premise, deconvolution of curve data was performed, the data pairs corresponding to the Peak 3 were used to apply isoconversional analysis methods and get E_a of 110 kJmol^{-1} and LnA of 19 min^{-1} .

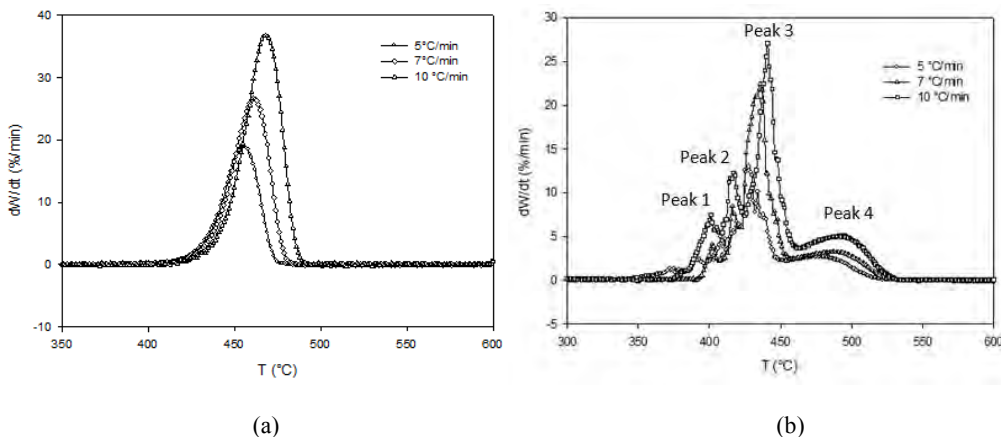


Figure 3. DTG curves of COC55. (a) Nitrogen atmosphere. (b) Oxygen atmosphere

Conclusions

As expected the T_g of the studied copolymers increased with the increment of norbornene in the main chain.

The reaction order of the degradation for the COC studied resins under nitrogen atmosphere is approximately of first order.

The tested copolymers in nitrogen atmosphere exhibit thermal stability above $400 \text{ }^{\circ}\text{C}$. The thermal stability order is $\text{COC30} > \text{COC38} > \text{COC55}$. It can be concluded that the presence of the tertiary carbons in the structure determine the thermal stability. The higher the concentration of this tertiary carbons, the lower the thermal stability.

The E_a for the thermal degradation of the copolymers tested are higher for those with lower content of norbornene. Their values calculated by isoconversional methods are between 230 kJmol^{-1} and 260 kJmol^{-1} .

The thermal degradation for the studied COC resins occurs in a single step reaction while the thermal oxidation presented a DTG multi peak curves that evidence a complex behavior with more than one reaction occurring simultaneously. Peak 3 of these curves represents the predominant reaction with E_a around 110 kJmol^{-1} .

Acknowledgments

The authors acknowledge to LCQ Ma. Guadalupe Méndez P. for her dedication at conducting thermal tests.

References

- [1] L. Barral, F. J. Díez, S. García-Garabal, J. López, B. Montero, R. Montes, C. Ramírez, and M. Rico, "Thermodegradation kinetics of a hybrid inorganic-organic epoxy system," *European Polymer Journal*, vol. 41, pp. 1662-1666, 2005.
- [2] T. C. K. Yang, S. S. Y. Lin, and T.-H. Chuang, "Kinetic analysis of the thermal oxidation of metallocene cyclic olefin copolymer (mCOC)/TiO₂ composites by FTIR microscopy and thermogravimetry (TG)," *Polymer Degradation and Stability*, vol. 78, pp. 525-532, 2002.
- [3] J. Woo Park, S. Cheon Oh, H. Pyeong Lee, H. Taik Kim, and K. Ok Yoo, "A kinetic analysis of thermal degradation of polymers using a dynamic method," *Polymer Degradation and Stability*, vol. 67, pp. 535-540, 2000.
- [4] C. Liu, J. Yu, X. Sun, J. Zhang, and J. He, "Thermal degradation studies of cyclic olefin copolymers," *Polymer Degradation and Stability*, vol. 81, pp. 197-205, 2003.
- [5] B. Jankovic, "Thermal characterization and detailed kinetic analysis of Cassava starch thermo-oxidative degradation," *Carbohydrate Polymers*, vol. 95, pp. 621-629, 2013.
- [6] R. Li, "Time-temperature superposition method for glass transition temperature of plastic materials," *Materials Science and Engineering: A*, vol. 278, pp. 36-45, 2000.
- [7] T. Rische, A. J. Waddon, L. C. Dickinson, and W. J. MacKnight, "Microstructure and Morphology of Cycloolefin Copolymers," *Macromolecules*, vol. 31, pp. 1871-1874, 2014/06/11 1998.
- [8] C. Delfolie, L. C. Dickinson, K. F. Freed, J. Dudowicz, and W. J. MacKnight, "Molecular Factors Affecting the Miscibility Behavior of Cycloolefin Copolymers," *Macromolecules*, vol. 32, pp. 7781-7789, 2014/06/24 1999.
- [9] C. Gamlin, N. Dutta, N. Roy-Choudhury, D. Kehoe, and J. Matisons, "Influence of ethylene - propylene ratio on the thermal degradation behaviour of EPDM elastomers," *Thermochimica Acta*, vol. 367 - 368, pp. 185-193, 2001.

THERMAL DECOMPOSITION OF PINACOLONE DIPEROXIDE (PDP) AND DIETHYL KETONE TRIPEROXIDE (DEKTP) IN METHYL METHACRYLATE AND ITS FURTHER POLYMERIZATION KINETIC STUDY

Karla Delgado Rodríguez,¹ Graciela Morales,^{1*} Javier Enríquez¹ and Gastón P. Barreto²

¹ *Síntesis de Polímeros. Centro de Investigación en Química Aplicada, Blvd. Enrique Reyna 140, C.P. 25294, Saltillo, México. *graciela.morales@ciqa.edu.mx*

² *Facultad de Ingeniería, Universidad Nacional del Centro de la Provincia de Buenos Aires. Avda. del Valle 5737, B7400JWI, Olavarría, Buenos Aires, Argentina*

Abstract

The thermal decomposition reactions of pinacolone diperoxide (PDP) and diethyl ketone triperoxide (DEKTP), in the temperature range of 110-140°C with an initiator concentration of 0.01 M were studied in pure methyl methacrylate (MMA). Furthermore, when PDP and/or DEKTP were used as initiators for the bulk polymerization of MMA, high molecular weights *c.a.* 400,000 to 1,200,000 g mol⁻¹ and conversions up to 99% were obtained, in relatively short polymerization time *c.a.* 30-60 min, depending on the initiator and the reaction temperature. Depending on the temperature used, the initiators can behave as multi-functional or classic radical initiators.

Introduction

Cyclic organic peroxides have gained great importance over the years due to their unusual reactivity. This can be explained by the relatively low energy of the O-O bond, ~45 kcal mol⁻¹, that makes them thermodynamically unstable compounds that can easily decompose by the homolytic cleavage of the peroxide bond, generating an intermediate bi-radical that in turn, can act as an initiator in the polymerization of vinyl monomers. This kind of initiators can give rise to higher polymerization rates and generate polymeric chains with higher molecular weights in comparison with the typically used noncyclic mono-functional peroxides.

There are numerous studies in the literature where it is evidenced that the thermal decomposition of this kind of peroxides is strongly affected not only by the respective ring substituents but also by the used solvent [1,2]. These studies revealed kinetic and thermodynamic data, mainly focused on the thermal decomposition, specially of PDP and DEKTP (Figure 1), in solution of different organic solvents [1-7] and mixtures of organic solvent-monomer (at a volume ratio of 50/50). Moreover, Barreto *et al.* reported the DEKTP thermal decomposition at 130°C in solutions 0.1 M and 1 M of MMA in ethylbenzene [7]. According to all these studies, and for the particular case of DEKTP, it has been demonstrated that it is thermally decomposed in solution by the homolytic cleavage of one of the O-O bonds, generating an intermediate bi-radical which can be, in later stages of the decomposition process, decomposed by different pathways [7].

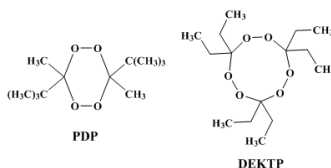


Figure 1. Structures of the cyclic peroxides PDP and DEKTP

However, reports related with the thermal decomposition and kinetic behavior of these cyclic multi-functional peroxides in the presence of a vinyl monomer as the solvent, are very limited.

On the other hand, both cyclic peroxides have been used for the bulk styrene (St) and MMA polymerizations yielding products at higher polymerization rates with elevated molecular weights [7,8]. In this study the decomposition of PDP and DEKTP in MMA is reported and their performances during MMA polymerization are evaluated and compared.

Experimental

Initiators Synthesis

PDP was prepared according to methods previously described in the literature [2]. The synthesis involves the reaction between 3,3-dimethyl-2-butanone and hydrogen peroxide (30% v/v) in sulfuric acid (70% v/v) at -15 to -20°C. DEKTP was also obtained according to methods reported in the literature [9]. Its synthesis involves the reaction between 3-pentanone and hydrogen peroxide (30 v/v) in sulfuric acid (70% v/v) at -15 to -20°C. The purity of the peroxides was confirmed by nuclear magnetic resonance (NMR) analysis.

Thermal decomposition of the initiators (PDP or DEKTP) in MMA

A stock solution of PDP or DEKTP 0.01 M in MMA was prepared with naphthalene (0.01% w/v) as an internal standard. The solution was transferred to pyrex glass ampoules to be thoroughly degassed under vacuum at -196°C (with liquid nitrogen) and then sealed with a flame torch. The ampoules were immersed in a thermostatic silicone oil bath stabilized at the selected temperature and they were withdrawn after predetermined times. The reaction was stopped by cooling the ampoules at 0°C. After that, the polymeric products were dissolved in THF and precipitated drop-wise over methanol (volume ratio 1:10). The polymer was decanted and the supernatant was analyzed by gas chromatography-mass spectrometry (GC-MS) using the internal standard method.

The pseudo-first order rate constant values (k_d) were calculated from the slope of the line obtained by a least mean square analysis of the experimental data by plotting the values of $\ln[\text{PDP or DEKTP}]$ concentration versus reaction time. The activation parameters were calculated using the Eyring equation (Equation 1):

$$\ln\left(\frac{k_d}{T}\right) = -\frac{\Delta H}{RT} + \frac{\Delta S}{R} + \ln\left(\frac{R}{N_A h}\right) \quad \text{Eq. 1}$$

where ΔH is the activation enthalpy, ΔS is the activation entropy, T is the temperature in K at which each constant (k_d) was determined, R is the general gas constant ($1.9872 \text{ cal mol}^{-1} \text{ K}^{-1}$), N_A is Avogadro's number ($6.023 \times 10^{23} \text{ mol}^{-1}$) and h is the Planck's constant ($1.5835 \times 10^{-34} \text{ cal s}^{-1}$).

Bulk polymerization of MMA initiated with PDP or DEKTP

Polymerization experiments were carried out in ampoules following the same degasification and reaction procedures previously detailed. The polymeric products were isolated by precipitation and dried under vacuum at room temperature until constant weight. Monomer conversion was determined gravimetrically and molecular weights were determined by size exclusion chromatography (SEC).

Analytical techniques

The PDP and DEKTP quantification in the solutions was carried out by GC-MS analysis in a BPX70 capillary column (70% cyanopropyl polysilphenylene-siloxane, 30 m, 0.25 mm I.D., 0.25 μm film thickness), installed in a Thermo Quest Trace 2000 GC model gas chromatograph with helium as the carried gas (1 mL min^{-1}) and injection port at 150°C in splitless mode. The detection was carried out with Finnigan Polaris Ion trap MS with transfer line at 210°C and ion source at 200°C.

The molecular weights of the polymer samples were determined by SEC at 40°C using a Hewlett-Packard instrument (HPLC series 1100) equipped with a refractive index detector. A series of three PLGel columns with porosities of 10^3 , 10^5 , and 10^6 \AA was used. Calibration was carried out with poly(methyl methacrylate) (PMMA) standards and THF (HPLC grade) was used as the eluent at a flow rate of 1 mL min^{-1} .

The PDP and DEKTP were characterized by ^1H and ^{13}C NMR using a JEOL Eclipse-300 MHz spectrometer. CDCl_3 was used as a solvent and the analysis were performed at room temperature.

Results and Discussion

Thermal decomposition of PDP and DEKTP. The kinetic studies of the thermal decomposition of PDP and DEKTP in MMA were carried out at 0.01 M, in the temperature range of 110 to 140°C (Table 1). The thermal decomposition reaction of PDP at the four different temperatures follows a pseudo first-order kinetic law up to at least 54% of the cyclic diperoxide conversion, meanwhile in the case of DEKTP it follows a pseudo-first-order kinetic law up to at least 52% of the triperoxide conversion.

The temperature effect on the k_d values (Table 1) can be represented by the Arrhenius equation in which the exhibited errors correspond to the standard deviations obtained through the kinetic data treatment with the least mean squares method (Equation 2 and 3 for PDP and DEKTP, respectively).

$$\ln k_d = -27.53 - \frac{2.68}{T} - (28,550 / 1066.69) \quad \text{Eq. 2}$$

$$\ln k_d = -25.13 - \frac{3.56}{T} - (26,741 / 1414.61) \quad \text{Eq. 3}$$

Table 1. Values corresponding to the thermal decomposition of PDP and DEKTP in MMA (0.01 M) at different temperatures

T (°C)	$k_d \times 10^5$ (s ⁻¹)	$t_{1/2}$ ^a (min)	PDP conv. (%)	r ^b	T (°C)	$k_d \times 10^5$ (s ⁻¹)	$t_{1/2}$ (min)	DEKTP conv. (%)	r
110	5.28	218.75	54	0.9949	110	4.50	256.6	55	0.9980
120	9.98	115.73	59	0.9953	120	9.87	117.0	52	0.9940
130	30.8	37.50	66	0.9983	130	33.48	34.5	70	0.9924
140	86.6	15.32	87	0.9972	140	50.64	22.7	72	0.9713

^a Half-life time

^b Linear correlation coefficient of the corresponding kinetics plots

The corresponding activation parameters, $\Delta H^\ddagger = 27.70 \pm 1.07$ kcal mol⁻¹ and $\Delta S^\ddagger = -4.45 \pm 2.68$ cal mol⁻¹ K⁻¹ in the case of PDP and, $\Delta H^\ddagger = 25.96 \pm 1.41$ kcal mol⁻¹ and $\Delta S^\ddagger = -9.14 \pm 3.55$ cal mol⁻¹ K⁻¹ for DEKTP, were obtained from the Eyring equation.

Comparing the reactivity of PDP and DEKTP in MMA, it can be observed that the $k_{d,PDP}$ is higher than the $k_{d,DEKTP}$ for all the evaluated temperatures. In order to explain this behavior, the different values of energy (i.e. variations in activation energies, activation enthalpies and entropies) were not considered due to their similar values (within the experimental error). However, the molecular arrangement of the initiators in the space has to be taken into account.

While both molecules are symmetrical and have a molecular arrangement in the space of the boat-chair type (most stable conformation), the conformational degrees of freedom of each molecule vary depending on the size of their substituents (see Figure 2). In the case of PDP, a substituted molecule with two tert-butyl (bulky groups), makes the molecule to restrict its conformational degrees of freedom (there is not twisting in the molecule and the possibility of only one conformer, according to studies by Molecular Dynamic). Thus, when PDP and MMA interact, it is difficult the rearrangement in the transition state due to the restriction in the mobility of PDP, which quickly leads to the scission of the O-O bonds, increasing the k_d values.

On the contrary, DEKTP molecule, a hexa-substituted molecule with ethyl groups, has greater conformational degrees of freedom (possibility of 350 conformers). Thus when DEKTP and MMA interact there is not difficulty to reach the transition state due to the greater degree of rotational and translational degree of freedom of DEKTP, whereby the DEKTP molecule is more stable and the scission of O-O bonds is less favored, justifying in this way the lowest k_d values.



Figure 2. Molecular boat-seat type arrangement in the space for PDP and DEKTP

MMA polymerization using PDP or DEKTP as initiators. Bulk polymerizations of MMA in the presence of PDP or DEKTP were carried out and the evolution of conversion and molecular weight as a function of time (Figures 3a and 3b, respectively) was evaluated. The peroxide concentration was in all cases 0.01 M and the temperature range was 110 to 130°C.

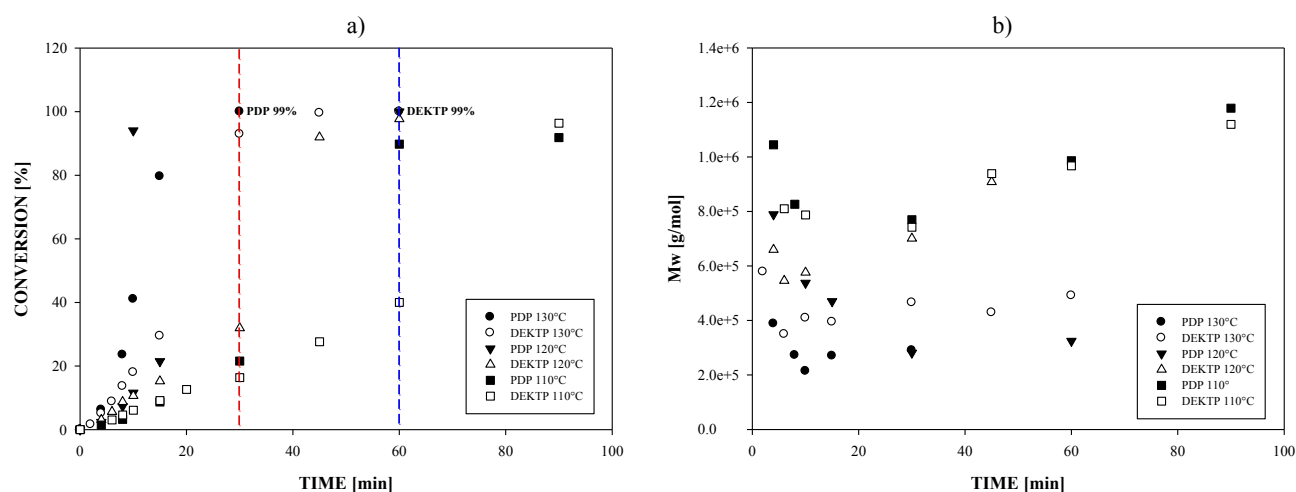


Figure 3. MMA bulk polymerization initiated with PDP or DEKTP at 110-130°C, a) conversion evolution, and b) molecular weight behavior as a function of reaction time

In both cases, the polymerization rate increases with temperature as expected, as a result of a higher radical concentration due to the faster initiators decomposition (Figure 3a). However, in the case of PDP, and at higher temperatures c.a. 130°C, the polymerization rate is higher than in the case of DEKTP which in principle can be attributed to the higher k_d of PDP. On the other hand, and as expected for a radical polymerization process, an increase in conversion results in a decrease in the molecular weights of the obtained materials (Figure 3b). However, at each evaluated temperature and especially at 120°C for PDP and 130°C for DEKTP, it can be observed an increase in molecular weight as polymerization reaction proceeds. On the contrary, at temperature of 130°C, in the case of PDP as the initiator, the molecular weight remains without changes throughout the polymerization.

The gradual increase in molecular weight during the polymerization can be justified considering the presence of O-O active sites once the initiators decomposed to form the initial intermediate bi-radical. So that, the initial growth can occur by addition of monomer molecules to the intermediate bi-radical and then the undecomposed O-O bonds within the polymer chains, re-initiate, propagate and terminate yielding polymers with high molecular weight. Meanwhile for the case of PDP at 130°C, the behavior is similar to that of a classical radical initiator.

Taking into account the above results, it was postulated a sequential scission mechanism for the O-O active sites of PDP during the MMA polymerization at 110-120 °C, meanwhile at 130°C a sequential-concerted decomposition mechanism could be postulated. In the case of DEKTP a sequential decomposition mechanism can be observed at the temperature range of 110-130°C.

On the other hand, the polymerization rates (R_p) were determined at low monomer conversions (less than 15%) for both initiators under the same experimental conditions described above (Table 2) and in accordance with the previous results obtained for the respective k_d 's, based on the conformational possibilities as well as the stability of the transition state, and the possibility of different decomposition mechanism with temperature, R_p for PDP evidences a higher increase with temperature and is higher than R_p for DEKTP, confirming all the above described.

Table 2. Polymerization rate values (R_p) calculated for MMA polymerizations initiated by PDP or DEKTP

Temperature (°C)	$R_p \times 10^{-4}$ (mol L ⁻¹ s ⁻¹) (PDP)	$R_p \times 10^{-4}$ (mol L ⁻¹ s ⁻¹) (DEKTP)
130	78.886	33.706
120	25.108	21.613
110	11.156	11.226

Conclusions

The differences in reactivity of PDP and DEKTP during MMA polymerization were interpreted taking into account their molecular arrangements in the space. On the other hand, PDP and DEKTP were effective initiators in the bulk polymerization of MMA, where the use of DEKTP as the initiator at 130°C allows MMA conversions ca. 99% in shorter periods of time (45 min) and a molecular weight increment behavior during the polymerization, due to a sequential decomposition mechanism at this temperature.

When PDP was used as the initiator, higher conversion values with lower molecular weights were obtained in comparison with DEKTP, and at temperatures above 120°C, its behavior is the typical of a classical radical initiator.

Acknowledgements

The authors would like to thank the Mexican National Council for Science and Technology (CONACYT) for Karla Delgado's scholarship granted 293911 and for the bilateral Cooperation México-Argentina Program through the Project N°190268, and to Pablo Acuña for his technical support in SEC analyses. Barreto is member of the Career of Scientific and Technological Research Council of the National Scientific and Technical Research (CONICET).

References

- [1]. A. I. Cañizo, Trends in Organic Chemistry, 11, 55 (2006).
- [2]. G. N. Eyler and A. I. Cañizo, Quimica Nova, 25, 364 (2002).
- [3]. G. N. Eyler, A. I. Cañizo, E. E. Alvarez and L. F. R. Cafferata. Anales de la Asociación Química Argentina, 82, 175 (1994).
- [4]. A. I. Cañizo, G. N. Eyler, G. Morales and J. R. Cerna, Journal of Physical Organic Chemistry, 17, 215 (2004).
- [5]. A. I. Cañizo, G. N. Eyler, C. M. Mateo, E. E. Alvarez and R. K. Nesprías, Heterocycles, 63, 2231 (2004).
- [6]. A. I. Cañizo and G. N. Eyler, Revista Latinoamericana de Quimica, 33/3, 103 (2005).
- [7]. P. Barreto and G. N. Eyler, Polymer Bulletin, 67, 1 (2011).
- [8]. J. R. Cerna, G. Morales, G. N. Eyler and A. I. Cañizo, Journal of Applied Polymer Science, 83, 1 (2002).
- [9]. G. N. Eyler, A. I. Cañizo, E. E. Alvarez and L. F. R. Cafferata. Tetrahedron Letters, 34, 1745 (1993).

Development of low shrinkage polymers by using expanding monomers

Ricardo Acosta Ortiz ¹, Marco Sangermano ², Amy Grace Savage Gomez ¹, Aida Esmeralda Garcia Valdez ¹, Maria Lydia Berlanga Duarte ¹

¹ Centro de Investigación en Química Avanzada, Blvd Enrique Reyna Hermosillo, 140, 25294. Saltillo, Coahuila, México

² Dipartimento di Scienza Applicata e Tecnologia, Politecnico di Torino, Cso. Duca degli Abruzzi, 24, 10129, Torino, Italia,

Abstract

In this review are presented the advances in the research related to the development of novel spiroorthocarbonates and the study of their performance to reduce or eliminate the shrinkage produced in the polymerization of epoxy and acrylic monomers

Key words: shrinkage, spiroorthocarbonate, epoxy polymers, acrylic polymer

1. Introduction

Shrinkage that occurs during the process of polymerization is often neglected. However, for certain applications that require dimensional stability is crucial to eliminate it or reduce it. The change in the bonding distance by passing from Van der Waals distance in the monomer (3.4 Å), to covalent distance in the polymer (1.54 Å), originates the shrinkage during the polymerization. Depending on the type of process of polymerization, the level of shrinkage could be as high as 50 % as in the case of polycondensation reactions, or as low as 3-5 % as in the case of ring-opening polymerizations. There has been reported several approaches to solve this problem, for instance, to use fillers in order to reduce physically the level of shrinkage, however, by doing so, a lot of stress is produced in the polymeric matrix, originating microvoids and microcrackings. Other method is to use prepolymers. As these species are partially polymerized, the level of shrinkage is reduced. The last approach is to use expanding monomers. These compounds polymerize with volume expansion. Spiro orthoesters (SOE) and spiro orthocarbonates (SOC) are the more studied expanding monomers. SOC are double cyclic acetals that polymerize under acidic catalysis but are stable under basic conditions. When these compounds polymerize by double ring opening polymerization poly (ether carbonates) are produced.

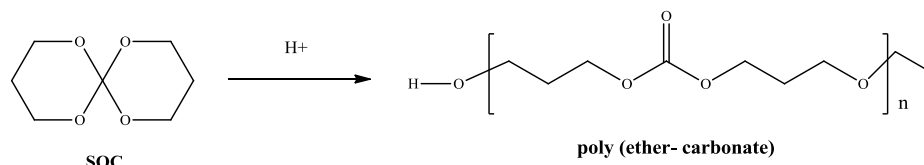


Figure 1. Cationic ring opening polymerization of a SOC

When added as additives to a formulation of epoxy or acrylic monomers, the flexibility of the produced poly (ether carbonates), reduces the shrinkage stress in the polymeric matrix.

Our research group has been engaged in the development of novel SOC, as the performance of these monomers exceeds that of the SOEs. In this paper we report our advances in this area

2. Experimental

In these studies were used epoxy monomers like the 3,4-epoxycyclohexylmethyl, 3', 4', epoxycyclohexancarboxylate (EP), and diglycidil ether of bisphenol A (DGEBA) as well as the oxetane monomer: bis[1-ethyl (3-oxetanyl)]methyl ether (OXT-221). The cationic photoinitiator (decyloxy phenyl)phenyl iodonium hexafluoro antimonate (DPPI) was used in all cases at 1 mol %. In the

case of the dental formulations were used the following dimethacrylate monomers: glycerolate of bisphenol A dimethacrylate (Bis-GMA), triethyleneglycol dimethacrylate (TEGDMA) and urethane dimethacrylate (UDMA). As radical photoinitiator was used the bis (2,4,6-trimethyl benzoyl) phenyl phosphine oxide (BAPO) at 1 mol % concentration; DPPI was also used at 1 mol %. In all cases the monomers were photopolymerized either with UV light as in the case of epoxy monomers or with visible light for the dental formulations.

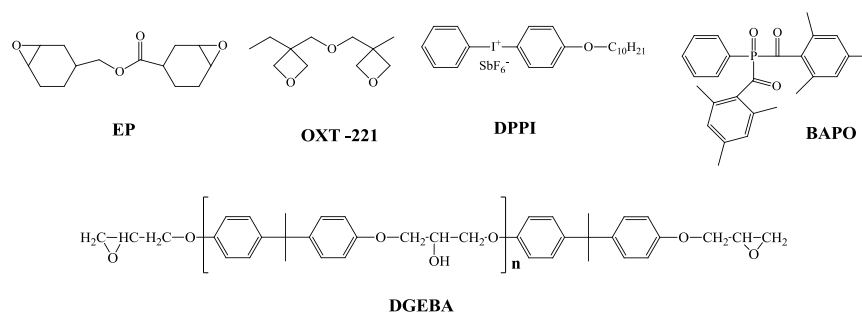


Figure 2. Chemical structure of all monomers and photoinitiators used in this study

3. Results

3.1. Functionalized SOC's

The structures of prepared functionalized spiroorthocarbonates I and II are shown in Figure 3. In these compounds our aim was to functionalize the spiroorthocarbonates with the same type of functional group of the base monomer, in order to get copolymers and in this way to enhance the performance of the SOC. For instance in the case of SOC I, this monomer was prepared through a series of reactions to introduce an epoxycyclo aliphatic group to the SOC, while in the case of monomer II, oxetane groups were attached to the SOC moiety. There were prepared formulations of EP with varying concentrations of monomer I (0-10 % w/w). It was found that at 10 % concentration of I there was an increase in the conversion of epoxy groups (70 %) in comparison with the blank sample (55 %) ^[1]. This effect is due to the flexibilizing effect that impart the poly (ether carbonates) generated in the polymerization of I, allowing higher mobility of the reacting cationic species. However, this flexibilizing effect brings as a consequence, a lower Tg temperature of the produced polymer in comparison with the blank sample. At the concentration of 10 % w/w not only was eliminated the shrinkage in the polymer, but volume expansion of 1.16 % in the resulting polymer was observed.

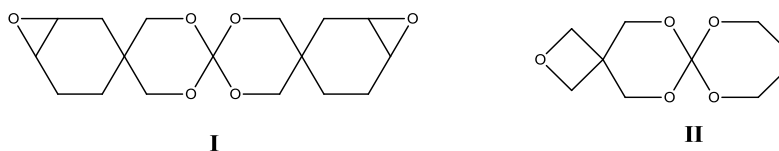


Figure 3. Chemical structures of functionalized SOC's

The presence of monomer II in a photocurable formulation 1:1 with OXT-221, enhanced the rate of photopolymerization of the oxetane monomer, achieving higher conversion than in the case of pristine OXT-221. This was due to the delay in the gelation of the high Tg of the formed network, by the presence of the poly (ether carbonates) produced in the polymerization of II. When a mixture 1:1 of monomer II and OXT 221 was assayed, it was observed zero shrinkage in the produced polymer ^[2].

3.2. SOC's that polymerize by ring opening and by the activated monomer mechanism

Other interesting spiroorthocarbonate monomers were prepared by a transesterification reaction of tetraethyl orthocarbonate with glycerol ^[3]. It was obtained a mixture 55:45 of compounds III and IV respectively, which could not be resolved and was used as such. In the case of the photopolymerization of EP with increasing concentration of a mixture 55:45 of III and IV as antishrinkage additives, it was found that the flexibility of the produced poly (ether carbonates), delayed the gelation of the polyethers generated in the cationic polymerization of EP, promoting an increase in the conversion of the epoxy groups, passing from 40 % for the

blank sample without SOC, to 75% when 20 mol % of the SOC were added to the formulation. The presence of the hydroxyl groups in the SOC resulted in an increase in the photopolymerization rate of EP, due to the involvement of the activated monomer mechanism. Additionally, it was observed that the elastic modulus increased due to crosslinking reaction induced by the bifunctionality of monomers III and IV. Shrinkage was reduced 88 % in comparison with a control sample.

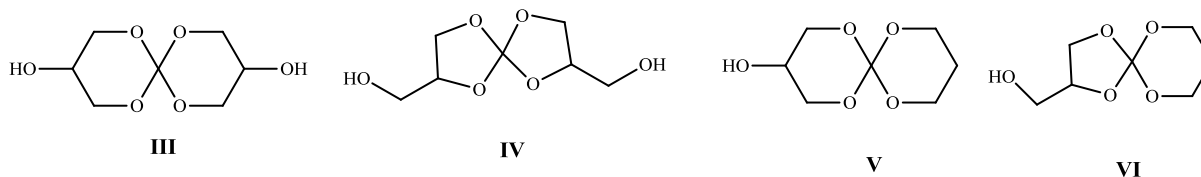


Figure 4. Chemical structures of hydroxy SOC

Monohydroxy SOC V and VI were also prepared by isolating the intermediate hemi spiroorthocarbonates of the reaction between glycerol and tetraethyl orthocarbonate and reacting them with 1,3-propanediol^[4]. In the case of the polymerization of EP with increasing concentrations of a mixture of V and VI, it was found that the shrinkage was reduced 40 % in comparison with a control sample. Regarding the elastic modulus, it was observed the opposite effect than in the case of formulations with III and IV, as it was found a decrease in the modulus as a result of the chain transfer reactions provoked by the presence of only one hydroxyl groups.

3.3. Bulky SOC

It was of interest to study the effect of introducing bulky groups to the SOC. It was prepared a cyclododecane functionalized SOC^[5]. Though the synthesis of this compound involved four stages, it was found that by introducing this bulky groups to the polyether carbonates formed in the ring opening polymerization of the SOC, not only was eliminated the shrinkage but a level of expansion of 5 % was obtained when the SOC VII was added at 8 mol % to the monomer EP. It was found that this concentration was the limit of solubility in the base monomer. It was also observed a shift in the Tg passing from 141 °C for the control sample without the SOC to 114 °C when VII was added at 8 mol %.

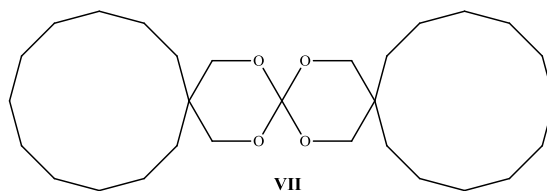


Figure 5. Chemical structure of a bulky SOC

3.4. Tetrafunctional SOC

Once that SOC V and VI were prepared, they were useful as a building block to prepare multifunctional SOC. The tetrafunctional SOC VIII and IX were prepared by reacting SOC V and VI with carbon tetrabromide in basic medium^[6].

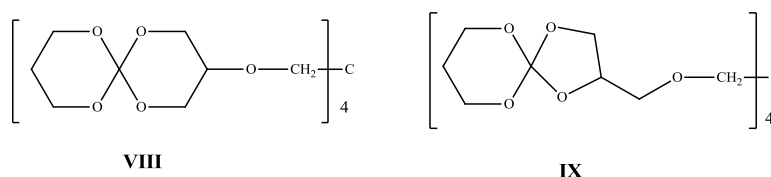


Figure 6. Chemical structures of tetrafunctional SOC

By using this monomers VIII and IX, in the photopolymerization of the EP monomer, in concentration as low as 5 mol %, it was observed an expansion level of 0.26 %, that increased to 2.16 % when the concentration of the mixture of VIII and IX was 7 mol

%. As the concentration level required of VIII and IX, to eliminate the shrinkage in polymers of EP, was relatively low, the viscoelastic properties of the formulated polymer were fairly preserved in comparison with a control sample without SOC. This effect can also be explained by the crosslinking induced by the tetrafunctional SOC.

3.5. SOC with photosensibilizing fluorene groups

Due to the fact that the cationic photoinitiator DPPI used to polymerize the SOC by ring opening, only undergo photolysis with UV light, it was thought that by introducing photosensitizers groups like fluorene, in the SOC, these groups could photosensitize the photolysis of DPPI, using visible light. The monomer IX was prepared by a transesterification reaction of 9H-fluorene-9, 9-dimethanol with tetraethyl orthocarbonate ^[7]. When this monomer was added at 10 mol % to a formulation with DGEBA, it was observed volume expansion of 0.19 %. Due to the presence of aromatic rings in DGEBA, it was not possible to photopolymerize it with visible light, but indeed, it was observed photopolymerization with visible light, changing the monomer to EP, which is an epoxycycloaliphatic monomer. In this monomer was also eliminated the shrinkage by using 10 mol % of SOC X.

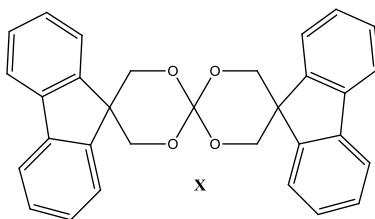


Figure 7. Chemical structure of fluorene SOC X

3.6. Reducing the shrinkage in dental resins

One of the main problems in polymeric dental restorative materials is the shrinkage that occurs during the polymerization of the dimethacrylate monomer used in this application. Shrinkage results in debonding between the tooth and the dental resin, originating microchannels. These bring as a consequence, secondary caries in the already restored tooth. We prepared monomers XI, XII with the aim of anchoring the SOC moiety in the acrylic network by the reaction of the allylic groups with the acrylic macroradicals ^[8]. These monomers were added as mixture 45:55 respectively, to a dental formulation with BIS-GMA:TEGDMA:UDMA 50:30:20 respectively, using DPPI as cationic photoinitiator at 1 mol % and BAPO also at 1 mol %. Here both, radical polymerization of the dimethacrylate groups as well as the cationic polymerization of the SOC proceeded simultaneously.

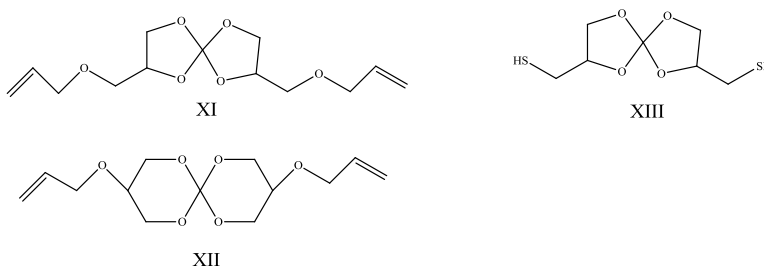


Figure 8. Chemical structures of SOC for dental resins

It was found that by adding increasing concentrations of the mixture XI and XII, the conversion of the dimethacrylate groups was enhanced, achieving 65 % conversion when 20 mol % of the mixture of SOC was added to the dental formulation, in comparison with 50 % for the control sample without SOC. The shrinkage was reduced 52 % when 20 mol % of XI and XII was added to

the dental formulation. Additionally, it was found an improvement in the mechanical properties of the obtained polymer due to the increase in the crosslink density originated by the ring opening polymerization of the SOC's.

Another approach to reduce the shrinkage of the acrylic network in the dental resin was to anchor the SOC moiety by means of thiol groups. These groups can react with the dimethacrylate monomers by means of the thiol-ene mechanism. Monomer XIII was prepared by transesterification reaction of 1-thioglycerol with tetraethyl orthocarbonate ^[9]. Here, it was also found an augment in conversion by adding increasing concentrations of monomer XIII, achieving 60 % conversion of the dimethacrylate groups with 30 mol % of XIII, against 45 % conversion of the control sample. The mechanical properties of the resulting materials were also improved by the further crosslinking attained by the cationic ring opening polymerization of the SOC. Shrinkage was reduced 60 % by using 30 mol % of XIII in the dental formulation.

4. Conclusions

Different types of SOC's were prepared with the aim to reduce or eliminate the shrinkage in the photopolymerization of epoxy and dimethacrylate monomers. Several approaches like attaching functional groups to the SOC moieties in order to enhance their performance when added to epoxy or oxetane monomers, or to increase the bulkiness, or photosensitivity of this monomers, were essayed with excellent results. Also, were evaluated SOCS functionalized with allylic or thiol groups in order to attach the SOC moiety to the acrylic network in dental resins, resulting in a decrease of the shrinkage and an improvement in the mechanical properties of the resulting materials.

Acknowledgments

The authors thank the Mexican National Council of Science and Technology (CONACYT) for funding the project 151489. Assistance in analysis and determination of mechanical properties of samples by Guadalupe Mendez, Judith Cabello, Jorge Felix Espinoza, Jose Luis Saucedo, and Francisco Zendejo is gratefully acknowledged

References

- [1] M. Sangermano, R. Acosta Ortiz, B.A. Puente Urbina; M.L. Berlanga Duarte; A.E. Garcia Valdez; R. Guerrero Santos; Synthesis of an epoxy functionalized spiroorthocarbonate used as low shrinkage additive in cationic UV curing of an epoxy resin; *European Polymer Journal*, 44, 1046-1052, (2008)
- [2] M. Sangermano, S. Giannelli, R. Acosta Ortiz, M.L. Berlanga Duarte, A.K. Rueda Gonzalez, A.E. Garcia Valdez; Synthesis of an Oxetane functionalized Hemi spiro ortho carbonate used as low shrinkage additive in cationic UV Curing of Oxetane Monomers; *Journal of Applied Polymer Science*, 112, 1780-1787, (2009).
- [3] R. Acosta Ortiz, M. L. Berlanga Duarte, A.G. Savage Gomez, M. Sangermano, A.E. Garcia Valdez; Novel Diol spiroorthocarbonates derived from glycerol as anti-shrinkage additives for the cationic photopolymerization of epoxy monomers; *Polymer International*, 59, 680-685, (2010)
- [4] R. Acosta Ortiz*, M.L. Berlanga Duarte, A.G. Savage Gomez, M. Sangermano; The effect of hydroxy-spiroorthocarbonates on the cationic photopolymerization of an epoxy resin and on the mechanical properties of the final polymer; *Polymer International*, 61, 587-595, (2012)
- [5] R.I. Lozano Palacios, BSc Thesis of Instituto Tecnológico de Saltillo, "Síntesis y caracterización de un nuevo monómero ortoespirocarbonato a partir de la ciclododecanona como agente antiencogimiento para la fotopolimerización catiónica de un monómero epoxi-cicloalifático", november (2011)
- [6] R. Acosta Ortiz, M. L. Berlanga Duarte, A.G. Savage Gomez, M. Sangermano, M. Perez; Novel tetraspiroorthocarbonates as successful antishrinking agents for the photopolymerization of epoxy monomers; *Journal of Macromolecular Science: part A. Pure and Applied Chemistry*, A49 (4), 361-368, (2012)
- [7] R. Acosta Ortiz, M. L. Berlanga Duarte, J. L. Robles Olivares, M. Sangermano; Synthesis of the fluorene spiroorthocarbonate and the evaluation of its antishrinking activity in the cationic photopolymerization of an epoxy resin, *Designed Monomers and Polymers*, 16 (4), 323-329, (2013)
- [8] R. Acosta Ortiz, L. A. Reyna Medina, M. L. Berlanga Duarte, L. Ibarra Ssamaniego, A.E. Garcia Valdez, Z. L. Garcia Mendez, L. Mendez Gonzalez; Synthesis of glycerol-derived diallyl spiroorthocarbonates and the study of their antishrinking properties in acrylic dental resins, *J. Mater. Sci.: Mater. Med.*, 24, 2077-2084, (2013)
- [9] R. Acosta Ortiz, A.G. Savage Gomez, M.L. Berlanga Duarte, A.E. Garcia Valdez, The Effect of a dithiol spiroorthocarbonate on mechanical properties and shrinkage of a dental resin, *Designed Monomer and Polymers*, DOI 10.1080/15685551.2014.947555, (2014)

DEGRADATION AND CHARACTERIZATION OF POLYETHYLENE TEREPHTHALATE (PET) FOR THE ELIMINATION OF LEAD (II) IN WATER.

Jesús Daniel Estrada Flores,¹ Nancy Adriana Pérez Rodríguez,² María Guadalupe Sánchez Anguiano,³ Perla Elizondo Martínez,⁴ Javier Rivera de la Rosa⁵

Universidad Autónoma de Nuevo León, UANL, Facultad de Ciencias Químicas, Av. Universidad S/N, Ciudad Universitaria, San Nicolás de los Garza, Nuevo León, C. P. 66451, México. Tel. 81-83294000

Abstract

In this work the adsorption capacity of the degradation product was evaluated polyethylene terephthalate (PET), deposited on metal spheres of a diameter of 2-4 mm using the technique of liquid-phase deposition. The oligomer was obtained by the degradation of PET with triethylene, the pH_{pzc} determined and was characterized by FTIR and GPC. The coated spheres were characterized by SEM and swelling studies. Ion adsorption Pb (II) was analyzed at different experimental conditions (metal concentration, pH, time). The Pb²⁺ ion adsorption reached a plateau at pH 6 at a concentration of Pb (II) 700 mg / L.

Introduction

The availability of good quality drinking water is vital to human life; however, the nature of today's consumer society has led to an exorbitant increase of pollutants emitted to the environment, among which you can find the heavy metals from a variety of activities such as mining, oil combustion, industrial processes, etc. Which are adsorbed on the floor incorporated into rivers and lakes water quality deteriorated.

One of the techniques used for the removal of these metals in water is adsorption which depends on temperature, pH and removal capacity of the adsorbent material. This technique has the advantage of easy operation, it is highly effective at very low concentrations of metal and does not generate sludge. In recent decades have been used polymers with functional groups capable of interacting with these metal ions present in water by ion competition. One material that can be used are low molecular weight polyesters which are obtained as partial degradation products of poly ethylene terephthalate (PET), which is a material used extensively in the manufacture of packaging and textiles.

Given the above, this research is intended to use a degradation product of PET to coat the surface of cellular materials and assessing the ability of removal to the Pb (II) ion present in water.

Experimental

Degradation: In a 3-necked flask 250 mL 32 g of triethylene glycol and PET, 0.05 stannous chloride and zinc stearate was added. Was stirred for 3.5 h at a temperature of 195 ° C. Subsequently washed with water at 70 ° C to remove residues of glycols and put on the stove for 24 h at 90 ° C. After drying, the product was characterized by infrared (FTIR) and gel permeation chromatography (GPC). Will finally determine the point of zero charge to the material.

Coating: First spheres coated previously weighed pickled and degreased. The oligomer is heated around 90 ° C and once the temperature reached was added ethanol at 70 ° C approximately 15 mL to disperse the

oligomer, when the solution is dispersed enough spheres were introduced for 5 minutes and then extracted to carry them to dry for 24 hours at 90 ° C.

Adsorption tests: Were carried out using a mass of 0.05 g oligomer added to flasks with 100 mL solution of $\text{Pb}(\text{NO}_3)_2$ with concentrations (10 -1000 mg/L). After, the flask was kept under stirring at 120 rpm, pH 6 (I present best pH adsorption capacities) for 2 h. The temperature was controlled at 25 ° C using a thermometer 250 ° C. The product was filtered and taken to analysis by Atomic Absorption Spectroscopy and its adsorption capacity calculated from the equation:

$$q = \frac{(C_0 - C_t)V}{M}$$

Q = Maximum adsorption capacity (mg / g).

C₀ = Concentración inicial (mg / L).

C_e = Cocentración equilibrium (mg / L).

V = Volume of solution (L).

M = Masadel adsorbent (g).

Results and discussion

In Figure 1 the oligomer was observed FTIR, where bands are shown characteristics of a polyester resin (Table 1), with the exception of the band at 3400 cm^{-1} corresponding to the OH groups it does not appear in the spectrum of PET without degrading, this signal increases because the OH groups from the TEG become part of the backbone of the oligomer in place of ethylene glycol so that the chain end groups contain more especially OH.

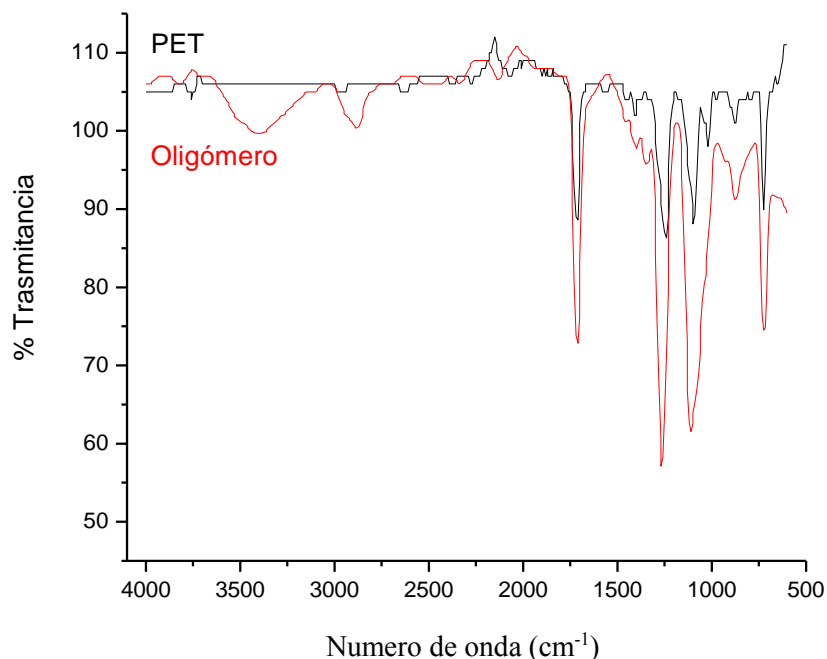


Table 1. Major Signs of the FTIR spectrum of the oligomer.

Longitud de onda cm^{-1}	Grupo
3400	OH
2900	C-H metilenos
1700	C=O carbonilo
1150	C-O Ester
600	Aromáticos

Figure 1. FT-IR spectrum of PET oligomer.

In the SEM images shown in Figure 2 the outer surface of the uncoated and coated areas were seen, shows that the polymer is deposited correctly, could also check the presence of the oligomer on the surface of the sphere forming a coating according to the EDS analysis shown in Tables 2 and 3, making possible its foray into the area of removal of metals from aqueous solutions.

Table 2. EDS analysis sphere uncoated

Element	Wt%	At%
CK	05.14	19.48
FeL	43.13	35.12
NiL	27.02	20.94
AlK	01.83	03.08
SiK	01.88	03.05
CrK	20.25	17.72
MnK	00.75	00.62
Totals	100.00	

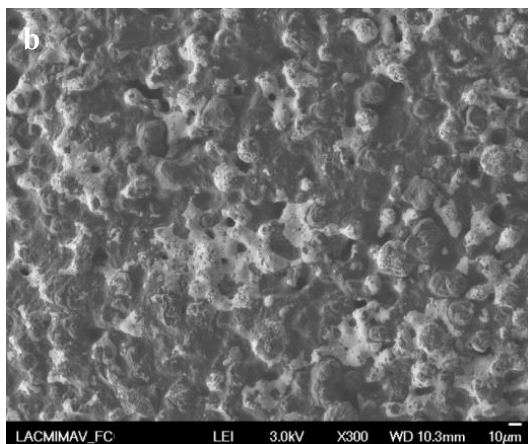
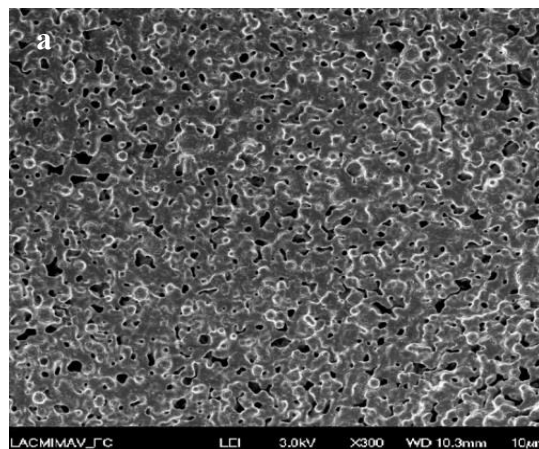


Table 3. EDS analysis sphere coated

Element	Weight%	Atomic%
C K	51.56	70.03
O K	21.55	21.98
Si K	0.41	0.24
Cr K	3.79	1.19
Fe L	18.11	5.29
Ni L	4.58	1.27
Totals	100.00	

Figure 2. SEM micrograph of sphere a) uncoated and b) covered.

With regard to GPC analysis oligomer conducted to observe the effect on the molecular mass distribution. Figure 3 and Table 4 indicate the results of the molecular mass of the product is 884, indicating that the polymer chain degradation starting PET short chains breaking containing 5 repeating units, also you can see the poly dispersity equal to 2.26 attributable to the different sizes of chain that are the product of degradation.

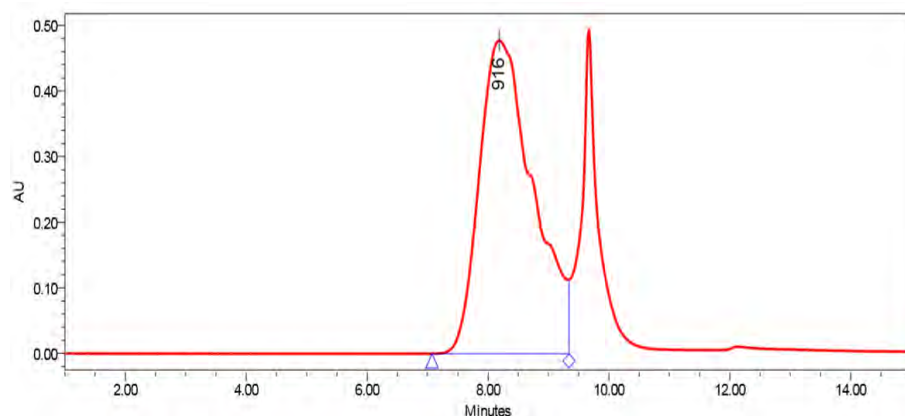


Table 4. GPC Parameters.

Tiempo (min)	8.18
Mn	390
Mw	884
Mp	916
PD	2.26

Figure 3. GPC analysis of PET oligomers.

Moreover, in Figure 4 the determination pH_{pzc} oligomer was observed, which has a net surface charge in a solution at pH 7.0, which leads us to assume that values above pH pH_{pzc} oligomer surface acquires a net negative charge and a net positive charge at below pH_{pzc} values.

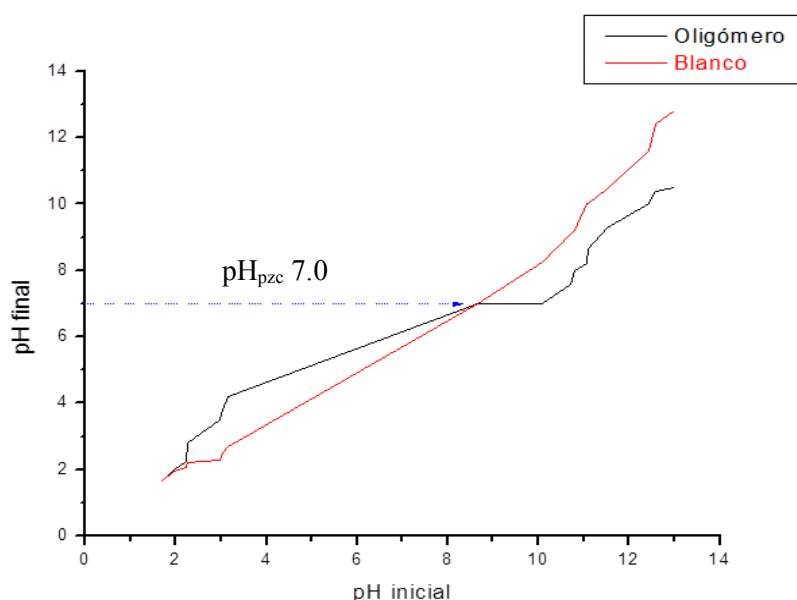


Figure 4. The pH_{pzc} determination to the oligomer solution (initial pH value; final pH value).

From the experimental data obtained in the curve of maximum capacity for Pb^{2+} shown in Figure 5, a maximum capacity of 309.32 mg / g at an initial concentration of 700 mg / L was obtained. From these data

were analyzed by the Langmuir model and Freundlich isotherms. The adsorption isotherm was best described by assuming a monolayer adsorption Freundlich where the value increases to reach that corresponding to the saturation monolayer formation.

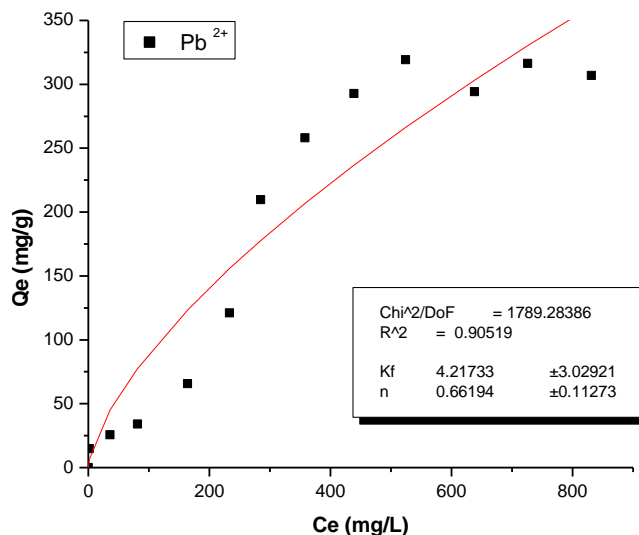


Figure 5. Maximum capacity curve of Pb^{2+} oligomer, pH 6 contact time of 2 h at 150 rpm.

Conclusions

As a result of degradation by glycolysis of PET, low molecular weight oligomers are obtained and as many OH terminations according to the infrared spectrum and GPC. Was achieved by coating the metal spheres the technique of liquid phase deposition as shown in the images obtained by SEM. According to the model Freundlich, the physical adsorption is multilayered and has reached its maximum capacity of 309 mg / g for Pb^{2+} .

Acknowledgements

The authors acknowledge the support of the CONACYT (03-6375-QMT-08-005) and the Faculty of Chemistry (UANL). Jesus Daniel Estrada Flores, thank CONACYT-Mexico for the scholarship for graduate study.

References

- [1] H. Jabeen, K. C. Kemp, V. Chandra. Journal of Environmental Management, 130, 429-435 (2013).
- [2] J. Wang, Li Xu, Cheng, Y. Meng. Chemical Engineering Journal, 193-194, 31-38 (2012).
- [3] Y. Meng, J. Wang, Li Xu, A. M. Li. Chinese Chemical Letters, 23, 496-499 (2012).
- [4] M. Najafi, Y. Yousefi, A. A. Rafati. Separation and Purification Technology, 85, 193-205 (2012).
- [5] J. Gong, X. Wang, X. Shao, S. Yuan. Talanta, 101, 45-52 (2012).

PREPARATION AND CHARACTERIZATION OF A THERMOPLASTIC MATRIX OF POLY-EPSILON-CAPROLACTONE WITH CHITOSAN FOR REMOVAL HEAVY METALS FROM WASTEWATER

Oscar Velasco¹, Miquel Gimeno³, Ricardo Beristain², Ricardo Rosas¹, Keiko Shirai^{1*}

¹ Universidad Autónoma Metropolitana, Biotechnology Department, Laboratory of Biopolymers. Av. San Rafael Atlixco No. 186. Col. Vicentina. C.P. 09340. México City

² Universidad Autónoma Metropolitana-Lerma. Departament of Land Resources. Hidalgo Poniente No. 46, Col. La Estación, C.P. 52006, Lerma de Villada, Estado de México

³ Depto. de Alimentos y Biotecnología. Facultad de Química. Universidad Nacional Autónoma de México. 04510 México DF.

*E-mail: smk@xanum.uam.mx

Abstract

This work aims to report a thermoplastic composite based on a matrix of poly- ϵ -caprolactone (PCL) (Mn 29.5 kDa), which was enzymatically synthesized using immobilized *Candida antarctica* lipase B (CALB) in a nontoxic compressed fluid media and chitosan (Ch) (degree of acetylation of 6.80% and Mv of 121.2 kDa), which was produced by mixing in an extruder. The product is moldable, reusable and biodegradable and it is useful to remove heavy metal contaminants as copper in wastewater treatment. The PCL:Ch ratio under study in this work were 1:1 and 5:1. The removal capacities of copper metal of the materials are presented.

Introduction

In the last decades of the past century the development, management and application of biodegradable materials has been a paradigm. The efforts have been directed toward synthesis of biodegradable polymers with certain characteristics to be applied specific areas.¹

Among these research areas, those focused to solve environmental problems have had particular interest, for instance, the depuration of polluted waters. In this regard, for the past 20 years the depuration methods have been based on various techniques such as application of chemical flocculants for removal metals, systems using ion exchange with resins and activated carbon absorbers.^{2,3}

Ch is a polysaccharide found in the cell wall of some fungi but it is mainly produced by N-deacetylation of chitin as the second most abundant biopolymer in nature after cellulose. Ch has chemical versatility due to changes in its structure which can acquire different properties⁴. Currently one of the applications of chitosan in variety of physical forms including fibers, films, membranes, gels nanoparticles and microspheres is in the treatment of polluted water.⁵ Its flocculant capacity is comparable to traditional chemicals employed for wastewater treatment. Ch has many advantages such its high efficiency in the reduction of organic matter, soluble solids (SS) and metal ions⁶. This pollution by metals is mainly associated with water discharges from industrial processes that end in the Lerma River. These metals alter aquatic systems which remain trapped and accumulated by sedimentation. The latter constitutes a serious problem for biological systems, for example in humans is a cause of gastrointestinal problems and dermatitis. The presence of metals in the microorganisms produces inhibition of the metabolic activity³. The biological process to attain chitin from crustacean wastes has been patented and it proved enhanced characteristics of both

chitin and derived resulting polymers, among them, increased crystallinities and low depolymerization besides of green and non-toxic biotechnology.⁷

On the other hand, PCL is among biodegradable polymers with exceptional biocompatibility and wide commercial use. PCL has a degradation time of 2 to 4 years, depending on the molecular weight, its degradation in the body to 6-hydroxyl caproic acid is to be converted to acetyl-CoA and incorporated into the Krebs cycle. PCL can be combined with other polymers to the desired new properties and management, an example is the application as a drug carrier, since we must mention that may be degraded by other microorganisms by hydrolytic degradation, but can be modified by copolymerization with lactones or glycolic / lactide to modify their degradative capacity⁸. PCL is a semi-crystalline hydrophobic homopolymer, the crystallinity tends to decrease with increasing molecular weight. In this regard, enzyme catalyzed synthesis is pointed to produce higher crystallinity polymers than conventional organometallic catalyst in addition to free non-toxic processes, which is worth to study in the present work. A novel process based on the use of low-boiling point and green fluorocarbons has been conducted to attain relatively high molecular weight semi crystalline PCL by enzymatic means.⁹

The aim of this work was to prepare and characterize a mixture of thermoplastic matrix of PCL with incorporated Ch, which retains its functionality in order to be applied in wastewater treatment for the removal of copper.

Experimental

Ch was obtained by heterogeneous *N*-deacetylation of chitin extracted by lactic acid fermentation from shrimp wastes^{7,10}. The molecular weight of the Ch was determined by intrinsic viscosity using as solvent acetic acid (2%) and sodium acetate (0.2M) with equation Mark Houwink-Sakurada.¹¹

PCL was synthesized by enzymatic polymerization of caprolactone at 2.5 MPa and 65 ° C for 24 h. Polymer was solubilized in chloroform, filtered and precipitated with methanol^{9, 12}. The molecular weight of PCL was determined by gel permeation chromatography (GPC) in HPLC with flow of 10 ml/min in a Shodex GPC KF-800 column using chloroform as mobile phase at 35 ° C, using polystyrenes as standards.⁹

Ch and PCL were previously dried in an oven at 30 °C to ensure they were free of moisture for 24 h. The formulations were prepared in order to obtain blends with ratios Ch:PCL of 1 to 1 and 1 to 5. Ch were mixed with the PCL and afterwards were extruded in an extruder Model LE-075.¹³

The adsorption of copper ion was carried out in a continuous system with a hydraulic residence time of 2 h for each mixture with a concentration of 70 mg/L and the analysis was carried out by atomic absorption using an Atomic Adsorption Spectrometer model SpectrAA 220 FS Varian.¹⁴

Results and Discussion

The PCL was obtained following a reported enzymatic reaction with some changes that was subsequently purified and corroborated with FTIR analysis. The molecular weight was determined by GPC/SEC) to obtain a *M_n* (Molecular number) 29.5 kDa upon polystyrene standards (Figure 1).

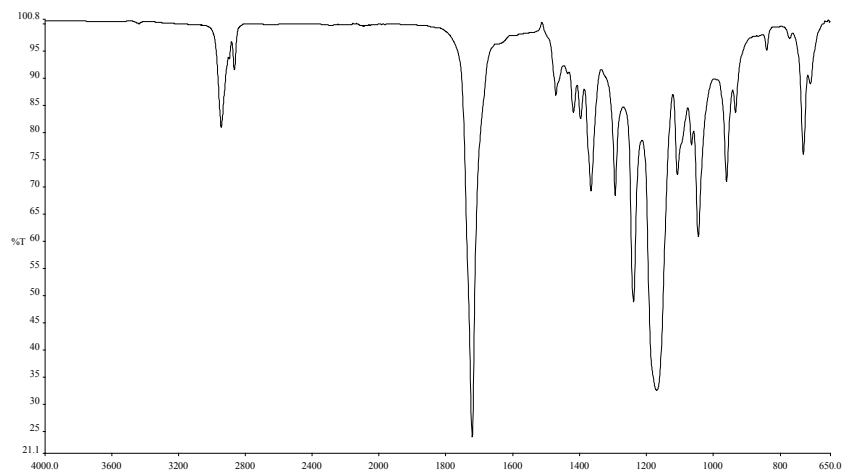


Figure 1. Infrared spectrum of PCL enzymatically synthesized

Chitin obtained by biological method was deacetylated by a termoalkaline reaction for a period of 3.5 hours, thereafter Ch was attained and assigned by FTIR analysis subsequently ^1H NMR studies gave a DA% of 6.80% and its M_v (Molecular Viscosity) determined by intrinsic viscosity an M_v was 121.2 kDa (Figure 2).

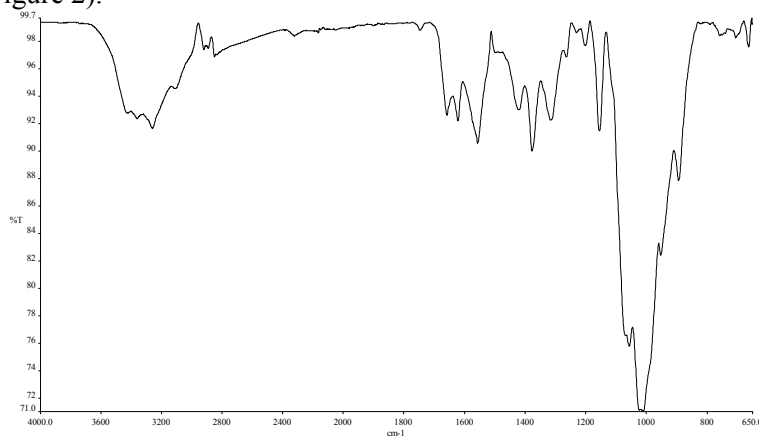


Figure 2. Infrared spectrum of Ch

The mixture of PCL and Ch was 5 to 1 and 1 to 1, respectively. The hydraulic retention time (HRT) evaluated was of 2 h, feeding with a solution containing copper concentration of 70 mg / L at pH 6: this concentration was selected because this concentrations are commonly found in the Lerma River of Toluca in the State of Mexico as a contaminant. Copper was presented in various sections of the river in a range of 60-80 mg Cu^{2+} / L and these concentrations are harmful to humans causing vomiting, nausea and diarrhea inclusive liver and kidney damages leading to death¹⁵. The copper adsorbed was monitored by FT IR analyses (Figures 3 and 4).

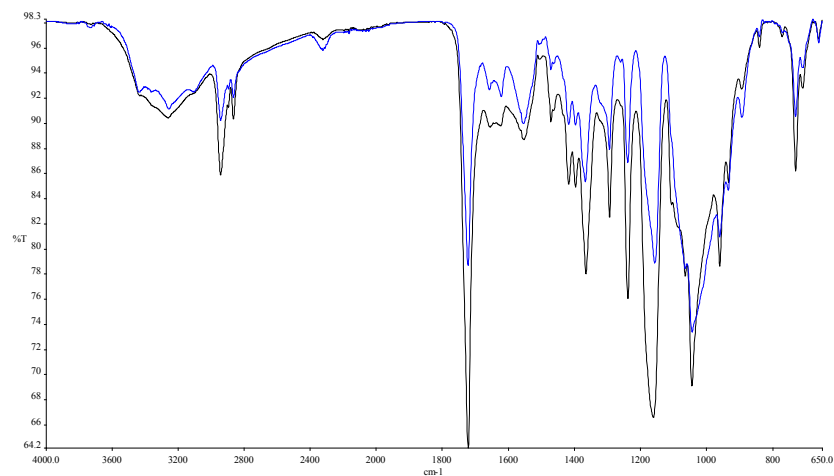


Figure 3. IR spectrum of PCL-Ch (5: 1) (black line) and the PCL-Ch after contact with copper in solution (blue line)

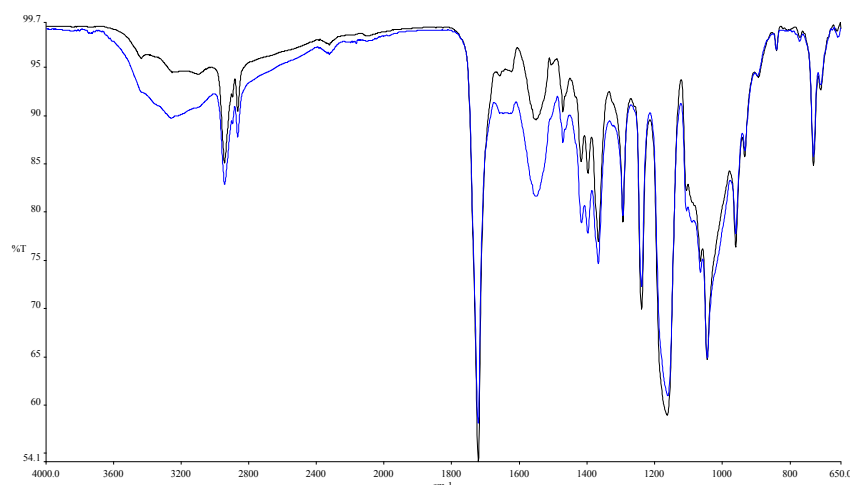


Figure 4. IR spectrum of PCL-Ch (1: 1) (blue line) and the PCL-Ch after contact with copper in solution (black line).

According to FTIR spectra for the samples, it can be observed a diminish in transmittance with interaction of groups of Ch located at 1655, 1620 and 1556 cm^{-1} and the hydroxyl group at 3280 cm^{-1} , this might be due to the ionic interaction between the hydroxyl group and encourage the copper ion.

In Table 1 is shown the adsorption capacity of the mixtures evaluated at different ratios. The mixture ratio of 5: 1 displayed an adsorption value of 1.77, whereas with the mixture ratio of 1:1 the adsorption capacity improved 9.1 fold-times; achieving adsorption efficiency of 54%. Similar results were reported by Wan et al. (2013); those authors reached an adsorption capacity of 18 mg Cu^{2+} / g adsorbent in a batch system. On the other hand, Popuri et al. (2009) reported in a continuous system an adsorption capacity of 87.9 mg Cu^{2+} / g adsorbent, the adsorption capacity was 5.5 times higher than the value achieved in the present work. Perhaps, it might have been due to the characteristics of the material, ie the ratio of the materials, since ah observed that PCL has no adsorption capacity so to be in more and to be a hydrophobic material causes a decrease in the adsorption as a barrier in areas of contact with chitosan, a fact that makes no mention Popuri is the adsorption performance of the material under the conditions of the study and the amount of support.

Table 1. Adsorption capacity of the composites at 2 h of HRT

PCL-Ch ratio	Adsorption Capacity		
	mg Cu ²⁺ / g adsorbent	Adsorption (%)	mg Cu ²⁺ / g Adsorbent*min
5:1	1.77	7.60	0.015
1:1	16.12	54.27	0.13

According to the results it can be said that the best value for adsorption capacity is the mixed ratio 1: 1. Compared to previous work by Popuri et al in 2009, our results are below their continuous system (87.9 mg Cu²⁺ / g adsorbent), however, our results with the 1: 1 (PCL:Ch) ratio are similar to the results from the batch system process reported by Wan et al (2013) (18 mg Cu²⁺ / g adsorbent).

Conclusions

This study showed that under our conditions the best value for copper removal is the PCL-chitosan (1:1) ratio, with an adsorption capacity of 16,123 mg Cu²⁺ / g adsorbent at pH 6 with a HRT of 2 h.

Acknowledgements

We thank Secretary of Science Technology and Innovation of Mexico City (SECITI) (PICO12-152) and CONACYT for scholarship (OVG).

References

- [1] S. N. Laksmi and T. L. Cato. Progress in Polym. Sci., 32, 762-798 (2007).
- [2] I. G. Lalov, I. I. Guerginov, M. A. Krysteva, K. Farstov. Water Research., 34 (5), 1503-1506 (2000).
- [3] F. Fenglian and W. Qi. J. Environmental Management, 92, 407-418 (2011).
- [4] W. Jian-Ping, C. Yong-Zhen, Y. Shi-Jie, S. Guo-Ping, Y. Han-Qing. Water research, 43, 5267-5275 (2009).
- [5] R. Laus, R. Geremias, H. L. Vasconcelos, M. C.M. Laranjeira, V. T. Fávere. J. Hazardous Materials 149, 471–474. (2007).
- [6] D. Zeng, J. Wu and J. Kennedy. Carbohydrate Polymers, 71, 135–139 (2008).
- [7] N. Pacheco, M. Garnica-Gonzalez, M. Gimeno, E. Barzana, S. Trombotto, L. David & K. Shirai, Biomacromolecules, 12, 3285–3290. (2011).
- [8] M. A. Woodruff and H. D. Werner. Progress in Polym. Sci., 35, 1217-1256 (2010).
- [9] R. García-Arrazola, M. Gimeno, and E. Bárzana. Macromolecules, 40, 4119-4120 (2007).
- [10] C. Juárez. Thesis Specialty Biotechnology UAM (2011).
- [11] S. Kobayashi, Proc. Jpn. Acad., Ser. B 86: 338-365. (2010).
- [12] D.R. Chen, J.Z. Bei, S.G. Wang. Polymer Degradation and Stability 67: 455-459. (2000).
- [13] D. E. Ramírez-Arreola, J. R. Robledo-Ortiz, F. Moscoso, A. Martín, D. Rodríguez, R. González-Núñez. J. Applied of Polym. Sci. 123, 179–190, (2011).
- [14] W. Meng-Wei, W. Chan-Ching, C. Chien-Min. International J. Environmental Sci. And Development. 4 (5), 545-551 (2013).
- [15] I. Barceló-Quintal, E. López-Galván, H. Solís-Correa, E. Domínguez-Mariani, S. Gómez-Salazar. J. Environmental Protection, 3, 878-888 (2012).

EFFECT OF THE HEIGHT OF THE BED IN A PACKED COLUMN WITH CHITOSAN CRYOGELS FOR SORPTION OF Cu^{2+} ION

Agustín Ostria Hernández¹, Anete Jessica Arcos Arévalo¹, Rosa Elvira Zavala-Arce¹, Pedro Ávila Pérez^{1,2}, Eric Guibal³, Beatriz García Gaitan¹, José Luis García Rivas¹

1Instituto Tecnológico de Toluca. Av. Tecnológico s/n Fracc. La Virgen, Metepec, Estado de México, México.

2Instituto Nacional de Investigaciones Nucleares. Carretera México-Toluca s/n, La Marquesa Ocoyoacac, Estado de México. México.

3Ecole des mines d'Alès, Centre des Matériaux des Mines d'Alès, 6 Avenue de Clavières, F-30319 Alès Cedex, France

Abstract

Heavy metals occur naturally in the earth's crust. These can become contaminants if its distribution in the environment is altered by human activities. One of them is copper that has wide and diverse uses. Waste treatment and disposal in many industries that use copper as raw material have not handled properly, representing a major source of pollution. In this work, chitosan, a biopolymer, esteemed as a good adsorbent for metal ions such as copper, has been used in the form of cryogel beads in order to study the metal sorption behavior in a continuous up-flow process using a packed column at different bed heights. Columns of 3 cm and 6 cm height bed of cryogel beads made of chitosan (Q) crosslinked with ethylene glycol diglycidyl ether (EGDE), were used. A inlet flowrate of 2 mL/min of a solution with an initial concentration of 20 mg Cu^{2+} /L, pH 5.0 and temperature of 25 °C. Results showed that at a bed height of 3 cm, saturation point was reached at 870 minutes, whereas for the 6 cm column bed was 1302 minutes. Sorption rate decreases by 6 cm column compared with the column 3 cm bed. So that, the bed height is an important factor on dynamic sorption for the material studied.

Introduction

Public health and ecosystems equilibrium depends on water quality, which restricts the supply of water and potential distribution for different uses. Water is associated with the transmission of diseases affecting human health, either directly or through contamination of food intake, so its quality is absolutely related to the population life quality [1]. Mexico currently faces serious problems of availability, waste and water pollution. Instituto Nacional de Estadística, Geografía e Informática (INEGI) [2] and Secretaría de Medio Ambiente y Recursos Naturales (SEMARNAT) [3] have reported that the most polluted and overexploited water resources are concentrated in the most populated areas of the country, where the lack of water is increasing daily, causing an inadequate quality of it for a variety of applications including human consumption [4]. An important trouble in water pollution are high concentrations of heavy metals because of human activities, which modifies natural conditions of water bodies. Copper has wide and diverse applications since it is used in the transportation industry, electronics, construction, agriculture, energy, health and new technologies. However, these process discharge large waste quantities without an adequate treatment causing several damages to the biota in rivers, lakes or ponds and bioaccumulation in the trophic chain. Many of these industries using copper as raw material were not properly handling the disposal of waste and its treatment, representing a major source of pollution because many of them dump them into rivers, lakes or ponds, or because confining their waste improperly presented a later infiltration into aquifers. It has been reported that chitosan has a high potential for the removal of metal ions, dyes, proteins and humic acid, among others. So that, currently it's been important to look for a solution for copper uptake from wastewaters and investigation reports have showed that chitosan has a high potential for the removal of metal ions,

dyes, proteins and humic acid, among others. This polymer is biodegradable, biocompatible and non-toxic because it does not produce immune response, besides its polycationic nature characteristic that allows using it in various applications. Chitosan is characterized by a high number of free amino groups, which are highly reactive for chelating metal cations at a pH close to neutrality. Studies have been carried out in sorption of Cu^{2+} ions, and other metals with chitosan have achieved acceptable results. The aim of this study was to evaluate the operating characteristics and dynamic sorption behavior in a fixed bed column packed with cryogel chitosan crosslinked with ethylene glycol diglycidyl ether (QE), for the removal capacity of Cu^{2+} ions in aqueous solution at different bed height.

Experimental

QE cryogel synthesis was performed using industrial grade Chitosan from America Alimentos Co. with a 65% of deacetylation. It was dissolved in a 3% acetic acid solution (Fermont brand), and then was crosslinked with 1% ethylene glycol diglycidyl ether (EGDE) solution (TCI brand) at a reaction time of 6 hours to achieve mechanical stability. QE cryogel beads were obtained dripping the aqueous gel solution in a liquid nitrogen bath, and then freeze-drying at $-57\text{ }^{\circ}\text{C}$ and a pressure of 0.018 mbar in a Heto Drywinner device. Lyophilization time was 24 hours [5, 6]. Removing impurities and unreacted reagents after the crosslinking reaction was an important step in order to avoid potential interferences with the chitosan functional groups responsible for adsorption process [6]. Beads were washed at first time with 1.5% acetic acid solution during 30 minutes, after that several washings were performed with deionized (DI), $30\text{ }^{\circ}\text{C}$ and 150 rpm constant shaking every 20 minutes until the wash water reached the pH of the initial deionized water. Cryogel beads obtained after swelling process were 2.696 mm diameter approximately. Continuous sorption was performed in an up-flow column packed QE cryogel beads, consisted of a glass column of 3 cm inside diameter and a 16 cm height [7.8]. The effect of height bed was studied using 3 and 6 cm. A solution of initial concentration of 20 mg Cu^{2+}/L , and pH of 5.0 was pumping at 2 mL/min flowrate at $25\text{ }^{\circ}\text{C}$. In order to ensure the formation of a complete breakthrough curve, experiments was running for 16 h and 26 h respectively for each column. Samples collected at column out were analyzed by an Perkin Elmer 100 AAnalyst spectrometer to determine Cu^{2+} concentrations.

Results and Discussion

Breakthrough curves were plotted by Origin 8.1®, and data were fitted to Thomas and Adams-Bohart mathematical models. Figure 1 shows the effluent sample respect to the influent initial concentration ratio (C/C_0) versus experiment running time, which each sample was collected.

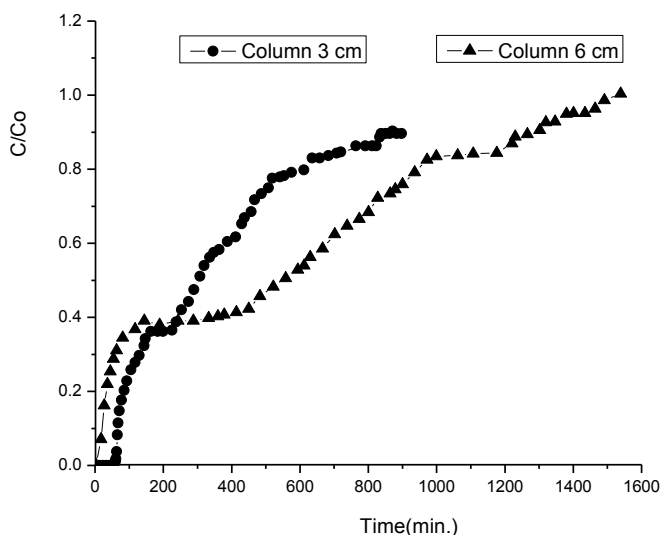


Figure 1. Breakthrough curves at 3 cm and 6 cm column height

The breakthrough curves of the two columns is seen that the start of the sorption is at a very rapid speed because the slopes of the rupture curves between 0 and 150 minutes is steep suggesting that the material of the cryogel QE of sipping rapidly reaching the breaking point (C/C_o) = 0.20 [9] for column 3 cm at 84 minutes to 6 cm column at 36 minutes. Following 150 minutes shows that this rate of sorption is considerably decreased to zero in (C/C_o) = 0.38, remaining unchanged at this point for a time of 70 minutes. After 220 minutes begin to sorb sorbent material but at a lower speed relative to the beginning of the process and gradually, except that for the column 3 cm to 6 cm is the sorption speed is higher. Saturation point (C/C_o) = 0.9 [10, 11] is obtained 870 minutes for the column 3 cm and 6 cm column of 1302 minutes is because the greater the amount of QE cryogel. See Table 1.

During the sorption process from 0 to 150 minutes there is a saturation of the Cu^{2+} ions on the surface of the cryogel QE at this point is reached at a ratio of (C/C_o) = 0.38, the sorption rate becomes zero at this point, for Cu^{2+} ions begin to migrate from the surface into the cryogel, which occurs between 150 to 220 minutes. Thereafter, when the inside of the sphere was already saturated, sip starts again on its surface but fewer and less speed [12].

BREAKING POINT		
PARAMETER	COLUMN 3 cm QE	COLUMN 6 cm QE
(C / Co)	0.2024	0.2173
Time (min)	84	36
SATURATION POINT		
PARAMETER	COLUMN 3 cm QE	COLUMN 6 cm QE
(C / Co)	0.9031	0.9038
Time (min)	870	1302

Table 1. Breakpoints and saturation of the columns of 3 cm and 6 cm QE cryogel bed.

Column experiments with mathematical models of Thomas and Adams-Bohart were analyzed. Table 2 shows the values obtained from both columns. It is observed that in the Thomas model rate constant (K_{th}) decreases with increasing bed height of cryogel QE, this shows that sorption behavior is controlled by the mass transport resistance [12]. The Adams-Bohart model is used to describe the initial part of the curve in the column break. Its validity is limited in the range of $C < 0.5C_0$ [12]. It is also observed in this model the kinetic constant of Adams-Bohart (K_{ab}) decreases with increasing bed height of cryogel QE, confirming what the model says Thomas. The amount of Cu^{2+} adsorbed (q_0) on the column 3 cm of bed is less compared with that of 6 cm of bed according to the model QE Thomas, this is because there is a greater mass of sorbent in column 6 cm in 3 cm. The Adams-Bohart model, there is little variation in the amount of Cu^{2+} adsorbed (N_0), in the initial part of the breakthrough curves, indicating that the behavior in this part of the curve is very similar.

The correlation factor R^2 Thomas model show that the model represents the behavior of the sorption process in the columns. In contrast, in the Adams-Bohart model, although the correlation factor R^2 indicates that this model can adequately represent the behavior in the first part of the breakthrough curve. However it is recommended to find another model that can better simulate the behavior in this area of the breakthrough curve.

The breaking point for both columns is very similar. However the point of saturation is reached faster on the columns, 3 cm bed of QE regarding 6cm QE bed because in the latter more material is used so it takes longer to reach this point.

PARAMETER	Column 3 cm QE	Column 6 cm QE
THOMAS MODEL		
K_{th} (mL/min.mg)	0.24475	0.12645
q_0 (mg /g)	13.296	20.764
R^2	0.9839	0.9598
ADAMS-BOHART MODEL		
K_{ab} (L/mg.min)	0.0034	0.00139
N_0 (mg/L)	96.116	92.943
R^2	0.8231	0.7865

Table 2. Models of Thomas and Adams-Bohart 3 cm column 6 cm bed and QE.

Conclusions

Curves shown in this resistance breaking takes place at 150 minutes, time in which the sorbent material is saturated in its surface, so it can not sorb more until the sorbate is sucked inside the material, so that the surface is free and begins to sorb more, which occurs at 220 minutes, but with a different sorption speed between the two columns.

After this time the behavior is different, achieving faster sorption column 3 cm to 6 cm of the bed, according to the setting data to the kinetic model.

Mathematical models of Thomas and Adams-Bohart show that the sorption process is controlled by the mass transport resistance of Cu^{2+} ions in the cryogel QE beads. Show that the rate of sorption decreases with increasing bed height column.

So we can conclude that the bed height of the material if it influences the sorption process of Cu^{2+} ions.

Acknowledgements

Instituto Tecnológico de Toluca, División de Estudios de Posgrado e Investigación.
Laboratorio de Investigación en Ingeniería Ambiental (LIIA) del Instituto Tecnológico de Toluca.
Dirección General de Educación Superior Tecnológica (DGEST). By financing the project with key 4625.12-P
Instituto Nacional de Investigaciones Nucleares (ININ).
Consejo Nacional de Ciencia y Tecnología (CONACYT), through a scholarship.
Consejo Mexiquense de Ciencia y Tecnología (COMECYT)

References

- [1] Instituto Nacional de Ecología y Cambio Climático, (INECC). 2005. El agua en México. Revista 11. pp 1-5, 46, 47.
- [2] Instituto Nacional de Estadística y Geografía (INEGI), 2005.
- [3] Secretaría del Medio Ambiente y Recursos Naturales (SEMARNAT), 2006.
- [4] Enciso, A. 2003. “Revela CAN problemas en abasto nacional de agua” la Jornada, 3 de Febrero de 2003. www.jornada.unam.mx/2003/feb/03/030203/oriente.html
- [5] Corral-Capulín, N.G. 2014. “Estudio de la competencia de sorción de los iones Cu(II) y Cd(II) en criogeles a base de quitosano”. Tesis de maestría. Instituto Tecnológico de Toluca.
- [6] Arcos-Arevalo, A. 2012. Síntesis y caracterización de un criogel a partir de quitosano y su estudio como adsorbente de iones Cu (II) en solución acuosa. Tesis de maestría. Instituto Tecnológico de Toluca.
- [7] Worch, Eckhard. 2012. Adsorption Technology in Water Treatment. Fundamentals, Processes and Modeling. De Gruyter. (6.2). pp. 175-178.
- [8] Raghvan, N., Rutven, D. M. 1983. Numerical simulation of a fixed bed sorption column by the method of ortogonal collocation. J. AIChE. Vol. 29. Pp. 922-925.
- [9] NOM-001-SEMARNAT-1996. Límites máximos permisibles de contaminantes en las descargas de aguas residuales en aguas y bienes nacionales.
- [10] Tenorio R., G. 2006. Caracterización de la biosorción de cromo con hueso de aceituna. Editorial de la Universidad de Granada. España. (Tesis Doctoral).
- [11] Han, R.; Zou, W.; Li, H.; Li, Y. and Shi, J. (2006). Copper (II) and lead (II) removal from aqueous solution in fixed-bed columns by manganese oxide coated zeolite. Journal of Hazard Materials. Elsevier.B137:934-942.
- [12] García, J.J., Solache, M., Martínez, V., Solís C. 2013. Removal of fluoride ions from drinking water and fluoride solutions by aluminum modified iron oxides in a column system. Journal of colloid and interface science. 407. Pp. 410-415.

THIN FILMS OF CHITOSAN/PYRROLIL QUINONE FOR ADSORPTION OF FLUORIDE AND NITRITES.

Melissa Tapia Juárez,¹ J.Betzabe González Campos,¹ Luis Chacón García¹

¹ *Instituto de Investigaciones Químico Biológicas, Universidad Michoacana de San Nicolás de Hidalgo, Morelia Mich, Mexico. Betzabe.gonzalez@yahoo.com.mx*

Abstract

The design of biomaterials with the ability to recognize anions is a potential area of investigation due to the indispensable role that anions play in nature; chitosan (CT) is a biopolymer capable of binding different type of ions and has the ability to form thin films, while recently the ability of anion recognition by pyrrolyl quinone (PQ) compounds has been demonstrated. Therefore, this work proposes to test the anion adsorption capacity of chitosan/pirrolyl-quinone composite in the form of thin films so that the addition of pyrrolil quinone to chitosan could strengthen its ability to recognize or absorb anions. The anions tested in this work are nitrite and fluoride.

Introduction

Detection of anions is of great importance because of the impact they have in biological systems, food and pharmaceutical industries among others [1]. Examples are nitrate and nitrite (NO₂⁻ and NO₃⁻) anions which are widely used in food industry, especially in meat products; at high concentrations these anions are highly toxic so that the monitoring of these ions is transcendental [2]. Another example is fluoride (F⁻), this anion has been detected in drinking water and high concentrations intake can be harmful to human health, leading to a condition called dental or skeletal fluorosis [3]. In this context, pyrrole compounds as a group are the most widely studied class of anion receptors, however the use of pyrrolyl quinone (PQ) compounds as anionic recognizers has been recently reported, so that their synthesis and anion selectivity (specifically by fluorine) is brand new [4]. On the other hand, there are reports showing that CT is an effective bio-absorbent of NO₂⁻ and NO₃⁻ ions, and also has the ability to remove fluoride excess in drinking water [2]. Therefore, it is expected that the combination of these two components (CT and PQ) allows obtaining an excellent composite material for the elimination and easy detection of different anions.

Experimental

Synthesis of 2-dipyrrolyl-2,5-dimethyl-p-benzoquinone (PQ).
2,5-dimethyl-1,4-benzoquinone (0.1 g, 0.73 mmol) and SiO₂ (1.3 g) were added into a solution of dipyrromethane (0.129 g, 0.74 mmol) dissolved in CH₂Cl₂ (2 ml), following by solvent removal. The reaction was kept at room temperature for 17 h. The residue was purified by flash column chromatography (Hex : EtOAc 9 : 1) to give compound 2 (PQ) as a purple solid.

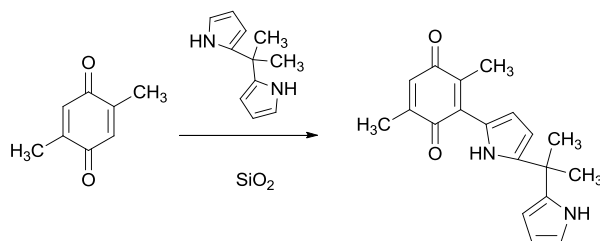


Figure 1. Schematic illustration of Synthesis of PQ.

Film preparation

Chitosan (CS) medium molecular weight ($M_w = 150,000$ g/gmol) and 82 % of degree of deacetylation (DD) reported by the supplier, was purchased from Sigma-Aldrich. Acetic acid from J.T. Baker was used as received. 1 wt % of chitosan was dissolved into a 0.4 M aqueous acetic acid solution with subsequent stirring during 24 hours to promote dissolution to obtain ure CT films. Subsequently, PQ (Figure 1) was added to the acid solution of CT at a concentration of 1.5% (w/v) to be mechanically stirred for 30 minutes, the mixture was further homogenized in an ultrasonic bath during 30 more minutes to subsequently be transferred to Petri dishes and dried at 60°C in an oven to evaporate the solvent. Finally the films were cut into small squares for better handling adsorption tests.

Absorption experiments:

Adsorption experiments were performed by triplicate at 30° , 40° and 50°C in a water bath. UV visible spectra (UV-Vis) were performed in a Jenway 6505 spectrophotometer, using a quartz cell for the study of solutions. In all experiments, deionized water was used. Anion solutions used were purchased from Sigma-Aldrich and Merck brand.

Adsorption tests of the CT/PQ combination was carried out by introducing a sample of the thin film composite into vials containing the anion solution at different concentrations. The vials were introduced to a water bath with recirculation during 1 hour at $30 \pm 2^\circ\text{C}$ for nitrite solutions and at $30 \pm 2^\circ\text{C}$, $40 \pm 2^\circ\text{C}$ and $50 \pm 2^\circ\text{C}$ for fluoride solutions. After contact time, each solution was analyzed by UV-Vis. The study of fluoride anions was determined by the SPANDS spectrophotometric method.

Results and Discussion

The analysis of the incorporation of PQ to CT was carried out by infrared spectra (IR) in order to evaluate a possible synergistic effect on the anion recognition capability. IR spectra show no apparent changes in the typical bands of CT shown in Figure 2, suggesting that there is no chemical interaction between both components.

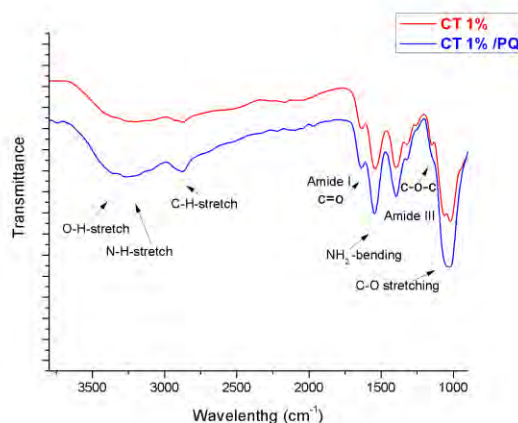


Figure 2: IR spectra obtained for: a) pure CT b) CT / 1.5% PQ .

Subsequently, the adsorption capacity of CT/PQ composite films was tested for fluoride and nitrite ions. The amount of anion adsorbed by the composite films (q_e) was calculated by mass balance according to equation (1).

$$q_e = \frac{V}{W} [C_0 - C_e] \quad (1)$$

Where C_0 and C_e are the initial and final concentrations (mg/L) of the anion in the solution respectively; V is the volume of the anion solution (L) and W is the sample weight (g). Table 1 details the initial (C_0) and final (C_e) concentrations, the difference between them ($C_0 - C_e$) and the q_e obtained for nitrite adsorption.

Table 1 Parameters used to obtain q_e for CT /1.5% PQ composite at 30°C.			
C_0 mg/L	C_e mg/L	$(C_0 - C_e)$ mg/L	q_e mg/g
189.5	179	10.5	6.84
289.5	278	11.5	7.64
389.4	378	11.4	6.96
489.3	478	11.3	6.37
589.3	578	11.3	7.09
689.2	678	11.2	6.46
789.2	778	11.2	6.55
889.2	878	11.2	7.05

Results indicate that in this concentration range the adsorbent material reaches saturation. At higher concentration of the anion solution, the capacity of the adsorbent reaches equilibrium adsorption; therefore the values of the adsorbed amount (q_e) remains between 6 and 7 mg/g, these results indicate that CT/PQ composite films removed between 10 and 11 mg/L of nitrite anions from the solution. Regarding pure CT films, they showed less adsorption capacity for nitrite anions compared with CTS/PQ composite.

The adsorption analysis of fluoride anions was carried out by the colorimetric method called SPANDS by the reaction between the fluoride anion and coloring zirconyl-SPANDS complex.

The results for fluorine experiments allowed us to obtain an adsorption isotherm, which describes the adsorption equilibrium and is a simple physical interpretation of the relationship between the adsorbed substance (sorbate) and the adsorbent phase once equilibrium has been

reached. In 1918 Irving Langmuir described this isotherm using a simplified model of a solid surface given by Equation 2:

$$\frac{C_e}{q_e} = \frac{1}{q_{\max} b} + \frac{C_e}{q_{\max}} \quad (2)$$

Where q_e is the amount of anion adsorbed solution (mg/g); C_e is the concentration at equilibrium of the anion solution (mg/L); q_{\max} the maximum adsorption capacity (mg/g); b coefficient related to the strength of adsorption.

The experimental data obtained for fluoride adsorption using CT and CT/PQ films could be fitted to Equation 2, showing a Type I Langmuir isotherm (Figure 3).

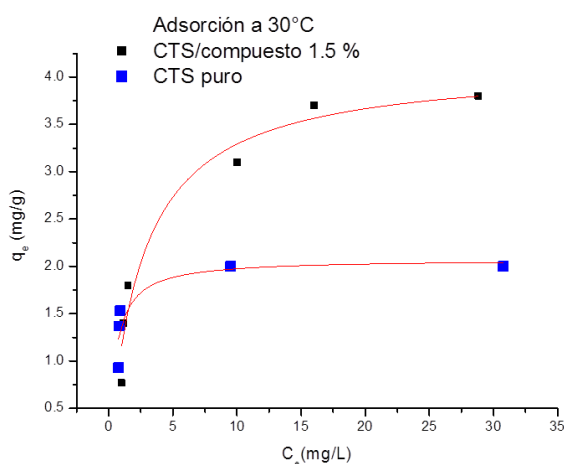


Figure 3. Adsorption isotherm of fluoride films CT/1.5% PQ at 30°C.

From Figure 3, it can be observed that the adsorption capacity at 30°C of CT was improved with the addition of PQ. It is noted that the q_e for pure CT films increases from 0.2 to 2 mg/g as the concentration of F^- increases, in the same way the values of q_e for CT/PQ films gradually increase from 0.77 to 3.8 mg/g according to the increase of the anion concentration. The values of the anion absorbed amount (q_e) are higher for CT/PT films compared with CT films; these results are expected since the PQ compound showed high affinity for F^- anions [4], and with the increase of the anion concentration, the film showed higher capacity and adsorption affinity. It is suggested that the adsorption process is performed through the binding sites (functional groups of the polymer OH, NH₂ and recognition sites of PQ) on the surface of the films, and is considered a monolayer adsorption.

The adsorption process is a thermodynamic equilibrium between the adsorbed solute and the solute in solution and for this reason it is temperature dependent. Temperature affects the balance because the interaction between the surface and molecules in solution are temperature dependent, therefore, the study of the temperature effect was performed at 30°C, 40°C and 50°C. The Langmuir isotherm comparing the three temperatures is shown in Figure 4.

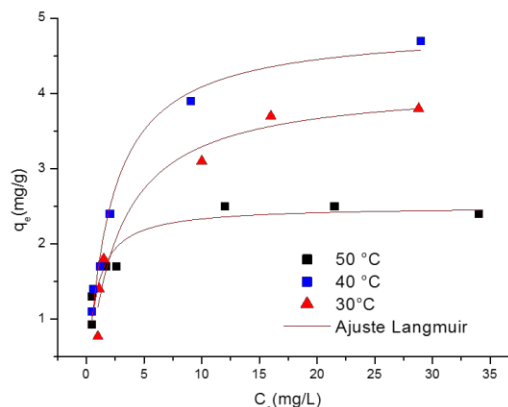


Figure 4. Fluorine adsorption isotherm for CT/PQ films at 30°C, 40°C and 50°C.

It can be clearly observed that the three isotherms shown in Figure 4 reach a saturation point, showing the greater amount of absorbed anion ($q_e = 24.7$) at 40°C. It is clear that the adsorption equilibrium is favored by the increment on the temperature from 30°C to 40°C, being the latter the optimum temperature for the adsorption of fluoride anions by CT/PQ films.

The adsorption process at 40°C indicates a strong bond between the adsorbent and the adsorbate, while an increase in temperature to 50°C may register one or more of the following three scenarios:

- (1) The bonding between the components is weaker.
- (2) The process of adsorption and desorption is faster.
- (3) The components of the CT/PQ composite may change in structure due to the increase in temperature.

Conclusions

The combination of CT with PQ proved to be effective for the adsorption of NO₂ and F⁻ ions, this methodology is very attractive because it is environmentally friendly, economic and easy to use.

References

- [1] G.E. Molau and H. Keskkula, J. Polym. Sci., Part A-1, 4, 1595 (1966).
- [2] G.M. Leal, J. M., Asua, Polymer, 50 (1), 68-76 (2009).
- P. D. Beer, P. A. Gale, Angew. Chem. Int. Ed. Engl, Vol 40, 486-516, (2001)
- M. J. Moorcrof, J. Davis, R. G. Compton, , Talanta, Vol 54, 785-803, (2001).
- S. P. Kamble, S. Jagtap, N. K. Labhsetwar, D. Thakare, Chemical Engineering Journal, Vol 129, 173-180, (2010).
- M. T.Juárez, J. B. González Campos, C. C. Celedón, D. Corona, E.Cuevas-Yañez, L. Chacón GarcíaRSC Adv, Vol 4,5660–5665, (2014).

SYNTHESIS OF NOVEL SEMICONDUCTING POLYURETHANE/POLYPYRROLE/POLYANILINE COMPOSITES FOR MICROORGANISM IMMOBILIZATION AND WASTEWATER TREATMENT

Iveth D. Antonio-Carmona,¹ Silvia Y. Martínez-Amador,¹ Víctor M. Ovando-Medina²

¹ *Departamento de Botánica, Universidad Autónoma Agraria Antonio Narro. Calzada Antonio Narro 1923, Buenavista, Saltillo, Coah., 25315. México.*

² *Ingeniería Química, COARA – Universidad Autónoma de San Luis Potosí, Carretera a Cedral KM 5+600, San José de las Trojes, Matehuala, SLP, México 78700. E-mail: ovandomedina@yahoo.com.mx.*

Abstract

The development of new materials for microorganism immobilization is very important in some areas as wastewater treatment. In this work polyurethane (PU) foams were modified polymerizing pyrrole (Py) and aniline (ANI) onto its surface by chemical oxidization in order to obtain PU/PPy, PU/PANI, and PU/(PPy-co-PANI) composites, used to immobilize microorganisms for municipal wastewater treatment in batch mode and continuous flow in two sequential (anaerobic/aerobic) packed bed reactors (PBR) at two hydraulic retention time (HRT). Composites were characterized by Fourier Transform Infrared (FTIR) spectroscopy and Scanning Electron Microscopy (SEM), and were tested in chemical oxygen demand (COD) removal during treatment. Batch wastewater treatment after 8 days showed higher COD removal efficiency (78%) on PU/(PPy-co-PANI) foam. Also, it was observed higher COD removal from the sequential PBR for 36 h HRT.

Introduction

Over the last century, continued population growth and industrialization have resulted in the pollution of various ecosystems on which human life relies on. In the case of ocean and river quality, such pollution is primarily caused by discharge of inadequately treated industrial and municipal wastewater. On initial discharge, these wastewaters can contain high levels of organic/inorganic pollutants which can be easily biodegradable, but whose impact load on the ecosystems, either in Total Suspended Solids (TSS), Biochemical Oxygen Demand (BOD), or Chemical Oxygen Demand (COD), may be in the tens of thousands mg/L [17, 19]. In the treatment of wastewater, biological process appears to be a promising technology; therefore, in recent years, considerable attention has been paid towards the development of reactors for anaerobic treatment of wastes leading to the conversion of organic molecules into biogas [10]. One way to improve anaerobic processes is microorganism immobilization onto solid supports. This technique is a powerful tool, which has very important industrial and research applications. Immobilization of any biosystem will depend on the type of bioactive material to be immobilized. The attachment of the active agent to a polymer matrix depends on the physical relationship between support and ligand. However, in biosystems immobilization, factors that influence the choice of the method to be used are generally empirical [9]. Particularly, it has been used a lot of synthetic materials as poly(vinyl alcohol) [7, 8], poly(methyl methacrylate) [13], polypropylene [15], polystyrene [6], PU [4, 18] and modified PU [5, 12]. Polyurethanes (PU) are one of the most versatile materials in the world today. It has been found to be applicable in the biochemical and biotechnological fields as a perfect support for enzyme immobilization [11, 16].

In this work, composites of PU/PPy, PU/PANI and PU/(PPy-co-PANI) were obtained by chemical oxidation. Composites were used for microorganism immobilization and tested in wastewater treatment. Composites were compared against the COD removal during a municipal wastewater

treatment in anaerobic batch reactors and in continuous flow in two sequential (anaerobic/aerobic) packed bed reactors. To the best of our knowledge, this is the first time that composites of PU with semiconducting PPy and PANI are used for microorganism immobilization in wastewater treatment.

Experimental

Materials

Py (>98%), ANI (>99%) and ammonium persulfate (APS, >98%) were purchased from Sigma-Aldrich and used as received. Polyurethane foam (PU) was purchased from a local market in Saltillo, Mexico. Distilled water was used in all polymerizations. Sulfuric acid (96-98%) and potassium dichromate (96-98%) were purchased from Analytika (Saltillo, Mexico); mercuric sulfate (>98%) and silver sulfate (>98%), from Jalmek-Científica, and potassium biphtalate (>99.95%) from Fermont (Monterrey, Mexico), these reagents were used for COD determinations.

Polymerizations

Polymerizations of Py and PANI onto PU foam surface was made as follows: 5 g of PU were cut in pieces of approximately 1 cm, and immersed in distilled water containing Py or ANI (copolymerizations of Py with ANI a molar ratio of these monomers was used) previously dissolved. Entrapped air bubbles were extracted from PU foams and allowed to saturate under magnetic stirring. APS was added, as the oxidizing agent, to reaction mixture to start polymerization. Coated PU foams were washed several times with distilled water to remove unreacted chemicals and dried in an oven at 60 °C until constant weight.

Microorganism immobilization onto composites

Municipal wastewater used in this study was obtained from the “Bosque Urbano Ejército Mexicano” from Saltillo, Coah., Mexico. Batch glass reactors with capacity of 500 ml marked as PU, PU/PPy, PU/PANI and PU/(PPy-co-PANI) were used, to which the composites were added, 20% of degranulated anaerobic sludge (v/v) and 40% (v/v) of wastewater as substrate. The systems were in batch mode for a month at 37°C under anaerobic conditions for biofilm formation. After this, the supernatant was removed along with the excess of sludge.

Batch anaerobic wastewater treatment

Kinetic experiments of COD removal were made at 37°C using the reactors containing composites with immobilized microorganisms (biofilm) with three replicates for each treatment, under anaerobic conditions, containing 40% (v/v) of municipal wastewater as substrate. Samples were taken of the aqueous phase each 48 h throughout 15 days to determine COD.

Continuous flow wastewater treatment in PBR

Pilot plant consisted of two sequential PBR of 5.8 L of working volume each, and packed with 20% wt/v of PU/(PPy-co-PANI) composite. The first reactor consisted of an anaerobic up-flow process, the output of this reactor was connected to other up-flow aerobic reactor (this last reactor was connected to an air pump at the bottom for the injection of air). Each reactor was conditioned with their respective sludge (anaerobic, aerobic) for biofilm attachment on the composite (7 days). At the end of this time, the sludges and wastewater were carefully taken out of each reactor, keeping the composite inside the reactors with their respective biofilms. Domestic wastewater was treated, using the system as a sequential PBR, for 15 days. Afterwards, sample of final effluent for the HRT was collected and analyzed.

Characterization

Composites of PU foam, PU/PPy, PU/PANI and PU/(PPy-co-PANI) were analyzed by FTIR-ATR spectroscopy (Agilent Tech., Cary 630) to determine chemical compositions and by scanning electron microscopy (SEM) (FEI, Quanta-3D FEG) to know surface morphology of composites. Determinations of COD removal during anaerobic wastewater treatment were measured as soluble in accordance with Standard Methods (1995) and NMX-AA-030-SCFI-2001. To establish the amount of biomass attached on the support, assessments were made as described by Di Trapani et al [3] obtaining the biomass weight per gram of support.

Results and Discussion

SEM images ($\times 33$), of different composites synthesized in this work, show that PU foam consisted of homogeneous surface of well-defined porous with average diameter of 500 μm . Sample of PU/PPy shows occluded pores with PPy; sample of PU/PANI shows less occluded pores than PU/PPy, whereas PU/(PPy-co-PANI) sample shows pores very slightly occluded pores, thus copolymer of PPy and PANI was deposited only on the surface of PU. However, when copolymer of PPy and PANI was deposited onto PU surface, very small spherical nanoparticles were formed with diameters between 80 and 150 nm ($\times 10,000$). This is a result of PPy which tends to form spherical morphology and a complex interaction of conducting polymers with PU foam surface (Fig. 1, 2).

The FTIR spectra of different materials synthesized and that of uncoated PU foam show: PU foam shows the characteristic signal of TDI; peak at 1715 cm^{-1} and at 1636 cm^{-1} correspond to C=O stretching in urethane, signal at 1600 cm^{-1} is due to C=C of aromatic ring, signal at 1228 cm^{-1} is ascribed to C–O, peak at 1080 cm^{-1} can be ascribed to C–O–C [2], which demonstrates that a TDI was used in the PU synthesis. The most important signals of PANI can be seen in Figure 3 (PU/PANI and PU/(PPy-co-PANI)).

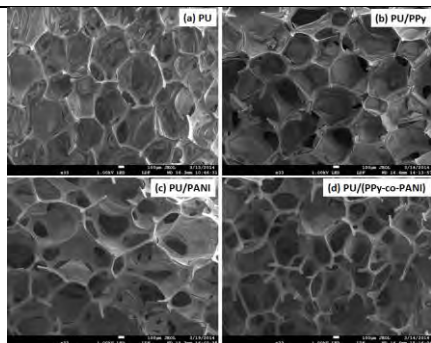


Figure 1. SEM images of PU foam and different composites synthesized at a magnification of 33 times.

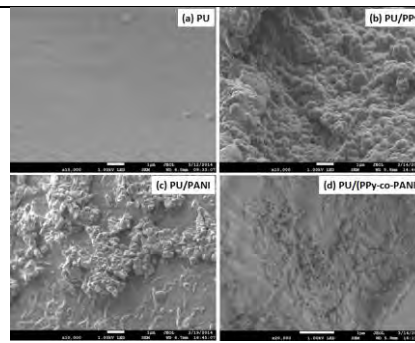


Figure 2. SEM images of PU foam and different composites synthesized at a magnification of 10,000 times (a), (b) and (c), and 20,000 times (d).

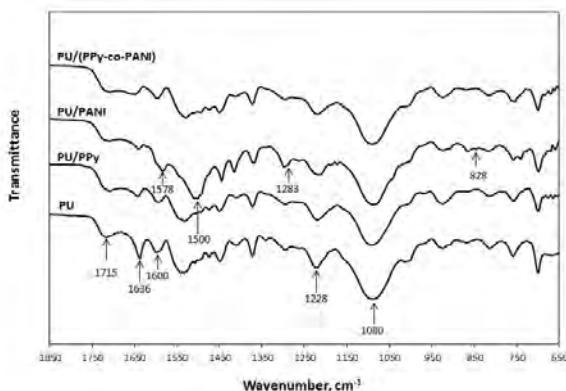


Figure 3. FTIR spectra of different composites of PU with PPy and PANI.

Percentage of efficiency in COD removal for PU foam, PU/PPy, PU/PANI and PU/(PPy-co-PANI) were 69%, 52%, 73% and 78%, respectively in a period of 8 days. The amount of biomass per gram of support were determined only for PU/(PPy-co-PANI) and for pure PU as described in the methodology section. The results are shown in Table 1.

Table 1: Amount of immobilized biomass in PU and PU/(PPy-co-PANI) supports in anaerobic and aerobic conditions.

Sample	g of biomass/g of support	Sample	g of biomass/g of support
PU, anaerobic	0.65	PU/(PPy-co-PANI), anaerobic	0.79
PU, aerobic	0.69	PU/(PPy-co-PANI), aerobic	0.84

COD removal efficiency increased with the COD in the influent (Table 2). It can be observed also, that when COD of the influent is very low (Run C/24 h in Table 2), COD removal efficiency decreased until 75%. On the other hand, by increasing the HRT to 36 h, higher efficiency was obtained (94%). It can also be observed that COD removal is mainly verified in the anaerobic section of PBR sequential system

Table 2: COD concentrations of influent and at the outlet of each reactor, and their respective removal efficiency.

Run/HRT	Influent, mg/L	Anaerobic reactor, mg/L	%	Aerobic reactor, mg/L	%	Overall, %
Run A/24 h	676	281	58	93	28	86
Run B/24 h	366	219	40	73	40	80
Run C/24 h	289	99	66	72	9	75
Run D/36 h	642	90	86	38	8	94

Conclusions

Combined mechanical properties of PU with biocompatibility of PPy and PANI, resulted in a material that was used for microorganism immobilization and applied in a domestic wastewater treatment, being PU/(PPy-co-PANI) the composite with the best COD removal of 78% (11% higher than pure PU) in batch mode, which was ascribed to the well coating of PU structures (not

so occluded pores) and smaller globular morphologies with enhanced superficial area, thus more microorganism were immobilized. Best COD removal efficiency on PBR sequential system was achieved at 36 h HRT (94%), due to more immobilized microorganisms on the foams, making it a good option for treating municipal wastewaters.

Acknowledgements

Author I.D.A.C. acknowledges to the Consejo Nacional de Ciencia y Tecnología, México (Scholarship #351801). This work was supported by the Consejo Nacional de Ciencia y Tecnología, México (Grant # SEP-80843).

References

- [1] American Public Health Association, Standard Methods for the Examination of Water and Wastewater, AWWA, WEF. APHA Publication (1995).
- [2] B.S. Gregori-Valdés, M. Guerra, G. Mieres, L. Alba, A. Brown, N.A. Rangel-Vázquez, M. Sosa and Y. de la Hoz. *Revista Iberoamericana de Polímeros*. 9, 377-388 (2008).
- [3] D. Di Trapani, G. Mannina, M. Torregrossa and G. Viviani. *Water Sci. Technol.* 61 (7), 1757-1766 (2010).
- [4] E. Quek, Y.P. Ting and H.M. Tan. *Bioresour. Technol.* 97, 32-8 (2006).
- [5] G. Robila, M. Ivanoiu, T. Buruiana and E.C. Buruiana. *J. Appl. Polym. Sci.* 66, 591-595. (1997).
- [6] H. Ullah, A.A. Shah, F. Hasan and A. Hameed. *Pak. J. Bot.* 42, 3357-3367 (2010).
- [7] I. Cruz, Y. Bashan, G. Hernandez-Carmona and L.E. de-Bashan. *Appl. Microbiol. Biot.* 97, 9847-9858 (2013).
- [8] J. Sun, J. Liu, Y. Liu, Z. Li and J. Nan. *Procedia Env. Sci.* 8, 166-172 (2011).
- [9] J.F. Kennedy, E.H.M. Melo and K. Jumel. *Biotechnol. Genet. Rev.* 7, 297-313 (1989).
- [10] K.V. Rajeshwari, M. Balakrishnan, A. Kansal, K. Lata and V.V.N. Kishore. *Renew. Sust. Energ. Rev.* 4, 135-156 (2000).
- [11] L. Kattimani, S. Amena, V. Nandareddy and P. Mujugond. *Iran. J. Biotechnol.* 7, 199-204 (2009).
- [12] L. Zhou, G. Li, T. An and Y. Li. *Res. Chem. Intermediat.* 36, 277-288 (2010).
- [13] M. Sousa, J. Azeredo, J. Feijó and R. Oliveira. *Biotechnol. Tech.* 11, 751-754 (1997).
- [14] NMX-AA-030-SCFI-2001. *Análisis de Agua*. México.
- [15] S.S. Naik and Y.P. Setty. *Int. J. Biol. Ecol. Environ. Sci.* 1, 42-45 (2012).
- [16] T. Romaskevicius, S. Budriene, K. Pielichowski and J. Pielichowski. *Chemija*. 17, 74-89 (2006).
- [17] W.J. Ng, *Industrial Wastewater Treatment*, World Scientific Publishing Company (2006).
- [18] Y.H. Lin, S.C.J. Hwang, W.C. Shih and K.C. Chen. *J. Appl. Polym. Sci.* 99, 738-743 (2006).
- [19] Y.J. Chan, M.F. Chong, C.L. Law and D.G. Hassell. *Chem Eng. J.*, 155, 1-18 (2009).

RED 2 DYE ADSORPTION BY CHITOSAN-BASED BIOADSORBENT: A KINETIC STUDY

¹Rosario Suárez-Reyes,¹ Alejandra Valdez-Zarco,¹ Celso Hernández-Tenorio, Rosa Elvira Zavala-Arce, José Luis García-Rivas,¹ Beatriz García-Gaitán

¹ *Instituto Tecnológico de Toluca, Av. Tecnológico S/N, Fraccionamiento La Virgen, Metepec, Edo. de México, México, C.P. 52149. Tel. +52 722 208 7224, beatrizggmx@yahoo.com*

Abstract

In this paper the synthesis of a chitosan-based bioadsorbent is presented, their characterization was completed by FTIR spectroscopy, scanning electron microscopy and surface area measurement; furthermore determination of the water content and adsorption kinetic at three temperatures were studied. Prior to the kinetic study, optimum conditions were determined: ratio of hydrogel mass-dye concentration also pH of adsorption. It was concluded that the bioadsorbent is capable of removing Red 2 dye from aqueous solutions at an acidic pH, and can be used for environmental remediation.

Introduction

Water pollution is caused by many chemical products, some of them are dyes [2], which are discharged into the atmosphere by industries that require to produce higher volumes for the sustenance of daily life, e.g.: pulp industry, paper, textile, food, wine, oil, metallurgy, tanning, metal finishing, pharmaceutical industry, etc. [1].

Effluents with high concentrations of azo dyes in water bodies has triggered a significant negative effect on human health, and a serious hazard for aquatic living organisms furthermore during the decomposition of dyes may occur amines, which are toxic compounds even more harmful than the dye itself. An application that is currently gaining importance has been the use of hydrogels as polishing treatment of wastewater by removing contaminants that have not removed on conventional treatments [3].

Hydrogels as being relatively new materials, still under investigation and characterization, lack of a precise definition of hydrogel, but it can be described as a polymeric material shaped three-dimensional cross-linked network of natural or synthetic origin, which swells in contact with the water giving rise to a soft, resilient material and that retains a significant fraction thereof in their structure without dissolving [4]. So that they have become very important due to their applications in the fields of biomedicine, optics, agriculture, engineering, food, agroforestry, environmental, and even more in recent years in the removal of synthetic dyes type azo which are generally toxic and carcinogenic, one such example is the dye Red 2.

Experimental

Experiments were carried out using the following reagents: commercial dye Red 2 was supplied by Sensient Co.; polyvinyl alcohol (PVA) USP grade high viscosity was purchased from Golden Bell; ethyleneglycol diglycidylether (EGDE) was acquired from Tokyo Chemical Industry Co. and used without further purification; chitosan (Q) was supplied by Alimentos America; all other utilized reagents were analytical-reagent grade. Distilled water was used to prepare all solutions.

Chitosan was dissolved in 0.4 M acetic acid and PVA in deionized (DI) water to obtain solutions at 3.1 wt% and 10.17, respectively. Subsequently both solutions were mixed, and then the resulting mixture was dropped into a 0.1 M NaOH solution and formed hydrogel beads (Q-PVA). Q-PVA beads in DI water at

basic pH; nitrogen atmosphere and chemical cross-linking reagent EGDE were mixed and shaken for 6 h at 70 °C in a water bath. Finally cross-linked Q-EGDE-PVA beads were washed with DI water until the wash water pH was equal to the DI water.

Hydrogel wetness content was determined by drying them to constant weight in an oven at 40 °C. Functional groups identification of Q and PVA was made by a spectrometer 640-IR Varian FTIR using 16 scans with a 4 cm⁻¹ resolution and a 4000-500 cm⁻¹ range. FTIR spectra have been recorded using ground and dried samples. Morphology of Q-EGDE-PVA beads was observed by scanning electron microscope JEOL JSM-6610LV using acceleration voltage of 10 KV and backscattered electrons. Samples were previously lyophilized (17 h, -50 °C and 1.5 mbar). Surface area and pore volume on beads previously freeze-drying have been measured operating a Brand Bel Model Sorp Max device and using nitrogen gas at 100 °C for 3 h. The isotherm adsorption/desorption was adjusted to BET method.

Experiments for determining dye concentration-hydrogel mass were carried out on several 15 mL capacity vials, which contained dye solutions of 100, 200 and 300 mg/L at pH 2 and 40 to 80 mg Q-PVA-EGDE hydrogel. All solutions were taken into contact to two different masses in triplicate under the following experimental conditions: 10 mL of dye solution were added to the hydrogel mass in corresponding vials, and were stirred using an orbital thermo-shaker at 30 °C and 150 rpm during 72 h. Once the contact time was completed, solutions were decanted and pH of supernatants was measured. Dye concentration was quantified by UV-vis spectrophotometry.

R2 dye 200 mg/L solutions were prepared and adjusted at pH to 2, 3, 4, 5, 6 and 7 respectively, each of the solutions were put contacted in triplicate using an orbital shaker in vials with 40 mg of the hydrogel; under the following experimental conditions: 10 mL of dye solution, 30 °C and 150 rpm for 72 h. At end of contact time proceeded in a manner analogous to that described above.

Kinetic studies have been performed after preliminary of pH optimum testing using those conditions and three temperatures, 30, 40 and 50 °C in order to determine the best percentage of R2 dye removal; therefore, from a concentration of 200 mg/L of dye solution R2 was adjusted to pH 3 and vials were prepared with 40 mg of Q-EGDE-PVA beads by triplicate which were put in contact to 10 ml of solution and stirring speed was 200 rpm in an orbital shaker for 72 h at 18 different sampling times. Results are presented in Figure 4.

Results and Discussion

Percentage of water retained in the areas analyzed was 97.8%, so that Q-EGDE-PVA hydrogel can be classified as a high-swelling hydrogel. This high water content allows high permeability and good surface properties for the adsorption of the Red 2 dye.

Figure 1 shows the FTIR spectrogram of synthesized material and chemically cross-linked Q-EGDE-PVA. It is observed that the characteristic bands of chitosan are kept at 3460 and 3417 cm⁻¹ belonging a stretching vibration of a primary and deformation amine belonging to the group NH₂ to 1593 cm⁻¹ and 1026 cm⁻¹, band corresponding to the characteristic bond of COC polysaccharides such as is observed at the chitosan.

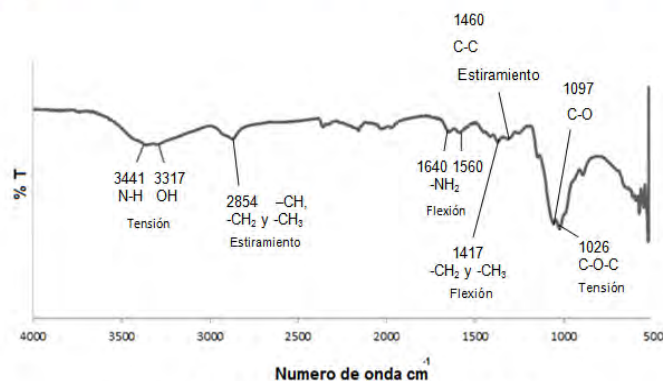


Figure 1. FTIR spectra of Q-EGDE-PVA beads.

Micrographs in Figure 2 show morphology of Q-EGDE-PVA beads, were taken by SEM at a magnification of 500X and 33X, both with an accelerating voltage of 10KV using backscattered electron; where is evident the material porosity, all pore have different diameters and some cracks (Figure 2b) on the bead surface were formed possibly either the freeze drying process previously carried out during the preparation of the sample or by vacuum which they were subjected in the SEM at the time of taking the micrographs.

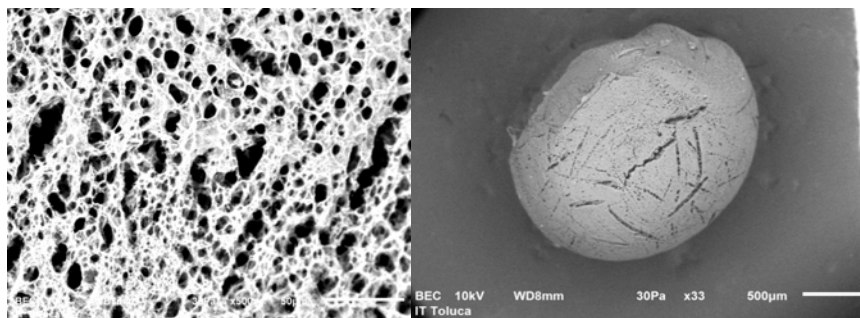


Figure 2. Micrograph of hydrogel Q-PVA EGDE amplified, a) at 500X and b) at 33X.

The surface area of the hydrogel Q-EDGE-PVA was determined by fitting the curve of isotherm adsorption-desorption obtained as measurement result by BET method, thereby obtaining a value of 65.85 m²/g of total surface area.

Results for determining dye concentration-hydrogel mass are presented in Table 1, which highlights the best adsorption conditions for Red 2 dye.

Table 1 Percentage removal at different concentrations of the dye Red 2 using different amounts of hydrogel.

Hydrogel mass (mg)	Percentage of removal at different concentrations of dye Red 2		
	100 mg/L	200 mg/L	300 mg/L
40	99.95	69.11	42.71
80	99.92	99.75	90.89

In Figure 3 shows results of the study of the behavior of the adsorption phenomenon of beads Q-EGDE-PVA varying the pH of the solutions containing Red 2 during a contact time of 72 hours, 150 rpm and 30 °C. The greater amount of dye adsorbed per gram of adsorbent material is in the range of pH 2 - 3, due to the high concentration of H^+ the active sites of the adsorbent were protonated so that the dye were negatively charged in aqueous media was attracted to the material being attached to it.

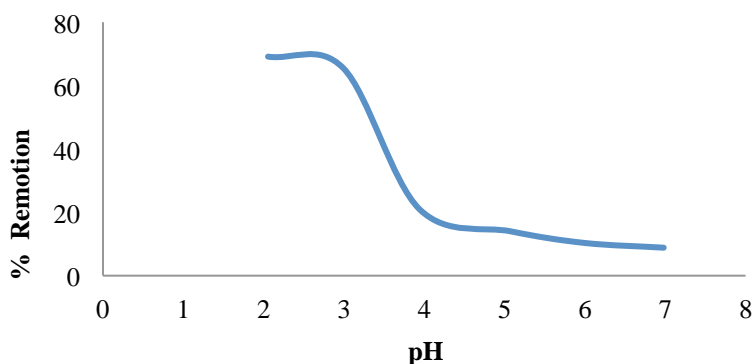


Figure 3 Effect of pH on the percentage of removal of dye R2 at 200 mg/L and 40 mg hydrogel.

Adsorption kinetics experimental data are presented in Figure 4, it is observed that the equilibrium was reached at 28 hours and kinetics behavior very similar for the three temperatures, which indicates that there are not an important dependence of temperature.

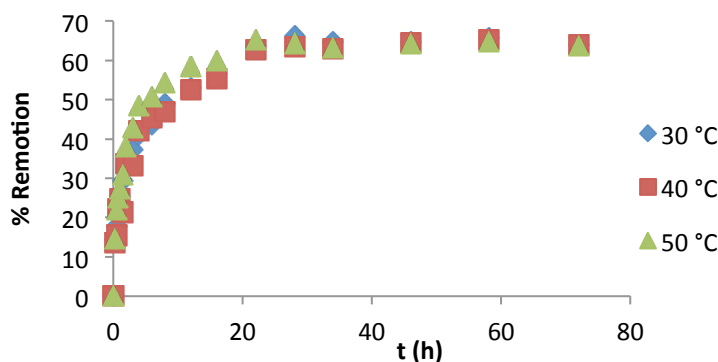


Figure 4. Percent dye removal R2 with respect to time at 30, 40 and 50 ° C

Conclusions

It is possible to perform the synthesis of hydrogel beads chitosan-based polyvinyl alcohol cross-linked with EGDE capable of adsorbing Red 2 dye at a pH between 2 and 3. The high percentage of water retained by the hydrogel synthesized favors the adsorptive capacity of Red 2. Using FTIR analysis it is possible to observe the major functional groups of each polymers. Characterization by SEM allowed knowing that hydrogel Q-EGDE-PVA is a porous material. Surface area was 65.85 m²/g. Adsorption tests showed that the best conditions to quantify the percentage of removal of dye were 200 mg/L of solution R2 at pH of 3 and 40 mg hydrogel. According to the results obtained the greatest percentage removal was 66.23%, achieving it at 30 ° C and 28 h.

Acknowledgements

Authors thank to DGEST for financial support to the project "Study of adsorption of red dye No. 2 areas of chitosan-PVA" (5219.14-P) and CONACYT for scholarships provided by Valdez-Zarco A. and Suarez-Reyes R.

References

- [1] Yuezhong W., Chensi S., Yanyan N., Shaoping T., Feng Y. 2012. "Glow discharge plasma in water: a green approach to enhancing ability of chitosan for dye removal". *Journal of Hazardous Materials*, Vol. 201-202, pp. 162-169.
- [2] Gupta V. K., Jain R., Nayak A., Agarwal S., Shrivastava M. 2011. "Removal of the hazardous dye-tartrazine by photodegradation on titanium dioxide surface", *Materials Science and Engineering*, Vol. C 31, pp. 1062-1067.
- [3] Wan N. W. S., Teong L. C., Hanafiah M. A. K. M. 2011. "Adsorption of dyes and heavy metal ions by chitosan composites: a review", *Carbohydrate Polymers*, Vol. 83(4), pp. 1446-1456.
- [4] Paipitak K., Pornpra T., Mongkontalang P., Techitdheer W., Pecharapa W. 2011. "Characterization of PVA-chitosan nanofibers prepared by electrospinning", *Procedia Engineering*, Vol. 8, pp. 101-105.
- [5] Katime I., Katime O., Katime D. *Los materiales inteligentes de este milenio: los hidrogeles macromoleculares. Síntesis, propiedades y aplicaciones*. 2004. Servicio Editorial de la Universidad del País Vasco. España. pp. 15-16.
- [6] García-Rivas L., García-Gaitán B., Antonio-Cruz R. C., Zavala-Arce R. E., Granados-García M., Dadó-Lujano I., Reyes-Gómez J., Luna-Bárcenas J. G. 2010. "Síntesis y caracterización de esferas de quitosano-EGDE-PVA para adsorción de Cu(II)", *Revista Iberoamericana de Polímeros*, Vol. 11(7), pp. 541-549.

SORPTION OF FLUORIDES USING CHITOSAN'S CRYOGELS

Arcos-Arévalo, A. J.¹, R.E. Zavala-Arce¹, P. Ávila-Pérez^{1,2}, B. García-Gaitán¹, J. L. García-Rivas¹ y M. L. Jiménez Núñez¹.

¹ *Tecnológico Nacional de México/Instituto Tecnológico de Toluca. Avenida Tecnológico S/N Fraccionamiento La Virgen, Metepec, México. C.P. 52149. zavalaarce@yahoo.com*

² *Dirección de Investigación Tecnológica, Instituto Nacional de Investigaciones Nucleares (ININ). Carretera México-Toluca S/N La Marquesa, Ocoyoacac, México. C.P. 52750.*

Abstract

Fluorine is a part of a lot of minerals, and through geochemical processes the salts containing fluoride are solubilized in aquifers, affecting the quality of drinking water and pose a risk to public health because its prolonged intake affects mainly the bone tissues, as well as increased susceptibility to kidney diseases and cancer, causes affectation in brain development and reduction IQ in school-aged children [1-3]. In Mexico more than five million people are chronically exposed to high concentrations of fluoride through water for human use and consumption. Whereby the present work, consisted in the synthesis of cryogels from chitosan cross-linked with ethylene glycol diglycidyl ether (QE) and their modification by carboxylation (QEC) and by impregnation with iron (QEH); and subsequent study of its capacity for removal of fluoride by conducting experiments in batch systems and assessing in turn the effect on the sorption capacity, the variation of the pH. Obtaining, the best sorption capacities of fluoride ions at pH 4; 17.52 mg F/g cryogel for QE, 12.51 mg F/g cryogel for QEC and 20.34 mg F/g cryogel for QEH.

Introduction

The fluorine content of the earth's crust is about 0.3 g/kg and is found in the form of fluorides in various minerals, and through geochemical processes the salts containing fluoride are solubilized in aquifers; therefore, most of the fluoride in drinking water is naturally occurring. In Mexico, there are regions where by the geological characteristics, the aquifers contain dissolved fluorine, affecting the quality of drinking water and assuming a risk to public. [1-5].

Although fluorine is too reactive to have some natural biological function, is incorporated into biologically active compounds; and if its intake is prolonged through water consumption, mainly affects bone tissues (bones and teeth), as well as the brain and spinal cord, has been shown that the accumulation of fluorides in the hippocampus of the brain causes degeneration of the neurons and decreased aerobic metabolism; as well as alteration of the metabolism of free radicals in the liver, kidney and heart [4-8].

The fluoride ions can be removed from water by using a suitable material to trap or retain such ions, ie by using a sorbent material; for which have been developed many synthetic resins. However, use of resins based on natural polymers is one interesting alternative because they are not toxic and their use can lower the cost of these treatments, as well as improve them [9-11]. One of these natural polymers is chitosan, since due to the presence of amino and hydroxyl groups in its structure, is able to interact with various ions. However, has a limited swelling in water which limits the accessibility to their groups; so to improve its effectiveness have been developed chemical and physical modifications, such as the preparation of cryogels; which provide a better structure due to the formation of macropores and microchannels, and by adding a crosslinking agent is possible to obtain a material more stable and resistant to interaction with aqueous solutions, providing better contact surface, which may contribute to increased efficiency in the adsorption process. Whereby the present work proposes the synthesis of chitosan's cryogels crosslinked with ethylene glycol diglycidyl ether, as well as modified by carboxylation and by impregnation with iron of these cryogels, in order to determine their performance as sorbents of fluorine ions present in water.

Experimental

In this paper were synthesized three cryogels, using for this, Industrial chitosan (American Food) with a deacetylation percentage of 67%; ethylene glycol diglycidyl ether (TCI), $\text{FeCl}_3 \cdot 6\text{H}_2\text{O}$ (Sigma-Aldrich), CH_2COOH (Meyer), ethanol (Meyer) and glacial acetic acid (Fermont). For the kinetic study NaF (Meyer) was used for preparing the solutions.

The QE cryogels's spheres were synthesized using the methodology described by [12], later in order to enhance the sorption capacity of these cryogels two modifications were made; which consisted of carboxylation of QE cryogels and the addition of Fe (III) to QE cryogels.

The carboxylation was performed by contacting the QE cryogels with a solution 0.5 M of CH_2COOH , with constant stirring and maintaining a pH of 8, later was washed until a neutral pH; to finally obtain the QEC cryogels [13].

The conditioning with iron was made with a 0.1 M solution of FeCl_3 , which was in contact with QE cryogels with constant stirring, for subsequent washing with ethanol, thus obtaining the QEH cryogels [14 and 15].

Finally were carried out comparative kinetics adsorption between the QE, QEC and QEH cryogels, the tests consisted on placing 0.1 g wet weight of spheres of each of the cryogels in contact with 10 mL of a solution of 10 mg/L fluorine, adjusting the pH of said solution to the following values: 4, 5, 6 and 7, at a temperature of 303.15 °K and evaluating different time intervals.

Results and Discussion

The results of the kinetic studies performed are shown below in figure 1. As can be seen in A), using a pH 7 none of the material reaches the sorption equilibrium; this behavior may be due to an interference of the OH ions from the fluorine solution.

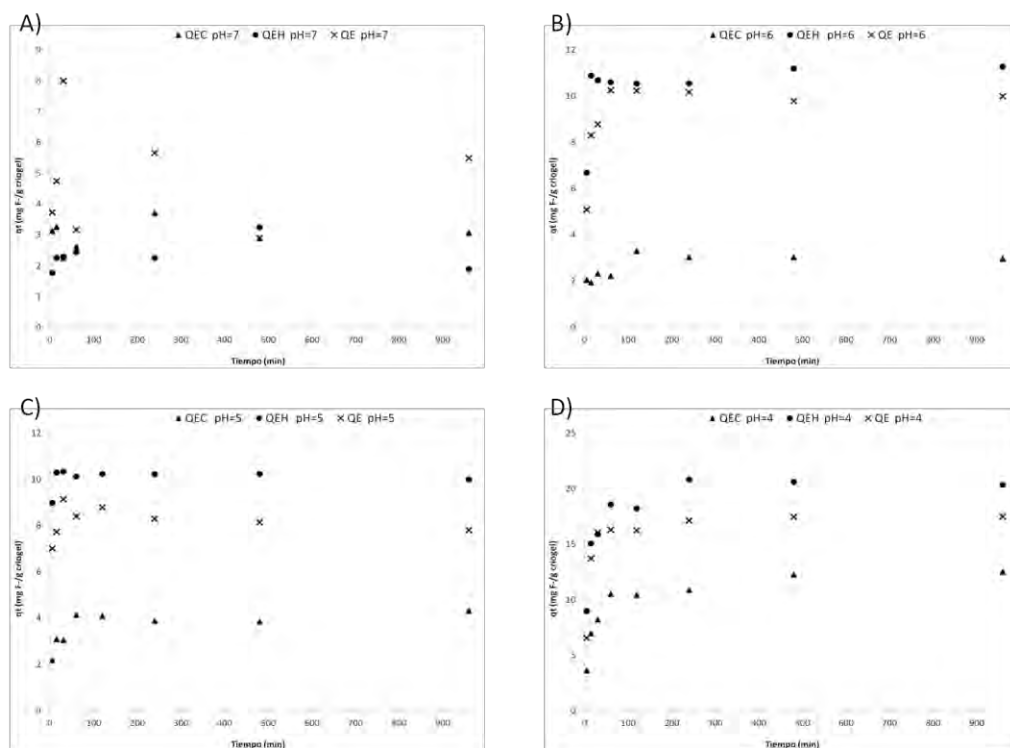


Figure 1. Kinetics studies

On the other hand in B), C) and D), it can be seen that the removal values are increasing during the first minutes of the experiment and then begin to stabilize until equilibrium is reached. The equilibrium time was taken as the time after which there was no significant change in the amount of fluorine captured by the materials; so it was determined that in general the equilibrium time for all cryogels is 480 min, since after this time the data show no significant changes.

Table 1. Summary of sorption capacity

Cryogel	pH 6	pH 5	pH 4
	q_e (mg F/g cryogel)	q_e (mg F/g cryogel)	q_e (mg F/g cryogel)
QE	10.2	8.0	17.5
QEC	3.0	4.3	12.5
QEH	11.3	10.1	20.4

As shown in Table 1, the highest sorption capacities are shown by the QEH cryogel for the three pH, followed by QE cryogel. It can also be seen that lowering the working pH until 4, the sorption capacities are increased significantly in all cryogels, particularly for the QEC cryogel, that increases about four times its sorption when compared to the capacity presented in the pH 6. This behavior can be attributed to protonation of the cryogels interacting with the acidic medium of the fluoride solutions, and in accordance with that reported by [7 and 15-18]; possible interactions between the fluoride ion and cryogels may be as shown in Figures 2, 3 and 4.

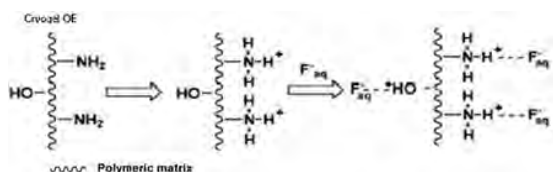


Figure 1. QE Cryogel

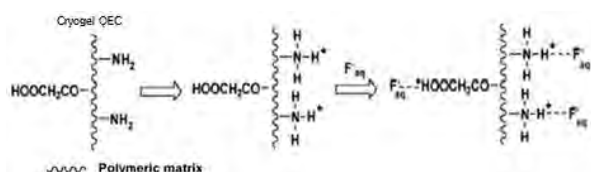


Figure 2. QEC Cryogel

Commonly in media with low acidity, the fluorine ions tend to interact with the hydroxyl or carboxyl groups present in the polymeric matrix, however, as shown in Figures 1 and 2, the amino groups present in the cryogels may be protonated in the acidic mediums, allowing that the fluoride ions can interact more easily with these groups, through the possible formation of hydrogen bonds, and by increasing the number of functional groups available for the removal of fluoride ions.

By other hand in Figure 3, it can be seen that the possible mechanism referred to by the authors aforementioned, is via the formation of complexes between the iron in the cryogel and the fluorine ions, as well as by electrostatic interactions or through interactions acid-base of Lewis, between iron and the fluorine ions. In this case it is possible that being in an acidic medium, the iron present in the QEH cryogel, present a greater affinity for fluoride ions.

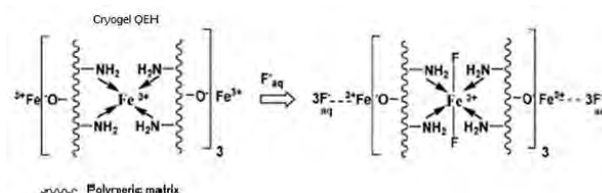


Figure 3. QEH Cryogel

As show the data in Table 1, the most appropriate pH for sorption of fluorine ions, is the pH 4, so below is presented the fit of the experimental data obtained from the three cryogels at this pH, for kinetic models of Lagergren and Ho through a nonlinear regression using the program Origin 8.1, a summary of the parameters obtained is showing in Table 2.

Table 2. Summary of kinetic models

Cryogel	<i>Lagergren model</i>			<i>Ho model</i>		
	R^2	$K_1 (min^{-1})$	$q_e (mg g^{-1})$	R^2	$K_2 (mg^{-1} min^{-1})$	$q_e (mg g^{-1})$
QE	0.99	-0.11	16.95	0.98	9.16×10^{-3}	17.83
QEC	0.95	-0.06	11.34	0.98	6.77×10^{-3}	12.14
QEH	0.96	-0.10	19.36	0.99	7.62×10^{-3}	20.47

While it can be assumed that the Lagergren model presents a slightly better fit for the QE cryogel, graphically the Ho model represents better the behavior of the experimental data of the three cryogels; this model suggests that in the sorption may be involved a chemical sorption and that sorption speed depends on the adsorption capacity in balance and not on the concentration of the adsorbate [19].

The sorption capacities obtained from the three synthesized materials, in the pH 4, 5 and 6 are competitive when compared with that reported by other authors as [6-8, 15-18 and 20-25]. Being the sorption capacities obtained at pH 4 of the three cryogels higher than the data previously reported by these authors; however it is also observed that the working pH chosen as optimal in these works range from pH 6 to 7; and when comparing the sorption capacities obtained at pH 6 in this work, it is observed that the QE and QEH cryogels have higher values than those of the other works, making them competitive and suitable materials to be used in the removal fluorine, being QEH cryogel the best suited of the three materials synthesized because it is the one with the higher sorption capacities.

Conclusions

The synthesized cryogels are suitable materials to be used as sorbents of fluoride ions. Being the QEH cryogel the most suitable of the three synthesized cryogels because this is the one with the highest sorption capacity. It was also observed that the optimum pH for removal of fluorides using these materials is pH 4.

Acknowledgements

To the Consejo Nacional de Ciencia y Tecnología (CONACYT), for the scholarship given.

To the la Dirección General de Estudios Superiores Tecnológicos (DGEST), for supporting the 5194.13-P project.

To the Instituto Nacional de Investigaciones Nucleares (ININ).

To the División de estudios de Posgrado e Investigación (DEPI) an the Laboratorio de Investigación en Ingeniería Ambiental del Instituto Tecnológico de Toluca.

References

- [1] Galicia-Chacón, L., Molina-Frechero, A., Oropeza-Oropeza, A., Gaona, E. and L. Juárez-López, Rev. Int. Contam. Ambie. 27, 4 (2011).
- [2] Trejo-Vázquez, R., J. R. Treviño-Díaz and E. García-Díaz, Conc. Tec. 36 (2008).
- [3] Vega-Gleason, S., Com. Nac. del Agua. Gerencia de Saneamiento y Calidad del Agua (2012)
- [4] ATSDR (2004).

- [5] WHO/OMS. Guías para la calidad del agua potable. 3rd. ed. vol. 1 (2006).
- [6] Viswanathan, N. and S. Meenakshi, J. of Col. and Int. Sci. 322 (2008).
- [7] Viswanathana, N, C. S. Sundaram and S. Meenakshi, Col. and Surf. B: Bioint. 68 (2009).
- [8] Viswanathan, N. and S. Meenakshi, Col. and Surf. B: Bioint. 72 (2009).
- [9] SIFYQA (2007).
- [10] García-Aragón, J. A., C. Díaz Delgado, P. Morales Reyes, P. Ávila Pérez, S. Tejeda Vega and G. Zarazúa Ortega, Ing. Hid. Méx. 38, 4 (2003).
- [11] García-Aragón, J. A., C. Díaz Delgado, E. Quentin, P. Ávila Pérez, S. Tejeda Vega and G. Zarazúa Ortega, Hidrobio. 17, 2 (2007).
- [12] Corral C., N. G., A. J. Arcos A., R.E. Zavala A., P. Ávila P., B. Garcia G., R. M. Gomez E. and R. I. Bartolo A., XIII Congreso Internacional y XIX Congreso Nacional de Ciencias Ambientales. Guerrero, México (2014).
- [13] Jeon, C. and W. H. Höll, Water Res. 37 (2003).
- [14] Chensi Shen, Hui Chen, Shaoshuai Wu, Yuezhong Wen, Lina Li , Zheng Jiang, Meichao Li and Weiping Liu, J. Haz. Mat. 244– 245 (2013).
- [15] Viswanathan N. and S. Meenakshi, J. Fluorine Chem. 129 (2008).
- [16] Viswanathan, N., C. Sairam Sundaram and S. Meenakshi, J. Haz. Mat. 161 (2009).
- [17] Huang, R., B. Yang, Q. Liu and K. Ding, J. Fluorine Chem. 141 (2012).
- [18] Viswanathan, N., C. S. Sundaram and S. Meenakshi, J. Haz. Mat. 167 (2009).
- [19] García-Mendieta, A., DEPI, ITToluca México, Tesis doctoral (2010).
- [20] Sahli, Menkouichi M.A., S. Annouar, M.Tahaikt, M. Mountadar, A. Soufiane and A. Elmidaoui, Desalination 212 (2007).
- [21] Kamble, S. P., S. Jagtap, N. K. Labhsetwar, D. Thakare, S. Godfrey, S. Devotta and S. S. Rayalu, Chem. Eng. J. 129 (2007).
- [22] Viswanathan, N. and S. Meenakshi, J. Haz. Mat. 178 (2010).
- [23] Dongre, D. N., Ghugal, J. S. Meshram and D. S. Ramteke, African J. Env. Sci. and Tec. 6, 2 (2012).
- [24] Kumar, E., A. Bhatnagar, M. Ji, W. Jung, S. Lee, S. Kim, G. Lee, H. Song, J. Choi, J. Yang and B. Jeon, Water Res. 43 (2009).
- [25] Gandhi, N., D. Sirisha, K.B. Chandra Shekar and S. Asthana, Int. J.ChemTech Res. 4, 4 (2012).

EVALUATION OF THE ADSORPTION OF RED 2 DYE IN AQUEOUS SOLUTION USING CHITOSAN-CELLULOSE HYDROGEL BEADS

J.I. Moreno-Puebla¹, C. Hernández-Tenorio¹, B. García-Gaitan¹, J.L. García-Rivas¹,
R.E. Zavala-Arce¹, J. H. Pacheco-Sánchez¹

¹ *Instituto Tecnológico de Toluca, Av. Tecnológico s/n. Fraccionamiento La Virgen
Metepéc, Edo. De México, México C.P. 52149.*

Abstract

The project aims to develop an effective material with the ability to remove water pollutants, specifically anionic dyes. Aqueous solutions of Red 2 dye were put in contact with chitosan-cellulose hydrogels cross-linked with ethylene glycol diglycidyl ether under different conditions. Then their adsorptive capacities were compared using different kinetic models to identify the mechanisms of the phenomenon and evaluate if the hydrogels removal capacity and speed are significant and justifies their use in a practical implementation of this technology.

Introduction

Water pollution of rivers and lakes is due mainly to substances that are used with increasing frequency. For example, the use of some household products (detergents), agriculture (pesticides, herbicides and fertilizers) and effluents from industries (dyes, heavy metals) in wastewater from population centers.

The dyes, especially those of synthetic origin that are present in wastewater, are responsible for many harmful effects to the environment, flora and aquatic fauna. Among the most important effects are: the reduction of dissolved oxygen, the formation of recalcitrant and toxic compounds to cells, obstructing the passage of light to the water bodies and aesthetic impairment [1]. Red No. 2 is an azo dye that may cause intolerance in people who are affected by salicylates. Moreover, it is a histamine liberator, and may intensify symptoms of asthma. It is also involved in cases of hyperactivity in children when used in combination with benzoates. A connection has been established between the consumption of Red No. 2 and tumor production by experiments in rats, but is not yet proven in humans. For these reasons, many countries like the United States have restricted its use [4].

Chitosan is an abundant and inexpensive polymer with desirable characteristics to be a good adsorbent of dyes, such as high adsorption capacity, easy access, low cost, mechanical stability, environmentally friendly and high selectivity to remove a wide range of dyes without requiring complicated modifications [2]. The chitosan-cellulose hydrogel maintains these properties along with a good surface area and mechanical resistance while having a size which allows it to be used in continuous flow systems.

The removal of dyes by adsorption is a good alternative because of its efficiency and hydrogels are becoming increasingly important in the removal of contaminants so the aim of this study is to evaluate the adsorption capacity of chitosan-cellulose hydrogel beads in Red No. 2 dye aqueous solutions by using kinetic models.

Experimental

The experiments were performed using chitosan from America Alimentos with a desacetylation rate of 67%, microgranular cellulose from Sigma-Aldrich and commercial Red No. 2 dye.

Synthesis

The hydrogel synthesis was based on the method described by Li and Bai [3] with some modifications to use food grade chitosan instead of reagent grade. Chitosan was dissolved in acetic acid solution with moderate stirring. After 4 hours of stirring cellulose was added and allowed to homogenize by stirring at medium speed with a mechanical propeller stirrer.

The mixture was dripped into a solution of NaOH to form the spheres, which were under constant agitation at room temperature for 12 hours. The beads were removed from the NaOH solution and washed with distilled water in a beaker to be agitated at a moderate rate using a magnetic stirrer plate until they were at the pH of distilled water. The beads were left at low temperature with distilled water until crosslinking.

Crosslinking

Distilled water was adjusted to pH = 12 and was placed in a round bottom flask together with the beads in a certain proportion. The flask was left in a thermostatic bath to a temperature of 70 ° C, then was added ethylene glycol diglycidyl ether using a micropipette. The crosslinking reaction was carried out for 6 hours under a nitrogen atmosphere, and then allowed to cool to room temperature. Beads were removed from the solution and they were washed with distilled water until they were at the pH of distilled water.

Preliminary tests

Red No.2 solutions adjusted to 100, 200 and 300 ppm were prepared at different pHs, (2, 3, 4, 5, 6 and 7), approximately 50 mg of the hydrogel were placed in vials and 10ml of the Red No. 2 solution were added were added 2 and stirred at 150 RPM at 30 ° C for 72 hours.

Kinetics

From the results of the preliminary tests it was determined that the kinetic would take place by using a solution of Red No. 2 with an initial concentration of 200 ppm and 30 mg of the hydrogel at 200 RPM, starting to determine concentration at 0.25 hours with varied intervals until 72 hours.

Results and Discussion

In the test performed by varying the pH of the solution with dye was found that less than in pH of 3 or inferior the removal of dye increased compared to the removal obtained at higher pHs so it was decided to conduct the kinetic experiments initiating at a value of pH 3 (Fig. 1):

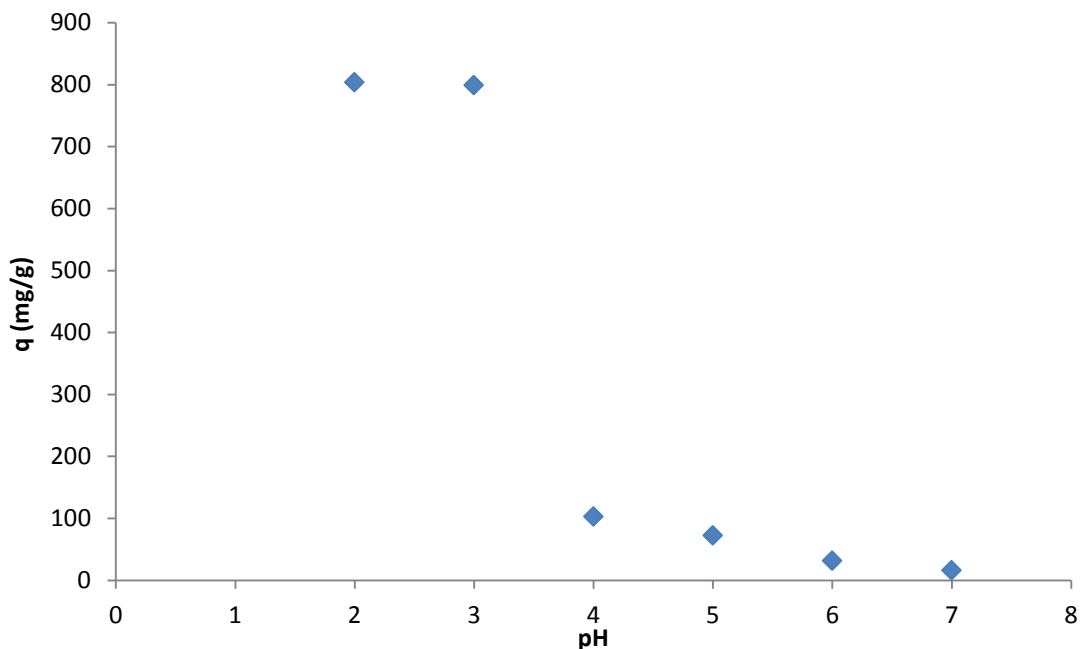


Fig.1. Graph of initial pH of the solution versus q obtained after 72 hours.

Upon completion of the kinetics experiments it was determined that the temperature increased slightly the removal of dye from the aqueous solution within the temperature range studied, although the temperature is seen to have little to no effect on the time taken to reach equilibrium, which was reached at 72 hours approximately with q_e values of 1005, 1048 and 1080 mg/g for the 30, 40 and 50°C temperatures respectively (Fig. 2):

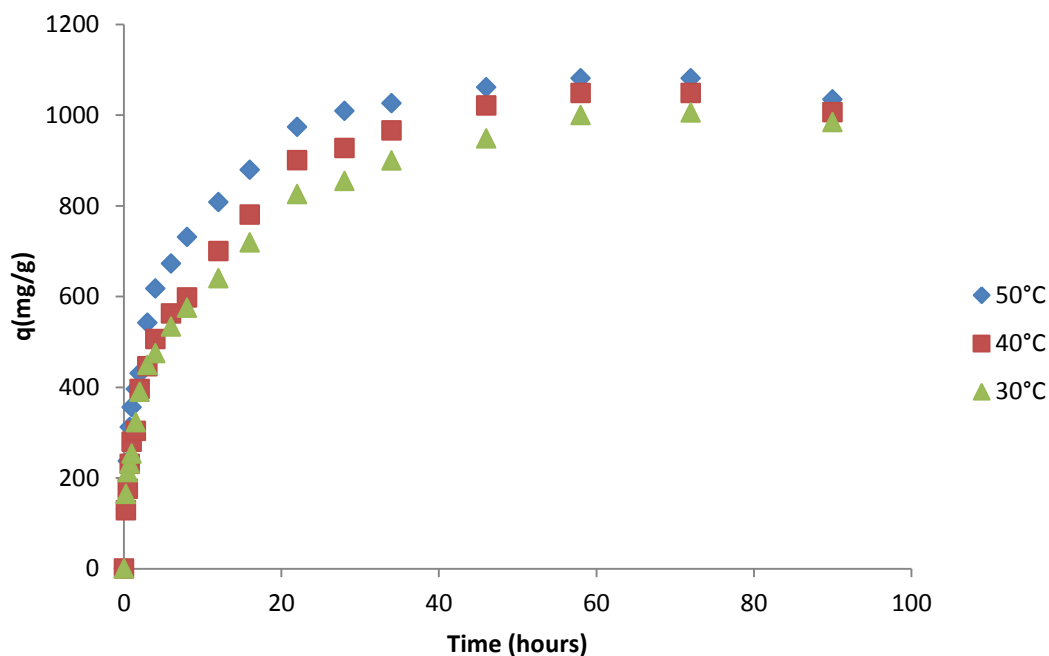


Fig.2. Graph comparing the three kinetic studies performed at different temperatures.

The data obtained from the kinetics were fitted to the models of Ho-McKay and Elovich yielding high adjusted correlation coefficients (Table 1), especially for the Elovich Model, the tight fitting can also be appreciated in the graph (Fig. 3):

	30°C	40°C	50°C
Ho-McKay	0.9430	0.9663	0.9736
Elovich	0.9765	0.9810	0.9912

Table 1: Adjusted correlation coefficients of the fittings.

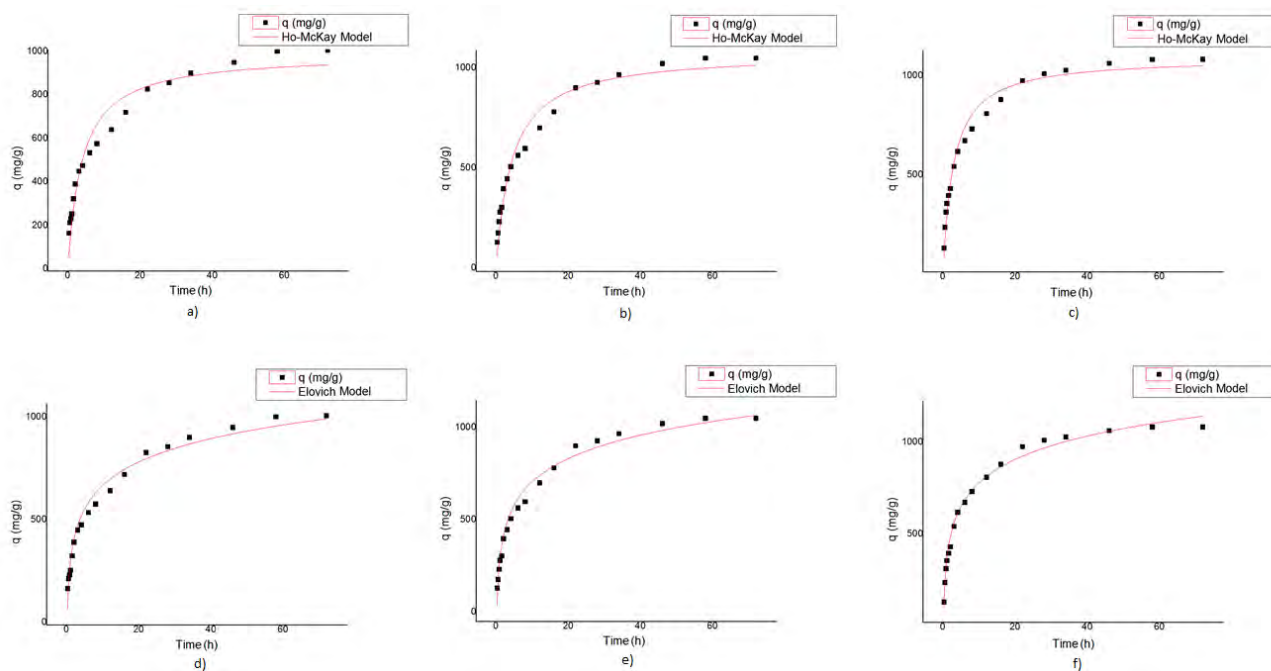


Fig. 3: Graphs of the fittings: a), b) and c) fittings to Ho-McKay model at 30, 40 and 50 ° C temperatures respectively, d), e) and f) fittings for Elovich model at 30, 40 and 50 ° C temperatures respectively.

Conclusions

The chitosan-cellulose hydrogel cross-linked with ethylene glycol diglycidyl ether has a good capacity for dye adsorption at acid pH but this capability significantly decreases as the pH approaches neutrality, it is presumed this is because the primary mechanism of adsorption of dye is due to the electrostatic attraction that occurs between the amino group protonated in acidic media with the dye dissociated in the solution that possesses a negative charge as it loses its sodium positive ions.

By performing the kinetic to three different temperatures and slight increase of dye removal in higher temperature was found in the range of temperatures studied, however, the temperature has little to no effect on the time it takes to reach equilibrium.

The data fitted with a high correlation coefficient to the models of Ho-McKay and Elovich being especially good for the latter which may indicate the presence of chemisorption, details about the specific mechanisms of adsorption of hydrogel require more experiments to determine the mediums that lead to removal of dye out of the solutions.

Acknowledgements

To the Instituto Tecnológico de Toluca and its División de Estudios de Posgrado e Investigación for providing the the instalations of the Laboratorio de Investigación en Ingeniería Ambiental to perform the experiments.

To the Dirección General de Educación Superior Tecnológica for providing the resources to develop the project through the “Estudios de sorción en sistemas de batch y continuo, con hidrogeles y criogeles a base de quitosano” project, code 4625.12-P.

To CONACYT and COMECYT for providing economic support.

References

- [1] A. Arango-Ruíz and L.F. Garcés-Giraldo, Remoción del colorante azoico amaranto de soluciones acuosas mediante electrocoagulación, *Lasallista de Investigación*, 6(2), 31-38 (2007).
- [2] G. Crini, Application of chitosan and its derivatives as adsorbents for dye removal from water and wastewater: A review, *Carbohydrate polymers* 113, 115–130 (2014).
- [3] N. Li and R. Bai, Copper adsorption on chitosan-cellulose hydrogel beads: behaviors and mechanisms. *Trans IchemE*, 76, Part B: 332-340 (2004).
- [4] S.L. Rodríguez-Amézquita, Identificación y cuantificación de colorantes artificiales en refrescos en polvo elaborados y/o distribuidos en Guatemala. Tesis de Licenciatura, Universidad de San Carlos, Guatemala, 13-14, (2008).

ENCAPSULATION OF EXTRACTANTS WITH BIOPOLYMERS FOR PALLADIUM RECOVERY

T. Imelda Saucedo Medina,¹ Ricardo Navarro Mendoza,¹ Mercy Dzul Erosa,¹ Esperanza García Vieyra,¹ María del Pilar González Muñoz,¹ Enrique Elorza Rodríguez,² Eric Guibal.³

¹ *Departamento de Química. Universidad de Guanajuato, México. E-mail: sauceti@ugto.mx*

² *Departamento de Ingeniería en Minas, Metalurgia y Geología. Universidad de Guanajuato, México.*

³ *Ecole des mines d'Alès, Francia.*

Abstract

A new generation of extractant impregnated resin has been elaborated by encapsulation of extractants in biopolymer capsules. The extractant forms the core of the spherical particle, while the biopolymer entraps the extractant in a shell. The immobilization can reduce the loss of extractant, and it makes possible the use of the system in simple fixed bed columns. Cyanex 302 (bis(2,4,4-trimethylpentyl)monothiophosphinic acid) was immobilized into alginate capsules prepared by ionotropic gelation in CaCl_2 solutions. The influence of a series of parameters on microcapsule preparation was investigated. Selected materials were tested for Pd(II) recovery from HCl solutions through equilibrium and kinetic sorption studies.

Introduction

Regardless of the application (environmental purpose or resource valorization), metal ions may be recovered from aqueous solutions through different techniques such as precipitation, membrane processes, electrodeposition, liquid-liquid extraction or ion-exchange/chelating resins.¹ The choice of the process is controlled by the characteristics of the effluents, the value of the metal, its concentration, the regulations concerning its discharge into the environment etc. Solvent extraction is frequently used because of its high selectivity for target metals.² The extractant can be used directly dissolved in the organic phase (liquid-liquid extraction) or impregnated on a polymeric support such as membranes (SLM, supported liquid membrane) or resins.³ Recently, several processes have been described for the encapsulation of extractants by incorporation a porous polymer matrix.^{4,5} These materials allow the extraction, the separation and the selective recovery of valuable metals with several advantages or benefits compared to conventional liquid-liquid extraction: stability of the extractant, easier operating conditions, limitation of extractant loss (due to mechanical or chemical effects) and prevention of the formation of ternary phases. The present work focuses on the encapsulation of Cyanex 302 (bis(2,2,4-trimethylpentyl)monothiophosphinic acid) in calcium alginate gel. The composite beads are prepared by ionotropic gelation of sodium alginate drops (which contain the extractant) into a CaCl_2 solutions. In this case, the encapsulation process consists in the embedment of extractant drops into a thin polymer layer that serves as a confinement barrier (which can be only crossed through by specific species which have appropriate affinity): the confinement barrier allows reducing the use of solvents, decreasing the possible loss of extractant and making easier the phase separation process. In a first step, the intrinsic parameters that control the formation of alginate gel beads (without extractant) have been investigated: type of alginate (viscosity), biopolymer concentration, concentration of the gelling agent (CaCl_2 concentration). The morphological and mechanical characteristics of the gel beads have been analyzed in order to select experimental conditions for the encapsulation of Cyanex 302. Different lots of composite beads (microcapsules) have been prepared (varying the proportions of extractant and alginate) and tested for Pd(II) recovery from HCl solutions.

Experimental

Three different samples of alginate were supplied by Sigma Aldrich; these three samples were characterized by their viscosity (measured at 40 °C, from 1 % w/w alginate/aqueous solutions): LVA (low viscosity alginate: 4.07 ± 0.05 cps), MVA (medium viscosity alginate: 4.93 ± 0.09 cps) and HVA (high viscosity alginate: 77.12 ± 0.25 cps). The extractant, Cyanex 302 (bis(2,2,4-trimethylpentyl)monothiophosphinic acid), was obtained from CYTEC (Canada).

Synthesis of alginate beads and microcapsules. Alginate gels beads and microcapsules were produced with an encapsulator (Büchi B-390) (Switzerland); this equipment allows the production of reproducible and standardized lots of beads and capsules making profit of the possibility to play simultaneously on the pressure (in the vessel containing the biopolymer), vibration frequency (at the level of the injector or nozzle), and the electrostatic charge of the beads (preventing their agglomeration). For the production of alginate gel beads, the vibration frequency was set to 300 Hz, the electrode potential was adjusted to 2,500 V, the pressure to 75-100 mbar, and the inner diameter of the nozzle was 750 μm . Different concentrations of alginate have been tested depending on their respective viscosity: for LVA alginate concentration was set to 1, 2, 3 and 4 % (w/w), for MVA alginate concentration was fixed to 1, 2 and 3 % (w/w) while for HVA the high viscosity of the biopolymer did not allow using higher concentration than 1 % (w/w). Three different concentrations of gelling agent (i.e., CaCl_2) have been carried out: 0.1, 0.5 and 1.0 M.

For the synthesis of microcapsules the experimental procedure changed: two concentric nozzles (300/500 μm ; i.e., diameter of the internal nozzle (extractant flow), and external nozzle (biopolymer solution), respectively). The vibration frequency was 350 Hz, the electrode potential was fixed to 2,500 V and the pressure was adjusted to 350 mbar. In this case only HVA was used at the concentration of 0.5 % with a flow rate of 15 mL min^{-1} . The extractant (i.e., Cyanex 302) was diluted in kerosene (1:1, v/v) and pumped with different flow rates: 1 mL min^{-1} (MC1), 1.5 mL min^{-1} (MC2), and 2 mL min^{-1} (MC3); the microcapsules were stabilized by ionotropic gelation using a 0.5 M CaCl_2 solution. The gel beads and the microcapsules were maintained in the ionotropic gelation solution for 24 h, before being rinsed with water. The stocks of beads and microcapsules were stored in 0.1 M CaCl_2 solution. Optical microscopy (160 X) was used for characterizing the macroscopic properties of the materials.

Study of extraction performance. The impact of HCl concentration on the efficiency of Pd(II) extraction was performed by contact for 48 hours of 40 mg of sorbent (MC1, m, g) with a 10 mL volume (V) of a 50 mg Pd L^{-1} solution (C_0) prepared from different HCl solutions ($C(\text{HCl})$: 0.01, 0.1, 0.5, 1, 2, 3, 4 and 5 M). Palladium residual concentration was determined by flame atomic absorption spectrometry (AAS) and the sorption capacity was determined by the mass balance equation. Systematically the sorbent dosage (SD, m/V) was set to 4 g L^{-1} . Agitation speed was 150 rpm and all the experiments were performed at 20 ± 1 °C.

Sorption isotherms were obtained by contact of the microcapsules (MC1) with Pd(II) solutions prepared from 0.5 M HCl solutions varying metal concentration from 10 to 250 mg Pd L^{-1} (SD: 4 g L^{-1}). Sorption isotherms were modeled with the Langmuir equation using non-linear regression facilities of Mathcad software (Version Plus 6.0, Mathsoft, Inc.).

Uptake kinetics were studied varying the sorbent dosage (SD: 4 and 10 g L^{-1}) by contact of the microcapsules (MC1) with 100 mL of a 50 mg Pd L^{-1} solution (prepared in 0.5 M HCl solution); samples (0.5 mL) were collected at fixed contact times, filtrated and analyzed for residual metal concentration.

Results and Discussion

Preparation of alginate gel beads. Prior to the manufacturing of microcapsules the influence of experimental parameters such as alginate concentration (depending on the viscosity and the type of sodium alginate: LVA, MVA, HVA) and CaCl_2 concentration was studied through a series of experiments with the objective of optimizing the morphology and the mechanical resistance of the encapsulating material. Table 1 reports the main conclusions of this preliminary study. With LVA sample, the increase in the concentration of alginate leads to the formation of beads that are more spherical and more homogeneous in size. The best alginate beads (with LVA) were obtained at alginate concentrations of 3 and 4 % with average diameters in the range 1.22-1.88 mm. With MVA sample it was more difficult obtaining spherical particles: actually they have an ovoid form (and even drop form with 1 % alginate concentration). When the concentration of the biopolymer increases the raise of the viscosity leads to the formation of very heterogeneous particles (both in size and form), especially with 3 % alginate concentration (where the beads tended to agglomerate). In the case of HVA sample (high viscosity alginate) the concentration was set to 1 % giving very spherical particles with appropriate mechanical properties (shown by good resistance to strong agitation). This alginate was selected for further experiments.

Figure 1 shows the results obtained with varying the concentration of CaCl_2 in the ionotropic gelation media (using 1 % HVA solution). When increasing CaCl_2 concentration the heterogeneity in size of the beads tends to decrease and concentrations of 0.5 M and 1 M seem the more appropriate for the ionotropic gelation of alginate solutions.

Table 1. Microphotographs of alginate gel beads for LVA (low viscosity), MVA (medium viscosity) and HVA (high viscosity) samples (0.1 M CaCl_2 ; nozzle: 750 μm ; alginate flow rate: 20-25 mL min^{-1}).

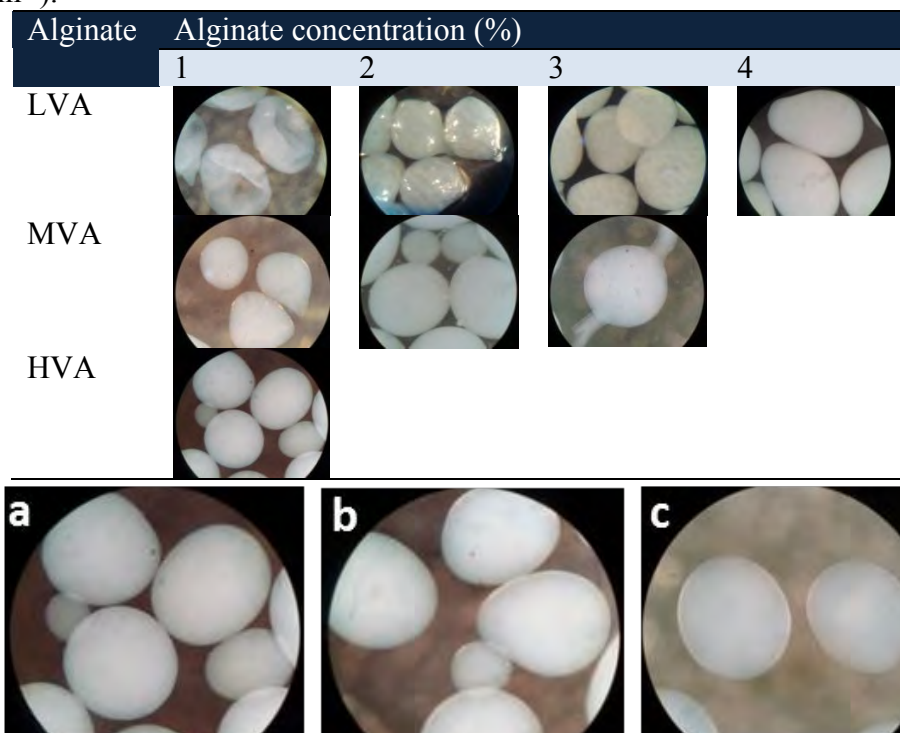


Figure 1. Effect of CaCl_2 concentration on the ionotropic gelation of alginate (HVA, 1 % w/w): a) 0.1 M; b) 0.5 M and c) 1.0 M (nozzle: 750 μm , alginate flow rate: 20-25 mL min^{-1}).

Preparation of alginate-Cyanex 302 microcapsules. Preliminary studies have shown that with alginate concentrations higher than 0.5 % (w/w) the microcapsules were heterogeneous both in size and morphology. On the basis of these preliminary observations and the results of the previous section, microcapsules were prepared using HVA at the concentration of 0.5 % (w/w); the ionotropic gelation being performed in 0.5 M CaCl_2 solutions. Figure 2 shows 3 lots of microcapsules prepared with different flow rates of extractant (MC1, MC2, MC3). Under these conditions the MCs are generally mononuclear, spherical and homogeneous in size: the size of the capsule varies in the range 0.69-0.74 mm while the extractant nucleus varies in the range 0.32-0.58 mm (depending on the flow rate of the extractant).

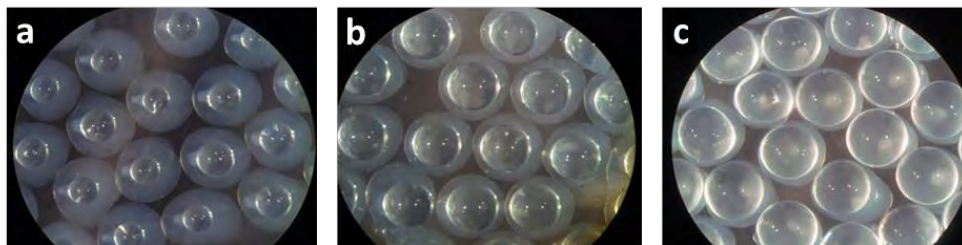


Figure 2. Microcapsules of Cyanex 302 prepared with HVA (0.5 % w/w and 0.5 M CaCl_2 as the ionotropic gelation solution; size of concentric nozzles: 300/500 μm ; alginate flow rate: 15 mL min^{-1} ; Cyanex 302 flow rate: a) MC1: 1.5, b) MC2: 2.0, c) MC3: 3.0 mL min^{-1}).

The mechanical stability of the MCs was investigated by contact of 0.1 g of MCs with 10 mL of HCl solutions (concentrations: 0.01, 0.5 and 5 M) for three days. While MC2 and MC3 materials were almost completely disrupted and destroyed after 1 day of agitation (regardless of HCl concentration), MC1 beads remained mechanically stable over the 3 days of agitation (with the exception of the experiment performed with 5 M HCl solutions, where the destruction of the MCs was observed at the third day of agitation). MC1 material was selected for further experiments on Pd(II) sorption.

Influence of HCl concentration on Pd(II) recovery. The extraction efficiency remained in the range 50-90 % and progressively decreased with increasing HCl concentration. For HCl concentration higher than 6 M the MC1 material was not stable and tended to disrupt.

Pd(II) sorption isotherms. Figure 3 (A) shows Pd(II) sorption isotherms using MC1 for 0.5 M HCl solutions. The solid line represents the modeling of the sorption isotherm with the Langmuir equation: this equation fits well experimental data. The isotherm is quasi irreversible: the initial slope of q vs C_{eq} is very steep followed by a progressive increase up to reach a saturation plateau.

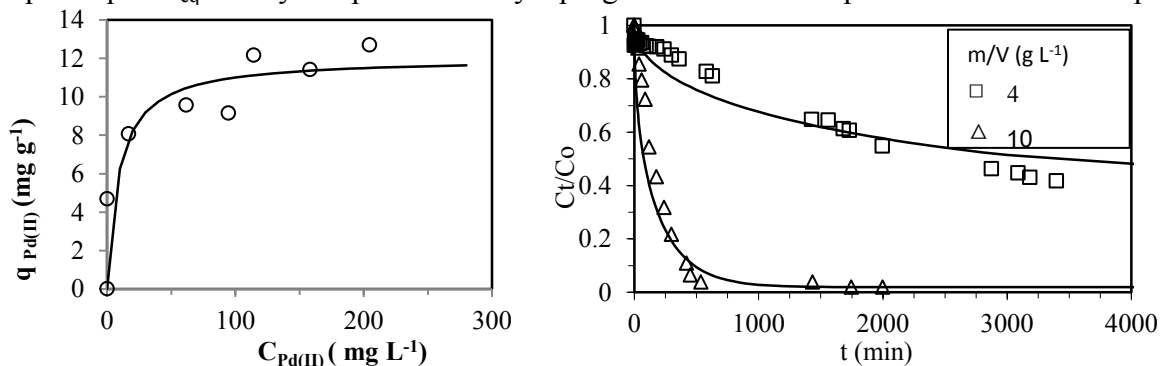


Figure 3. (A) Pd(II) sorption isotherm (B) Pd(II) uptake kinetics (C_0 : 50 mg Pd L^{-1}). MC1 material; SD: 4 g L^{-1} ; $C(\text{HCl})$: 0.5 M; T: 20 $^{\circ}\text{C}$.

The maximum sorption capacity is close to $12 \text{ mg Pd g}^{-1} \text{ MC1}$ while the affinity coefficient is found to be close to 0.108 L mg^{-1} . Taking into account the humidity of the MC1 particles (i.e., 92.6 %) the maximum sorption capacity reaches $143 \text{ mg Pd g}^{-1} \text{ MC1}_{\text{dry}}$. This value is higher than the levels reached using similar materials with an immobilization of the extractant in the matrix of the polymer: 77 mg Pd g^{-1} .⁵

Pd(II) uptake kinetics. Figure 3 (B) shows the kinetic profiles for the recovery of Pd(II) from 0.5 M HCl solutions using MC1. The solid line shows the modeling of intraparticle diffusion using the model described by Zhu and Sengupta.⁶ Regardless of the experimental conditions (sorbent dosage), the model of resistance to intraparticle diffusion fits well experimental profiles. For the highest SD (i.e., 10 g L^{-1}) more than 90 % of the sorption occurred within the first 500 min while the full equilibrium required about 24 h of contact: the second phase in the sorption process was much slower. On the opposite hand, for the lowest SD (i.e., 4 g L^{-1}) the uptake kinetics was quite slow: two days of contact were necessary to reach the equilibrium. The coefficients of intraparticle diffusion were calculated, giving values of 5.63×10^{-12} and $7.76 \times 10^{-11} \text{ m}^2 \text{ min}^{-1}$ for SD: 4 and 10 g L^{-1} , respectively. These values should be taken as indicative but can be used to compare with alternative systems. In the case of Pd(II) extraction (from HNO_3 solutions) using Cyanex 302 encapsulated in alginate (matrix immobilization) 50 h were necessary for reaching the equilibrium,⁵ while for Cyphos IL 101 immobilized in microcapsules of alginate the equilibrium time was close to 72 h.⁴

Conclusions

Cyanex 302 can be efficiently encapsulated in alginate gel providing the type of alginate is appropriately selected: an alginate of high viscosoty (HVA) reveals efficient (at the concentration of 0.5 % w/w) for immobilizaing the extractant. Mononuclear particles can be obtained; however, the amount of extractant immobilized is to be appropriately selected for maintaining the mechanical stability of the encapsulated material: MC1 seems to be a good compromise (corresponding to the lowest extractant loading among the values tested in the present work). The maximum sorption capacity reaches 12 mg Pd g^{-1} (143 mg Pd g^{-1} , refering to sorbent dry weight). The sorbent dosage influences the time required for reaching the equilibrium: about 24 h for SD: 10 g L^{-1} , and about 48 h at the lowest SD (i.e., 4 g L^{-1}). These materials can be considered a promising alternative to conventional systems for the recovery of valuable or toxic metal ions from HCl solutions. Future work will focus on the improvement of physico-chemical stability of the composite materials and the enhancement of diffusion properties.

Acknowledgements

Authors acknowledge the financial support from the University of Guanajuato (CIAI 2013, 279/13) and PROMEP, SEP (Recuperación de metales preciosos contenidos en disoluciones acuosas provenientes de fuentes secundarias).

References

- [1] F. L. Bernardi, R. A. Grant, D. C. Sherrington. *React.Funct. Polym.*, 65 (3), 205-217 (2005).
- [2] S. G. Sarkar, P. M. Dahdke. *Indian J. Chem. Techn.*, 7 (3), 109-111 (2000).
- [3] R. Navarro, I. Saucedo, C. González, E. Guibal. *Chem. Eng. J.*, 185– 186, 226– 235 (2012).
- [4] T. Vincent, A. Parodi, E. Guibal. *React. Funct. Polym.*, 68 (7), 1159–1169 (2008).
- [5] H. Mimura, H. Ohta, k. Akiba, Y. Onodera. *J. Nucl. Sci. Technol.*, 38 (5), 342-348 (2001).
- [6] Y. Zhu, A. Sengupta. *Environ. Sci. Technol.*, 26 (10), 1990-1998 (1992).

THERMODYNAMIC PARAMETERS OF FLUORIDE ION ADSORPTION BY A BIOPOLYMER

Beatriz Magdalena Millán-Olvera¹, José Luis García-Rivas¹, Rosa Elvira Zavala-Arce¹, Beatriz García-Gaitán¹

¹ *Instituto Tecnológico de Toluca, Av. Tecnológico S/N, Fraccionamiento La Virgen, Metepec, Edo. de México, México, C.P. 52149. Tel. +52 722 208 7224, lgrivas230@yahoo.com.mx*

Abstract

Chitosan-PVA beads modified by cross-linking were synthesized and characterized using FTIR analysis. Hydrogel beads were used for batch experiments in order to obtain the maximum fluoride ion adsorption capacity varying contact time, pH and temperature. The thermodynamic parameters were calculated from equilibrium data, negative values obtained for Gibbs free energy and enthalpy suggest that the process is exothermic and spontaneous. In case of calculated entropy, a negative value is an indicative of the adsorption process. Besides, Gibbs free energy values increased with an increase in temperature, which indicates that the reaction slows down with a rise in temperature.

Introduction

In recent years the world has greatly increased concern about the presence of fluoride ions in drinking water due to natural and anthropogenic activities. In the northern of Mexico there are communities that use groundwater sources to supply water for human use and consumption without being given a treatment of drinking water, which leads to a significant health risk [1]. Previous studies show that these water sources contain high concentrations of fluorides when ingested by people cause dental and skeletal fluorosis mainly. NOM-127-SSA1-1994 marks as maximum permissible limit (MPL) 1.5 mg/L of fluoride in drinking water [2]. In recent years, the use of natural polymers as adsorbents has been an effective method to provide new polymeric materials. Chitosan is obtained from chitin and is known as an excellent biosorbent, which has been applied to the study of the adsorption of pollutants. Therefore, in this paper the feasibility of removing fluoride ions from aqueous solutions by beads of hydrogel based on chitosan (Q) and polyvinyl alcohol (PVA) cross-linked with ethylene glycol diglycidyl ether (EGDE) was examined.

Experimental

2.1. Reagents

For synthesis and adsorption experiments was used deionized (DI) water. Chitosan (Q) with 68% deacetylation degree was supplied by Alimentos America; poly(vinyl alcohol) (PVA) USP grade high viscosity purchased from Golden Bell; ethyleneglycol diglycidyl ether (EGDE) 100% purity was purchased from Tokyo Chemical Industry Co. and used without further purification; TISAB Solution II (prepared in the laboratory with NaOH, NaCl and glacial acetic acid 100% were of analytical grade used without further purification). NaF 99% purity was obtained from Meyer.

2.2. Synthesis

The synthesis of Q-PVA beads cross-linked with EGDE (Q-EGDE-PVA) was made following the methodology proposed by Garcia-Rivas et al. [3] with some modifications. Initially solutions of Q in 0.4 M acetic acid at 3.1 %wt and PVA in DI water at 10%wt were prepared. Then these solutions were mixed and were added dropwise to a solution of NaOH 1 M to generate Q-PVA beads, once the drip process was completed the beads were left under constant stirring for 2 h, at the end of this time beads were washed until wash water pH was equal to the pH of the DI water. Finally, the crosslinking reaction was carried out using EGDE on a round bottom flask at 70 °C, 125 rpm, in inert atmosphere of N₂ for 6 h. After the reaction, Q-EGDE-PVA beads were cooled to 15 °C and washed with DI water until the solution pH became the same as that of the fresh DI water. The beads were then stored in DI water for further use.

2.3. FTIR spectroscopy

Q-EGDE-PVA beads were characterized by Fourier transform infrared spectroscopy (FTIR) to identify functional groups. Varian 640 ATR spectrometer was used. The spectrum was obtained with 16 scans at a resolution of 4 cm⁻¹ using a frequency range of 4000 to 550 cm⁻¹.

2.4. Adsorption experiments

Adsorption experiments were carried out by the batch method in triplicate. To determine optimum pH on adsorption of fluorides about 0.5 g of beads was added into 10 mL of 10 mg/L sodium fluoride solution with desired pH value (range 2 to 8). The mixture was shaken in an orbital shaker (Heidolph model UNIMAX 1010-Inkubator 1000) at 200 rpm and 30 °C. Once obtained optimum pH, adsorption kinetics was carried out at contact times of 5, 10, 15, 30, 45 and 60 min and 2, 4, 8, 16, 24, 48 and 72 h. The kinetic study were performed with an initial concentration of 10 mg/L sodium fluoride solution, 10 mL solution, 0.5 g beads, 200 rpm and fixed temperature (30, 40 and 50 °C). pH was adjusted only at the beginning of the experiment. Subsequently adsorption capacity was determined for each contact time (q_t) by $q_t = V(C_0 - C_t)/m$, where C_0 is the initial concentration, C_t is the concentration at time t , V is the volume of the solution m is the mass of adsorbent. The experimental data were fitted using OriginPro 8.1 software to kinetic models of pseudo-first order $q_t = q_e(1 - e^{-k_1 t})$ and pseudo-second order $q_t = k_2 q_e^2 t / (1 + k_2 q_e t)$, where k_1 and k_2 are the sorption rate constants, q_t is the adsorption capacity at time t and q_e represents the adsorption capacity at equilibrium.

2.5 Thermodynamic parameters

The thermodynamic parameters were obtained by $\ln(q_e/C_e) = -\Delta H^\circ/RT + \Delta S^\circ/R$ where q_e is concentration of the adsorbate at equilibrium on the surface of the adsorbent and C_e is the concentration in the solution at equilibrium [5].

Results and Discussion

3.1. FTIR Analysis

In Figure 1, spectra of Q-EGDE-PVA beads before and after adsorption of fluoride ions are shown. The major bands of Q-EGDE-PVA beads are: 3350 cm⁻¹ (stretching vibrations of -OH and -NH₂ groups), 2850 cm⁻¹ (-CH stretching vibrations in -CH and -CH₂), 1652 cm⁻¹ (-NH₂ bending vibration), 1379 cm⁻¹ (-CH bending vibrations in -CHOH-), 1067 and 1028 cm⁻¹ (-CO stretching vibration in -COH). Hydrogen bonding in amines is weaker than that of hydroxyl

groups, so -NH_2 stretching bands are not as broad or intense as -OH stretching bands. A slight broadening of -NH_2 stretching band in Q-EGDE-PVA beads adsorbed with fluoride ions can be taken as indicative of a hydrogen bond between protonated amine (NH_3^+) and fluoride ion [6].

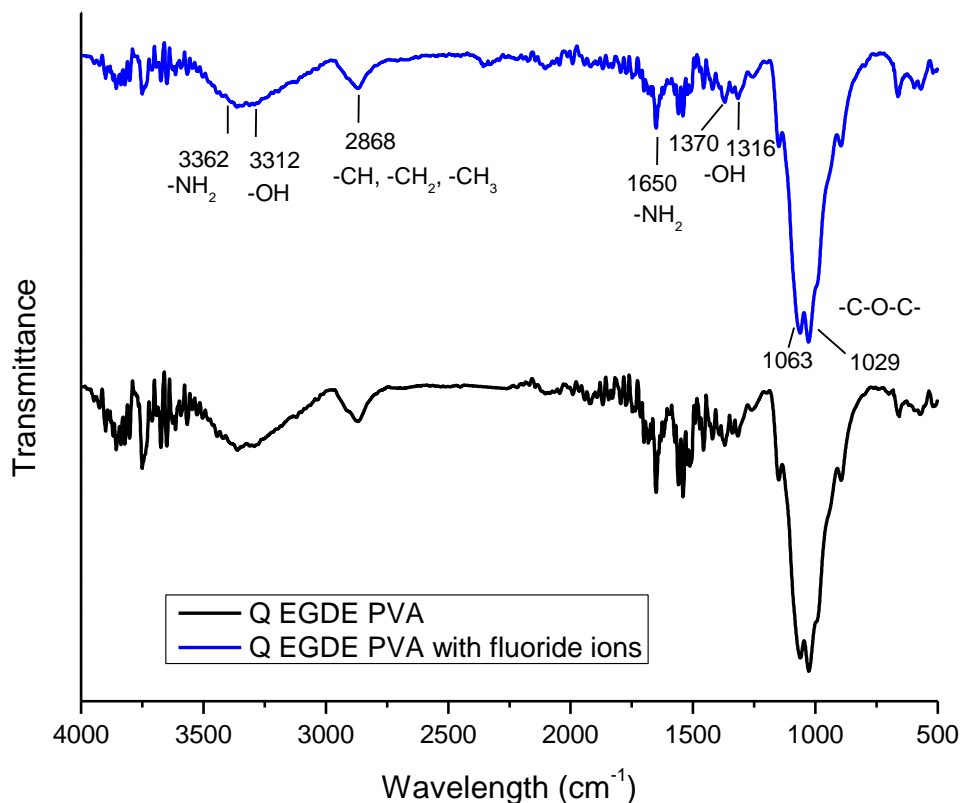


Figure 1. FTIR spectra.

3.2 Effect of pH

The effect of varying pH on fluoride ions adsorption capacity using Q-EGDE-PVA beads can be seen in Figure 2, which clearly shows that at pH 3 the greatest capacity adsorption is obtained.

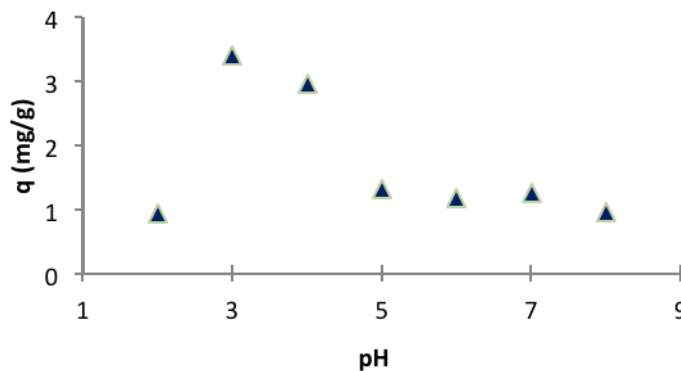


Figure 2. Effect of pH.

3.3. Adsorption kinetics

The adsorption kinetics obtained is shown in Figure 3. The data correspond to average adsorption capacity ($q_{t\ prom}$) calculated based on dry mass of the beads used. As seen, maximum adsorption occurs at 30 °C and in the three tested temperatures equilibrium is reached after 120 min of contact.

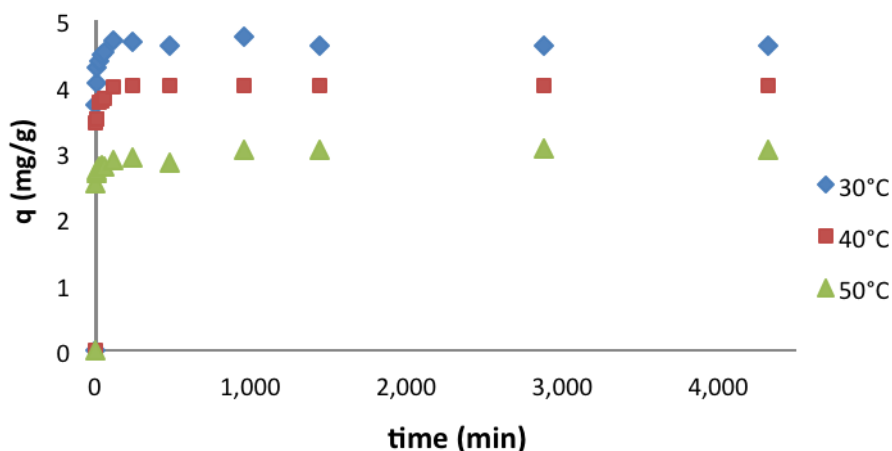


Figure 3. Effect of contact time on adsorption capacity.

The values of parameters obtained in each of the two models, as well as the correlation coefficients obtained are shown in Table 1. Values show that pseudo-second order kinetics model fits well with the experimental data.

Table 1. Kinetic parameters.

Temperature (°C)	Pseudo-primer order			Pseudo-segundo order		
	k_1 (min ⁻¹)	q_e (mg g ⁻¹)	R ²	k_2 (min ⁻¹)	q_e (mg g ⁻¹)	R ²
30	0.3085	4.5	0.986	0.1595	4.7	0.998
40	0.4103	3.9	0.976	0.2520	4.0	0.992
50	0.4069	2.9	0.984	0.3932	2.9	0.993

3.4. Thermodynamic parameters

Standard changes of energy, enthalpy and entropy are shown in Table 2. Negative values of ΔG° indicate that adsorption of fluoride ions in Q-EGDE-PVA beads is spontaneous. Negative value of ΔH° suggests that the process is exothermic, so an decrease of temperature encourages fluoride ion adsorption. The values of the enthalpy of adsorption process can be used to distinguish between physical and chemical adsorption, chemical adsorption to the range of values of the enthalpy is 83 to 830 kJmol⁻¹, while for the physical adsorption range is from 8 to 25 kJ mol⁻¹. On the basis of the above distinction, it is concluded that adsorption of the fluoride ions is a physical process [5].

Table 2. Thermodynamic parameters.

ΔG° (J mol ⁻¹)			ΔH°	ΔS°
30°C	40°C	50°C	(kJ mol ⁻¹)	(J mol ⁻¹ K ⁻¹)
-2227	-609	-166	-33.6	-104

Conclusions

The Q-EGDE-PVA beads are a good material for fluoride ions removal. The values of the thermodynamic parameters confirm spontaneity of the process and exothermic nature of the adsorption of fluoride ions, which is advantageous because at lower temperatures the beads remove more ions. The adsorption kinetics follows pseudo-second order. Due to precursors homopolymers from Q-EGDE-PVA beads, this adsorbent has characteristics of being a biodegradable, non-toxic and low cost, contributing these properties to place it as a good biosorbent of fluoride ions.

Acknowledgements

The authors are thankful to Dirección General de Educación Superior Tecnológica (project 4625.12) for the provision of financial support to carry out this research work and thank to CONACYT for the scholarship No. 34194 granted to B.M.M.O.

References

- [1] Trejo R. y Bonilla A., "Análisis del riesgo para la salud pública ocasionado por la exposición a fluoruros en el estado de Aguascalientes México", *Revista Internacional de Contaminación Ambiental*, Vol. 18, No. 4, p.171-177, 2002.
- NOM-127-SSA1-1994. "Salud ambiental, agua para uso y consumo humano-límites permisibles de calidad y tratamientos a que debe someterse el agua para su potabilización", *Diario oficial de la federación*, 1994.
- Bhatnagar A., Kumara E., Sillanpääb M, "Fluoride removal from water by adsorption", *Chemical Engineering Journal*, Vol. 171, No. 3, p. 811-840, 2011.
- García-Rivas L., García-Gaitán B., Antonio-Cruz R. C., Zavala-Arce R. E., Granados- García M., Dadó- Lujano I. I., Reyes- Gómez J., Luna-Bárceñas J. G., "Síntesis y caracterización de esferas de quitosano- EGDE-PVA para la adsorción de Cu(II)". *Revista Iberoamericana de Polímeros*, Vol. 11, No. 7, p. 541-549, 2010.
- Aravind V., Elango K.P."Adsorption of fluoride onto magnesita-Equilibrium and thermodynamic study". *Indian Journal of Chemical Technology*, Vol. 13, pp 476-483 (2006).
- Viswanathan, N., Meenakshi, S. "Enriched fluoride sorption using alumina/chitosan composite. *Journal of Hazardous Materials*, Vol. 178, p.226-232.(2010).

SYNTHESIS AND CHARACTERIZATION OF SOME POLYMERIZABLE SURFACTANTS (SURFMERS)

González-Pluma Marisol; Elizalde-Herrera Luis E. ^{*}; Saldivar-Guerra Enrique

**Department of Polymer Synthesis, Centro de Investigación en Química Aplicada, Saltillo Coahuila, México C.P. 25254. luis.elizalde@ciqua.edu.mx*

Abstract

A series of bifunctional vinyl-terminated surfmer having EO blocks were synthesized. These compounds were successfully synthesized by the condensation of poly (ethylene oxide) (PEO) with different molecular weights from 200 to 8000 g/mol ω -methyleted with 3-isopropenyl- α , α -dimethylbenzyl isocyanate. The chemical structure of the prepared compounds was confirmed using elemental analysis, FTIR and NMR spectra. The complete consumption of 3-isopropenyl- α , α -dimethylbenzyl isocyanate was monitored by isocyanate peaks using FTIR, and the structure of the surfmer was confirmed by NMR. The critical micelle concentration (CMC) of the surfmers was carried out by density, and the measurements confirm that the obtained surfmers are potential candidate for emulsion polymerization.

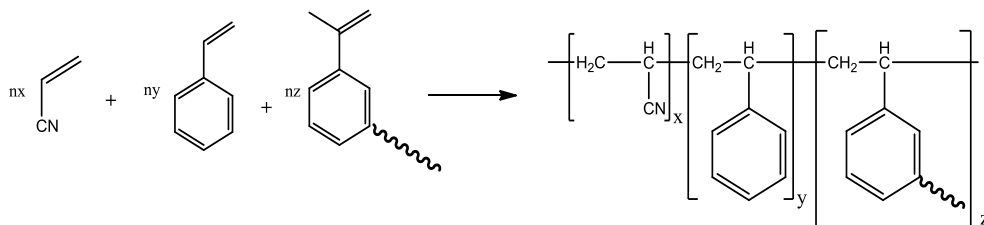
Introduction

Free-radical graft copolymerization of styrene (St) and acrylonitrile (AN) in the presence of polyether polyols has been used to prepare polymer polyols in industry, which are important raw material of performance flexible polyurethane foams ^[1,2]. The graft copolymerization modification can improve the load-bearing characteristic and the cell opening behavior of polyurethane foams. In the industry, the polyurethanes are formed through the reaction between isocyanate compounds and a graft polyol (polymer polyol). This graft polyol is a copolymer of poly (styrene-acrylonitrile) dissolved in a polyol carrier. This copolymer is prepared through the random polymerization of this co-monomers in the presence of a polymerizable surfactant which is used as a surfactant and this stabilizes the polymeric particles (dispersed phase) in a polyol carries (continuous phase) ^[3, 4] (Scheme 1).

The interest in polymeric surfactants for heterogeneous polymerization has increased in recent years. In emulsion polymerization, surfactant plays an important role in the process, since they control the nucleation process as well as the stabilization of the polymer particle during the polymerization and storage of the latexes. Polymeric emulsifiers and stabilizers are promising alternatives to the traditional low molecular weights surfactants. Traditional surfactants are not reactive in the polymerization process and thus are not covalently linked onto the particle surface resulting in negative effects on the properties of emulsion latexes, mainly caused by desorption of the surfactant from the polymer particles surface ^[5,6]. In fact, it has been reported that the migration of the surfactant through the polymer particles surface can modify adhesion, water sensitivity and the optical properties ^[7-9].

To avoid these problems, the use of polymerizable surfactants, referred as surfmers. Polymeric surfactants have only a limited possibility to migrate because of their much lower diffusion rate. If copolymerizable surfactants are used there is no migration possible. The surfmers remain covalently linked to the polymer, preventing migration during storage and film formation. The surfmers can copolymerize with the vinyl monomers to produce strong sterically stabilized latexes monomers via aqueous emulsion polymerization. The areas of improvements using surfmers are: mechanical stability of the latex, very high solids contents, water resistance, adhesivity and control of surface charge density and application in films, which indicates a decrease of surfactant migration ^[10].

The first vinyl monomer syntheses, which also function as emulsifying agent, were reported in 1958 ^[11] however the term “surfmer” is recently used and is defined as the compound able to polymerize and contains in the same molecule an hydrophilic moiety which can act as a surfactant.



Scheme 1. Schematic representation of the synthesis of St-AN stabilized latex using a surfmer as a reactive stabilizer.

One of the main applications of the surfmers, and more popular, are in emulsion polymerization or related processes, with the peculiarity that surfmer molecule, at the end of the process, are covalent connected and partly buried into the particles obtained and generate improvements in the quality of the latexes due to prevents the migration during storage and film formation, moreover and improves resistance to freezing and to shearing^[12-14].

There were a significant number of studies on the polymerization of surfmers^[15, 16]. These molecules combines the physical behavior of a traditional surfactant and the reactivity of monomers, in order to produce particles latex with high colloidal stability, allowing the preparation of high solid latexes, control on the particle size and distribution, surface charge density and surface functionality.

The most extensively studied macromonomers are based on EO blocks functionalized with styryl, mathacryloyl, thiol, maleate, vinyl, and *p*-vinylphenylalkyl reactive groups. The main reason to use EO refers to the good solubility in water as well as various alcohols. We now report the synthesis of bifunctional vinyl-terminated surfmer having EO blocks. These compounds were successfully synthesized by the condensation of poly (ethylene oxide) (PEO) with different molecular weights from 200 to 8000 g/mol ω -methylated with 3-isopropenyl- α , α -dimethylbenzyl isocyanate.

Experimental

Chemicals

The samples of the ω -methylated poli(ethylene oxide) (PEO) of different molecular weights (200, 600, 1500, 4000 and 8000 g mol⁻¹) were provided by POLIOLES S.A. de C.V. Ethylene glycol monoethyl ether, 3-isopropenyl- α , α -dimethylbenzyl isocyanate (TMI), zinc chloride (ZnCl₂) were purchased form Aldrich. The THF was distilled over sodium.

Analysis

The structure of the surfmers was confirmed by NMR (500 MHz) spectrophotometer Bruker ADVANCED III using chloroform-*d* as solvent and tetramethylsilane as internal reference. Chemical shifts were expressed in parts per million. FTIR spectra were taken in a Nicolet Magna 550 Infrared spectrophotometer equipped with an optical interferometer of potassium bromide. The critical micelle concentration (CMC) of the surfmers was carried out by density using an AMVn Automated Microviscometer equipped with an Anton Paar DMA 5000 oscillating U-tube densitometer at 25°C.

Synthesis of the vinyl terminated-PEO surfmer (VT-PEO)

The designs of the surfmer were based on a nonionic surfactant and select the poly (ethylene oxide) as the group which can interact with the water in the emulsion polymerization. The reactions of the different ω -methylated-PEO with 3-isopropenyl- α , α -dimethylbenzyl isocyanate (Scheme 2) provide a new type of surfmers based on PEO. The synthesis of different surfmers carried out using PEO with 200, 600, 1500, 4000 and 8000 g/mol in reaction with 3-isopropenyl- α , α -dimethyl benzyl isocyanate in a molar ratio 1:1.2 respectively in THF as solvent and ZnCl₂ in catalytic amounts at 70 °C. The reaction mixture was refluxed

for 24 h. The reaction was performed in a 250 ml 3-neck flask fitted with a condenser and an addition funnel. The system was flamed with vacuum (1 mmHg) and filled with nitrogen (Ultra High Purity grade). Then, 10 g (6.66 mmol) of PEO (1500 g mol⁻¹) and 60 ml of dry THF were added under constant stirring. Once the PEO was completely dissolved, 1.61 g (8.0 mmol) of 3-isopropenyl- α , α -dimethylbenzyl isocyanate in 25 ml of dry THF was added through a dropping funnel. A catalytic amount of ZnCl₂ was added, and the reaction mixture was allowed to react for 24 h under inert atmosphere at reflux. The complete consumption of 3-isopropenyl- α , α -dimethylbenzyl isocyanate was monitored by isocyanate peaks using FTIR. The product was concentrated by evaporation. The same procedure was implemented with all others PEO.

Spectroscopic Properties.

3a Viscous liquid 98% yield. **¹H-RMN** (500 Mhz, CDCl₃) δ (ppm): 7.94 (s, 1H, **NH**), 7.3 (m, 4H, **CH** Ar-H), 5.3 (s, 1H, **CH₂=C**), 5.0 (s, 1H, **CH₂=C**), 3.6 (s, 4H, 2**CH₂-O**), 2.10 (s, 3H, **CH₃-C**), 1.62 (s, 6H, 2**CH₃**). **¹³C-RMN** (125.686 Mhz, CDCl₃) δ : 153.5, 146, 142.5, 140.5, 127, 123, 121, 112, 70, 62.5, 61, 54.5, 28.5, 21.

FT-IR (pellet KBr, cm⁻¹): 2874, 1724, 1458, 1351, 1252, 953.

3b Viscous liquid 97% yield. **¹H-RMN** (500 Mhz, CDCl₃) δ : 7.94 (s, 1H, **NH**), 7.3 (m, 4H, **CH** Ar-H), 5.3 (s, 1H, **CH₂=C**), 5.0 (s, 1H, **CH₂=C**), 3.6 (s, 20H, 2**CH₂-O**), 2.10 (s, 3H, **CH₃-C**), 1.62 (s, 6H, 2**CH₃**). **¹³C-RMN** (125.686 Mhz, CDCl₃) δ : 153.5, 146, 142.5, 140.5, 127, 123, 121, 112, 70, 62.5, 61, 54.5, 28.5, 21.

FT-IR (pellet KBr, cm⁻¹): 2874, 1724, 1458, 1351, 1252, 953.

3c Viscous liquid 98% yield. **¹H-RMN** (500 Mhz, CDCl₃) δ : 7.94 (s, 1H, **NH**), 7.3 (m, 4H, **CH** Ar-H), 5.3 (s, 1H, **CH₂=C**), 5.0 (s, 1H, **CH₂=C**), 3.6 (s, 56H, 2**CH₂-O**), 2.10 (s, 3H, **CH₃-C**), 1.62 (s, 6H, 2**CH₃**). **¹³C-RMN** (125.686 Mhz, CDCl₃) δ : 153.5, 146, 142.5, 140.5, 127, 123, 121, 112, 70, 62.5, 61, 54.5, 28.5, 21.

FT-IR (pellet KBr, cm⁻¹): 2874, 1724, 1458, 1351, 1252, 953.

3d solid white 95% yield. **¹H-RMN** (500 Mhz, CDCl₃) δ : 7.94 (s, 1H, **NH**), 7.3 (m, 4H, **CH** Ar-H), 5.3 (s, 1H, **CH₂=C**), 5.0 (s, 1H, **CH₂=C**), 3.6 (s, 136H, 2**CH₂-O**), 2.10 (s, 3H, **CH₃-C**), 1.62 (s, 6H, 2**CH₃**). **¹³C-RMN** (125.686 Mhz, CDCl₃) δ : 153.5, 146, 142.5, 140.5, 127, 123, 121, 112, 70, 62.5, 61, 54.5, 28.5, 21.

FT-IR (pellet KBr, cm⁻¹): 2874, 1724, 1458, 1351, 1252, 953.

3e Solid white 95% yield. **¹H-NMR** (500 Mhz, CDCl₃) δ : 7.94 (s, 1H, **NH**), 7.3 (m, 4H, **CH** Ar-H), 5.3 (s, 1H, **CH₂=C**), 5.0 (s, 1H, **CH₂=C**), 3.6 (s, 364H, 2**CH₂-O**), 2.10 (s, 3H, **CH₃-C**), 1.62 (s, 6H, 2**CH₃**). **¹³C-RMN** (125.686 Mhz, CDCl₃) δ : 153.5, 146, 142.5, 140.5, 127, 123, 121, 112, 70, 62.5, 61, 54.5, 28.5, 21.

FT-IR (pellet KBr, cm⁻¹): 2874, 1724, 1458, 1351, 1252, 953.

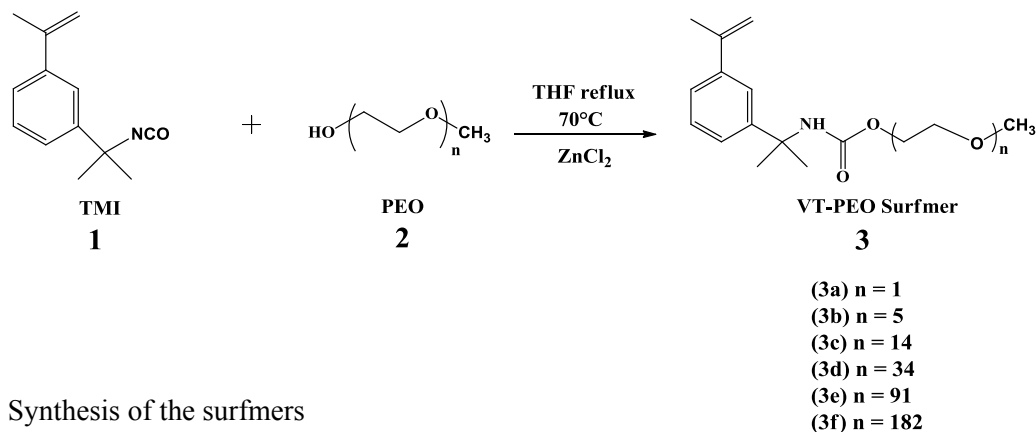
3f Solid white 96% yield. **¹H-RMN** (500 Mhz, CDCl₃) δ : 7.94 (s, 1H, **NH**), 7.3 (m, 4H, **CH** Ar-H), 5.3 (s, 1H, **CH₂=C**), 5.0 (s, 1H, **CH₂=C**), 3.6 (s, 728H, 2**CH₂-O**), 2.10 (s, 3H, **CH₃-C**), 1.62 (s, 6H, 2**CH₃**). **¹³C-RMN** (125.686 Mhz, CDCl₃) δ : 153.5, 146, 142.5, 140.5, 127, 123, 121, 112, 70, 62.5, 61, 54.5, 28.5, 21.

FT-IR (pellet KBr, cm⁻¹): 2874, 1724, 1458, 1351, 1252, 953.

Results and Discussion

In the present study six series of surfmers with different content of EO were synthesized according to the Scheme 2. Methyl groups were chosen in the EO reactant in order to prevent a possible dimerization product in the surfmer. These compounds include in their structure a vinyl group that is necessary for

further copolymerization reaction. The synthesis was achieved using two different catalysts: zinc chloride and zinc acetate. However, zinc chloride is preferred in the surfmer preparation due to their highest activity.



Scheme 2. Synthesis of the surfmers

The surfmer formation was demonstrated by FTIR, this analysis shows the disappearance of the band at 2256 cm^{-1} attributed to the stretching of the isocyanate group in the starting material and the appearance of the band at 1724 cm^{-1} corresponding to the stretching of the C=O of the urethane group (Figure 1).

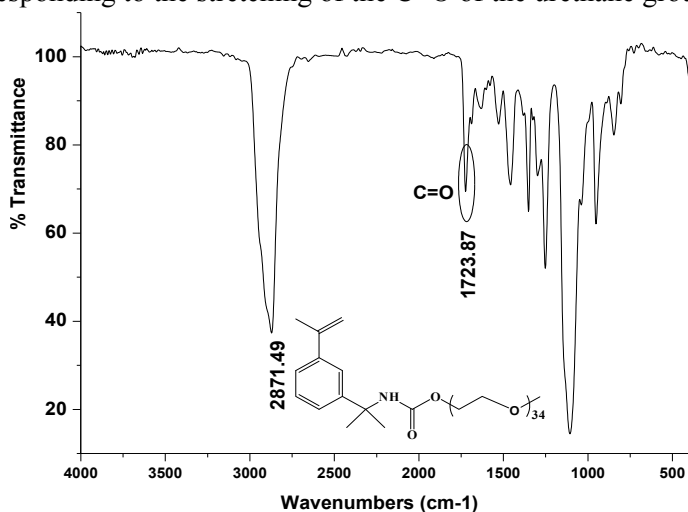


Figure 1. FT-IR spectrum of 3d Surfmer

Further characterization was achieved by ^1H NMR spectroscopy (surfmer 3d) where is observed a strong resonance at 3.6 ppm characteristic for the two methylene group in the of EO block ($-\text{CH}_2-\text{CH}_2\text{O}-$) n , the aromatic protons are observed at 7.3 ppm and the resonance detected in the range between 5.0 and 5.3 ppm are assigned to the vinyl protons. The signal at 2.1 ppm is a characteristic peak of the methyl protons ($-\text{CH}_3$). The proton in the urethane group ($-\text{NHCOO}-$) appears at 7.94 ppm. A diffusion order spectroscopy (DOSY) NMR experiments were carried out to confirm the presence of the surfmers. The DOSY RMN experiments provide two dimensional maps in which the signals are separated according to their chemical shift in one dimension and by its diffusion coefficients in the other. At the 2D-DOSY RMN spectrum, present one diffusion coefficient, shows that all chemical functionalities presents in the RMN spectra are covalent linked in a single surfmer molecule.

An important data in the emulsion polymerization is the critical micelle concentration (CMC); this value in these new surfmer molecules was determined by density (ρ) according to ASTM-D4052 ^[17]. The CMC values are present in the Table 1. The value of the CMC itself is largely governed by the hydrophobic part, i.e., the length of the benzylic sequence: the longer that sequence, the smaller the CMC. The hydrophilic

part, also gives the same effect, consider for instance the comparison of the CMC values of 3a and 3f surfmers with the 0.60 and 1.24 wt. % respectively, the length of the hydrophilic poly (ethylene oxide) increased moderately the CMC.

	<i>VT-PEO surfmers</i>	
		<i>CMC</i> <i>wt. %</i>
Table 1. Critical Micelle Concentration of the VT-PEO surfmers determined by density method	3a	0.60
	3c	0.85
	3d	0.92
	3e	1.04
	3f	1.24

Conclusions

The synthesis of the surfmers was achieved by the reaction of different ω -methylated-PEO with 3-isopropenyl- α , α -dimethylbenzyl isocyanate using a molar ratio of 1.0: 1.2 respectively were ZnCl₂ works better, due to their highest activity. The new synthesis of vinyl terminated-PEO surfmers (VT-PEO) described in this paper was synthesized from various molecular weights of PEO (hydrophilic part) and (hydrophobic part), yield above 95% in all cases, calculated by gravimetry and finally their characterization by FT-IR and NMR confirmed their synthesis. The CMC analysis showed that the VT-PEO surfmers can be potential candidates for emulsion polymerization reactions.

Acknowledgements

The authors are grateful to the Mexican Council of Science and Technology (CONACYT) for financial support provided through the doctoral graduate program of the Centre for Research in Applied Chemistry (CIQA).

References

- [1] D.A. Heyman and O.M. Grace, *Journal of Cellular Plastics*, 21 (1985) 101-104.
- [2] Mihail Ionescu, *Chemistry and Technology of Polyols for Polyurethanes*, Rapra Technology Limited, 2005.
- [3] A. Rath, W. Apichatachutapan, R. Gummaraju, R. Neff and D. Heyman, *Journal of Cellular Plastics*, 39 (2003) 387.
- [4] G.G. Ramlow, D.A. Heyman and O.M. Grace, *Journal of Cellular Plastics*, (1983) 237.
- [5] D. Urban, K. Takamura, *Polymer Dispersions and Their Industrial Applications*; Wiley-VCH; Weinheim, Germany, 2002
- [6] S. C. Thickett, R. G. Gilbert, *Polymer* 48 (2007) 6965-6991.
- [7] I. Piirma, *Makromol. Chem. Macromol. Symp.* 35–36 (1990) 467-475.
- [8] K. Holmberg, *Prog. Org. Coat.* 20 (1992) 325.
- [9] J.M. Asua, H.A.S. Schoonbrood, *Acta Polym.* 49 (1999) 671.
- [10] S. A. Chen and H. S. Chang, *J. Polym. Sci., Polym. Chem. Ed.*, 23 (1985) 2615.
- [11] H. H. Freedman, J. P. Mason, A. I. Medalia, *J Org Chem* 23 (1958) 76-82.
- [12] S. Voronov, A. Kohut, I. Tarnavchyk, A. Voronov, *Current Opinion in Colloid & Interface Science* 19 (2014) 95–121.
- [13] A. Guyot, K. Tauer, *Adv. Polym. Sci.* 111 (1994) 43-65.
- [14] A. Guyot, *Advances in Colloid and Interface Science* 108 –109 (2004) 3–22.
- [15] O. Soula, A. Guyot, N. Williams, J. Grade, & T. Blease, *J. Polym. Sci. Part A: Polym. Chem.* 37 (1999) 4205–4217.
- [16] M. Summers, J. Eastoe, *Advances in Colloid and Interface Science* 100 –102 (2003) 137–152.
- [17] *ASTM D4052-11*, Standard Test Method for Density, Relative Density, and API Gravity of Liquids by Digital Density Meter, 2011

DEGRADATION OF PLASTICS BY PLASMA IN A RADIO FREQUENCY REACTOR.

Erick de Jesus Silva Valenciano,¹ Maria Guadalupe Neira Velazquez,² Yadira Karina Reyes Acosta,¹ Claudia Guadalupe Hernández Ramos,² Maria Guadalupe Mendez Padilla²

¹*Facultad de Ciencias Químicas de la Universidad Autónoma de Coahuila
Blvd. Venustiano Carranza s/n, Colonia Republica Oriente, Saltillo, Coahuila, México. CP. 25280
ericksilvaig@outlook.com*

²*Centro de Investigación en Química Aplicada (CIQA), Blvd. Enrique Reyna Hermosillo No. 140, Colonia San José de Los Cerritos Saltillo, Coah., México, CP. 25249 2guadalupe.neira@ciqa.edu.mx*

Abstract

The main objective of this study is to know the behavior of four plastics, after being degraded in a plasma reactor, Low Density Polyethylene (LDPE), Polypropylene (PP), Polyethylene terephthalate (PET) and polylactic acid (PLA), they were treated at different conditions: time (1.5h, 2.5h), power (150w, 200w and 250w) and system pressure (0.7 mbar, 0.8 mbar and 1 mbar). Mass losses were compared and only the samples that had the highest degradation of each polymer were analyzed with techniques such as Thermo Gravimetric Analysis (TGA) and Infrared Spectroscopy (IR).

Introduction

The fraction of plastics solid wastes in the cities is increasing continuously in recent years. Plastics usually account for about 7% in weight of the total municipal solid waste and much more by volume.^[1] Most of plastics aren't biodegradables so its natural decomposition takes too long and all the waste and high environmental pollution is a serious problem today.

In order to minimize the times of plastics degradation exist many process for example the traditional pyrolysis of polyethylene and polypropylene has been studied by Faravella et al.^[2] Plasma pyrolysis is a new technology that has unique advantages.^[1] Characterization of pyrolysis performance of waste plastics to generate energy or products of high added value Plasma technology to degrade or decompose plastics is commonly used because the treatments take only a few minutes, and the chemical treatments are consistent and reproducible and no special chemicals or waste removal procedures are needed since gaseous by products can be collected at the exit of the plasma chamber.^[3]

Polypropylene (PP) has become one of the most popular thermoplastic and present faster growth than other polymers, since has very good properties and low cost. In the other hand, polyethylenterephthalat (PET) it is one of the most widely used plastic in the industry of packaging of liquids. Polylactic acid (PLA) is a biodegradable polymer produced by condensation polymerization, the lactic acid used to produce PLA is extracted from renewable sources such as corn, sugar or rice, furthermore bags of low density polyethylene (LDPE) are used in grocery stores to transport the merchandise and LDPE is generally used for its low cost.^[4]

The aim of this study was to degrade the described polymer in a radiofrequency (RF) plasma reactor and analyze the polymers before and after the plasma treatment in order to evaluate the effect of the plasma treatment on the chemical structure of the polymers.

Experimental

The system used in this work is shown in Figure 1, it is a cylindrical glass reactor with aluminum caps, the reactor it is connected to a vacuum pump, this pump creates the low pressure in the system to remove any contaminants in the environment of reaction. A generator of radio frequency it is also connected to the glass reactor and generates the plasma inside the reactor. In this study air from the environment was used to perform the degradation of the polymers. The polymers were degraded at different time and pressure of air.

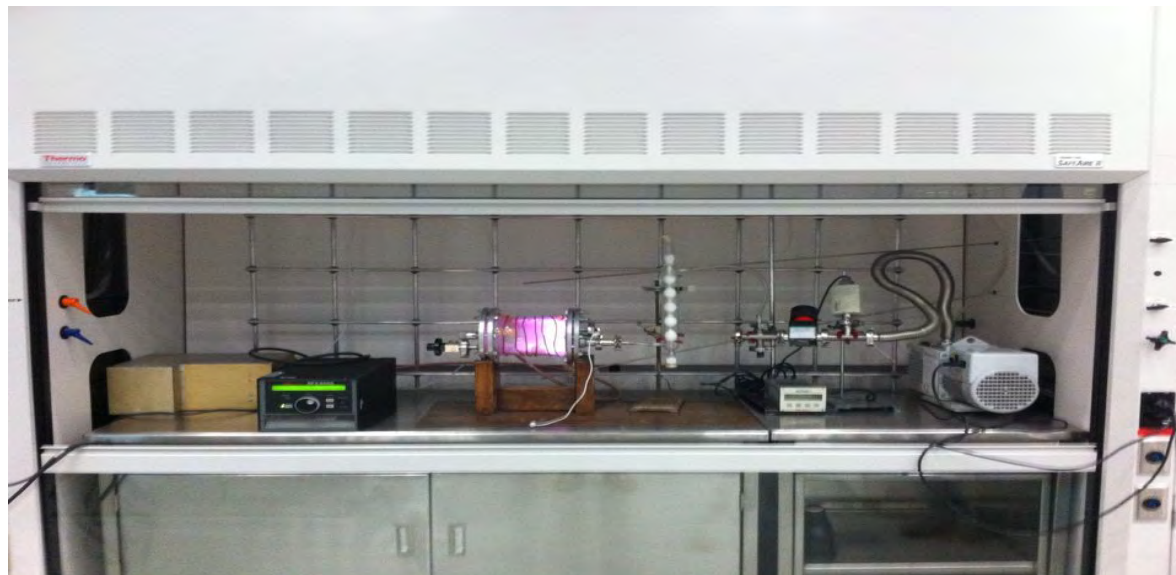


Figure 1. System of plastics degradation (right to left), generator of radio frequency, reactor, condenser, pressure sensor, and vacuum pump.

Four films of each polymer were degraded in each experiment, the area of these films was of 4 cm². The films were deposited on top of microscope glass slides. We experimented with different plasma conditions. Pressure: 0.7 mbar, 0.8 mbar and 1 mbar; time of degradation: 1.5 and 2.5 hours and plasma input power of 200 watts (W).

In order to evaluate the degradation of each plastic, samples were weighted before and after plasma treatment and the percentage of weight loss was calculated for each plastic in every treatment using the Equation 1.

$$\% \text{ weight loss} = \left(\frac{(w_o - w_f)}{w_o} * 100 \right) \quad \text{Equation 1.}$$

Equation 1. Calculus of weight loss for each plastic, where w_o was the initial weight and w_f was the final weight.

Technical characterization used was: Fourier transform infrared spectroscopy (FTIR) and thermogravimetric analysis.

Results and Discussion

Table 1. Shows the percentage of weight loss under different conditions of the different plastic degraded. It is appreciated that the plastics that degrade more easily are PP and PLA, in contrast LDPE and PET because of their stable chemical structure stable, are more difficult to degrade under the action of air plasma. It was decided to take a general percentage of all plastics and the results of this average are presented at the end of the Table. It is also important to highlight that polymers treated at 2.5 hours in general degraded more that the polymers treated at 1.5 hours, so the time of exposure of the plastics played an important role in the degradation of the polymers. The effect of the pressure on the level of the degradation was not straight forward, since the polymers did not showed a specific behavior of degradation as a function of pressure.

Table 1. Degradation of different plastics under different plasma conditions.

	200 Watts					
	1.5 hrs			2.5hrs		
	0.7mbar	0.8mbar	1mbar	0.7mbar	0.8mbar	1mbar
PET	13.41	8.60	8.97	34.46	29.23	12.39
PP	79.50	84.64	96.22	81.30	73.84	98.86
LDPE	13.39	16.39	18.52	21.59	11.34	17.02
PLA	35.40	27.24	32.69	95.66	92.77	54.80
Total	35.40	34.2	39.10	58.20	51.80	45.70

Figure 2 and Figure 3 shows the FTIR spectra of LDPE and PP respectively. FTIR analysis of the LDPE in Figure 2 shows some differences between the virgin and plasma degraded polymer. For instance, the peaks located between 2800 and 2920 cm^{-1} are smaller in LDPE treated under plasma, these peaks correspond to the presence of CH_2 and CH_3 groups, indicating that many of these groups disappeared due to the degradation of the polymers in presence on the plasma. On the other side, the band located at 1050 cm^{-1} represents CH_2 groups that are related to the crystallinity of this polymer and was also affected (was increased) during the plasma degradation process.

In relation to the FTIR analysis of PP (in Figure 3) we can observe some important differences between the virgin and the plasma treated PP, to start with, the degraded PP present a curve located between 3500 - 3400 cm^{-1} and it represent the O-H formation, since oxygen is presented during the plasma degradation of this polymer, another region of the plasma treated PP, shows a decrease of the bands located between 2800 and 2920 cm^{-1} are attributable to symmetric and asymmetric stretching vibrations of CH_2 and CH_3 ^[8], it is well known that during degradation, PP experience chain scissions mainly in the tertiary carbon on the chain, and that is the reason why, the peaks located between 2800 and 2920 cm^{-1} showed a decrease of their intensity. In virgin PP two intense peaks located at 1460 and 1378 cm^{-1} , the first peak is caused by CH_3 asymmetrical deformation vibrations of CH_2 , while the peak located at 1378 cm^{-1} is due to the symmetric deformation vibrations^[8] of CH_3 . It is appreciated in the FTIR spectrum of PP plasma degraded that these two peaks (located at 1460 and 1378 cm^{-1}) merge in just one peak located at

1460 cm^{-1} , this results provokes the deformation of the polymer. In general can be pointed out that there are important chemical differences between the FTIR spectra of virgin and plasma degraded polymers, as is appreciated in Figures 2 and 3.

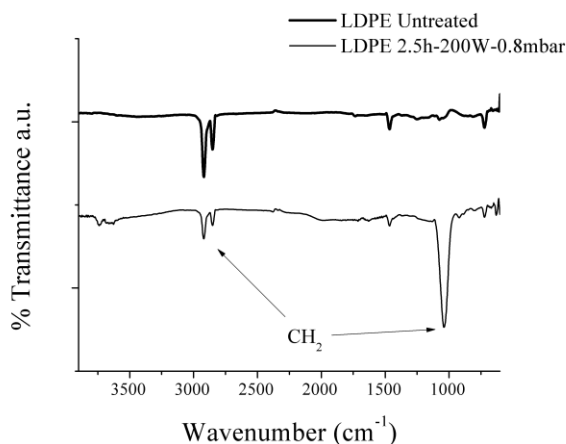


Figure 2. Spectrum of FTIR of LDPE virgin and degraded.

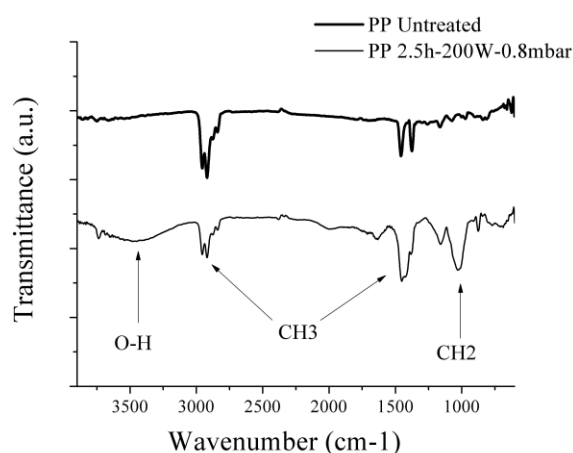


Figure 3. Spectrum of FTIR of PP untreated and degraded.

Figures 4 and Figure 5 shows TGA thermograms of PLA and PET untreated and plasma degraded. It is appreciated in both cases that the polymers exposed to plasma presented lower thermal stability than virgin polymers, the plasma treatment breaks the polymer chains, leaving macromolecules with lower molecular weight and with presence of certain chemical groups that are more susceptible to experience degradation when heated. As is appreciated plasma treated PET and PLA experiment weight loss at lower temperatures than virgin polymers.

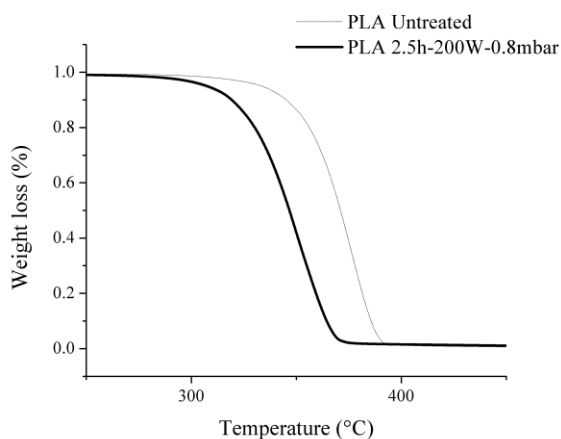


Figure 4. TGA curves of PLA plasma degraded and virgin

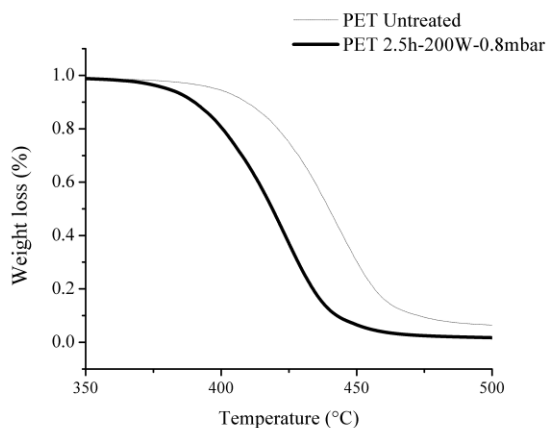


Figure 5. TGA curves of PET degraded by plasma and virgin

Conclusions

Percent weight loss is a function of certain variables of the plasma system, like for example, the time of residence, but the major factor is the chemical structure of each plastic. For instance, in this study; PP and PLA experienced higher degradation than LDPE and PET.

The results also showed that plasma is an efficient technique to carry out polymer degradation, and also is a technique that is friendly with the environment.

Degradation or pyrolysis of plastics by plasma is another alternative to recycling because with plasma it is possible to produce syngas as a product of the pyrolysis, which can be converted into energy or fuel or other products of high value and the implementation of this technology at industrial scale could generate great benefits.

Acknowledgements

We acknowledge the Centro de Investigacion en Quimica Aplicada (CIQA), for all the facilities provided with the materials and equipment used in this study, the company ECOTERRA S.A. de C.V. and its representative: Lic. Raul Hernandez Ojeda and INADEM are also acknowledged for their financial support provided to carry out this work.

References

- [1] L.Tang, J. Huang, Fuel Processing Technology, 88(6), 549-556 (2007).
- [2] E.Ranzi, M. Dente, T. Faravelli, Kinetic modeling of polyethylene and polypropylene thermal degradation, 40(41), 305-319, (1997)
- [3] N.Patra, J. Hladik, M. Pavlatová, Investigation of plasma-induced thermal, structural and wettability changes on low density polyethylene powder, 98(8), 1489-1494 (2013)
- [4] D. G. Papageorgiou, D.N. Bikiaris, K. Chrissafis. Effect of crystalline structure of polypropylene random copolymers on mechanical properties and thermal degradation kinetics, 543, 288-294 (2012)
- [5] H.Rajandas, S. Parimannan, K. Sathasivam. A novel FTIR-ATR spectroscopy based technique for the estimation of low-density polyethylene biodegradation. 31(8) 1094-1099 (2012)
- [6] C. Vasile, M. Pascu. Practical guide to polyethylene, Rapra Technology Limited, 77 (2005).
- [7] A. Nazarov, F.Balestra, V.Kilchytsk, Functional nanomaterials and devices for electronics, sensors and energy harvesting, 303 (2014)
- [8] R.Morent, N. De Geyter, C.Leys, L.Gengembre, E.Payen. Comparison between XPS and FTIR analysis of plasma-treated polypropylene film surfaces, 40, 597-600, (2008)
- [9] N. Miskolczi, L. Bartha, G.Deak, B. Jover. Thermal degradation of municipal plastic waste for production like hydrocarbons, 86(2) 357-366 (2004)
- [10] Q. Zhang, Y. Wu, L.Dor, W.Yang, W. Blasiak, A thermodynamic analysis of solid waste gasification in the Plasma Gasification Melting process 112, 405-413 (2013).

METATHESIS DEPOLYMERIZATION OF CHICOZAPOTE (MANILKARA ZAPOTA)

Sonia Reyes-Gómez,¹ Mikhail Tlenkopatchev¹

¹ *Instituto de Investigaciones en Materiales, Universidad Nacional Autónoma de México, Apartado Postal 70-360, CU, Coyoacán, México D.F. 04510, México*

Abstract

This work reports, the metathesis depolymerization of chicozapote (*Manilkara zapota*), which is a mixture of *cis*-1,4 (20%), *trans*-1,4 (73%) and 3,4 (7%) polyisoprenes; it also contains calcium oxalate monohydrate and a resinous fraction. The reactions were performed using 2nd generation Grubbs and Hoveyda-Grubbs catalysts, with olefins: dimethyl maleate, diethyl maleate and methyl methacrylate, as chain transfer agents, in toluene at 45°C. There were obtained well defined diester or methyl ester telechelic oligomers with average molecular weight M_n from 1729 to 3990 g/mol, determined by GPC.

Introduction

The chicozapote (*Manilkara zapota*) is a source of natural chewing gum. It is obtained from the area of the Yucatan peninsula, comprising Guatemala, Honduras and the southeasternmost tip of Mexico. The latex, also called “crude chicle” is obtained by tapping the bark of the tree. And then is boiled in an open vessel with constant stirring to reduce the water content to below 40%. The concentrated latex is then poured into molds to form, on cooling, blocks of about 20 to 25 pounds each [1], this is called the “gum base”. The latex containing both, *cis*- and *trans*-polyisoprenes, at ratios of either 1:1, 1:4 or 3:7 in the commercial chicle resin, and 1:1 in the single tree [2]. It also contained calcium oxalate monohydrate and a resinous fraction [3].

Olefin metathesis is a very versatile approach to obtain value added chemical intermediates from renewable raw materials. In this context, the metathesis degradation of polyalkenamers and their cross-metathesis (CM) with linear olefins as chain transfer agents (CTAs) to produce cyclic oligomers and end-functionalized polymers (telechelics) has been studied for over 30 years [4-5]. The installation of structural elements within complex natural products and the CM of electron deficient substrates, such as acrylic acid and its esters can now be accomplished using active and functional group tolerant metathesis catalysts [6].

In the present study, we investigated the natural chicle (NC) metathesis degradation, in the presence of high functionalized olefins: dimethyl maleate (DMM), diethyl maleate (DEM), methyl methacrylate (MMA) as chain transfer agents (CTAs); using 2nd generation Grubbs (G2) and Hoveyda Grubbs (H-G2) catalysts, to achieve the synthesis of low-molecular-weight telechelic oligomers in a well-controlled manner. These products represent valuable starting materials for the synthesis of detergents.

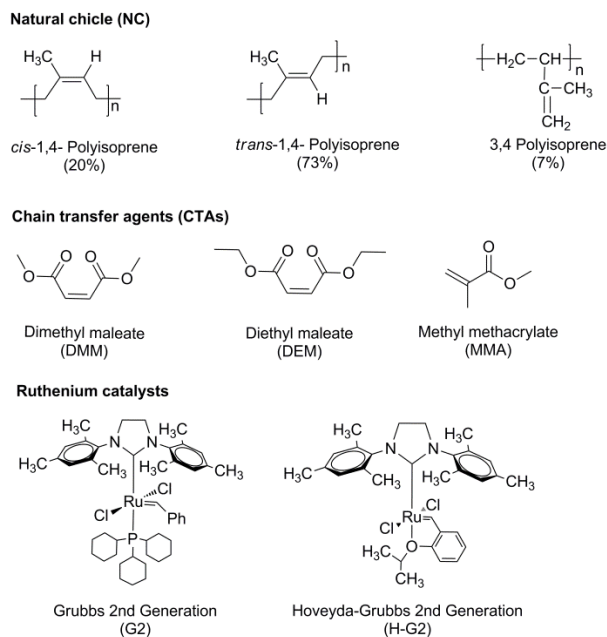
Experimental

Reagents

Natural chicle gum base (NC) from Chetumal Mexico, was tapped from chicozapote tree (*Manilkara zapota*). ($M_n = 1.4 \cdot 10^4$; PDI = 2.5). It was determined by ¹H NMR, that NC is a

mixture of *cis*-1,4 (20%), *trans*-1,4 (73%) and 3,4 (7%) polyisoprenes (Fig. 2) [7].

Dimethyl maleate (DMM), diethyl maleate (DEM), methyl methacrylate (MMA), toluene anhydrous, methanol; benzylidene [1,3-bis(2,4,6-trimethylphenyl)-2-imidazolidinylidene] dichloro (tricyclohexylphosphine) ruthenium (Grubbs catalyst 2nd generation) (G2) and (1,3-Bis-(2,4,6-trimethylphenyl)-2-imidazolidinylidene)dichloro(o-isopropoxyphenylmethylene)ruthenium (Hoveyda-Grubbs catalyst 2nd Generation) (HG2) were purchased from Sigma-Aldrich and used as received. Other solvents were of reagent grade and used without further purification (Schem. 1).



Scheme 1. Reagents used for the metathesis reactions.

Purification of natural chicle (NC)

In order to evaluate the reactivity of these catalysts, the metathesis degradation was performed using natural chicle gum base (NC) as received and purified.

NC was precipitated into methanol and then dried under vacuum before use (NCP).

Inorganic constituents and carbohydrates were separated from the chicle hydrocarbons and resins by dissolving NC in toluene and precipitated into methanol, and then dried under vacuum before use. The purified NCT was analyzed by ^1H NMR (CDCl_3) according to literature (Fig. 2) [7].

cis-1,4-PI δ (ppm): 5.12; 2.03; 1.7. *trans*-1,4-PI δ (ppm): 5.12; 2.00; 1.60. 3,4-PI δ (ppm): 4.69; 1.9 and 1.6. Corresponding to (m, mH, $\text{CH}=\text{C}(\text{CH}_3)\text{CH}_2$), (m, 4 mH, $\text{CH}_2\text{CH}_2\text{C}(\text{CH}_3)=\text{CHCH}_2\text{CH}_2$), (s, 3 mH, $\text{CH}=\text{C}(\text{CH}_3)\text{CH}_2$), respectively.

Characterization

FTIR spectra were recorded at room temperature on a Nicolet 5700 spectrophotometer with a diamond tip as a dispersing agent. ^1H and ^{13}C NMR spectra were recorded on a Varian Inova Unit 300 (300 and 75MHz, respectively) spectrometer. CDCl_3 was used as solvent. Chemical shifts are reported in ppm downfield from tetramethylsilane (TMS, $\delta=0.00\text{ppm}$).

Average molecular weight (M_n) and molecular weight distributions (PDI) were determined by gel

permeation chromatography (GPC). The GPC analysis was performed at 35°C in THF (0.3ml/min) using a Waters ALLIANCE 2695 Separation Module equipped with 2 columns: Waters Styragel HR 4E (M_w $5 \cdot 10^2$ to $1 \cdot 10^5$) and Styragel HR 5E (M_w $2 \cdot 10^3$ a $4 \cdot 10^6$). Narrow molecular weight linear polystyrene standards (ranging from $3.70 \cdot 10^2$ to $4.290 \cdot 10^6$) were used to calibrate the GPC.

Degradation procedure

All the experiments were performed under nitrogen atmosphere in a glass vial. The reaction vial temperature was controlled using a thermostat and an oil bath. Metathesis degradation of NC (0.5g) was performed using DMM, DEM and MMA as CTAs, with the molar ratio $[C=C]/[CTA]=1:1$. The catalysts Grubbs 2nd generation (G2) or Hoveyda-Grubbs 2nd Generation (H-G2); were added in molar ratio $[C=C]/\text{catalyst}=250$. The degradation was performed in bulk; the solvent (toluene) was added only with the catalyst. The metathesis reaction products were stabilized by adding N-phenyl-1 naphthylamine to the solution and then were precipitated using an excess of methanol. The products were dried under vacuum at room temperature and characterized by FT-IR, 1H , ^{13}C -NMR and GPC.

Results and Discussion

Table 1 reports the degradation of the NC in the presence of DMM, DEM and MMA as CTAs, using catalysts G2 and H-G2. The initial molecular weight of natural chicle was $M_n = 1.4 \cdot 10^4$; PDI = 2.5. The yields of the products were in the range of 90–99%.

Table 1. NC metathesis degradation in bulk, with DMM, DEM and MMA as CTAs, using catalysts G2 and H-G2. (NC/CTA=1:1; $[C=C]/\text{catalyst}=250$; temperature=45°C; time=24h, toluene as solvent).

Entry	Rubber	Catalyst	CTA	M_n (theor.) ^a	M_n (GPC) ^b	PDI (GPC) ^b
	NCT	-	-	-	14557	2.49
1	NCT	G2	DMM	212	2243	1.65
2	NCP	G2	DMM	212	2500	1.43
3	NC	G2	DMM	212	2656	1.41
4	NC	H-G2	DMM	212	3414	1.52
5	NCP	G2	DEM	240	2468	1.41
6	NC	G2	DEM	240	3990	1.79
7	NCP	H-G2	DEM	240	2259	1.32
8	NC	H-G2	DEM	240	3153	1.40
9	NCT	G2	MMA	168	1729	1.05
10	NCP	G2	MMA	168	1980	1.03
11	NC	G2	MMA	168	2035	1.13
12	NC	H-G2	MMA	168	1866	1.03

NC: Natural chicle without purification. NCT: Natural chicle dissolved in toluene and precipitated into methanol before use. NCP: Natural chicle precipitated into methanol before use.

G2: 2nd generation Grubbs catalyst. H-G2: 2nd generation Hoveyda-Grubbs catalyst.

a: Theoretical MW based on complete NC and CTA conversion.

b: Determined by GPC with THF as the eluent. Values reported relative to polystyrene standards.

Figure 1 depicts the NC and the telechelic oligomers (TNC) characterized by FT-IR (Table 1, entries 2, 5 and 10). All the IR spectra of the degraded TNC products show the strong peak centered at $\nu = 1741 \text{ cm}^{-1}$ which indicates the presence of the carbonyl group (C=O).

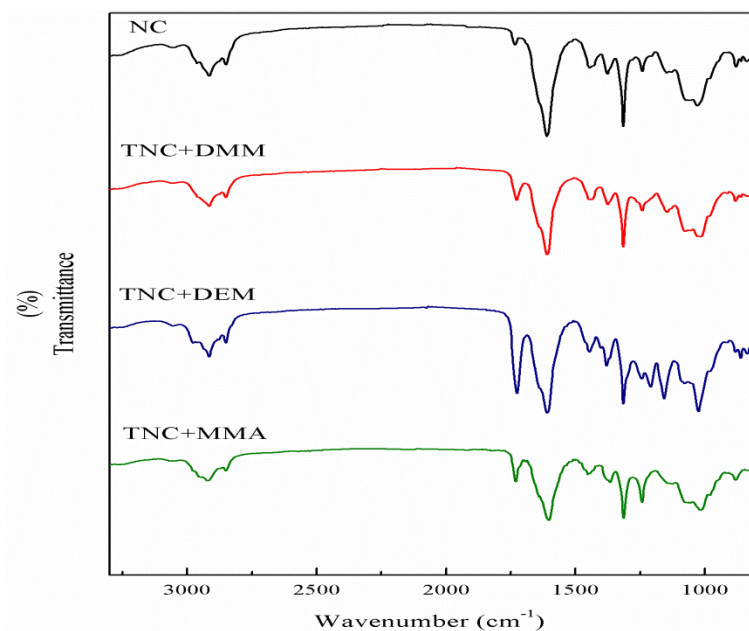


Figure 1. FT-IR spectra of the CN and the products of degradation via cross-metathesis with DMM, DEM and MMA.

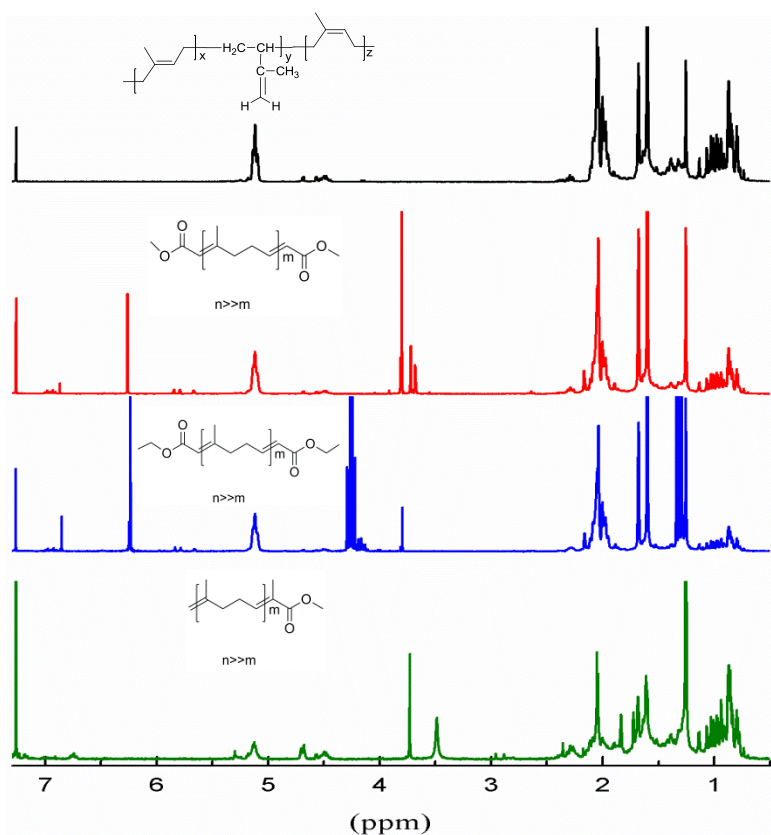


Figure 2. ^1H NMR spectra of the CNT and the telechelic oligoisoprenes using DMM, DEM and MMA as CTAs.

^1H NMR spectra (Fig. 2) of the NC and the products (Table 1; entries 2, 5 and 10) after 24h show that the signals of the ethylene, methyl and methylene protons of the *cis* and *trans* polyisoprene units have not changed from those detected for NC. When DMM was used as CTA, new signals were observed at $\delta=5.84\text{--}5.67$ (H) and 3.79 ppm ($\text{CH}_3\text{-OCO}$). For DEM, the new peaks appeared at $\delta=5.84\text{--}5.67$ (H); 4.29–4.22 (CH_2); 1.337–1.253 ppm (methyl in $\text{CH}_2\text{-CH}_3\text{-OCO}$). Finally, when using MMA, the spectrum show new peaks at $\delta=4.70\text{--}4.67$ (C=CH_2) and 3.73 ppm ($\text{CH}_3\text{-OCO}$). These observations confirmed the formation of diester or methyl ester terminated isoprene oligomers.

Conclusions

Degradation of NC via cross-metathesis with high functionalized olefins DMM, DEM and MMA, using 2nd generation Grubbs and Hoveyda-Grubbs catalysts, can be performed in bulk conditions, avoiding large amounts of organic solvent. Reactions proceeded to give diester or methyl ester telechelics with masses in the range of 1729 to 3990 g/mol determined by GPC. The yields of the oligomers were good and ranged between 90 and 99%. The obtained products can significantly contribute to a sustainable supply for detergents.

Acknowledgements

This work was supported by CONACYT (Ph.D. Scholarship to S. R). The authors thank Alejandrina Acosta and Salvador Pe for their assistance in MR and measurements.

References

- [1]. W. Schelesinger, H. M. Leeper, Ind. and Eng. Chem. (1951), 398–403.
- [2]. Y. Tanaka, J. T. Sakdapipanich, Chemical Structure and Occurrence of Natural Polyisoprenes, Wiley-VCH Verlag GmbH & Co. KGaA, Published Online (2005).
- [3]. E. Azpeitia, A. Bowers, P. Crabbé, O. Mancera, J. S. Matthews, J. Reynoso, J. Salazar, Canadian J. of Chem. 30, (1961), 2321–2323.
- [4]. Ivin KJ, Mol JC. Olefin Metathesis and Metathesis Polymerization; Academic Press: San Diego, CA, 1997, chapter 16.
- [5]. S. Uribe, M. A. Tlenkopatchev. Suplemento de la Revista Latinoamericana de Metalurgia y Materiales 2009 S1 (4): 1463–1467.
- [6]. A. K. Chatterjee, T.-L. Choi, D. P. Sanders and R. H. Grubbs, J. Am. Chem. Soc., 125, (2003), 11360–11370.
- [7]. D. Chen, H. Shao, W. Yao, B. Huang. International Journal of Polymer Science, 2013, (2013), 1–5. DOI:10.1155/2013/937284.